

Materials Forming, Machining and Tribology

Harshit K. Dave
J. Paulo Davim *Editors*

Fused Deposition Modeling Based 3D Printing

 Springer

Materials Forming, Machining and Tribology

Series Editor

J. Paulo Davim, Department of Mechanical Engineering, University of Aveiro,
Aveiro, Portugal

This series fosters information exchange and discussion on all aspects of materials forming, machining and tribology. This series focuses on materials forming and machining processes, namely, metal casting, rolling, forging, extrusion, drawing, sheet metal forming, microforming, hydroforming, thermoforming, incremental forming, joining, powder metallurgy and ceramics processing, shaping processes for plastics/composites, traditional machining (turning, drilling, milling, broaching, etc.), non-traditional machining (EDM, ECM, USM, LAM, etc.), grinding and others abrasive processes, hard part machining, high speed machining, high efficiency machining, micro and nanomachining, among others. The formability and machinability of all materials will be considered, including metals, polymers, ceramics, composites, biomaterials, nanomaterials, special materials, etc. The series covers the full range of tribological aspects such as surface integrity, friction and wear, lubrication and multiscale tribology including biomedical systems and manufacturing processes. It also covers modelling and optimization techniques applied in materials forming, machining and tribology. Contributions to this book series are welcome on all subjects of “green” materials forming, machining and tribology. To submit a proposal or request further information, please contact Dr. Mayra Castro, Publishing Editor Applied Sciences, via mayra.castro@springer.com or Professor J. Paulo Davim, Book Series Editor, via pdavim@ua.pt.

More information about this series at <http://www.springer.com/series/11181>


Harshit K. Dave · J. Paulo Davim
Editors

Fused Deposition Modeling Based 3D Printing

 Springer

Editors

Harshit K. Dave 
S. V. National Institute of Technology
Surat, India

J. Paulo Davim 
Department of Mechanical Engineering
Campus Santiago
University of Aveiro
Aveiro, Portugal

ISSN 2195-0911 ISSN 2195-092X (electronic)
Materials Forming, Machining and Tribology
ISBN 978-3-030-68023-7 ISBN 978-3-030-68024-4 (eBook)
<https://doi.org/10.1007/978-3-030-68024-4>

© The Editor(s) (if applicable) and The Author(s), under exclusive license to Springer Nature Switzerland AG 2021

This work is subject to copyright. All rights are solely and exclusively licensed by the Publisher, whether the whole or part of the material is concerned, specifically the rights of translation, reprinting, reuse of illustrations, recitation, broadcasting, reproduction on microfilms or in any other physical way, and transmission or information storage and retrieval, electronic adaptation, computer software, or by similar or dissimilar methodology now known or hereafter developed.

The use of general descriptive names, registered names, trademarks, service marks, etc. in this publication does not imply, even in the absence of a specific statement, that such names are exempt from the relevant protective laws and regulations and therefore free for general use.

The publisher, the authors and the editors are safe to assume that the advice and information in this book are believed to be true and accurate at the date of publication. Neither the publisher nor the authors or the editors give a warranty, expressed or implied, with respect to the material contained herein or for any errors or omissions that may have been made. The publisher remains neutral with regard to jurisdictional claims in published maps and institutional affiliations.

This Springer imprint is published by the registered company Springer Nature Switzerland AG
The registered company address is: Gewerbestrasse 11, 6330 Cham, Switzerland

Preface

3D printing is the common term used for a variety of additive manufacturing processes in which a three-dimensional object is constructed using a CAD model. Earlier, this process was considered suitable for producing prototypes only. However, in recent times, with the improvement of precision and repeatability, few of the 3D printing processes have become viable as an industrial production technology. Fused deposition modelling is a term used for the 3D printing process, wherein a continuous filament is fed from a spool through a hot extruder head and deposited layer by layer. FDM-based 3D printing is, at present, the most popular 3D printing process owing to its cost and flexibility. Other 3D printing techniques may offer better results, but they are far costlier than the FDM process.

An attempt has been made in this book to provide a thorough understanding of the FDM-based 3D printing process followed by recent studies on experimental investigations, specific applications as well as modelling and optimization of the process. The book consists of 25 chapters. The first two chapters of this book provide a basic outline of the FDM-based 3D printing process. These include the full description of the technique, types of machines and raw materials, process parameters, defects, design variations and simulation methods. The next six chapters (third to eighth chapters) include a vast range of experimental investigations that include studies on process improvement, microstructure study, mechanical testing and characterization. The post-processing of 3D printing part is an important stage of preparing functional parts. The next two chapters (ninth and tenth chapters) are dedicated to the post-processing stage of 3D printing. As 3D printing substantially reduces waste, it is considered to be better in enhancing the sustainability of the products than most of the other existing manufacturing processes. There are two chapters (eleventh and twelfth chapters) dedicated to sustainability concerns in the FDM process. There are wide-scale applications of the FDM process in 3D printing ranging from composites to health care and electronics applications. Seven chapters (thirteenth to nineteenth chapters) discuss various applications like composites, external medical devices, drug delivery system, orthotic inserts, watertight components, etc. Specifically, the nineteenth chapter is dedicated to 4D printing using the FDM process. Though 3D printing is widely

used in present days, the understanding of the theoretical aspects through modelling and optimization is finding immense interest. The last six chapters (twentieth to twenty-fifth chapters) are exclusively dedicated to modelling and optimization study of the FDM process. There is an interesting discussion on computational models, evolutionary algorithms, tool path optimization, layout optimization along with the application of machine learning and metaheuristic approaches in the FDM process.

This book is primarily aimed at graduate-level researchers and educators studying 3D printing. There is sufficient depth for research students with many references to provide direction towards their chosen research area. Researchers will also benefit from the book to know about opportunities for further research.

We are sincerely thankful to Springer for providing this opportunity as well as their professional support throughout the process. Last but not the least, we extend our heartfelt gratitude to all the contributors for their valuable contributions to this book especially during the pandemic situation all around the world which largely restricted access to our laboratories and other resources.

Surat, India
Aveiro, Portugal
April 2021

Harshit K. Dave
J. Paulo Davim

Contents

Introduction to Fused Deposition Modeling Based 3D Printing Process	1
Harshit K. Dave and Sandip T. Patel	
Fused Deposition Modeling Based 3D Printing: Design, Ideas, Simulations	23
Md. Hazrat Ali and Anuar Abilgazyev	
Calorimetry, Structure and Morphology of Printed Samples from Biodegradable Materials Using FDM 3D Printing Technology	43
Dumitru Nedelcu and Andrei-Danut Mazurchevici	
Experimental Investigation on FDM Fabricated Tetra Chiral Auxetic Structures Under Uniaxial Compressive Loading	63
Shailendra Kumar, Swapnil Vyavahare, Soham Teraiya, and Labh Chand Dhakar	
Experimental Study of Drilling 3D Printed Polylactic Acid (PLA) in FDM Process	85
Mohammadreza Lalegani Dezaki, M. K. A. Mohd Ariffin, and B. T. H. T. Baharuddin	
Mechanical Properties of 3D-Printed Elastomers Produced by Fused Deposition Modeling	107
A. Alperen Bakır, Roozbeh Neshani, and Sezer Özerinç	
Mechanical Characterization of Fused Deposition Modeling (FDM) 3D Printed Parts	131
Davood Rahmatabadi, Ahmad Aminzadeh, Mohammad Aberoumand, and Mahmoud Moradi	
Mechanical and Tribological Characteristics of Polymer Composites Developed by Fused Filament Fabrication	151
Vijay Tambrallimath, R. Keshavamurthy, Arun Patil, and H. Adarsha	

The Surface Quality Improvement Methods for FDM Printed Parts: A Review	167
Abdul Wahab Hashmi, Harlal Singh Mali, and Anoj Meena	
Post-processing of FDM 3D-Printed Polylactic Acid Parts by CNC Trimming	195
Mohammadreza Lalegani Dezaki and M. K. A. Mohd Ariffin	
Sustainable Product Development by Fused Deposition Modelling Process	213
R. Keshavamurthy, Vijay Tambrallimath, G. Ugrasen, and D. P. Girish	
Sustainability Analysis of Fused Deposition Modelling Process	227
Faladrum Sharma and U. S. Dixit	
Fabrication of Composite Structures via 3D Printing	255
Madhukar Somireddy	
Use of FDM Technology in Healthcare Applications: Recent Advances	277
Irene Buj-Corral, Aitor Tejo-Otero, and Felip Fenollosa-Artés	
Fused Filament Fabrication for External Medical Devices	299
C. P. Paul, K. Dileep, A. N. Jinoop, A. C. Paul, and K. S. Bindra	
Potential Advanced Drug Delivery Systems Based on Hydrogels in 3D Printing Technology for Cancer Treatment	323
Agnieszka M. Jankowska, Magdalena B. Łabowska, Izabela Michalak, Patrycja Szymczyk-Ziółkowska, Julita Kulbacka, and Jerzy Detyna	
3D Printed Personalized Orthotic Inserts Using Photogrammetry and FDM Technology	349
T. Ravi, Rajesh Ranganathan, S. P. Ramesh, and Devendra Singh Dandotiya	
Manufacturing of Watertight Housing for Electronic Equipment by Fused Deposition Modeling	363
Pablo E. Romero, Antonio Agulló, and Esther Molero	
4D Printing by Fused Deposition Modeling (FDM)	377
Mohammad Aberoumand, Davood Rahmatabadi, Ahmad Aminzadeh, and Mahmoud Moradi	
Computational Models: 3D Printing, Materials and Structures	403
Ashish R. Prajapati, Shilpesh R. Rajpurohit, and Madhukar Somireddy	
Multi-Objective Optimization for FDM Process Parameters with Evolutionary Algorithms	419
Nita Yodo and Arup Dey	

**Application of Machine Learning in Fused Deposition Modeling:
A Review** 445
A. Equbal, S. Akhter, Md. A. Equbal, and A. K. Sood

**Tool-Path Optimization in Material Extrusion Additive
Manufacturing** 465
Neri Volpato and Tiago Rodrigues Weller

**Metaheuristic Approaches for Modeling and Optimization
of FDM Process** 483
Ahmad Aminzadeh, Mohammad Aberoumand, Davood Rahmatabadi,
and Mahmoud Moradi

**Layout Optimization for FDM Process by Multi-objective
Optimization Using RSM and GRA** 505
Sandeep Rathee and Manu Srivastava

Introduction to Fused Deposition Modeling Based 3D Printing Process



Harshit K. Dave and Sandip T. Patel

Abstract Fused deposition modeling (FDM) or fused filament fabrication (FFF) is one of the most popular 3D printing technologies for variety of applications. It's ease of use and affordable cost makes it popular among diverse group of users. In this chapter basics of FDM technology is discussed to cater all types of readers. The process parameters and its effects are also included in this chapter.

1 3D Printing

3D printing (3DP) is commercially existing from 80's, but still today it resembles technology from the science fiction movie. Today 3D printers have begin to enter into household as an essential article, similar to computer.

Another accepted technical term for 3DP is additive manufacturing (AM). According to ISO/ASTM [1], 3DP is defined as process of joining material feedstock to make desired shape part from 3D model data, usually layer upon layer. In this definition, feedstock means bulk raw material and layer means process of laying out the feedstock material to create a surface. The shape of layer is generally planar in order to reduce complexity of much complex 3DP procedure. Addition to this, it is worth mentioning that layer should be adequately thin. 3D model data requirements render computer essential for 3DP, unlike subtractive- and formative-manufacturing.

H. K. Dave

Department of Mechanical Engineering, Sardar Vallabhbhai National
Institute of Technology, Surat, Gujarat, India
e-mail: harshitkumar@yahoo.com

S. T. Patel (✉)

Department of Mechanical Engineering, Government Engineering College,
Valsad, Gujarat, India
e-mail: stpatel1983@gmail.com

There are many well-established 3DP processes exist today and still new processes are getting invented and developed. Principle difference between these processes lies in two operations:

- i. how layer of feedstock material is created, and
- ii. how subsequent layer are bonded or fused

These operations mainly depend on type of feedstock material (i.e. metal, polymer, ceramics, composite etc.) and form of feedstock material (i.e. powder, sheet, filament, liquid, slurry, paste etc.). All these factors determine the working principle and machine architecture of particular 3DP process. Based on fundamental working principle, 3DP processes can be broadly categorised into seven types as depicted in Fig. 1.

2 Material Extrusion

According to ISO/ASTM 52900:2015 [1], material extrusion is the umbrella term for 3DP processes in which material is selectively dispensed through a nozzle or orifice to build parts. In simple terms, it is analogous to computer controlled hot glue gun used to build three-dimensional shape by dispensing glue layer upon layer.

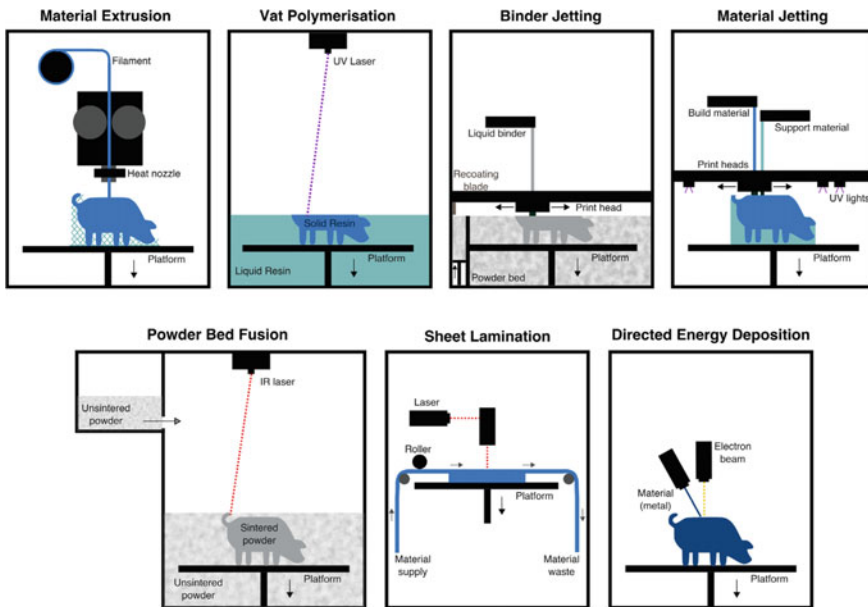


Fig. 1 Illustrations of the seven categories of 3DP processes (Image permission under the Creative Commons Attribution License 4.0 [2])

Extrusion in conventional manufacturing is forming operation to create uniform cross section objects by continuously pushing out heated material through die. The shaping of object finalizes when material came out of a die. Material extrusion in context of 3DP is not related to forming, as shaping of object is not finalized when material is pushed out of nozzle. Object shape is finalized by in situ deposition of material as per the CAD data. The continuous strand of material came out of nozzle gives distinguish characteristic to the object, which differentiate material extrusion from other 3DP processes.

Material extrusion is generally used for polymer materials. Conceptually any material which can flow continuously out of nozzle and then harden can be used for material extrusion. So, there are variety of materials that can be used such as polymer, polymer matrix composite, clay, concrete, food, hydrogels etc. In theory the same process can be used for metals by heating them at high temperature. Due to high surface tension of molten metal it will form droplets coming out of nozzle and not continuous strand of metal, which cannot be considered as material extrusion.

The sole focus of this book is on the fused deposition modeling (FDM) technology. Thus, rest of the topics are concentrated on FDM technology.

3 Introduction of Fused Deposition Modeling

Fused deposition modeling (FDM) is most prevailing material extrusion type 3DP technology. It is the reason that majority presumes material extrusion as FDM. The term FDM is coined and trademarked by, its inventor and co-founder of Stratatsys, Scott Crump. Fused filament fabrication (FFF) is another term used as synonym to fused deposition modeling. The term FFF had coined by the makers of RepRap project [3] and advocated by members of open source community to prevent legal issues related to intellectual property rights (IPR). In this chapter the term FDM is used to be interpreted as FFF/FDM for convenience.

FDM can be defined as filament based material extrusion 3DP process in which polymer (usually thermoplastic) filament is melted using heated nozzle and selectively dispensed layer by layer to build parts [4, 5]. There is no standard definition exist for FDM by national or international standards. Due to this reason, many times other material extrusion techniques are falsely considered as FDM. The distinct feature of FDM is filament based material extrusion, wherein filament also act as a machine element. Solid filament perform function of a piston to push molten material in heated nozzle.

FDM is the most extensively employed 3DP technology in terms of number of 3D printers worldwide actively installed [6, 7]. It is most affordable 3D printing technology at desktop scale, which makes it first choice for domestic consumers, hobbyist and education institutes.

4 FDM Process and Working Principle

Overall FDM printing process is depicted in Fig. 2. Similar to generic 3DP process, it starts with creation of CAD model with aid of any CAD software. The 3D CAD model is prepared by designer using design inputs and in case of reverse engineered design, using scanned data of a geometry. Then native CAD model is converted into file format which can be understood by 3D printing software, commonly known as slicing software. These common file formats are respectively STL, OBJ, AMF and 3MF. The STL format is the most used file format. It has become unofficially accepted standard representation in the 3DP industry [8].

In next step, the tessellation CAD model is imported in slicing software. Nowadays, few commercially available slicing software are capable of importing native 3D files from CAD software, which improves the accuracy of CAD model. Slic3r, Cura and Repetier are few popular and freely available slicing software. The main function of slicing software is to convert imported 3D CAD models into printing instructions for a given 3D printer to build an object. The slicing software performs numbers of tasks including: (i) slicing CAD model into thin horizontal layers, (ii) infill generation, (iii) support structure generation for overhangs, and (iv) tool path generation for each layer; based on user inputs for build orientation, slicing parameters (i.e. raster width, raster orientation, infill, layer thickness etc.) and machine parameters (i.e. deposition speed, extrusion temperature, build platform temperature etc.). All of this necessary process-relevant data to convert a digital model into a physical model is then recorded in the G-code file. This G-code file can afterwards be sent to FDM printer.

The controller unit of FDM printer directs the printhead to build a part with layer by layer deposition of material as per instruction recorded in G-code file. The typical FDM printer schematic is depicted in Fig. 3. During printing, the filament

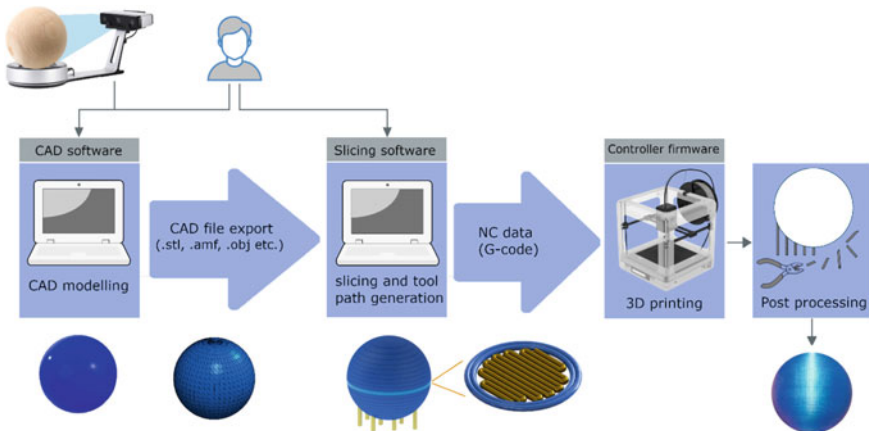


Fig. 2 FDM printing process

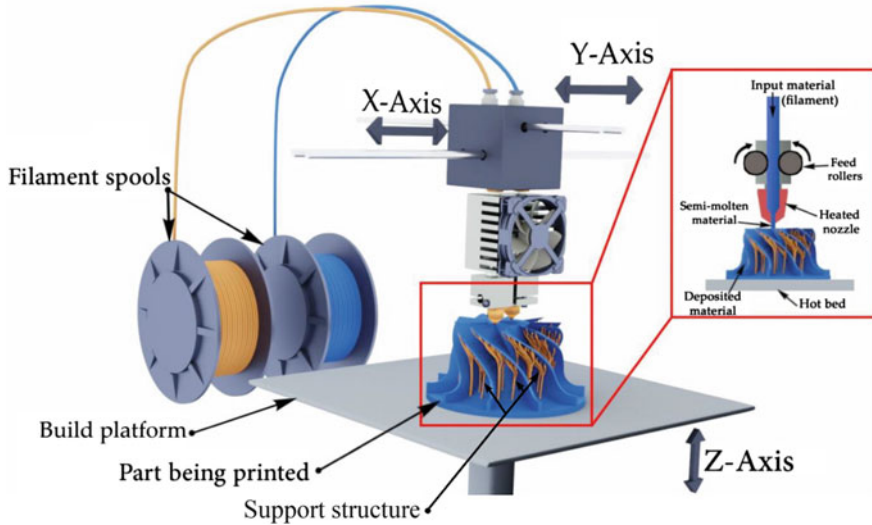


Fig. 3 FDM printer schematic (Image permission under the Creative Commons Attribution License 4.0 [10])

based feedstock material is unwound from spool and fed to printhead, which heats the filament into semiliquid state above its glass transition temperature. It is then extruded out of a nozzle in form of fine bead and deposited on built platform of printer. Here, moving solid filament perform function of a piston to push molten filament out of nozzle [9]. The force exerted by filament to extrude the melt must be adequate to overcome the pressure drop across the printhead, which depends on the rheological properties of the melted material and the geometry of the flow path. Thus, filament must be rigid enough and should not fail under buckling. Filament acting as a machine element simplifies and reduce the size of extrusion mechanism of FDM printer. The printhead (or the build platform) can travel in X- and Y- axis, which enable depositing the molten material to form 2D layers of the build part. On completion of each layer, starting from the bottom layer, the build platform (or the printhead) will travel in the Z axis by amount of selected layer thickness, which enable depositing the following layer on top of the preceding layer. The hot semiliquid state of the material deposited from the nozzle tip enables adjacent layers and adjacent beads to fuse together. The nozzle tip pressed the extruded molten material against the previous layer. Due to pressure and the high temperature, the surface of the previous layer re-melts. This enables the fusion of the new layer with the previously printed substrates. The material solidifies quickly after being deposited. The layer by layer deposition process is continue until the part is finish. Dual extrusion head printers are also available, in which one nozzle dispense base material to build part while second nozzle dispense material for support structure.

In last step, the completed part is removed from the FDM printer and post processing operations are carried out as per the requirement. Generally, the

objective of post processing is to remove support structure, improve aesthetics and improve surface quality. The support structure material is either insoluble or soluble type. Insoluble Support structures are removed by breaking them away, as they are printed in a more fragile state. While, soluble support structure material dissolve in water or specific chemicals, such as PVA (soluble in water) and HIPS (soluble in d-Limonene). Variety of other optional post processing operations which can be performed on FDM printed part are sanding, polishing, painting, metal plating, epoxy coating, dipping, vapor smoothing, etc.

5 FDM Printer Types

Variety of FDM printers are available in different sizes, configuration and mechanisms. Their classification according to configuration and technology source is discussed.

5.1 Printer Types as Per Configuration

FDM printers can be classified into four types according to their configuration viz. cartesian, delta, polar, and robotic arm, as depicted in Fig. 4.

5.1.1 Cartesian FDM Printers

The most common FDM 3D printer configuration is cartesian. This type of printer operates using cartesian coordinate system. The build volume shape is rectangular prism and for that reason shape of build platform is kept rectangular or square. This type of printer has three linear carriages in X-, Y-, and Z- axis to place a printhead in the correct position during printing. This is accomplished by either moving

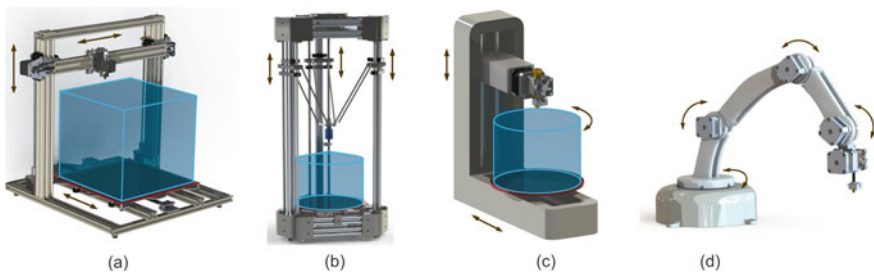


Fig. 4 Types of FDM printers as per configuration, **a** cartesian, **b** delta, **c** polar, and **d** robotic arm, the build volume is shown in blue

printhead or moving both printhead and build platform, driven by linear carriages. There are three popular variants of cartesian 3D printer, as listed below along with example of few 3D printer models available in recent times.

- i. Printhead move in X-Y plane and build platform move along Z axis. Examples of 3D printer models: Stratasys F123, Ultimaker S5, MakerBot Replicator+.
- ii. Printhead move in X- and Z- axis, while built platform move in Y axis. Examples of 3D printer models: Original prusa mini, LulzBot Mini, da Vinci Jr. 2.0.
- iii. Printhead move in X-, Y- and Z- axis, while built platform is stationary. Examples of 3D printer models: BigRep ONE, Cincinnati MAAM.

5.1.2 Delta FDM Printers

Delta configuration 3D printers typically have three arms attached to vertical rails. The printhead is suspended above build platform by these arms in a triangular layout, where the printhead is connected to the end of each arm with spheroidal joints. The coordinated movement of arms on vertical rails adjust the position of printhead relative to the build platform in 3D build envelope. The built platform is kept stationary. The build volume shape is almost cylindrical and for that reason shape of build platform is kept circular.

The delta configuration printers are cheaper and faster but less accurate compared to cartesian configuration printers. Example of popular delta 3D printers are Delta WASP, Anycubic Predator, Mass Portal XD, etc.

5.1.3 Polar FDM Printers

This type of printer operates using polar coordinate system. They are least popular among all other configuration. The build volume shape is cylindrical and for that reason shape of build platform is kept circular. Generally, the printhead can move in Z-axis. The position of printhead is defined by polar coordinate system in horizontal plane, where each point on a plane is determined by a distance from a center point of build platform and an angle from a reference direction. This is achieved by rotating the build platform and linear lateral movement of the build platform (or the printhead). Example of polar configuration printers are Polar 3D and Sculpto PRO2.

5.1.4 Robotic Arm FDM Printers

This category of FDM printer is an industrial robotic arm attached with printhead as an end effector. Robotic arm is more expensive than any other configuration of FDM printer. Still, they are gaining popularity due to their speed and ability to print geometrically complex parts. Example of Robotic arm FDM printers are Dobot Magician and Rotrics DexArm.

5.2 Printer Types as Per Technology Source

There are two types of FDM printer technology available viz. open-source and closed-source. Closed-source or Proprietary technology is closely guarded by means of IPR. As oppose to proprietary technology, open-source technology is freely available for everyone. Under RepRap project many open-source printer designs and its software were developed and available to everyone. On contrary, Stratasys being the pioneers in FDM have the majority of the patent related to FDM and hold on radical technology.

6 Material Feedstock

FDM feedstock is solid filament usually made of thermoplastic material. Filament is characterized by extreme length relative to its uniform cross section. Most commonly available filament diameter sizes are 1.75 and 2.85 mm. There are great variety of materials to choose from and absolutely new materials are emerging regularly in the 3D Printing market. Feedstock materials are available from all category of thermoplastic pyramid including commodity-, engineering- and high-performance- thermoplastics, as depicted in Fig. 5.

As material directly affects the physical properties and printing behavior of printed part, it is important to consider material selection before CAD modeling. The comparison of few popular pure thermoplastic filament material is depicted in Fig. 6. FDM printer filaments available in a variety of polymer material as well polymer based composite consist of fibre- and particle- reinforcement. Variety of reinforcement material can be premixed with thermoplastic to make filament, for example carbon fibre, glass fibre, kevlar, wood, metal powder etc. Continuous fibre reinforcement is also made possible by various similar technology.

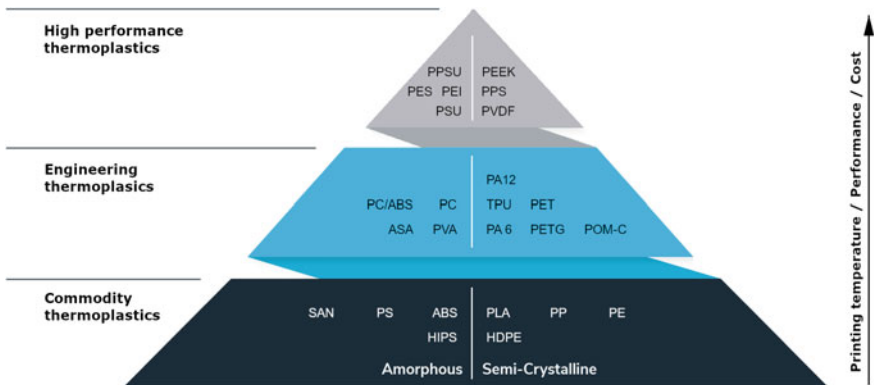


Fig. 5 Thermoplastic material pyramid for FDM filament materials

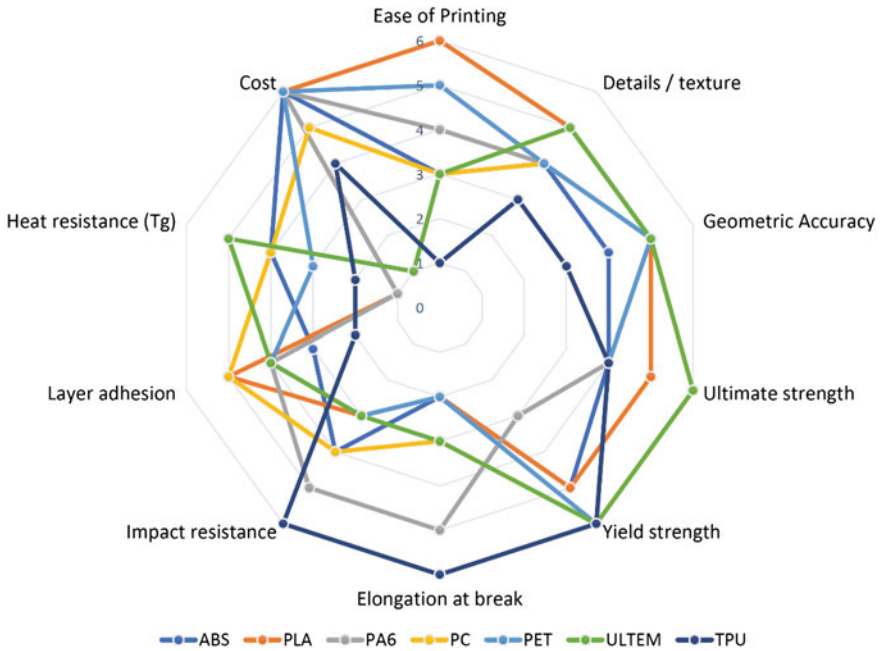


Fig. 6 Ranking of FDM 3D printing polymers on six-point ranking scale (1-being less preferable to 6-being highly preferable) along the different criteria including process-, quality-, thermal- and mechanical- performance

7 Process Parameters

FDM offers various process parameters, and they have a great effect on build time, quality and mechanical characteristics of printed parts [11–13]. Selecting proper combination of process parameters enables predication and control of part characteristics. Which allow the user to select optimum combination of process parameters to achieve part with desired characteristics. These process parameters are related to build orientation, machine parameters (i.e. deposition speed, build chamber temperature, extrusion temperature, build platform temperature etc.) and slicing parameters (i.e. layer thickness, raster width, infill, raster orientation, air gaps etc.) as depicted in Fig. 7.

7.1 Extrusion Temperature

Extrusion temperature is referred to the temperature at which the filament material is heated in the liquefier before extrusion [13].

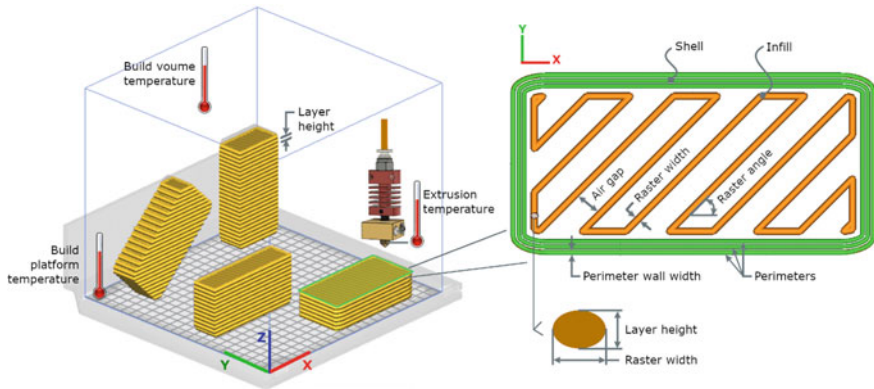


Fig. 7 FDM process parameters

The viscosity of molten material coming out from the nozzle is controlled by extrusion temperature. With increase in extrusion temperature, the viscosity of molten material decreases. This allows melt to flow more easily through the printhead with a smaller pressure drop. Increase in extrusion temperature also improves fusion between successive beads or raster of extruded material, that enhance the mechanical strength of printed part [14]. At higher temperature some polymer degrades quickly and left residue inside the nozzle that would contaminate further melt [15].

7.2 Nozzle Diameter

Nozzle diameter is referred to the internal diameter of extruder nozzle opening. Typical nozzle sizes are 0.15, 0.2, 0.25, 0.3, 0.35, 0.4, 0.5, 0.6, 0.8 and 1.0 in mm. It is much obvious that a larger nozzle will extrude more material than a smaller nozzle, hence reduce the build time.

7.3 Build Orientation

Build orientation is referred to the orientation of printing part with reference to machine coordinate system in a build envelope, as depicted in Fig. 7.

Build orientation is one of the key process parameter which has significant impact on the staircase effect and volume of support structure generation [4, 17, 18]. Staircase effect is partially responsible for dimensional accuracy and surface finish of printed part. While the support structure generation contribute to post-processing requirement, material amount and build time [17, 18]. An example of support

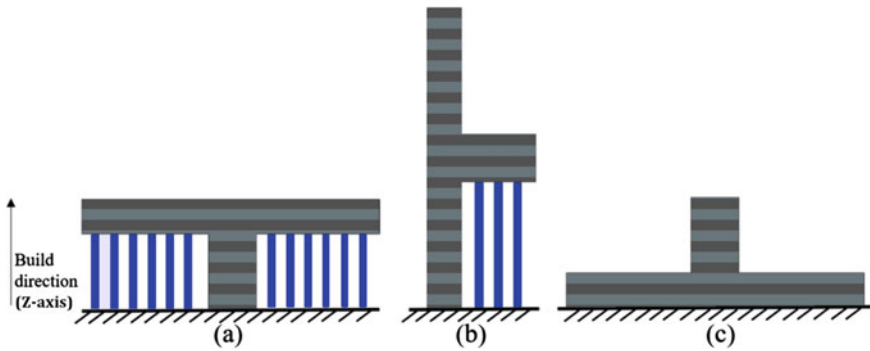


Fig. 8 Support structure (blue) volume requirement for different build orientation of T shaped part (gray): **a** highest, **b** medium, and **c** zero (Image permission under the Creative Commons Attribution License 4.0, adapted from [16])

structure generation for various build orientation of T shaped part is depicted in Fig. 8. Furthermore, build orientation defines the direction in which the mechanical properties of part show anisotropic behavior [18, 19]. This is due to the fact that in FDM, Z-axis anisotropy is highest due to poor inter layer bonding.

7.4 Layer Thickness

Layer thickness is referred to the thickness of the deposited layers along the Z-axis of FDM printer. Typical layer thickness for FDM varies from 0.05 to 0.4 mm [19]. Usually, it is smaller than the printhead nozzle diameter. A rule of thumb suggests, layer thickness should be within 0.25–0.8 times nozzle diameter. The minimum possible layer thickness of FDM printer is called printing resolution on Z-axis or vertical resolution. It is different from printing resolution, which is size of the smallest possible detail on X- and Y-axis.

Layer thickness directly affects surface quality and build time of the printed part. With reduction in layer thickness the staircase effect is minimized, while the build time increases [4, 13]. Smaller layer thickness produced more detailed part having high surface finishing. Furthermore, more precise and accurate slicing of CAD model is made by slicer software for smaller layer thickness, which eventually eliminates potential voids and gaps [19]. It is observed that smaller values of layer thickness enhance the tensile strength [11, 13].

7.5 Raster Width

Raster width is referred to the width of the bead deposited from the nozzle. It depends on the extrusion nozzle diameter, flow rate and print speed. It is observed that smaller values of raster width enhance the tensile strength [11].

7.6 Raster Angle

Raster angle is referred to the angle between the deposition raster and the X-axis of build platform. Thus, Raster angle decides the tool path direction with respect to X-axis of the printer. It should not confuse with raster orientation corresponding to loading condition. The positive direction for raster angle is in anti-clockwise from X-axis.

In reality, combine effect of build orientation and raster angle defines raster arrangement within the part. In simple words, for same layer- and raster-arrangement for a FDM printed part, multiple combination of build orientation and raster angle exists. An example for said condition is depicted in Fig. 9.

7.7 Shell and Associated Parameters

Shell is outermost solid wall of FDM printed parts. Top and bottom wall/shell of part is usually printed by completely filled solid layers. They may be chosen to keep open also.

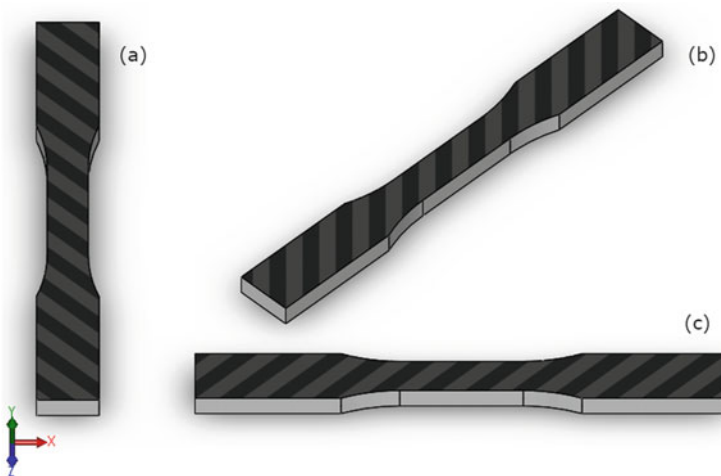


Fig. 9 Tensile test specimens for combination of three build orientations in xy plane and three raster angles viz, **a** 135°, **b** 90°, and **c** 45°; producing same part

The outlines of each layer create the vertical shell. Perimeters is referred to the number of outlines in each layer, which creates vertical shell. While, perimeter wall width is width of the bead deposited in perimeter or outlines in each layer.

7.8 Infill Pattern

In order to decrease build time and save material, FDM parts are generally not printed fully solid. Parts are printed with porous internal structure which is called as infill. The geometry of infill is referred as infill pattern. Selection of infill pattern is generally made based on its printing time, strength and flexibility. Verity of infill patterns are available in various slicer software. There are two types of infill patterns: 2D and 3D. The most commonly used infill patterns are depicted in Fig. 10.

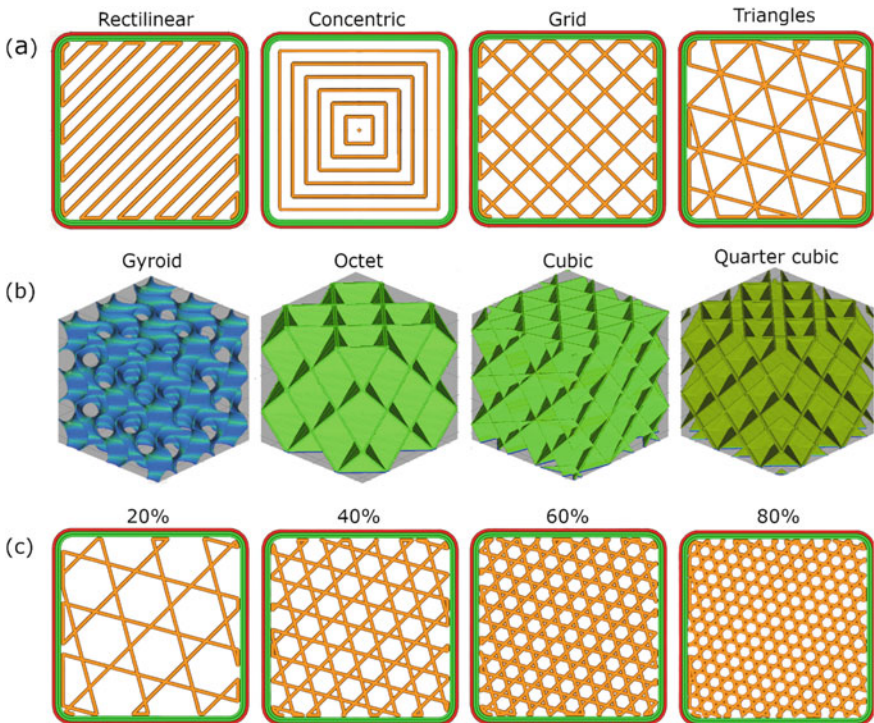


Fig. 10 Commonly found infill types in open software, **a** 2D infill patterns, **b** 3D infill patterns, and **c** various infill density for tri-hexagon/stars pattern

7.9 Infill Density

Infill density is defined as the percentage of infill volume with filament material. It can range from 0% (completely hollow) to 100% (completely solid). Higher infill density means that there is more material, hence higher strength and weight of part. Comparison of different infill density are depicted in Fig. 10c.

7.10 Air Gap

Air gap is referred to the gap between two adjacent beads on a deposited layer. In slicer software generally three kinds of air gap can be specified in a layer, which includes gap between two adjacent perimeter; gap between two adjacent interior raster; and gap between innermost perimeter and outermost interior raster. The value of air gap can be either positive, zero or negative, as depicted in Fig. 11. In case of zero air gap, the two adjacent raster just touch. A positive air gap means that two adjacent raster do not touch, which creates less dense structure having faster build time. Negative air gap means that two adjacent raster overlap on each other, which creates relatively dense structure with higher build time. Generally negative air gap is preferred to improve mechanical properties [11].

7.11 Print Speed

Print speed is referred to the travel speed of the printhead along the XY plane while extruding. Typical print speed for FDM printer varies from 30 to 80 mm/s.

Print speed affects the build time of printed part. With increase in the print speed, build time reduced. Low print speed is recommended to gain a higher print precision, as at higher speed dynamic effect of drive system increases, which give rise to jerky motion [13]. Speed is also constrained by maximum volumetric flow rate of extruder head. The maximum speed can be calculated by following Eq. (1) [15].

$$\text{Max. print speed} = \frac{\text{Max. volumetric flow rate}}{\text{Layer height} \times \text{Raster width}} \quad (1)$$

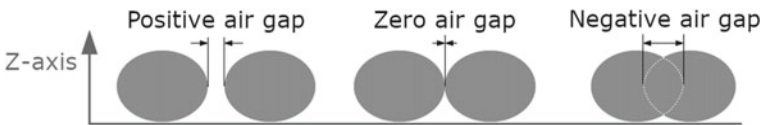


Fig. 11 A schematic representation of two adjacent raster cross-section, showing different airgap conditions

7.12 *Build Volume Temperature*

The build volume temperature can only be maintained when printer is with enclosures. Enclosures can improve printing performance by keeping dust and wind out and heat in. Not much research has been made to check effect of build volume temperature on FDM printed parts.

7.13 *Build Platform Temperature*

The build platform is generally heated to improve adhesion of first layer of the part to the build platform. The build platform temperature is recommended to kept slightly above the glass transition temperature of the filament material to achieve the optimal adhesion [20].

7.14 *Skirt and Brim*

Brim is referred to an extra area outside part boundary, attached to extreme edges of part in a first layer, as depicted in Fig. 12a. It is provided to increase surface area for the better adhesion of printed part to the build platform. It also reduces warping. Once the print it is finished, brim is cut away.

The skirt is a printed outline at a short distance away from the perimeter of the object, as depicted in Fig. 12b. The skirt is deposited on the build platform before starting to print the part in order to ensure that the material is flowing smoothly from the printhead.

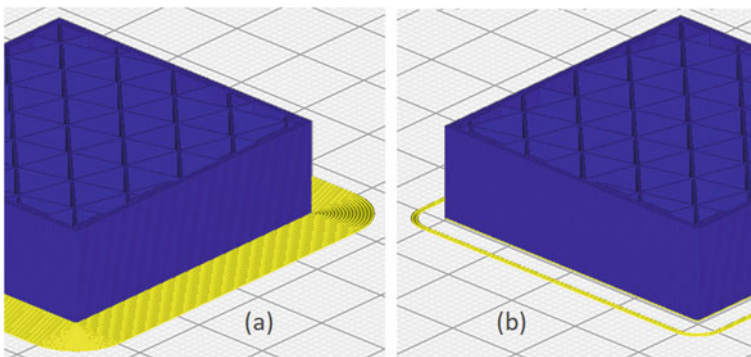


Fig. 12 FDM printed part (blue) with **a** Brim (yellow) and **b** skirt (yellow)

7.15 Processing Parameter Correlations

Processing-structure-property relationships in FDM are complex, nonlinear and poorly understood [21]. Understanding of this correlation having key significance to lead a way for standardizing the process and maximizing adaptation by industry [12]. Various process parameters influence the build time, mechanical characteristics, surface quality and dimensional accuracy of printed part in indirect or direct manner. Nevertheless, not all process parameters have same impact on various outcome, some process parameters have strong effect while other have smaller impact. Researchers focusing on some key parameters, which are illustrated with aid of ishikawa diagram as depicted in Fig. 13.

Due to unavailability of standards for FDM machine, materials and test procedures, benchmarking of results obtained from a variety of research studies focused on process parameters is complex task. In other words, for current research status, generalizing the results obtained from various research is almost impossible due to complex correlations among process parameters [11]. Although, few common takeaways confirmed by majority of studies are listed below.

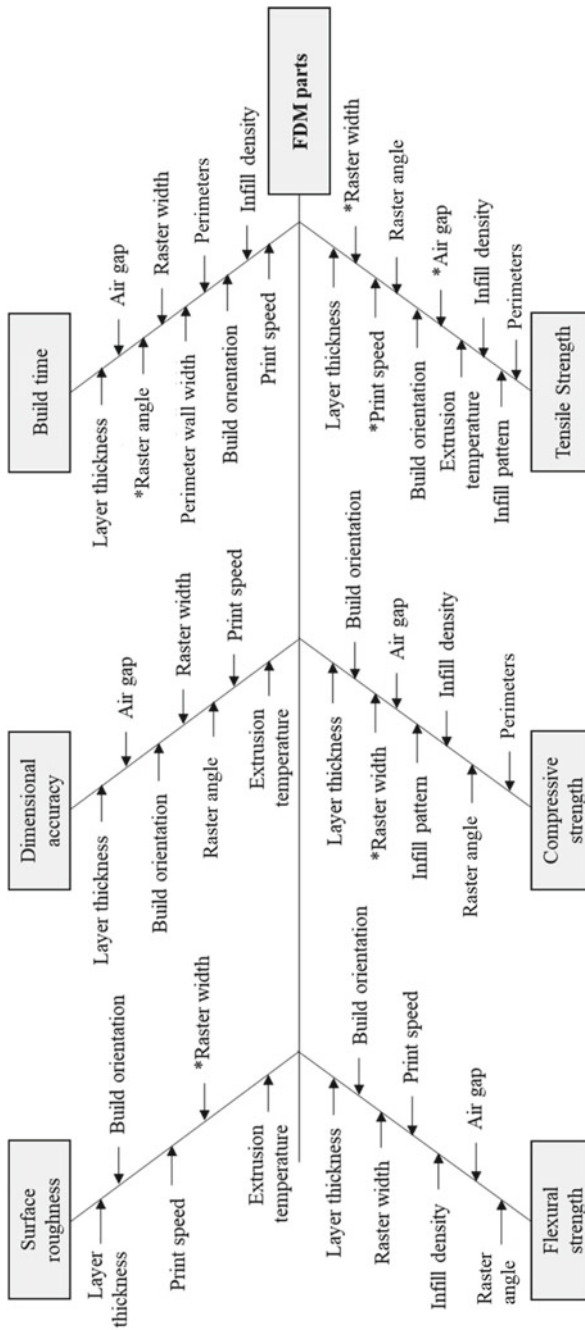
- Extrusion temperature, build platform temperature, build volume temperature, infill pattern, perimeters, perimeter wall width and nozzle diameter are currently insufficiently studied in the literature [11, 13].
- Layer thickness, build orientation, raster angle, infill pattern, infill density and air gap are the key parameters having significant effect on mechanical properties of FDM printed parts [11, 21, 22].
- Tensile strength is increased with rise in infill density and perimeters [14].
- Tensile strength is maximum when the direction of extruded raster of part are parallel to the direction of the applied force [11, 23–26]. This can be achieved by proper combination of build orientation and raster angle.
- Build time is found minimum at higher layer thickness, low infill density, zero raster angle and build orientation having minimum support structure [13].

Further research is needed to investigate combined effect of process parameters on compressive strength, flexural strength and fatigue strength.

8 Defects in FDM Printed Parts

There are few common defects associated with FDM (as depicted in Fig. 14) due to variety of reasons, including and not limited to poor calibration of printer, selection of wrong operation parameters etc.

Warping is most usual quality issue in FDM printed parts. In warping, generally base of the printing part is bent upwards due to thermal contraction of the upper layers. This occurs due to variation in cooling rates between different layers of the print. It can be prevented by increasing the adhesion between the part and the build



* Indicates still unknown whether a parameter is significant for a part characteristic or not

Fig. 13 An Ishikawa diagram to illustrate the effects of FDM process parameters on part characteristic (Image permission under the Creative Commons Attribution License 4.0, adapted from [13])

platform, and maintaining proper temperature of the FDM system. Another similar defect, called elephant's foot, occurred on base layers of part where material build-up occurs in the X-Y plane. It occurs when the nozzle is very close to the build platform or the temperature of the build platform is very high.

Layer shifting or layer misalignment is a displacement of print layers at a certain height from their intended positions in the X-Y plane. FDM printers with an open-loop control system, generally have this problem. The printer cannot detect wrong position of printhead if for any reason a servo motor loses steps, and print will continue with a wrong position.

Stringing or oozing is hairy strings of plastic that sometimes occurs in open area between two sections of print. Stringing happens when a small amount of plastic leaks and drips out of the nozzle, leaving a small thread stick to two sections in open area. This problem is usually caused by inaccurate settings used during the slicing process. It can be prevented by reducing extrusion temperature and proper filament retraction setting.

Ringing is a wavy pattern that may appear on the surface of printed part. It occurs due to printer vibrations, which are usually caused by the inertia of the printhead and when there are sudden direction changes. Reduction in the printing speed will reduce the ringing. Mechanical vibrations due to loosen and damaged machine components should be fixed to reduce the ringing.

Z-wobble is usually spotted when the printed layers are not perfectly aligned laterally with their adjacent layers above and below. Z-wobble may appear to look like ridges or lines appear in a repeating pattern on the sides of part. This problem is may be due to mechanical issues, temperature fluctuations or poor filament quality.

Curling or overheating occurs due to melting material at a very hot temperature, that will cause deformation in the part having curled corners and sagged layers. This

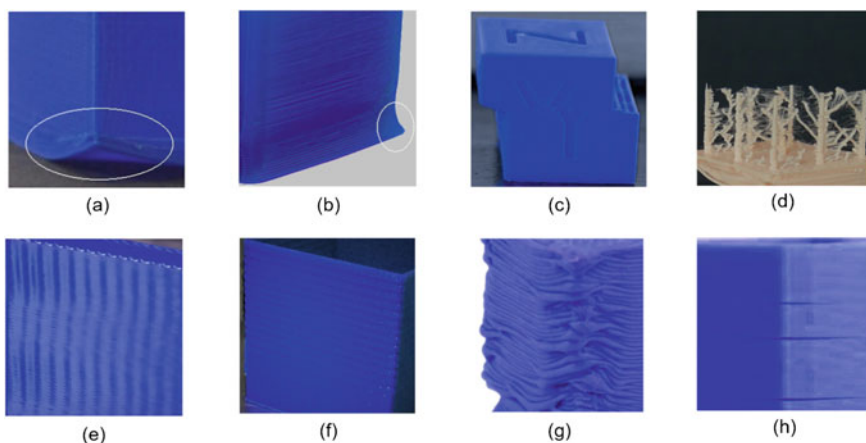


Fig. 14 Defects in FDM printed parts, **a** warping, **b** elephant's foot, **c** layer shifting, **d** stringing, **e** ringing, **f** z-wobble, **g** curling, and **h** layer separation

occurs as high temperature melt does not solidify and retain its shape in time, which cause layers to collapse or sag. This problem can be simply resolved by reducing printing temperature and increasing cooling.

Layer separation occurs when the layers of a part do not bond, resulting in these layers being separated. This defect occurs due to poor bonding between the layers. This can be resolved by increasing the print temperature or reducing the layer fan speed.

9 Advantages and Limitations

The advantages associated with FDM are as listed below.

- Compare to other major 3D printing methods, FDM is more affordable, accessible and cost-effective. Due to these reasons it is most used 3DP technology and best suited for beginners.
- FDM printer is relatively simple to operate and maintain.
- The process is relatively clean, safe and doesn't require the use of harsh chemicals.
- Feedstock materials are very diverse, readily available and affordable.
- Broad range of thermoplastic materials and exotic filaments can be printed with no or relatively few alterations on any FDM printer.
- Design of FDM printer can be scaled easily compare to other 3DP technology. They are available in size that can fit on a desktop to size of large wardrobe.

The limitations associated with FDM are as listed below.

- The major limitation of FDM is part strength and anisotropy. Parts build by FDM are not fully dense and z-axis anisotropy arises as inter-layer bonding is not as strong as intra-layer bonding.
- Surface quality (including volumetric error, shape deviation and surface finish) of FDM is not as good as other major 3D printing methods.
- High detail prints are hard to achieve.
- Unsuitable for thin-walled products. As per thumb rule, recommended minimum wall thickness for horizontal/vertical wall is 1 mm, while curved and slant wall will require more thickness.
- FDM is primarily limited to thermoplastics based pure- and composite- materials. Metal and ceramic material printing is possible by using thermoplastics-based metal/ceramic reinforced filament, but it requires secondary sintering operation and resultant part will not be fully dense.

References

1. ISO/TC 261 (2015) ISO/ASTM 52900:2015. Additive manufacturing—general principles—Part 1: terminology
2. Carew RM, Errickson D (2020) An overview of 3D printing in forensic science: the tangible third-dimension. *J Forensic Sci* 65:1752–1760. <https://doi.org/10.1111/1556-4029.14442>
3. RepRap (2019) (2020) Fused filament fabrication—RepRap. In: Reprap.org. https://reprap.org/wiki/Fused_filament_fabrication. Accessed 16 Nov 2020
4. Masood SH (2014) Advances in fused deposition modeling. In: *Advances in additive manufacturing and tooling. Comprehensive materials processing, vol 10*, pp 69–91. Elsevier
5. Mwema FM, Akinlabi ET (2020) Basics of fused deposition modelling (FDM). In: *fused deposition modeling*, pp 1–15. Springer
6. Varotsis AB (2020) Introduction to FDM 3D printing| 3D Hubs. In: 3D Hubs. <https://www.3dhubs.com/knowledge-base/introduction-fdm-3d-printing/>. Accessed 16 Nov 2020
7. Moreau C (2020) The state of 3D printing. <https://www.sculpteo.com/blog/2020/06/02/download-our-state-of-3d-printing-2020-for-free/>. Accessed 16 Nov 2020
8. Qin Y, Qi Q, Scott PJ, Jiang X (2019) Status, comparison, and future of the representations of additive manufacturing data. *Comput Aided Des* 111:44–64. <https://doi.org/10.1016/j.cad.2019.02.004>
9. Kumar S (2020) Other solid deposition processes. *Additive manufacturing processes*. Springer, Cham, pp 111–130
10. Elkaseer A, Schneider S, Scholz SG (2020) Experiment-based process modeling and optimization for high-quality and resource-efficient FFF 3D printing. *Appl Sci* 10:2899. <https://doi.org/10.3390/app10082899>
11. Popescu D, Zapciu A, Amza C et al (2018) FDM process parameters influence over the mechanical properties of polymer specimens: a review. *Polym Testing* 69:157–166. <https://doi.org/10.1016/j.polymertesting.2018.05.020>
12. Dizon JRC, Espera AH Jr, Chen Q, Advincula RC (2018) Mechanical characterization of 3D-printed polymers. *Addit Manuf* 20:44–67. <https://doi.org/10.1016/j.addma.2017.12.002>
13. Dey A, Yodo N (2019) A systematic survey of FDM process parameter optimization and their influence on part characteristics. *J Manuf Mater Process* 3:64. <https://doi.org/10.3390/jmmp3030064>
14. Turner BN, Strong R, Gold SA (2014) A review of melt extrusion additive manufacturing processes: I. Process design and modeling. *Rapid Prototyp J* 20:192–204. <https://doi.org/10.1108/rpj-01-2013-0012>
15. Gibson I, Rosen D, Stucker B (2015) *Extrusion-based systems. Additive manufacturing technologies*. Springer, New York, pp 147–173
16. Jiang J, Xu X, Stringer J (2018) Support structures for additive manufacturing: a review. *J Manuf Mater Process* 2:64. <https://doi.org/10.3390/jmmp2040064>
17. Das P, Mhapsekar K, Chowdhury S et al (2017) Selection of build orientation for optimal support structures and minimum part errors in additive manufacturing. *Computer-Aided Des Appl* 14:1–13. <https://doi.org/10.1080/16864360.2017.1308074>
18. Di Angelo L, Di Stefano P, Guardiani E (2020) Search for the optimal build direction in additive manufacturing technologies: a review. *J Manuf Mater Process* 4:71. <https://doi.org/10.3390/jmmp4030071>
19. Bikas H, Lianos AK, Stavropoulos P (2019) A design framework for additive manufacturing. *Int J Adv Manuf Technol* 103:3769–3783. <https://doi.org/10.1007/s00170-019-03627-z>
20. Spoerk M, Gonzalez-Gutierrez J, Sapkota J, Schuschnigg S, Holzer C (2017) Effect of the printing bed temperature on the adhesion of parts produced by fused filament fabrication. *Plast, Rubber Compos* 47:17–24. <https://doi.org/10.1080/14658011.2017.1399531>
21. Braconnier DJ, Jensen RE, Peterson AM (2020) Processing parameter correlations in material extrusion additive manufacturing. *Addit Manuf* 31:100924. <https://doi.org/10.1016/j.addma.2019.100924>

22. Mohamed OA, Masood SH, Bhowmik JL (2015) Optimization of fused deposition modeling process parameters: a review of current research and future prospects. *Adv Manuf* 3:42–53. <https://doi.org/10.1007/s40436-014-0097-7>
23. Rajpurohit SR, Dave HK (2018) Effect of process parameters on tensile strength of FDM printed PLA part. *Rapid Prototyp J* 24:1317–1324. <https://doi.org/10.1108/rpj-06-2017-0134>
24. Domingo-Espin M, Puigoriol-Forcada JM, Garcia-Granada A-A, Llumà J, Borros S, Reyes G (2015) Mechanical property characterization and simulation of fused deposition modeling Polycarbonate parts. *Mater Des* 83:670–677. <https://doi.org/10.1016/j.matdes.2015.06.074>
25. Durgun I, Ertan R (2014) Experimental investigation of FDM process for improvement of mechanical properties and production cost. *Rapid Prototyp journal* 20:228–235. <https://doi.org/10.1108/rpj-10-2012-0091>
26. Ziemian C, Sharma M, Ziemi S (2012) Anisotropic mechanical properties of ABS parts fabricated by fused deposition modelling. In: *Mechanical engineering. InTech*

Fused Deposition Modeling Based 3D Printing: Design, Ideas, Simulations



Md. Hazrat Ali and Anuar Abilgaziyeu

Abstract The capability of printing real three-dimensional (3D) objects from digital data is a sophisticated technology. 3D printing (3DP) technology has proliferated in the last several decades by attracting more manufacturers globally. It enables users to make parts without almost any geometrical restrictions. This chapter discusses Fused Deposition Modeling (FDM) technology, its types, applications, and prospects. It also discusses the latest introduced technologies and energy consumption in 3D printing.

1 Introduction

Additive technologies are currently one of the most dynamically correct uses of digital manufacturing. These technologies possess great prospects in the manufacturing of mechanical engineering and biomedicine products and repair work. Among all basic principles of 3D printing, the extrusion-based system where the material is selectively fed through a nozzle is the most widespread in current days.

This chapter discusses the fused filament fabrication (FFF) type of 3D printer that belongs to the extrusion-based systems in additive manufacturing. Along with the abbreviation FFF, FDM (fused deposition modeling) is also used to denote this technology. However, legally the term FDM is trademarked by Stratasys Company [1, 2]. In order to design 3D printers with these working principles, companies should use a different name.

Md. Hazrat Ali (✉) · A. Abilgaziyeu
Department of Mechanical and Aerospace Engineering, School of Engineering
and Digital Sciences, Nazarbayev University, Nur-Sultan, Kazakhstan
e-mail: md.ali@nu.edu.kz

A. Abilgaziyeu
e-mail: aabilgaziyeu@nu.edu.kz

Currently, there are several dozens of different companies offering their products based on this technology. The wide use of FDM printing is explained by the financial reason for this type, i.e., the low cost of both printer itself and its supplies. Another reason is the wide range for printing capabilities of various types of products and the availability of components for assembling FDM printers without the support. There are three main types of FDM printers based on price and advancement: home desktop, professional and industrial ones. The FDM technique, with some modifications depending on the purpose of use, is successfully applied in many fields, such as medicine [3, 4], food [5], and even construction engineering [6, 7].

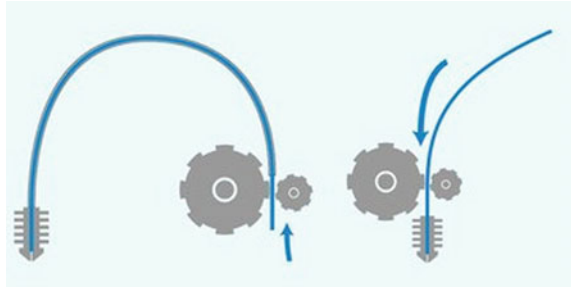
It should be noted that FFF technology has a lot of significant characteristics and features that make it possible to value its advantages over other types of 3DP technologies, namely:

- the most simple printing principle and easy implementation on the bases of standard electronic components
- relatively high resolution (up to 20 microns)
- the possibility to print simultaneously with several materials or several colors
- the possibility of using a wide range of thermoplastic materials with different characteristics (e.g., carbon-reinforced plastics, electrically conductive materials, etc.), including those that are safe for health (both during the process and the use of the finished product) and that do not require special storage and handling conditions
- implementation in the form of compact personal printing devices that do not require specific technical knowledge of installation, connection, and operation
- prototyping of objects with complex geometry and cavities that are beyond the power of other technologies
- lack of noise pollution and industrial waste requiring disposal or special places for installation
- low cost of both the devices themselves and the materials used
- the possibility of self-assembly or DIY of the printing device from a ready-made kit or a set of components
- printed products have high-performance characteristics and can be used as serial products;
- the openness of the technology and open-source hardware and software allows for the improvement and implementation of 3D printing devices in various fields.

FDM printers use a feeding mechanism to push a filament into the extrusion chamber to create a high pressure that would push out melted material through the nozzle. The feeding mechanism generally consists of two roller wheels that clamp filament. One wheel is controlled by a driving motor to generate the translation movement of the filament. The second one is to create high friction between the filament and the driving motor wheel.

The extruders are classified as a direct and Bowden extrusion based on the location of the feeding mechanism. In the direct extrusion system, the feeding

Fig. 1 Schematics of Bowden and direct extrusion systems [8]



mechanism is mounted on the moving extrusion hot-end, whereas Bowden one has the feeding mechanism located on the frame of the printer and has a Bowden cable which works as a guide for the filament is driven to the hot-end through it (Fig. 1). Bowden type extrusion makes the printer lighter, especially when the printer has more nozzles or extrusions.

2 Design Variations

The most common arrangement used for FDM is a Cartesian coordinate system. Built on Cartesian coordinates, this technology works based on three axes (X, Y, and Z). One or more of these axes move the mechanical print head of the equipment, i.e., the coordinates specified along the axes implement movement and position of the extrusion system relative to the platform (Fig. 2). Of all kinds of kinematic schemes of FDM 3D printers, the Cartesian system shows relatively high stability of results.

Another popular schematic arrangement is Delta. In this kinematic scheme, the print head's movement occurs along with three parallel guides (Fig. 2). The change in coordinates along the Z-axis takes place when the angle between the drives changes. The workspace in printers with this system is usually much larger vertically. They also come in open and closed cases. The Delta scheme's advantages include higher printing speed but less accuracy at the model's edges than the Cartesian scheme. This is because all three attachment points are involved in the movement of the extruder. The electric motors operate simultaneously, which leads to the accumulation of errors in coordinate positioning.

A kinetic scheme like Polar is a reasonably new scheme introduced by the company of the same name, Polar. It uses a polar coordinate system. Its fundamental difference from the Cartesian scheme is that the extruder moves in the X and Y planes not linearly but in a circle relative to the platform. The platform of such a scheme of 3D printers has a circular shape, rotates in a circle, and moves entirely along one horizontal axis, and the extruder moves up and down (Fig. 3). It is faster than the Cartesian type.

3D printers with robotic arms (SCARA) are designed with a mechanical programmable arm-grripper, replaceable extruder. SCARA is a kinetic scheme designed

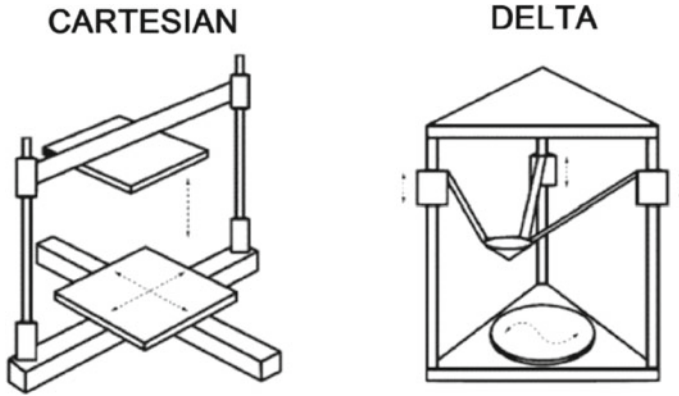
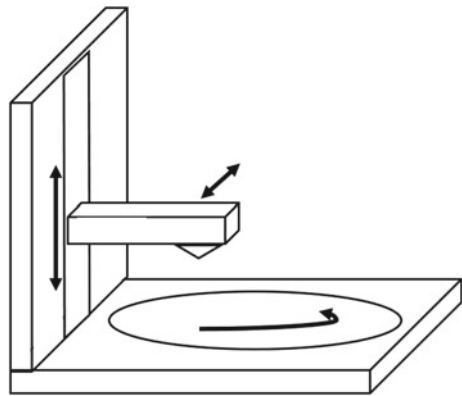


Fig. 2 Cartesian and delta type FDM printers [9]

Fig. 3 Polar type printer



for manipulators with limited mobility with increased accuracy and rigidity. In this scheme, the extruder is located at the end of the manipulator, which moves due to lever joints along the XY axes and a separate drive along the Z-axis. According to this scheme, the devices built are distinguished by very high accuracy and repeatability, low noise and vibration levels, and compactness. Among the disadvantages is the complicated software compared to the Cartesian ones.

3 Latest Process Variation and Process Mechanisms

3.1 Polymer Printing

Polymer printing is the most popular process variation among all process variations. In polymer printing, there is a wide range of available materials. The material range

includes thermoplastics (e.g., ABS, PLA), engineering polymers (e.g., PA (Nylon), TPU, PETG), high-performance thermoplastics (e.g., PEEK, PEI), and other composite materials (carbon-reinforced thermoplastic, electrically conductive materials).

The polymer FDM technology is quite simple and works based on the melted polymer filament's extrusion from a coil. The extrusion system has a nozzle with a heater that melts the filament and has a feeder mechanism that generates pressure inside the nozzle to facilitate pushing the molten material out of the nozzle (Fig. 4). The constant pressure application ensures a constant flow rate, whereas the extrusion mechanism's constant movement implies even fabrication of an object's layers.

Ideally, the melted polymer material after the extrusion process should keep its shape and size. However, external factors such as gravity and tension may cause the change of the shape and size. The material also shrinks and gets porous upon the solidification process, affecting the printed parts' quality.

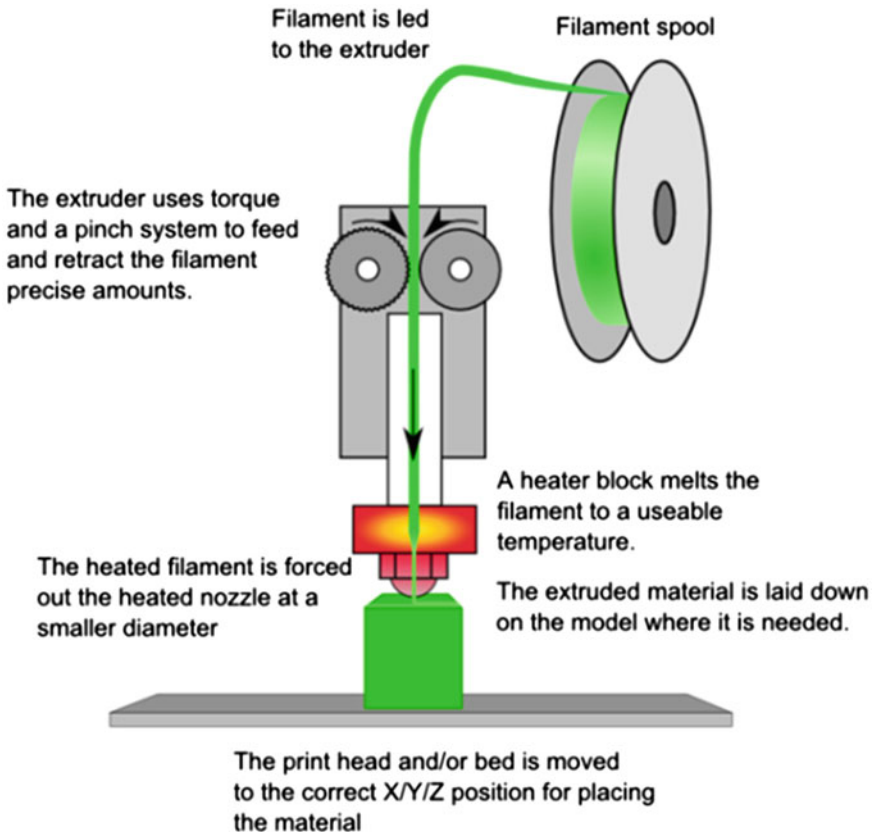


Fig. 4 Schematic of FDM [10]

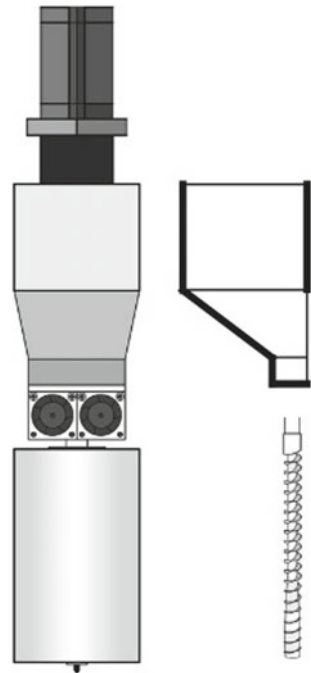
A new extruder system called Gigabot X for polymers was introduced on Kickstarter by re 3D company [11]. The company believes that thermoplastics' novel extrusion system could decrease dependent on current polymer filaments and reduce material waste. The input of the extrusion system is polymer granules, not usual filaments. There is a screw inside a heated barrel in the extrusion system that drives pelletized plastics and extruded through a small nozzle (Fig. 5). The waste materials after printing can be recycled and pelletized to be reused again in the printer.

3.2 Food Printing

Currently, 3D printing technology opened new directions, even beyond food production. Further development prospects can be defined from its benefits such as sustainability, food aesthetics, and nutrition control. It helps with the demand for special food customer groups such as sportsmen, older people, pregnant women, and children.

There are three additive manufacturing techniques used in food printing, which is extrusion, selective laser sintering, and binder jetting. The extrusion system is the most popular one in food printing [5]. It is a digitized engineering solution that helps to prepare food with different designs and customized nutrition proportions. It

Fig. 5 Extrusion system of Gigabot X [12]



uses the same coordinate systems as FDM does Cartesian, Delta, Polar, and Scara. However, food printers use distinct extrusion systems from FDM that are syringe, air pressure, and screw-type systems.

The popularity of using the FDM system in food printing is achieved firstly due to a relatively wide range of material appropriate for the extrusion through a nozzle. Secondly, more complex designs can be achieved as it eliminates molding. Thirdly, the elimination of molding narrows the overall expenses to the cost of machines and ingredients.

Soft self-supporting edible materials such as dough, meat paste, and processed cheese can be used to create 3D printed food. The choice of the material's viscosity is crucial, enabling the material to be extruded through a tiny nozzle and strong enough to hold its structure [13].

Lipton et al. [14] successfully printed multi-material constructs of turkey meat and celery. Then the printed materials were able to be slow cooked or deep-fried. The extrusion system technique is also used to create customized 3D chocolate products [15]. Researchers from Netherland Organization for Applied Scientific Research (TNO) made use of a soft-materials extrusion system to print-rich diversity of food. They used meat purees, carbohydrates, proteins, and other nutrients from alternative sources such as algae, grass, and insects [16].

Currently, many researchers and companies are focusing on improving the extrusion type of food printing. The majority of current 3D printers can print unique and complex shapes without controlling at the macro-nutritional level. Combining these two values to the final food is very significant. It needs to be addressed to improve food printing technology to have a healthy life and the growing population's sustenance.

3.3 *Live-Cell Printing*

Extrusion-based system printing is also used to extrusion living cells, which is also known as bioprinting. It is already used in tissue engineering to print parts such as cells, tissues, bones, cartilage, bi-layered skin [17], artificial organs [18]. In bioprinting, bioink is the material dispensed by extrusion or a deposition system controlled by a computer. There are three types of deposition systems in bioprinting: pneumatic, piston-driven, and screw-driven extrusion systems [17].

The main challenge of bioprinting for use in medicine is biocompatibility and non-toxicity of materials. The main materials that have been successfully applied are hydrogels and composite materials. 3D bioprinters offer faster fabrication of drugs at a lower cost.

Visser et al. [19] used in-air microfluidics to print biostructures with living cells. This technique can help to fabricate micro-building blocks that could be a major boost in tissue engineering advancement, and it will be able to fix the damaged tissues. Cubo et al. [20] with collaboration with BioDan, developed an extrusion-based 3D printer capable of fabricating functional human skin.

4 Printing Methods and Technologies

According to Ali et al. [21], in 2016, there were only a few technologies available that can perform multi-material and multi-color printing, and their performances were relatively poor. Companies and researchers have often designed dual or multi-extrusion systems to fabricate multi-material parts simultaneously. They just literally increased the number of nozzles and extrusion systems to facilitate multi-color and/or multi-material printing. This method of solving mono-color printing is not practical since adding more nozzles requires more heaters and more feeding motors, making the printer bulky and heavy. This slows printing speed and print volume significantly. Moreover, this solution consumes high energy and limits the number of materials and/or colors depending on the number of nozzles installed. Multi-extruders also decrease the printing area, which is available for single-nozzle printing.

Nevertheless, currently, there are many proposed novel systems proposed by different research groups and companies that attempted to tackle these issues.

4.1 Single-Nozzle Multi-material Printers

There have been proposed reinforced polymer material printing for FDM printers to improve the mechanical properties of printed objects [22]. Tian et al. [23] developed a novel fabrication approach technique is particularly suitable for reinforced composite plastic materials that consist of polylactic acid as the matrix and carbon fiber. The extruder head has only one nozzle but two inputs for two different filament materials (Fig. 6).

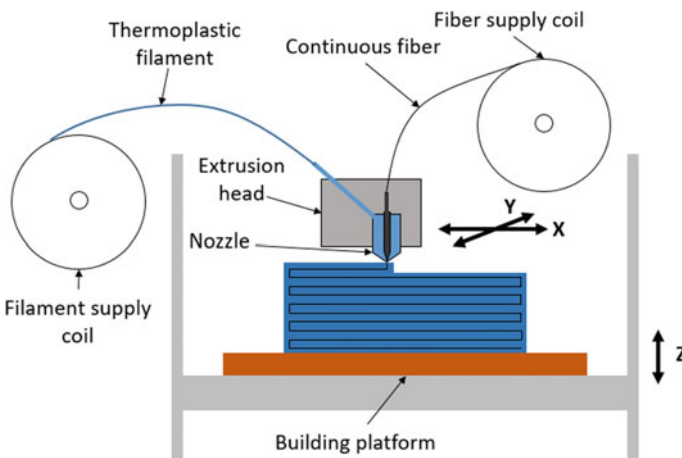


Fig. 6 Schematic of FDM 3DP for continuous carbon-reinforced PLA composites

This method is performed by providing matrix and fiber filaments simultaneously. The major challenge is the bonding between the two materials.

4.2 Multi-nozzle Printers

Ali et al. [21, 24] have proposed a novel multi-extrusion system for five different material/color FDM printing. They utilize only two motors for the whole feeding mechanism. This novel system's main feature is that there is only one feeding mechanism for the whole system. In order to drive the specific filament, it rotates and switches to the needed filament. The extrusion system consists of five nozzles and only one feeding motor, so it is much lighter than conventional multi-material systems.

4.3 Full-Color Printers

Some companies have already proposed new systems to design full-color FDM printers.

Da Vinci Color Mini 3D printer introduced by Taiwanese company XYZPrinting can print full-color objects. The printer utilizes CMYK inkjet technology that enables to produce infinite color palette. The printer uses a special color-absorbing PLA filament and mixes magenta, cyan, and yellow ink droplets to print objects with millions of colors. This 3D printer is the world's first full-color FDM 3D printer (Fig. 7) [25].

The Polish company OVE collaborating with the American company Memjet has developed a full-color FDM 3D printer (Fig. 8). OVE printer uses a transparent PLA filament, and after printing one layer, the platform is moved to the side where the printing object is painted by Memjet printhead [26].

The PlaySmart 3D printer by Polaroid has an option to print with multiple colors. It has only one nozzle, and it has a smart software that pauses the printing process to allow the user to change the filament to the needed color [28].

4.4 Parallel FDM Printing

Parallel FDM printing is a novel method of printing where multiple independently printing extruders are used simultaneously. This approach allows us to achieve a high printing speed proportional to the number of printing elements. Before designing a 3D printer using FDM parallel printing technology, developing the printer design and the parallel printing algorithm for independently moving extruders is necessary.



Fig. 7 Da Vinci Color Mini 3D printer [25]



Fig. 8 OVE printer [27]

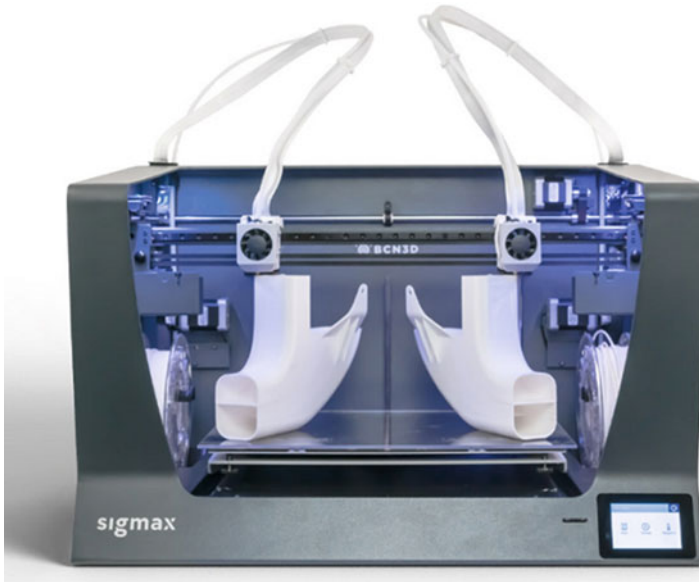


Fig. 9 Sigmax printer [30]

The Spanish company BCN3D Technologies made available to the public all the drawings and instructions necessary for self-assembly of the latest proprietary 3D printer FDM BCN3D Sigmax [29], equipped with two extruders with parallel kinematics (Fig. 9). A distinctive feature of all Sigma 3D printers is parallel-kinematics: the devices are equipped with two extruders with an independent X-axis stroke, making it possible to simultaneously print two identical parts, or mirror models, for example, halves of an assembled product.

Different extruders can print different plastic colors to produce different colored layers of the model, making it much easier to change the plastic required with a single extruder. Each extruder has its printable area, resulting in two main areas.

Before this, only one extrusion system at a time was used as the standard for FDM printing. Some designs have multiple extruders moving together and printing separately at different times. There are printers with two extruders (MakerBot Replicator 2X, WANHAO Duplicator 4X, etc.). The main extruder grows the central part of the model, and the additional one prints the supporting structures using soluble plastic. These printers can also be used for double-color printing. However, these multiple extruders were assembled in one extrusion system and could not print two different parts in parallel.

5 Simulations

Otepbergenov et al. [31] conducted a study to analyze a customized ankle-foot orthosis for patients to rehabilitate from the foot drop disease. For their study, the researchers used a multi-material FDM 3D printer. They changed the high stress concentrated regions with Nylon 12 material to reduce the stress and make a longer lifetime for the orthosis. They performed experimental and numerical FEA analyses. Figure 10 shows simulation results, and the force applied is on the zone with the red color in the figure.

Figure 11 shows the obtained experimental results.

The results showed significant improvement by decreasing the equivalent stress by nearly 50% and decreasing total deformation by 35% and 70%.

Sabyrov et al. [32] created a flexible neck orthosis design using an FDM printer for rehabilitation with regular usage. The digital model of the patient allowed them to design the neck orthosis with high accuracy.

The finite element analysis method found in ANSYS software was used to assess the model's mechanical behavior. The numerical simulation approach shows an applied force on the object and consequent displacement and load distribution along with the model. The initial step begins with setting filament parameters in the software. Thermoplastic elastomer (TPE) material has both features of plastic and rubber. TPE fabricated orthosis includes strong, flexible, and durable properties.

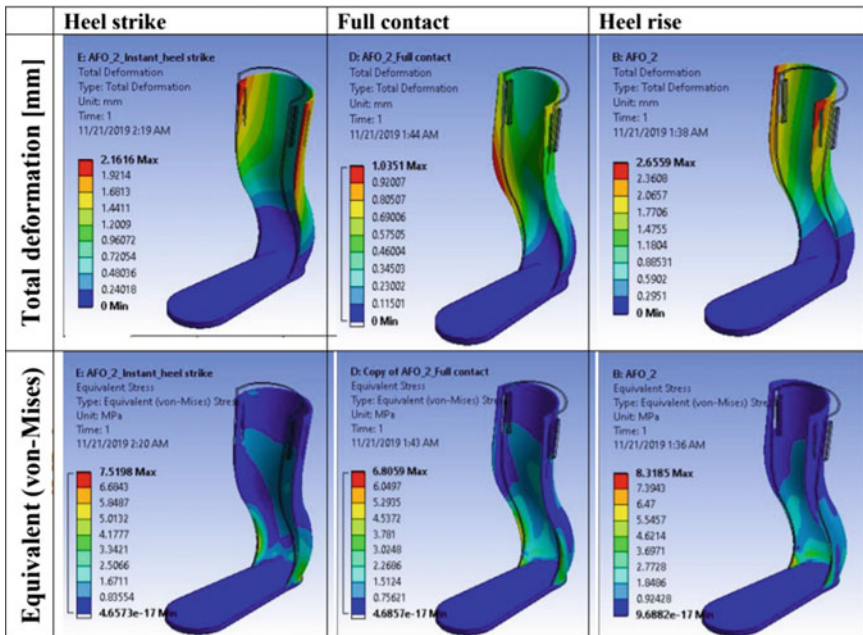


Fig. 10 Simulation results at each gain instance [31]

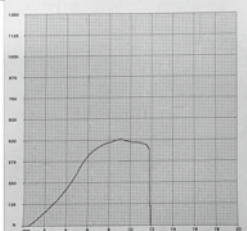
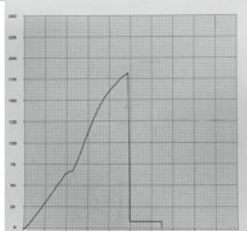
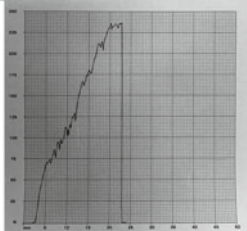
	Benchmark	Modified model 1	Modified model 2
Graph of load vs. deformation			
Ultimate load	505 N	183 N	237 N
Max. deform.	12 mm	7.5 mm	23.5 mm

Fig. 11 Experimental results of the compression testing [31]

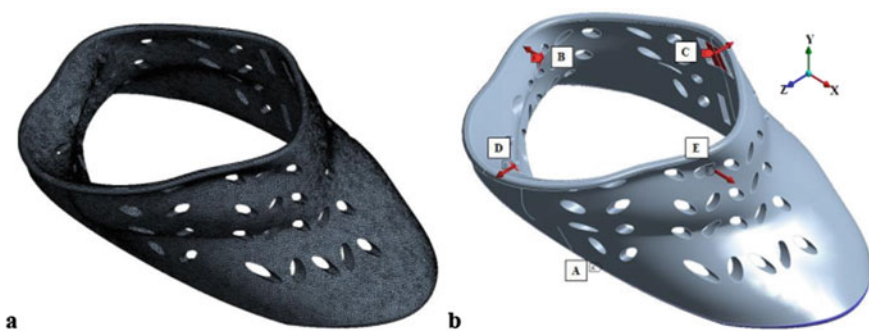


Fig. 12 a mesh view of the design model and b applied force directions and boundary conditions [32]

The purpose of numerical assessment is to observe how the neck orthosis behaves under an applied force. The fine mesh formed by 799,699 elements and 1,208,407 nodes ensure accurate simulation (see Fig. 12a).

Figure 12b illustrates the directions of forces; the letter “B” and “E” corresponds to lateral bending (left and right side of orthosis). Extension force relates to the letter “C” and the backside of the model. To the forward part of the neck is applied the flexion force (“D”).

The model’s lower edge was chosen as a fixed boundary, indicated with the letter “A” and blue color region. The value of forces applied from the inner surface for flexion, extension, and lateral bending are 210, 190, and 165 N, respectively.

The influence of the applied force on stress distribution is represented in Fig. 13 in the iso-color view. On the left side of Fig. 13a is shown a color-bar, where the



Fig. 13 Stress distribution along the model: **a** front, **b** left-side, and **c** back views [32]

highest pressure is represented with red color, whereas the lowest corresponds to blue color. The unit of stress parameter is “MPa”. It could be seen that the region most affected by pressure is the backside of the model, while on the left and the front side, the effect is minor.

Figure 14 shows that the maximum displacement caused by applied force is 1.4685 mm. Similar to stress distribution, the highest total displacement occurred on the backside of the model. The left side has almost 0.5 mm enlargement, while deformation on the front side is negligible.

According to simulation analysis, it can be concluded that the weakest part of the model is the backside region. Nevertheless, the small deformation value is reasonably small. Moreover, on the nape side are oriented rectangular holes for Velcro, designed for comfortable dressing. During wear, the printed neck model could be regulated and tied comfortably.

The model was tested via ANSYS software, which highlighted the orthosis’s durability under an applied force.

Ali and Batai [33] researched the sandwiched structures’ deformation and mechanical strength with a honeycomb cover. Face sheets were made of ABS, whereas honeycomb core was made of PLA material.

ANSYS is used to study the sandwich structures’ mechanical properties with various cores under the bending load ranging from 200 to 2000 N. To be more specific; the load is line load. The boundary conditions and meshing are shown in Fig. 15. The load is applied to the indenter while the bottom of the support is fixed. Moreover, the mesh size is 1 mm. In this study, stress distribution on the sandwich structures is characterized using Von-Mises stress. Simultaneously, total deformation is taken as another indication of the mechanical behavior while subject to the bending loads (Fig. 16).

According to the stress distribution on the sandwich structures with various cores, the sandwich composite with honeycomb core presents relatively lower maximum stress than the one with the solid plate core of the same weight as its, while the composite structure with the core of the same thickness as its shows a bit



Fig. 14 Deformation (displacement) along the model: a front, b left-side, and c back views [32]

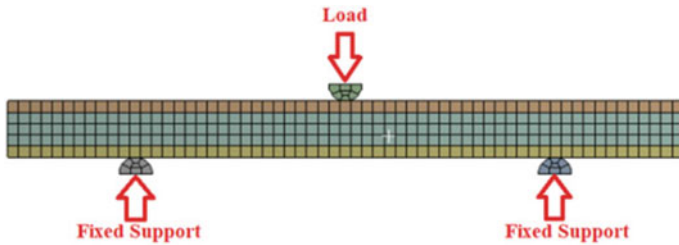


Fig. 15 3-point bendings (boundary conditions and meshing): each fixed support is located 10 mm away from the nearest free end [33]

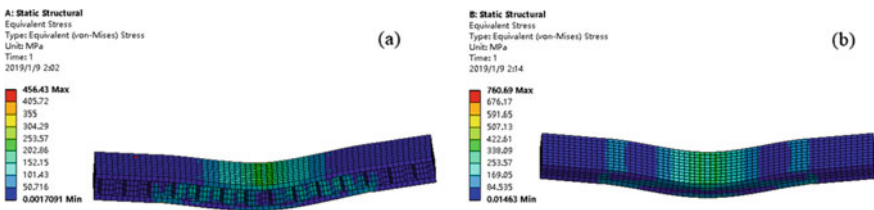


Fig. 16 Von-Mises stress distribution under the load of 1 kN: a sandwich structure with honeycomb core stress distribution, and b sandwich structure with solid plate core with a thickness of 1.08 mm stress distribution [33]

higher maximum stress value than it. Figure 17 shows the sandwich structure with a honeycomb core (SH) deforms more than the SSP (3 mm) having the same weight. SH's deformation pattern is even closer to the structure's deformation pattern with the same thickness's solid core.

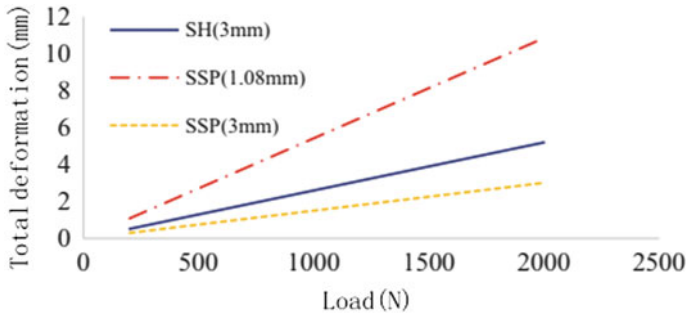


Fig. 17 Maximum total deformation of the sandwich composites under the bending loads from 200 to 2000 N [33]

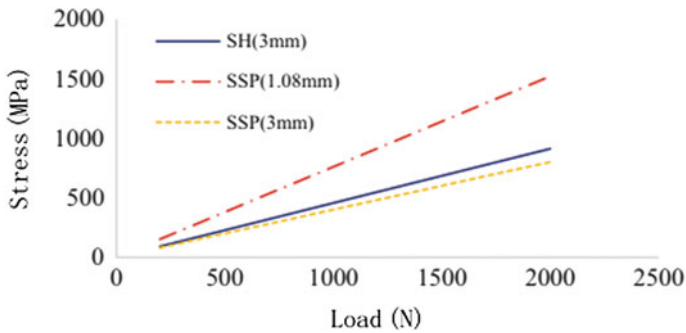


Fig. 18 Maximum Von-Mises stress on the sandwich structure of different cores under the loads from 200 to 2000 N [33]

As shown in Fig. 18, SH undergoes significantly less stress than SFP (1.08 mm) under the loading from 200 to 2000 N. While they differ in thickness, they are the same in weight. It can be inferred that honeycomb core undergoes less stress than the solid plate core of the same weight. As for SSP (3 mm) and SH (3 mm), these two specimens are of the same thickness, while the SSP (3 mm) is three times heavier than the SH (3 mm). Despite this, they demonstrate more or less the same stress resistance performance. Therefore, while keeping the same mechanical performance, the honeycomb structure can substitute heavier solid structures.

6 Energy Efficiency

The traditional manufacturing systems use a high amount of energy and water and produce high-level waste materials, which negatively impacts the environment. Therefore, there is a need for more sustainable manufacturing processes with less

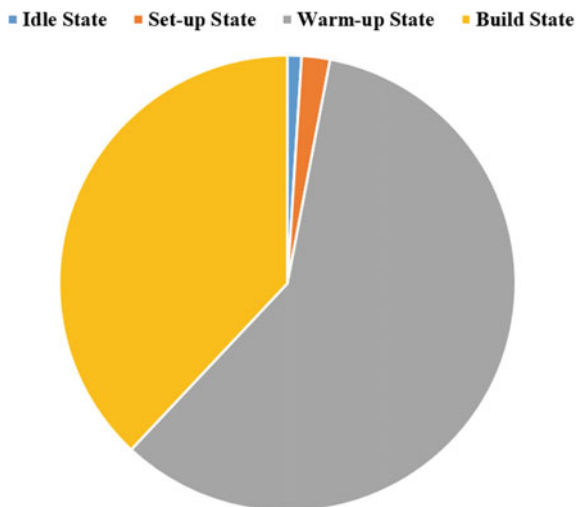
energy consumption. 3DP is one of the solutions that minimize waste of materials in the production of 3D objects. Even the material used to support overhanging parts or complex geometries removed after parts are printing can be recycled to be reused again with filament extruder equipment. Meanwhile, traditional subtractive manufacturing machines remove materials from a block, leading to more material waste in the production process. The ratio of waste materials with the final part material can get up to 19:1 [34]. However, some people argue that waste materials can be recycled to be reused again. Even though it is, the recycling process demands lots of energy and resources, which impacts the environment.

3D printing impacts the environment comparatively lower than traditional manufacturing methods due to less energy usage. According to Kreiger et al. [35], 41–64% of energy reduction occurs during the manufacturing of polymer products with low-cost FDM 3D printers. Moreover, the fabrication of objects with 3D printers does not require any extra special tooling as traditional manufacturing does, and it makes 3D printers more sustainable than the other one [36].

On the other hand, some researchers have disagreed with these points. For instance, Kurman et al. [37] stated that 3D printing uses an extremely high amount of electrical energy, according to researchers at Loughborough University. The researchers compared the energy consumed to manufacture similar objects by industrial 3D printers and injection molding machines. The estimation showed that the 3D printer uses 50–100 times more electrical than the other one. Other authors stated that FDM printing affects human health and the environment when printing with ABS and PLA materials, and it generates 1.61×10^{10} ea/min and $4.27-4.89 \times 10^8$ ea/min emissions [38].

3DP needs energy and material as consumables in order to fabricate 3D objects. Usually, the whole needed energy is converted from electrical energy, and it is divided into three groups: thermal, mechanical, and auxiliary energies [39]. The energy distribution of FDM sub-processes [40] is shown in Fig. 19.

Fig. 19 Energy distribution of the FDM process



7 Conclusion

Additive manufacturing is already widely applied in various areas as a manufacturing technique, and it facilitates the production processes of fabrication of parts. FDM is one of the first invented 3D printing technologies and keeps on to be one of the most popular techniques because of its key advantages: the most simple and easy-to-use printing principle, variety of materials, and low cost.

This book chapter discusses a review of FDM 3D printing technology in terms of technologies and energy consumption. Lots of researches were conducted on the invention of strong materials and multi-material or multi-color printing. Results revealed that FDM is a promising technology with high potential. However, researchers still need to carry out on topics of limitations of the technology in order to fully make FDM technologies to be a practical, reliable, and effective solution.

References

1. Stratasys (2019) Legal Documents. Stratasys [Online]
2. United States Patent and Trademark Office, “Trademark Search” [Online]. Available: https://tsdr.uspto.gov/#caseNumber=4325106&caseSearchType=US_APPLICATION&caseType=DEFAULT&searchType=statusSearch
3. Honigmann P, Sharma N, Okolo B, Popp U, Msallem B, Thieringer FM (2018) Patient-specific surgical implants made of 3D printed PEEK: material, technology, and scope of surgical application. *BioMed Res Int* 4520636
4. Tejo-Otero A, Buj-Corral I, Fenollosa-Artes F (2019) 3D printing in medicine for preoperative surgical planning: a review. *Ann Biomed Eng* 48:536–555
5. Sun J, Zhou W, Yan L, Huang D, Lin L (2018) Extrusion-based food printing for digitalized food design and nutrition control. *J Food Eng* 220:1–11
6. Paolini A, Kollmannsberger S, Rank E (2019) Additive manufacturing in construction: a review on processes, applications, and digital planning methods. *Addit Manuf* 30
7. Khoshnevis B, Dutton R (1998) Innovative rapid prototyping process makes large sized, smooth surfaced complex shapes in a wide variety of materials. *Mater Technol* 13(2):53–56
8. Heulette T (2020) Direct vs. Bowden extruder: does it make a difference? All3DP, 10 Jan 2020 [Online]. Available: <https://all3dp.com/2/direct-vs-bowden-extruder-technology-shootout/>
9. Alafaghani A, Qattawi A, Ablat MA (2017) Design consideration for additive manufacturing: fused deposition modelling. *Open J. Appl. Sci.* 7(6):291–318
10. RepRap Wiki, “File:FFF.png,” 30 Aug 2012 [Online]. Available: <https://reprap.org/wiki/File:FFF.png>
11. Re3D, “Gigabot X,” Re3D [Online]. Available: <https://re3d.org/gigabotx-release/>
12. Re3D, “Gigabot X: Large-Scale, Recycled Plastic Pellet 3D Printer,” Kickstarter [Online]. Available: <https://www.kickstarter.com/projects/re3d/gigabot-x-your-direct-pellet-extrusion-3d-printer>
13. Godoi FC, Prakash S, Bhandari BR (2016) 3d printing technologies applied for food design: status and prospects. *J Food Eng* 179:44–54
14. Lipton J, Arnold D, Nigl F, Lopez N, Cohen D, Noren N, Lipson H (2010) Mutli-material food printing with complex internal structure suitable for conventional post-processing. In: Paper presented at 21st annual international solid freeform fabrication symposium—an additive manufacturing conference (2010)

15. Hao L, Mellor S, Seaman O, Henderson J, Sewell N, Sloan M (2010) Material characterisation and process development for chocolate additive layer manufacturing. *Virtual Phys Prototyp* 5(2)
16. Van der Linden D (2015) 3D food printing Creating shapes and textures [Online]. Available: https://www.tno.nl/media/5517/3d_food_printing_march_2015.pdf
17. Derakhshanfar S, Mbeleck R, Xu K, Zhang X, Zhong W, Xing M (2018) 3D bioprinting for biomedical devices and tissue engineering: a review of recent trends and advances. *Bioactive Mater* 3(2):144–156
18. Rastogi P, Kandasubramanian B (2019) Review of alginate-based hydrogel bioprinting for application in tissue engineering. *Biofabrication* 11(4):042001
19. Visser CW, Kamperman T, Karbaat LP, Lohse D, Karperien M (2018) In-air microfluidics enables rapid fabrication of emulsions, suspensions, and 3D modular (bio)materials. *Sci Adv* 4(1):eaao1175
20. Cubo N, Garcia M, del Canizo JF, Velasco D, Jorcano JL (2017) 3D bioprinting of functional human skin: production and in vivo analysis. *Biofabrication* 9(1):015006
21. Ali MH, Mir-Nasiri N, Ko WL (2016) Multi-nozzle extrusion system for 3D printer and its control mechanism. *Int J Adv Manuf Technol* 86:999–1010
22. Ali MH, Abilgazyev A, Adair D (2019) 4D printing: a critical review of current developments and future prospects. *Int J Adv Manuf Technol* 105:701–717
23. Tian X, Liu T, Yang C, Wang Q, Li D (2016) Interface and performance of 3D printed continuous carbon fiber reinforced PLA composites. *Compos A Appl Sci Manuf* 88:198–205
24. Abilgazyev A, Kulzhan T, Raissov N, Ali MH, Ko WL, Mir-Nasiri N (2015) Design and development of multi-nozzle extrusion system for 3D printer. In: Paper presented at international conference on informatics, electronics & vision (ICIEV)
25. XYZPrinting, “da Vinci Color,” XYZPrinting [Online]. Available: <https://www.xyzprinting.com/en/product/da-vinci-color>
26. Stevenson K (2019) A different full color 3D printing solution from OVE. Fabbaloo, 9 Sep 2019 [Online]. Available: <https://www.fabbaloo.com/blog/2019/9/9/a-different-full-color-3d-printing-solution-from-ove>
27. Vialva T (2019) OVE and memjet introduce fast, full-color FFF 3D printer. 3D printing industry, 5 Sep 2019 [Online]. Available: <https://3dprintingindustry.com/news/ove-and-memjet-introduce-fast-full-color-fff-3d-printer-161216/>
28. Polaroid, “PlaySmart,” Polaroid [Online]. Available: <https://www.polaroid3d.com/en/playsmart3dprinter/>
29. Dynamism, “BCN3D Sigmax,” Dynamism [Online]. Available: https://www.dynamism.com/3d-printers/bcn3d-sigma.html?gclid=CjwKCAjw8MD7BRAReiwAGZsrBVW3QNnMmG9n1zI1yDhVFs35BU-I9EFcOZ3S9hMxGay2ONVe_j9nUxoCdscQAvD_BwE
30. DToday.ru, “BCN3D has released blueprints for the latest Sigmax 3D printer,” 3DToday.ru [Online]. Available: <https://3dtoday.ru/blogs/news3dtoday/the-company-bcn3d-posted-in-open-access-drawings-of-the-latest-3d-print/>
31. Otepbergenov T, Smagulov Z, Abilgazyev A, Kurokawa S, Ali MH (2019) Numerical and experimental analysis of the 3D printed multi-material ankle-foot orthosis. In: Paper presented at the 10th Asia conference on mechanical and aerospace engineering, Bangkok
32. Sabyrov N, Sotsial Z, Abilgazyev A, Adair D, Ali MH (2020) Design a flexible neck orthosis using an FDM printer for rehabilitation with regular usage. In: Paper presented at procedia computer science, Elsevier
33. Ali MH, Batai S (2020) Bending behavior of sandwich composite structures of 3D-printed materials. *Adv Mater Manuf Eng* 281–287
34. Liu Z, Jiang Q, Zhang Y, Li T, Zhang H-C (2016) Sustainability of 3D printing: a critical review and recommendations. Volume 2: materials; biomanufacturing; properties, applications, and systems; sustainable manufacturing

35. Kreiger M, Pearce JM (2013) Environmental life cycle analysis of distributed three-dimensional printing and conventional manufacturing of polymer products. *ACS Sustain Chem Eng* 1(12):1511–1519
36. Mani M, Lyons KW, Gupta SK (2014) Sustainability characterization for additive manufacturing. *J Res Nat Inst Stand Technol* 119:419–428
37. Kurman M, Lipson H (2013) Is eco-friendly 3D printing a myth? (Op-Ed). *LiveScience*, 20 July 2013 [Online]. Available: <https://www.livescience.com/38323-is-3d-printing-eco-friendly.html>
38. Kim Y, Yoon C, Ham S, Park J, Kim S, Kwon O, Tsai P-J (2015) Emissions of nanoparticles and gaseous material from 3D printer operation. *Environ Sci Technol* 49(20):12044–12053
39. Xu J, Wang K, Sheng H, Gao M, Zhang S, Tan J (2019) Energy efficiency optimization for ecological 3D printing based on adaptive multi-layer customization. *J Cleaner Prod* 245:118826
40. Yoon H-S, Lee J-Y, Kim H-S, Kim M-S, Kim E-S, Shin Y-J et al (2014) A comparison of energy consumption in bulk forming, subtractive, and additive processes: review and case study. *Int J Precis Eng Manuf-Green Technol* 1(3):261–279

Calorimetry, Structure and Morphology of Printed Samples from Biodegradable Materials Using FDM 3D Printing Technology



Dumitru Nedelcu  and Andrei-Danut Mazurchevici 

Abstract The current concerns of researchers worldwide are focused on the study of top technologies and materials that have minimal impact on life quality. Thus, merging the most used 3D printing technology, FDM-Fused Deposition Modeling, with biodegradable polymeric materials from renewable resources is one of the current topics in the field of industrial research. The aim of the present study is the analysis of FDM printed samples from biodegradable polymers like Extrudr GreenTec Anthracite, Extrudr BDP Pearl, bioFila Linen and bioFila Silk. The used materials for 3D printing, according to the manufacturer and to the obtained results, from morphological investigations point of view, have a high rate of decomposition into chemical elements that are found naturally in nature. The performed analyses were SEM (Scanning Electron Microscopy), EDX—Energy Dispersive X-ray Analysis, XRD—X-Ray Diffraction Analysis and DSC—Differential Scanning Calorimetry analyses in order to identify their elemental composition, the phase transitions suffered by the materials during heating and aspects regarding the adhesion between layers specific to the additive manufacturing. The obtained results support the researchers by providing valuable information that helps to establish some process parameters (melting temperature, printing direction, etc.) but also to understand the materials behavior that take place during the heating process. From a thermal, morphological and structural point of view, 3D printed biodegradable materials can be used in various fields of activity, being able to replace nonbiodegradable polymers that are so harmful to the environment and health.

D. Nedelcu (✉) · A.-D. Mazurchevici
Department of Machine Manufacturing Technology, “Gheorghe Asachi” Technical
University of Iasi, Blvd. Mangeron, No. 59A, 700050 Iasi, Romania
e-mail: dnedelcu@tuiasi.ro

D. Nedelcu
Academy of Romanian Scientists, Str. Ilfov, Nr. 3, Sector 5, 010164 Bucharest, Romania

© The Author(s), under exclusive license to Springer Nature Switzerland AG 2021
H. K. Dave and J. P. Davim (eds.), *Fused Deposition Modeling Based 3D Printing*,
Materials Forming, Machining and Tribology,
https://doi.org/10.1007/978-3-030-68024-4_3

1 Introduction

The persistence of fossil fuel based plastics in the environment, the lack of storage space for waste, the concern about emissions during incineration, as well as the dangers of ingestion of these materials have stimulated efforts to develop new biodegradable materials. To be competitive, biodegradable plastics must have properties similar to conventional plastics. Existing biodegradable product lines need to be expanded to meet specific physical requirements and other forms of polymers need to be further researched and modified so that the degradation time varies according to climatic differences and performance requirements. Among the most important factors in the development of a successful biodegradable polymer industry are cost reduction, as well as public and political acceptance [1].

Within the scientific community, it requires the optimization and development of new processes and technologies, which will allow the sustainable production of materials, recyclable, biocompatible and biodegradable, from renewable natural resources. The main challenges in order to convert and obtain industrial materials from bio resources are sustainability, durability, compatibility and accessibility to the new developed materials.

Rapid prototyping is an additive manufacturing technology that determines raw material savings but also the possibility to obtain a prototype in a very short time without the involvement of other conventional processing technologies. The constant need to develop and improve technologies, whether it refers to modern manufacturing technologies or to technologies for obtaining materials with a low impact on the environment, has led to the creation of sustainable products globally [2].

The most widespread technology for obtaining parts by additive manufacturing is Fused Deposition Modeling (FDM), which offers the possibility of obtaining prototypes, of various sizes in a very short time, compared to the possibilities offered by traditional manufacturing technologies, a sketch of this method can be seen in Fig. 1. Parts can be obtained using solid state thermoplastic filaments. The filament is pushed through a heated nozzle where it is melted. The printer continuously moves the nozzle, placing the molten material in precise locations, following a predetermined path. The construction of the part is realised by depositing melted thermoplastic material layer by layer until this one it is completed [2].

The main advantages of FDM technology are: obtaining prototypes in a short time and a low manufacturing cost. However, the technology also has some limitations, among which we mention: low dimensional accuracy for small parts; lower surface quality and lower print speed compared to other printing methods [3]. FDM technology is widely used in various industries for printing parts from the class of electronic enclosures, clamping and fixing devices, injection molds, etc.

Joining the modern technology used for the parts fabrication with the biodegradable materials from renewable resources, leads to obtaining multiple advantages due to the ease of printing biodegradable parts, functional and able to successfully replace conventional plastic ones [3].

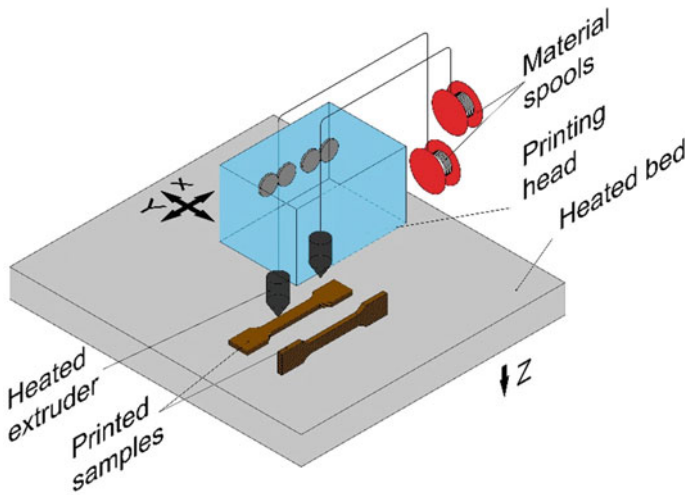


Fig. 1 FDM technology—sketch and model construction

Determining and understanding the functional characteristics of biodegradable materials that can be used in additive manufacturing is essential because only in this manner can be achieved the correct and optimal selection of the material which is thus able to match the application from the targeted field.

In the last decade, due to the need to reduce environmental pollution as a cause of the massive use of exhaustible resources in various industries. Numerous research studies have been conducted on the possibility of replacing polluting materials with biodegradable, compostable or recyclable ones. Thus, 3D printing of biodegradable polymeric materials has been and continues to be a major interest research topic, the biodegradable thermoplastics materials used mainly in FDM printing are PLA (Poly lactic acid) [4–7], PLA-based composite [8–13], PHB—polyhydroxybutyrate [14], PCL—polyhydroxybutyrate [15], lignin based polymers as Arboblend V2 Nature, Arbofill Fichte [16], etc. The results obtained from the carried out studies regarding various properties of 3D printed biodegradable materials certifies the possibility of substituting polymeric materials based on nonbiodegradable resources.

The need of the present paper comes from the total lack of scientific research on the structural and thermal properties of the Extrudr GreenTec Anthracite, Extrudr BDP Pearl, bioFila Linen and bioFila Silk biodegradable materials. So far, no results are known regarding the samples or parts 3D printed from the mentioned materials. Therefore, was necessary the knowledge of these biodegradable thermoplastics characteristics in order to make some recommendations to replace certain parts made from conventional plastics and which are used in spread activity sectors.

2 Materials and Methods


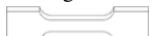
3D printing of the samples required for thermal, structural and morphological determinations was performed using a number of four biodegradable polymeric materials selected according to their usefulness and the possibility of replacing nonbiodegradable synthetic plastics [4, 17]. The biodegradable materials used were Extrudr BDP Green-TEC Anthracite, Extrudr BDP Pearl, bioFila Linen and bioFila Silk.

Extrudr Green-TEC Anthracite and Extrudr BDP Pearl filaments are produced by Extrudr company (Lauterach, Austria). *Extrudr Green-TEC Anthracite* is a BIO performance product (from renewable raw materials—contains PLA—Polylactic acid (based on corn starch, sugar cane or tapioca roots), copolyester and additives) [5], biodegradable according to DIN EN ISO 14855, suitable for applications that require high tensile strength (excellent flexural strength), low deformation and high product surface quality. Also, the material has no smell and is safe for the use industry food. *Extrudr BDP Pearl* is a material 100% from renewable resources, used mainly in applications where the aesthetic part is important (BIO design product) and with mechanical and thermal characteristics comparable to those of PLA. According to the manufacturer its chemical composition is similar to that of Extrudr Green-TEC Anthracite material [18].

The filaments from the purchased bioFila Linen material are totally biodegradable, having higher resistance than other biodegradable materials, it is also characterized by a linen cloth exture, being suitable for projects where the aesthetic part is very important. bioFila Linen is also completely biodegradable, this polymer having a fine and shiny texture reminiscent of silk texture, being ideal for decorations. These two types of filaments are produced by the twoBEars company from Vielank, Germany [19].

3D printing of the samples specific to the tensile test (dumbbell shape—ISO 527 standard) was realised using Raise3D Pro2Plus printing equipment, from the Fine Mechanics and Nanotechnologies Laborator, Faculty of Machine Manufacturing and Industrial Management, “Gheorghe Asachi” Technical University of Iasi. The samples were printed using a 0.4 mm nozzle diameter, 2 or 3 contours (2 for “on edge” orientation and 3 for “flat” orientation) in the shell area—rectilinear type, in the raster area, the set infill type was “grid” but, according to a previous study realized by the research team [20], it was found that for an infilling percentage higher then 95%, the ideaMaker software used by the printing equipment, no longer takes into account the programmer established pattern, automatically switching to the rectilinear pattern. The infilling degree in the raster area was 100%. The rectilinear infilling type results from the superposition of two successive layers in which for the first layer the movement of the printing head is made rectilinearly at an angle of $+45^\circ$ and for the deposition of the next layer the head movement is also made rectilinearly but in the -45° direction. There is no movement of the head in the same layer after the grid route. It should also be mentioned that the printing of

Table 1 Printing parameters used to prototype samples from biodegradable materials

Printing temperatures			Process factors		
Material	<i>Nt</i> (°C)	<i>Pt</i> (°C)	<i>So</i>	<i>Is</i> (mm/s)	<i>Lt</i> (mm)
Extrudr Green-TEC Anthracite	220	60	Flat	40	0.1
Extrudr BDP Pearl	180	55			
bioFila Linen	215	65	On edge	80	0.2
bioFila Silk	220	65			

Nt Nozzle temperature, *Pt* Printing bed temperature, *So* sample orientation on the printing bed, *Is* infill speed, *Lt* layer thickness

the samples was performed using a complete factorial experimental plan, the process factors being varied on two levels, Table 1.

For DSC (Differential scanning calorimetry) experiments, tensile test sample fragments of up to 5 mm from all types of materials, with weighing less than 50 mg were cut. For this purpose, a NETZSCH differential scanning calorimeter type DSC 200 F3 Maya was used, with <1 W sensitivity, 0.1 K thermal accuracy and <1% enthalpy accuracy—generally. The equipment has been calibrated according to Bi—Bismut, In—Indium, Sn—Tin and Zn—Zinc standards. Temperature scans were performed between (20–200) °C with a heating rate of 10 K/min, in a Ar—Argon protective atmosphere, the thermal analysis was completed before the samples began to deteriorate, carbonize. The DSC thermograms recorded during heating were evaluated using the Proteus program, provided by NETZSCH using the tangent method. Temperatures were determined where the half of the transformation took place (T50), as well as the amount of heat dissipated or absorbed.

Structural and morphological analysis was performed using SEM and EDX methods on a QUANTA 200 3D electron microscope. For the surface analysis, in order to the realization micrographic maps, samples from the experiments where the highest value of the tensile strength was reached were chosen. The SEM analysis was performed on the surface area of tensile tested samples and for the areas where the complete ruptures occurred, in the cross-section of the samples.

The QUANTA 200 3D electron microscope (also equipped with an EDX detector) was used for SEM (Scanning Electron Microscopy) analysis. The images were obtained taking into account the following parameters: 10–20 kV acceleration voltage of the secondary electrons; 100×–500× magnification power; 15 mm working distance; Large Field Detector (LFD) used for the analysis of non-conductive samples (polymers, textile fibers, powders, etc.); 0° tilt angle; 60 Pa pressure inside the microscope chamber.

X-ray diffraction analysis (XRD) is the most commonly used technique to characterize the crystallinity and phase purity of a material. The X'Pert Pro MRD X-ray diffractometer was used for the X-ray diffractographic analysis. This equipment is equipped with a Cu $k\alpha$ $\lambda = 1.54$ Å, Panalytical equipment (Netherlands), to which a 45 kV voltage was applied, the diffraction angle (2θ) varying between 5° and 90° The data obtained were processed using the X'Pert

Data Collector, X'Pert High Score Plus and X'Pert Data Viewer programs, being finally rendered in the diffractograms form in diffraction 2θ angle coordinates and using the absolute intensity of the maximum diffraction.

3 Results and Discussions

3.1 Calorimetric Analysis (DSC) for Printed Samples from Biodegradable Materials

DSC analysis was performed on samples cutted from specific tensile samples printed using the FDM method. The samples printing temperature is an input parameter which in the case of biodegradable polymeric materials printing cannot be varied much, maximum 10–15 °C, considering the own experience accumulated in this field. Thus, our recommendation is to perform a DSC analysis, before starting the printing process, just to see, first of all, the material melting point which can then be correlated with the technical specifications provided by the manufacturer. They generally offer a longer thermal printing range.

The biodegradable material Extrudr GreenTec Anthracite shows peaks associated with the following phase transitions, Fig. 2: water evaporation from the base matrix (probably lignin) highlighted by an endothermic peak at 64.1 °C, with a quantity of heat absorbed of -6.45 J/g; material crystallization or lignin reorganization (major component of the material structure) at a temperature of 85.2 °C through an exothermic peak, with 18.56 J/g heat release; melting of a constituent element of the biodegradable material highlighted by an endothermic peak at a temperature of 116.6 °C, with a heat consumption of -21.6 J/g; melting point of the material through an endothermic peak at 177.2 °C, with -25.43 J/g amount of heat absorbed.

The printed sample from Extrudr BDP Pearl exhibit after calorimetric analysis three representative peaks, Fig. 3, two endotherms and one exotherm associated as follows: first endothermic peak at 63.6 °C is associated with water evaporation from the base matrix of the material (probably lignin) with heat absorption in the amount of -6.92 J/g; at a temperature of 93.6 °C there is an exothermic peak that corresponds to the material crystallization or can be assigned to a lignin reorganization, a transformation that takes place with 18.53 J/g heat release; at a temperature of 156 °C there is an endothermic peak associated with the melting point of the material and which needed -17.43 J/g to achieve.

The thermal characterization of the biodegradable material bioFila Linen is represented in Fig. 4 which shows two endothermic peaks and an exothermic peak. The endothermic peaks are associated with the water evaporation from the base matrix at a temperature of 63.5 °C (-8.63 J/g absorbed heat) and the melting point of the material at a temperature of 156.6 °C, in the temperature range of (140–165) °C, with the absorption of -17.8 J/g heat. The exothermic peak, at a

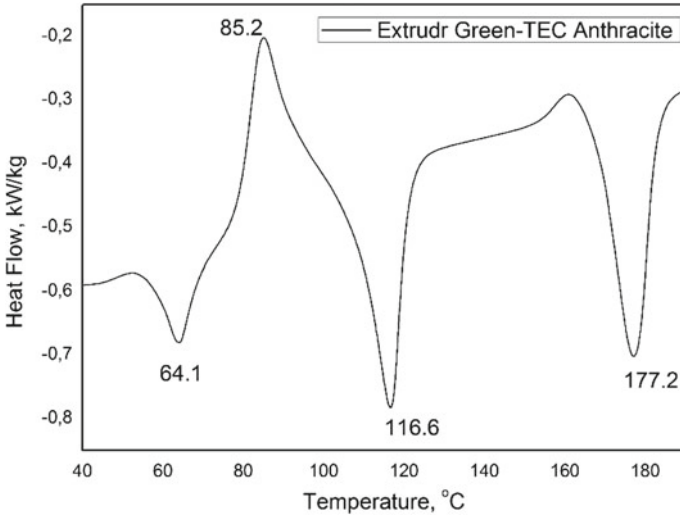


Fig. 2 Highlighting the main thermal behavior of the printed sample from Extrudr Green-TEC Anthracite

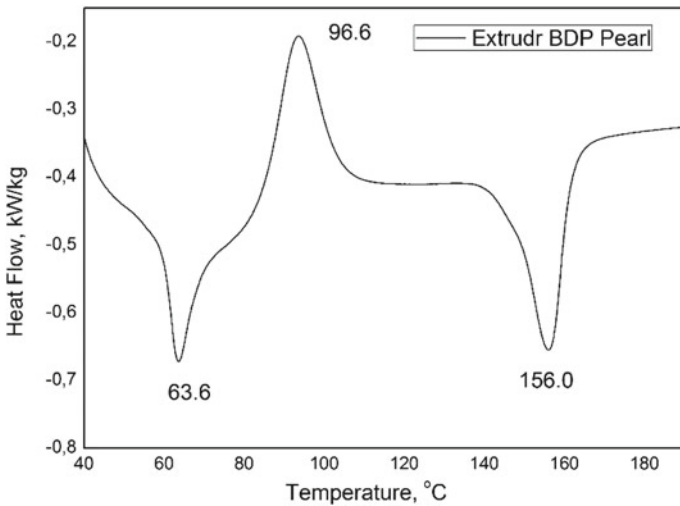


Fig. 3 Highlighting the main thermal behavior of the printed sample from Extrudr BDP Pearl

temperature of 112.9 °C, corresponds to the material crystallization/a lignin reorganization and takes place with the release of heat in a fairly large amount, 17.97 J/g.

For the biodegradable thermoplastic material bioFila Silk, three peaks, two endotherms and one exotherm were highlighted, corresponding to the following

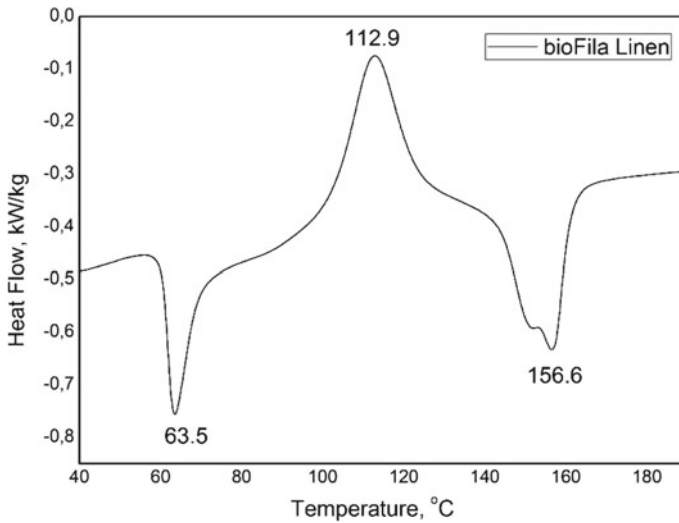


Fig. 4 Highlighting the main thermal behavior of the printed sample from bioFila Linen

transformations that took place during the heating of the sample up to a temperature of 200 °C, Fig. 5: an endothermic peak at a temperature of 64.9 °C associated with the water evaporation from the base matrix, with heat absorption in the amount of -10.18 J/g; an exothermic peak corresponding to the material crystallization or as well as in the case of the other analyzed materials to a lignin reorganization at a temperature of 95 °C, transformation which took place with heat release, 23.54 J/g; second endothermic peak, at a temperature of 154.7 °C associated to melting point of the bioFila Silk material, with -22.7 J/g heat absorption.

3.2 Surface and Structure Analysis for Printed Samples from Biodegradable Materials

For the surface analysis, in order to realize micrographic maps, tensile tests specific samples were chosen, the SEM analysis being performed for the surface area of the samples and for the area where the complete rupture occurred.

Figure 6 shows the SEM images of the sample from Extruder Green-TEC Anthracite, images in which the slightly uneven profile of the deposited filament can be observed, when making a layer. Due to the nozzle pressure, during printing the melted filament in the upper layer is flattened especially in the area where two filaments on different layers are superimposed, Fig. 6a. In the breaking area, Fig. 6b, reveals a homogeneous structure with filaments specific to printing at +45°/-45°, rectilinear type but also can be observed elongated filaments due to deformation occurred during the tensile test, the material showing breaking filaments

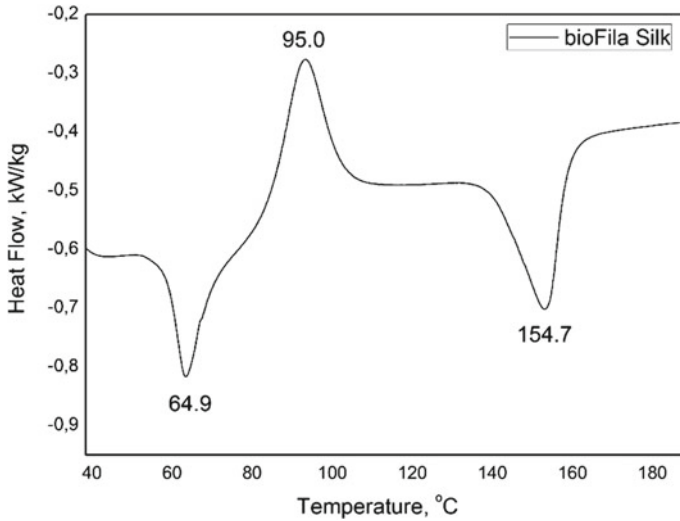


Fig. 5 Highlighting the main thermal behavior of the printed sample from bioFila Silk

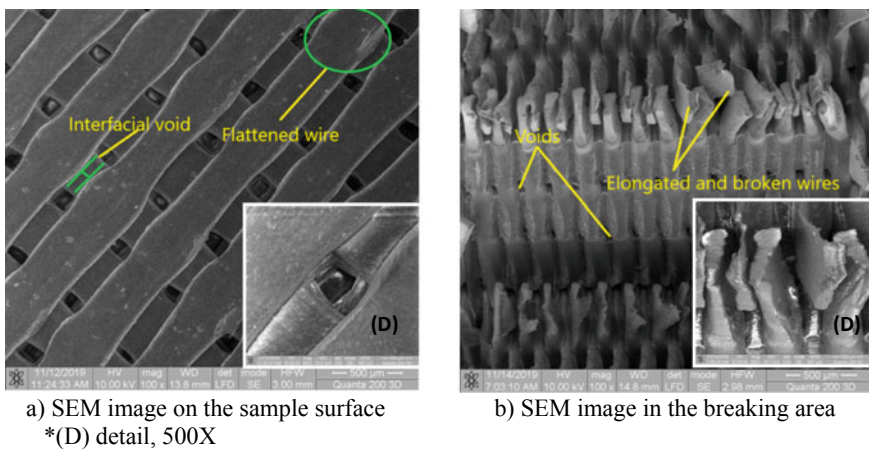


Fig. 6 SEM images of the printed sample from Extrudr Green-TEC Anthracite, “flat” orientation on the printing bed: **a** SEM image on the sample surface *(D) detail, 500×, **b** SEM image in the breaking area

specific to elastic polymers. In detail (D), it is observed that in the first phase the outer part of the filament yields, after which the inner, the raster part lengthens until it breaks.

Figure 7a shows the surface structure of the printed sample made of Extrudr BDP Pearl, rectilinear infill pattern, +45°/−45° deposition angle. An uneven profile of the deposited filaments can be observed, when making a layer,

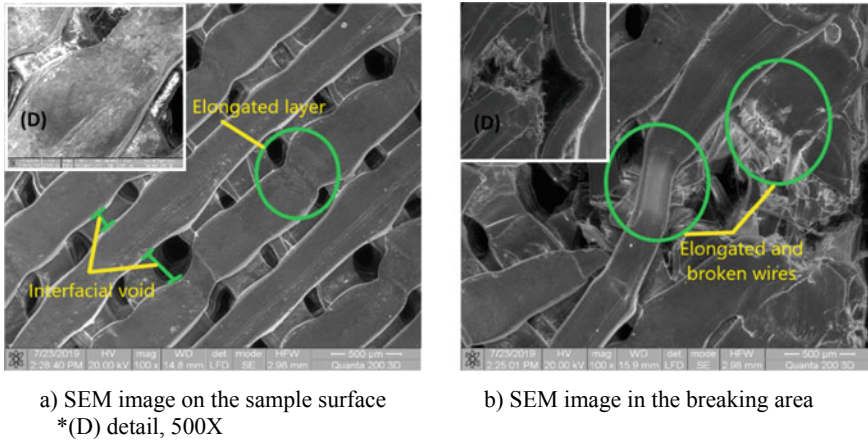


Fig. 7 SEM images of the printed sample from Extrudr BDP Pearl, “flat” orientation on the printing bed: **a** SEM image on the sample surface *(D) detail, 500 \times , **b** SEM image in the breaking area

these not being adjacent. It is also possible to observe an almost perfect deposition between the deposited filaments on each layer. There is also a non-uniformity of the extruded filament, filament deformation (detail marked with (D)) in the upper layer more than in the free space created between the deposited filaments. There was also an elongation of the deposited filament in the upper layer due to the space between the deposited filaments on the lower layer, but probably also due to the slow cooling of the deposited filaments.

In the breaking area of the sample, Fig. 7b, there are elongated and broken filaments due to the action of the forces involved in the tensile test. Looking at the figure detail, it can be seen that the filaments breaking is characteristic to ductile materials. Another aspect to be mentioned is that the outer layer of the sample (shell layer) failed first during the test, detaching from the raster area of the sample due to the different structure (printing mode).

In the case of the bioFila Linen material, the surface image of the sample, Fig. 8a, reveals a homogeneous surface with lines specific to the contour area since the sample was printed “on edge” so, the shell area becoming its surface. Damaged areas can also be observed, areas that probably appeared as a result of handling or tensile tests (during sample catching between the tanks).

Regarding the analysis of the sample in the breaking zone, Fig. 8b, it was found that the outer shell has a porous structure due to the large size of the rhomboidal voids between the deposited layers. In the raster area the adhesion between the layers is much higher, the porosity decreases a lot. The way the filaments breaks, detail—D, is one specific to rigid materials, behavior also revealed by the specific curves of tensile and bending tests [17].

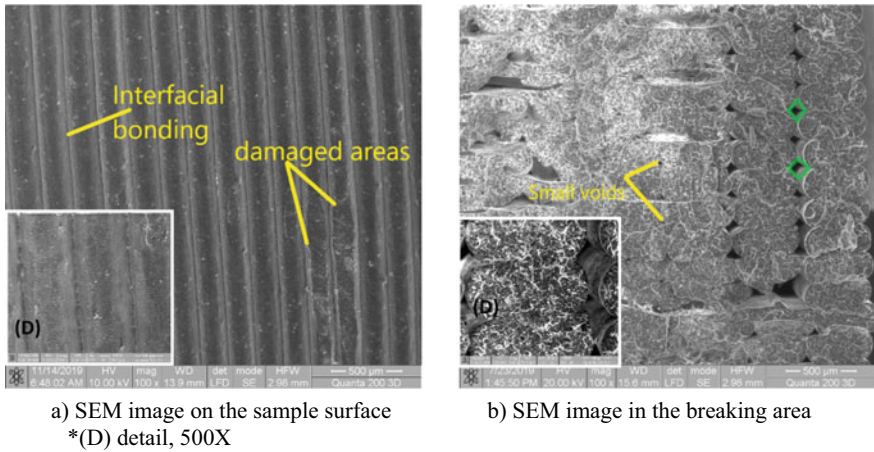


Fig. 8 SEM images of the printed sample from bioFila Linen, “on-edge” orientation on the printing bed: **a** SEM image on the sample surface *(D) detail, 500×, **b** SEM image in the breaking area

For the bioFila Silk material, the surface image of the sample, Fig. 9a, reveals a homogeneous surface with perfectly bonded filaments. At the same time, the adhesion between the extruded and deposited filaments is observed in the detailed image.

For the cross-sectional analysis, Fig. 9b, comparing the size of the triangular gaps in the raster area and the size of the rhomboidal/diamond-shaped gaps in the shell area of the sample was observed contrary to expectations, that in the raster

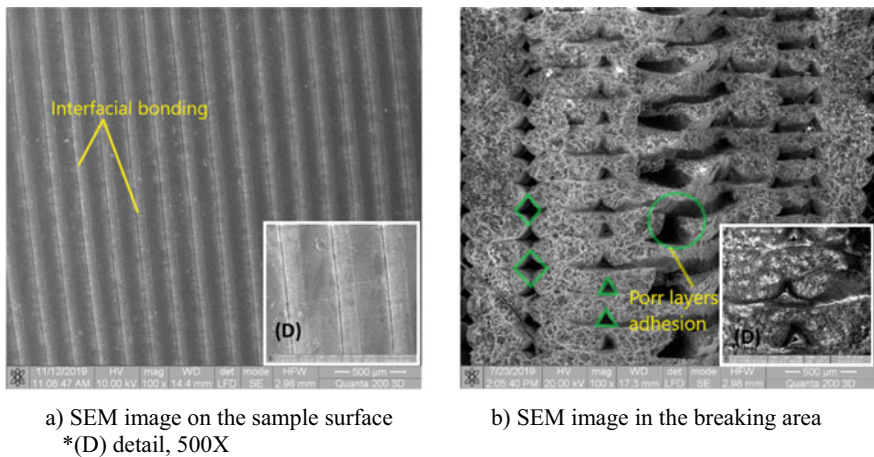


Fig. 9 SEM images of te printed sample from bioFila Silk, “on edge” orientation on the printing bed: **a** SEM image on the sample surface *(D) detail, 500×, **b** SEM image in the breaking area

area the specimen has higher porosity and in some places lack of layers. This inner structure indicates a material rapid cooling, which prevented the extruded filament from filling the free space of the model.

For the samples printed “on edge”, Figs. 8 and 9 the view reveals the layers, one below the other, being the contour, the deposited filaments are perpendicular to the Z direction of the printer, while in the case of “flat” orientation of the sample, Figs. 6 and 7, the view captures the XY plane in which the first layer has the +45° direction, so the SEM images of the surface capturing only this type of layer placement.

Analysing the SEM images of the samples cross-section it can be seen that the *sample orientation on the printing bed* influences their structure and implicitly will influence the provided mechanical responses. Thus, for the samples printed “on edge”, in the raster area the adhesion between the deposited filaments/layers is much compact, Fig. 8b, then in the case of the “flat” printed samples, Fig. 6b. But, the adhesion between the raster area and the shell area is much weaker in the case of “on edge” printing, which is characterized by rather large voids, but which are specific to FDM printing. It should also be taken into account that for “on edge” printed samples the shell percentage is much higher than for “flat” printed specimens, which gives them better mechanical strength because the loading direction and the arrangement direction of the deposited filaments are parallel.

The *layer thickness* influences the mechanical characteristics of the samples but also the surface ones because the thinner the deposited layer is, the higher the sample density and the surface quality will be, Fig. 6 compared to Fig. 7.

The *infill speed* also had a visible influence on the sample from Fig. 7a since compared to Fig. 6a it presents deformed filaments, because during to a layer deposition, the previously deposited filaments fails to solidify completely (being a little thicker) until a new filament is laid. Thus, due to the specific FDM voids and to the filaments weigh, they were deformed.

3.3 EDX Chemical Analysis for Printed Samples Made of Biodegradable Materials

The following figures show electron microscopy images over which were superimposed line graphs of chemical analysis but also graphs that chemically characterize the printed samples from the studied materials, for experiments with the best results of tensile strength (printed samples).

Figure 10 shows the specific composition highlighted by the prototyped samples from: Extrudr Green-TEC Anthracite and Extrudr BDP Pearl. The main chemical elements identified both in the EDX graph and in the in-line analysis of a portion of the sample were carbon and oxygen in mass and atomic percentages of 54% oxygen, 46% carbon for the Extrudr Green-TEC Anthracite sample and approximately equal proportions of oxygen and carbon for Extrudr BDP Pearl material.

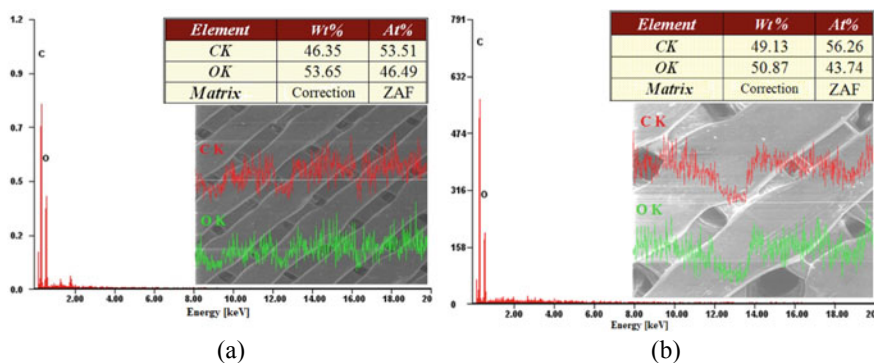


Fig. 10 EDX spectroscopic analysis for 3D printed materials: **a** Extruder Green-TEC Anthracite, **b** Extruder BDP Pearl

The in-line analysis reflects the structural homogeneity of the printed samples. This analysis also confirms the biodegradable content (biodegradable raw materials—plants) of the materials listed above.

EDX spectroscopic analysis of printed samples from bioFila Linen material, Fig. 11a, and bioFila Silk, Fig. 11b showed that they have in composition similar chemical elements to samples presented above (Extruder Green-TEC Anthracite, Extruder BDP Pearl) but the sample from bioFila Linen has in its mass and atomic composition calcium, in proportion of 12.76% and respectively 4.92%. The presence of calcium could most likely be due to the manufacturer's use of it in order to fine increase the mechanical performance of the material or to reduce the production cost by decreasing the polymer resin amount [21].

In-line EDX analysis in the cross-section of the analyzed samples showed that the materials have a homogeneous structure, with numerous carbon and oxygen bonds.

In-line EDX analyzes, presented in the form of diagrams that are superimposed over the SEM images in the cross section of the filaments, offer the possibility to identify both the constituent elements of the sample and the possibility of locating them. Their location is achieved by tracking the amplitude of the peaks. Thus, for example, in Fig. 11b, it can be easily seen that when the amplitude of the peaks for the carbon distribution diagram (C) is increased, the diagram for oxygen (O) at those points records minimums. This situation is associated with the presence of natural plant fibers that have in their composition a very high amount of carbon. There is also the possibility that the chemical elements have the same amplitude of the peaks for a certain area/point, a case associated with the identification of a carbon-oxygen bond(s).

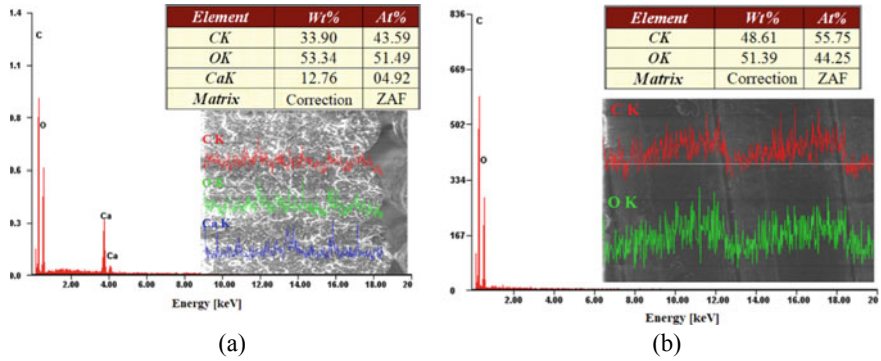


Fig. 11 EDX spectroscopic analysis for 3D printed materials: **a** bioFila Linen, **b** bioFila Silk

3.4 XRD Analysis

XRD analysis, for the study of the materials structure, was used to identify the crystalline phases present in a material and, thus, was revealed information regarding their chemical composition. Phase identification is done by comparing the obtained data with those in the databases reference.

In Fig. 12 are presented the XRD analyzes of Extrudr Green-TEC Anthracite (Fig. 12a) and Extrudr BDP Pearl (Fig. 12b) materials, which reflect their different structure.

The predominant peak noted with 1 for the XRD spectrum of the *Extrudr Green-TEC Anthracite* material is recorded at 2θ of 28.68° (intensity 41,424) and can be associated with calcium carbonate particles [21, 22], or taking into account that the EDX analysis did not identify calcium element in the chemical composition of the material, another variant would be polyvinyl chloride [23]. For the peak noted by 2 at an angle 2θ of 9.5° and with an intensity of 34,050, according to the literature

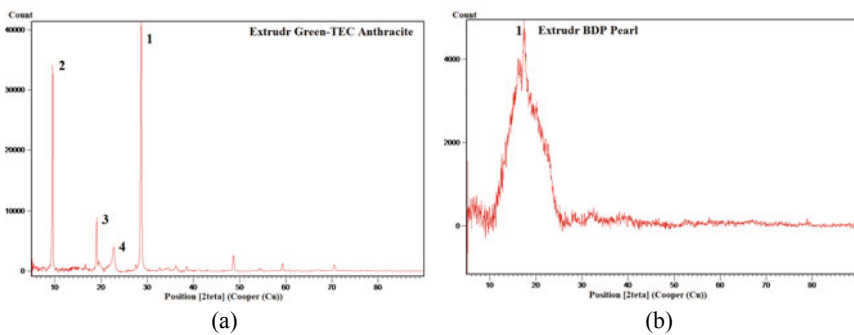


Fig. 12 XRD analysis for samples printed from: **a** Extrudr Green-TEC Anthracite, **b** Extrudr BDP Pearl

could coincide with the crystallization phase of graphene oxide (GO) [24], which is a biodegradable compound, non-toxic, soluble in water and used in the reinforcement of polymers or composites [25]. There was also a peak, noted with 3, which is similar to that obtained by the authors of the paper [26] at 19.1° angles, intensity 9834, a peak that may be caused by the presence in the composition of lignin or natural fibers. The peak marked with 4 at an angle of 22.5° , corresponds to the area of cellulose crystallization, similar results being obtained by the authors of the papers [27, 28].

The spectrum of *Extrudr BDP Pearl* material shows a major peak, noted by 1, at an angle of 18.23° with a very high intensity (compared to the other studied materials) of 4951. This maximum could be associated with the presence of polyvinylidene fluoride ($(C_2H_2F_2)_n$) known by the acronym PVDF and is used by manufacturers to increase the purity, resistance to solvents, acids and hydrocarbons of the material [29, 30].

The *Extrudr BDP Pearl* material is a semi-crystalline one and the *Extrudr Green-TEC Anthracite* material is a material with a high degree of crystallinity, characterized by narrow peaks and high intensity.

Figure 13 shows the XRD diagrams of the biodegradable materials *bioFila Linen*, Fig. 13a, and *bioFila Silk*, Fig. 13b. The *bioFila Linen* material has a major peak at an angle of 29.42° , noted by 1, at a maximum intensity of 22,417, which according to the authors in references [22, 31] but also to the EDX analysis presented in the previous subsection, may be associated to the calcium carbonate compound ($CaCO_3$). This compound is used by many manufacturers to increase both impact resistance and material rigidity—a requirement that becomes important at high temperatures of use. For example, it is used to make products from PVC (polyvinyl chloride), polypropylene, ABS (Acrylonitrile butadiene styrene) and other ingredients, in order to improve mechanical, electrical and implicitly thermal characteristics such as tensile strength and elongation [21]. Also, the sample from the *bioFillLinen* shows other peaks of much lower intensity which could correspond to the cellulose crystallization [27, 28], polyvinyl chloride or carbon from natural vegetable fibers [26] and others of even lower intensity.

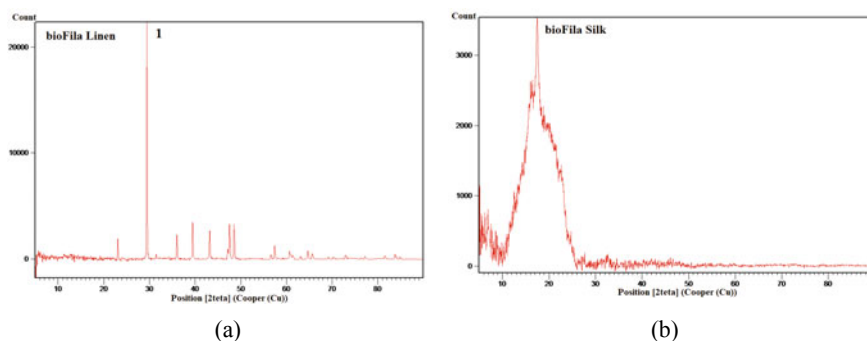


Fig. 13 XRD analysis for samples printed from: **a** *bioFila Linen*, **b** *bioFila Silk*

The spectrum of the bioFila Silk material shows a maximum diffraction at a 2θ angle of 17.47° with an absolute intensity of 3547 and which could correspond to polyvinylidene fluoride [29, 30]. The bioFila Linen material is a material with a high degree of crystallinity, but the bioFila Silk material has a semicrystalline structure, being characterized by a wide peak and low intensity compared to the bioFila Linen material.

The rigid behavior of the bioFila Linen material visible in the breaking area of the tensile test specimen (Fig. 8b) is confirmed by the EDX and XRD analyzes which reveal that the material contains calcium carbonate in a percentage of approximately 12%, an additive that confers rigidity to the material [31].

4 Conclusions

The calorimetric analysis revealed the thermal behavior of the studied biodegradable materials, thus, identifying specific transitions that took place during a polymer heating: water evaporation from the basic matrices in the first heating part in the case of all samples; crystallizations—which occurs in the case of semicrystalline, crystalline or high crystalline materials and which has also been confirmed by XRD analysis; melting points—necessary to establish the printing temperature but also to observe the materials thermal stability up to the temperature of 200°C . Another aspect that should be mentioned is the rather low melting point, between $(154\text{--}176)^\circ\text{C}$ compared to that of synthetic plastics that have melting points above 200°C , this aspect leading to significant energy reductions during the manufacturing process.

The surface and transversal analyze of the printed samples highlighted their rigid (bioFila Linen and bioFila Silk) or elasto-plastic (Extrudr GreenTec Anthracite and Extrudr BDP Pearl) structure, but also aspects related to the established process parameters, the orientation of the sample on the printing bed having a major influence on the sample physical structure and most likely also on the mechanical characteristics due to the different arrangement of the layers. Infill speed and layer thickness have influenced the surface quality but also the adhesion between the deposited filaments/layers.

EDX and X-ray diffraction analysis highlighted the presence of oxygen and carbon elements (in approximately equal atomic and mass percentages), these ones are found in abundance in plants and annual plant fibers. In the case of bioFila Linen, the material has revealed the presence of calcium carbonate, in a proportion of approximately 13% of the total mass. This filler was used by the manufacturer to fine increase the mechanical performance of this material and to decrease its price with the decrease of the resin amount.

Other information obtained from XRD analysis is closely related to the mechanical responses provided by the printed specimens during the tests reported by the authors of references [4, 17].

Following the performed studies, on the selected biodegradable thermoplastics some recommendations on the possibility of replacing different synthetic polymers in various fields of activity can be done. So, the Extrudr Green-TEC Anthracite, Extrudr BDP Pearl, bioFila Linen, bioFila Silk highlighted a high degree of biodegradability and has thermal, structural, and morphological behavior comparable to that of non-biodegradable polymeric materials, as Acrylonitrile butadiene styrene (ABS), Polyethylene (PET), Polypropylene (PP), Polycarbonate (PC) [32–37], which from this point of view makes them able to substitute the mentioned conventional materials and not only.

Acknowledgements This work was supported by a grant of the Romanian Ministry of Research and Innovation, CCCDI—UEFISDI, project number PN-III-P1.2-PCCDI-0446/82PCCDI/2018, acronym TFI PMAIAA/FAMCRIFA, within PNCI III.

References

1. Pilla S (2011) Engineering applications of bioplastics and biocomposites—an overview, handbook of bioplastics and biocomposites engineering applications. Wiley, New Jersey, pp 1–14
2. Redwood B, Schöffner F, Garret B (2017) The 3D printing handbook technologies, design and applications, Hardcover, pp 24–50
3. Mazurchevici S-N, Mazurchevici A-D, Nedelcu D (2020) Dynamical mechanical and thermal analyses of biodegradable raw materials for additive manufacturing. *Materials* 13:1819. <https://dx.doi.org/10.3390/ma13081819>
4. Mazurchevici A-D, Popa R, Carausu C, Comaneci R, Mazurchevici S-N, Nedelcu D (2020) Basic mechanical analysis of biodegradable materials. In: Paper accepted for publication in proceedings of NewTech2020 international conference, IOP conference series: materials science and engineering
5. Sin LT, Rahmat AR, Rahman WAWA (2012) Polylactic acid: PLA biopolymer technology and applications, 1st ed. Elsevier, Great Britain, pp 22–28
6. CuiFFo MA, Snyder J, Elliott AM, Nicholas Romero N, Kannan S, Halada GP (2017) Impact of the fused deposition (FDM) printing process on polylactic acid (PLA) chemistry and structure. *Appl Sci* 7(6):579. <https://doi.org/10.3390/app7060579>
7. Mazzanti V, Malagutti L, Mollica F (2019) FDM 3D printing of polymers containing natural fillers: a review of their mechanical properties. *Polymers* 11:1094. <https://doi.org/10.3390/polym11071094>
8. van den Oever MJA, Beck B, Müssig J (2010) Agrofibre reinforced poly-(lactic acid) composites: effect of moisture on degradation and mechanical properties. *Compos Part A* 41:1628–1635
9. Gkartzou E, Koumoulos EP, Charitidis CA (2017) Production and 3D printing processing of bio-based thermoplastic filament. *Manuf Rev* 4:2016020
10. Guo R, Ren Z, Bi H, Song Y, Xu M (2018) Effect of toughening agents on the properties of poplar wood flour/poly (lactic acid) composites fabricated with fused deposition modeling. *Eur Polym J* 107:34–45
11. Depuydt D, Balthazar M, Hendrickx K, Six W, Ferraris E, Desplentere F, Ivens J, Van Vuure AW (2019) Production and characterization of bamboo and flax fiber reinforced polylactic acid filaments for fused deposition modeling (FDM). *Polym Compos* 40:1951–1963

12. Liu H, He H, Peng X, Huang B, Li J (2019) Three-dimensional printing of poly (lactic acid) bio-based composites with sugarcane bagasse fiber: effect of printing orientation on tensile performance. *Polym Adv Technol* 30:910–922
13. Stoof D, Pickering K, Zhang Y (2017) Fused deposition modelling of natural fibre/polylactic acid composites. *J Compos Sci* 1:8
14. Vaidya AA, Collet C, Gaugler M, Lloyd-Jones G (2019) Integrating softwood biorefinery lignin into polyhydroxybutyrate composites and application in 3D printing. *Mater Today Commun* 19:286–296
15. Tran TN, Bayer IS, Heredia-Guerrero JA, Frugone M, Lagomarsino M, Maggio F, Athanassiou A (2017) Cocoa shell waste biofilaments for 3D printing applications. *Macromol Mater Eng* 302:1700219
16. Mazurchevici S-N, Mazurchevici A-D, Nedelcu D (2020) Dynamical mechanical and thermal analyses of biodegradable raw materials for additive manufacturing. *Materials* 13:1819. <https://doi.org/10.3390/ma13081819>
17. Carausu C, Mazurchevici S-N, Mazurchevici A-D, Andrusca L, Comaneci R, Popa R, Nedelcu D (2020) mechanical characterization of additive manufactured samples from biodegradable materials. In: Paper accepted for publication in proceedings of ModTech2020 international conference, IOP conference series: materials science and engineering
18. Extrudr. <https://www.extrudr.com/en>. Accessed 09 Nov 2019
19. Two-bears. <http://www.two-bears.eu>. Accessed 09 Nov 2019
20. Mazurchevici A-D, Carausu C, Ciofu C, Popa R, Mazurchevici S-N, Nedelcu D (2019) Infill and type influence on tensile strength of pla biodegradable material using FDM technology. *Int J Modern Manuf Technol* XI 2:44–49
21. Plastic technology. <https://www.ptonline.com/knowledgecenter/plastics-feeding/application-profiles>. Accessed 09 Nov 2019
22. Facchinetto SE, Bortolotto T, Neumann GE, Vieira JCB, de Menezes BB, Giacomelli C, Vanessa Schmidt V (2017) Synthesis of submicrometer calcium carbonate particles from inorganic salts using linear polymers as crystallization modifiers. *J Braz Chem Soc* 28 (4):547–556
23. Wankasi D, Dikio E D (2014) Polyvinyl chloride waste as an adsorbent for the sorption of Pb^{2+} from aqueous solution. *J Chem* 817527. <https://dx.doi.org/10.1155/2014/817527>
24. Vargas LR, Poli AK, de Cássia Lazzarini Dutra R, de Souza CB, Ribeiro Baldan M, Gonçalves ES (2017) Formation of composite polyaniline and graphene oxide by physical mixture method. *J Aerosp Technol Manag São José dos Campos* 9(5 1):29–38
25. Hielscher ultrasunete tehnologie. <https://www.hielscher.com/ro/graphene-oxide-ultrasonic-exfoliation-and-dispersion.htm>. Accessed 09 Nov 2019
26. Wu C-S (2004) Analysis of mechanical, thermal, and morphological behavior of polycaprolactone/wood flour blends. *J Appl Polymer Sci* 94:1000–1006. <https://dx.doi.org/10.1002/app.20837>
27. Poletto M, Ornaghi Júnior HL, Zattera AJ (2014) Native cellulose: structure, characterization and thermal properties. *Materials* 7:6105–6119. <https://dx.doi.org/10.3390/ma7096105>
28. Kaushik VK, Kumar A, Kalia S (2012) Effect of mercerization and benzoyl peroxide treatment on morphology, thermal stability and crystallinity of sisal fibers. *Int J Textile Sci I* (6):101–105. <https://dx.doi.org/10.5923/j.textile.20120106.07>
29. Cai Xiaomei, Lei Tingping, Sund Daoheng, Linde Liwei (2017) A critical analysis of the a, b and g phases in poly (vinylidene fluoride) using FTIR. *RSC Adv* 7:15382
30. Janakiraman S, Surendran Abhijith, Ghosh Sudipto, Anandhan S, Venimadhav A (2016) Electroactive poly (vinylidene fluoride) fluoride separator for sodium ion battery with high coulombic efficiency. *Solid State Ionics* 292:130–135
31. Helmia FM, Elmitwallib HR, Elnagdy SM, El-Hagrassy AF (2016) Calcium carbonate precipitation induced by ureolytic bacteria *Bacillus licheniformis*. *Ecol Eng* 90:367–371. <https://doi.org/10.1016/j.ecoleng.2016.01.044>
32. Trhliková L, Zmeskal O, Psencik P, Florian P (2016) Study of the thermal properties of filaments for 3D printing. *AIP Conf Proc* 1752:040027. <https://doi.org/10.1063/1.4955258>

33. Elkholy A, Rouby M, Kempers R (2019) Characterization of the anisotropic thermal conductivity of additively manufactured components by fused filament fabrication. *Progress Addit Manuf* 4:497–515
34. Ngo Ich-Long, Jeon Sangwoo, Byon Chan (2016) Thermal conductivity of transparent and flexible polymers containing fillers: a literature review. *Int J Heat Mass Transf* 98:219–226. <https://doi.org/10.1016/j.ijheatmasstransfer.2016.02.082>
35. Garzon-Hernandez S, Garcia-Gonzalez D, Jérusalem A, Arias A (2019) Design of FDM 3D printed polymers: an experimental-modelling methodology for the prediction of mechanical properties. *Mater Des* 188:108414. <https://doi.org/10.1016/j.matdes.2019.108414>
36. Abeykoon C, Sri-Amphorn P, Fernando A (2020) Optimization of fused deposition modeling parameters for improved PLA and ABS 3D printed structures. *Int J Lightweight Mater Manuf* 3(3):284–297. <https://doi.org/10.1016/j.ijlmm.2020.03.003>
37. Wojtyła S, Klama P, Baran T (2017) Is 3D printing safe? Analysis of the thermal treatment of thermoplastics: ABS, PLA, PET, and nylon. *J Occup Environ Hyg* 14(6):D80–D85. <https://doi.org/10.1080/15459624.2017.1285489>

Experimental Investigation on FDM Fabricated Tetra Chiral Auxetic Structures Under Uniaxial Compressive Loading



Shailendra Kumar , Swapnil Vyavahare , Soham Teraiya ,
and Labh Chand Dhakar 

Abstract This chapter describes an experimental investigation on tetra chiral auxetic structures subjected to uniaxial compressive loading. The structures of polyethylene terephthalate glycol-modified (PET-G) material are manufactured by material extrusion technique, fused deposition modeling (FDM). The influence of geometric parameters of structures on responses namely strength, stiffness, plateau stress and specific energy absorption (SEA) under compressive loading is investigated. Two geometric parameters namely thickness of ligament (t) and radius of cylinder (r) are considered. Full factorial design is used for designing the experiments and then experimental results are analysed using analysis of variance. It is found that the radius of cylinder has significant effect on structure's compressive strength and compressive modulus. With increase in radius of cylinder, compressive strength and compressive modulus decrease. Both thickness and radius are found influential for plateau stress. As the thickness increases the plateau stress decreases but with an increase in radius the plateau stress increases. Both parameters are found significant for SEA of structure. As the thickness increases, the SEA decreases, but with an increase in radius SEA initially decreases and then increases. Predictive models are also developed to correlate responses with parameters. Further, multi-objective optimization is performed for maximization of responses.

S. Kumar (✉) · S. Vyavahare · S. Teraiya · L. C. Dhakar
Department of Mechanical Engineering, Sardar Vallabhbhai National Institute of
Technology, Surat, Gujarat, India
e-mail: skbudhwar@med.svnit.ac.in

S. Vyavahare
e-mail: swapnil.vyavahre@gmail.com

S. Teraiya
e-mail: sohamteraiya@gmail.com

L. C. Dhakar
e-mail: lcdhakar@gmail.com

1 Introduction

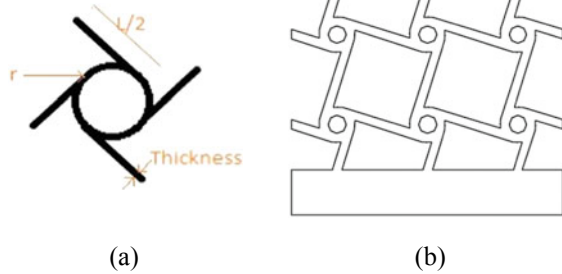
Additive manufacturing (AM) involves layer-by-layer construction of the intricate design. AM generally classified in seven categories such as stereolithography (SLA), liquid polymerization (LP), fused deposition modeling (FDM), ballistic particle manufacturing (BPM), selective laser sintering (SLS), laser engineered net-shaping (LENS), and binder jet printing (BJP) [1, 2]. Nowadays, parts produced by AM are used in aerospace, defense, and automobile industries. The USA launched new 3D printed Volvo trucks for checking its fuel efficiency. Many researchers worked on application-based problems such as smart filter [3], mechanical absorber [4], auxetic polymer matrix for enhanced device sensitivity [5], dilator for the opening of cavity an artery [6], aerodynamic surface [7]. Among all AM techniques, FDM is most popular because of its cost-effectiveness, a wide range of material availability, and its capability of manufacturing parts having good strength [8]. Different types of AM techniques are used to manufacture complex structures and tailorable mechanical properties are obtained.

Lightweight structures are required in automobile, aerospace, and medical domains. With recently developed meta-materials, counterintuitive properties can be produced. These mechanical meta-materials are classified depending upon mechanical properties they target, i.e. Young's modulus, shear modulus, Poisson's ratio [9]. These materials have anomalous mechanical properties due to their structural design i.e. vanishing shear modulus, negative compressibility, zero/negative/switchable Poisson's ratio.

Auxetic or negative Poisson's ratio structure, is a class of meta-material, are of great research interest as it demonstrates high strength to weight ratio, improved mechanical properties such as higher in-plane indentation resistance, impact resistance, bending stiffness, fracture toughness, synclastic curvature, vibration damping, hardness, excellent shock absorption capability and transverse shear modulus over conventional structure having a positive Poisson's ratio [10, 11]. These structures are classified depending upon the geometry of the unit cell unit cell i.e. re-entrant, chiral, origami, 3D buckliball etc. Among these structures, chiral structures are popular due to their unique deformation mechanism i.e. clockwise or anti-clockwise rotation of cylinder around its center depends upon the place of attachment of struts to the cylinder. This causes gradual distribution of load to the neighbouring unit cells resulting in global deformation rather than local failure. Chiral structure are further classified depending upon number of ligaments attached to cylindrical geometry tangentially and direction of this attachment. In tetra chiral auxetic structure four ligaments are attached to cylindrical geometry tangentially as shown in Fig. 1. These structures are difficult to fabricate using conventional manufacturing techniques such as casting, welding, metal forming, and powder metallurgy [12]. AM can easily overcome the limitations of conventional manufacturing in fabrication of the auxetic structure.

Researchers have studied various structures manufactured using different AM techniques. Grima et al. [13] conducted experiments on 3, 4, and 6 arrow star

Fig. 1 **a** Unit cell, and
b drawing of tetra chiral
auxetic structure



structures for auxetic behavior. They concluded that rotational symmetry of star shape containing 4 and 6 unit cells have better auxetic behavior than structures having 3 unit cells. Alderson et al. [14] investigated structures made of crystalline silica for the deformation mechanism at a molecular level. They observed that when the structure goes under the application of negative hydrostatic pressure, there is variation in Poisson's ratio from negative to positive. Alderson et al. [15] conducted experiments to compute the elastic property of a cylinder having different types of ligaments. They concluded that a higher number of ligaments with chiral geometry resulted in more elastic moduli. Javadi et al. [16] proposed the numerical method which is a combination of finite element and genetic algorithm to identify auxetic structure with a wide range of Poisson's ratio for 2D and 3D cellular structures. They developed a new design with different Poisson's ratio structures and auxetic materials. Assidi and Ganghoffer [17] derived the collapse mechanism for tetra chiral and hexa chiral cellular structures and investigated the main influencing parameters for auxeticity. They observed that effective tensile modulus is more effective in a definite direction. Chen et al. [18] described the in-plane and out-of-plane behavior of anti-tetra chiral structure with the theoretical, numerical, and experimental method. They concluded that the most significant parameters for NPR are the length of ligaments in X and Y direction. Ge et al. [19] studied the impact behavior of hexagonal honeycomb structure in X and Y direction with parameters such as cell wall angle, crushing velocity, and relative density of the structures. They concluded that X-direction breaking mainly influences by the deformation mode, while Y-directional breaking mainly influences by crushing strength. Fanfan et al. [20] studied honeycomb structure for dynamic strength by analytical and numerical simulation. They found that the honeycomb structure is dynamic sensitive in Y-direction. Carneiro et al. [21] performed the numerical investigation of the re-entrant structure and shown the effect of geometrical constraints on auxetic behavior. They found that NPR depends on geometry and base material of the structure. Yang et al. [22] investigated the use of the deflection

beam model and the Timoshenko model in an analytical solution for 3D re-entrant honeycomb auxetic cellular structure, to get modulus, Poisson's ratio, and yield strength in principle direction. They compared finite element analysis (FEA) results with the experimental results and found that developed models had reasonable accuracy in predicting all the responses. Li et al. [2] investigated the influence of process variables on NPR structures made of metal alloy mixture fabricated by using the SLS method. They used the method of linear energy density, which proved useful in identifying the process window in designed structures and achieved the highest NPR of -2 for these structures. Habib et al. [23] investigated the effect of cell thickness on compressive behavior and energy absorption capability of the Nylon-12 honeycomb structure made by FDM. They observed that an increase in ratio of thickness and length increased compressive modulus, plateau stress, and energy absorption capacity and decreased densification strain. Li et al. [24] studied different structures such as hexagonal, mixed honeycomb, and re-entrant for in-plane uniaxial and bi-axial crushing properties. They concluded that the plateau stress values in re-entrant structures are more compared to the hexagonal honeycombs. Alomarah et al. [25] investigated a new auxetic structure, re-entrant chiral honeycomb (RCA) for compression tests and compared its performance with other auxetic structures. They found that RCA outperformed other auxetic structures in the compressive strength and energy absorption if it is subjected to load in the Y direction. Qi et al. [26] investigated the compressive strength of tetra chiral subjected to static and dynamic conditions experimentally as well as numerically. They concluded that the effect of geometric parameters and cell wall thickness is significant for crushing strength. Gebrehiwot et al. [27] studied flexural properties of FDM manufactured beams containing various types of stiffeners numerically and experimentally. They observed that honeycomb and square stiffener has the highest and lowest calculated area moment of inertia respectively. Fashanu et al. [28] examined possibility of adoption numerical unit-cell homogenization as a predictive tool and found that predictive results are in accordance with experimental results.

The literature review shows that limited attempts are made to investigate the effect of geometric variables on the tetra chiral auxetic structure's mechanical properties. Also, there is limited literature is available on investigating the mechanical properties of tetra chiral auxetic structures of polyethylene terephthalate glycol-modified (PET-G) material. Therefore, in the present work, efforts are made to investigate the mechanical properties of FDM fabricated auxetic structures of PET-G material. PET-G is an excellent material for the applications that require more durability than poly-lactic acid (PLA) and acrylonitrile butadiene styrene (ABS) materials. The objectives of the current experimental investigation are as follows—(i) to study the effect of geometric variables/parameters on responses namely strength, stiffness, plateau stress and SEA under compressive loading, (ii) to develop regression models for the responses using single objective optimization, and (iii) to perform multi-objective optimization by combining all the responses.

2 Methodology

Following steps are involved in the present experiential investigation—(i) Design of Experiment, (ii) Modeling of configurations of structure, (iii) FDM fabrication, and (iv) Response measurement.

2.1 Design of Experiment

In the present study, two geometric parameters of tetra chiral auxetic structure, namely thickness of ligament (t) and radius of cylinder (r), are investigated as shown in Fig. 2. Levels of selected parameters (Table 1) are taken by following the ASTM C365 standard. A comprehensive experimental study is planned using a full factorial design and Stat-Ease Inc developed Design-Expert 11 software. Experimental design suggested a total of 9 experiments with the repetition of each experiment as listed in Table 2.

Density ratio (relative density) plays an important role in NPR cellular structures [29]. In the present investigation, its value is kept constant at 25% for all structures. Depth of all configurations of structure is kept as 25 mm [25]. Length of ligaments (L) is calculated using Eq. (1) [30]. All parameters of tetra chiral are defined in non-dimensional format such as α and β ; where α is L/r , β is t/r .

$$\frac{\rho}{\rho_{core}} = \frac{\beta[2\alpha + \pi(2 - \beta)] - 2[\phi - (1 - \beta) \sin \phi]}{4 \left[\left(1 - \frac{\beta}{2}\right)^2 + \frac{\alpha^2}{2} \right]} \tag{1}$$

where,

ϕ is the angle for overlapping

ρ is the density of the auxetic structure

ρ_{core} is the density of solid material

$\frac{\rho}{\rho_{core}}$ is the density ratio for structure

Fig. 2 Angle and the overlapping area

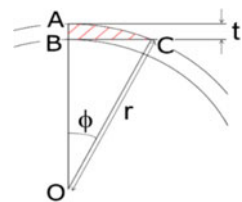


Table 1 Geometric parameters and their levels

Levels	1	2	3
Thickness of ligament, t (mm)	1.4	1.7	2
Radius of chiral geometry, r (mm)	4	5	6

Table 2 Design of experiment

Run no.	Value of geometric parameter	
	Thickness of ligament (t)	Radius of chiral geometry (r)
1	1.4	4
2	1.4	5
3	1.4	6
4	1.7	4
5	1.7	5
6	1.7	6
7	2	4
8	2	5
9	2	6

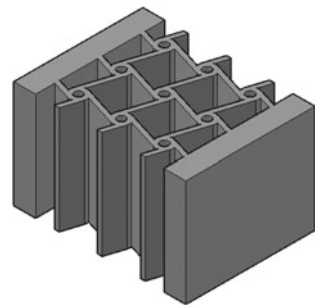
2.2 Modeling of Configurations of Structure

The tetra chiral auxetic structures are designed with the help of Solidworks 2020 software. Figure 3 shows the representative computer-aided design (CAD) model of auxetic structure having tetra chiral configuration.

2.3 FDM Fabrication

The design of structure is in such a way that the cellular core is sandwiched between two plates (top and bottom). Both the plates is kept at 5 mm thickness so that there will be negligible deformation of plates while testing. Tetra chiral unit cell contains

Fig. 3 CAD model of tetra chiral auxetic structure



four ligaments and one cylinder, so the overall structure displays the symmetry in the X and Y direction. The CAD models are sliced using CURA 4.2.1 software and then fed to the Delta 2040, FDM machine manufactured by Wasp, Italy, which has a 0.4 mm nozzle diameter [31]. Feedstock material (i.e. PET-G) is in the form of filament having diameter as 1.75; which is provided by M/s Positron Additive Ltd., Pune, India,. Values of constant process parameters used in fabrication of all configurations is listed in Table 3. Using design of experiment (Table 2), total nine configurations of tetra chiral auxetic structure are fabricated on FDM machine. These fabricated configurations are depicted in Fig. 4.

2.4 Response Measurement

After fabrication of configurations, uniaxial static compressive tests are performed in the compression testing machine at a speed of 5 mm/min as shown in Fig. 5. The applied force is measured by the machine load cell. Load-displacement curves, initial stiffness, energy absorbed are evaluated. Flatwise compression properties of sandwich cores are measured according to a standard test method, ASTM C365 [32, 33]. Two specimens are tested for each configuration of the structure as shown in Fig. 6. The load-displacement curves assessed from the compression tests are translated in the stress-strain curves by gaging sizes of the specimens. Stiffness is calculated from the initial linear region of the stress-strain curve. Structures are tested till 60% strain.

Table 3 Values of constant process parameters

Process parameter	Value
Layer thickness (mm)	0.2
Wall thickness (mm)	0.4
Top and bottom thickness (mm)	0.3
Print speed (mm/s)	40
Infill density (%)	100
Cooling fan speed (%)	100
Nozzle temperature (°C)	240
Bed temperature (°C)	100

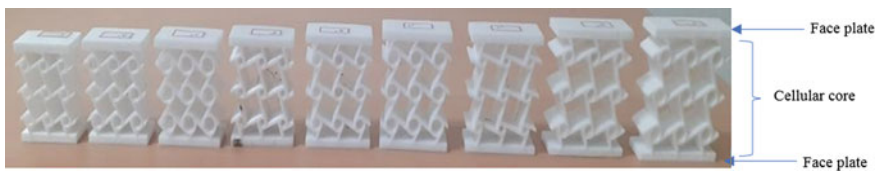


Fig. 4 FDM fabricated tetra chiral auxetic structures



Fig. 5 Compression testing machine

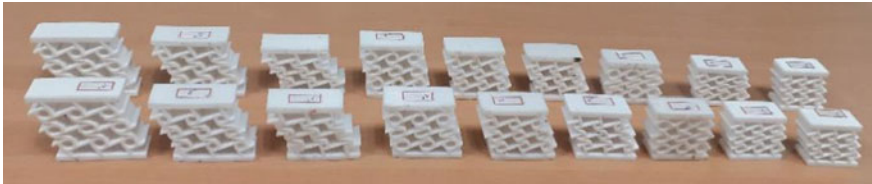


Fig. 6 Tetra chiral auxetic structures after compression testing

From stress-strain data, the curve is plotted using MATLAB software, and basic curve-fitting is applied to the curve to obtain tenth-degree polynomial as shown in Fig. 7, so that the energy absorption and plateau stress can be easily calculated. The compressive modulus is analysed from the initial elastic region of this curve from Eq. (2).

$$\sigma = E\varepsilon \quad (2)$$

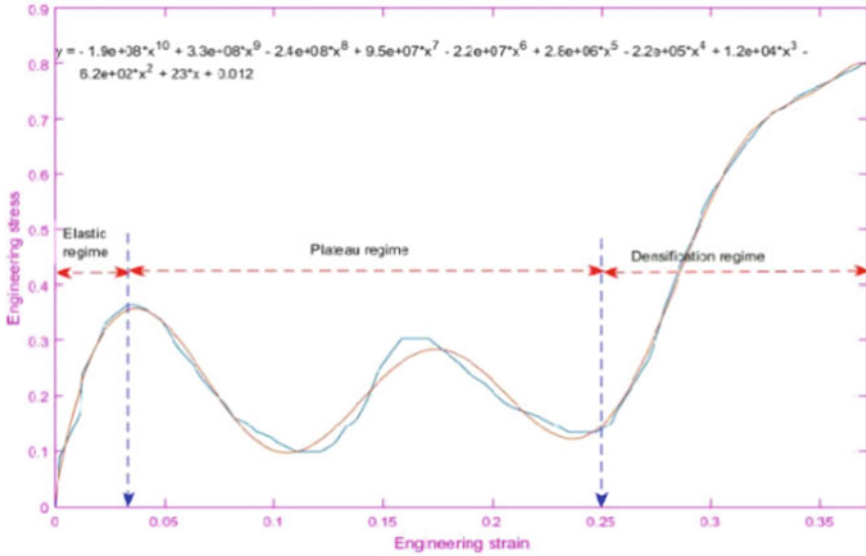


Fig. 7 Representative stress-strain curve (Run no. 1)

where σ is stress, δ is the movement of the plate, ϵ is strain value, and E is the compressive modulus of the specimen.

Compressive strength is a stress value that can be taken from the stress-strain curve before 10% of strain near to yield strength. If the yield point does not appear in the stress-strain curve, then compressive strength is taken at 10% of strain value [34]. Energy absorption is calculated from Eq. (3) and SEA by Eqs. (4) and (5).

$$E = \int_0^{\epsilon_d} \sigma(\epsilon) d\epsilon \tag{3}$$

$$SEA(m) = \frac{E}{m} \tag{4}$$

$$SEA(v) = \frac{E}{v} \tag{5}$$

The plateau stress is calculated using Eq. (6), because the relation between stress-strain is fluctuating, a single stress value from the graph cannot be considered [25].

$$\sigma_{pl} = \frac{\int_{\epsilon_y}^{\epsilon_d} \sigma(\epsilon) d\epsilon}{\epsilon_d - \epsilon_y} \tag{6}$$

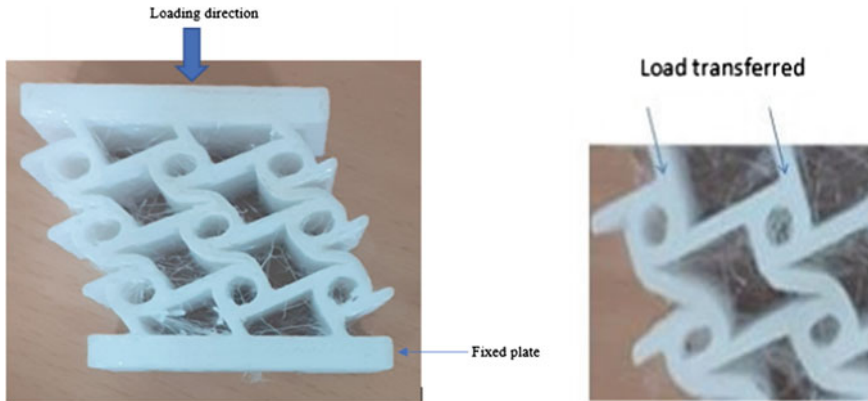


Fig. 8 Deformation of tetra chiral auxetic structure

Under compressive loading, force is applied perpendicularly to the face plate, then it is transferred to the ligaments as shown in Fig. 8. As load transfers through the ligaments, torque acts on the circular sections. As a result, the ligaments wrap around the circular sections and hence deformation occurs. Due to this deformation, the first layer of unit cells occupies the space of second layer unit cells and second layer occupies the space of third layer unit cells; and thus densification of structure takes place.

3 Results and Discussion

As shown in Fig. 7, three major regimes are observed in the stress-strain curves of all the structures such as elastic regime, plateau regime, and densification regime. Elastic behavior is considered up to the end of the straight line of the curve. The second region is called a plateau regime where the curve fluctuates like a waveform, and numbers of crest and trough are formed because of the sequential collapse of the unit cells row-by-row. The third region is called the densification regime where all unit cells have been collapsed and thus load increases sharply. This point also considers as a failure point of specimens [25]. Experimental results are given in Table 4. Stress-strain curves are fitted with the regression models using polynomial curves. For fitting the curve and calculation of area under the stress-strain curve, MATLAB software is used.

Table 4 Experimental results for auxetic structures

Sr. No.	t (mm)	r (mm)	l (mm)	E (MPa)	S (MPa)	PS (MPa)	EV (KJ/m ³)	EM (J/gm)
1	1.4	4	44.077	18.919	0.365	0.202	51.9	128.195
2	1.4	4	46.841	20.449	0.445	0.272	67.4	166.480
3	1.4	5	48.977	18.835	0.494	0.487	109.1	253.778
4	1.4	5	50.671	18.587	0.678	0.643	140.5	312.564
5	1.4	6	53.957	12.012	0.513	0.545	149.2	324.290
6	1.4	6	56.702	16.647	0.713	0.777	266.2	578.593
7	1.7	4	56.947	39.24	0.774	0.509	128.3	306.871
8	1.7	4	60.644	44.445	1.084	0.725	203.8	470.892
9	1.7	5	63.829	12.435	0.494	0.448	122.5	301.309
10	1.7	5	44.077	14.715	0.531	0.548	124	304.999
11	1.7	6	46.841	11.501	0.304	0.277	51.1	112.999
12	1.7	6	48.977	11.246	0.291	0.339	48.6	110.867
13	2	4	50.671	22.836	0.572	0.323	120.5	332.344
14	2	4	53.957	16.622	0.551	0.321	107	295.110
15	2	5	56.702	15.431	0.349	0.255	65.3	163.382
16	2	5	56.947	17.028	0.336	0.232	60	150.121
17	2	6	60.644	17.351	0.547	0.4926	113.5	281.966
18	2	6	63.829	15.626	0.541	0.489	108.9	263.729

t thickness of ligament, *r* radius of cylinder, *l* length of ligament, *E* Modulus, *S* Strength, *PS* Plateau stress, *EV* Energy absorption per unit volume, *EM* Energy absorption per unit mass

3.1 Effect of Geometric Parameters on Responses

3.1.1 Effect of Ligaments Thickness and Chiral Radius on Compressive Modulus and Strength

It is observed from Figs. 9 and 10 that radius has a significant effect on the modulus of tetra chiral geometry. As the thickness of ligaments increases modulus and strength increase till a thickness value of 1.7 mm, but with further increase in thickness, modulus decreases as flexural strength of ligament decreases. Compressive load is inversely proportional to thickness therefore easy bending is occurred during testing. As the radius of the chiral topology increases, modulus decreases. This is due to a decrease in a torque acting on the cylinder.

3.1.2 Effect of Ligaments Thickness and Chiral Radius on Plateau Stress

Plateau stress is the average value of stress between yield strain to densification strain. It mainly depends on the length of ligaments. It is observed from the result

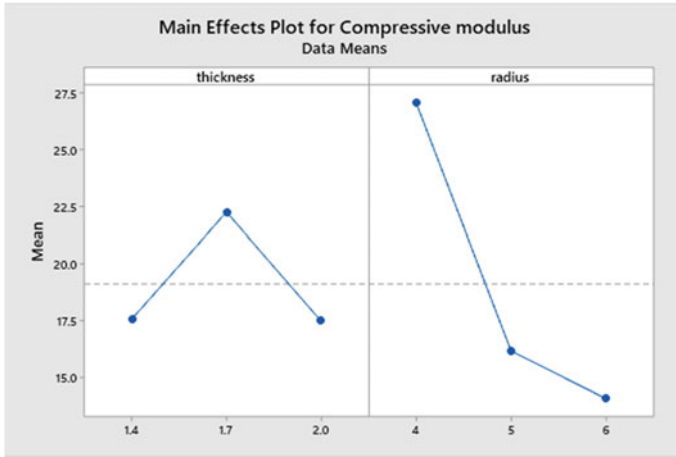


Fig. 9 Mean effect plot for compressive modulus

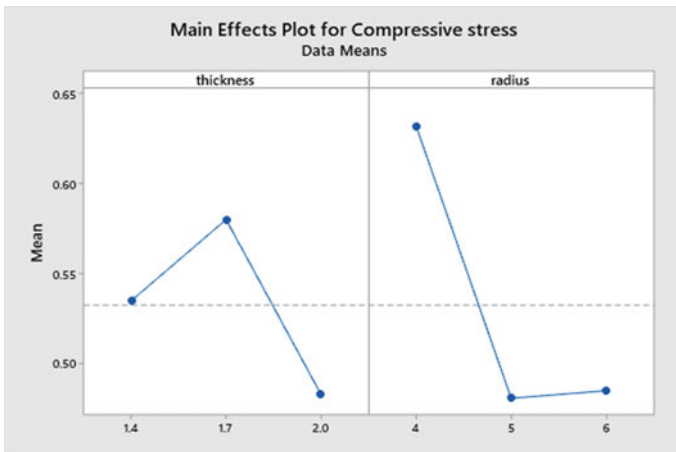


Fig. 10 Mean effect plot for compressive strength

that the length of ligaments increases with increases in thickness, and it decreases with increase in a radius of the chiral cylinder. As shown in Fig. 11, as thickness increases plateau stress decreases. With a higher value of ligament length load reduces and a lower value of ligament length results in lesser difference value of densification and yield strain. However, with an increase in the radius, plateau stress increases because during the quasi-static compression test densification regime starts earlier as compared to other structures. From Fig. 9, it is observed that variation in plateau stress is significant with the change in thickness and radius.

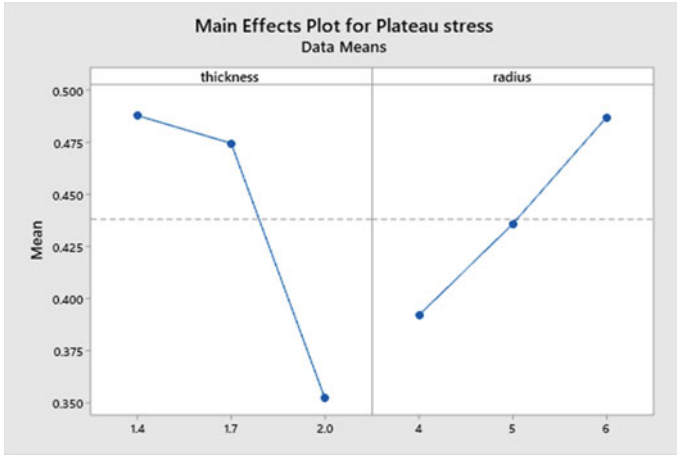


Fig. 11 Mean effect plot for plateau stress

3.1.3 Effect of Ligaments Thickness and Chiral Radius on SEA

From Figs. 12 and 13, it is found that as the thickness of ligaments increases, the mean values of SEA (i.e. energy absorption per unit volume as well as energy absorption per unit mass) decrease. This is due to high fluctuation in the stress-strain curve. Due to it less area is covered under the stress-strain curve. For an increase in radius from 4 to 5 mm energy absorption decreases, and with further increase in the radius of chiral topology, energy absorption per unit volume increases. The effect of thickness is more than the radius for energy absorption per

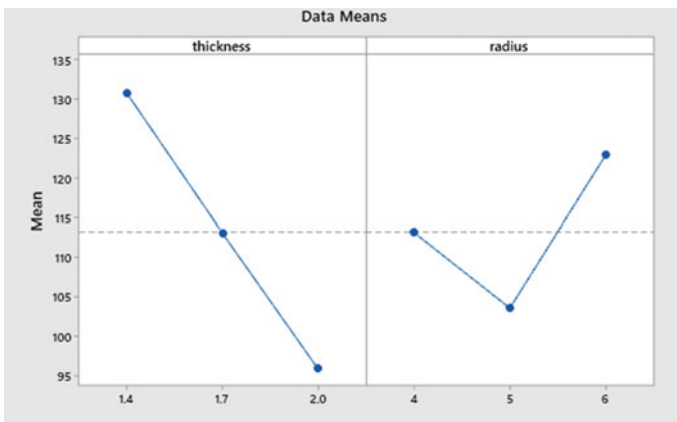


Fig. 12 Mean effect for energy absorption per unit volume

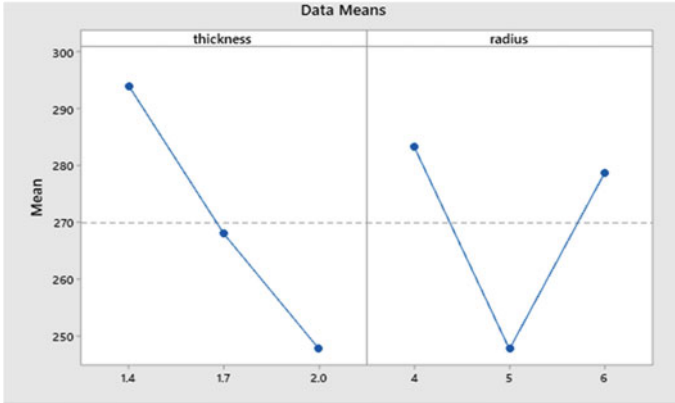


Fig. 13 Mean effect for energy unit mass

unit volume, because thickness mathematical models for each response is developed in the next section.

3.2 Predictive Models for Responses

Regression models of responses of auxetic structures of PET-G material are generated using ANOVA in the software.

3.2.1 Predictive Model of Compressive Modulus

From Table 4, it is observed that compressive modulus values range from 11.246 to 44.445 MPa. Compressive modulus is derived as a function of t and r . The regression model of the compressive modulus is given in Eq. (7).

$$\begin{aligned} \text{Compressive modulus} = & -2139 + 2642 \times t + 708 \times r - 1044 \times t \times r + 94.42 \\ & \times t^2 \times r^2 - 6.196 \times t^2 \times r^3 - 64.3 \times r \times t^3 \end{aligned} \quad (7)$$

3.2.2 Predictive Model for Compressive Strength

The compressive strength of tetra chiral structures is listed in Table 4, which shows the lowest and highest values of strength as 0.2908 to 1.0841 MPa. The regression model for compressive strength is given in Eq. (8).

$$\begin{aligned} \text{Compressive strength} = & -77.83 + 83.83 \times t + 19.03 \times r - 20.98 \times t^2 - 0.7363 \times r^2 \\ & - 18.7 \times t \times r + 4.037 \times t^2 \times r + 0.4788 \times r^2 \times t \end{aligned} \quad (8)$$

3.2.3 Predictive Model for Plateau Stress

Plateau stress is calculated as an average value over the plateau region because there is no single point is available for stress. The regression model given in Eq. (9) is in good agreement with experimental data as it has R^2 and Adjusted R^2 , such as 99.26 and 94.12% respectively.

$$\begin{aligned} \text{Plateau stress} = & -69.62 + 71.34 \times t + 17.78 \times r - 17.41 \times t^2 - 0.7858 \times r^2 \\ & - 16.29 \times t \times r + 3.362 \times t^2 \times r + 0.4644 \times r^2 \times t \end{aligned} \quad (9)$$

3.2.4 Predictive Model for Energy Absorption Per Unit Volume

From Table 4, it is observed that energy absorption per unit volume for tetra chiral structures are lowest of 51.1 kJ/m³, and highest 266.2 kJ/m³. The regression model for the energy absorbed per unit volume is given in Eq. (10).

$$\begin{aligned} \text{Energy absorption/volume} = & -1.557 \times 10^4 + 1.81 \times 10^4 \times t + 3221 \times r - 5148 \times t^2 \\ & - 3.212 \times r^2 - 3695 \times t \times r + 1050 \times t^2 \times r \end{aligned} \quad (10)$$

3.2.5 Predictive Model for Energy Absorption Per Unit Mass

Energy absorption per unit mass (SEA) have lowest and highest values from 110.867 to 578.5931 J/gm, respectively. The regression model for the energy absorbed per unit mass is given in Eq. 11.

$$\begin{aligned} \text{Energy absorption/mass} = & -1.817 \times 10^4 + 1.792 \times 10^4 \times t + 2964 \times r - 2136 \times t \\ & \times r - 3548 \times t^2 - 39.96 \times r^2 + 21.1 \times t^3 \times r^2 \end{aligned} \quad (11)$$

Comparison between experimental and predicted values of responses is given in Table 5. Predictive models are validated by using R^2 and adjusted R^2 values, as shown in Table 6.

Table 5 Comparison between experimental and predicted values of responses

Sr. No.	t (mm)	r (mm)	l (mm)	E (exp) (MPa)	E (prd) (Mpa)	S (exp) (Mpa)	S (prd) (MPa)	PS (exp) (MPa)	PS (prd) (MPa)	EV (exp) (KJ/ m ³)	EV (prd) (KJ/ m ³)	EM (exp) (J/ gm)	EV (prd) (J/ gm)
1	1.4	4	44.07	19.68	23.42	0.40	0.40	0.23	0.21	59.65	52.52	147.33	145.33
2	1.4	5	46.84	18.71	18.16	0.58	0.53	0.56	0.55	124.8	129.62	283.17	280.38
3	1.4	6	48.97	14.32	18.70	0.61	0.61	0.66	0.63	207.7	200.28	451.44	451.30
4	1.7	4	50.67	41.84	41.54	0.92	0.91	0.61	0.61	166.05	166.88	388.88	390.74
5	1.7	5	53.95	13.57	22.41	0.51	0.52	0.49	0.45	123.25	111.98	303.15	296.88
6	1.7	6	56.70	11.37	11.83	0.29	0.28	0.30	0.29	49.85	50.64	111.93	330.43
7	2	4	56.94	19.72	24.10	0.56	0.56	0.32	0.3	113.75	110.60	313.72	307.44
8	2	5	60.64	16.23	17	0.34	0.33	0.24	0.23	62.65	112.7	156.75	159
9	2	6	63.82	16.48	21.73	0.54	0.54	0.49	0.45	111.2	108.36	272.84	268.24

t thickness of ligament, r radius of cylinder, l length of ligament, E Modulus, S Strength, PS Plateau stress, EV Energy absorption per unit volume, EM Energy absorption per unit mass, exp Experimental value, prd Predicted value

Table 6 Model summary

Response	RMSE	R ²	Adjusted R ²
Compressive modulus	1.9247	0.9939	0.9576
Compressive strength	0.0230	0.9981	0.9846
Plateau stress	0.0936	0.9926	0.9412
Energy absorption per unit volume	13.9574	0.9895	0.9264
Energy absorption per unit volume	8.8099	0.9990	0.9928

Root mean square error (RMSE) values are calculated using Eq. (12) with R² and Adjusted R² values. RMSE shows the standard deviation of residuals, and this residual value describes how far it is from actual values. RMSE also gives a summary of how great concentration of points near to the fitted regression line. Model predictions found to be in accordance with experimental outcomes; which is shown in Table 6.

$$RMS = \sqrt{\frac{\sum_{n=1}^{n=9} (y - y_1)^2}{n}} \tag{12}$$

3.3 Single-Objective Optimization

Single-objective optimization is performed using the JAYA algorithm [35] in MATLAB software to calculate set of optimized variables for maximization of each output individually. Optimization results are listed in Table 7.

Table 7 Optimized parameters for single objective optimization of responses

Response	t (mm)	r (mm)	Optimized value of responses
Compressive modulus (MPa)	1.755	4	42.239
Compressive strength (MPa)	1.727	4	0.922
Plateau stress (MPa)	1.4	5.763	0.638
Energy absorption per unit volume (KJ/M ³)	1.4	6	200.288
Energy absorption per unit mass (J/gm)	1.4	6	451.302

Table 8 Multi-objective optimization

Combined objective function (COF) value = 0.937139		
t = 1.741 mm, r = 4 mm	E	42.193
	S	0.921
	PS	0.613
	EV	169.271
	EM	397.574

t thickness of ligament, *r* radius of cylinder, *E* Modulus, *S* Strength, *PS* Plateau stress, *EV* Energy absorption per unit volume, *EM* Energy absorption per unit mass

3.4 Multi-objective Optimization

Multi-objective optimization of tetra chiral auxetic structure is also performed to optimize both geometric parameters. For this, the combined multi-objective function is prepared as given in Eq. (13) [35].

$$\text{Max } (Z) = \frac{w_1 \times Y(\text{CM})}{\text{CM}_{\text{max}}} + \frac{w_2 \times Y(\text{CS})}{\text{CS}_{\text{max}}} + \frac{w_3 \times Y(\text{PS})}{\text{PS}_{\text{max}}} + \frac{w_4 \times Y(\text{EV})}{\text{EV}_{\text{max}}} + \frac{w_5 \times Y(\text{EM})}{\text{EM}_{\text{max}}} \quad (13)$$

where, CM = Compressive Modulus, CS = Compressive strength, PS = Plateau Stress, EV = Energy absorbed per unit volume, EM = Energy absorbed per unit mass, Y(CM), Y(CS), Y(PS), Y(EV), Y(EM) are response surface equations for each response, w_1, w_2, \dots, w_5 are weight values assigned to each response. These weight values are assigned as per the requirement of the application, and the aggregate of all the weights should be 1. Here, equal weights for all the responses are considered, i.e., $w_1 = w_2 = w_3 = w_4 = w_5 = 0.2$.

The combined objective function value is found to be 0.937, and corresponding levels of design parameters are 1.741 and 4 for *t* and *r*, respectively as given in Table 8.

It is found that at thickness of ligament 1.741 mm and radius of chiral geometry 4 mm; both geometric parameters are optimized simultaneously for all responses.

4 Conclusion

An experimental investigation on strength, stiffness, plateau stress, and SEA of FDM fabricated tetra chiral auxetic structures of PET-G material under compressive loading is described in this chapter. Followings are the findings of present work:

- (i) Radius of the cylinder has a significant influence on compressive strength and modulus. As the radius of cylinder increases, compressive strength and modulus decrease.

- (ii) Both thickness and radius are found influential for plateau stress. As the thickness increases the plateau stress decreases, but with an increase in radius, the plateau stress increases.
- (iii) The influence of thickness and radius on energy absorption per unit volume and energy absorption per unit mass is significant. As the thickness increases, the energy absorption per unit volume and energy absorption per unit mass decrease, but with an increase in radius, both responses initially decrease and then increases.
- (iv) Tetra chiral structures exhibit elastic-plastic deformation behavior under in-plane compression loading.

Further, regression models are also generated to calculate strength, stiffness, plateau stress, and SEA of auxetic structures. Also, optimization of geometric variables is achieved to maximize each response individually. Also, a multi-objective optimization is performed to optimize geometric parameters.

The conclusions of the present investigation are useful to fabricate tailor-made auxetic structures of maximum strength, stiffness, plateau stress and SEA. Future research will be directed towards studying the strength, stiffness and SEA of auxetic structures made by FDM subjected to various types of loading.

References

1. Gibson I, Rosen DW, Stucker B (2014) Additive manufacturing technologies, vol 17. Springer, New York
2. Li S, Hassanin H, Attallah MM, Adkins NJ, Essa K (2016) The development of TiNi-based negative Poisson's ratio structure using selective laser melting. *Acta Mater* 105:75–83
3. Alderson A, Rasburn J, Ameer-Beg S, Mullarkey PG, Perrie W, Evans KE (2000) An auxetic filter: a tuneable filter displaying enhanced size selectivity or defouling properties. *Ind Eng Chem Res* 39:654–665. <https://doi.org/10.1021/ie990572w>
4. Bezazi A, Scarpa F (2007) Mechanical behaviour of conventional and negative poisson's ratio thermoplastic polyurethane foams under compressive cyclic loading. *Int J Fatigue* 29:922–930. <https://doi.org/10.1016/j.ijfatigue.2006.07.015>
5. Nicolais Jour L, Mir M, Ali MN, Sami J, Ansari U (2014) Review of mechanics and applications of auxetic structures SP—753496 VL-2014
6. Mir M, Ali MN, Sami J, Ansari U (2014) Review of mechanics and applications of auxetic structures. *Adv Mater Sci Eng*
7. Bettini P, Airoidi A, Sala G, Di Landro L, Ruzzene M, Spadoni A (2010) Composite chiral structures for morphing airfoils: numerical analyses and development of a manufacturing process. *Compos B Eng* 41(2):133–147
8. Vyavahare S, Teraiya S, Panghal D, Kumar S (2019) Fused deposition modeling: a review. *Rapid Prototyp J*. <https://doi.org/10.1108/RPJ-04-2019-0106>
9. Yu X, Zhou J, Liang H, Jiang Z, Wu L (2018) Mechanical metamaterials associated with stiffness, rigidity and compressibility: a brief review. *Prog Mater Sci* 94:114–173
10. Elipe JCÁ, Lantada AD (2012) Comparative study of auxetic geometries by means of computer-aided design and engineering. *Smart Mater Struct* 21(10):105004
11. Zhang X, Yang D (2016) Mechanical properties of auxetic cellular material consisting of re-entrant hexagonal honeycombs. *Materials* 9(11):900

12. Faludi J, Bayley C, Bhogal S, Iribarne M (2014) Comparing environmental impacts of additive manufacturing vs. traditional machining via life-cycle assessment. Laboratory for Manufacturing and Sustainability, UC, Berkeley
13. Grima JN, Gatt R, Alderson A, Evans KE (2005) On the potential of connected stars as auxetic systems. *Mol Simul* 31(13):925–935
14. Alderson A, Alderson KL, Evans KE, Grima J. N, Williams MS (2005) Modelling of negative Poisson's ratio nanomaterials: deformation mechanisms, structure-property relationships and applications. *J Metastable Nanocrystalline Mater* 23:55–58. Trans Tech Publications
15. Alderson A, Alderson KL, Attard D, Evans KE, Gatt R, Grima JN, Zied K (2010) Elastic constants of 3-, 4- and 6-connected chiral and anti-chiral honeycombs subject to uniaxial in-plane loading. *Compos Sci Technol* 70(7):1042–1048
16. Javadi AA, Faramarzi A, Farmani R (2012) Design and optimization of the microstructure of auxetic materials. *Eng Comput* 29(3):260–276
17. Assidi M, Ganghoffer JF (2012) Composites with auxetic inclusions showing both an auxetic behavior and enhancement of their mechanical properties. *Compos Struct* 94(8):2373–2382
18. Chen YJ, Scarpa F, Liu YJ, Leng JS (2013) Elasticity of anti-tetrachiral anisotropic lattices. *Int J Solids Struct* 50(6):996–1004
19. Ge Z, Hu H (2013) Innovative three-dimensional fabric structure with negative Poisson's ratio for composite reinforcement. *Text Res J* 83(5):543–550
20. Fanfan Y, Lingling H, Tongxi Y (2013) Effect of cell-wall angle on the in-plane crushing behaviour of hexagonal honeycombs. *Mater Des* 46:511–523. ISSN 0261-3069
21. Carneiro VH, Puga H, Meireles J (2016) Analysis of the geometrical dependence of auxetic behavior in re-entrant structures by finite elements. *Acta Mechanica Sinica* 32(2):295–300
22. Yang L, Harrysson O, West H, Cormier D (2015) Mechanical properties of 3D re-entrant honeycomb auxetic structures realized via additive manufacturing. *Int J Solids Struct* 69:475–490
23. Habib FN, Iovenitti P, Masood SH, Nikzad M (2017) In-plane energy absorption evaluation of 3D printed polymeric honeycombs. *Virtual Phys Prototyp* 12(2):117–131
24. Li X, Lu Z, Yang Z, Yang C (2018) Anisotropic in-plane mechanical behavior of square honeycombs under off-axis loading. *Mater Des* 158:88–97
25. Alomarah A, Masood SH, Sbarski I, Faisal B, Gao Z, Ruan D (2019) Compressive properties of 3D printed auxetic structures: experimental and numerical studies. *Virtual Phys Prototyp* 1–21
26. Qi C, Jiang F, Yu C, Yang S (2019) In-plane crushing response of tetra-chiral honeycombs. *Int J Impact Eng* 130:247–265
27. Gebrehiwot SZ, Leonardo EL, Eickhoff JN et al (2020) The influence of stiffener geometry on flexural properties of 3D printed polylactic acid (PLA) beams. *Prog Addit Manuf.* <https://doi.org/10.1007/s40964-020-00146-2>
28. Fashanu O, Murphy D, Spratt M et al (2020) Effective elastic properties of additively manufactured metallic cellular structures using numerical unit-cell homogenization. *Prog Addit Manuf.* <https://doi.org/10.1007/s40964-020-00141-7>
29. Gibson LJ, Ashby MF (1999) Cellular solids: structure and properties. Cambridge University Press, New York
30. Lorato A, Innocenti P, Scarpa F et al (2010) The transverse elastic properties of chiral honeycombs. *Compos Sci Technol* 70 (7):1057–1063. ISSN 0266-3538
31. Vyavahare S, Kumar S, Panghal D (2020) Experimental study of surface roughness and dimensional accuracy of parts produced by Fused Deposition Modelling. *Rapid Prototyp J.* <https://doi.org/10.1108/RPJ-12-2019-0315>
32. Scarpa F, Blain S, Lew T, Perrott D, Ruzzene M, Yates JR (2007) Elastic buckling of hexagonal chiral cell honeycombs. *Compos A Appl Sci Manuf* 38(2):280–289
33. Xu J, Wu Y, Wang L, Li J, Yang Y, Tian Y, Gong Z, Zhang P, Nutt S, Yin S (2018) Compressive properties of hollow lattice truss reinforced honeycombs (Honeytubes) by additive manufacturing: patterning and tube alignment effects. *Mater Des* 156:446–457

34. Raeisi S, Tapkir P, Ansari F, Tovar A (2019) Design of a hybrid honeycomb unit cell with enhanced in-plane mechanical properties (No. 2019-01-0710). SAE Technical Paper
35. Rao RV (2016) Jaya: a simple and new optimization algorithm for solving constrained and unconstrained optimization problems. *Int J Ind Eng Comput* 7(1):19–34

Experimental Study of Drilling 3D Printed Polylactic Acid (PLA) in FDM Process



Mohammadreza Lalegani Dezaki, M. K. A. Mohd Ariffin ,
and B. T. H. T. Baharuddin

Abstract In the current technology, a 3D printer machine can fabricate and duplicate almost anything. Technology is available for the usage of all-purpose mostly in manufacturing industry. 3D printing or additive manufacturing is a process of making three dimensional solid objects from 3D CAD data. In this research, the effects of drilling parameters on FDM products are investigated. The surface texture of 3D printed samples is examined to find out the effects of build orientation. Average surface roughness (R_a) and average maximum height of the profile (R_z) are investigated to determine the effects of printing and drilling processes. Results show surface roughness becomes worse by increasing build orientation. Therefore, horizontal specimen such as 0° sample has the best surface quality compared to perpendicular ones. Moderate feed rate with the value of 1100 mm/min and 800 rpm to 1000 rpm spindle speed showed the best quality in drilled holes. Besides, the quality of holes in 0° sample has the lowest R_a and R_z value compared to other specimens. Further, build orientation also affects surface quality in the drilling process due to the printing angle. After drilling process, results showed the effect of feed rate and spindle speed are significant.

1 Introduction

Additive manufacturing (AM) is a powerful process to make different products. This process is key to the next industrial revolution due to its features and capabilities. Freeform design, complex structure, fast process, and lower cost are the

M. Lalegani Dezaki · M. K. A. Mohd Ariffin (✉) · B. T. H. T. Baharuddin
Advance Manufacturing Research Group, Department of Mechanical and Manufacturing
Engineering, Universiti Putra Malaysia, 43400 Seri Kembangan, Selangor, Malaysia
e-mail: khairol@upm.edu.my

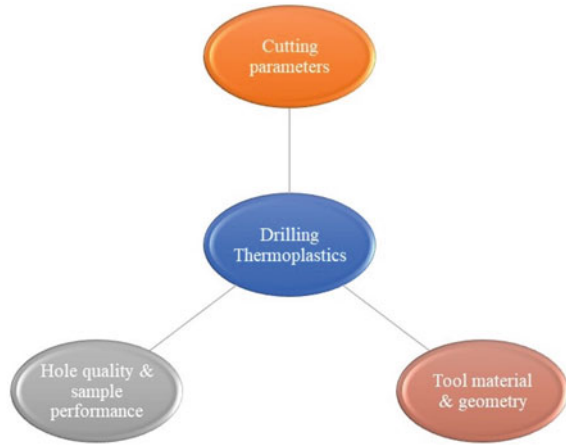
M. Lalegani Dezaki
e-mail: lalegani.mr@gmail.com

B. T. H. T. Baharuddin
e-mail: hangtuah@upm.edu.my

capabilities of AM process [1]. However, issues like poor surface quality, mass production, shrinkage, and warpage have been existed [2]. Customize production is another advantage that machines can build structures in which conventional manufacturing is not possible to make them. Capability to print various materials from polymers to metal alloys and composites let engineers and scientists use AM in different applications, for example, aerospace [3], manufacturing [4], medical [5], and construction [6]. Computer-aided design (CAD) shows although it is possible to design complex product, this is not easy to produce these products with traditional methods such as milling, turning, and drilling. By AM, impossible parts can be produced faster in high volume with high quality. AM also allows reducing part count and replacing complex assemblies with single parts that are lighter [7]. Due to the printing characteristics, AM process is divided into different categories. Binder jetting, directed energy deposition, material extrusion, powder bed fusion, and vat polymerization are the most common AM processes which have been used to fulfill customer's demands [8]. Material can be used in different shapes from liquid, powder, and solid based on process requirements [9, 10]. These processes start to build products layer by layer from bottom to the top. In contrast to subtractive process that removes material to reach the final product, AM builds samples by adding material by following G-codes by reading stereolithography (STL) file and completing the sample layer by layer [11]. AM processes need to build products by using support that can be from the same or different materials. This support structure depends on build orientation which is highly important in these processes [12, 13]. Various factors like layer thickness, temperature, infill pattern, infill percentage, build orientation, and printing speed affect surface quality and mechanical properties [14, 15]. Printing time can be affected by the product's size or process parameters that are mentioned before [16]. One of the common AM processes is fused deposition modelling (FDM) which is used in the majority of desktop 3D printing due to the most accessible process with low cost, feedstock, and simple operating conditions [17]. It involves the extrusion of thermoplastic typically in form of a filament in a layer by layer structure. Parts are built from the bottom-up in a crude way like a glue gun. In this process, there is a nozzle which is dispensing molten thermoplastic onto a build platform. The nozzle has three axis of motion (X, Y, and Z) and by that coordination, curvilinear layers and complex geometries can be built from the bottom-up. In FDM machines, sense of the real-time speed of the print head is touchable and how it needs to stop and start very quickly can be seen clearly. The filament is fed from the cartridges into the build chamber where the extrusion nozzle receives it. Extruder heats the filament and deposit onto the build platform. In addition, some machines have more than one nozzle, one for printing material and another one for support material. Filaments have been existed in different colors and are made of thermoplastics and composite polymers [18]. Thermoplastic materials can be acrylonitrile butadiene styrene (ABS), polylactic acid (PLA), thermoplastic polyolefins (TPO), polycarbonate (PC), polypropylene (PP) which are highly used in FDM process due to their reliable mechanical properties [9]. One of the most common materials in this process is PLA which is a biodegraded thermoplastic material and is made of

renewable resources [19]. Non-toxic material, good for food packaging and medical applications, and recyclable products are the main advantages of PLA products but issues like being brittle, slow decomposition, lower strength compared to ABS material, and shrinkage have existed. Few past decades, researchers have investigated printing PLA material by FDM process to find out optimal printing conditions [20–22]. Similar to other AM processes, various parameters can affect surface accuracy and mechanical characteristics in FDM process. The most critical elements that have an extraordinary impact on parts are nozzle diameter, nozzle temperature, build orientation, layer thickness, and bed temperature. Samples can be hollow or solid by modifying infill density based on needs [23]. The main advantages of FDM is freedom of design which products can be produced in different shapes and geometries with high accuracy. FDM machine does not need any expensive tooling what usually called the AM potential elimination of tooling. Besides, cost of assembly and production can be reduced in this process because material price is cheaper compared to other AM processes like selective laser melting (SLM) [24]. On the other hand, there are obviously some disadvantages in FDM. This process is slow that can penalize production volume. Another drawback is poor surface quality due to layer structure [25]. This issue has a negative effect on mechanical properties and aesthetic features. Alsoufi et al. [26] investigated the infill and build orientation parameters on 3D printed PLA + material to determine the effects of parameters on surface texture. Additionally, Hyndhavi et al. [27] examined build orientation, layer thickness, and raster angle parameters to identify their impacts on the surface. 90° orientation, 200 microns layer thickness, and 0° raster angle showed better quality in ABS material. Pandey et al. [28] investigated the effects of build orientation in FDM process by developing a genetic algorithm. It was founded that build orientation had a great influence on surface quality and mechanical properties and horizontal and vertical angles had better surface quality compared to perpendiculars due to the less support and stable deposition angle [28]. Pre-processing and post-processing are the key elements in FDM process to achieve high quality products [29]. These techniques help to enhance products by eliminating obstacles such as staircase defects, warpage, and shrinkage. Slicing methods [30], process parameters [31], and accuracy prediction [32] are categorized in pre-processing while post-processing techniques are a vast range of processes from machining to chemical processes [33]. These methods have been used to enhance surface texture and quality of products after printing process. As an example, Galantucci et al. [34] used chemical finishing process to enhance surface roughness of ABS products. Although FDM is a capable process to print different features, sometimes printing specific details with tight tolerances is not achievable. High speed machining (HCM) is used as post-processing or secondary process to enhance the product's features [35]. Milling, turning, and drilling are the main processes that are used to improve tolerances and increase the quality of samples. Drilling is a machining process carried out by rotating cutting tool to make circular holes in solid material [36]. This process can be used in dental applications, for example, Ovidiu et al. [37] described a method to drill 3D printed PLA for implants by using cone beam computed tomography (CBCT). A drill bit or twist drill is the

Fig. 1 Aspects of drilling thermoplastics



tool that makes hole in this process and this process is capable to drill blind and through holes. The most common cutting tool in drilling process is twist drill [38]. Various drilling machines can be used to make holes with specific features, for example, portable drilling, bench drilling, radial drilling, and multiple drilling [39]. Parameters are divided into two categories which are machining parameters such as feed rate, spindle speed, and cutting speed and tool parameters like tool geometry, tool material, and tool type. As shown in Fig. 1, these parameters affect hole quality and accuracy. To obtain the optimum quality in drilling operation, selecting proper parameters is necessary to enhance mechanical properties [40, 41]. When quality of the holes is critical, tool geometry plays an important role in drilling process. Besides, tool material is also effective in this process, for example, stainless steel or solid carbide tool can be used to drill thermoplastics.

Thermoplastic machining is a way to eliminate issues in molding and forming process. These issues are high cost, time-consuming process, and sometimes it is not possible to make complex shapes. Machining process can be used to reach high-quality products and close tolerances from plastics to composites and metals [42–44]. There have been developments in CNC machining process itself by increasing axis or jointed-arm robots which leads to higher accuracy and quality [45–47]. For example, Amanullah et al. [48] developed a hybrid machine by a combination of FDM and CNC milling process. Machining or more specifically drilling process, in this case, helps to eliminate these obstacles while there are problems in drilling thermoplastics, for instance, plastics are started to melt during the drilling process due to high temperature, the product may crack because of high tooling pressure [49, 50], and other issues such as non-optimized process parameters or collision due to complex features [51]. Al Quran [52] analyzed drilling effects on teflon material based on thermal conductivity. By increasing the cutting speed, the temperature was increased in a specific zone and 200 m/min cutting speed with pressurized air can be used to drill thermoplastics. In addition, Altan et al. [53] evaluated the effects of drilling process on burr formation in ultra-high molecular weight polyethylene (UHMWPE) material by

using Taguchi method. Less deformation and lower burr were found at 0.025 mm/rev feed rate and 30 m/min cutting speed. In another study, Endo et al. [54] investigated drilling small holes (1 mm) on polyetherimide (PEI) and polyacetal (POM) thermoplastics. Adeniji et al. [55] also investigated the slot milling on polycarbonate (PC) thermoplastic material. They found out tool type and feed rate were the most critical factors while the effects of depth of cut was insignificant. It should be noted many researches have investigated the surface texture and dimensional accuracy of FDM products after using post processing or secondary process [56], for example, Taufik et al. [57] developed CNC-assisted selective melting as a post-processing technique to improve surface roughness. Results showed that there was a major improvement in all samples' surface. In addition, lower build angle showed poor surface quality compared to higher angles while low feed rate was needed to finish the process. Also, Nsengimana et al. [58] investigated the dimensional accuracy of ABS P400 sample by using tumbling, shot peening, hand finishing, spray painting, CNC machining, or chemical treatment. However, post-processing techniques showed enhancement thoroughly, negative deviation range (± 0.1 mm) was found out which was close to the target for CNC machining and this result was due to poor calibration and cutting parameters. Due to the vast range of materials that are used in FDM process, Abdul Shukor et al. [59] applied Taguchi and signal to noise ratio methods to find out the optimum milling process parameters on 3D printed PP material. The results showed 0.599 μm roughness by combining 4138 rpm cutting speed with 1241 mm/min feed rate and 0.5 mm depth of cut. Another study conducted by Pandey et al. [60] to investigate the effects of hot cutter machining on FDM products. Major improvement for surface roughness was recorded with 87% confidence level. In addition, impact of CNC milling machining on 3D printed PLA products was investigated to find out the influence of build orientation on surface roughness in both FDM and CNC machining processes [61]. In this research, 0° build orientation had the best surface quality among samples in printing and machining processes while the perpendicular ones were worst. Also, Dhokia et al. [62] investigated the effects of machining process on 3D printed PP material to find out optimum parameters. Neural networks (NNs) was developed to predict milling operation to examine surface roughness. Based on details, maximum spindle speed, maximum feed rate, and maximum depth of cut were led to higher average surface roughness (R_a). Moreover, Prakasvudhisarn et al. [63] found out the optimal CNC machining process by applying particle swarm optimization (PSO) and support vector machines (SVMs) method. Consistent results were conducted by PSO algorithm for end-mill process which was shown the method was capable to be used for machining process. Tomal et al. [64] examined R_a of 3D printed samples by a combination of abrasive milling machining and FDM process. There was a major improvement by using milling process in all samples and 0.1 mm layer thickness parameter had the best surface quality among samples. As well, Pămărac et al. [65] investigated the influence on end-mill process on 3D printed ABS and PLA materials to find out optimum process parameters.

It should be noted many factors are effective in 3D printing and machining process. Thus, finding proper tooling and optimum process parameter is vital to eliminate issues. Unfortunately, not many researches have been done on drilling 3D

printed thermoplastics. FDM is a capable process to print different features but dimensional accuracy is not as good as machining process to reach tight tolerances. Hence, this article analysed a combination of FDM and drilling process (CNC process) to find out the impacts of drilling parameters on 3D printed PLA samples in perpendicular build orientations. Specifically, this method is helpful for hybrid machining to enhance product quality when it comes to assembly process. Surface roughness measurement such as average surface roughness (R_a) and average maximum height of the profile (R_z) conducted to measure the quality of the holes and find out the optimum drilling parameters.

2 Methodology

This article was a combination of FDM process and drilling process. To conduct this research, samples were printed in different orientations due to its impacts on surface quality and mechanical properties in AM. First of all, a rectangular block was designed in Solidworks[®] to be printed. As shown in Fig. 2, dimensions of the sample were 85 mm length, 85 mm width, and 40 mm height. This sample was used for printing process. The artefacts were printed by FDM machine for further progress which was drilling by CNC machine.

The Ultimaker 2+ machine was used to print samples in various build orientations. First, the design was sliced by Cura[®] software to generate G-codes. Layer by layer behavior in AM process affects surface quality and part's structures. Hence, samples show different qualities when it comes to printing process. Based on past

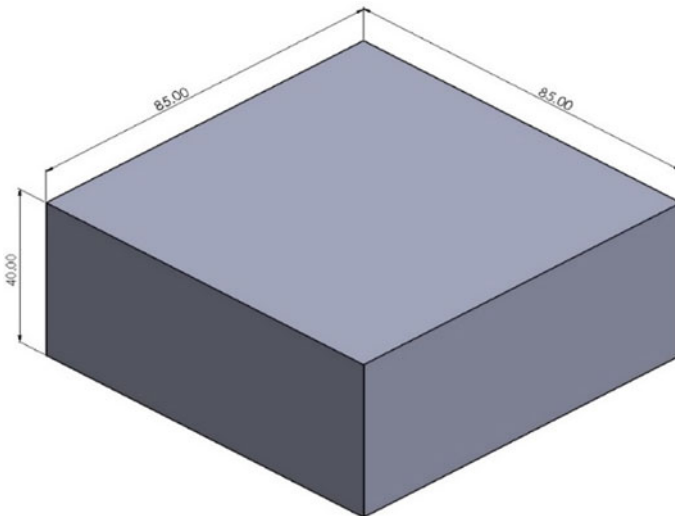


Fig. 2 Schematic of block design

Table 1 Printing parameters for blocks

Samples no.	1	2	3	4
Build orientation (degree)	0	15	45	75
Extruder diameter (mm)	0.4	0.4	0.4	0.4
Filament diameter (mm)	2.85	2.85	2.85	2.85
Filament colour	white	white	white	white
Layer thickness (mm)	0.15	0.15	0.15	0.15
Infill density (%)	100	100	100	100
Infill pattern	Linear	Linear	Linear	Linear
Extruder temp. (°C)	200	200	200	200
Bed temp. (°C)	60	60	60	60
Fan	ON	ON	ON	ON
Weight with support (gram) ±2	352	371.50	392.30	357
Weight without support (gram) ±2	352	352.50	352.80	352

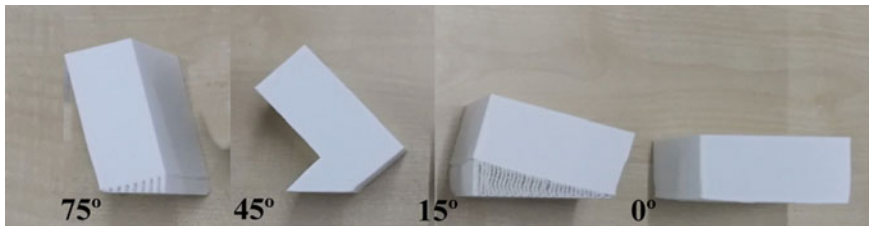


Fig. 3 Printed blocks in three orientations

researches, horizontal and vertical specimens had better surface quality compared to perpendiculars [12, 16, 61]. In this study, four angles were the main elements to find out the best surface quality after drilling holes. Sometimes, printing in these angles are suitable for complex structures and reducing material waste. Meanwhile, white PLA material from PolyLite™ was used and the process parameters were recorded in Table 1. Almost two days were needed to print each sample due to their solid infill and slow process which was one of the drawbacks of FDM process. Specimens were printed in four different angles which were 0°, 15°, 45°, and 75°, as shown in Fig. 3. Default printing settings were chosen due to their stability. After printing process, holes were designed to be machined by CNC.

The following step was to design holes on these cubes for drilling process by Solidworks®. Okuma MX-45VA CNC milling machine was used due to the high accuracy and stability compared to manual millings. 18 holes with 20 mm diameter and 15 mm depth were designed both sides of the samples which were side A and side B (see Fig. 4). Unfortunately, there have not been researchers on drilling 3D printed PLA products; therefore, a barrage range of drilling parameters was chosen to investigate the optimum elements and their effects on holes quality, as shown in

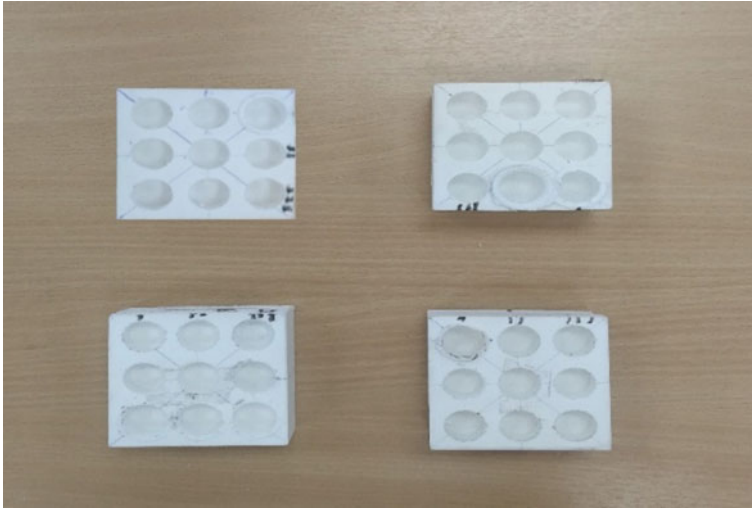


Fig. 4 Drilled PLA samples

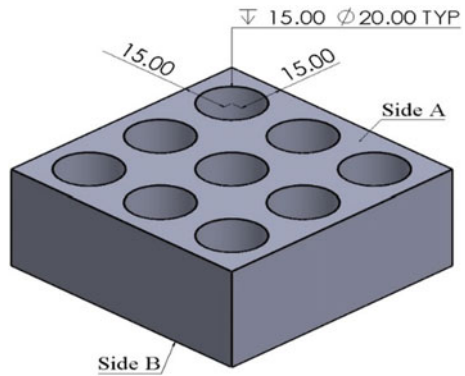
Table 2. Stainless steel twisted drilling tools with 12 mm and 20 mm diameter were used to drill plain holes. The first cutting tool (12 mm \varnothing) was used to avoid cracks in drilling holes due to the large diameter and brittle characteristics of PLA material. Also, pressurized air was used for cooling to avoid material melting. PLA material absorbs moisture and water; thus, fluid cooling may affect surface quality. Mastercam[®] software was used to generate G-codes for drilling. Spindle speed with the value of 600 rpm was constant while feed rate was chosen from a range of 200 mm/min to 1800 mm/min for side A. In addition, spindle speed from 1000 rpm to 3400 rpm with a constant 1000 mm/min feed rate were applied in this research for side B. Holes were numbered from 1 to 18 for surface roughness measurement to determine the effects of drilling parameters on PLA material. Moreover, specimens were drilled by following the drilling parameters step by step and were ready for measurement as shown in Fig. 5.

Surface measurement was conducted to determine the quality and texture of holes. Waviness and profiles were affected due to drilling and printing processes. Layer by layer binding in FDM process and various parameters in machining led to different surface characteristics. Thus, Mahr Perthometer S2 machine was used to measure average surface roughness (R_a) and average maximum height of the profile (R_z) for 3D printed blocks and each hole. The machine was capable to measure point by point so four points inside the holes and on the printed samples' surface were measured and average value of each point was recorded (see Fig. 6a, b). Tracing length (L_t) with 5.6 mm value and 4.0 mm evaluation length (L_n) were chosen to measure specimens with high accuracy. Each point was measured twice to find out accurate results for further progress due to the error that may happen during measurement.

Table 2 Drilling parameters

Side	Hole number	Feed rate (mm/min)	Spindle speed (rpm)
A	1	200	600
	2	400	
	3	600	
	4	800	
	5	1000	
	6	1200	
	7	1400	
	8	1600	
	9	1800	
B	10	550	1000
	11		1300
	12		1600
	13		1900
	14		2200
	15		2500
	16		2800
	17		3100
	18		3400

Fig. 5 Holes' details



3 Results and Discussion

After printing the blocks, their surfaces were measured point by point separately. The value of surface parameters is recorded in Table 3. Each point was measured and Fig. 7 shows the average value of recorded R_a and R_z of five chosen points. The surface texture was smooth if the value of surface parameters was the lowest or vice versa. The main goal was to measure one side of the cube due to the drilling

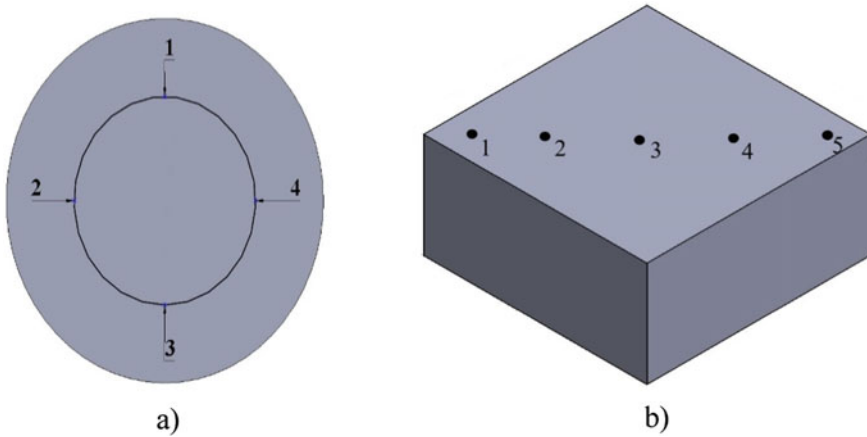


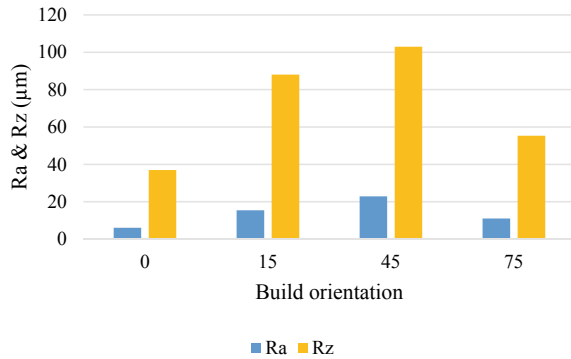
Fig. 6 (a) Points for hole measurement and (b) points for 3D printed samples

process. Data showed by increasing the build orientation, R_a and R_z increased as well. The best surface quality was for 0° with $6.07 \mu\text{m } R_a$ and $36.96 \mu\text{m } R_z$. Layer by layer structure was almost invisible in this sample. In contrast, the value of parameters increased slightly to 45° orientation samples. The worst surface texture was for 45° due to the large value of R_a and R_z . Further, there was a sharp decrease to $11.05 \mu\text{m } R_a$ and $55.34 \mu\text{m } R_z$ for 75° sample. This means by achieving stable printing, the quality of products enhances gradually. 3D printers used support structure to print perpendicular samples. This support affects surface texture and mechanical properties while for printing horizontal and vertical samples, building support is not necessary. Therefore, the quality of 0° products was much better compared to 15° , 45° , and 75° [66].

Table 3 Surface condition for 3D printed blocks

Sample	Profile	R_a (μm)	R_z (μm)	Sample	Profile	R_a (μm)	R_z (μm)
0°	1	6.01	36.5	45°	1	23.13	102
	2	5.58	33.3		2	22.79	101
	3	5.99	38.4		3	20.65	98
	4	5.95	32.9		4	23.63	105
	5	6.83	43.7		5	24.08	109
	Average	6.07	36.96		Average	22.86	103
15°	1	13.59	81.8	75°	1	11.91	53.8
	2	15.37	81.7		2	11.68	52.7
	3	14.58	87.5		3	11.42	53.3
	4	15.11	90.3		4	10.79	48.9
	5	18.48	98.8		5	9.45	68
	Average	15.43	88.02		Average	11.05	55.34

Fig. 7 R_a and R_z value for 3D printed blocks



Surface measurement was done on all specimens and R_a and R_z value were recorded to examine the drilling process on PLA thermoplastic. The main issue in drilling 3D printed plastic is to avoid cracks and fatigue during the process. It may happen due to the poor adhesion between layers and by pressing the cutting tool on the sample, the part is cracked easily. Hence, a 12 mm tool was chosen to drill holes one by one to reduce the pressure due to the large diameter. After drilling the samples, the R_a and R_z values for each hole based on chosen points for side A are recorded in Table 4 and Table 5. The data is scattered for 4 points for each hole to examine each side. The minimum value of R_a belonged to 0° sample for hole number 6 which was $8.48 \mu\text{m}$. In contrast, hole 3 in the sample with 15° build orientation had the largest value of R_a and R_z ($19.15 \mu\text{m}$ and $89.68 \mu\text{m}$). As shown in these Tables, the average values of R_a and R_z are fluctuating in a wide range in different build orientations. Due to the poor feed rate or spindle speed, the surface integrity of some holes was not uniform based on variance and standard deviation such as hole 8 at 45° sample. This issue happened due to the small melted material that stucked to the cutting tool because of the poor feed rate. Hence, after drilling one hole, process was stopped to remove the material from the cutting tool. Also, differences were observed inside the holes while the feed rate was lowest or highest. Based on data, by increasing the build orientation, the value of R_a and R_z increased as well. This means build orientation plays an important role in drilling process due to the layer binding and the angle of material deposition. Therefore, the horizontal sample had the best surface quality in all holes for side A compared to perpendicular ones. Moreover, the results showed by increasing the feed rate, the surface quality decreased but at the highest feed rate which was 1800 mm/min, the quality of texture was getting worse. Beside of drilling parameters, many factors affected the quality such as cooling system. As far as PLA absorbs moisture from liquid, it was not possible to use fluid cooling in drilling process. In this case, 15° had the worst quality in the majority of holes from number 1 to 9 except hole 7 and 9.

To attain a better understanding of drilling parameters MATLAB was used to plot 2D and 3D graphs to show the results better. As shown in Figs. 8 and 9 the differences between each sample and hole are visible clearly. 1400 mm/min and

Table 4 The value of R_a for holes on side A

Hole number	Build orientation (°)	R_a (µm)				Average	Std dev.	Variance
		1	2	3	4			
1	0	9.50	10.80	11.60	10.50	10.60	0.75	0.57
	15	15.50	13.70	16.30	12.80	14.58	1.39	1.94
	45	14.80	18.50	18.80	10.90	15.75	3.21	10.32
	75	16.40	11.20	12.30	14.14	13.51	1.97	3.89
2	0	10.80	11.80	11.50	11.70	11.45	0.39	0.15
	15	15.30	16.70	13.80	18.30	16.03	1.67	2.78
	45	15.30	10.90	12.20	9.90	12.08	2.03	4.13
	75	14.43	10.76	10.82	11.50	11.88	1.50	2.26
3	0	13.30	11.60	14.20	10.30	12.35	1.51	2.27
	15	23.20	21.50	15.10	16.80	19.15	3.31	10.96
	45	13.10	16.60	15.70	12.90	14.58	1.61	2.59
	75	13.00	13.40	14.15	13.70	13.56	0.42	0.18
4	0	10.20	8.50	9.70	8.70	9.28	0.70	0.49
	15	18.90	14.70	17.80	11.70	15.78	2.81	7.91
	45	11.00	7.60	8.40	14.90	10.48	2.85	8.11
	75	8.40	10.60	7.80	11.30	9.53	1.46	2.14
5	0	9.50	10.40	8.90	11.30	10.03	0.91	0.83
	15	19.90	20.80	12.40	11.90	16.25	4.12	16.94
	45	14.20	13.80	13.60	14.90	14.13	0.50	0.25
	75	10.30	9.80	12.20	12.10	11.10	1.07	1.14
6	0	8.70	8.10	7.60	9.50	8.48	0.71	0.50
	15	12.60	18.50	19.40	14.10	16.15	2.87	8.22
	45	6.70	8.90	11.70	13.40	10.18	2.57	6.61
	75	9.60	9.80	8.10	9.30	9.20	0.66	0.44
7	0	14.30	15.20	13.80	15.10	14.60	0.58	0.33
	15	17.30	17.20	14.80	15.50	16.20	1.08	1.17
	45	18.10	14.10	12.80	17.00	15.50	2.14	4.57
	75	23.70	13.50	17.40	14.50	17.28	3.98	15.81
8	0	12.80	13.10	10.60	11.20	11.93	1.05	1.11
	15	16.20	14.60	17.30	16.80	16.23	1.02	1.03
	45	13.00	11.50	21.10	18.90	16.13	3.99	15.90
	75	17.70	10.80	12.60	13.57	13.67	2.53	6.41
9	0	13.40	14.60	12.30	11.90	13.05	1.05	1.10
	15	13.90	14.80	15.00	16.26	14.99	0.84	0.71
	45	12.40	13.60	13.50	19.60	14.78	2.83	7.98
	75	13.90	14.40	17.90	16.30	15.63	1.59	2.53

Table 5 The value of R_z for holes on side A

Hole number	Build orientation (°)	R_z (µm)				Average	Std dev.	Variance
		1	2	3	4			
1	0	60.20	53.60	50.70	55.30	54.95	3.45	11.89
	15	71.20	81.80	73.70	66.70	73.35	5.49	30.09
	45	80.30	92.20	93.20	75.30	85.25	7.67	58.75
	75	78.50	67.10	72.30	78.50	74.10	4.77	22.74
2	0	58.60	63.00	55.10	59.20	58.98	2.80	7.85
	15	71.10	75.10	68.60	86.20	75.25	6.73	45.34
	45	79.00	56.20	60.70	56.70	63.15	9.32	86.78
	75	72.00	54.30	56.80	63.20	61.58	6.84	46.76
3	0	65.30	58.00	77.30	53.40	63.50	9.03	81.48
	15	113.00	101.00	65.90	78.80	89.68	18.41	338.96
	45	61.60	77.90	73.40	63.50	69.10	6.77	45.89
	75	62.80	88.80	60.10	59.50	67.80	12.19	148.55
4	0	51.20	42.60	47.20	39.80	45.20	4.36	18.98
	15	97.70	74.80	91.00	61.40	81.23	14.15	200.32
	45	52.90	44.40	46.10	65.90	52.33	8.46	71.54
	75	43.60	51.20	40.30	58.50	48.40	7.04	49.62
5	0	48.30	53.60	45.20	56.50	50.90	4.41	19.48
	15	83.50	64.90	89.50	69.60	76.88	10.00	99.90
	45	67.50	82.10	73.40	74.50	74.38	5.19	26.98
	75	67.40	45.90	62.50	66.40	60.55	8.65	74.89
6	0	40.30	38.60	36.20	42.00	39.28	2.14	4.60
	15	54.00	80.90	81.00	71.70	71.90	11.00	121.07
	45	40.10	47.30	63.30	62.10	53.20	9.84	96.91
	75	45.00	42.30	38.60	53.10	44.75	5.33	28.40
7	0	69.80	74.50	60.20	73.20	69.43	5.60	31.31
	15	77.90	83.30	72.00	72.80	76.50	4.53	20.54
	45	108.00	74.50	58.10	99.10	84.93	19.76	390.41
	75	103.00	93.80	68.50	67.20	83.13	15.62	244.12
8	0	65.20	66.90	56.50	58.60	61.80	4.36	18.98
	15	77.50	88.50	64.00	86.50	79.13	9.67	93.42
	45	67.40	58.20	99.00	79.20	75.95	15.25	232.51
	75	85.00	60.60	80.00	51.20	69.20	13.82	191.06
9	0	68.30	74.00	65.30	58.30	66.48	5.66	32.04
	15	73.20	66.50	70.10	85.60	73.85	7.19	51.64
	45	57.50	64.00	67.10	84.70	68.33	10.07	101.38
	75	73.30	73.30	85.50	81.20	78.33	5.25	27.56

1800 mm/min feed rate showed the highest value of surface parameters compared to other values. Results showed the quality of holes was lowest while the feed rate exceeded 1400 mm/min. Furthermore, feed rate values that are less than 800 mm/min were also achieved poor surface quality. On the other hand, feed rate between 800 mm/min and 1200 mm/min showed uniform surface texture while the best quality was achieved at 1200 mm/min feed rate with 600 rpm constant spindle speed. Also, there was a major improvement in drilling for all samples in surface

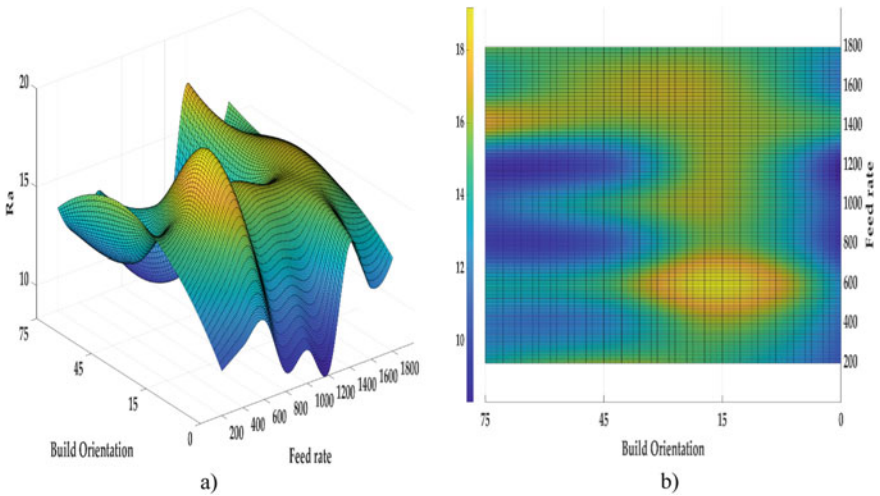


Fig. 8 The average value of R_a for side A in (a) 3D schematic and (b) 2D schematic design

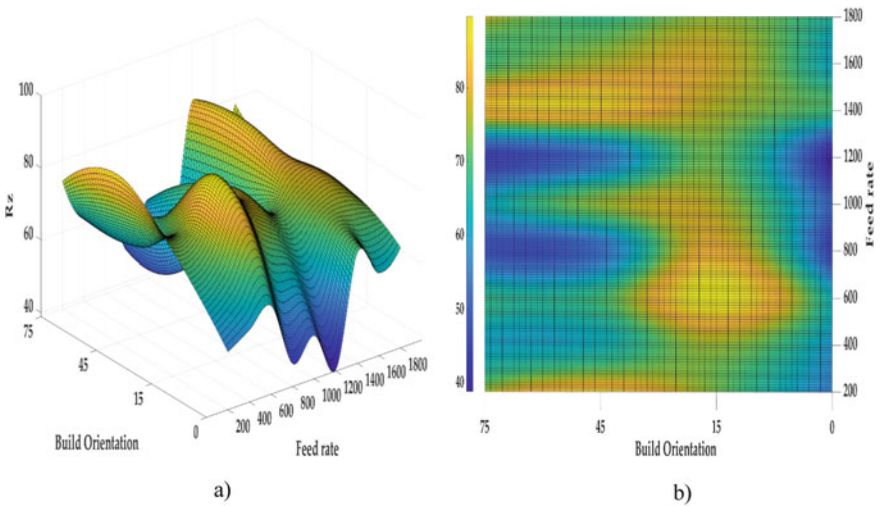


Fig. 9 The average value of R_z for side A in (a) 3D schematic and (b) 2D schematic design

quality except 0° because the quality of printed and drilled samples was almost the same. However, increasing surface quality in drilling and machining can be achievable if smooth machining was used. In brief, a moderate feed rate is recommended to have the best surface quality. Besides, choosing proper spindle speed is also necessary to achieve the highest quality without defects and errors. Meanwhile, the spindle speed was also examined in side B to find out the effects and issues for further progress.

In order to find out drilling parameters, Table 2 is described in methodology section. Moreover, the influence of spindle speed should be analysed to find out at what range the drilling process is optimum. A barrage range of data was recorded for side B as well to determine the characteristics of each hole after drilling. Tables 6 and 7 show the average, standard deviation, and the variance of R_a and R_z for each hole. The minimum R_a and R_z values were for hole number 10 in 0° sample with 7.03 μm and 38.85 μm . In contrast, hole number 17 in 15° sample had a maximum value of 16.40 μm R_a and 86.30 μm R_z , respectively. It followed the same direction as feed rate followed which was by increasing the spindle speed, the quality of holes became worse. Also, variance and standard deviation showed quality of some holes is not consistent due to the poor spindle speed value. In

Table 6 The value of R_a for holes on side B

Hole number	Build orientation (°)	R_a (μm)				Average	Std dev.	Variance
		1	2	3	4			
10	0	7.50	6.30	6.80	7.50	7.03	0.51	0.26
	15	9.01	8.30	11.20	8.70	9.30	1.12	1.26
	45	9.12	9.16	8.02	8.96	8.82	0.47	0.22
	75	8.76	8.90	8.55	10.92	9.28	0.95	0.91
11	0	8.33	7.87	7.05	8.60	7.96	0.59	0.35
	15	12.82	10.51	11.18	13.61	12.03	1.24	1.54
	45	16.44	10.96	9.65	14.90	12.99	2.78	7.71
	75	8.84	9.52	8.24	8.47	8.77	0.48	0.23
12	0	9.77	8.90	9.52	10.01	9.55	0.41	0.17
	15	17.32	10.29	8.61	11.98	12.05	3.27	10.68
	45	8.52	10.59	9.51	14.54	10.79	2.29	5.22
	75	11.75	9.94	8.30	10.12	10.03	1.22	1.49
13	0	12.50	13.20	11.90	12.12	12.43	0.49	0.24
	15	16.93	12.30	10.80	16.39	14.11	2.62	6.85
	45	10.12	12.97	13.12	17.19	13.35	2.52	6.34
	75	18.54	14.43	9.51	9.76	13.06	3.72	13.85
14	0	8.06	9.20	7.88	8.50	8.41	0.51	0.26
	15	9.18	9.30	8.70	8.37	8.89	0.37	0.14
	45	9.76	6.36	7.20	13.60	9.23	2.82	7.93
	75	10.55	9.36	10.87	8.57	9.84	0.92	0.85

(continued)

Table 6 (continued)

Hole number	Build orientation (°)	R _a (μm)				Average	Std dev.	Variance
		1	2	3	4			
15	0	10.50	11.60	10.87	11.80	11.19	0.53	0.28
	15	14.36	15.21	11.84	16.62	14.51	1.74	3.02
	45	12.80	11.69	13.30	10.50	12.07	1.08	1.16
	75	17.06	9.80	17.60	13.24	14.43	3.16	9.95
16	0	11.80	11.66	12.06	12.88	12.10	0.47	0.22
	15	14.65	17.59	13.81	10.39	14.11	2.57	6.58
	45	13.94	10.83	15.34	14.58	13.67	1.71	2.94
	75	16.23	10.18	10.46	14.48	12.84	2.59	6.73
17	0	13.80	14.33	13.60	14.23	13.99	0.30	0.09
	15	17.39	17.81	17.68	12.72	16.40	2.13	4.54
	45	8.17	17.50	18.31	15.40	14.85	4.00	15.98
	75	12.26	16.44	15.07	16.14	14.98	1.65	2.72
18	0	12.30	11.20	12.80	11.89	12.05	0.59	0.34
	15	10.43	9.98	14.82	10.41	11.41	1.98	3.91
	45	13.50	14.58	16.96	18.10	15.79	1.83	3.35
	75	17.32	11.70	14.76	15.29	14.77	2.01	4.05

Table 7 The value of R_z for holes on side B

Hole number	Build orientation (°)	R _z (μm)				Average	Std dev.	Variance
		1	2	3	4			
10	0	41.20	37.50	35.90	40.80	38.85	2.23	4.96
	15	49.30	41.60	56.30	45.20	48.10	5.46	29.84
	45	46.30	48.50	42.20	46.60	45.90	2.30	5.28
	75	50.70	51.30	42.55	75.90	55.11	12.49	155.99
11	0	43.50	40.80	40.20	44.20	42.18	1.71	2.91
	15	64.20	79.90	52.70	77.10	68.48	10.86	118.01
	45	71.30	48.60	44.50	79.00	60.85	14.63	214.00
	75	49.80	51.70	42.60	45.10	47.30	3.62	13.14
12	0	48.90	46.20	46.00	50.10	47.80	1.75	3.08
	15	77.40	55.20	49.10	65.30	61.75	10.73	115.11
	45	53.20	54.40	43.60	85.50	59.18	15.76	248.52
	75	57.60	52.60	48.90	55.70	53.70	3.30	10.87
13	0	52.30	59.80	48.60	51.90	53.15	4.10	16.80
	15	100.00	50.30	39.20	79.40	67.23	23.95	573.57
	45	54.40	64.90	60.50	84.00	65.95	11.07	122.50
	75	91.20	65.30	40.20	63.50	65.05	18.05	325.95

(continued)

Table 7 (continued)

Hole number	Build orientation (°)	R _z (µm)				Average	Std dev.	Variance
		1	2	3	4			
14	0	39.80	43.50	35.60	41.80	40.18	2.95	8.69
	15	44.00	48.20	41.80	39.70	43.43	3.15	9.91
	45	49.70	33.40	45.70	74.70	50.88	15.01	225.29
	75	53.60	50.10	55.60	46.50	51.45	3.47	12.04
15	0	51.20	56.60	53.60	55.80	54.30	2.10	4.41
	15	69.30	83.00	58.50	93.80	76.15	13.39	179.22
	45	58.80	54.90	65.90	47.70	56.83	6.58	43.31
	75	68.40	46.90	88.50	71.60	68.85	14.80	218.92
16	0	55.80	56.70	59.80	59.30	57.90	1.69	2.86
	15	70.20	93.60	66.60	47.90	69.58	16.25	264.06
	45	103.00	61.70	74.80	66.60	76.53	15.99	255.55
	75	74.20	53.50	56.60	72.70	64.25	9.28	86.12
17	0	65.10	68.20	65.90	68.00	66.80	1.33	1.78
	15	92.30	102.00	82.10	68.80	86.30	12.31	151.60
	45	68.30	79.30	89.50	89.90	81.75	8.85	78.35
	75	75.30	84.90	80.20	73.90	78.58	4.34	18.81
18	0	70.10	64.30	72.40	67.50	68.58	3.02	9.10
	15	66.10	68.70	74.70	10.41	54.98	25.92	671.81
	45	68.50	71.60	93.50	93.30	81.73	11.73	137.51
	75	81.00	59.40	67.20	84.60	73.05	10.21	104.29

addition, this issue affected the drilling process by melting the material as shown in Fig. 10. Undoubtedly, melted material affected surface texture. However, when the spindle speed was in optimum range the holes' quality was consistent without defects. Further, by increasing the build orientation, the surface smoothness became poorer as well. It means holes in 0° sample had the best surface texture.

As shown in Figs. 11 and 12, 2200 rpm and slower spindle speed show lower R_a and R_z values compared to the faster one. The differences between 1000 rpm and 2200 rpm were insignificant except for sample 15° which the hole quality increased by 4%. Figures show lowest R_a and R_z values belong to hole 10 for all samples with the range from 7.03 µm to 9.30 µm for R_a and 38.85 µm to 55.11 µm for R_z. Therefore, the values were fluctuated before 2500 rpm but at 1000 spindle speed and 1000 mm/min feed rate showed the best quality in all build orientations. Also, holes had good quality at 2200 rpm spindle speed while at 3100 rpm spindle speed, the worst surface quality was observed and the largest surface parameters were recorded for both R_a and R_z. As shown in Table 6, by increasing the spindle speed to 3100 rpm, the value of R_a increases by 40% for all samples. Surprisingly, there was no effect of layer structure inside the holes while inside the poor-quality holes, there were small shattered materials that stucked to the holes' walls. This defect

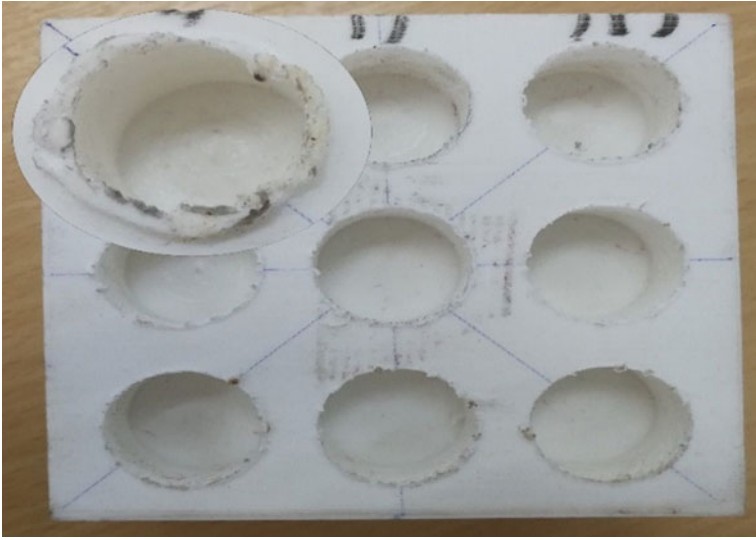


Fig. 10 Melted hole due to the poor feed rate or spindle speed

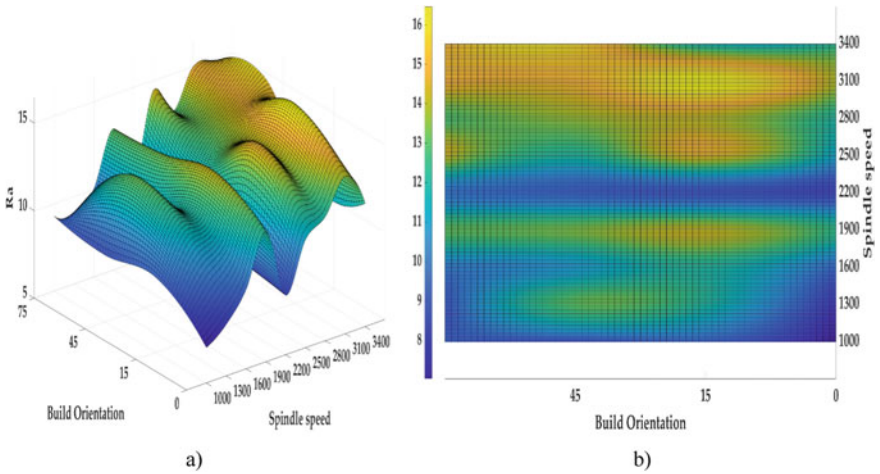


Fig. 11 The average value of R_a for side B in (a) 3D schematic and (b) 2D schematic design

happened because of non-optimised spindle speed or feed rate. The results showed the quality of holes in side B was better compared to side A. In brief, an increase in spindle speed leads to poorer surface for holes with 20 mm diameter.

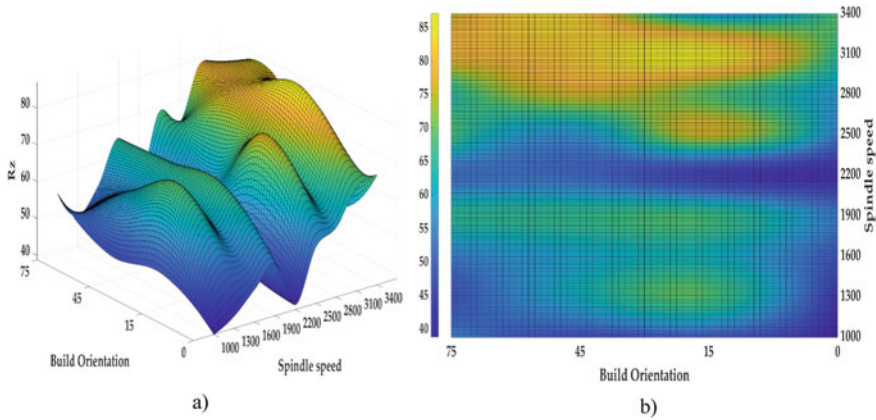


Fig. 12 The average value of Rz for side B in (a) 3D schematic and (b) 2D schematic design

4 Conclusion

FDM is capable to print complex structure in proper time without sacrificing material properties. However, printing metal alloys and materials which have a high melting temperature is not possible due to the process limitation. Also, the surface quality of final products in FDM is not as good as other AM processes such as SLM. Hence, by using machining processes as a secondary or a post-processing technique, improving surface texture is possible. Also, this research is helpful for hybrid machining (HM) due to the combination of machining and AM. In this study, the drilling effects on 3D printed PLA products were investigated to examine the surface texture after and before drilling process. A summary of the results is listed as follows.

- The 0° build orientation sample had the best surface condition among printed samples.
- Ra and Rz increased by increasing in build orientation and they decreased by reaching to 90°.
- The effects of spindle speed and feed rate were significant in drilling process.
- Low spindle speed (between 700 rpm and 1000 rpm) was the optimum range of drilling holes with 20 mm diameter.
- By increasing the spindle speed (more than 3000 rpm), the surface condition became the worst.
- Moderate feed rate which was 1100 mm/min showed the lowest Ra and Rz in the range of 7.03 μm–9.30 μm.
- Low feed rate and high feed rate showed poor surface quality in all samples.
- Same to the printing process, holes in the 0° sample had the best surface quality.

References

1. Gebhardt A, Hötter J-S, (2016) 4—Rapid prototyping, in additive manufacturing. In Gebhardt A, Hötter J-S (eds). Hanser. pp 291–352
2. Ngo TD, Kashani A, Imbalzano G, Nguyen KT, Hui DJCPBE (2018) Additive manufacturing (3D printing): A review of materials, methods, applications and challenges 143:172–196
3. Kobryn P, Ontko N, Perkins L, Tiley J (2006) Additive manufacturing of aerospace alloys for aircraft structures. Air Force Research Lab Wright-Patterson AFB OH Materials and Manufacturing
4. Kruth J-P, Leu M-C, Nakagawa TJCA (1998) Progress in additive manufacturing and rapid prototyping. CIRP Ann-Manuf Technol 47(2):525–540
5. Yan Q, Dong H, Su J, Han J, Song B, Wei Q, Shi Y (2018) A review of 3D printing technology for medical applications. Engineering 4(5):729–742
6. Ghaffar SH, Corker J, Fan MJAIC (2018) Additive manufacturing technology and its implementation in construction as an eco-innovative solution 93:1–11
7. Cuellar JS, Smit G, Plettenburg D, Zadpoor A (2018) Additive manufacturing of non-assembly mechanisms. Addit Manuf 21:150–158
8. Gibson I, Rosen DW, Stucker B (2014) Additive manufacturing technologies, vol 17. Springer
9. Bourell D, Kruth JP, Leu M, Levy G, Rosen D, Beese AM, Clare AJCA (2017) Materials for additive manufacturing. CIRP Annals 66(2):659–681
10. Frazier WE (2014) Metal Additive Manufacturing: A Review. J Mater Eng Perform 23 (6):1917–1928
11. Wong KV, Hernandez A (2012) A review of additive manufacturing. ISRN Mech Eng 2012:208760
12. Taufik M, Jain PK (2013) Role of build orientation in layered manufacturing: a review. Int J Manuf Technol Manage 27(1–3):47–73
13. Pérez CJL (2002) Analysis of the surface roughness and dimensional accuracy capability of fused deposition modelling processes. Int J Prod Res 40(12):2865–2881
14. Calignano F, Manfredi D, Ambrosio EP, Biamino S, Lombardi M, Atzeni E, Salmi A, Minetola P, Iuliano L, Fino P (2017) Overview on Additive Manufacturing Technologies. Proc IEEE 105(4):593–612
15. Lecký Š, Václav S, Michal D, Hrušecký R, Košťál P, Molnár I (2019) Assembly Tool Manufacturing and Optimization for Poly(lactic acid) Additive Manufacturing. Mater Sci Forum 952:153–162
16. Salmi M, Ituarte IF, Chekurov S, Huotilainen E (2016) Effect of build orientation in 3D printing production for material extrusion, material jetting, binder jetting, sheet object lamination, vat photopolymerisation, and powder bed fusion. Int J Collab Enterp 5(3–4): 218–231
17. Nováková-Marcin inová U, Kurj I (2012) Basic and advanced materials for fused deposition modeling rapid prototyping technology
18. Li N, Huang S, Zhang G, Qin R, Liu W, Xiong H, Shi G, Blackburn J (2019) Progress in additive manufacturing on new materials: A review. J Mater Sci Technol 35(2):242–269
19. Pang X, Zhuang Z, Fau X, Tang X, Tang Z, Fau-Chen, and Chen X Poly(lactic acid) (PLA): research, development and industrialization. (1860-7314 (Electronic))
20. Zhou X, Hsieh S-J, Sun Y (2017) Experimental and numerical investigation of the thermal behaviour of poly(lactic acid) during the fused deposition process. Virtual Phys Prototyp 12 (3):221–233
21. Sukindar NA, Baharuddin B, Jaafar CNA, Ismail MIS, Ariffin M, Anwar MK (2016) Analyzing the effect of nozzle diameter in fused deposition modeling for extruding poly(lactic acid) using open source 3D printing

22. Afrose MF, Masood SH, Iovenitti P, Nikzad M, Sbarski I (2016) Effects of part build orientations on fatigue behaviour of FDM-processed PLA material. *Prog Addit Manuf* 1(1):21–28
23. Alafaghani AA, Qattawi A (2018) Investigating the effect of fused deposition modeling processing parameters using Taguchi design of experiment method vol 36, 164–174
24. Olakanmi EO, Cochrane R, Dalgarno K (2015) A review on selective laser sintering/melting (SLS/SLM) of aluminium alloy powders: Processing, microstructure, and properties. *Prog Mater Sci* 74:401–477
25. Reddy V, Flys O, Chaparala A, Berrimi CE, Amogh V, Rosen BG (2018) Study on surface texture of Fused Deposition Modeling. *Procedia Manuf* 25:389–396
26. Alsoufi MS, Elsayed AE (2017) How surface roughness performance of printed parts manufactured by desktop FDM 3D printer with PLA + is influenced by measuring direction. *Am J Mech Eng* 5(5):211–222
27. Hyndhavi D, Babu GR, Murthy SB (2018) Investigation of Dimensional Accuracy and Material Performance in Fused Deposition Modeling. *Mater Today: Proc* 5(11):23508–23517
28. Pandey PM, Thrimurthulu K, Reddy NV, Optimal part deposition orientation in FDM by using a multicriteria genetic algorithm. *Int J Prod Res* 42(19):4069–4089
29. Chohan JS, Singh R (2017) Pre and post processing techniques to improve surface characteristics of FDM parts: a state of art review and future applications. *Rapid Prototyp J* 23(3):495–513
30. Ariffin, MM, Sukindar N, Baharudin BH, Jaafar C, Ismail M (2018) Slicer method comparison using Open-source 3D printer. In: *IOP Conference Series: Earth and Environmental Science*. IOP Publishing
31. Mohamed OA, Masood SH, Bhowmik JLJAiM (2015) Optimization of fused deposition modeling process parameters: a review of current research and future prospects 3(1):42–53
32. Boschetto A, Bottini (2014) Accuracy prediction in fused deposition modeling 73(5–8):913–928
33. Vyavahare S, Teraiya S, Panghal D, Kumar S (2020) Fused deposition modelling: a review. *Rapid Prototyp J* 26(1):176–201
34. Galantucci LM, Lavecchia F, Percoco G (2009) Experimental study aiming to enhance the surface finish of fused deposition modeled parts. *CIRP Ann* 58(1):189–192
35. Hällgren S, Pejryd L, Ekengren J (2016) Additive Manufacturing and High Speed Machining-Cost comparison of short lead time manufacturing methods. *Procedia CIRP* 50:384–389
36. Subramanian J, Baskar N, Ganesan M, Padmanaban MRA, Hariharan B, Arunagirinathan R, Kavin P, Hariharan S (2018) Study on Drilling Process Parameters—Review. *Int J Eng Res Technol* 6
37. Ovidiu D, Szuhaneck C, Tuce R, David A, Leretter M (2017) Polylactic Acid 3D Printed Drill Guide for Dental Implants Using CBCT. *Rev Chim-Buchar-Orig Ed* - 68:341–342
38. Talapatra S, Islam I (2016) Optimization of grinding parameters for minimum surface roughness using Taguchi method. In: *International Conference on Emerging Trends in Engineering & Management*
39. Jayendran A (1994) Drills and drilling machines. In: Jayendran A (ed) *Englisch für Maschinenbauer*. Vieweg + Teubner Verlag, Wiesbaden, pp 81–87
40. Kalpakjian S, Schmid SR, Sekar KSV (2016) Manufacturing engineering and technology
41. Raju KVMK, Janardhana GR, Kumar PN, Rao VDP (2011) Optimization of cutting conditions for surface roughness in CNC end milling. *Int J Precis Eng Manuf* 12(3):383–391
42. Peng T, Xu X (2014) Energy-efficient machining systems: a critical review. *Int J Adv Manuf Technol* 72(9–12):1389–1406
43. Alexander I, Vladimir G, Petr P, Mihail K, Yuriy I, Andrey V (2016) Machining of thin-walled parts produced by additive manufacturing technologies. *Procedia CIRP* 41:1023–1026
44. Caggiano A (2018) Machining of fibre reinforced plastic composite materials. *Materials* 11(3):442

45. Popan A, Bâlc N, Luca B, Popan A, Carean A (2015). The Accuracy of the Plastic Parts Milling Process Executed by a Six Axes Robot. In: *Applied Mechanics and Materials*. Trans Tech Publ
46. Jun C-S, Cha K, Lee Y-S (2003) Optimizing tool orientations for 5-axis machining by configuration-space search method. *Comput Aided Des* 35(6):549–566
47. Lee W-C, Wei C-C, Chung S-C (2014) Development of a hybrid rapid prototyping system using low-cost fused deposition modeling and five-axis machining. *J Mater Process Technol* 214(11):2366–2374
48. Amanullah ANM, Saleh T, Khan R (2017) Design and development of a hybrid machine combining rapid prototyping and CNC milling operation. *Procedia Engineering* 184:163–170
49. Alauddin M, Choudhury I, El Baradie M, Hashmi M (1995) Plastics and their machining: a review. *J Mater Process Technol* 54(1–4):40–46
50. Maxwell AS, Turnbull A (2003) Measurement of residual stress in engineering plastics using the hole-drilling technique. *Polym Testing* 22(2):231–233
51. Hatna A, Grieve RJ, Broomhead P (1998) Automatic CNC milling of pockets: geometric and technological issues. *Comput Integr Manuf Syst* 11(4):309–330
52. Al Quran FM (2007) Machining accuracy and stability during drilling of thermoplastics. *J. Appl. Sci* 7:141–144
53. Altan M, Altan E (2014) Investigation of burr formation and surface roughness in drilling engineering plastics. *J Braz Soc Mech Sci Eng* 36(2):347–354
54. Endo H, Marui E (2006) Small-hole drilling in engineering plastics sheet and its accuracy estimation. *Int J Mach Tools Manuf* 46(6):575–579
55. Adeniji D, Schoop J, Gunawardena S, Hanson C, Jahan M (2020) Characterization and Modeling of Surface Roughness and Burr Formation in Slot Milling of Polycarbonate. *J Manuf Mater Process* 4:59
56. Kumbhar NN, Mulay AV (2018) Post Processing Methods used to Improve Surface Finish of Products which are Manufactured by Additive Manufacturing Technologies: A Review. *J Inst Eng (India): Ser C* 99(4):481–487
57. Taufik M, Jain PK (2016) CNC-assisted selective melting for improved surface finish of FDM parts. *Virtual Phys Prototyp* 11(4):319–341
58. Nsengimana J, Van der Walt J, Pei E, Miah M (2019) Effect of post-processing on the dimensional accuracy of small plastic additive manufactured parts. *Rapid Prototyp J* 25(1):1–12
59. Abdul Shukor J, Said S, Harun R, Husin S, Kadir A (2016) Optimising of machining parameters of plastic material using Taguchi method. *Adv Mater Process Technol* 2(1):50–56
60. Pandey PM, Reddy NV, Dhande SG (2003) Improvement of surface finish by staircase machining in fused deposition modeling. *J Mater Process Technol* 132(1–3):323–331
61. Lalegani Dezaki M, Mohd Ariffin MKA, Ismail MIS (2020) Effects of CNC machining on surface roughness in fused deposition modelling (FDM) products. *Materials* 13(11):2608
62. Dhokia V, Kumar S, Vichare P, Newman S, Allen R (2008) Surface roughness prediction model for CNC machining of polypropylene. *Proc Inst Mech Eng, Part B: J Eng Manuf* 222(2):137–157
63. Prakashvudhisarn C, Kunnapadeelert S, Yenradee P (2009) Optimal cutting condition determination for desired surface roughness in end milling. *Int J Adv Manuf Technol* 41(5–6):440
64. Tomal ANMA, Saleh Ceng MimechE T, Khan MR (2018) Combination of fused deposition modelling with abrasive milling for attaining higher dimensional accuracy and better surface finish. *IIUM Engineering J* 19:221–231
65. Pămărac R, Petrușe R (2018) Study Regarding the Optimal Milling Parameters for Finishing 3D Printed Parts from ABS and PLA Materials. *ACTA Universitatis Cibiniensis* 70:66–72
66. Buj-Corral I, Domínguez-Fernández A, Durán-Llucià R (2019) Influence of print orientation on surface roughness in fused deposition modeling (FDM) processes. *Materials* 12(23):3834

Mechanical Properties of 3D-Printed Elastomers Produced by Fused Deposition Modeling



A. Alperen Bakır , Roozbeh Neshani , and Sezer Özerinç 

Abstract Recent advances in the development of elastomeric thermoplastic filaments have enabled the production of elastomeric components using fused deposition modeling. The unique mechanical properties of elastomers and the vast design space of additive manufacturing provide new opportunities to develop structural parts with tailored mechanical behavior. Understanding the mechanical behavior of FDM-produced elastomers is an essential part of realizing these opportunities and ensuring the reliable operation of printed parts in service. This chapter presents an overview of the current knowledge about the mechanical behavior of FDM-produced elastomers. The chapter first presents some introductory information about FDM and the mechanical behavior of elastomers. The subsequent discussion presents the effects of the primary process parameters, namely, nozzle temperature, raster orientation, build orientation, and infill ratio on the mechanical properties. Finally, recent findings on elastomeric composites and cellular structures are discussed, and future research directions are proposed.

A. A. Bakır

Department of Mechanical, Materials and Manufacturing Engineering,
University of Nottingham, Nottingham, UK
e-mail: alialperenbakir@gmail.com

R. Neshani · S. Özerinç

Department of Mechanical Engineering, Middle East Technical University,
Ankara, Turkey
e-mail: roozbeh.neshani@metu.edu.tr

S. Özerinç (✉)

Department of Micro and Nanotechnology, Middle East Technical University,
Ankara, Turkey
e-mail: ozeric@metu.edu.tr

1 Introduction

Fused deposition modeling (FDM) is an additive manufacturing technology based on the principle of plastic extrusion, where a nozzle deposits the heated thermoplastic on a printing bed in the desired trajectory. FDM's additive nature enables the production of unique and complicated structures that are very costly or impossible to produce by conventional techniques.

FDM's earlier use has been mostly limited to rapid prototyping activities for design iterations [1]. However, the recent advances in the filament material technology combined with the decreasing cost and increasing performance of FDM-based printers have rendered the FDM-production of actual load-bearing components feasible. This relatively new and broader application field requires a better understanding of FDM-produced parts' mechanical behavior. The lack of knowledge on this topic triggered numerous studies in the literature, investigating the structure-process-property relationship in FDM-produced parts.

Acrylonitrile butadiene styrene (ABS) and polylactic acid-based (PLA) thermoplastics have been the primary filament materials since the beginning of the FDM technology. As a result, most studies in the literature have focused on these materials while evaluating the mechanical behavior of FDM-produced parts. Extensive reviews on the subject summarize the current knowledge and gaps in the literature for the FDM-printing of ABS and PLA [2–5]. On the other hand, the recent advances in filament technology have also enabled the use of elastomeric thermoplastics with FDM, which adds new capabilities to this printing technology.

Elastomers are a particular class of amorphous polymers that exhibit extreme elasticity. In the unstressed state, the long molecules of the elastomer are irregularly coiled and twisted. Upon tensile loading, the molecules uncoil, untwist and straighten, corresponding to a low-entropy state. With the loading release, the molecules go back to their original state due to the energetically favorable high-entropy configuration. Therefore, as opposed to the energy-elastic materials such as metals and ceramics, elastomers exhibit entropy-elastic behavior.

The entropy-elasticity results in the unique mechanical behavior of low elastic modulus and extreme strain recovery, making elastomers suitable for a wide range of applications requiring damping, sealing, insulation, and adhesion.

Both thermoset polymers and thermoplastic polymers include some types that exhibit elastomeric behavior. However, only thermoplastic elastomers are relevant for FDM, as the FDM technique requires the raw material to exhibit thermoplasticity.

Understanding the mechanical behavior of FDM-produced elastomers is essential for the best utilization of the capabilities of FDM and the unique properties of elastomers. As mentioned above, there has been an accumulation of detailed knowledge about the structure-process-property relationships for FDM-produced parts based on materials such as PLA and ABS. However, similar studies on elastomers are quite limited in the literature.

This chapter aims to provide an overview of the current knowledge on the mechanical behavior of FDM-produced elastomeric parts, with a focus on process-property relationships. Section 2 starts with basic information about the mechanical properties of elastomers in general. Section 3 presents a list of studies in the literature, summarizing the elastomeric materials used and mechanical testing techniques utilized so far. Section 4 provides a detailed discussion of the effect of FDM process parameters such as nozzle temperature, raster orientation, build orientation, and infill ratio on printed parts' mechanical performance. Section 5 summarizes the key findings and proposes new research directions based on the observed gaps in the literature.

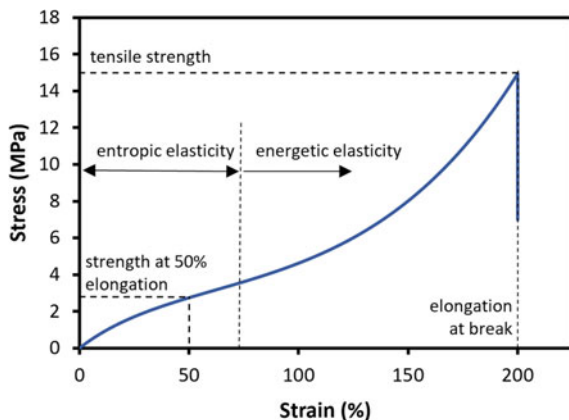
2 Mechanical Behavior of Elastomers

Figure 1 shows a generic stress-strain curve for an elastomeric material under uniaxial tensile load. The stress-strain curve exhibits a nonlinear and smooth behavior with no apparent transition between elastic and plastic deformation. On the other hand, the curve has an inflection point that defines the transition from entropic elasticity to energetic elasticity. One can use secant or tangent lines to define the modulus of elasticity for relatively small strains. Other key parameters are the stresses at certain strain levels (such as 50% and 100%), tensile strength (at the point of failure), and elongation at failure. In addition, glass transition temperature (T_g) is a critical parameter, below which elastomers start losing their rubber-like behavior.

The stress-strain behavior of elastomers is strain rate and temperature-dependent, making the analysis further complicated. Hyperelastic models use strain energy density function, W , to describe the elastic response as follows.

$$W = W(\lambda_1, \lambda_2, \lambda_3) = W(I_1, I_2, I_3) \tag{1}$$

Fig. 1 Stress-strain behavior of an elastomeric specimen under uniaxial tension



$$I_1 = \lambda_1^2 + \lambda_2^2 + \lambda_3^2 \quad (2)$$

$$I_2 = \lambda_1^2 \lambda_2^2 + \lambda_2^2 \lambda_3^2 + \lambda_1^2 \lambda_3^2 \quad (3)$$

$$I_3 = \lambda_1^2 \lambda_2^2 \lambda_3^2 \quad (4)$$

In these equations, I terms are the invariants of Cauchy-Green deformation tensor, and λ_i terms are principal stretches.

Since most elastomeric materials are virtually incompressible (Poisson's ratio = 0.5), I_3 becomes unity, and the model only depends on the first and second invariants. Then one can define the material response in terms of the first Piola-Kirchhoff stress as follows.

Uniaxial tension:

$$P_{11} = P = 2 \left(\lambda - \frac{1}{\lambda^2} \right) \left(\frac{\partial W}{\partial I_1} + \frac{\partial W}{\partial I_2} \frac{1}{\lambda} \right), \quad P_{22} = P_{33} = 0 \quad (5, 6)$$

Equi-biaxial tension:

$$P_{11} = P_{22} = P = 2 \left(\lambda - \frac{1}{\lambda^5} \right) \left(\frac{\partial W}{\partial I_1} + \frac{\partial W}{\partial I_2} \frac{1}{\lambda^2} \right), \quad P_{33} = 0 \quad (7, 8)$$

Pure shear:

$$P_{11} = P_1 = 2 \left(\lambda - \frac{1}{\lambda^3} \right) \left(\frac{\partial W}{\partial I_1} + \frac{\partial W}{\partial I_2} \right) \quad (9)$$

$$P_{22} = P_2 = 2 \left(1 - \frac{1}{\lambda^2} \right) \left(\frac{\partial W}{\partial I_1} + \frac{\partial W}{\partial I_2} \lambda^2 \right), \quad P_{33} = 0 \quad (10, 11)$$

Table 1 summarizes some of the most common hyperelastic constitutive models used to describe the mechanical response of elastomers. This chapter focuses more on the fused deposition modeling of elastomers rather than the fundamentals of elastomeric mechanical behavior. Therefore, for further information, we refer the readers to detailed reviews on this subject [6–8].

Figure 2a presents the experimental stress-strain behavior of FDM-printed elastomeric specimens based on a thermoplastic polyurethane (TPU) filament (Ninjaflex by Fenner Inc., USA) [18]. The figure shows the predictions of four different models, namely, two-term Ogden, Neo-Hookean, Yeoh, and Mooney-Rivlin. Overall, the Ogden model provides the most accurate prediction for the whole strain range. On the other hand, the Neo-Hookean model presents a simple and effective approach for small strains. Figure 2b presents a similar comparison for the case of true stress and compares the predictions of Mooney-Rivlin and Neo-Hookean models.

Table 1 A summary of some common hyperelastic models in the literature

Model	Year	Expression	References
Mooney-Rivlin	1940	$W = \sum_{i+j=1}^N C_{ij}(I_1 - 3)^i (I_2 - 3)^j$	[9, 10]
Neo-Hookean	1943	$W = C_1(I_1 - 3), 2C_1 = \mu(\text{shear modulus})$	[11]
Valanis and Landel	1967	$W = w(\lambda_1) + w(\lambda_2) + w(\lambda_3), \frac{dw}{d\lambda} = 2\mu \ln(\lambda)$	[12]
Ogden	1972	$W = \sum_{N=1}^P \frac{\mu_N}{\alpha_N} (\lambda_1^{\alpha_N} + \lambda_2^{\alpha_N} + \lambda_3^{\alpha_N} - 3)$	[13]
Van der Waals	1986	$W = G \left\{ -(\lambda_m^2 - 3) [\ln(1 - \Theta) - \Theta] - \frac{2}{3} \left(\frac{I_1 - 3}{2} \right)^{\frac{3}{2}} \right\}$	[14, 15]
Yeoh	1990	$W = \sum_{i=1}^3 C_i (I_1 - 3)^i$	[16]
8-chain	1993	$\sigma_i(\text{cauchy stress}) = \frac{nkT\sqrt{N}}{3} \frac{\lambda_i^2}{\lambda_{ch}} \mathcal{L}^{-1} \left(\frac{\lambda_{ch}}{\sqrt{N}} \right)$	[17]

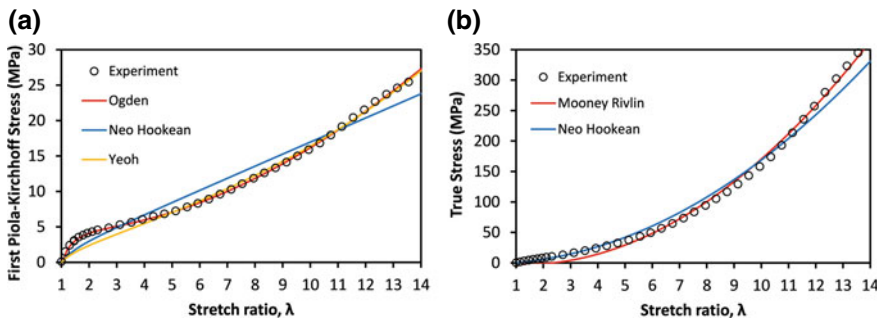


Fig. 2 Stress-strain behavior of an FDM-produced TPU specimen utilizing Ninjaflex filament [18]. Markers represent experimental data, and curves show model predictions. (a) and (b) shows the engineering and true stress versions of the data, respectively. Stretch ratio is defined as the ratio of the final gauge length to the initial gauge length, $\lambda = l/l_0$

Elastomers also exhibit time-dependent mechanical response due to their viscoelastic characteristics. Linear viscoelastic models (LVM) consider this response as a combination of an elastic solid and a viscous fluid [19]. Figure 3 represents four common models based on different combinations of dashpots and springs. Table 2 summarizes the main equations for these models [20].

Linear models provide simple expressions; however, they are applicable only for small strains. There also exist nonlinear models, especially for the predictions at higher strains. These models’ details are beyond this chapter’s scope and are covered in detail in several review articles [21–23].

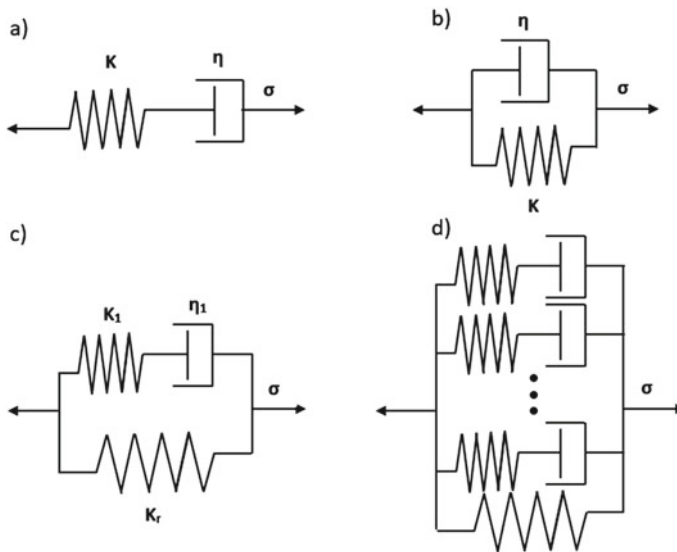


Fig. 3 Schematic representations of common linear viscoelastic models; (a) Maxwell Model, (b) Kelvin-Voigt Model, (c) Standard Linear Solid (SLS) Model, (d) Generalized Maxwell Model

Table 2 A summary of the linear viscoelastic models (LVM)

Model	Equation ^a
Maxwell	$\frac{\sigma}{\eta} + \frac{1}{k} \frac{d\sigma}{dt} = \frac{d\varepsilon}{dt}$
Kelvin-Voigt	$\sigma = k\varepsilon + \eta \frac{d\varepsilon}{dt}$
Standard Linear Solid	$\sigma + \frac{\eta_1}{k_1} \frac{d\sigma}{dt} = k_r \left(\varepsilon + \eta_1 \frac{k_r + k_1}{k_r k_1} \frac{d\varepsilon}{dt} \right)$
n-term Prony Series	$G(t) = G_0 + \sum_{i=1}^N G_i \exp\left(-\frac{t}{\tau_i}\right)$
Boltzmann Superposition Principle	$\sigma(t) = k_r \varepsilon(t) + \int_0^t K(t-s) \frac{d\varepsilon(s)}{ds} ds$

^a σ is stress, K is elastic modulus, and η is viscosity

3 FDM-Printed Elastomers and Testing

Table 3 shows a summary of elastomeric FDM filaments reported in the literature and the commercially available alternatives. In earlier studies, researchers produced custom filaments from elastomeric pellets by twin-screw extrusion [24, 25]. Later on, numerous filament manufacturers have developed elastomeric filaments optimized for the FDM process. Most of these filaments are based on thermoplastic polyurethane (TPU)—a class of polyurethane widely used in the industry.

The FDM process enables the net-shape manufacturing of any custom geometry. Therefore, specimen preparation for a wide range of mechanical tests is

Table 3 Elastomeric FDM filaments reported in the literature and commercial filaments available in the market

Type of Elastomer	Manufacturer and Product Name/ Production Technique	Tensile Strength (MPa)	References
Thermoplastic Polyurethane (TPU)	Fenner Inc., Ninjaflex	26	[26]
	Fenner Inc., Cheetah	39	[27]
	Dddrop BV., TPU	50	[28]
	FormFutura BV., PhytonFlex	50	[29]
	ColorFabb BV., NGEN FLEX	3–7	[30]
Thermoplastic Copolyester (TPC)	FormFutura BV., FlexiFil	24	[31]
Thermoplastic Elastomer (TPE)	DuPont Inc., Hytrel 3D4000FL	13–19	[32]
	Recreus Industries S. L, FilaFlex	13–15	[33]
	Fenner Inc., NinjaTek TPE	25–30	[33]
Polypropylene/Styrene-Ethylene Butylene-Styrene (PP/SEBS)	Twin-screw extrusion	20–25	[34]
Thermoplastic Polyurethane/ Multi-Walled Carbon Nanotube (TPU/MWCNT)	Twin-screw extrusion	25–30	[24]
Thermoplastic Polyurethane/Wood Flour Composite (TPU/WF)	Twin-screw extrusion	12–28	[25]

straightforward and does not require any subsequent manufacturing step. Table 4 summarizes the mechanical characterization studies performed so far on FDM-produced elastomeric parts. The table also indicates the associated ASTM and ISO standards utilized during these tests and the process parameters investigated in each study.

Tensile testing has been the most frequently used method to assess the mechanical properties of printed elastomers. Studies about the impact, fatigue, and fracture behavior of FDM-produced elastomers are quite limited, indicating the need for further work in this field.

Table 4 A summary of mechanical characterization studies on elastomeric materials produced by FDM. For each study, the investigated parameters and the utilized testing standards are listed

Test method	References	Standard	Investigated parameters				Layer thickness
			Nozzle temperature	Raster orientation	Build orientation	Infill ratio	
Tensile	Chaudhry [30]	ASTM D638		X		X	X
	Hohimer et al. [24]	ASTM D638	X	X			X
	Kepekci et al. [35]	ASTM D638	X				
	Messimer et al. [36]	ASTM D638			X		
	Miller et al. [37]	Custom				X	
	Bakır et al. [38]	ASTM D638	X			X	X
	Hohimer et al. [39]	ASTM 3039	X	X			X
	Chaudry [30]	ASTM 695		X		X	X
	Yarwindran [33]	ASTM D2240				X	
Flexural	Yarwidran [33]	ASTM D790				X	
Fracture toughness	Messimer et al. [36]	ASTM D5045			X	X	

4 Effect of Process Parameters on the Mechanical Properties

4.1 Comparison with Injection Molding

One of FDM's biggest challenges is the production of parts whose strength can reach those of injection molded parts. Figure 4 shows the stress-strain behavior of FDM-produced and injection-molded polypropylene (PP) and styrene-(ethylene-butylene)-styrene (SEBS) blends as an example [34]. FDM-produced part utilized an infill ratio of 100% and a raster angle of 45° —common parameters for load-bearing applications (these parameters will be further explained in the subsequent sections). The results show that the FDM-produced part's tensile strength is almost 40% lower than that of the injection-molded specimen.

A significant difference between the mechanical performance of FDM-produced polymers and those produced by conventional methods is a common observation [40]. The relatively low strength of printed parts has been the main driving force for numerous studies in the literature to optimize the mechanical performance.

In the below sections, we discuss the effects of key printing parameters that influence the mechanical properties of printed parts, namely, nozzle temperature, raster and build orientation, layer height, and infill ratio. Finally, we present the effect of additives and secondary phases on the mechanical behavior.

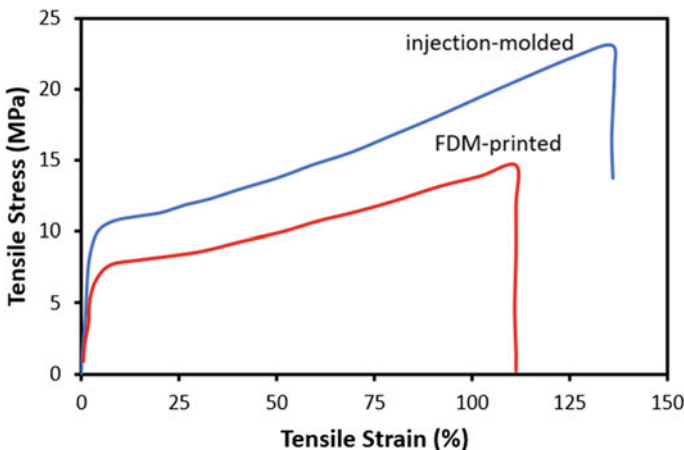


Fig. 4 Comparison of the stress-strain behavior of an FDM-produced and an injection-molded specimen [34]. For the FDM-produced specimen, the infill ratio is 100%, the nozzle temperature is 220 °C, the raster angle is 45° , and the nozzle diameter is 0.4 mm

4.2 Nozzle Temperature

Nozzle temperature is one of the most critical parameters that directly influence the polymer's flow dynamics as it is extruded through the nozzle. The optimization of the temperature is usually based on the printing quality. At low temperatures, nozzle clogging, and incomplete fusion between the layers deteriorate the printing quality. On the other hand, at high temperatures, warping [41] and polymer degradation [42] becomes an issue. In addition, most low-cost FDM printers have a maximum nozzle temperature of around 260 °C. Therefore, there usually exists an optimum temperature that provides the best results.

Figure 5 shows the effect of nozzle temperature on the stress-strain behavior of a commercial elastomeric filament, Ninjaflex (Fenner Inc. USA) [35]. The initial response of the elastomer is mostly independent of temperature. However, at large elongations, the curves start to differ. 230 °C specimen shows a considerably higher tensile strength and elongation at break.

The fusion between the printed layers is the primary phenomenon that generates the nozzle temperature-dependent strength [43]. As temperature increases, the viscosity of the polymer decreases, and the fusion quality improves. The results presented in Fig. 5 suggest that the printed specimens exhibit some flaws at the nozzle temperatures of 220 °C and 225 °C due to incomplete fusion.

On the other hand, there are also findings suggesting that the nozzle temperature is not very effective on strength. Figure 6 demonstrates this behavior for the tensile strength of an FDM-produced TPU based on Elastollan 1185A TPU (BASF, Germany) [39]. The figure shows the tensile strength for various combinations of nozzle temperature, raster orientation, and air gap. The trends are a complicated

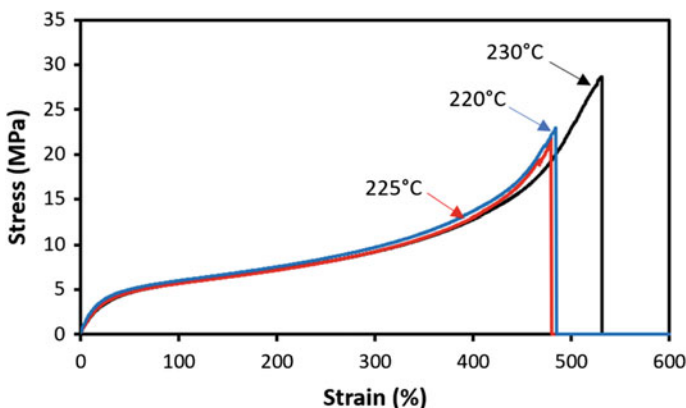


Fig. 5 Tensile stress-strain behavior of FDM-produced elastomeric specimens made of Ninjaflex filament [35]. Layer height is 0.2 mm, nozzle diameter is 0.4 mm, bed temperature is 40 °C, printing speed is 5 mm/s, and air gap is negative. The curves are averaged trends based on multiple specimens with a range of raster orientations

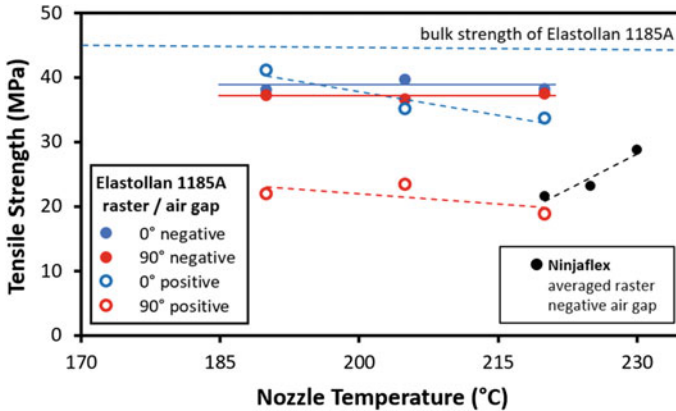


Fig. 6 Effect of nozzle temperature on the tensile strength of FDM-produced TPU parts [35, 39]. For the Elastollan 1185A based specimens, the layer height is 0.2 mm, the nozzle diameter is 0.6 mm, and no bed heating was used. For Ninjaflex based specimens, layer height is 0.2 mm, and bed temperature is 40 °C

function of the raster orientation and air gap, as discussed further in Sect. 4.3. However, there is no apparent effect of the nozzle temperature on strength. The figure also shows the strength of Ninjaflex TPU based on the data of Fig. 5, exhibiting significant strengthening with increasing nozzle temperature. The results suggest that some other process parameters might dominate the mechanical response in certain circumstances, and as a consequence, the effect of nozzle temperature might become negligible.

4.3 Raster and Build Orientation

Raster orientation describes the trajectory of the printing head within a layer, and the build orientation defines the orientation of the part with respect to the printing bed. Figure 7 shows a schematic description of the most common combinations of raster and build orientations.

Three primary raster orientations are parallel, perpendicular, and diagonal. These orientations are defined with respect to the loading axis of the tensile specimen. Therefore, the parallel, perpendicular, and diagonal raster orientations result in 0°, 90°, and 45° angles between the loading axis and the printed lines, respectively. When it comes to the build orientation, the most common configurations are horizontal, on-edge, and vertical. For vertical specimens, the raster orientation does not directly define the orientation of the printed lines with respect to the loading axis, which forms an exception to these conventions.

Another parameter that influences the effects of raster and build orientation on mechanical behavior is the air gap. The air gap defines the spacing between the

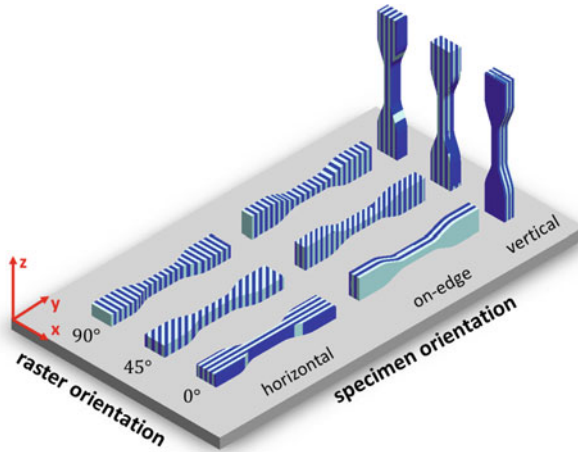


Fig. 7 Schematic descriptions of various combinations of raster orientation and build orientation. Blue and white colors represent the adjacent lines of the raster. The schematic exaggerates the widths of printed lines and does not show the individual layers for clarity. Note that the definition of 0° and 90° raster is somewhat arbitrary for vertical specimens

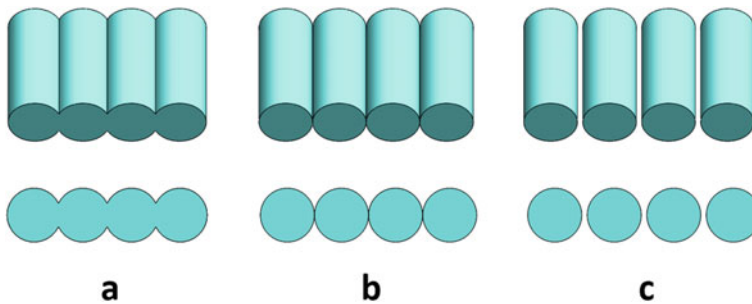


Fig. 8 Schematic representation of different air gap values (a) Negative air gap, (b) zero air gap (no air gap), (c) positive air gap

printed lines, as demonstrated in Fig. 8. For air gaps comparable to or larger than the printed line width, the part becomes a cellular structure. Section 4.5 discusses this scenario in further detail in terms of the effect of the infill ratio. This section will focus on small positive and negative air gaps, as shown in Fig. 8. A positive air gap increases the distance between the printed lines, whereas a negative air gap results in slightly overlapping lines.

Based on the above definitions of raster orientation, build orientation, and air gap, literature data provide insight into the mechanics of printed parts. As an example, Fig. 9 shows the tensile strength of FDM-produced specimens based on Elastollan 1185A (BASF, Germany) and those based on Ninjaflex (Fenner Inc., USA) as a function of raster orientation [35, 39]. For Elastollan 1185A, strength is

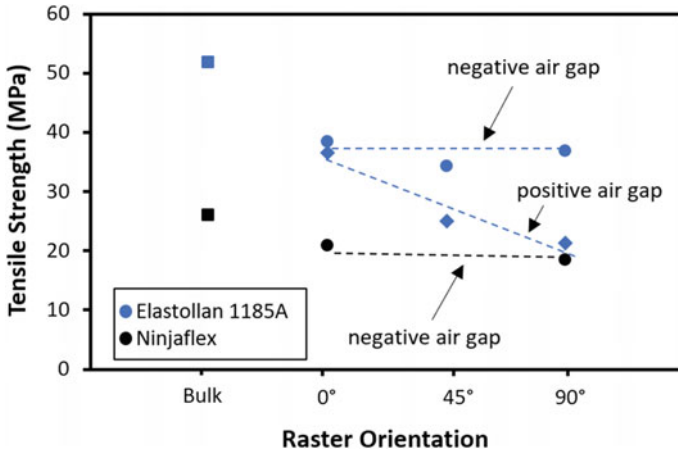


Fig. 9 Effect of raster orientation on the tensile strength for negative and positive air gaps [35, 39]. The filament materials are based on Elastollan 1185A (BASF, Germany) and Ninjaflex (Fenner Inc., USA). For Elastollan 1185A, the nozzle temperature is 235 °C, layer height is 0.2 mm, and printing speed is 10 mm/s, with no bed heating. For Ninjaflex, layer height is 0.2 mm, printing speed is 5 mm/s, and bed temperature is 40 °C. Ninjaflex results are the average values for a range of nozzle temperatures

highest for the parallel orientation (0°) and becomes lower for the diagonal (45°) and perpendicular raster (90°) cases. An interesting observation is the dependence of this trend on the air gap. The effect of orientation is less pronounced for the negative air gap; perpendicular and diagonal cases have approximately the same strength. However, for the positive air gap, the orientation affects the strength by almost 50%. The results of Ninjaflex TPU exhibit a similar trend, where the negative air gap renders the strength orientation independent.

The influence of fusion sites on the load-bearing capacity can explain the observed results. The flow is smooth along the printed lines and results in continuous polymer segments with adequate mechanical integrity. On the other hand, the cohesion between the printed lines relies on fusion quality during printing [44]. As a result, fusion sites are usually weaker than the printed lines themselves. For the case of the parallel raster, the printed lines are parallel to the loading direction. In this case, the printed lines carry most of the load, and weak-fusion sites do not play a significant role in determining the strength. On the other hand, for perpendicular raster, tensile testing puts the fusion lines under pure tension, resulting in stress concentrations and reduced load-bearing capacity.

When the air gap is positive, the separation between the printed lines becomes larger, resulting in lower fusion temperatures and smaller hydrostatic pressures. The results in Fig. 9 support this argument; the positive air gap amplifies the raster orientation effect on the strength. Therefore, in load-bearing applications, a negative air gap is a more conservative approach that reduces the strength anisotropy of the printed parts.

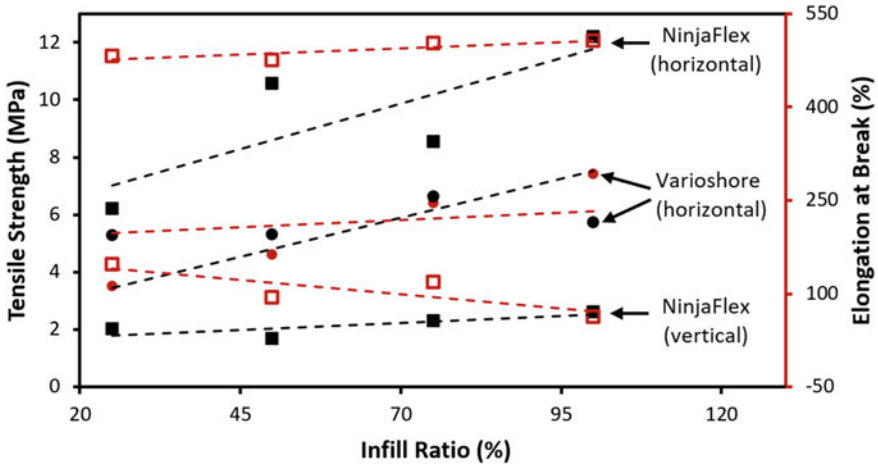


Fig. 10 Effect of built orientation on the mechanical properties of FDM-produced specimens made of Ninjaflex TPU filament (Fenner Inc., USA) and Varioshore TPU filament (Colorfabb, Netherlands). For Ninjaflex-based specimens, the nozzle temperature is 225 °C, the bed temperature is 60 °C, layer height is 0.32 mm, and raster orientation is 45°/−45° [36]. For Varioshore specimens, the nozzle temperature is 240°C, layer thickness is 0.4 mm, bed temperature is 45 °C, raster orientation is 45°, infill ratio is 100%, and feed rate is 100% [38]

The build orientation affects the strength through mechanisms similar to those of raster orientation. In the case of build orientation, the primary parameter is the fusion level between the layers. Figure 10 shows the mechanical properties of horizontal and vertical build orientation specimens as a function of the infill ratio for Ninjaflex TPU-based specimens [36]. Both the strength and the ductility of vertical specimens are considerably lower than the horizontal counterparts. For comparison purposes, the figure also shows the results of horizontal build orientation specimens based on the Varioshore TPU filament (Colorfabb, Netherlands). This comparison demonstrate that large variations can occur in between different filament materials, although the base material is the same.

Comparison of the effects of raster orientation (Fig. 9) and build orientation (Fig. 10) indicates that build orientation's effect is more severe on mechanical behavior. This observation is consistent with the previous findings on thermoplastic filaments, such as PLA and ABS [45].

4.4 Layer Height

Layer height defines the layer thickness of each printing cycle. In other words, the layer height determines the number of layers along the build direction (z-direction).

Figure 11 shows the effect of layer height on the tensile strength for FDM-produced TPU parts [30]. While the trends are not very clear, there is an overall monotonic reduction in strength with increasing layer height.

As the layer height increases, fusion surfaces become wider, generating more space for defects and void generation. The associated stress concentrations might explain the observed reduction in strength. Microscopical observation of the cross-sections can provide further insight into the problem.

While layer height has an apparent influence on the tensile strength, its effect on the compressive strength is less evident. Figure 12 exemplifies this behavior for the case of cylindrical compression specimens made of TPU [30]. The compressive strength is virtually independent of the layer thickness for three different infill ratios in the range of 80–100%, considering the experimental uncertainties.

The difference between the tensile and compressive behavior is an indication of printing defects and associated stress concentrations. The partly fused sites and defective regions can still provide adequate load carrying capacity under compression. However, these sites become stress concentrators under tension, which reduces the material’s strength.

Overall, the literature data suggest that the layer height effect is not as significant as raster orientation and build orientation. The implications of layer height might become more pronounced in the case of vertical build orientation. However, there is no study to date that reports the effect of layer height on the strength of vertical specimens, whose analysis should be among the future research directions.

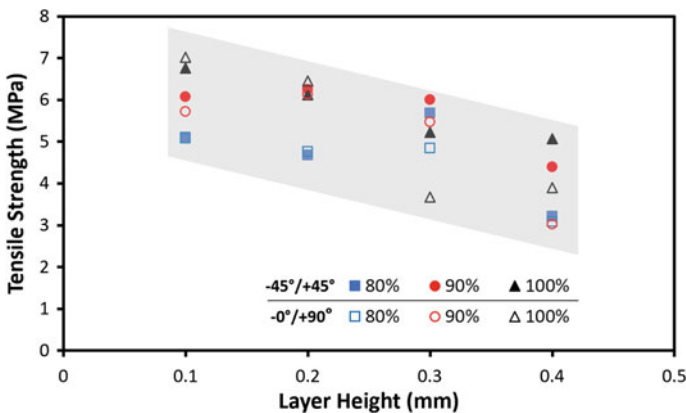


Fig. 11 Variation of the tensile strength of TPU as a function of infill ratio and layer height [30]. Open and filled markers indicate raster orientations of 0°/90°, and 45°/-45°, respectively. The build orientation is horizontal, the nozzle temperature is 230 °C, and the nozzle diameter is 0.4 mm. The gray parallelogram emphasizes the trend of decreasing strength with increasing layer height

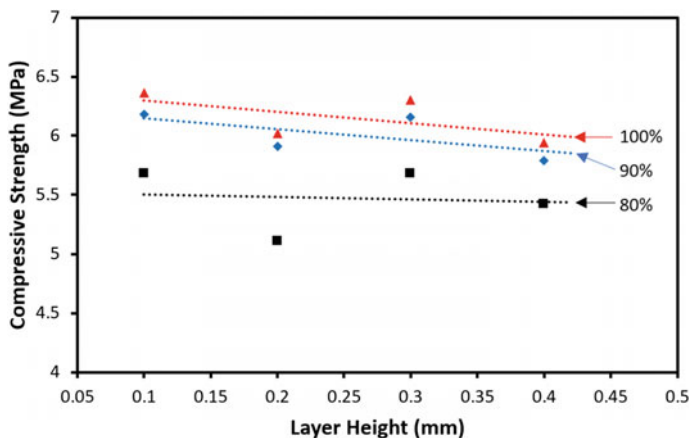


Fig. 12 Effect of layer height on the compressive strength of TPU parts for three different infill ratios [30]. The build orientation is horizontal, nozzle diameter is 0.4 mm and the nozzle temperature is 230 °C

4.5 Infill Ratio/Cellular Structures

The infill ratio is one of the most critical parameters in FDM. As FDM is a relatively slow process, a low infill ratio is desirable for reducing the printing time and manufacturing cost [46]. On the other hand, the compromise between the strength and the infill ratio requires proper optimization for load-bearing components' reliable operation.

Interestingly, the studies on the effect of infill ratio are quite limited in the literature for elastomers. Yarwindran et al. [33] measured the hardness of specimens printed by using two TPU-based commercial filaments, Filaflex (Recreus S.L., Spain), and Ninjaflex (Fenner Inc., USA) [33]. The study utilized a honeycomb infill pattern, whose dimensions were varied for tuning the infill ratio. The results indicate a monotonic increase in hardness with an increasing infill ratio. When infill ratio increases from 10% to 100%, Shore D hardness of Ninjaflex increases from 23 to 56. Over the same range, Filaflex exhibits a larger hardness variation, ranging from 8 to 30.

Figure 13 shows the tensile strength variation of cellular specimens made of Carbothane AC-4095A (Lubrizol, USA). The study employed a crosshatch pattern for generating a range of infill ratios. Tensile strength monotonically increases with increasing infill ratio. The figure compares the FDM results with those of the Continuous Liquid Interface Production (CLIP) process that uses the Carbon 3D printer and Carbon's EPU40 resin [37]. FDM-produced parts' normalized strength values are close to those of CLIP—a recent photopolymerization-based 3D printing technology that employs considerably more expensive equipment and raw material [47]. The close results show the great potential of FDM in economically producing advanced parts.

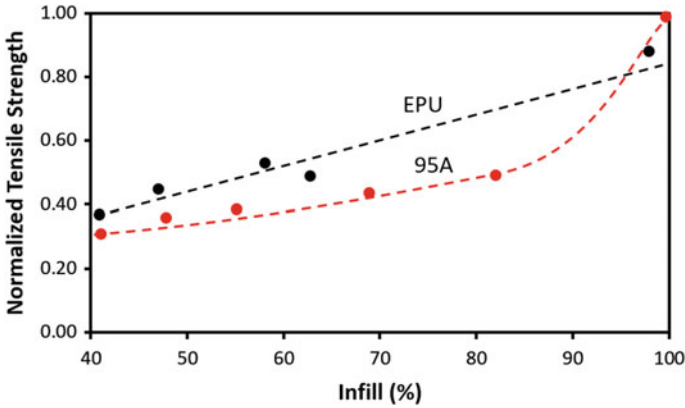


Fig. 13 Tensile strength of elastomeric specimens produced by FDM (95A) and CLIP (EPU40) as a function of infill ratio [37]. Tensile strength is normalized by the strength of the respective specimens with 100% infill ratio

The mechanical behavior of porous and cellular structures does not solely depend on the infill ratio. The morphology and distribution of the pores and voids also affect the behavior. Gibson and Ashby proposed a simple relationship for this purpose [48]:

$$\frac{\sigma}{\sigma_s} = C_1 \left(\frac{\rho}{\rho_s} \right)^{C_2} \tag{12}$$

In this equation, σ is the strength, and ρ is the density of the cellular structure. σ_s and ρ_s are the corresponding properties of the fully dense material (100% infill). The model takes the effect of cell geometry into account through constants C_1 and C_2 . Equation (12) can also be used for the elastic modulus by replacing σ with E .

For open and closed-cell structures, Gibson and Ashby propose C_2 values of 1.5 and 2, respectively [48]. However, the hardness measurements of Yarwindran et al. [33] mentioned above and those presented in Fig. 13 show approximately linear behavior with a rapid rise in strength towards 100% infill ratio. The additional support provided by the solid frame defining the specimen’s circumference might explain this deviation from the model. This structure, called shell (or inwall), is commonly employed in 3D printing as it maintains adequate printing quality and provides better impact resistance. Bakır et al. [49] proposed a modified Gibson-Ashby relationship to take the inwall effect into account, as follows.

$$\frac{\sigma}{\sigma_s} = C_0 + C_1 \left(\frac{\rho}{\rho_s} \right)^{C_2} \tag{13}$$

where C_0 represents the additional support provided by the inwall structure.

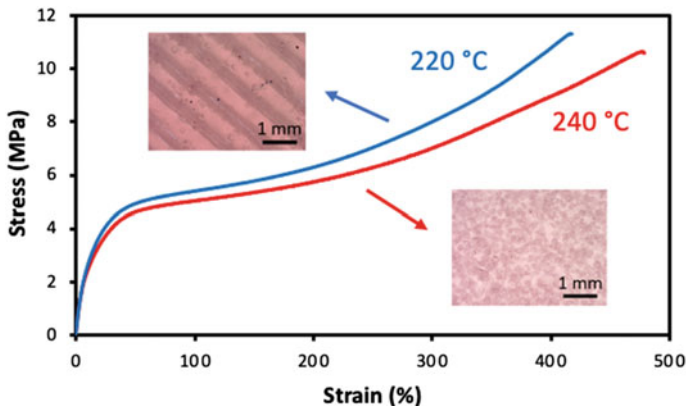


Fig. 14 Stress-strain curves and optical microscopy images of foaming TPU specimens printed using two different nozzle temperatures [38]. The layer thickness is 0.4 mm, the infill ratio is 100%, and the bed temperature is 40 °C

A recently developed foaming filament provides a new approach to the manufacturing of porous structures through FDM. The Varioshore TPU filament (Colorfabb, Netherlands) is an elastomeric filament that foams upon heating. The nozzle temperature and feed rate control the extent of foaming, enabling the tuning of the strength and stiffness. Figure 14 shows the mechanical behavior and optical microscopy images of specimens printed at two different temperatures [38]. The nozzle temperature of 220 °C exhibits more than 50% higher tensile strength and ductility compared to the case of 240 °C. The microstructure provides insight into the observed behavior. At 220 °C, the foaming is negligible, and the printing lines are visible. When the nozzle temperature is 240 °C, the polymer exhibits a porous structure with uniformly distributed voids. Such a small temperature rise is not expected to alter the microstructure of the elastomer. Therefore, the lower density and the associated reduction in load-bearing capacity can explain the findings.

The results discussed in this chapter show the great application potential of cellular elastomeric materials for the design and manufacturing of lightweight and compliant parts. However, the limited data in the literature prevents a thorough assessment of this opportunity. Future studies should focus on identifying the relationships between the infill ratio, cell geometry, and mechanical properties in a systematic fashion.

4.6 Composites and Polymer Blends

Elastomers in pure form have the lowest strength among polymers. There are continuing efforts towards the development of stronger elastomers through

secondary particle and phase additions. There are extensive reviews on the subject, such as those focusing on the effect of carbon nanotube additions [50] and blending [51].

When it comes to the FDM process, the extrusion-based working principle enables a wide range of opportunities to incorporate secondary phases and additives to the filament material. Figure 15 shows the effect of wood flour additions on the mechanical properties of TPU-based printed parts [25]. Upon the addition of wood flour, the strength first decreases and then increases. Overall, the additions do not result in an improvement over the pure-TPU specimen. In the meantime, the elongation at break considerably decreases. This study’s focus was altering the cosmetic appearance of the printed parts; therefore, some reduction in strength might be acceptable. Nevertheless, the findings emphasize the importance of the proper additive choice and careful engineering of the polymer matrix-particle interface for superior mechanical performance.

The polymer blending approach is another route to optimizing the mechanical properties and achieving pure elastomeric behavior. Figure 16 shows the stress-strain behavior of polypropylene/styrene-(ethylene-butylene)-styrene (PP/SEBS) blends with varying composition. When the SEBS content is 20 and 40 wt%, the blend behaves as a thermoplastic. When the SEBS content reaches 60 wt%, elastomeric behavior is achieved. Elastomeric behavior also results in a significant reduction in strength. The study considered carbon black additions as a solution to this problem. Figure 16 shows that as carbon black content increases, the strength monotonically increases. However, the ductility decreases in the meantime, exhibiting the classical strength-ductility trade-off in engineering materials.

Nozzle diameters of most FDM printers range between 0.2 and 0.6 mm, limiting the size of reinforcement particles added to the elastomeric matrix. When the particle size becomes comparable to the nozzle diameter, severe clogging and

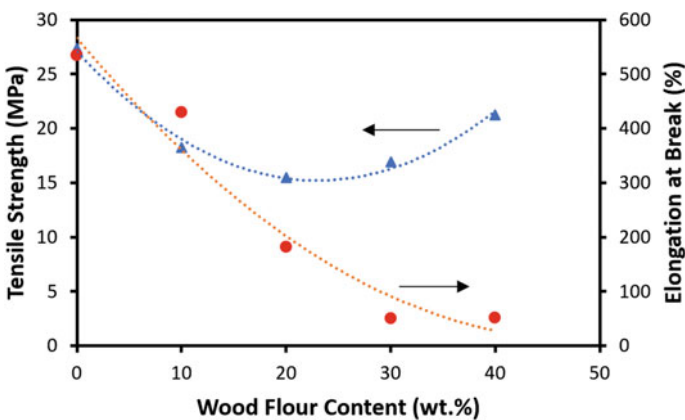


Fig. 15 Effect of wood flour content on the mechanical behavior of printed TPU specimens [25]. The study did not provide the details of the FDM process parameters

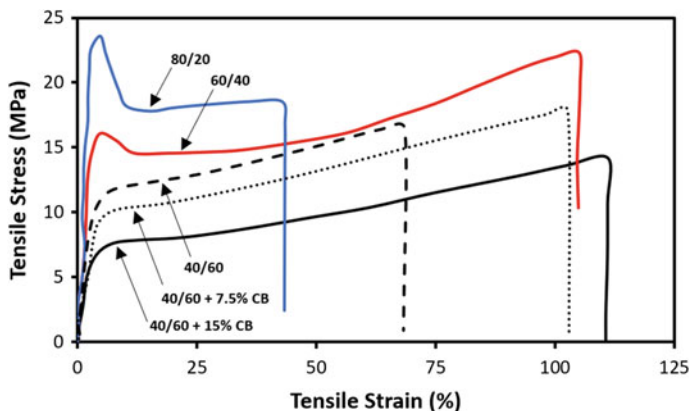


Fig. 16 Tensile stress-strain behavior of FDM-produced PP/SEBS blends [34]. The 40/60 + 15% CB indicates a 40% PP and 60% SEBS blend with 15 wt% carbon black additions

nozzle wear become an issue. Carbon nanotubes can eliminate these problems due to their submicron size. Furthermore, they can serve as an ultra-high-strength secondary phase. Table 5 shows the tensile strength of TPU/multi-walled carbon nanotube (MWCNT) composites as a function of MWCNT content. As MWCNT content increases, elastic modulus considerably improves. On the other hand, the strength decreases dramatically upon the addition of MWCNT to the matrix. There is a need for further studies investigating the interactions between the composite parameters and FDM process parameters, which will enable the optimization of the mechanical properties.

5 Conclusions and Future Research Directions

The unique mechanical properties of elastomeric filaments provide a new design space for the wider use of FDM-printed polymers in structural applications. Understanding the mechanical behavior of printed elastomeric parts is crucial for realizing the full potential of this opportunity.

Table 5 Mechanical properties of printed TPU parts with varying multi-walled carbon nanotubes (MWCNT) content [24]

	MWCNT Content (wt%)		
	0.0	1.0	2.0
Tensile strength (MPa)	36.2	28.8	23.7
Elastic modulus (MPa)	11.5	21.4	25.1
Elongation at break (%)	665	645	597

The nozzle temperature is 235°C, the bed temperature is room temperature, the nozzle diameter is 0.6 mm, and the layer height is 0.2 mm

The literature findings show that the primary parameters that influence the strength of FDM-produced elastomeric parts are nozzle temperature, raster orientation, build orientation, layer thickness, and infill ratio. Careful optimization of these parameters can lead to printed parts with strength values close to injection-molded counterparts.

Another promising capability of FDM is the manufacturing of lightweight and compliant cellular structures. The combination of this capability with the unique properties of elastomers has great potential towards the development of new generation lightweight structural parts, impact absorbers, and similar. Foaming filaments provide an additional tool for the further optimization of such structures by enabling a hierarchical architecture.

Most studies in the literature about the mechanics of FDM-produced parts focus on commonly used thermoplastics such as PLA and ABS. Mechanical properties of FDM-produced elastomeric parts have only recently gained attention, and there are a very limited number of studies in the literature at the moment. Therefore, there are numerous unanswered questions about the mechanical behavior of printed elastomeric parts:

1. There is not sufficient systematic data about the effect of nozzle temperature, build orientation, and infill ratio on the mechanical behavior of printed elastomers. The possible interactions between these parameters are not well understood.
2. Elastomeric materials have very complicated temperature and strain rate-dependent mechanical behavior. Implications of these for the FDM technology are not studied in detail.
3. Combining the ideas of elastomer-printing and cellular structures is very promising for developing new generation compliant structural parts. There is a vast design space to be explored in this field.
4. The development of elastomer-based composites and elastomeric polymer blends with enhanced properties and functionality are active research topics. Combining the recent advances in these fields with the capabilities of FDM can lead to novel structures with unique mechanical properties.

Systematic studies on these matters will provide guidelines to researchers and engineers towards the development of novel elastomeric parts and structures.

References

1. Masood SH (1996) Intelligent rapid prototyping with fused deposition modelling. *Rapid Prototyp J* 2:24–33. <https://doi.org/10.1108/13552549610109054>
2. Mohamed OA, Masood SH, Bhowmik JL (2015) Optimization of fused deposition modeling process parameters: a review of current research and future prospects. *Adv Manuf* 3:42–53. <https://doi.org/10.1007/s40436-014-0097-7>

3. Liu Z, Wang Y, Wu B, Cui C, Guo Y, Yan C (2019) A critical review of fused deposition modeling 3D printing technology in manufacturing polylactic acid parts. *Int J Adv Manuf Technol* 102:2877–2889. <https://doi.org/10.1007/s00170-019-03332-x>
4. Jaisingh Sheoran A, Kumar H (2020) Fused Deposition modeling process parameters optimization and effect on mechanical properties and part quality: Review and reflection on present research. *Mater Today: Proc* 21:1659–1672. <https://doi.org/10.1016/j.matpr.2019.11.296>
5. Rahim TNAT, Abdullah AM, Akil HM (2019) Recent Developments in Fused Deposition Modeling-Based 3D Printing of Polymers and Their Composites. *Polym Rev* 59:589–624. <https://doi.org/10.1080/15583724.2019.1597883>
6. Beda T (2007) Modeling hyperelastic behavior of rubber: A novel invariant-based and a review of constitutive models. *J Polym Sci, Part B: Polym Phys* 45:1713–1732. <https://doi.org/10.1002/polb.20928>
7. Marckmann G, Verron E (2006) Comparison of hyperelastic models for rubber-like materials. *Rubber Chem Technol* 79:835–858. <https://doi.org/10.5254/1.3547969>
8. Dal H, Gültekin O, Açıkgöz K (2020) An extended eight-chain model for hyperelastic and finite viscoelastic response of rubberlike materials: Theory, experiments and numerical aspects. *J Mech Phys Solids* 145:104159. <https://doi.org/10.1016/j.jmps.2020.104159>
9. Mooney M (1940) A theory of large elastic deformation. *J Appl Phys* 11:582–592. <https://doi.org/10.1063/1.1712836>
10. Rivlin RS (1948) Large elastic deformations of isotropic materials IV. further developments of the general theory. *Phil Trans R Soc Lond A* 241:379–397. <https://doi.org/10.1098/rsta.1948.0024>
11. Treloar LRG (1943) The elasticity of a network of long-chain molecules—II. *Trans Faraday Soc* 39:241–246. <https://doi.org/10.1039/TF9433900241>
12. Valanis KC, Landel RF (1967) The strain-energy function of a hyperelastic material in terms of the extension ratios. *J Appl Phys* 38:2997–3002. <https://doi.org/10.1063/1.1710039>
13. Ogden RW, Hill R (1972) Large deformation isotropic elasticity—on the correlation of theory and experiment for incompressible rubberlike solids. *Proc R Soc Lond Math Phys Sci* 326:565–584. <https://doi.org/10.1098/rspa.1972.0026>
14. Kilian H-G (1981) Equation of state of real networks. *Polymer* 22:209–217. [https://doi.org/10.1016/0032-3861\(81\)90200-7](https://doi.org/10.1016/0032-3861(81)90200-7)
15. Kilian H-G, Enderle HF, Unseld K (1986) The use of the van der Waals model to elucidate universal aspects of structure-property relationships in simply extended dry and swollen rubbers. *Colloid & Polymer Sci* 264:866–876. <https://doi.org/10.1007/BF01410637>
16. Yeoh OH (1990) Characterization of elastic properties of carbon-black-filled rubber vulcanizates. *Rubber Chem Technol* 63:792–805. <https://doi.org/10.5254/1.3538289>
17. Arruda EM, Boyce MC (1993) A three-dimensional constitutive model for the large stretch behavior of rubber elastic materials. *J Mech Phys Solids* 41:389–412. [https://doi.org/10.1016/0022-5096\(93\)90013-6](https://doi.org/10.1016/0022-5096(93)90013-6)
18. Reppel T, Weinberg K (2018) Identification of hyper- and viscoelastic properties of different flexible FDM printed specimens. *Proc Appl Math Mech* 18. <https://doi.org/10.1002/pamm.201800382>
19. Markovitz H Boltzmann and the Beginnings of Linear Viscoelasticity| Kopernio. <https://kopernio.com/viewer?doi=10.1122%2F1.549444&token=WzE2MDE1ODksJjEwLjExMjlvMS41NDk0NDQiXQ.qXZt8MCPiE1eeRuZ2Zg1vZWf08Y>. Accessed 16 October 2020
20. Banks H, Hu S, Kenz Z (2011) A Brief Review of Elasticity and Viscoelasticity. *Adv Appl Math Mech* 3. <https://doi.org/10.4208/aamm.10-m1030>
21. Drapaca CS, Sivaloganathan S, Tenti G Nonlinear constitutive laws in viscoelasticity| Kopernio. https://kopernio.com/viewer?doi=10.1177%2F1081286506062450&token=WzE2MDE1ODksJjEwLjExNzcvMTA4MTI4NjUwNjA2MjQ1MCIjId._AmW8IxAy6fQ8QMkuPrH0KAU0Fk. Accessed 16 October 2020
22. Wineman A (2009) Nonlinear viscoelastic solids—A review. *Math Mech Solids* 14:300–366. <https://doi.org/10.1177/1081286509103660>

23. Christensen RM (1980) A nonlinear theory of viscoelasticity for application to elastomers. *J Appl Mech* 47:762–768. <https://doi.org/10.1115/1.3153787>
24. Hohimer C, Aliheidari N, Mo C, Ameli A (2017) Mechanical Behavior of 3D Printed Multiwalled Carbon Nanotube/Thermoplastic Polyurethane Nanocomposites. *Proceedings of the ASME Conference on Smart Materials, Adaptive Structures and Intelligent Systems*
25. Bi H, Ren Z, Guo R, Xu M, Song Y (2018) Fabrication of flexible wood flour/thermoplastic polyurethane elastomer composites using fused deposition molding. *Ind Crops Prod* 122:76–84. <https://doi.org/10.1016/j.indcrop.2018.05.059>
26. Fenner Inc. N (2019) Technical Specifications of NinjaFlex 3D printing filament
27. Fenner Inc. N (2018) Technical Specifications of Cheetah 3D printing filament
28. dddrop BV. (2020) Technical Datasheet for TPU Filament
29. Herzberger J, Sirrine JM, Williams CB, Long TE (2019) Polymer Design for 3D Printing Elastomers: Recent Advances in Structure, Properties, and Printing. *Prog Polym Sci*. <https://doi.org/10.1016/j.progpolymsci.2019.101144>
30. Chaudhry MS, Czekanski A (2020) Evaluating FDM Process Parameter Sensitive Mechanical Performance of Elastomers at Various Strain Rates of Loading. *Materials* 13:3202. <https://doi.org/10.3390/ma13143202>
31. Formfutura BV. (2016) Technical Datasheet for Flexifil Filament
32. E.I. du Pont de Nemours and Company (2017) DuPont™ Hytrel® 3D4000FL NC010 product information
33. Yarwindran M, Sa'aban NA, Ibrahim M, Periyasamy R (2016) Thermoplastic elastomer infill pattern impact on mechanical properties 3D printed customized orthotic insole. *ARPN Journal of Engineering and Applied Sciences*. 11:7
34. Banerjee SS, Burbine S, Kodihalli Shivaprakash N, Mead J (2019) 3D-Printable PP/SEBS Thermoplastic Elastomeric Blends: Preparation and Properties. *Polymers* 11:347. <https://doi.org/10.3390/polym11020347>
35. Kepenekci M, Özerinç S (2020) Unpublished work
36. Messimer P, O'Toole B, Trabia M (2020) Identification of the Mechanical Characteristics of 3D Printed NinjaFlex®. *American Society of Mechanical Engineers Digital Collection*
37. Miller AT, Safranski DL, Wood C, Guldborg RE, Gall K (2017) Deformation and fatigue of tough 3D printed elastomer scaffolds processed by fused deposition modeling and continuous liquid interface production. *J Mech Behav Biomed Mater* 75:1–13. <https://doi.org/10.1016/j.jmbbm.2017.06.038>
38. Bakır A, Özerinç S (2020) Unpublished work
39. Hohimer C, Christ J, Aliheidari N, Mo C, Ameli A (2017) 3D printed thermoplastic polyurethane with isotropic material properties. *Proceedings of SPIE Vol. 10165 Behavior and Mechanics of Multifunctional Materials and Composites 2017*
40. Popescu D, Zapciu A, Amza C, Baciu F, Marinescu R (2018) FDM process parameters influence over the mechanical properties of polymer specimens: A review. *Polym Testing* 69:157–166. <https://doi.org/10.1016/j.polymertesting.2018.05.020>
41. Bakır AA, Atik R, Özerinç S (2021) Effect of fused deposition modeling process parameters on the mechanical properties of recycled polyethylene terephthalate parts. *J Appl Polym Sci* 138:49709. <https://doi.org/10.1002/app.49709>
42. Kaygusuz B, Özerinç S (2019) Improving the ductility of polylactic acid parts produced by fused deposition modeling through polyhydroxyalkanoate additions. *J Appl Polym Sci* 136:48154. <https://doi.org/10.1002/app.48154>
43. Ahn S, Montero M, Odell D, Roundy S, Wright PK (2002) Anisotropic material properties of fused deposition modeling ABS. *Rapid Prototyp J* 8:248–257. <https://doi.org/10.1108/13552540210441166>
44. Bellehumeur C, Li L, Sun Q, Gu P (2004) Modeling of Bond Formation Between Polymer Filaments in the Fused Deposition Modeling Process. *J Manuf Process* 6:170–178. [https://doi.org/10.1016/S1526-6125\(04\)70071-7](https://doi.org/10.1016/S1526-6125(04)70071-7)
45. Bakır AA, Atik R, Özerinç S (2020) Mechanical Properties of Thermoplastic Parts Produced by Fused Deposition Modeling: A Review. *Rapid Prototyp J*

46. Baich L, Manogharan G, Marie H (2015) Study of infill print design on production cost-time of 3D printed ABS parts. *Int J Rapid Manuf* 5:308–319. <https://doi.org/10.1504/IJRAPIDM.2015.074809>
47. Tumbleston JR, Shirvanyants D, Ermoshkin N, Januszewicz R, Johnson AR, Kelly D, Chen K, Pinschmidt R, Rolland JP, Ermoshkin A, Samulski ET, DeSimone JM (2015) Continuous liquid interface production of 3D objects. *Science* 347:1349–1352. <https://doi.org/10.1126/science.aaa2397>
48. Gibson IJ, Ashby MF (1982) The mechanics of three-dimensional cellular materials. *Proc R Soc Lond Math Phys Sci* 382:43–59. <https://doi.org/10.1098/rspa.1982.0088>
49. Bakır AA, Atik R, Özerinç S Effect of fused deposition modeling process parameters on the mechanical properties of recycled polyethylene terephthalate parts. *J Appl Polym Sci*. <https://doi.org/10.1002/app.49709>
50. Bokobza L (2007) Multiwall carbon nanotube elastomeric composites: A review. *Polymer* 48:4907–4920. <https://doi.org/10.1016/j.polymer.2007.06.046>
51. Mangaraj D (2002) Elastomer Blends. *Rubber Chem Technol* 75:365–427. <https://doi.org/10.5254/1.3547677>

Mechanical Characterization of Fused Deposition Modeling (FDM) 3D Printed Parts



Davood Rahmatabadi¹, Ahmad Aminzadeh²,
Mohammad Aberoumand, and Mahmoud Moradi³

Abstract The objective of this chapter presents the mechanical characterization of fused deposition modeling (FDM) as a famous and the most used technology in 3D printing or rapid prototyping process. The availability and cheapness of raw materials and the simplicity of these types of printers have led to their widespread use for various applications. In contrast, there are challenges in this method, like other methods of additive manufacturing (AM), one of the most important of which is the selection of print parameters and its impact on mechanical properties significantly. In this chapter, three subject are discussed; thermoplastic filament used, introduction of printing parameters and the impact of them on mechanical properties. Due to the widespread use of various thermoplastic filament as raw materials for FDM printers, the most widely used ones are introduced. Then the strong impact of the FDM printing parameters on the mechanical properties of produced specimens is fully explored as the main topic of this chapter.

D. Rahmatabadi · M. Aberoumand
School of Mechanical Engineering, University of Tehran, Tehran, Iran
e-mail: d.rahmatabadi@ut.ac.ir

M. Aberoumand
e-mail: m.aberoumand@ut.ac.ir

A. Aminzadeh
Department of Mathematics, Computer Science and Engineering,
Université du Québec à Rimouski, Rimouski, Québec, Canada
e-mail: ahmad.aminzadeh@uqar.ca

M. Moradi (✉)
School of Mechanical, Aerospace and Automotive Engineering, Faculty of Engineering,
Environment and Computing, Coventry University, Gulson Road, Coventry CV1 2JH, UK
e-mail: moradi@malayeru.ac.ir; moradi.malayeru@gmail.com

Department of Mechanical Engineering, Faculty of Engineering, Malayer University,
Malayer, Iran

1 Introduction

The term of Additive manufacturing (AM) or 3D printing is defined as the novel technology used to generate the 3D/4D parts with the help of layer-upon-layer addition of various types of materials such as polymers, metals, ceramics, and composites [1]. In other words, as one of the most famous and common techniques in the third industrial revolution. Also, AM is perfect for complex forms of fabrication and mass production that could not be manufactured via a conventional manufacturing process and it is sharply utilized in industry applications such as aerospace, automotive, and custom-made production in biomechanics science. Consequently, designers and manufacturing units must define and understand material characterization and mechanical loads. Based on ISO/ASTM standards and literature [2] AM techniques are generally categorized as: directed energy deposition (LENS) [3], material jetting (Objet) [4], vat polymerization (SLA) [5], binder jetting (3DP) [6], material extrusion (ME/FDM) [7], sheet lamination (LOM) [8], and powder bed fusion (SLM/SLS) [9]. Among all AM technics, fused filament fabrication (FFF) or fused deposit melting (FDM) is the most common method that applies in engineering and manufacturing units. Due to the process condition, FFF/FDM is a quite complicated and highly flexible process with several factors, as well as a limitation that affects mechanical and quality-related properties. The main advantage of FDM technology is the effective mechanical properties of resulting parts manufactured using this method and the range of materials. In other words, among all polymer-based additive manufacturing processes, FDM parts have the strongest mechanical property. In contrast, the major drawback of using this technology is the build speed [10]. To this end, it is necessary to explore and define the mechanical properties and behavior of FDM for different categories of materials and sets of process parameters/manufacturing conditions. Figure 1 show the process scheme and the most advantages and disadvantages of FDM process are demonstrated in Fig. 2. There are three main steps in the physics of the FDM process, and this chapter will describe the basic perspective of material characterization and mechanical properties of the FDM process.

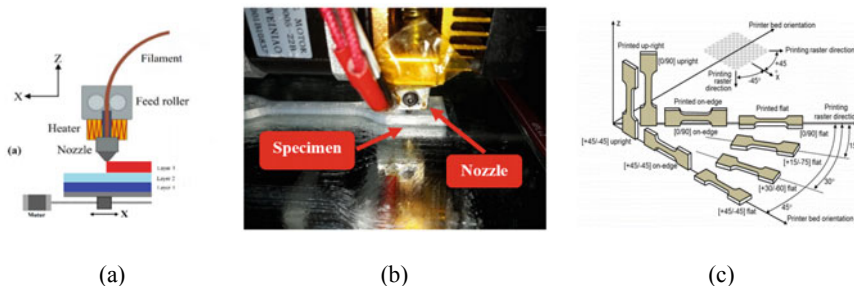


Fig. 1 FDM process (a) The scheme of FEM process (b) FDM printing machine and (c) Graphic representation of the printer bed orientations [11]

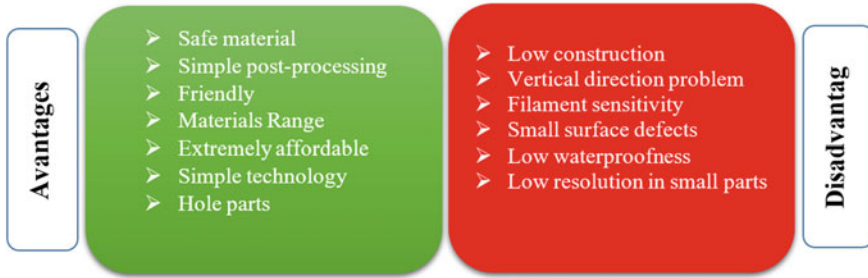


Fig. 2 Advantage and disadvantage of FDM process

- First, when the nozzle has received the desired temperature by the sensors, the filament is fed to the extrusion head and in the nozzle.
- Second, the melted material is deposited layer-by-layer in bed location, where it cools and solidifies.
- Third, once a layer is created, the build platform moves down, and a new layer is deposited.

The challenge of achieving best mechanical properties is the main subject of researches in this field, which aims to determine and set the printing parameters to get high speed, high quality, mechanical properties and surface roughness and low cost. Due to the strong dependence of printing parameters on mechanical properties, predicting it is not an easy task and has always been done experimentally and in previous researches the effect of these parameters on mechanical properties has been investigated. The most important of these parameters can be raster angle [12–18], orientation [12–16, 18], layer thickness [15, 17–19], pattern [20], density [15, 16] and etc. [14, 17]. Therefore, the main focus of this chapter is on investigating the effect of print parameters on mechanical properties during FDM process.

2 Filament Materials

In the FDM process, the thermoplastic material used by printers comes in the form of a plastic filament that passes through a nozzle. Thermoplastics are flexible and formable and easily molded. To the best of the author's knowledge, thermoplastics are easily molded and formed if exposed to heat, but it will melt if exposed to high temperatures. For this reason, these materials are used in printers. In addition, low density, recyclability, low price, a wide range of properties, high ductility are the most important advantages of these materials. Thermoplastics are classified based on chemical composition, crystallinity percentage, transition and melting temperatures. As most of these materials have a low percentage of crystallinity and one of the most essential parameters on their mechanical properties and operating

temperature is the amount of crystallinity. For this purpose, they are classified into two categories: semi-crystalline and amorphous. The elasticity due to the amorphous regions and the ability to be vital come from the crystalline regions to the material. Note that if the temperature is above the melting point, the crystalline regions will disappear. In fact, one of the most critical factors affecting the mechanical, metallurgical, and physical properties, as well as surface quality, is the filament material properties. Based on applications, there are a wide of filaments as briefly describe bellow. Filaments are usually sold in spools and generally provided by the machine manufacturers, even though there are more and more generic filament manufacturers. Currently, there is a wide variety in filament material. However, the most common FDM materials are the acrylonitrile butadiene styrene (ABS) and poly lactic acid (PLA) since they are the ones applied in the most elementary 3D printers they are also the most rationally priced.

3 Printing Parameters in FDM

The dependence of the properties of the final part on the printing parameters in FDM process is very high and each of these parameters can lead to a wide range of mechanical properties, surface roughness, consumption volume and manufacturing time. Therefore, recognizing the printing parameters to examine how they affect the final features is the first step to achieve the desired properties. Printing parameters are usually divided into three categories, which are the extruder parameters, which is actually the geometry of the extruder. The second category is processing parameters that; in fact, it can be said that there are parameters that are determined by the device and the consumable material. The third category of parameters, which are called structural, and in fact, due to the lack of limitations and applicability for all materials, have a wide range that strongly affects the properties of the final part. In this section, all three categories of parameters are explained.

3.1 Extruder Geometry

As the name implies, this parameter is the geometry of the extruder, in this section, changing the input parameters is not easy. The two main parameters that fall into this category are the nozzle diameter and its width. The nozzle diameter (the diameter of the extruder nozzle) are usually considered constant and many types of research have not been discussed in this field and, by default, for most FDM printers, nozzle diameter of 0.4 mm is used. However, it has a great effect on mechanical properties, surface smoothness and manufacturing time, and usually for complex parts the nozzle diameter less than 0.4 mm and for larger parts to reduce printing time, nozzles with a diameter greater than 0.4 mm are used.

3.2 Processing Parameters

Processing parameters usually are selected based on the materials and type of printer. Nozzle and bed temperatures, printing and retraction speeds are included in this category. For example, most polymers that have good adhesion use lower bed temperatures, and higher temperatures are usually used for better adhesion of the first layer. The nozzle temperature usually depends on the melting temperature of the used filament and usually affects the fluidity, adhesion of layers, increase the density of the material and reduce cavities.

3.3 Structural Parameters

Two basic features of printing methods are layer-by-layer fabrication and porous production capability, which are the main reason for the emergence of structural parameters. The third category of printing parameters is structural parameters, which is more extensive than the other two categories and have no restrictions on the use of different materials. Figure 3, structural printing parameters are presented. In the following, each of them is introduced in detail.

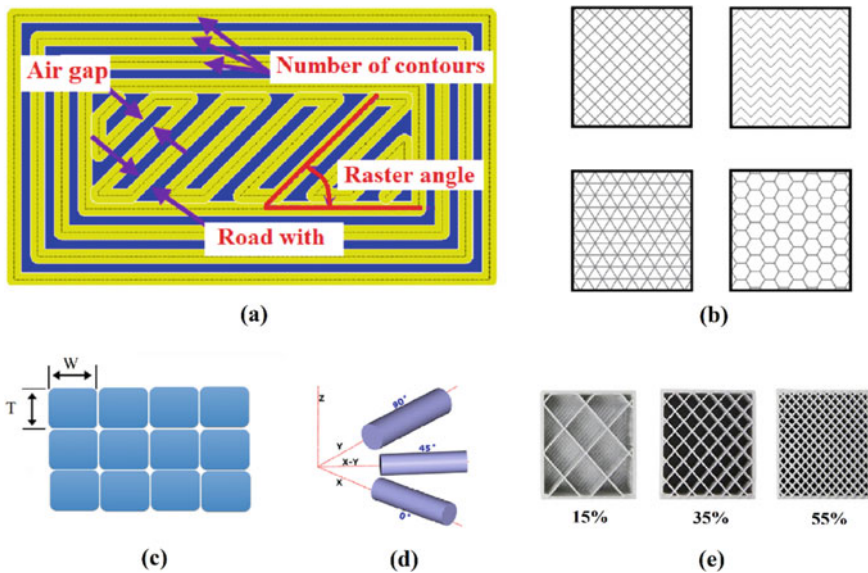


Fig. 3 Structural printing parameters for FDM process: (a) raster angle and air gap (b) infill pattern (c) number of contour (d) build orientation and (e) infill percentage

3.3.1 Orientation

The first parameter of this category is the build direction or orientation. For each sample produced by the FDM method, there are at least three different positions depending on the slicing and printing angle in terms of length, width and height of the sample. As mentioned, based on the sample geometry, production time and the desired mechanical properties, the sample can be sliced in all three dimensions and the layer layout can be applied in the selected direction. Usually, for samples with simple geometry where mechanical properties are not a priority in the direction in which most material is used in one layer, the part is cut and printed. Thus, print time is increased because the number of layers is dramatically increased, and as the number of layers decreases, the printing time also decreases.

3.3.2 Raster Angle

The raster angle means the nozzle movement angle for printing each layer on top of each other relative to applied force direction. Raster angle has a significant role in the mechanical properties and anisotropy of FDM printed parts, and by changing it, the strength, toughness or failure mechanism can be controlled and adjusted according to the intended purpose [21]. Fixed and alternating raster angles, as the most common and widely used, are included in all FDM printers. A fixed raster angle or unidirectional raster angle can vary between 0 and 90 degrees. In the second category, the layer up was done alternately with 90 degrees' change compared to the previous layer and is present by default in most FDM printers. The most commonly used are 0/90 and 30/-60, and 45/-45.

3.3.3 Layer Thickness

Layer thickness is the height of each print layer, and in the first, the upper and inner layers are defined in the FDM process. This parameter is strongly influenced by the nozzle diameter, and the nozzle diameter affects the layers and walls thickness; and it is recommended that the thickness of the layers be considered to be a maximum of 80% of the nozzle diameter and the best suggestion is half nozzle diameters.

3.3.4 Infill Density, Infill Pattern and Air Gap

One of the advantages and necessities of 3D printing is that the parts can be hollow in different degrees. From a production point of view, this not only reduces material consumption and costs but also reduces the final weight of the body (it will also save time). Different section of FDM part are included peripheral walls or shell, top and bottom layers, and infill each of which can be adjusted separately due to its effect on mechanical and physical properties. According to the mechanical

properties and the priorities of the final part, the percentage of filling is determined, the other three sections are always considered as solid, and only the thickness of each is determined by a factor of the layer thickness. The Fig. 4 shows four examples of available infill patterning in all software. According to the print direction of the fibers in relation to the loading direction and adhesion between the layers as well as the fibers, the effect of the printing pattern on the mechanical properties is determined. To optimize this process, most parts are printed with solid shells and filled with a certain percentage of material. Also, air gap as another effective parameter is the empty space between the fibers and is somewhat opposite to overlap. This parameter is mostly used for simple geometries.

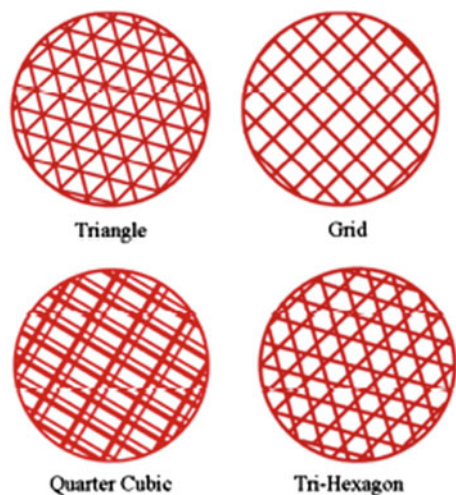
3.3.5 Printing Speed

The printing speed of the layers affects the thermal cycle of each layer, and by increasing the printing speed, the time required to arrange the next layer decreases. Increasing the printing speed reduces the cooling rate because the next layer will be printed (high temperature) on it in less time, and through this, it can affect the mechanical properties.

4 Mechanical Properties

This section presents the effect of print parameters on mechanical properties. Mechanical properties are the results of tensile, flexural, compressive, and fatigue tests, from which the mechanical properties of the material, including tensile

Fig. 4 Different infill pattern in FDM software [22]



strength, yield strength, compressive strength, fatigue life, elongation, strain energy toughness, are derived. Table 1 attempts to present a number of recent studies by using materials, variable printing parameters, and outputs. Because some of the print parameters have the same or reciprocal effects on the mechanical properties, both or three parameters are considered as a group. After presenting the effect of printing parameters individually or in groups and analyzing each parameter, the last researches are reported on a case-by-case basis.

4.1 Nozzle Diameter and Layer Thickness

The effect of nozzle diameter and layer thickness on mechanical properties, surface smoothness, fabrication time and consumables is almost a trend. For this reason, these two parameters are examined together. The two main challenges in the final part of the FDM process are surface smoothness (stair-stepping) that the nozzle diameter and layer thickness have the most impact on it and with decreasing the nozzle diameter and layer thickness, this defect is less visible. Yang et al. investigated the effect of nozzle diameter on mechanical properties, surface roughness and fabrication time investigated. It was reported that by changing the nozzle diameter from 0.2 to 0.6 mm, the tensile strength improved by 19%, and the production time was reduced from 3.81 to 1.30 h, but on the opposite side, the surface roughness quality decreased by 108% [33].

4.2 Orientation and Raster Angle

Raster angle has a great role in the mechanical properties and anisotropy of FDM printed parts. By changing it, the strength, toughness, or failure mechanism can be controlled and adjusted according to the intended purpose [21]. Figures 5, 6, and 7 show the dependence of mechanical properties and failure mechanisms on the raster angle [21]. The results of most researches for different materials printed with FDM show the same trend of the effect of raster angle on mechanical properties, which is obtained the highest and the lowest at angles of 0 and 90 degrees, respectively, and for the middle raster angles (0–90), as the angle increases, the strength gradually decreases [21].

Higher-strength is usually obtained at the raster angle in the same direction as loading, and alternating the print angle allows achievement control strength, elongation, and toughness. For example, the higher elongation value for the FDM printed specimen is obtained at lower raster angles relative to the applied force due to the change of fiber direction towards the loading direction. In other words, when the relative angle between the arrangement of the fibers and the loading is not horizontal or vertical, the fibers first try to rotate perpendicular to the loading direction, and with that, the number of elongation increases. Interestingly, in the

Table 1 Investigations focused on the effect of printing parameters on the mechanical properties

Material	First author	Inputs	Levels	Outputs	References
ABS	Ahn	Air Gap (mm) Raster width (mm) Nozzle temperature (°C) Orientation (°)	0, -0.0508, 0.508, 1, 270, 280, 0, 90	Tensile strength Compressive strength	[16]
ABS	Samykano	Layer thickness (mm) Raster angle (°) Infill density	0.35, 0.4, 0.5 45, 55, 65 40, 60, 80	Tensile strength Yield strength Elongation	[23]
ABS	Chin Ang	Air gap (mm) Raster width (mm) Orientation (°)	0, 1.27 0.305, 0.98 0, 90	Yield strength Compressive strength Porosity	[24]
ABS	Rayegani	Orientation (°) Air gap (mm) Raster angle (°) Raster width (mm)	0, 90 -0.0025, 0.5588 0, 45 0.2034, 0.5588	Tensile strength	[25]
ABS	Sood	Layer thickness (mm) Orientation (°) Air gap (mm) Raster angle (°) Raster width (mm)	0.1270, 0.1780, 0.2540 0, 15, 30 0, 0.0040, 0.0080 0, 30, 60 0.4064, 0.4564, 0.5064	Tensile strength Impact strength Flexural strength	[26]
ABS	Domingo-Espin	Printing speed (mm/s) Layer thickness (mm) Infill density (%) Nozzle diameter (mm) Infill pattern	25, 30, 35 0.1, 0.2, 0.3 25, 50, 75 0.3, 0.4, 0.5 Rectilinear, Honeycomb	Fractography Fatigue properties	[27]
ABS	Percoco	Raster angle (°) Raster width (mm)	0, 30, 60 0.404, 0.479, 0.554	Compressive strength	[28]

(continued)

Table 1 (continued)

Material	First author	Inputs	Levels	Outputs	References
ABS/Cu	Nabipour	Nozzle temperature (°C) Raster angle (°) Nozzle diameter (mm) Layer thickness (mm)	230, 240, 250 +45/-45, 0/90, 30/60 0.5, 1, 1.5 0.1, 0.2, 0.3	Build time Tensile strength Density	[29]
PLA	Afrose	Orientation (°)	0, 45, 90	Tensile strength Fatigue life Strain energy	[13]
PLA	Moradi	Nozzle temperature (°C) Infill density (%) Layer thickness (mm)	190, 200, 210, 220, 230 10, 20, 30, 40, 50 0.1, 0.15, 0.2, 0.25, 0.3	Tensile strength Density Build time Elongation	[30]
PLA	Deshwal	Nozzle temperature (°C) Infill density (%) Printing speed (mm/s)	190, 210 20, 100 50, 150	Tensile strength	[31]
PLA	Akhoundi	Nozzle temperature (°C)	210, 220, 230, 240, 250	Tensile strength Tensile modulus	[32]
PLA	Aloyaydi	Infill pattern	Grid, Triangular, Quarter cubic, Tri-Hexagonal	Impact strength Compressive strength	[22]
PLA	Yang	Nozzle temperature (°C) Printing speed (mm/s) Nozzle diameter (mm) Layer thickness (mm)	200, 215, 230 20, 30, 40 0.2, 0.4, 0.6 0.1, 0.2, 0.3	Build time Tensile strength Surface roughness	[33]
Bronze PLA	Moradi	Nozzle temperature (°C) Infill density (%) Layer thickness (mm)	190, 205, 220, 235, 250 15, 25, 35, 45, 55 0.15, 0.25, 0.35, 0.45, 0.55	Tensile strength Density Build time Elongation Fracture mechanism	[34]

(continued)

Table 1 (continued)

Material	First author	Inputs	Levels	Outputs	References
PEEK	Wang	Nozzle diameter (mm) Nozzle temperature (°C) Layer thickness (mm)	0.4, 0.6, 0.8 360, 380, 400, 420, 440, 460 0.25, 0.3, 0.35, 0.4	Tensile strength Surface roughness Density	[35]
PEEK	Wu	Layer thickness (mm) Raster angle (°)	0.2, 0.3, 0.4 0, 30, 45	Tensile strength Flexural strength Compressive strength	[18]
PEEK	Ding	Nozzle temperature (°C) Orientation (°)	360, 370, 380, 390, 400, 410, 420 0, 90	Density Flexural strength Tensile strength Elongation	[36]
PEEK	Ei Magri	Nozzle temperature (°C) Printing speed (mm/s)	380, 390, 400, 410, 420 20, 30, 40	Tensile strength Elongation	[37]
PEI	Ding	Nozzle temperature (°C) Orientation (°)	360, 370, 380, 390, 400, 410, 420 0, 90	Density Flexural strength Tensile strength Elongation	[36]
PETG	Srinivasan	Infill density (%)	20, 30, 40, 50, 60, 70, 80, 90, 100	Tensile strength Surface roughness Flexural strength	[38]
Nylon	Kamoona	Air gap (mm) Raster angle (°) Orientation (°)	0, 0.1, 0.2 0, 30, 60 0, 45, 90	Flexural strength	[39]

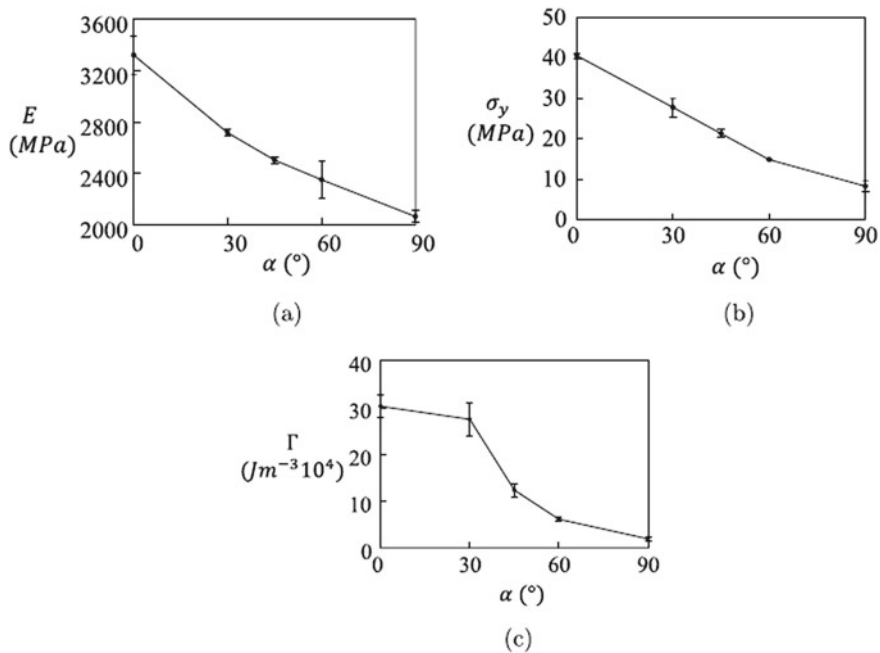


Fig. 5 Changes in mechanical properties in terms of raster angle [21]

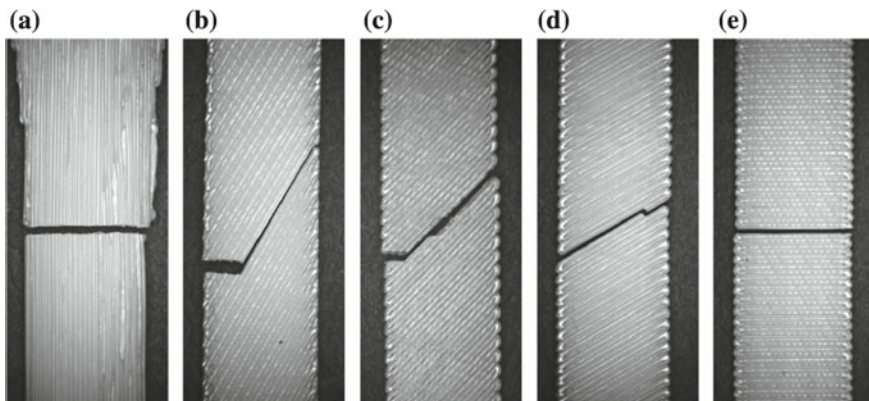


Fig. 6 Failure mechanism for unidirectional or fixed raster angle at different angle: (a) 0° (b) 3° (c) 45° (d) 60° and (e) 90° [21]

unidirectional raster angle, this amount of growth is limited because the separation of fiber through all the layers causes a sudden fracture. In the alternating arrangement of the layers, it is possible to achieve more rotation of the fibers and prevent premature failure, and it is possible to achieve a more excellent elongation.

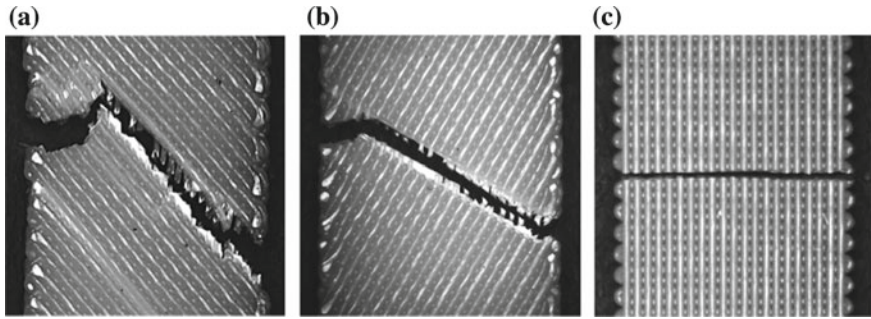


Fig. 7 Failure mechanism for altering raster angle at different angle (a) $[45^\circ/-45^\circ]$ (b) $[30^\circ/-60^\circ]$ and (c) $[0^\circ/90^\circ]$ [21]

In addition to these two general categories (unidirectional and altering raster angles), there are various other modes for how the layers are arranged, and in general, different properties can be used to control the mechanical properties and the failure mechanism. Both orientation and raster angle parameters are very influential on mechanical properties and when the direction of applied force and stress is perpendicular to the direction of the nozzle movement, the minimum amount of strength is obtained because in this case, the most stress is applied to the bonds that form the layers. Also, this mode can be adjusted and controlled by manipulating both orientation and raster angle parameters in FDM process, and it should be noted that the effect of orientation on mechanical properties is much greater than the raster angle.

Afrose et al. [13] investigated the effect of build orientation on the tensile strength and fatigue properties. They used PLA filament, and all standard samples were printed in the three build directions of 00, 450, and 900, and after applying the tensile test, the fatigue assessed at four levels of UTS (50–80% of UTS). As expected, tensile strength was maximized at build direction of 0° , but, fatigue life was maximized at build direction of 45° at all levels of cyclic loading. Also, they calculated absorbed strain energy during the cyclic test and concluded that the trend of strain energy was similar to the number of the life cycle, and the highest value was achieved in the orientation of 450.

In the other attempt, Ziemian et al. [40, 41] conducted that, by selecting the raster aligned along the longest dimension, the highest tensile strength was achieved. Also, they investigated the flexural strength and found for the 0° fiber orientation, $+45^\circ/-45^\circ$, and 90° orientations that the ultimate strength value was highest. Based on the literature [42–44], the raster angle plays an important role in anisotropy, and in fact, the presence of a printing angle causes anisotropy, and another challenge of the FDM method is the existence of severe anisotropy in the parts produced with it. In this regard, the raster angle is one of the most critical parameters deal with the strength of FDM parts. Once the raster angle was set on 0° , both stiffness and strength were reported at the highest level. However, stiffness and strength gradually decreased by increasing the raster angle. In order to achieve the

increased strength in ABS [45, 46] and PLA [47] materials, raster width and the layer thickness should be minimal.

As mentioned in the previous discussions, printing parameters are very influential on the failure mechanism during the tensile test and by changing the mechanism and the failure process, it affects the mechanical properties. Due to the effect of printing parameters such as build orientation, raster angle, pattern, nozzle temperature, etc. on the bonding, in all printed parts by FDM, complex mechanisms are governed. There are two main failure mechanisms, one is a rupture in the fibers, and the other is the separation or debonding in the fibers [21, 48] and according to the strength of each of the two, the mechanical properties depend on it. Figure 8 shows the failure mechanism in the two cases mentioned. In Fig. 8a, the direction of applied force and fibers is the same, or in other words, the filling angle is zero degrees, and failure occurs when the fibers rupture, but in Fig. 8b, the direction of applied force and fiber interfaces is the same, and the crack growth starts from the interfaces. Most of the time, due to the higher strength of the fibers than the bonding between them, failure begins at the interfaces between the layers [18, 27]. By changing the build direction or raster angle, the direction of stress concentration can be easily adjusted so that the applied force is in the direction of the fibers, and in the case of the first mechanism, more strength is obtained. This is why the fibers show the greatest strength when the fibers are in the direction of applied forces [25]. In the second mechanism, it occurs when the direction of the fibers is perpendicular to the direction of the applied force, or in other words, the direction of the applied force is in line with the interfaces of fibers. In this case, usually, the minimum amount of strength is obtained, and the stress concentration is on the bonding interfaces. In this case, by changing other parameters such as increasing the nozzle temperature to increase fluidity, heat treatment after printing to improve the quality of the interfaces bonding between fibers, increase the width of the fibers to increase the overlap of the fibers to boost the bonding between fibers. To increase strength without changing the direction of construction. The third state of the failure mechanism occurs when the fiber angles relative to applied forces are not 0 and 90 degrees, in which case, with the rotation of the fibers to one of these angles, the failure mechanism is a combination of the two fundamental mechanisms. In Fig. 9, the third case of the failure mechanism is quite clear. In this figure, tensile

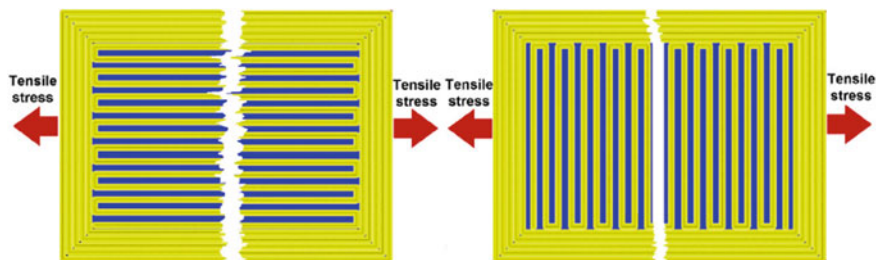


Fig. 8 Fracture mechanism for raster angle of 0° and 90° [48]

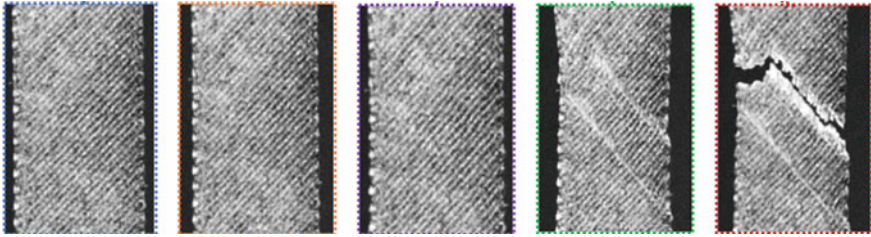


Fig. 9 Tensile specimens at different strain levels [21]

specimens are presented at different strain levels which with increasing force, the fibers try to rotate and be in the direction of applying force, and on the other hand, failure in the interfaces causes another failure mechanism, and as seen in Fig. 9, after failure, some of the fibers are in the direction of applying force, which increases the toughness and elongation. The degree of rotation of the fibers can lead to delayed failure, increased toughness, and elongation.

4.3 Infill Patterning and Density

Infill density has a great effect on mechanical properties and surface, and as it is known, with increasing infill density, the empty space decreases, and an increase in strength and density and a decrease in surface roughness are obtained [38]. A comprehensive study of the effect of infill density on tensile strength and surface roughness for PETG was performed, and the results of their work showed that increasing the density increases the strength and improves the surface roughness, but in return, increases the time and cost [38].

One of the advantages and necessities of 3D printing is that the parts can be hollow in different degrees. From a production point of view, this not only reduces material consumption and costs but also reduces the final weight of the body (it will also save time). According to the print direction of the fibers in relation to the loading direction and adhesion between the layers and the fibers, the effect of the printing pattern on the mechanical properties is determined. In this regard, the cross-section of the printed PLA sample with different patterns, and the image shows the raster, cavities, and adhesions between the layers is illustrated in Fig. 10. The grid pattern is a specific two-dimensional pattern, and its most important advantage over other patterns is its simplicity and less time. The second pattern is triangular, which is a two-dimensional grid made of triangles, and its main advantage is that when a vertical force is applied to the surface of the object, this pattern shows high resistance. This pattern is also suitable for thin rectangular pieces because there is little contact between the walls in these objects.

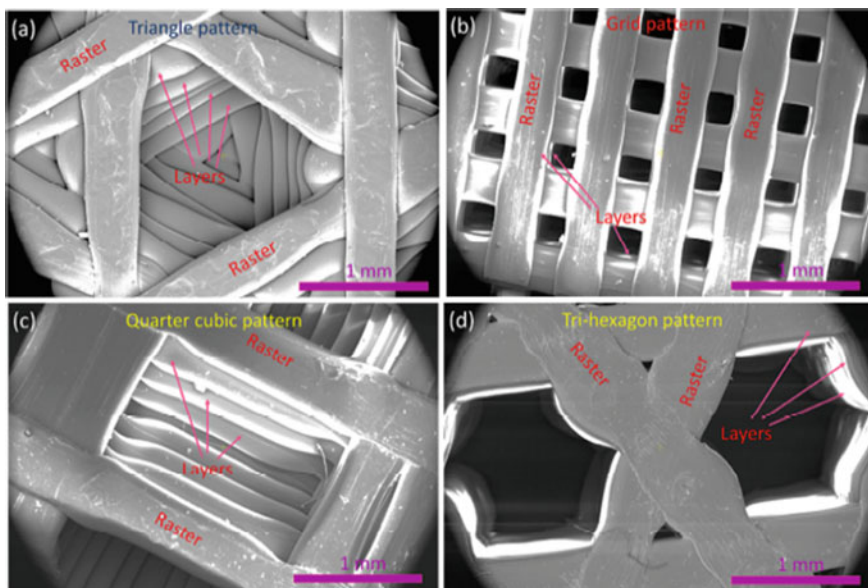


Fig. 10 SEM images of different infill pattern: (a) triangle (b) grid (c) quarter cubic and (d) tri-hexagon pattern [22]

4.4 Nozzle Temperature

Another essential parameter is the nozzle temperature, which affects the mechanical properties by affecting the solidification of the layers, fluidity, and velocity. As the nozzle temperature increases, due to the higher energy level, more crystallinity is reported, and the peak of cold recrystallization appears. Also, increasing the nozzle temperature causes better fluidity in the arrangement of the layers and increases the relative density by reducing the air pores. Relative density is usually used as a basic criterion for evaluating the print quality and printability of polymers in the FDM process [36]. Ding et al. concluded that by raising the nozzle temperature for PEEK and PEI, the relative density and flexural strength increased gradually [36]. Akhouni et al. have found that by raising the nozzle temperature from 210–250 °C for PLA, the tensile strength and elastic modulus increased because the bonding between the layers and fibers was boosted [32].

5 Conclusion

In this chapter, the main goal was to try comprehensively introduce the FDM printing parameters and study the effect of the significant parameters on the mechanical properties in detail. Highlighted results can be summarized as follows:

1. Despite the simplicity and cheapness of the FDM process, the challenge of material preparation, achieving mechanical properties, adjusting printing parameters and considering their interaction complicates this process. Other factors such as anisotropy, surface smoothness, fabrication time, and volume of consumables should be considered as the main challenges of this process for selecting and adjusting parameters.
2. ABS and PLA are two popular materials in this method, and due to the need of different industries for better properties, more and more materials are being marketed with different reinforcements, which multiplies the identification of print parameters.
3. The raster angle and orientation were recognized as the two main printing parameters on the mechanical properties, by adjusting it, the desired mechanical properties can be achieved, and almost the failure mechanism changes drastically with these two parameters.
4. Decreasing the layer thickness, increasing the relative density and increasing the temperature significantly increase the mechanical properties because of improving fluidity to reduce cavities.

References

1. Abedi HR, Hanzaki AZ, Azami M et al (2019) The high temperature flow behavior of additively manufactured Inconel 625 superalloy. *Mater Res Express* 6:116514. <https://doi.org/10.1088/2053-1591/ab44f6>
2. Vyavahare S, Teraiya S, Panghal D, Kumar S (2020) Fused deposition modelling: a review. *Rapid Prototyp. J.* 26:176–201
3. Dávila JL, Neto PI, Noritomi PY, et al (2020) Hybrid manufacturing: a review of the synergy between directed energy deposition and subtractive processes. *Int J Adv Manuf Technol*, 1–14
4. O'Reilly M, Hoff M, Friedman SD et al (2020) Simulating tissues with 3D-printed and castable materials. *J Digit Imaging* 1–12:1280–1291. <https://doi.org/10.1007/s10278-020-00358-6>
5. Brighenti R, Cosma MP, Marsavina L et al (2020) Laser-based additively manufactured polymers: a review on processes and mechanical models. *J Mater Sci.* <https://doi.org/10.1007/s10853-020-05254-6>
6. Yadav P, Fu Z, Knorr M, Travitzky N (2020) Binder Jetting 3D Printing of Titanium Aluminides Based Materials: A Feasibility Study 22. <https://doi.org/10.1002/adem.202000408>
7. Wiese M, Thiede S, Herrmann C (2020) Rapid manufacturing of automotive polymer series parts: A systematic review of processes, materials and challenges. *Addit. Manuf.* 36:101582

8. Gupta R, Dalakoti M, Narasimhulu A (2020) A critical review of process parameters in laminated object manufacturing process. In: *Advances in materials Engineering and Manufacturing Processes*. Springer, pp 31–39
9. MP (2020) Additive manufacturing of Tungsten Carbide hardmetal parts by selective laser melting (SLM), selective laser sintering (SLS) and binder jet 3D printing (BJ3DP) techniques. *Lasers Manuf Mater Process*. 7:338–371
10. Gibson I, Rosen D, Stucker B, et al (2015) Applications for Additive Manufacture. In: *Additive Manufacturing Technologies*. Springer, pp 451–474
11. Rohde S, Cantrell J, Jerez A et al (2018) Experimental characterization of the shear properties of 3D-printed ABS and polycarbonate parts. *Exp Mech* 58:871–884. <https://doi.org/10.1007/s11340-017-0343-6>
12. Cantrell JT, Rohde S, Damiani D et al (2017) Experimental characterization of the mechanical properties of 3D-printed ABS and polycarbonate parts. *Rapid Prototyp J* 23:811–824. <https://doi.org/10.1108/RPJ-03-2016-0042>
13. Afrose MF, Masood SH, Iovenitti P, et al (2016) Effects of part build orientations on fatigue behaviour of FDM-processed PLA material. *Prog Addit Manuf* 1:21–28. <https://doi.org/10.1007/s40964-015-0002-3>
14. Torrado AR, Roberson DA (2016) Failure analysis and anisotropy evaluation of 3D-printed tensile test specimens of different geometries and print raster patterns. *J Fail Anal Prev* 16:154–164. <https://doi.org/10.1007/s11668-016-0067-4>
15. Melenka GW, Schofield JS, Dawson MR, Carey JP (2015) Evaluation of dimensional accuracy and material properties of the MakerBot 3D desktop printer. *Rapid Prototyp J* 21:618–627. <https://doi.org/10.1108/RPJ-09-2013-0093>
16. Ahn S-HH, Montero M, Odell D, et al (2002) Anisotropic material properties of fused deposition modeling ABS 8:248–257. <https://doi.org/10.1108/13552540210441166>
17. Domingo-Espin M, Borros S, Agullo N, et al (2014) Influence of Building Parameters on the Dynamic Mechanical Properties of Polycarbonate Fused Deposition Modeling Parts. *3D Print Addit Manuf* 1:70–77. <https://doi.org/10.1089/3dp.2013.0007>
18. Wu W, Geng P, Li G et al (2015) Influence of layer thickness and raster angle on the mechanical properties of 3D-printed PEEK and a comparative mechanical study between PEEK and ABS. *Mat (Basel)* 8:5834–5846. <https://doi.org/10.3390/ma8095271>
19. Chacón JM, Caminero MA, García-Plaza E, Núñez PJ (2017) Additive manufacturing of PLA structures using fused deposition modelling: Effect of process parameters on mechanical properties and their optimal selection. *Mater Des* 124:143–157. <https://doi.org/10.1016/j.matdes.2017.03.065>
20. Smith WC, Dean RW (2013) Structural characteristics of fused deposition modeling polycarbonate material. *Polym Test* 32:1306–1312. <https://doi.org/10.1016/j.polymertesting.2013.07.014>
21. Kiendl J, Gao C (2020) Controlling toughness and strength of FDM 3D-printed PLA components through the raster layout. *Compos Part B Eng* 180:107562. <https://doi.org/10.1016/j.compositesb.2019.107562>
22. Aloyaydi B, Sivasankaran S, Mustafa A (2020) Investigation of infill-patterns on mechanical response of 3D printed poly-lactic-acid. *Polym Test* 87:106557. <https://doi.org/10.1016/j.polymertesting.2020.106557>
23. Samykano M, Kanagaraj G, Selvamani SK et al (2019) Mechanical property of FDM printed ABS: influence of printing parameters. *Int J Adv Manuf Technol* 102:2779–2796. <https://doi.org/10.1007/s00170-019-03313-0>
24. Ang KC, Leong KF, Chua CK, Chandrasekaran M (2006) Investigation of the mechanical properties and porosity relationships in fused deposition modelling-fabricated porous structures. *Rapid Prototyp J* 12:100–105. <https://doi.org/10.1108/13552540610652447>
25. Rayegani F, Onwubolu GC (2014) Fused deposition modelling (fdm) process parameter prediction and optimization using group method for data handling (gmdh) and differential evolution (de). *Int J Adv Manuf Technol* 73:509–519. <https://doi.org/10.1007/s00170-014-5835-2>

26. Sood AK, Ohdar RK, Mahapatra SS (2010) Parametric appraisal of mechanical property of fused deposition modelling processed parts. *Mater Des* 31:287–295. <https://doi.org/10.1016/j.matdes.2009.06.016>
27. Domingo-Espin M, Travieso-Rodriguez JA, Jerez-Mesa R, Lluma-Fuentes J (2018) Fatigue performance of ABS specimens obtained by fused filament fabrication. *Mat (Basel)* 11:2521. <https://doi.org/10.3390/ma11122521>
28. Percoco G, Lavecchia F, Galantucci LM (2012) Compressive properties of FDM rapid prototypes treated with a low cost chemical finishing. *Res J Appl Sci Eng Technol* 4:3838–3842
29. Nabipour M, Akhoundi B (2020) An experimental study of FDM parameters effects on tensile strength, density, and production time of ABS/Cu composites. *J Elastomers Plast* 009524432091683. <https://doi.org/10.1177/0095244320916838>
30. Moradi M, Meiabadi S, Kaplan A (2019) 3D printed parts with honeycomb internal pattern by fused deposition modelling; experimental characterization and production optimization. *Met Mater Int* 25:1312–1325. <https://doi.org/10.1007/s12540-019-00272-9>
31. Deshwal S, Kumar A, Chhabra D (2020) Exercising hybrid statistical tools GA-RSM, GA-ANN and GA-ANFIS to optimize FDM process parameters for tensile strength improvement. *CIRP J Manuf Sci Technol*. <https://doi.org/10.1016/j.cirpj.2020.05.009>
32. Akhoundi B, Nabipour M, Hajami F, Shakoori D (2020) An experimental study of nozzle temperature and heat treatment (annealing) effects on mechanical properties of high-temperature polylactic acid in fused deposition modeling. *Polym Eng Sci* 1–9:979–987. <https://doi.org/10.1002/pen.25353>
33. Yang L, Li S, Li Y et al (2019) Experimental investigations for optimizing the extrusion parameters on FDM PLA printed parts. *J Mater Eng Perform* 28:169–182. <https://doi.org/10.1007/s11665-018-3784-x>
34. Moradi M, Karami Moghadam M, Shamsborhan M et al (2020) The synergic effects of FDM 3D printing parameters on mechanical behaviors of bronze poly lactic acid composites. *J Compos Sci* 4:17. <https://doi.org/10.3390/jcs4010017>
35. Wang P, Zou B, Xiao H et al (2019) Effects of printing parameters of fused deposition modeling on mechanical properties, surface quality, and microstructure of PEEK. *J Mater Process Technol* 271:62–74. <https://doi.org/10.1016/j.jmatprotec.2019.03.016>
36. Ding S, Zou B, Wang P, Ding H (2019) Effects of nozzle temperature and building orientation on mechanical properties and microstructure of PEEK and PEI printed by 3D-FDM. *Polym Test* 78:105948. <https://doi.org/10.1016/j.polymertesting.2019.105948>
37. El Magri A, El Mabrouk K, Vaudreuil S et al (2020) Optimization of printing parameters for improvement of mechanical and thermal performances of 3D printed poly(ether ether ketone) parts. *J Appl Polym Sci* 137:1–14. <https://doi.org/10.1002/app.49087>
38. Srinivasan R, Ruban W, Deepanraj A et al (2020) Effect on infill density on mechanical properties of PETG part fabricated by fused deposition modelling. *Mater Today Proc* 27:3–7. <https://doi.org/10.1016/j.matpr.2020.03.797>
39. Kamoona SN, Masood SH, Mohamed OA (2018) Experimental investigation on flexural properties of FDM processed Nylon 12 parts using RSM. In: *IOP Conference Series: Materials Science and Engineering*
40. Ziemian S, Okwara M, Ziemian CW (2015) Tensile and fatigue behavior of layered acrylonitrile butadiene styrene. *Rapid Prototyp J* 21:270–278. <https://doi.org/10.1108/RPJ-09-2013-0086>
41. Ziemian C, Sharma M, Ziemi S (2012) Anisotropic Mechanical Properties of ABS Parts Fabricated by Fused Deposition Modelling. In: *Mechanical Engineering*. InTech Charlotte, NC
42. Es-Said OS, Foyos J, Noorani R et al (2000) Effect of layer orientation on mechanical properties of rapid prototyped samples. *Mater Manuf Process* 15:107–122. <https://doi.org/10.1080/10426910008912976>
43. Mendricky R, Fris D (2020) Analysis of the accuracy and the surface roughness of fdm/fff technology and optimisation of process parameters. *Teh Vjesn* 27:1166–1173. <https://doi.org/10.17559/TV-20190320142210>

44. Masood SH, Mau K, Song WQ (2010) Tensile properties of processed FDM polycarbonate material. In: Materials Science Forum. pp 2556–2559
45. Onwubolu GC, Rayegani F (2014) Characterization and optimization of mechanical properties of ABS parts manufactured by the fused deposition modelling process. *Int J Manuf Eng* 2014:1–13. <https://doi.org/10.1155/2014/598531>
46. Durgun I, Ertan R (2014) Experimental investigation of FDM process for improvement of mechanical properties and production cost. *Rapid Prototyp J* 20:228–235. <https://doi.org/10.1108/RPJ-10-2012-0091>
47. Torres J, Cotelo J, Karl J, Gordon AP (2015) Mechanical property optimization of FDM PLA in shear with multiple objectives. *JOM* 67:1183–1193. <https://doi.org/10.1007/s11837-015-1367-y>
48. Mohamed OA, Masood SH, Bhowmik JL (2017) Experimental investigation of time-dependent mechanical properties of PC-ABS prototypes processed by FDM additive manufacturing process. *Mater Lett* 193:58–62

Mechanical and Tribological Characteristics of Polymer Composites Developed by Fused Filament Fabrication



Vijay Tambrallimath, R. Keshavamurthy, Arun Patil,
and H. Adarsha

Abstract The concept of 3D printing also known as Additive Manufacturing (AM) is gaining huge importance from industrialists as well as researchers. Fused Filament Fabrication (FFF) is a major share holder of AM in the present market, which uses polymer in the form of filament to be used as a raw material for development of either prototype or functional models. The creation of any complex model can be easily fabricated by FFF. The model to be printed is first developed in any CAD form and then converted to .stl file format, which is later sliced and then added as an input to the 3D printer. The option of using AM is opening a wide way, for enhancement in design properties and quick printing. There remains a certain constraint with usage of these polymers alone in attainment of required properties. Therefore, the need for enhancement of properties of fabricated parts is of much necessary, which could be possible by addition of filler material. Polymer alone would not be able to provide required mechanical properties therefore the filler material either in the form of macro or micro particles or even in the form of nano particles is used to enhance the properties. Several researchers have tried various combination of filler material with the matrix for increase in specified properties. This chapter provides an insight towards FFF and its necessity, discusses the various polymer composites used in FFF, mechanical and tribological behaviour of polymer composites with variety of reinforcement addition and its potential applications and scope of FFF in near future.

V. Tambrallimath (✉)

Automobile Engineering, Dayananda Sagar College of Engineering, Bangalore 560078, India
e-mail: vijay.tambrallimath@gmail.com

R. Keshavamurthy

Mechanical Engineering, Dayananda Sagar College of Engineering, Bangalore 560078, India
e-mail: keshavamurthy.r@gmail.com

A. Patil

School of Mechanical Engineering, KLE Technological University, Hubballi 580021, India
e-mail: patilarun7@gmail.com

H. Adarsha

School of Mechanical and Automobile Engineering, Jain University, Bangalore, India
e-mail: h.adarsha@jainuniversity.ac.in

1 Introduction

The evolution of humans has seen an unprecedented agreeableness towards greater comfort and quality of life; this has been possible with the evolution of various materials in our utilization in day-to-day life. Since ages, humans have developed numerous strata of materials with the help of different processes, science and technology. We have developed an inherent character in utilizing and transforming the nature according to our desires. Materials had an important parameter in the society that decided the progress. The classification of ages as well is dependent on the types of materials being used and the classification is being done as Stone Age, Bronze Age and Iron Age. Plastic and lives of performance material has seen an advent in twentieth century that has created a huge significant impact in structuring the national economy and people's lives. Depending on the properties and requirements of usage, materials are broadly classified into 3 categories, they are; (i) metallic materials exhibiting metallic bonds (ii) polymer materials having covalent bonds and (iii) ceramic materials involving either ionic or covalent or a combination of both. Classification based on applicability can be classified into (i) structural materials; which have more significant properties in terms of strength, stiffness, deformation and so on (ii) functional materials; in which properties such as magnetism, sound, light, electricity and heat are primarily looked into.

The advantages of composite materials compared with conventional materials are higher; however, these materials' limitations cannot be neglected. Composites being relatively a new material, there has to be a comprehensive experience and prior knowledge required to bring these materials as a product of usage. Composites and their complexities in terms of manufacturing, the involvement of greater cost in development and curing of composites and their complexities in terms of manufacturing have become greater challenge to the designers of composites. The development of composite parts does not reach the real net shape, the utilization of certain machining process is necessary. For moulds with complex shapes, addition of excess material has to be done for identification and fixturing. Machining is a major process involved in removing these extra materials. Hence, machining is considered one of the important processes in developing composite materials through conventional process [1].

There are numerous ways in which manufacturing can be done for the development of various parts. Among the recent developments in manufacturing, one of the widely and continually evolving technologies is 3D printing technology that helps in the fabrication of complex and lightweight structures, which would have been a difficult task for other manufacturing systems. Figure 1 indicates AM usage in numerous categories such as prototype, production, research, and parts manufacturing for mechanical components. The figure indicates the more extensive utilization of AM, particularly in production and has increased exponentially in research sector from 2015 to 2019.

The establishment of AM application is intricate in fields like aerospace, medical, automotive, food, and engineering has seen greater involvement due to the

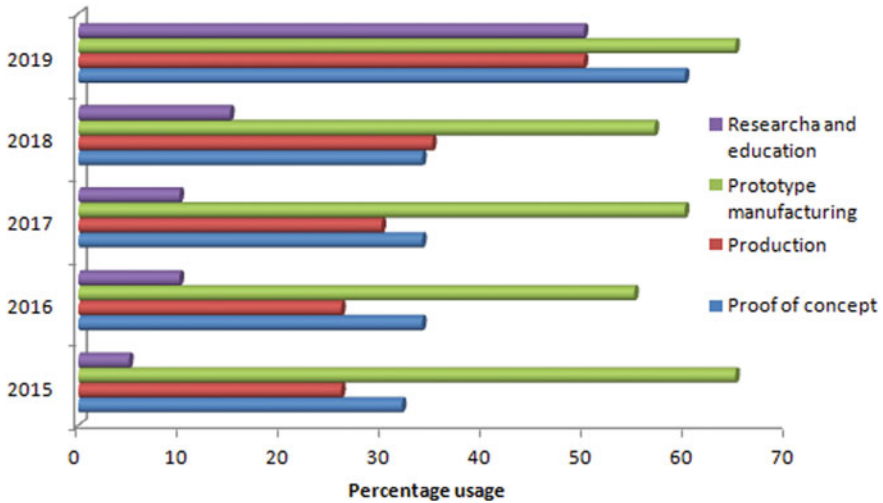


Fig. 1 Utilization of AM in various sectors [2]

viability in the production of intricate designs, cost-effectiveness, less lead time, and repeatability [3, 4]. The medical sector industry has started to try-out development of tissues, organs, and structures related to cells by using the methods of 3D printing [5, 6]. The involvement of 3D printing technology in the automotive industry helps reduce cost and time, which would involve tooling. The parts required for high-end equipment with low volume can be easily manufactured with 3D printing. The aeronautics sector has benefited at more considerable amount with development of parts light in weight, flexible and improved structures of geometry, which helps reduce fuel consumption and wastage of material. The compound annual growth rate (CAGR) of 3D printing would have been developed to 18.2% in medical, 29.07% in automobile, 22.17% in aerospace, and 32.05% in food industries by 2026. Figure 2 indicates the graphical representation of this growth.

Numerous materials can be included in the process of AM such as polymers, ceramics, metals and composites, which could be in the state of solid, semi-liquid or powder form depending on the type of 3D printing process [3, 9, 10].

The advent of 3D printing can be traced back to 1980s. Since then numerous processes have been developed in 3D printing. The acceptance of this manufacturing process is vast, due to a reduction in raw material usage, ease off reparability, development of products only when required, large saving energy consumption and enhanced product life cycle. The 3D printing process’s major classifications are selective laser sintering, fused filament fabrication, stereolithography, laminated object manufacturing and solvent cast direct writing [11, 12]. Stereolithography is considered to be one of the initial manufacturing processes in the category of 3D printing. The process involved the development of products by using ultraviolet light curable resins. The product is developed layer by layer by passing the

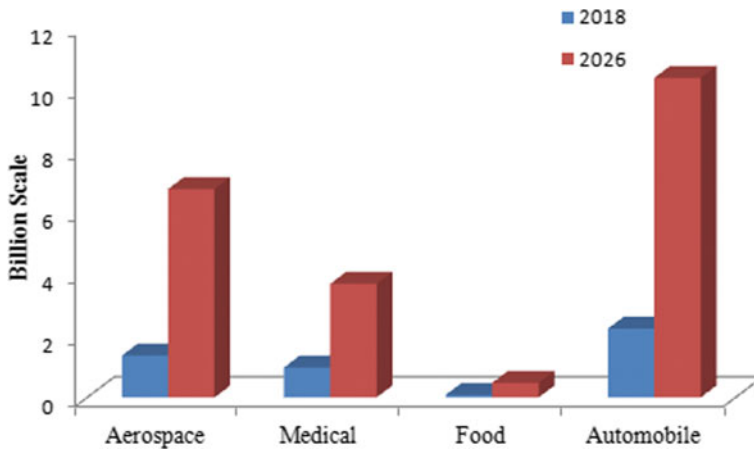


Fig. 2 Expected growth of AM industry in various sectors until 2026 [7, 8]

ultraviolet laser beam in a guided path according to the design; the laser beam will harden the resin to form the shape as per the design [13]. The process of selective laser sintering uses the method of powder bed printing technology. The solid product is formed by laser beam movement over the Powder particles which sinter to form a product [14]. The heat generated by the laser beam fuses the Powder particles to each other and in turn forms the layer. Each layer is then fused to another layer by same principle [15]. In laminated object manufacturing sheets are used as raw materials brought to the desired shape either by laser or mechanical cutters. The lamination of these sheets can happen after they are cut or first the lamination can be done and the sheets can be cut to desired structure. The cost involvement in this towards material and machining is less in comparison to other processes [16].

In the solvent cast direct writing (SC-DW) method, a polymer with dissolvable property is used to mix with rapid solvent evaporation process that helps in development of complex geometries at room temperature [17]. The most widely used form of 3D printing process is fused filament fabrication. In this process the nozzle is heated to a desired temperature to convert a thermoplastic filament to its semi-molten state and then extruded to develop a structure in a layer-by-layer manner [18]. The discussion of this process is elaborately done in the following sections of the chapter.

Fused filament fabrication stands apart from other manufacturing process in cost effectiveness and hence numerous researchers are aligning themselves towards this process. The utilisation of this process at a greater industrial scale led to various demands and requirements which have been addressed by industries. Most of printer manufacturing companies such as Stratasys, Ultimaker, Markforged, XYZprinting, Zortax, German RepRap and Dagoma are continually involved in improving the printers, while software companies such as Autodesk, Siemens PLM

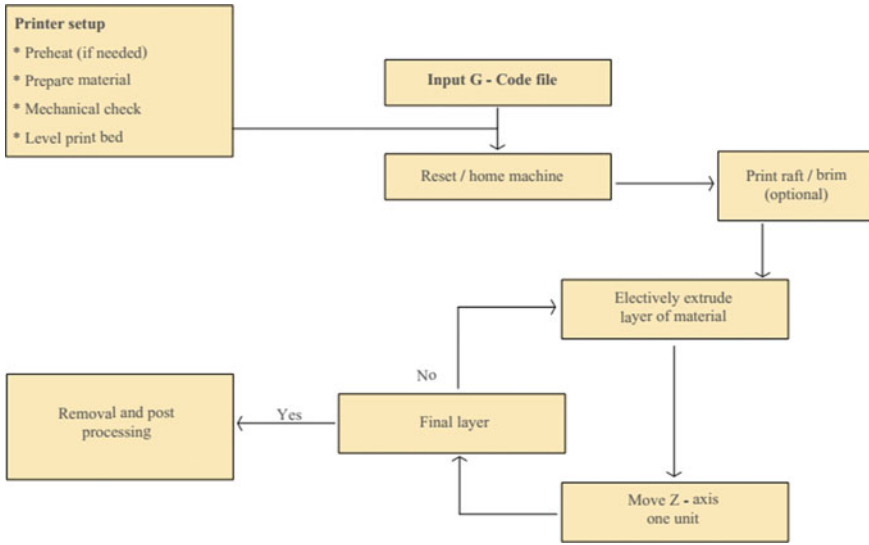


Fig. 3 Algorithm followed by FFF

software and Dassault systems are budding in development of new CAD software to be well-suited with the new printers. There still arise numerous technical issues concerning fused filament fabrication during the process of printing; it may be related to kind of quality of print or even the consistency of the parts. This kind of hindrance causes numerous defects in the printed samples and also numerous studies have also come forward to mitigate these complications in the process. The process algorithm of the FFF is mentioned in Fig. 3.

2 Synthesis of Polymer Composites in FFF

The advancement of AM technology has seen an immense growth in recent years and this trend continues in the recent manufacturing sector due to its affordability and adaptable applications in wide sector. The growth of this industry has seen to have a multi dollar business due to credible features added with its ability to fabricate complex structures and also have an ability to build parts with resolution in micrometers [19, 20]. Among the various available AM technologies extrusion based process of AM has seen its maturity at early stages due to capability of producing cost effective parts with ease of operation combined with design freedom. In this category of AM process, Fused Filament Fabrication (FFF) has seen wide scale acceptance and utilization [21].

Growth in the industry of additive manufacturing is seen in the present days and will continue with the same rate due to its ease of operatability and low cost for the

development of prototypes and functional products. The growth of additive manufacturing industry would be a multi-billion dollar in the near future due to its various advantages and its ability to customise complex monolithic structures and geometries, with the resolution of micrometre [19, 20]. Among the various methods of additive manufacturing the process of extrusion-based additive manufacturing has matured in the industry in recent times. This kind of manufacturing process provides cost effective and simple mode of functioning with advantages and freedom of design in additive manufacturing. Fused filament fabrication is an extrusion-based additive manufacturing process that has been well developed and embraced by various production processes [21]. The extraction of filament can be done by either using a single screw or twin screw extruder to extract a specified diameter filament which is used in FFF 3D printer. This filament extraction process involves the maintenance of a certain amount of screw speed, pressure, and temperature to extract a filament of a polymer's desired diameter [22, 23]. These key parameters in the process of extrusion, plays an essential role in the extraction of filament. The material used in the extraction process should have the ability to sustain the pressure to be extracted out as a filament. If the material would not withstand the application of pressure, it would lead to buckling of the filament during extrusion. Melt viscosity of the material helps understand the ability to withstand extrusion pressure and the elastic modulus helps determine load carrying capacity [24].

Figure 4 shows the simplified process of fused filament fabrication. This printing process takes place at an average speed and uses low melting point [25]. The advantages of this process are very high in comparison to its drawbacks. It paves the path towards high reliability, utilization of low cost materials, easy availability, low maintenance and lower investment cost [26, 27].

The methodology of FFF can be utilized in development of parts using polymers, polymer matrix composites, bio composites, nano composites, fibre reinforced composites and polymer ceramic composites [28]. Among the wide variety of polymers available for printing the most commonly used polymers are Acrylonitrile Butadiene Styrene, Polylactic acid, nylon, Acrylonitrile Styrene Acrylate, Polycarbonate and Polyethylene Terephthalate. The category of polymers used as high performing polymers are Polyether Ether Ketone and Polyetheramide. Newly developed polymer known as thermoplastic elastomer is used for developing flexible parts using FFF. Apart from polymers a wide variety of reinforced polymers can be used in FFF, some of the reinforcements used are carbon nanotubes,



Fig. 4 Simplified 3D printing process

graphene, copper, iron, glass and Kevlar. The variation of mechanical properties and development of certain defects are completely dependent on both matrix and reinforcement.

Numerous researchers have carried out various studies on using variety of filaments for FFF. Vijay et al. [29] in their study of synthesis and characterization of PC-ABS reinforced with graphene has successfully extracted the filament of 1.75 mm required for FFF. Graphene as reinforcement was added from 0.2 to 0.8 wt% in increment of 0.2 wt%. The suitability of usage of FFF filament was analysed by macro inspection. It was found that there were no cracks or flaws present in the filament. An interesting observation was made; pores reduction was observed with increase in filler content. The graphene reinforcement aggregation is also not noticed which predicts the efficient property of graphene in 2D lattice. It also has well defined structural and surface to area volume ratio.

Gray et al. [30] made an attempt to augment the tensile properties of the polymer composites and use it as functional component by adding thermotropic liquid crystalline polymers (TLCP) with PP matrix to be used in FFF. The study was focused on analysing the tensile and morphological properties for parts developed using filaments extracted by dual extrusion process. Zhong et al. [31] carried out a successful study on using short fibre reinforcement in ABS matrix. The developed composite filament had greater strength to be used for FFF. The studies were further extended to evaluate the effects of plasticizer and compatibilizer in analysis of variation of properties. Shofner et al. [32] developed a polymer composite by addition of single wall carbon nanotubes to ABS matrix.

G. Melenka et al. [33] carried out an experimental study on developing a polymer composite by addition of continuous Kevlar fibres to ABS matrix. The study was carried out in understanding the variation of tensile properties by varying filler material. Kevlar fibre was added in 4.04, 8.08 and 10.1% respectively. It was noted that with incremental addition of reinforcement the tensile strength increased along with young's modulus and strain. Perez et al. [34] made a comparative study for the analysis of variation in tensile strength for addition of various filler material. Samples were prepared by choosing ABS as a matrix material. TiO₂, jute fibre and thermo plastic elastomer (TPE) were added separately which were compared with pure ABS sample. Tensile strength increased for the ABS-TiO₂ when compared to pure ABS; however, there was a reduction in tensile strength for jute fiber and TPE. The combination of two polymers will have an improved effect on certain properties. The most commonly used blends are polycarbonate and acrylonitrile butadiene styrene. The combination of these materials have enhanced the thermal stability, processing characters and provided good impact results. Hence, this polymer material gives an improved mechanical property and makes it a stable and well applied material in polymer industry [35]. The usage of these materials has been largely seen in industries like automotive and appliances [36, 37].

3 Tensile and Impact Strength of Parts Developed by FFF

Polymer alone would not be able to provide required mechanical properties therefore the filler material either in the form of macro or micro particles or even in the form of nano particles is used to enhance the properties. Several researchers have tried various combination of filler material with the matrix for analysis of mechanical properties.

Ning et al. [38] examined the physical properties of carbon fibre reinforced with ABS by addition of varied weight percent of reinforcement developed by FFF. Addition of 5 and 7.5 wt% of carbon fibre exhibited a remarkable improvement in tensile strength and young's modulus. It was also observed that addition of long carbon fibres enhances the tensile strength and young's modulus, however, the value of toughness and ductility would be affected. Addition of 30 wt% of carbon fibre to ABS matrix had shown an improvement in tensile strength by 115% and young's modulus by 700%. These results exhibited enhanced specific strength greater than that of Aluminium.

Melenka et al. [33] studied the effect of addition mechanical properties by addition of Kevlar fibre to Nylon matrix. The developed filaments were fabricated using FFF. Increased addition of Kevlar fibre showed an incremental result in tensile strength and stiffness. The enhancement of fatigue life and strength was done by addition of carbon fibre in-between the layers of the matrix. Further enhancement of mechanical properties was carried out by thermal treatment [39]. Another study by Van Der Klift et al. [40] exhibited that an increase in number of layers of carbon fibre leads in formation of large voids resulting in decremental impact on tensile strength. The suitable amalgamation of carbon fibre to polymer would be achieved by maintaining the temperature range of 200–230 °C. An excellent bonding strength between the layers is observed when the thickness of layer is maintained between 0.4 and 0.6 mm and having hatch spacing of 0.6 mm. These conditions provided maximum flexural strength of 335 MPa and flexural modulus of 30 GPa. The effect of layer height along with FFF printing plate temperature on toughness was analysed by Lu et al. [41]. The studies were carried out for PLA, which exhibited appreciable bonding strength with less porosity when the plate's temperature was maintained at 160 °C. Layer height was maintained at 0.2 mm. These were considered suitable conditions in which no warpage was observed and parts were fabricated with high precision. However, pores in interface were not completely removed.

Patel et al. [42] examined the variation of tensile strength with varying density along with infill patterns of lines, grid and concentric. It is evident from the experimental values that 60% density with line infill pattern gave highest value of tensile strength for PLA parts developed through FFF. Whereas, 40% density with infill pattern of concentric gave minimal tensile strength.

Weng et al. [43] developed a polymer composite by addition of 1, 3 and 5 wt% of organic modified montmorillonite (OMMT) to ABS polymer to be used in FFF. The fabricated parts were investigated for tensile and flexural properties using

dynamic mechanical and thermal expansion tests. It was observed that incremental addition of OMMT to ABS matrix led to increase in tensile strength and modulus, flexural strength and modulus along with storage modulus. Linear thermal expansion was reduced. There was an increase with respect to decomposition and glass transition temperature with addition of OMMT. The reduction in elongation at break is due to the changes in molecular arrangement in ABS due to addition of OMMT.

Hanon et al. [44] investigated on mechanical properties with variation of process parameters in FFF. The results showed the ductile nature for specimens built flat, brittle for parts built upright and the strangest was for parts built on-edge. The specimens developed on edge have more stress bearing capacity than the specimens built on flat or upright direction. The application of tensile force over flat specimens is in parallel direction. The infill pattern was built with long lines at an angle of 45° with optimal number of layers with intent of increasing the elongation at higher strain rates. The specimens built on edge had complex structures with minimal size of contours having greater layers and short lines. The geometry of development of these samples gave high strength during testing. When looked into the samples built in upright direction the samples are built vertically upwards without having interlocking between the printed lines but rather are held by adhesive forces between the layers. With these abilities during building of specimens the ability for withstanding greater load is reduced drastically and hence it acts brittle in nature. Zaldivar et al. [45] studied the effect of print orientation on mechanical behaviour by using ULTEM 9085. The highest tensile strength was obtained in models developed on edge which was 84% greater than the specimens developed in upright manner. The specimens developed in flat form have an increased tensile strength by 21% than upright orientation. These findings prove an almost similar trend in terms of print orientation compared with the current work.

Mechanical characters of the samples fabricated by polycarbonate material were studied by Domingo-Espin et al. [36]. The study was carried out in determining the deformation behaviour of the specimens fabricated in numerous orientations. The samples developed in flat and on edge manner showed an ample plastic behaviour when the application of force is seen to be in same direction as that of layer deposition. The specimens developed in upright manner showed no much plastic deformation and hence were determined to be fragile in nature. This phenomenon was proven to be applicable when the load application was perpendicular to the built layer.

4 Tribological Characteristics of FFF Parts

Certain applications require sliding elements along with less friction and wear. However, certain other applications require high friction and low wear properties, such as brakes and clutches. Large amount of research and studies have concluded that the properties of wear and friction are inter dependent. The whole system of

these understandings depends on the tribological system, which involves microstructure studies, involvement of stress and speed and numerous other parameters [46, 47]. The material should have the ability to meet certain conditions in their applications, polymer composites are one class of materials which have proven to be flexible in development through various compositions, tailoring microstructure and in turn producing the desired properties towards friction and wear performance. The polymer products are well suited for tribological applications as they possess unique properties such as self lubrication, ability to dampen vibration, and resistance to corrosion [48]. With all these abundance properties, there are very nominal amounts of studies carried out to understand the tribological behaviour of 3D printed parts [49, 50].

Bustillos et al. [51] analysed the properties of wear and friction of parts developed by 3D printed PLA composite reinforced with graphene. The addition of graphene improved wear resistance by 14% and reduced friction coefficient by 65% compared with pure PLA. Such high standard led the authors to provide the utilization of these polymer composites for orthopaedic scaffold application. In another study bio-carbon reinforced PLA filaments were developed to analyse the structural and tribological properties by Ertane et al. [52]. Addition of 30 vol.% of carbon has significantly reduced the wear volume. Some of the mechanisms involved were predicted as to occurrence of fatigue and abrasive wear mechanism. The value of friction coefficient was maintained near 0.5 without much fluctuation.

Bai et al. [53] attempted to investigate the tribological properties with respect to surface orientation of polyamide 12. Anisotropic behaviour was noted for wear property studies. The surface analyses proved that the friction coefficient was smaller on side surfaces and wear resistance was greater and more remarkable compared to top surfaces.

Hanon et al. [54] examined the tribological properties of 3D printed polymers of different colours. The friction coefficient was measured to be in range of 0.5 and depth of wear was measured to be 150 μm . Application of load of 30 N led to wear rate of $3.2 \times 10^{-9} \text{mm}^3/\text{N}\cdot\text{mm}$. similar studies were noted by other researchers which predicted addition of bronze would lead to improved wear behaviour and the friction coefficient would be maintained almost constant [55–57]. Guo et al. [58] examined the authority of post-processing on behaviour related to tribology and surface characters of polyamide 12 (PA12). The process was carried out using the method of selective laser sintering. The process of post processing involving the method of magnetic field assisted finishing proved to have better surface finish and tribological characters by demonstrating better wear resistance and lesser friction coefficient. Involvement of certain post processing characters towards 3D printed parts helps in enhancing the tribological and surface properties.

Wear and friction are vital parameters to address in modern industrial sector. Research and studies in these fields by utilizing polymer composites have been well quantified in recent years. Reliable tribological characters, flexibility in usage of multi polymer composites using a wide spectrum of reinforcements, have led to the

development of a cost-efficient method of developing novel tribological materials. The fundamental understanding of these mechanisms leads to application in automobile and aerospace and development of products through 3D printing process.

5 Scope of Filaments in Near Future

Since the inception of FFF process, polymers and filaments made of polymers and its composites have played a major role in the domain of usage of raw materials. Resourcefulness and feasibility of development of filaments have led major companies to development of new filaments. The filaments were developed to provide better flow ability and shape by Weiste [59]. A tribo polymer filament was developed by Igus company was used for fabrication of functional prototypes [60]. A new polymer composition was named as PRIMALLOY developed by Verbatim which exhibited greater alterations to heat, oil and chemicals [61]. A German company RepRap developed a filament made of PLA which provides aesthetically agreeable finish during printing itself [62]. Superior strength PLA filaments were developed by Taulman3D to augment the clarity of the fabricated products [62]. PLA is also used for printing cartridge for mobile phones [63]. New materials are researched and developed for replacement of ABS in numerous applications [64]. SABIC is developing new combinations of materials for high performance for various combinations of PE, PC and ABS [65]. Filament developed by Polypropylene (PP) in Japan offers greater resistance to heat, chemical and fatigue. This also provides greater stiffness, tensile strength along smooth surface finish [66]. PLA material property enhancement was done by FLoreon 3D company as well [67]. Verbatim and Dupont developed varied polymer matrix filaments for high performance [68, 69]. Another company filamentum developed a PLA filament with addition of vertigo grey that enhances the look [70]. With suitable usage of certain filaments depending on application the modifications can be carried out. The modified application can be used as stacking pitch for orthotropic framework with uni-axial loading, developed with ABS [71], and much more effectively multi-layer polymer-dispersed liquid-crystal elastomers (PDLCEs) is used rather than traditional method [72]. Standard polymer filaments are used to develop models for the medical industries like skulls, which provide an in-depth view for analysis [73].

The development of filaments using natural materials began in 2010. These materials are biodegradable and recyclable in nature along with providing greater stability to the fabricated parts. The filament was developed using seaweed [74]. Lime stones and wood were also used in development of filaments [75]. The filament's color texture was modified by using the waste material of coffee towards development of filament [76]. WillowFlex company developed a recycled organic waste into bio-plastic filament [77]. Yet another bio-plastic was developed by Facilan which demonstrated exceptional mechanical properties and provided better finish with soft touch. Numerous researchers and industries have started using reinforcements as bio materials. It is also known that using bio materials as

reinforcement has been enhanced at greater extent in last few years. These materials have shown the development of sustainable materials and help achieve the desired physical and mechanical properties [78].

6 Conclusions

The manufacturing process by the method of Additive Manufacturing would be a turning point in the field of the manufacturing sector. The ability to convert the material to near net shape through 3D printing to control the properties has paved a greater rush for exponential growth of this field. The possibility of exploration in the fabrication of new composite materials and required customization through AM has led to the exploration of this field for researchers and developers. The advantages of using composite materials in 3D printing are controlling the physical, thermal, optical and electrochemical properties. Also there is wide opportunity of transforming the shape of these materials through 4D printing.

There are certain drawbacks in utilizing composite materials through AM process which needs to be set on track to adopt this method as mainstream manufacturing method. Some of the present issues faced in FFF are poor adhesion of reinforcement to the polymer matrix, void formation, difficulty in the utilization of continuous fiber as reinforcement and clogging of nozzle. The existing FFF machines are set to print only specified form of materials in the specific temperature range.

References

1. Sheikh-Ahmad JY (2009) Machining of polymer composites. Springer Science+Business Media LLC. <https://doi.org/10.1007/978-0-387-68619-6>
2. Columbus L (2019) The state of 3D printing. Available online: <https://www.forbes.com/sites/louiscolumbus/2019/05/27/the-state-of-3d-printing-2019/#fb942fb46c2c>. Accessed on 30 September 2020
3. Calignano F, Manfredi D, Ambrosio EP, Biamino S, Lombardi M, Atzeni E, Salmi A, Minetola P, Iuliano L (2017) Fino, overview on additive manufacturing technologies. *Proc IEEE* 105:593–612
4. Parandoush P, Lin D (2017) A review on additive manufacturing of polymer-fiber composites. *Compos Struct* 182:36–53
5. Chu C, Graf G, Rosen DW (2008) Design for additive manufacturing of cellular structures. *Comput Aided Des Appl* 5:686–696
6. Melchels FP, Domingos MA, Klein TJ, Malda J, Bartolo PJ, Huttmacher DW (2012) Additive manufacturing of tissues and organs. *Prog Polym Sci* 37:1079–1104
7. Allied Market Research. Allied Market Research. 3D Printing Healthcare Market to Reach \$3.69 Bn, Globally, by 2026 at 18.2% CAGR. Available online: <https://www.prnswire.com/news-releases/3d-printinghealthcare-market-to-reach-3-69-bn-globally-by-2026-at-18-2-cagr-allied-market-research-300944847.html>. Accessed on 6 October 2020

8. Business Wire. Outlook on the worldwide edible 3D printing market to 2025. Available online: <https://www.businesswire.com/news/home/20200407005584/en/Outlook-Worldwide-Edible-3DPrinting-Market-2025>. Accessed on 6 October 2020
9. Selvamani SK, Samykano M, Subramaniam SR, Ngui WK, Kadrigama K, Kanagaraj G, Idris MS (2019) 3D printing: Overview of ABS evolvement. AIP Conf Proc 2059:020041
10. Tee YL, Peng C, Pille P, Leary M, Tran P (2020) 3D Printing of Composite Materials: Experimental and Modelling Approach. J Miner Met Mater Soc (Tms) 72:1105–1117
11. Despeisse M, Ford S (2015) The role of additive manufacturing in improving resource efficiency and sustainability. In: Proceedings of the IFIP International Conference on Advances in Production Management Systems, Tokyo, Japan, 7–9 September 2015; Springer, Berlin, Germany, pp 129–136
12. Keshavamurthy R, Tambrallimath V, Prabhakar K, Sekhar N (2019) Additive manufacturing processes and their applications for green technology. In: Davim P, Kumaran ST, Jo Ko T, Arvind Raj S, Uthayakumar M (eds) Handbook of research on green engineering techniques for modern manufacturing. IGI Global, USA, November 2018. <https://doi.org/10.4018/978-1-5225-5445-5>
13. Manapat JZ, Chen Q, Ye P, Advincula RC (2017) Advincula, and engineering. 3D printing of polymer nanocomposites via stereolithography. Macromol Mater Eng 302:1600553
14. Peng C, Tran P (2020) Bioinspired functionally graded gyroid sandwich panel subjected to impulsive loadings. Compos Part B Eng 188:107773
15. Kruth JP, Mercelis P, Vaerenbergh JV, Froyen L, Rombouts M (2005) Binding mechanisms in selective laser sintering and selective laser melting. Rapid Prototyp J 11:26–36
16. Gao W, Zhang Y, Ramanujan D, Ramani K, Chen Y, Williams CB, Wang CC, Shin YC, Zhang S, Zavattieri PD (2015) The status, challenges, and future of additive manufacturing in engineering. Comput Aided Des Appl 69:65–89
17. Guo SZ, Gosselin F, Guerin N, Lanouette AM, Heuzey MC, Theriault D (2013) Solvent-cast three-dimensional printing of multifunctional microsystems. Nano Micro Small 9:4118–4122
18. Ahn SH, Montero M, Odell D, Roundy S, Wright PK (2002) Anisotropic material properties of fused deposition modeling ABS. Rapid Prototyp J 8:248–257
19. Horn TJ, Harrysson OLA (2012) Overview of current additive manufacturing technologies and selected applications. Sci Progress 95:255
20. Wong KV, Hernandez A (2012) A review of additive manufacturing. ISRN Mech Eng 2012:10
21. Crump SS (June) Apparatus and method for creating three-dimensional objects. U.S. Patent 5,121,329, 9 June
22. Gkartzou E, Koumoulos EP, Charitidis CA (2017) Production and 3D printing processing of bio-based thermoplastic filament. Manuf Rev 4:1. <https://doi.org/10.1051/mfreview/2016020>
23. Dudek P (2013) FDM 3D printing technology in manufacturing composite elements. Arch Metall Mater 58(4):1415–1418. <https://doi.org/10.2478/amm-2013-0186>
24. Liu J, Sun L, Xu W, Wang Q, Yu S, Sun J (2019) Current advances and future perspectives of 3D printing natural-derived biopolymers. Carbohydr Polym 207:297–316. <https://doi.org/10.1016/j.carbpol.2018.11.077>
25. Carneiro OS, Silva AF, Gomes R (2015) Fused deposition modeling with polypropylene. Mater Des 83:768–776
26. Durgun I, Ertan R (2014) Experimental investigation of FDM process for improvement of mechanical properties and production cost. Rapid Prototyp J 20:228–235
27. Masood SH, Song WQ (2004) Development of new metal/polymer materials for rapid tooling using fused deposition modelling. Mater Des 25:587–594
28. Mohan N, Senthil P, Vinodh S, Jayanth N (2017) A review on composite materials and process parameters optimisation for the fused deposition modelling process. Virtual Phys Prototyp 12:47–59

29. Tambrallimath V, Keshavamurthy R, Saravanbavan D, Pradeepkumar G S, Harish Kumar M (2019) Synthesis and characterization of graphene filled PC-ABS filament for FDM applications. In: *Advances in Polymer Composites: Mechanics, Characterization and Applications* AIP Conf. Proc. 2057, 020039-1–020039-8
30. Gray IV RW, Baird DG, Bøhn JH (1998) Effects of processing conditions on short TLCP fiber reinforced FDM parts. *Rapid Prototype J* 4(1):14–25
31. Zhong W et al (2001) Short fiber reinforced composites for fused deposition modeling. *Mater Sci Eng, A* 301(2):125–130
32. Shofner ML et al (2003) Nanofiber-reinforced polymers prepared by fused deposition modeling. *J Appl Polym Sci* 89(11):3081–3090
33. Melenka G, Cheung B, Schofield J, Dawson M, Carey J (2016) Evaluation and prediction of the tensile properties of continuous fiber-reinforced 3D printed structures. *Compos Struct* 153:866–875
34. Perez ART, Roberson DA, Wicker RB (2014) Fracture surface analysis of 3D-Printed tensile specimens of novel ABS- based materials. *J Fail Anal Prev* 14:343–353
35. Francis V, Jain PK (2018) A filament modification approach for in situ ABS/OMMT nanocomposite development in extrusion-based 3D printing. *J Braz Soc Mech Sci Eng* 40(7):361–373
36. Domingo-Espin M, Puigoriol-Forcada JM, GarciaGranada AA, Lluma J, Borros S, Reyes G (2015) Mechanical property characterization and simulation of fused deposition modeling polycarbonate parts. *Mater Des* 83:670–677
37. Greco R, Astarita MF, Dong L, Sorrentino A (1994) Polycarbonate/ABS blends: Processability, thermal properties, and mechanical and impact behavior. *Adv Polym Technol* 13:259–274
38. Ning F, Cong W, Qiu J, Wei J, Wang S (2015) Additive manufacturing of carbon fiber reinforced thermoplastic composites using fused deposition modeling. *Compos B Eng* 80:369–378
39. Mori K-I, Maeno T, Nakagawa Y (2014) Dieless forming of carbon fibre reinforced plastic parts using 3D printer. *Procedia Eng* 81:1595–1600
40. Van Der Klift F, Koga Y, Todoroki A, Ueda M, Hirano Y, Matsuzaki R (2015) 3D printing of continuous carbon fibre reinforced thermo-plastic (CFRTP) tensile test specimens. *Open J Compos Mater* 6:18
41. Lu W, William G, Gardner M, Douglas J (2017) Improving the impact strength of poly(lactic acid) (PLA) in fused layer modeling (FLM). *Polymer* 114:242–248
42. Patel DM (2017) Effects of infill patterns on time, surface roughness and tensile strength in 3D printing. *IJEDR* 5(3):2321–2341
43. Weng Z, Wang J, Senthil T, Wu L (2016) Mechanical and thermal properties of ABS/montmorillonite nanocomposites for fused deposition modeling 3D printing. *Mater Design* 102:276–283. <https://doi.org/10.1016/j.matdes.2016.04.045>
44. Hanon Muammel M, Alshammas Yazan, Zsidai László (2020) Effect of print orientation and bronze existence on tribological and mechanical properties of 3D-printed bronze/PLA composite. *Int J Adv Manuf Technol* 108:553–570. <https://doi.org/10.1007/s00170-020-05391-x>
45. Zaldivar RJ, Witkin DB, McLouth T, Patel DN, Schmitt K, Nokes JP (2017) Influence of processing and orientation print effects on the mechanical and thermal behavior of 3D-printed ULTEM® 9085 Material. *Addit Manuf* 13:71–80. <https://doi.org/10.1016/j.addma.2016.11.007>
46. Myshkin NK, Petrokovets MI et al (2005) Tribology of polymers: Adhesion, friction, wear, and mass-transfer. *Tribol Int* 38(11–12):910–921
47. Oster F, Hauptert F et al (2004) Tribologische Hochleistungs-beschichtungen aus neuartigen polyetheretherketon (PEEK)-compounds. *Tribol Schmierungstech* 51(3):17–24
48. Briscoe BJ, Sinha SK (2013) Tribological applications of polymers and their composites—past, present and future prospects

49. Hong Y, Zhang P, Lee K-H, Lee C-H (2017) Friction and wear of textured surfaces produced by 3D printing. *Sci China Technol Sci* 60:1400–1406
50. Hanon MM, Marczis R, Zsidai L (2020) Impact of 3D-printing structure on the tribological properties of polymers. *Ind Lubr Tribol*
51. Bustillos J, Montero D, Nautiyal P, Loganathan A, Boesl B, Agarwal A (2017) Integration of graphene in poly(lactic) acid by 3D printing to develop creep and wear-resistant hierarchical nanocomposites. *Polym Compos* 16:101–113
52. Ertane EG, Dorner-Reisel A, Baran O, Welzel T, Matner V, Svoboda S (2018) Processing and wear behaviour of 3D printed PLA reinforced with biogenic carbon. *Adv Tribol* 2018:1–11
53. Bai J, Yuan S, Chow W, Chua CK, Zhou K, Wei J (2015) Effect of surface orientation on the tribological properties of laser sintered polyamide 12. *Polym Test* 48:111–114
54. Hanon MM, Kovács M, Zsidai L (2019) Tribology behaviour investigation of 3D printed polymers. *Int Rev Appl Sci Eng* 10:173–181
55. Bajpai PK, Singh I, Madaan J (2013) Tribological behavior of natural fiber reinforced PLA composites. *Wear* 297:829–840
56. Ünlü BS, Uzkut M, Atik E (2010) Tribological behaviors of polymer-based particle-reinforced PTFE composite bearings. *J Reinf Plast Compos* 29:1353–1358
57. Unal H, Kurtulus E, Mimaroglu A, Aydin M (2010) Tribological performance of PTFE bronze filled composites under wide range of application conditions. *J Reinf Plast Compos* 29:2184–2191
58. Guo J, Bai J, Liu K, Wei J (2018) Surface quality improvement of selective laser sintered polyamide 12 by precision grinding and magnetic field-assisted finishing. *Mater Des* 138:39–45
59. Accreate Technology (2014) TCT magazine, Weistek exhibits 3D printers and filaments at CES. Accessed on 2 January 2020
60. Griffiths L (2014) TCT magazine, Igu introduces world's first tribo-filament for 3D printing. Accessed on 15 October 2014
61. Griffiths L (2014) TCT magazine, Verbatim Unveils PRIMALLOY 3D printing filament. Accessed on 10 September 2020
62. Griffiths L (2015) TCT magazine, German RepRap releases new performance PLA. Accessed on 19 January 2020
63. Pirnstill CW, Coté GL (2015) Malaria diagnosis using a mobile phone polarized microscope. *Sci Rep*. <https://doi.org/10.1038/srep13368>
64. Griffiths L (2016) TCT magazine, Algix 3D launches new filament to replace ABS. Accessed on 20 September 2020
65. SABIC (2017) TCT magazine, SABIC unveils new portfolio of high-performance filament grades for FDM 3D printing. Accessed on 10 May 2020
66. Davies S (2017) TCT magazine, Verbatim unveils new polypropylene 3D printing material. Accessed on 4 April 2020
67. Davies S (2017) TCT magazine, Floreon 3D begins search for partners to bring patented PLA filament technology to market. Accessed on 5 September 2020
68. Furomoto S (2017) TCT magazine, Verbatim introduces new PRIMALLOY BLACK high-performance 3D printing filament. Accessed on 12 September 2020
69. Coex LLC (2017) TCT magazine, DuPont high performance 3D printing materials available in EMEA through German RepRap. Accessed on 5 October 2020
70. Davies S (2017) TCT magazine, Fillamentum releases PLA Extrafill Vertigo Galaxy FDM 3D printing filament. Accessed on 6 October 2020
71. Tanaka T et al (2017) Orthotropic laminated open-cell frameworks retaining strong auxeticity under large uniaxial loading. *Sci Rep*. <https://doi.org/10.1038/srep39816>
72. Rešetič A et al (2016) Polymer-dispersed liquid crystal elastomers. *Nat Commun*. <https://doi.org/10.1038/ncomms13140>
73. Chen S et al (2017) The role of three-dimensional printed models of skull in anatomy education: a randomized controlled trail. *Sci Rep*. <https://doi.org/10.1038/s41598-017-00647-1>

74. O'Connor D (2013) TCT magazine, 3D printing with seaweed. Accessed on 3 December 2013
75. O'Connor D (2015) TCT magazine, MakerBot to launch four new filaments including metal, wood and limestone. Accessed on 26 September 2020
76. Griffiths L (2015) TCT magazine, 3Dom USA launches coffeebased bio-material for eco-friendly 3D printing. Accessed on 26 September 2020
77. Griffiths L (2015) TCT magazine, WillowFlex 3D printing filament to lead organic material evolution. Accessed on 26 September 2020
78. Facilan (2017) TCT magazine, 3D4Makers and Perstorp partner to launch Facilan FDM 3D printing filament portfolio. Accessed on 26 September 2020

The Surface Quality Improvement Methods for FDM Printed Parts: A Review



Abdul Wahab Hashmi, Harlal Singh Mali, and Anoj Meena

Abstract The implementation of traditional manufacturing processes is majorly limited by the scale of the manufacturing process and by the shape, size and geometrical nature of the part, and therefore manufacturing industries are sometimes obliged to use equipment and processes to decrease the final costs for the part. Nonetheless, the Fused deposition modeling technique is usually the most favorable additive manufacturing technique that is usually capable of overcoming certain special challenges, including physical properties, bad surface quality, and the use of various products for processing. The fact that the fused deposition modeling technique is best suited to the structure and custom nature of the component to be made, gives them a major competitive advantage. There have been several attempts to enhance surface quality by controlling various process parameters of the fused deposition modeling technique and using specific post-processing and pre-processing techniques including surface finishing methods. The purpose of this analysis is to report on a systemic literary examination of the general field of surface quality improvement methods used for fused deposition modeling printed parts.

1 Introduction

The additive manufacturing (AM) process is commonly called a layered manufacturing technique because, in this AM process, the materials join in a consecutive layer by layer to produce the desired part. The AM processes are completely numeric-controlled and automatic, utilized to produce the prototypes with the minimum intervention of human beings [1]. AM or direct digital manufacturing (DDM) can produce 3D physical parts simply using the computer-aided design (CAD) without making tools for specific parts [2, 3].

A. W. Hashmi · H. S. Mali · A. Meena (✉)

Advanced Manufacturing and Mechatronics Lab, Department of Mechanical Engineering, Malaviya National Institute of Technology, Jaipur 302017, India
e-mail: ameena.mech@mnit.ac.in

AM processes include extensive additive techniques varying from material jetting i.e. multi-jet modeling (MJM), binder jetting i.e. 3D printing (3DP), vat photopolymerization i.e. stereolithography apparatus (SLA), powder bed fusion i.e. selective laser sintering (SLS) process, direct energy deposition i.e. laser engineered net shaping (LENS) sheet lamination i.e. laminated object manufacturing (LOM) to hybrid AM techniques. It also involves the material extrusion-based processes like fused deposition modeling (FDM) and fused filament fabrication (FFF) [4].

AM may be used to print the extensive varieties of materials such as polymers, metals, and ceramics, as shown in Fig. 1. Nowadays, the most popular AM process material is polymer because of its low price and wide availability [5]. There is a huge potential for material choice and design, concerning the AM processes. There are many metals and alloys such as steel, steel alloys like stainless steel, tungsten, superalloys i.e. nickel-based alloy like Inconel 718, and titanium, that are specially applicable for the metal-based AM techniques. On the other hand, subtractive manufacturing is a very time consuming and expensive process [6]. AM technique called FDM process is quite efficient in producing plastic parts [7]. AM processes are completely numeric-controlled and automatic which are utilized to produce the prototypes with the minimum intervention of human beings [8]. The AM process involves the following three steps which include:

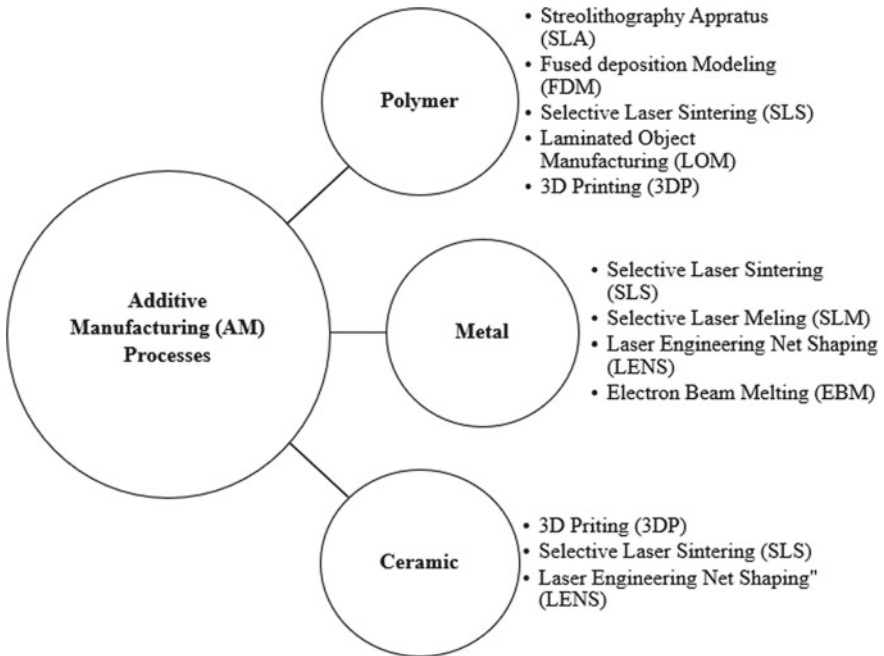


Fig. 1 AM processes classification based on raw materials

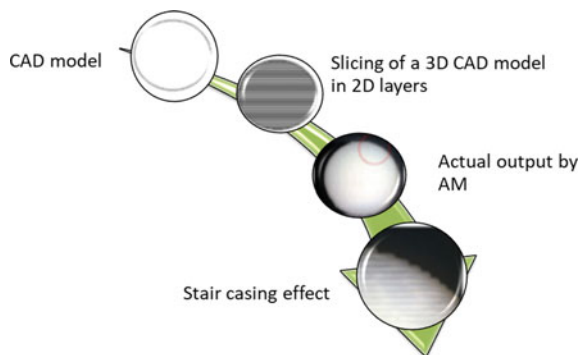
- (a) Computer-aided design (CAD) model in three-dimensional (3D) file format (3D-CAD) created with the help of available any commercial CAD software i.e. AUTOCAD, AUTODESK FUSION 360, SOLIDWORKS, PTC Creo, etc.
- (b) 3D-CAD model sliced into 2D layers,
- (c) G-code instruction file created with the help of any available slicing software i.e. Simplify 3D, Cura, Slic3r, Meshmixer, etc., and generating output by gradually stacking those 2D layers one after one by AM technique [9], as shown in Fig. 2.

For all applications, there is a great importance of dimensional accuracy, aesthetic appearance, and surface roughness [10]. Due to the surface roughness of the AM part, the aesthetic, as well as surface functionality becomes challenging. Various influential process parameters like raster angle, raster and contour angle, orientation angle, air gap, and layer thickness, etc. affect the resolution and accuracy of the AM printed part, and these factors also affect the surface roughness [11]. The roughness found on the AM part's surface is caused due to the stair-casing/stair-stepping effect of the layer manufacturing [9, 12]. This effect is generated mainly due to the method of the slice, in which one layer of molten polymer filament adheres to the previous layer, causes a predictable roughness on the end surface of the FDM part [13]. Alike all AM processes, the surface roughness is the major issue with FDM printed parts, as shown in Fig. 2. Before understanding the surface, improvement issues in FDM printed parts, the following section deliberates the FDM process.

2 FDM: The Most Widely Used AM Process

The processes are classified into polymer-based and metal-based AM processes. Although metal-based AM processes are growing up to the large extent in the current scenario but polymer-based AM techniques are well established and are used for manufacturing directly usable parts. Hence, only Polymer-based AM

Fig. 2 Sequence of the AM process and related stair casing/stair-stepping effect



techniques are discussed here in detail. Polymer-based AM techniques include the processes like material extrusion i.e. fused deposition modeling (FDM), direct ink writing (DIW), material jetting i.e. continuous ink printing (CIP), vat photopolymerization i.e. stereo lithography apparatus (SLA) and digital light processing (DLP), binder jetting i.e. 3D Printing (3DP), sheet lamination i.e. laminated object manufacturing (LOM), powder bed fusion i.e. selective laser sintering (SLS). The further classification of AM processes based on metals and polymers is shown in Fig. 3.

Few AM processes that have become the most popular manufacturing process for the product design industry such as FFF and FDM in the Polymer-based category are economical, easy to operate, the simplest type of AM process, hence being taken here for review. FDM is the world’s most flourishing and accepted AM process just because of its flexibility and simplicity in manufacturing as compared to the other AM techniques [14]. The process starts with the manufacturing of a 3D-CAD model by using appropriate CAD modeling software and converts it into a standard triangulation language or standard tessellation language (STL) file format that is recognized by the FDM machine [15]. Polylactic acid (PLA) and acrylonitrile butadiene styrene (ABS) are generally processed as the build material instead of nylon, wax, etc. Scaffolding is a water-soluble support material i.e. extruded through

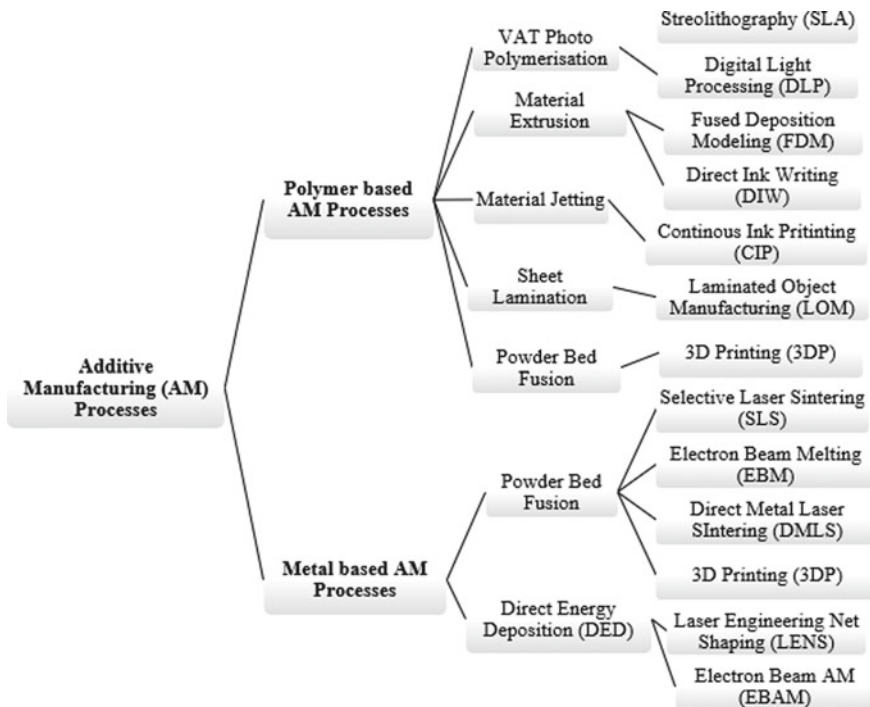


Fig. 3 AM processes: further classified based on polymers and metals

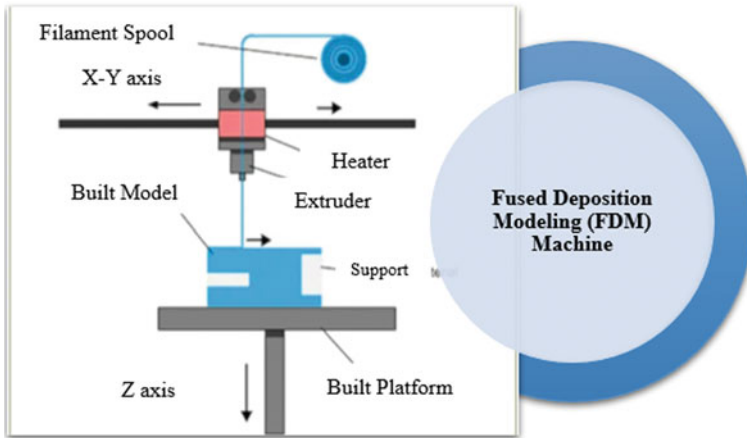


Fig. 4 Schematic diagram of the FDM machine

the second nozzle of the FDM Printer and flushed off from the surface with the help of chemicals like acetone [16]. Many other researchers have found commercial biomedical implant and device fabrication successfully by the investment casting of replicas produced by the FDM process. It has been utilized in a broad range of medical fields such as orthopedics, maxillofacial surgery, dental surgery, tissue engineering, neurosurgery, prosthesis, and orthosis [17]. FDM technology provides cost-effective, custom-made, and quick biomedical implants and devices based on real-time patient data to find out the particular geometrical information and clinical constraints. However, the poor surface quality and inaccurate dimensions hinder the use of these applications [18]. The schematic illustration of the FDM machine is presented in Fig. 4, describes the several components of the machine i.e. filament spool, heater, extruder, support, built platform, built model, and x-y-z-axis.

Different studies have been done on the different FDM process parameters such as build orientation, the orientation of material deposition, and layer thickness, to investigate the “stair-casing/stair-stepping effect.” Furthermore, various post-processing and pre-processing techniques have been discussed to obtain better results [14]. The following section deliberates the surface finish improvement issues of FDM printed parts.

3 Surface Finish Improvement Techniques for the FDM Printed Parts

The surface finish of the product is referring to the quality of mechanical products. The cracks start to build from the surface if the surface of the product is rough and it starts to propagate. If the surface of the product is smooth, then the crack resists its

initiation. The corrosion resistance property of the product also depends on surface quality [19]. It is a fact that FDM printing of a completely smooth surface is quite a difficult and challenging task. FDM process can't produce a completely smooth surface of the part. Many researchers tried to do it at different levels of parameters and modifying the slicing techniques but remain unsuccessful [20]. Two techniques are used to improve the finishing of the surface one is pre-processing, and another is post-processing [21].

3.1 Pre-processing Techniques for Improving the Surface Quality of FDM Printed Parts

The surface quality of the FDM printed product or part can be enhanced by optimizing the FDM process parameters like raster angle, raster and contour angle, built orientation, air gap, and layer thickness, etc. [22]. The pre-processing techniques are further classified into two branches, namely In-process Techniques and Adaptive Slicing, and these two branches are further divided into six and two branches respectively, as shown in Fig. 5.

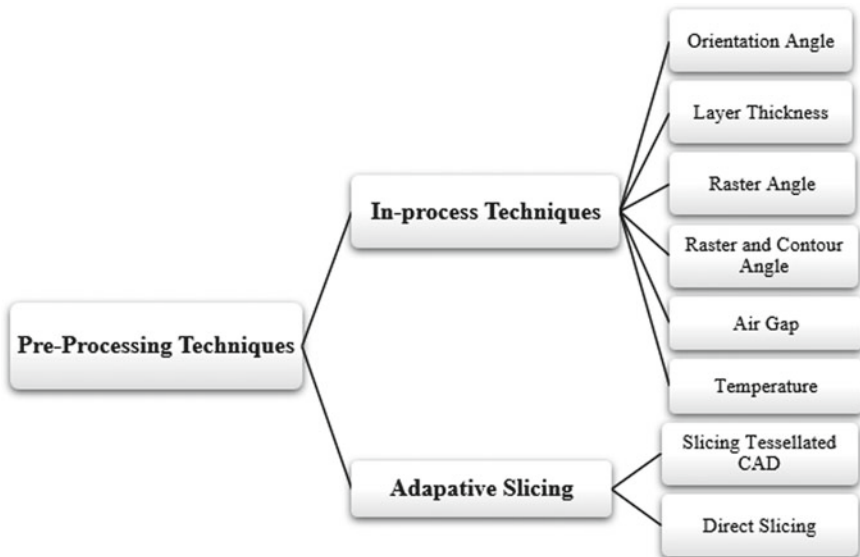


Fig. 5 Classification of pre-processing techniques for improving the surface quality of FDM printed parts

3.1.1 In-Process Techniques

In-process techniques involve the following process parameters during the conversion of 3D CAD file into G-code instructions file for FDM process:

Build Orientation

Researchers studied that the best pre-processing parameter to obtain the best surface quality is known as build orientation; it is also known as the deposition angle or angle of orientation. To obtain the desired results, the concerned CAD model can be changed [23]. The main objective of a build orientation is to obtain the best surface finishing of the FDM printed part. So, the optimization of the finishing process can be taken place at a particular build orientation and its respective angle on all positions of the FDM part [24].

Layer Thickness

The layer thickness is the layer height of the fused filament during the FDM printing process, which is deposited with the help of the extrusion heating nozzle, and this process is highly influential on the surface finish of the FDM printed part [25]. Before starting the process, there should be a trade-off between the thickness of the layer and build times. The increase in the build time increase in the stair-stepping, which should be fixed by the post-processing technique [26]. Nevertheless, the minimum value of layer thickness is essentially required to perform the FDM printing process [27].

Raster Width and Contour Width

The width of the molten filament, which deposit on the FDM printer bed, is known as raster width. When the raster width is minimum then the surface finishing and dimensional accuracy are maximum for the finishing FDM parts. It is also known as the smaller path width also plays a most important role in improving the surface finish as well as mechanical properties of FDM printed parts. On the other hand, the width of the outermost layer of the part is said to be Contour width. The wider the contour width, the better will be the dimensional accuracy and surface finishing. The direction of the raster, contour width, and filling strategy depend on tool paths, which are produce during the FDM printing process, affect the surface quality and mechanical features of the FDM part [28].

Air Gap

The air gap is the gap between two adjacent paths on the same fused filament layer. It is taken zero at the ends of the two nearest ends of the fused layer. The minimum surface finish is observed at the zero air gaps while the finishing of the surface increases at both the positive and negative air gaps [23].

Raster Angle

The direction of the raster plane with the x-axis is known as the raster angle. Researchers adopted two different raster angle strategies, one is criss-cross ($45^\circ/45^\circ$), and the other is cross ($0^\circ/90^\circ$). For the optimization of different outputs, some researchers changed the raster angle by $30^\circ/60^\circ$ [29].

Model Temperature

Model temperature is the specific temperature at which heating material extrusion nozzles are set to diffuse the outgoing FDM printer filament. The fluidity affects the surface roughness of the product; the change in model temperature can cause a change in fluidity. The high temperature of the model results in outstanding surface smoothness while the dimensional accuracy of the FDM printed part may be poor. The low temperature prevents the adhesion between the base plate and part material; as a result, the part can be replaced easily, but it reduces the finishing of the surface [30].

3.1.2 Adaptive Slicing

A technique which is the balancing agent between the build time and finishing of the surface is called as adaptive slicing technique [22]. In this technique, algorithms change the height of the slice and reduce the time of production; it also creates variable tool paths, depends on the minimum roughness of surface and geometry [31].

Slicing of the Three-Dimensional-Computer-Aided Design (3D-CAD) Tessellated Model

Kulkarni and Dutta studied and introduced the cusp height concept, which decides the fused filament layer thickness, and it further controls the surface roughness of the 3D printed part. The limit of the cusp height will be set by the user, and the algorithm will slice the CAD within the provided range. In this method, the cusp height and surface roughness are homogeneously restrictions for the complete surface [32].

Direct Slicing Software

Direct slicing software is utilized for slicing the CAD model directly with more accuracy and lesser time. It requires less storage for memory. In this software, the file is saved as an analytical surface such as parabolic, rectangular, and trapezoidal [33].

It can be said that adaptive slicing is a widely used process that develops algorithms to enhance the finishing of the surface of the parts. In addition to this, the quality of the surface can be enhanced only to a particular level, and it depends on the software and hardware [31, 34].

The FDM printed part mechanical properties and surface quality are dependent on the selection of optimum process parameters. Figure 6 represents the pre-processing and working process parameters of the process that must be optimized. Usually, pre-processing parameters can be categorized into two classes i.e. In-process parameters i.e. raster angle, raster and contour angle, raster width, built orientation, part infill style, and percentage, air gap, slice height, etc. and adaptive slicing i.e. slicing of the 3D-CAD tessellated model and direct slicing.

3.2 Post-processing Techniques for Improving the Surface Quality of FDM Printed Parts

Several post-processing techniques are used to perform the task for improving surface finish after the completion of the printing of the FDM part. These post-processing techniques are further classified into four different types, as shown in Fig. 7.

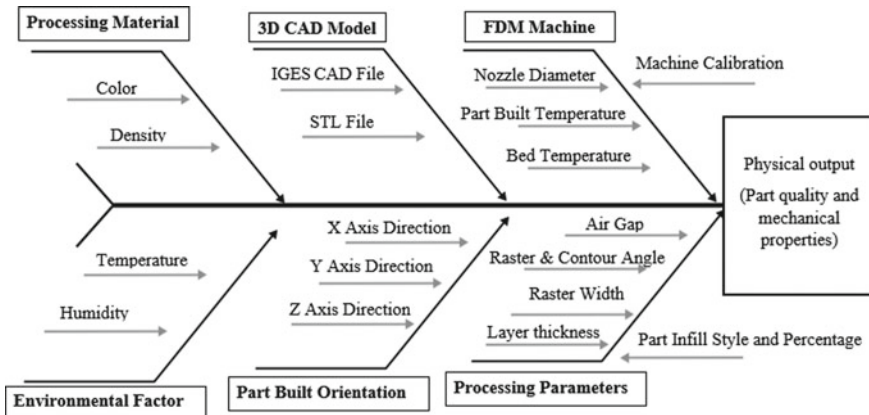


Fig. 6 Fishbone diagram for FDM process of AM

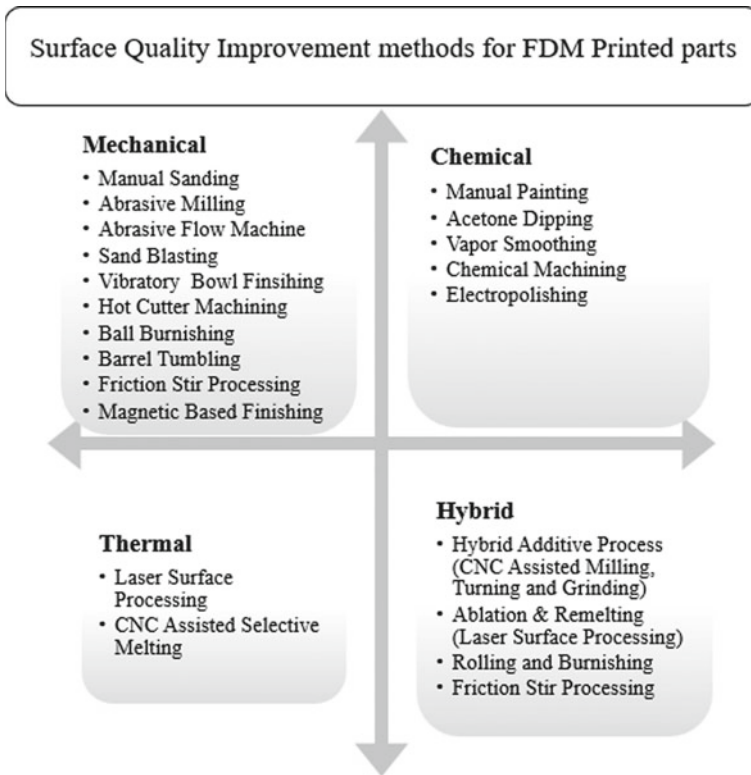


Fig. 7 Classification of surface quality improvement methods for the FDM printed parts

3.2.1 Mechanical finishing Techniques

In the mechanical finishing technique, the FDM part's surface profile is cut mechanically, or sometimes their peaks are pressed to improve the surface quality of the parts. This technique is similar to the technique of conventional metal finishing, but it quite differs when it comes in contact with the ABS plastics in comparison to metals. During this process of mass finishing, due to the abrasive action, remove the excess material from the corners and edges of the parts, and produce a good surface finishing [32].

Manual Sanding

This is a mechanical finishing technique. Several hand tools consisting of steel wool brushes and sandpapers of 120–320 grit sizes are used for finishing [33]. Furthermore, manual finishing isn't effective when the part has intricate shapes.

Only a skilled operator can perform manual sanding on FDM printed parts as the process cannot be controlled, is not consistent and accurate measurement is a challenge [35].

Abrasive Flow Machining (AFM)

Abrasive flow finishing (AFF) or abrasive flow machining (AFM) is a non-conventional finishing process for complicated parts where abrasive laden visco-elastic media is utilized to polish the parts' surface under the influence of extrusion pressure. The abrasion needs to be guided over the surfaces to be finished by component-specific tooling. During the process, abrasives impinging take place on the burrs and rough surface until a smooth surface is obtained. Since gives freedom to print complicated parts, AFM is naturally a suitable process of finishing parts printed by AM in general and FDM in particular. Mali et al. have investigated the AFF process for surface finishing of the ABS parts printed by the FDM process. A sustainable polymer abrasive gel-based media (SPAGM) was developed by mixing abrasive particles i.e. SiC, a natural polymer as a base material, and natural additives as a liquid synthesizer in a different percentage of proportion and size, then various properties of prepared SPAGM media were experimentally checked by their material characterization methods. Maximum improvement of surface finish was found ΔRa 6.27 μm for the internal surface and ΔRa 21.37 μm for the external surface [36]. The schematic diagram of abrasive flow machining (AFM) for the finishing of the FDM printed part is presented in Fig. 8, describes the several components of the machine i.e. upper and lower hydraulic cylinder, upper and lower abrasive media cylinder, a fixture for holding the FDM printed part.

Abrasive Jet Deburring

Abrasive Jet Deburring investigated by the researchers for the Stereo Lithography Apparatus (SLA) based printed polymer parts. However, there is a disadvantage to this method, as it removes the material unevenly because it can't control the pressure. As a result, the weight loss of the part is observed about 5.85% and a reduction in thickness is also observed [37].

Sandblasting

There is an industrially popular technique called sandblasting. It provides a 96% improvement in surface roughness; it is generally applied after the vapor smoothing process. According to the industrialists, sandblasting is an ultra-fine finishing process. It can provide matte finishing to the parts because the glossy surface is emanated due to the chemical and vapor exposure [38]. The schematic diagram of

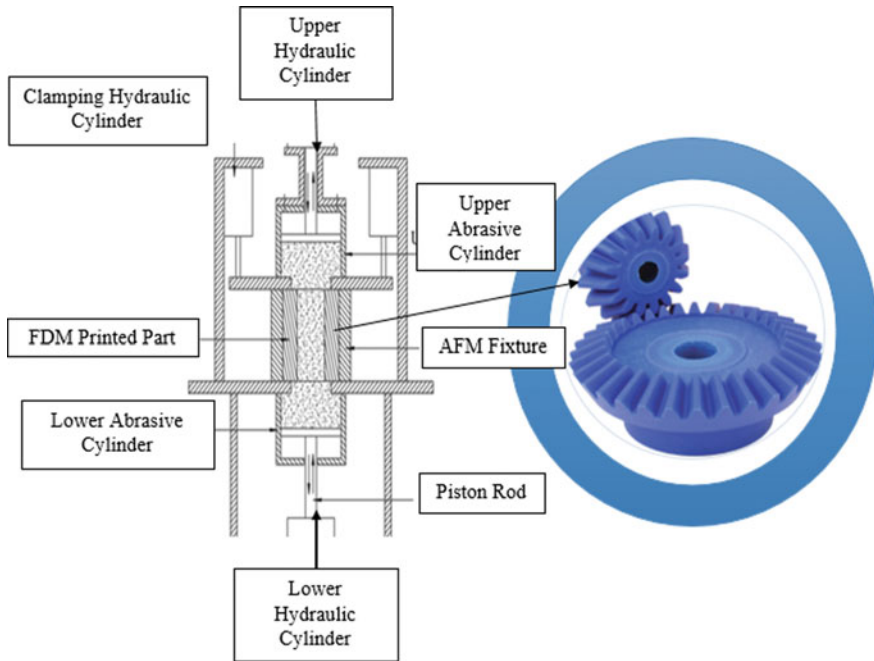


Fig. 8 Schematic diagram of the abrasive flow machine (AFM)

sandblasting of the FDM printed part is presented in Fig. 9, which describes the several components of the machine i.e. grit feeder, vacuum chamber, compressor, and nozzle to finish the FDM Printed part.

Vibratory Bowl finishing

In the vibratory bowl finishing process, the mass finishing of the FDM printed part takes place by the mixture of abrasive grit and water via a vibrating spring-mass system. The removal rates of different materials are found quite different, and it depends upon several factors, including the shape, media size, weight, and compounds [39]. At the end of the shaft, it is found that there are two eccentric weights group attached. For the ABS plastic parts, it is better to keep the media weight low and run the machine for a longer period [40]. The schematic diagram of vibratory bowl finishing of the FDM printed part is presented in Fig. 10, describes the several components of the machine i.e. vibratory bowl, orienting device grit feeder, tracker to finish the FDM printed part.

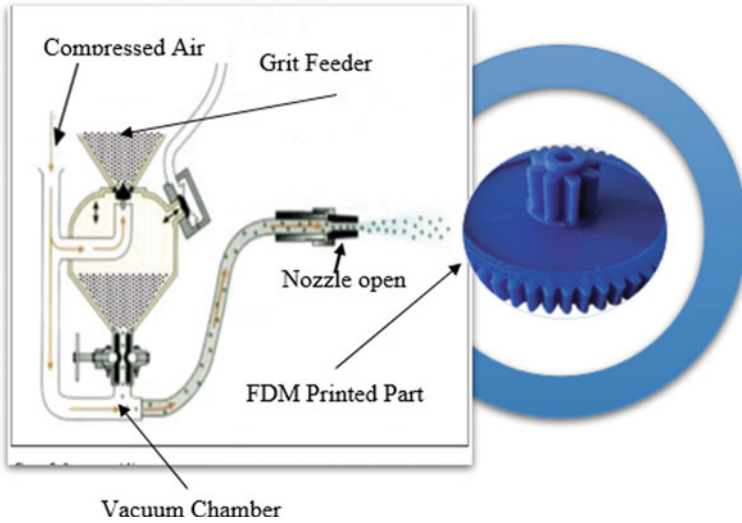


Fig. 9 Schematic diagram of the sandblasting

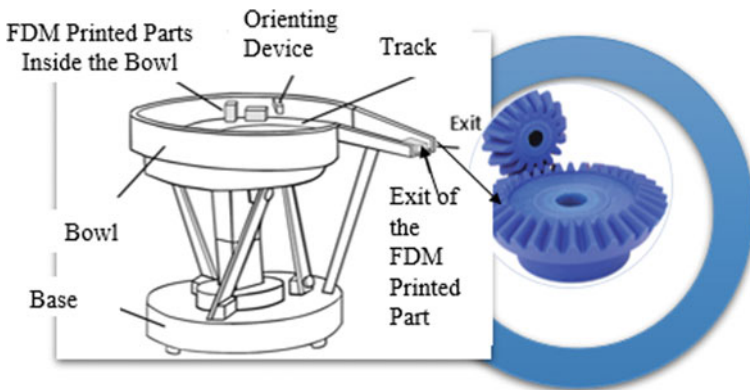


Fig. 10 Schematic diagram of the vibratory bowl finishing barrel tumbling

Barrel Tumbling

The Barrel Tumbling is the process of mass surface finishing of the FDM printed part that is used for the debarring, fine finishing, and surface modification. Some factors control the removal rate, including machining time, rotation speed, and media size and shape [41]. During barrel tumbling, parts are put in the closed rotating tube with media, abrasive compound, and water. There is a quite low initial cost for maintenance and operation [7]. The schematic diagram of barrel tumbling

of the FDM printed part is presented in Fig. 11, describes the several components of the barrel tumbling machine i.e. water and compound, abrasives, rotating barrel, and tumbler to finish the FDM printed part.

Hot Cutter Machining

The technique of hot cutter machining is quite successful in improving the surface finish of the FDM printed part. The cutting direction and rake angle are two major factors that impact the process [42]. For the concern about the construction, the hot cutters have different shapes that are fastened with the numerically controlled machine that is making traverse motion in the X-Y direction with the slice's periphery. The simulation can be achieved with this technique, which will suggest an improvement in the surface roughness. There is also a disadvantage that it will take a higher cost and time [22]. The illustrative line diagram of hot cutter machining of the FDM printed part is presented in Fig. 12, describes the several components of the hot cutter machine i.e. hot milling cutter, rotation of the tool, normal force to finish the FDM printed part.

Ball Burnishing Process

The ball burnishing process is used to fill out the valleys and press the peaks of the surface of the parts. The work is held between the head and tailstock. Few factors can help in improving the finishing of surfaces, such as an increase in the speed of the spindle, and the penetration depth for ABS parts. As the force of the burnishing tool increase, the hardness is also increased [43]. The schematic diagram of ball burnishing of the FDM printed part is presented in Fig. 13, which describes the several components of the ball burnishing machine i.e. Normal force, roller rotation, and burnishing roller to finish the FDM Printed part.

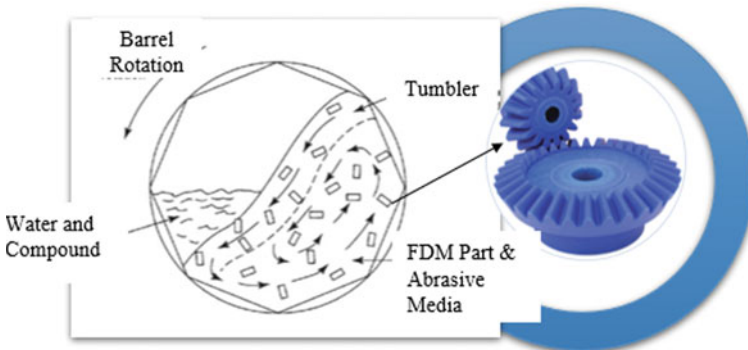


Fig. 11 Schematic diagram of the barrel tumbling

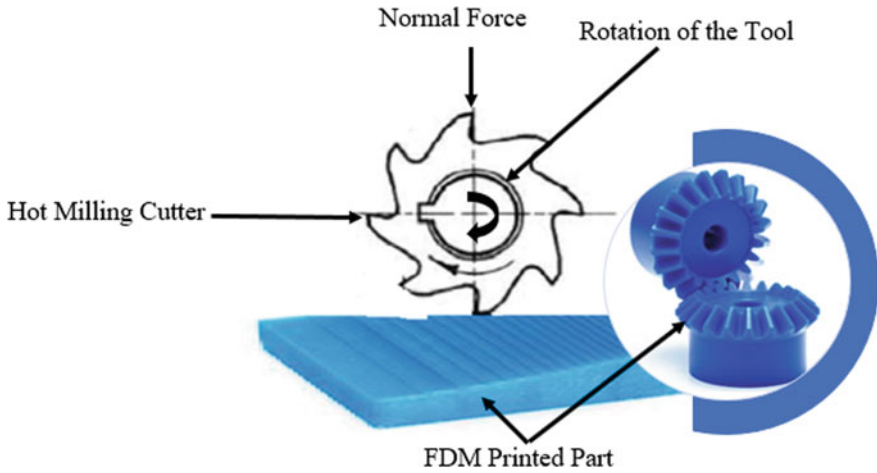


Fig. 12 Schematic diagram of the hot cutter machining

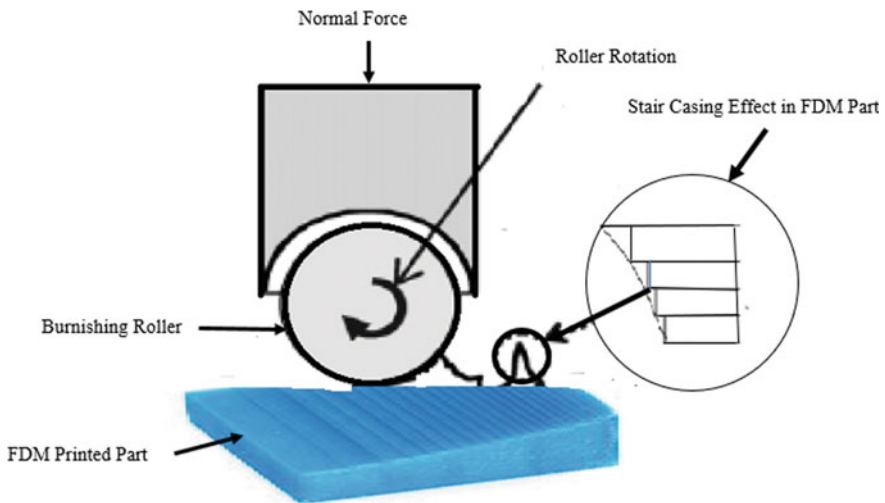


Fig. 13 Schematic diagram of the ball burnishing

Magnetic Abrasive Finishing (MAF)

Magnet abrasive finishing (MAF) is the most suitable way to increase the quality of the surface on both non-metallic and metallic surfaces. It can be utilized for complex product finishing, which is quite difficult by using conventional processes. In this process, the abrasive and magnetic properties of media can remove the tooling allowance by using a magnetic field that acts as a grain binder [42]. MAF has a lot of advantages, such as no dressing, and compensation is required for the finishing tool,

self-sharpening, controllability, and self-adaptability [44]. The illustrative line diagram of the magnetic abrasive finishing (MAF) of the FDM printed part is presented in Fig. 14, describes the several components of the machine i.e. magnetic tool, flexible magnetic abrasive brush to finish the FDM Printed part.

Friction Stir Processing (FSP)

The process of surface modification is employed for improving the mechanical properties of FDM printed parts and enhance surface integrity, which is called friction stir processing (FSP) [45]. This method is to work on the principle of friction stir welding, which is a solid-state based welding process. The characterization of friction stir processing may be done by low-temperature processing, mixing of surface layers, fine-grain microstructure, and healing of casting defects [46]. In addition to this, FSP is an environmentally friendly technique that doesn't require a high amount of heat to operate, and it doesn't produce different gases, radiations, and fumes that can cause safety hazards for human life [47]. The illustrative line diagram of friction stir processing of the FDM printed part is presented in Fig. 15, describes the several components of the machine i.e. tool rotation, torque, traveling force, and friction stir tool to finish the FDM Printed part.

3.2.2 Chemical Finishing Techniques

There is a better finishing technique for the plastics, where the surface can be improved just by the action of chemicals. This technique doesn't require any tool to be in contact with the surface; as a result, there will be no change in the dimension of parts [48].

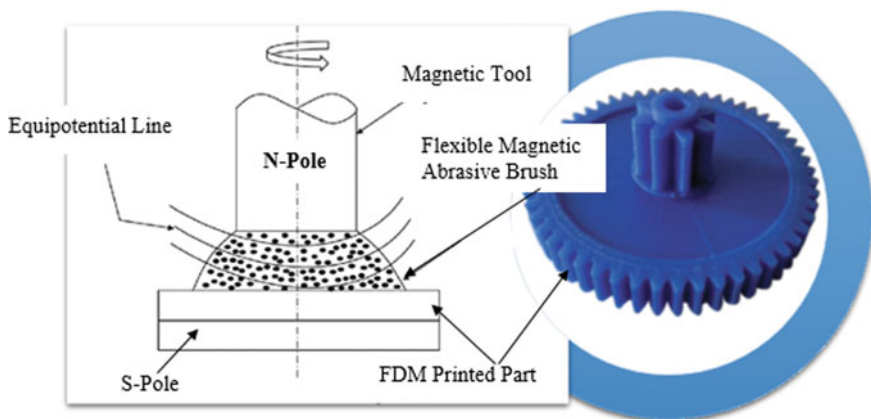


Fig. 14 Schematic diagram of the magnetic abrasive finishing

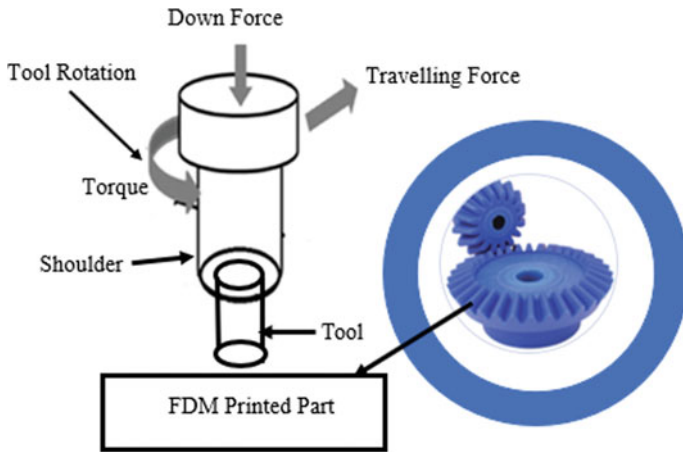


Fig. 15 Schematic diagram of the friction stir processing

Manual Painting

Few chemicals can be used for the smoothness of ABS parts, including thinner, acetone, toluene, and heptane. This method dissolves the extra edges and connects the layers [49]. These chemicals can be manually used for painting, it will save time and money, but the manual painting isn't consistent as the automatic painting, so there will be uneven surface finishing.

Acetone Dipping

The acetone dipping is another way to improve the finishing of the surface, FDM parts dipped into the aqueous solution of acetone for a particular time. It also has an excellent peeling property of the surface [50]. In the post-processing techniques, acetone dipping is quite an easy, effective, quick, and cost-effective way to improve surface finishing. There is a danger that the parts can be dissolved in the solution if it keeps dipped for a long time. If someone wants to keep it dipped for a longer period, have to use a diluted solution [51]. The illustrative line diagram of acetone dipping of the FDM printed part is presented in Fig. 16, describes the several components of the acetone dipping machine i.e. closed container, Platform, and liquid acetone to finish the FDM Printed part.

Vapor Smoothing

The Vapour smoothing technique is an advanced technique to improve the aesthetic appearance, dimensional accuracy, and surface quality of the FDM printed parts. In

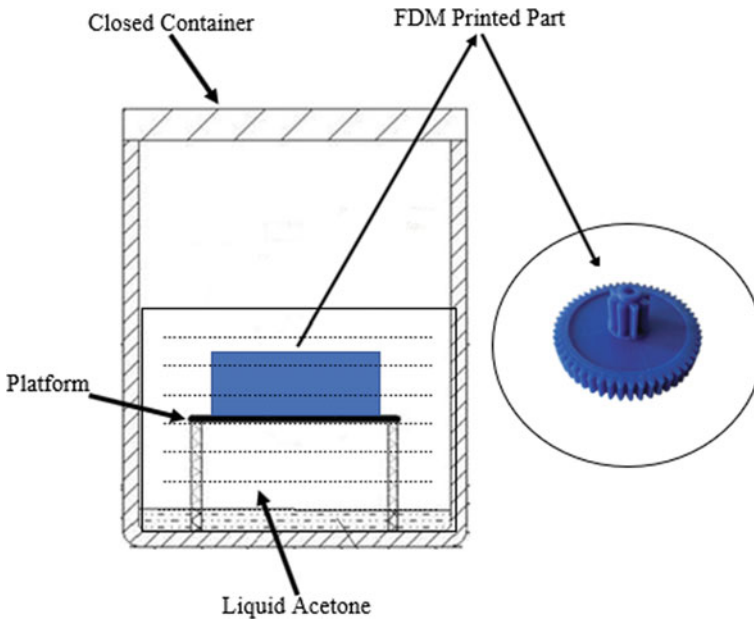


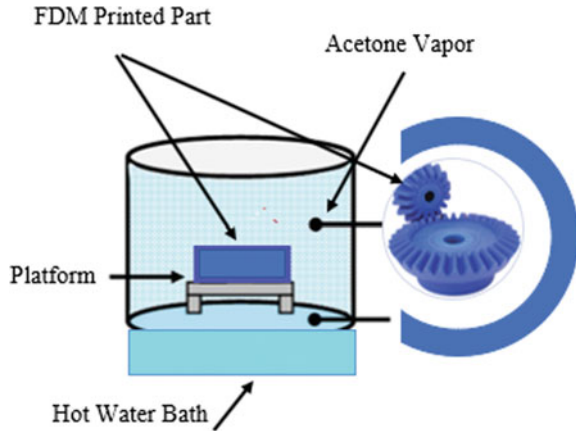
Fig. 16 Schematic diagram of the acetone dipping

this process, the part's surface temporarily reflows by the application of excess heat of chemicals within the controlled environment. It is used for the ABS parts surface finishing. In this process, the parts first cooled in the drying chamber; after this, it hangs inside the smoothing chamber where a particular amount of solvent is heated; as a result, the chemical vapor rise inside the chamber. These vapors rise and deposit on the surface of ABS parts where the condensation and infuse take place on the surface and make it temporarily flattened due to the surface tension. This process continues and completes three cycles; after this, it is put into the blasting of baking soda. Where the readings at the beginnings and end of the process cause great smoothness on the surface but produce a little change in dimensions [52]. The schematic diagram of vapor smoothing of the FDM printed part is presented in Fig. 17, which describes the several components of the vapor smoothing machine i.e. hot water bath, platform, and acetone vapor to finish the FDM Printed part.

Electroplating

Electroplating is another way to improve the roughness of the surface; in this method, first clean the surface and coat with palladium, here the palladium performs the functions of the bonding agent. By using this method, a thin chromium layer is deposited, which more durable and increases the wear assistance, mechanical strength, and surface finish [53]. There are some limitations to this process, and one

Fig. 17 Schematic diagram of the vapor smoothing



is that it is quite a cost to process, and the next one is its limited application in the industry. This method provides better hardness and mechanical strength, but it also changes the dimensions of parts [54].

3.2.3 Thermal Finishing Techniques

Thermal finishing techniques use the application of thermal energy to improve dimensional accuracy and surface quality of FDM parts. Researchers have used Laser-based surface Processing methods for finishing the FDM parts. These methods are discussed below:

Laser-Based Surface Processing

The FDM part surface is melted by the implication of laser energy is known as laser re-melting (LR) or laser-based surface processing. A melt pool gets created when a laser beam strikes the surface of the FDM part. Here, the surface tension and gravity adjust the level of the melt pool. As the beam of the laser was removed from the surface of the FDM part, there was a rapid reduction of temperature occurs and the melt pool rapidly solidifies with the reduction in the roughness of the surface, as shown in Fig. 18. This technique is applied to several metallic materials such as steel, and aluminum, titanium, nickel, their respective alloys, etc. as well as polymer materials such as ABS and PLA, etc. [55].

Chai et al. have investigated the laser-based surface processing of FDM parts by employing contactless laser scanning equipment to improve dimensional accuracy and surface quality of FDM printed thermoplastics. It was experimented on the thermoplastics, analyzed the final results, and found a 68% reduction in the final surface roughness [56]. Taufik et al. have investigated the laser-based surface

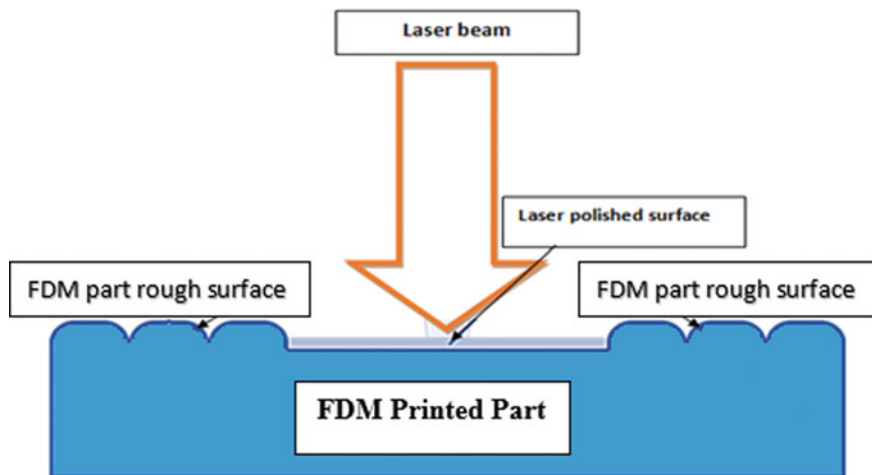


Fig. 18 Laser-based surface processing

processing of the FDM printed parts. The 120 W power of pulsed mode CO₂ laser was employed to finish the ABS printed parts by FDM technique. The Design of Experiment (DOE) and statistical analysis were employed to investigate the effect of various post-processing and pre-processing parameters like build orientation, skewness, kurtosis, and surface roughness. The results show that laser-based surface finishing is ten times more effective than other post-processing methods for FDM printed parts [57]. F. Lambiase et al. have investigated the laser-based surface processing of PLA parts produced by the MakerBot FDM printer. The continuous wave (CW) mode CO₂ laser of 30 W was employed for improving the surface finish of PLA parts. The initial surface roughness ΔRa 16 μm was improved up to the optimal value of ΔRa 0.3 μm [58]. Chen et al. have investigated laser polishing for improving the surface finish of Al/PLA printed parts by FDM technique. The fiber laser with 1070 nm wavelength and 200 W power was employed for laser polishing. The initial surface roughness was reduced from the ΔRa 5.64 μm to ΔRa 0.32 μm [59]. Kumbhar et al. investigated the laser-based surface processing of FDM parts. The CO₂ laser with 40 W power and 10.6 μm wavelength was employed for improving the surface finish of ABS plastic FDM printed parts. The initial surface roughness reduced from ΔRa 4.2484 μm to ΔRa 0.228 μm after the laser-based surface processing [60]. Chen et al. have investigated the laser polishing of Cu/PLA printed parts by FDM technique. A fiber laser with 1,070 nm wavelength and 200 W power was employed for laser-based surface processing. The initial surface roughness reduced from ΔRa 10.52 μm to ΔRa 0.87 μm after the laser polishing and reduced by more than 91% at the optimum polishing parameters [61]. Krishna et al. investigated the combined effect of different post-processing techniques i.e. acetone vapor smoothening, laser-assisted finishing, and shot-blasting methods for FDM parts. The combined effect of different

post-processing techniques including laser-based finishing was not only improved the surface roughness but also intensify the aesthetic properties of the ABS printed parts. The initial surface roughness was reduced from ΔRa 10.52 μm to ΔRa 0.87 for 0° surface, and from ΔRa 9.84 μm to ΔRa 2.2 μm for 90° surface [62].

CNC Assisted Selective Melting (SM) Tool

M. Taufik et al. have suggested the unique idea of the selective melting (SM) tool. Selective melting (SM) is defined as a novel post finishing CNC-assisted tool that has been designed and developed for built parts of FDM. The peak to valley height reduces the materials in chips form have been removed, unlike the conventional post-finishing process. The material of semi-solidified peaks fills inside the neighboring valleys by SM tool to reduce the surface roughness of FDM parts. The issues like location error effect, inner defect, scallop's minimization, and formation of post finishing irregular patterns have been overcoming by this study. By implementing this process FDM built parts surface finishing condition improved [63]. The illustrative diagram of the CNC-assisted SM tool for finishing the FDM parts is presented in Fig. 19.

3.2.4 Hybrid-Based Surface Finishing

Hybridization is one of the essential approaches for developing an efficient and flexible manufacturing process. This strategy combines two different tools or

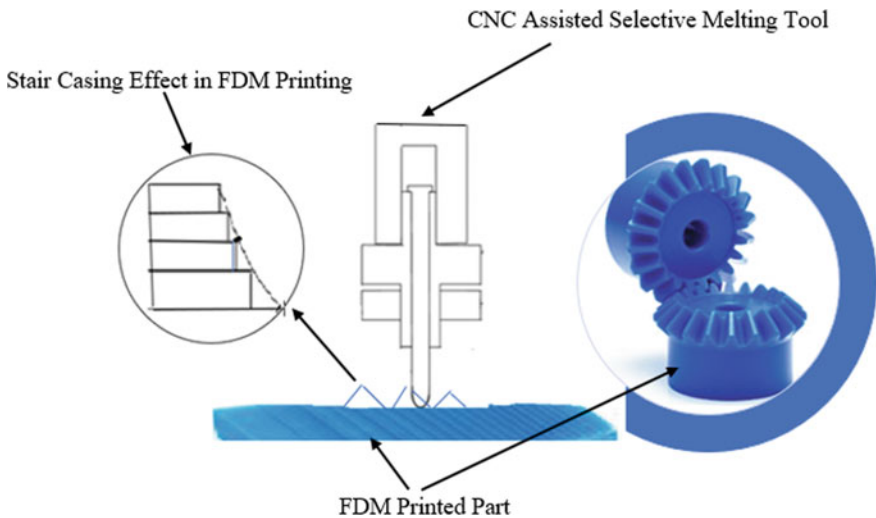


Fig. 19 Schematic diagram of the CNC assisted selective melting tool

energy sources. The additive technique is combined with CNC milling; thus, external and internal surfaces are machined by traditional or CNC machines. With the help of the RP and CNC method, a new optimum manufacturing solution, namely hybrid RP or ECLIPSE-RP, has been proposed. The accuracy from CNC and one setup process from RP have been combined to obtain better results in a single station. This new proposed hybrid system produced trimmed FDM with high accuracy, and excellent surface completion [64]. As it is reviewed, the main defect that arises from the FDM part is due to the staircase/stair-stepping effect that would require post-processing techniques and pre-processing techniques to reduce these defects. The difficulty is the accessibility to complex geometrical features and undercuts. In this research, the various surface finishing methods have been discussed. The new proposed RP system has decreased the build time and enhanced the accuracy of shape and size.

Lee et al. proposed a new hybrid RP system using an FDM machine, placed on each end of the five-axis machine. This new proposed hybrid system produced a trimmed FDM part with high accuracy and excellent surface finish. It leads to stability. This method reduced the build time by 44% and 58%, respectively [65].

According to the study of laser-based surface processing, there are many varieties of laser present in the manufacturing industries for material processing. Among them, the Carbon Dioxide Laser (CO_2) is the most popular one because it consists of high efficiency, high average power, and rugged construction. Besides this, Nd: YAG is also the most popular solid-state laser employed in the manufacturing industries. There are four types of this laser-based on different wavelengths, such as 1,064, 532, 355, 266 nm, and along with this, if there is a limitation of diffraction, it should be spot on with simple external beam steering optics so, the copper laser is the best option. This laser required much more maintenance and have a short lifetime as compared to the Nd: YAG. The excimer laser is also widely used for the application of materials processing. The most popular excimer laser are XeF, KrF, ArF, and F2. These lasers emit the radiation of the wavelength of 351 nm, 249 nm, 193 nm, and 157 nm, respectively. According to laser scientists, surface ablation occurs on the material surface by high beam intensities laser because of the short pulse, short wavelength. It provides crisp and clean features in glasses, ceramics, metals, composites, and polymers. This method makes these mentioned materials quite flexible for the applications of micro manufacturing [66]. Vispute et al. investigated a unique approach named the hybrid additive subtractive manufacturing (HASM) process for improving the dimensional accuracy and surface finish of the FDM parts. The novel material deposition tool (MDT) was fabricated for printing the polymer parts as similar to the FDM technique. The indigenous G-code tool path instruction file was created by following the HASM process approach on the MATLAB software. The final roughness of the MDT printed polymer part was reduced from ΔRa 19.495 μm to ΔRa 2.068 μm after machining [67].

4 Conclusions

The review of various surface quality improvement methods for FDM printed parts presented in this chapter described that various research on the field of surface finishing of FDM printed parts are still in its progressive phases and many hurdles are needed to be removed to get the best desired results for commercial application requirements. The staircase effect is the most challenging issue that occurs during any of the layer manufacturing processes, so it also comes into the picture during the FDM printing process, so it needs to be removed or minimize as possible by using any pre-processing or post-processing techniques includes surface quality improvement methods for FDM printed parts which are systematically elaborated in this chapter. The review showed that the surface roughness of the FDM Printed part is very high as compared to the other AM processed part. Several researchers have implemented various kinds of surface finishing techniques for improving the aesthetic appearance, dimensional accuracy, and surface quality of FDM Printed parts. In this Chapter, literature has been reviewed on different surface finishing techniques of the FDM Printed part. There are various methods to improve surface finishing and reduce the roughness of FDM printed parts. Figure 20 represents the various surface quality improvement methods for FDM printed parts that must have to be adopted at the end stage of the FDM printing process. Based on the review carried out, surface quality improvement methods for FDM printed parts can be categorized into four groups based on the physics and mechanism used in the process i.e. mechanical, chemical, thermal, and hybrid surface finishing techniques.

Since the problem of poor surface quality is part of FDM printed parts, it is quite important to select the most suitable surface quality improvement method as per the conditions and requirements. In this review, the applications, advantages, and limitations of both “pre-processing” and “post-processing” finishing techniques are discussed. Conclusively, it can be said that the dimensional accuracy and surface finish of FDM printed parts can be effectively improved by the abrasive flow

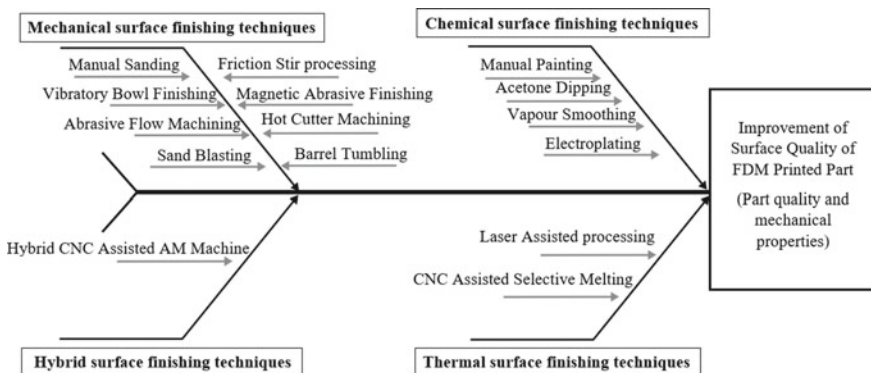


Fig. 20 Fishbone diagram for various surface quality improvement methods for FDM printed part

finishing (AFF) process for any freeform surfaces having functional surface requirements. For flat surfaces, Laser polishing techniques are best in use. At the same time, the chemical finishing technique is best for complex structures and geometries. In the end, it can be said that there is a great future for the development of AM surface improvement technologies, and more effective ways to improve the dimensional accuracy and surface finish of the AM parts not only in polymers but also in metals.

5 Future Scope

The research of various pre-processing and post-processing techniques leads to an understanding of the importance of surface finish in FDM printed parts. Therefore, it is imminent to obtain a good surface finish of products for every scale of the product. Some of the future challenges and dimensions in the surface finishing of FDM Printed parts are identified below:

- Surface roughness at nano-scales has not been a subject of consideration in major researches. There is still room for investigation on the nanoscale surface finish to attain better properties in an FDM Printed object.
- A comparison of in-built surface finishing techniques and separate procedures to carry out the surface finish of the product in terms of empirical analysis is also not widely researched.
- Another domain is the investigation of the effect of different surface finishing techniques for the FDM Printed smart materials, including self-cleaning and self-healing surfaces.
- Abrasive flow machining (AFM) may be a promising solution for improving the aesthetic appearance, dimensional accuracy, and surface finish of FDM printed parts. It needs to further investigate the optimum process parameters for a better surface finish.

References

1. Hassanin H, Elshaer A, Benhadj-Djilali R, Modica F, Fassi I (2018) Surface finish improvement of additive manufactured metal parts. In: Gupta K (ed) Micro and precision manufacturing. Engineering Materials. Springer International Publishing, Cham, pp 145–164. https://doi.org/10.1007/978-3-319-68801-5_7
2. Kumbhar NN, Mulay AV (2018) Post processing methods used to improve surface finish of products which are manufactured by additive manufacturing technologies: a review. J Inst Eng India Ser C 99(4):481–487. <https://doi.org/10.1007/s40032-016-0340-z>
3. Wong CH, Fung E (2015) More toxic goods stored near Tianjin homes. Wall Street J

4. Campbell RI, Martorelli M, Lee HS (2002) Surface roughness visualisation for rapid prototyping models. *Comput Aided Des* 34(10):717–725. [https://doi.org/10.1016/S0010-4485\(01\)00201-9](https://doi.org/10.1016/S0010-4485(01)00201-9)
5. Yang S, Li W (2018) Surface quality and finishing technology. In: *Surface finishing theory and new technology*. Springer Berlin Heidelberg, Berlin, Heidelberg, pp 1–64. https://doi.org/10.1007/978-3-662-54133-3_1
6. Thomas DS, Gilbert SW (2014) Costs and cost effectiveness of additive manufacturing. NIST SP 1176. National Institute of Standards and Technology, p NIST SP 1176. <https://doi.org/10.6028/NIST.SP.1176>
7. Boschetto A, Bottini L (2015) Surface improvement of fused deposition modeling parts by barrel finishing. *Rapid Prototyping J* 21(6):686–696. <https://doi.org/10.1108/RPJ-10-2013-0105>
8. Dutta D, Prinz FB, Rosen D, Weiss L (2001) Layered manufacturing: current status and future trends. *J Comput Inf Sci Eng* 1(1):60–71. <https://doi.org/10.1115/1.1355029>
9. Gross BC, Erkal JL, Lockwood SY, Chen C, Spence DM (2014) Evaluation of 3D printing and its potential impact on biotechnology and the chemical sciences. *Anal Chem* 86(7):3240–3253. <https://doi.org/10.1021/ac403397r>
10. Chohan JS, Singh R (2017) Pre and post processing techniques to improve surface characteristics of FDM parts: a state of art review and future applications. *Rapid Prototyping J* 23(3):495–513. <https://doi.org/10.1108/RPJ-05-2015-0059>
11. Frazier WE (2014) Metal additive manufacturing: a review. *J Mater Eng Perform* 23(6):1917–1928. <https://doi.org/10.1007/s11665-014-0958-z>
12. Seifi M, Salem A, Beuth J, Harrysson O, Lewandowski JJ (2016) Overview of materials qualification needs for metal additive manufacturing. *JOM* 68(3):747–764
13. Tyberg J (1998) Local adaptive slicing for layered manufacturing. Thesis, Virginia Tech
14. Jain P, Kuthe AM (2013) Feasibility study of manufacturing using rapid prototyping: fdm approach. *Procedia Eng* 63:4–11. <https://doi.org/10.1016/j.proeng.2013.08.275>
15. Lee J, Huang A (2013) Fatigue analysis of FDM materials. *Rapid Prototyping J* 19(4):291–299. <https://doi.org/10.1108/13552541311323290>
16. Singh R, Singh S, Kapoor P (2016) Investigating the surface roughness of implant prepared by combining fused deposition modeling and investment casting. *Proc Inst Mech Eng Part E: J Process Mech Eng* 230(5):403–410. <https://doi.org/10.1177/0954408914557374>
17. Hanus A, Špirutová N, Beňo J (2011) Surface quality of foundry pattern manufactured by FDM method-rapid prototyping. *Arch Foundry Eng* 11(1):15–20
18. Körner C (2016) Additive manufacturing of metallic components by selective electron beam melting—a review. *Int Mater Rev* 61(5):361–377. <https://doi.org/10.1080/09506608.2016.1176289>
19. Carter EM, Caldwell B (1993) *Return of the mentor: strategies for workplace learning (education policy perspectives)*. Falmer Press
20. Yadollahi A, Shamsaei N (2017) Additive manufacturing of fatigue resistant materials: challenges and opportunities. *Int J Fatigue* 98:14–31. <https://doi.org/10.1016/j.ijfatigue.2017.01.001>
21. Grzenda M, Bustillo A (2013) The evolutionary development of roughness prediction models. *Appl Soft Comput* 13(5):2913–2922. <https://doi.org/10.1016/j.asoc.2012.03.070>
22. Pandey PM, Thirumurthulu K, Reddy NV (2004) Optimal part deposition orientation in FDM by using a multicriteria genetic algorithm. *Int J Prod Res* 42(19):4069–4089. <https://doi.org/10.1080/00207540410001708470>
23. Sood AK (2011) Study on parametric optimization of fused deposition modelling (FDM) Process. PhD
24. Gurralla PK, Regalla SP (2014) DOE based parametric study of volumetric change of FDM parts. *Procedia Mater Sci* 6:354–360. <https://doi.org/10.1016/j.mspro.2014.07.045>
25. Vasudevarao B, Natarajan DP, Henderson M, Razdan A (2000) Sensitivity of RP surface finish to process parameter variation 251. <https://doi.org/10.26153/TSW/3045>

26. Vijay P, Danaiah P, Rajesh K (2011) Critical parameters effecting the rapid prototyping surface finish. *J Mech Eng Autom* 1(1):17–20
27. Nanchariaiah T, Raju DR, Raju VR (2010) An experimental investigation on surface quality and dimensional accuracy of FDM components. *Int J Emerg Technol* 1(2):106–111
28. Peng AH (2012) Methods of improving part accuracy during rapid prototyping. *AMR* 430–432:760–763. <https://doi.org/10.4028/www.scientific.net/AMR.430-432.760>
29. Ahn D, Kim H, Lee S (2009) Surface roughness prediction using measured data and interpolation in layered manufacturing. *J Mater Process Technol* 209(2):664–671. <https://doi.org/10.1016/j.jmatprotec.2008.02.050>
30. Luzanin O, Movrin D, Plancak M (2013) Experimental investigation of extrusion speed and temperature effects on arithmetic mean. *J Technol Plast* 38(2)
31. Mohan Pandey P, Venkata Reddy N, Dhande SG (2003) Slicing procedures in layered manufacturing: a review. *Rapid Prototyping J* 9(5):274–288. <https://doi.org/10.1108/13552540310502185>
32. Mani K, Kulkarni P, Dutta D (1999) Region-based adaptive slicing. *Comput Aided Des* 31(5):317–333. [https://doi.org/10.1016/S0010-4485\(99\)00033-0](https://doi.org/10.1016/S0010-4485(99)00033-0)
33. Boschetto A, Giordano V, Veniali F (2012) Modelling micro geometrical profiles in fused deposition process. *Int J Adv Manuf Technol* 61(9–12):945–956. <https://doi.org/10.1007/s00170-011-3744-1>
34. Pandey PM, Reddy NV, Dhande SG (2003) Real time adaptive slicing for fused deposition modelling. *Int J Mach Tools Manuf* 43(1):61–71. [https://doi.org/10.1016/S0890-6955\(02\)00164-5](https://doi.org/10.1016/S0890-6955(02)00164-5)
35. Spencer JD, Cobb R, Dickens P (1993) Surface finishing techniques for rapid prototyping. *Tech Pap Soc Manuf Eng Series*
36. Mali HS, Prajwal B, Gupta D, Kishan J (2018) Abrasive flow finishing of FDM printed parts using a sustainable media. *Rapid Prototyping J*
37. Leong KF, Chua CK, Chua GS, Tan CH (1998) Abrasive jet deburring of jewellery models built by stereolithography apparatus (SLA). *J Mater Process Technol* 83(1–3):36–47. [https://doi.org/10.1016/S0924-0136\(98\)00041-7](https://doi.org/10.1016/S0924-0136(98)00041-7)
38. Wennerberg A (1996) Experimental study of turned and grit-blasted screw-shaped implants with special emphasis on effects of blasting material and surface topography. *Biomaterials* 17(1):15–22. [https://doi.org/10.1016/0142-9612\(96\)80750-2](https://doi.org/10.1016/0142-9612(96)80750-2)
39. Schmid M, Simon C, Levy G (2009) Finishing of SLS-parts for rapid manufacturing (RM)—a comprehensive approach. *Proceedings SFF*, pp 1–10
40. Borrás L, Mohr S, Brandt P-Y, Gilliéron C, Eytan A, Huguélet P (2007) Religious beliefs in schizophrenia: their relevance for adherence to treatment. *Schizophr Bull* 33(5):1238–1246
41. Fischer M, Schöppner V (2013) Some investigations regarding the surface treatment of Ultem* 9085 parts manufactured with fused deposition modeling. In: 24th annual international solid freeform fabrication symposium, Austin, pp 12–14
42. Pandey PM, Venkata Reddy N, Dhande SG (2006) Virtual hybrid-FDM system to enhance surface finish. *Virtual Phys Prototyping* 1(2):101–116. <https://doi.org/10.1080/17452750600763905>
43. Vinitha M, Rao A, Mallik M (2012) Optimization of speed parameters in burnishing of samples fabricated by fused deposition modeling. *Int J Mech Ind Eng* 2(2):10–12
44. Debnath S, Kunar S, Anasane SS, Bhattacharyya B (2017) Non-traditional micromachining processes: opportunities and challenges. In: *Non-traditional micromachining processes*. Kibria G, Bhattacharyya B, Davim JP (eds) *Materials forming, machining and tribology*. Springer International Publishing, Cham, pp 1–59. https://doi.org/10.1007/978-3-319-52009-4_1
45. Bauri R, Yadav D, Suhas G (2011) Effect of friction stir processing (FSP) on microstructure and properties of Al–TiC in situ composite. *Mater Sci Eng A* 528(13–14):4732–4739. <https://doi.org/10.1016/j.msea.2011.02.085>
46. Rodelas JM (2012) Friction stir processing of Nickel-Base alloys. The Ohio State University

47. Mukherjee A, Patel NV, Gurjar KC (2017) Review paper on friction stir welding and its impact on environment. *IRJET* 4:1481–1490
48. Lyczkowska E, Szymczyk P, Dybala B, Chlebus E (2014) Chemical polishing of scaffolds made of Ti-6Al-7Nb alloy by additive manufacturing. *Arch Civil Mech Eng* 14:586–594
49. Pyka G, Burakowski A, Kerckhofs G, Moesen M, Van Bael S, Schrooten J, Wevers M (2012) Surface modification of Ti6Al4V open porous structures produced by additive manufacturing. *Adv Eng Mater* 14(6):363–370. <https://doi.org/10.1002/adem.201100344>
50. Percoco G, Lavecchia F, Galantucci LM (2012) Compressive properties of FDM rapid prototypes treated with a low cost chemical finishing. *Res J Appl Sci Eng Technol* 4 (19):3838–3842
51. McCullough EJ, Yadavalli VK (2013) Surface modification of fused deposition modeling abs to enable rapid prototyping of biomedical microdevices. *J Mater Process Technol* 213(6):947–954. <https://doi.org/10.1016/j.jmatprotec.2012.12.015>
52. Espalin D, Medina F, Arcaute K, Zinniel B, Hoppe T, Wicker R (2009) Effects of vapor smoothing on ABS part dimensions. In: Proceedings from rapid 2009 conference and exposition, Schaumburg, IL
53. Daneshmand S, Aghanajafi C, Ahmadi Nadooshan A (2010) The effect of chromium coating in RP technology for airfoil manufacturing. *Sadhana* 35(5):569–584. <https://doi.org/10.1007/s12046-010-0036-7>
54. Impens D, Urbanic RJ (2016) A comprehensive assessment on the impact of post-processing variables on tensile, compressive and bending characteristics for 3D Printed components. *Rapid Prototyping J* 22(3):591–608. <https://doi.org/10.1108/RPJ-02-2015-0018>
55. Ross I, Kumstel J, Bremen S, Willenborg E (2015) Laser polishing of laser additive manufactured surfaces made from Inconel 718 and ASTM F75. *Proc ASPE Spring Top Meet Achiev Precis Toler Addit Manuf* 60:136–140. <https://doi.org/10.3390/app10010183>
56. Chai Y, Li RW, Perriman DM, Chen S, Qin Q-H, Smith PN (2018) Laser polishing of thermoplastics fabricated using fused deposition modelling. *Int J Adv Manuf Technol* 96(9–12):4295–4302. <https://doi.org/10.1007/s00170-018-1901-5>
57. Taufik M, Jain PK (2017) Laser assisted finishing process for improved surface finish of fused deposition modelled parts. *J Manuf Process* 30:161–177. <https://doi.org/10.1016/j.jmapro.2017.09.020>
58. Lambiase F, Genna S, Leone C (2020) Laser finishing of 3D printed parts produced by material extrusion. *Optics Lasers Eng* 124:105801. <https://doi.org/10.1016/j.optlaseng.2019.105801>
59. Chen L, Zhang X (2019) Modification the surface quality and mechanical properties by laser polishing of Al/PLA part manufactured by fused deposition modeling. *Appl Surf Sci* 492 (February):765–775. <https://doi.org/10.1016/j.apsusc.2019.06.252>
60. Kumbhar NN, Mulay AV (2016) Finishing of fused deposition modelling (FDM) printed parts by CO₂ laser. In: 6th International and 27th all india manufacturing technology, design and research conference (AIMTDR-2016), college of engineering. Pune, Maharashtra, India. Finishing, pp 63–67
61. Chen L, Zhang X, Wang Y, Osswald TA (2020) Laser polishing of Cu/PLA composite parts fabricated by fused deposition modeling: analysis of surface finish and mechanical properties. *Polym Compos* 41(4):1356–1368. <https://doi.org/10.1002/pc.25459>
62. Krishna AV, Faulcon M, Timmers B, Reddy VV, Barth H, Nilsson G, Rosén BG (2020) Influence of different post-processing methods on surface topography of fused deposition modelling samples. *Surf Topogr Metrol Prop* 8(1). <https://doi.org/10.1088/2051-672X/ab77d7>
63. Taufik M, Jain PK (2016) CNC-assisted selective melting for improved surface finish of FDM parts. *Virtual Phys Prototyping* 11(4):319–341
64. Kim J, Cho KS, Hwang JC, Iurascu CC, Park FC (2002) Eclipse-RP: a new RP machine based on repeated deposition and machining. *Proc Inst Mech Eng Part K J Multi-Body Dyn* 216(1):13–20. <https://doi.org/10.1243/146441902760029357>

65. Lee W-C, Wei C-C, Chung S-C (2014) Development of a hybrid rapid prototyping system using low-cost fused deposition modeling and five-axis machining. *J Mater Process Technol* 214(11):2366–2374. <https://doi.org/10.1016/j.jmatprotec.2014.05.004>
66. Applications ITS (2016) Theory and practice theory and practice. *J Pastoral Care Coun* 30
67. Gowthaman CLYS (2018) Innovative design, analysis and development practices 1

Post-processing of FDM 3D-Printed Poly-lactic Acid Parts by CNC Trimming



Mohammadreza Lalegani Dezaki and M. K. A. Mohd Ariffin

Abstract 3D printing is the next industrial revolution which has brought many advantages over conventional methods. Fused deposition modelling (FDM) is a 3D printing process that prints products by extruding molten thermoplastic layer by layer. The process is highly capable to print different products but achieving smooth surface quality without layer structure is still challenging. Hence, post-processing techniques are useful to enhance mechanical properties and also surface texture. In this study, Computer numerical control (CNC) trimming was used as a post-processing technology to find out its effects on 3D printed Poly-lactic acid (PLA) products. In FDM process, samples were printed in different build orientations from 0° to 90° and analysed their surface texture to understand the influence of build orientation on surface quality. The goal of this study is to examine trimming parameters on printed PLA products. Furthermore, specimens were trimmed with a wide range of feed rates and spindle speeds. Surface roughness measurement (in this case average surface roughness (R_a) and average maximum peak to valley (R_z)) was conducted to determine the surface characteristics. Finally, it was found out that 1,200 mm/min feed rate with 3,500 rpm spindle speed reached the best surface quality. There was an extraordinary improvement in all samples after trimming reach to 97.18% compared to printing process. Also, results showed 0° had the lowest range of R_a and R_z among samples. This means the printing direction is highly effective in both printing and trimming processes.

M. Lalegani Dezaki · M. K. A. Mohd Ariffin (✉)
Advance Manufacturing Research Group, Department of Mechanical and Manufacturing Engineering, Universiti Putra Malaysia, Seri Kembangan, Selangor 43400, Malaysia
e-mail: khairol@upm.edu.my

M. Lalegani Dezaki
e-mail: lalegani.mr@gmail.com

© The Author(s), under exclusive license to Springer Nature Switzerland AG 2021
H. K. Dave and J. P. Davim (eds.), *Fused Deposition Modeling Based 3D Printing*,
Materials Forming, Machining and Tribology,
https://doi.org/10.1007/978-3-030-68024-4_11

1 Introduction

Additive manufacturing (AM) is a combination of technologies, which is invented in the late 1980s, used to produce end-use or prototype products [1]. Design complexity and freeform design are produced without material wastage and sacrificing mechanical properties. A wide range of materials can be used in AM process due to their capabilities and specific features. It is divided into different categories that refer to the American Society for Testing and Materials (ASTM F42-). Vat photopolymerisation [2], Material extrusion [3], Material jetting [4], Powder bed fusion [5], Sheet lamination [6], Binder jetting [7], and Direct energy deposition [8] are the AM processes which cover a vast range of applications. Solid, powder, and liquid materials can be printed by using these processes depends on requirements and needs. They are able to print materials from thermoplastics to metal alloys and concrete for medical [9], aerospace [10], construction [11], and manufacturing industries [12]. This process eliminates obstacles in conventional manufacturing processes such as milling, casting, forging, and so on [13]. Building samples without tooling and faster let engineers go beyond the limitations that were faced in the past. Producing structure is conducted by layer binding from bottom to the top. 3D printers receive the .STL file format which is generated by slicing software. The machine starts to build the product by following generated G-codes to print layer by layer to finish it. Each process has specific features and details, for example laser is used in Stereolithography (SLA) process to sinter liquid material [14]. Also, Selective laser melting (SLM) uses laser to print specimens, however, the material is metal or composite powder [15]. These processes use support structure to build products with high accuracy and quality. In addition, supports can avoid material dropping during the printing. Support structures are made from the same or different material. However, supports affects surface quality and removing them needs post processing techniques [16]. Surface quality and mechanical properties of products depend on many parameters. Various elements affect final products but the common factors among these processes are build orientation, layer thickness, temperature, and infill density [17]. By choosing optimum factors, high accuracy could be achieved.

Fused deposition modelling (FDM) is a common AM process which is widely used in domestic and industries [18]. This process is based on material extrusion and consists of different components. Stepper motors feed filament through nozzle and it melts filament shape material and follows generated G-codes by Computer numerical control (CNC) system. Then, the extruder deposits the material on the bed. The molten material solidifies at chamber temperature which is below the thermoplastics melting point. This process is repeated layer by layer until the product is finished [19]. Subsequently, support structure may be needed based on the product's features. The support material can be different if the machine uses two extruders. A vast range of thermoplastics and polymer composites can be used for printing in shape of filament with different colors. Nylon, Acrylonitrile butadiene styrene (ABS), Polylactic acid (PLA), Polypropylene (PP), and Polycarbonate

(PC) are the most common engineered plastics and highly used for different purposes [20]. Printing these materials depends on elements that are vital in FDM. The most important component in this system is the nozzle [21]. Other factors affect product quality and properties, for example, build orientation, nozzle temperature, nozzle diameter, layer thickness, and infill pattern [22]. Taufik and Jain [23] addressed the importance of build orientation in AM process and how affected product quality. Further, another research on build orientation has been investigated by Salmi et al. [24] and a comparison between AM technologies has been conducted. The results showed how build orientation can affect texture and mechanical properties. In addition, Pérez et al. [25] analyzed layer and wall thickness effects on 3D printed PLA products. Results showed by increasing both parameters, surface quality became worse. A review has been written by Jaisingh Sheoran et al. [26] to identify the impacts of other parameters such as infill, air gap, raster angle, etc., by using different techniques such as Analyze of variance (ANOVA), Design of experiment (DOE) on FDM products. Meanwhile, Alsoufi and Elsayed [27] found out nozzle diameter and layer height had an important role in printing PLA+ material. Briefly, controlling parameters and proposing new techniques for slicing procedure lead to better properties while issues could be eliminated as well [28]. Despite FDM is a capable system to print various objects, defects have still existed that need to be examined. In microstructure investigation, void between each layer happens due to layer binding which is an issue that affects mechanical properties [29]. Undoubtedly, staircase defect is another important drawback in FDM due to process characteristics [30]. Warpage and shrinkage are also made problems because of overheating and non-optimized parameters [31]. By developing the FDM machine to a multi axis or mobile system, issues like staircase can be eliminated [32]. Additionally, a hybrid rapid prototyping FDM machine was developed by Lee et al. [33] which showed a significant improvement in printing products. Besides, post-processing techniques and secondary processes have been used to enhance products features such as chemical or machining processes [34, 35]. Adel et al. [36] was used hot air jet as a secondary process to enhance surface of FDM 3D printed samples. Low jet velocity and high temperature showed better quality in polishing products.

Many techniques and developments have been conducted to improve surface quality and properties of 3D printed products. These techniques can be simple as using plier, sanding, and acetone washing to remove support and make the products' surface smoother, or can be done by complicated processes such as chemical treatment. CNC machining is one of the most common processes in manufacturing and has been widely used to reach tight tolerances and high accuracy [37]. Thus, reaching better tolerances and quality after printing products are achievable by using CNC as a secondary process because FDM is not the best option while it comes to tight tolerances and high accuracy [38]. CNC trimming process has been used to cut different products from metal alloys to polymers. It has been used to cut excess material or making slot and holes on products. Different cutters are used to produce specific features on samples in machining. Each cutter can be used for various purposes based on requirements. Unfortunately, not much researches have

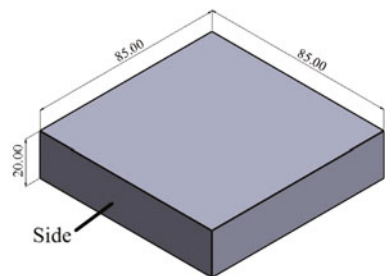
been conducted on CNC trimming of 3D printed products itself but CNC machining has been used as a main- or secondary process on thermoplastic. Hällgren et al. [39] made a comparison between CNC and AM process to find out the time and cost in both processes. It has been found a combination of these processes, which is known as Hybrid manufacturing (HM), led to higher accuracy and short processing time. Therefore, HM might be a potential substitution for FDM due to its features but position tracking and interpolation may make trouble in accuracy. Another post-processing technique by developing CNC-assisted selective melting and proposing a mathematical model of selective melting (SM) process has been done by Taufik and Jain [40]. By measuring average surface roughness (R_a), the results showed there was a major improvement for 3D printed samples. Also, feed rate affected the quality of specimens while lower build angle showed poor surface texture compared to higher ones. Nsengimana et al. [41] worked on post-processing technique's effects on surface quality and accuracy of ABS products. Tumbling, CNC machining, spray painting, hand finishing, and chemical treatment were examined and major improvements were conducted in all secondary processes. It should be noted machining calibration should be considered to avoid issues and defects on texture. On the other hand, machining parameters also have an extraordinary effect on thermoplastics. Hence, Abdul Shukor et al. [42] studied the influence of feed rate, cutting speed, and depth of cut on Polypropylene (PP) by using Taguchi signal/noise ratio in milling process. The best result was conducted by 4138 rpm cutting speed, 1241 mm/min feed rate, and 0.5 mm depth of cut. Therefore, by finding optimum cutting factors in machining 3D printed plastics, staircase defects could be eliminated [43]. All parameters should be uniform to avoid issues. Cooling in plastic machining is a vital element to reduce heat during the process but the liquid should not be used for those polymers which absorb moisture and water such as PLA [44]. Also, tools should be chosen properly to eliminate friction and crack [45]. Dhokia et al. [46] developed Neural networks (NNs) method to prognosticate the effects of machining parameters on surface roughness. Results showed minimum surface roughness was achieved at maximum feed and intermediate feed and speed while by increasing feed rate, roughness became worse. In another research, feed rate effects on surface roughness was significant and by decreasing its value, roughness decreased as well [47]. Another study evaluated surface roughness by developing support vector machine and particle swarm optimization algorithm to determine the optimal cutting condition in end-mill process [48]. Lalegani Dezaki et al. [49] investigated the impacts of machining on PLA material in different build orientations. They found out 0° sample had the best surface quality in both high-speed machining and printing process. Moreover, Pămărac and Petrusse [50] examined end-milling effects on 3D printed ABS and PLA material to determine the optimum parameters by analyzing average distance between the highest peak and lowest valley in each sampling length (R_t), average maximum peak to valley (R_z), and R_a [51]. Based on this study, feed rate and cutting speed played an important role in machining 3D printed products.

In brief, finding optimal conditions in machining is based on different factors that need to be considered to reach the best surface quality and accuracy. It has been founded, FDM process is capable to print different features but not in obtaining tight tolerances, machining could be a potential option to enhance products' quality. The reason why many parameters affect product development is a combination of two processes. However, literature showed by modifying elements, issues such as stairstep could be eliminated. Analyzing the effects of CNC trimming on 3D printed PLA samples are the main goal of this research. This study investigates the impacts of CNC trimming parameters on different build orientations in FDM products. This research helps to increase the performance of HM process when it comes to a combination of AM and machining. Hence, surface roughness analysis (R_a and R_z) was conducted to find out the best surface quality before and after post-processing (in this case CNC trimming).

2 Methodology

As discussed in the introduction many parameters affect surface quality in both processes. By controlling FDM elements, issues are eliminated while achieving tight tolerances and producibility can be done by a secondary process such as machining. Due to layer by layer structure, void and anisotropic are the main issues while mechanical properties of 3D printed samples after machining are affected as well. Surface roughness analysis is a way to investigate the condition of surface texture in various products [52]. Therefore, this research consists of two processes which are 3D printing and machining. Finding optimum CNC trimming parameters was conducted by printing specimens in different orientations. As shown in Fig. 1, a block with 85 mm length, 85 mm width, and 20 mm thickness was designed in Solidworks® software. In addition, the side of the sample which was investigated in this study is marked in Fig. 1. This artefact was used for printing process to print samples in different angles. This size was chosen to have stable machining and achieving the highest accuracy to machine the exact position. Also, due to the limitation to hold the sample during machining, this size was assigned to minimize errors and defects during the trimming process.

Fig. 1 Geometries of CAD design



The artefact was printed by FDM in 4 build orientations to analyze the surface roughness before and after cutting. CuraEngine[®] software was used to slice the sample and generated G-codes for printing process. Default printing settings were chosen to print each specimen separately. Critical parameters were constant for all samples while the build orientation was changed which was the most important factor in FDM process. As shown in Table 1, four samples were printed in 0°, 30°, 60°, and 90°. The point was to understand the behavior of FDM in printing parts in different angles. As mentioned in the literature, horizontal and vertical samples had the best surface quality compared to perpendicular [49]. Thus, the impact of trimming process on various build orientation is the goal of this study and find out which angle has the best texture after CNC trimming process. The Ultimaker 2+ machine was used to build specimens and due to the large volume and solid infill, each sample took 2 days to be printed completely, as shown in Fig. 2. White Polylactic acid (PLA) material from PolyLite[™] was the main material in this study. PLA is a biodegradable material which is extract from natural resources such as corn [53]. It is widely used in FDM due to good mechanical properties and reasonable price. The properties of this material are 37 MPa tensile strength, 6% elongation, 4 GPa flexural modulus, and 1.3 g/cm³ density [54]. As mentioned before, the surface texture of FDM products is not as good as other processes while printing PLA shows poorer dimensional accuracy compared to other materials.

Finding optimum trimming parameters (feed rate and spindle speed in this case) and their effects on surface texture of 3D printed products were the main goal of this study. Thus, each sample was cut into 8 pieces by CNC milling machine (see Fig. 3). CNC machine was used because it is a stable process and higher accuracy can be achieved compared to the manual milling machine. Okuma MX-45VA CNC machine was used to cut the sample into same size pieces. The machine's features are a table with 760 mm length and 460 mm width, maximum 7,000 rpm spindle speed, and 500 kg maximum work-piece weight. The value of each parameter for

Table 1 Blocks' printing parameters

Samples No.	1	2	3	4
Build orientation (degree)	0	30	60	90
Extruder diameter (mm)	0.4	0.4	0.4	0.4
Filament diameter (mm)	2.85	2.85	2.85	2.85
Filament colour	white	white	white	white
Layer thickness (mm)	0.15	0.15	0.15	0.15
Infill density (%)	100	100	100	100
Infill pattern	Linear	Linear	Linear	Linear
Extruder temp. (°C)	200	200	200	200
Bed temp. (°C)	60	60	60	60
Fan	ON	ON	ON	ON
Weight with support (gram) ± 2	176.5	189.4	179.2	176
Weight without support (gram) ± 2	176.50	175.5	176	176

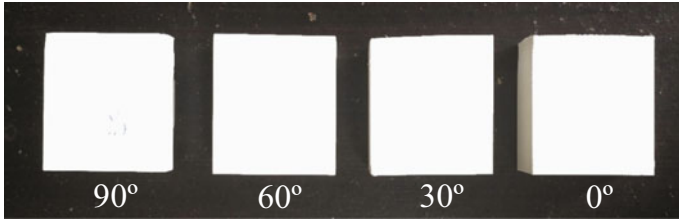
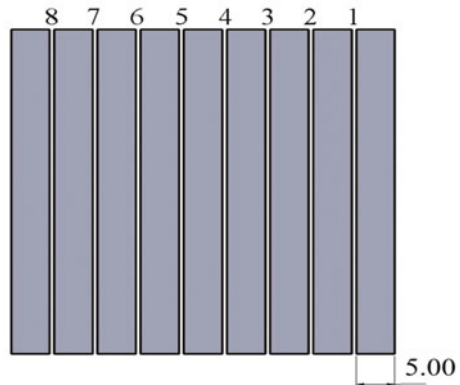


Fig. 2 Printed blocks

Fig. 3 Schematic of cutting procedure



trimming is written in Table 2. Heating might melt the sample during the machining, therefore pressurized air was a good option to reduce the temperature. PLA absorbs water and moisture and this causes changing in mechanical properties and surface quality. Therefore, using liquid in trimming process may affect surface quality and mechanical properties. Each specimen was machined separately by following the same parameters' value. Four flute cutting tool with 12 mm diameter was used to cut blocks with high accuracy without cracking the specimens. The material of the cutter was solid carbide which is highly effective to cut plastics with high quality. One side of the sample was clamped with the gripper and the other side machined step by step. Two runs were determined to analyze the effects of machining parameters. For the first four cuts, the feed rate was changing while for the next four, it was constant and spindle speed values were changing. The size of each trimming was 5 mm due to the limitation to hold the samples properly.

To determine the effects CNC trimming process on surface texture, surface roughness measurement was applied by Mahr Perthometer MarSurf PS1 machine. The machine had a probe to contact surface and measure the value of R_a and R_z . Point by point measurement was conducted due to the machine limitations to find out the condition of each piece. Five points as shown in Fig. 4 were chosen to be measured one by one before and after the trimming process. Each point was measured twice to obtain accurate results. The average value was calculated for

Table 2 Machining parameters

Run	Cutting number	Depth of cut (mm)	Feed rate (mm/min)	Spindle speed (rpm)
1	1	20	600	3,500
	2		800	
	3		1,000	
	4		1,200	
2	5	20	1,100	1,000
	6			2,000
	7			3,000
	8			4,000

Fig. 4 Surface measurement points



each surface to find out the influence of machining on 3D printed products. Layer binding in AM affects surface quality while by cutting the sample, layered structure is changed. By analyzing samples before and after machining, this binding is affected and values are changed. To determine the measurement, Evaluation length (L_n) was set on 4.0 mm with 5.6 mm Tracing length (L_t) [55].

3 Results and Discussion

By analysing 3D printed samples, it was found out that FDM process is a capable process to make products while there were limitations that prevent high quality in surface texture. Therefore, surface roughness of printed cubes was measured to find out the differences in various build orientations before trimming process, and layers after printing were observed in all build orientations. This staircase defect affected surface integrity and quality of texture. Thus, elimination of this issue leads to better adhesion and higher surface quality. Surfaces were measured in four build orientations and each point was measured twice to achieve an accurate result. Table 3 shows the value of R_a and R_z for printed specimens. As shown in Table 3, a wide range of values are recorded and cubes showed different conditions based on their printing structures. Figure 5 shows the diversity of values in different angles. This means by increasing the build orientation from 0° to perpendicular angles such as 60° , the value of R_a and R_z increased as well [56]. This happens due to the printing structure in which the sample is not stable compared to 0° and 90° . In contrast, after 60° orientation, there was a sharp decrease for 90° sample that the surface texture became better. Hence, it was founded in printed samples, 0° had the best surface

Table 3 R_a and R_z values for printed samples

Surface parameter	Build orientation (degree)	Points					Average
		1	2	3	4	5	
R_a (μm)	0	9.51	9.42	9.37	9.49	9.92	9.54
	30	15.01	15.41	15.64	15.53	15.67	15.45
	60	30.1	31.28	31.86	31.98	33.09	31.66
	90	10.17	11.81	7.52	13.32	12.98	11.16
R_z (μm)	0	50.85	46.65	47.05	48.95	50.9	48.88
	30	77.6	80.15	79.45	76.8	75.2	77.84
	60	115	111.5	118	117	124	117.1
	90	52.95	62.85	45.13	66.9	70.13	59.59

quality while the worst quality was for perpendicular samples (in this case 60°). Based on the information that Table 3 is provided, the surface roughness of 90° sample is reliable as well. Thus, it can be used for printing products based on design and requirement which cannot be printed at 0° angle. In brief, horizontal and vertical samples showed better layer structure and surface quality compared to perpendicular ones [57].

Moreover, surface texture of samples was analysed after the trimming process to find out the effects of machining on texture and layer structures. Therefore, the surface roughness parameters were measured and recorded after trimming. The limitations in this process were after one cut, measurements should be done to find out the differences between each parameter. Also, the cutting tool became like a melting tool if the trimming parameters were poor (e.g., excessive heat). For the first four runs, the feed rate was changing from 600 mm/min to 1,200 mm/min. Table 4 shows the value of R_a for each sample while the spindle speed was constant at 3,500 rpm. MATLAB was used to plot 2D graph to understand the effects of feed rate and spindle speed. By increasing the feed rate the surface quality became better (see Fig. 6). R_a values start at $1.5 \mu\text{m}$ for 60° to $0.624 \mu\text{m}$ for 0° . It shows by increasing the feed rate the surface quality becomes better and smooth. Also, the same result happened for all specimens and major improvements were observed compared to the printing process. The results were same for R_z values as well which Fig. 7 and Table 5 show by increasing feed rate, R_z values decrease slightly. The minimum value of R_a and R_z was assigned for 0° with 1,200 mm/min feed rate. In contrast, the maximums belonged to 60° orientation which had the poorest surface quality among specimens. Besides, a higher feed rate showed a drastic improvement in all samples compared to printed ones. In contrast, the largest value of R_a and R_z was for 600 mm/min feed rate.

On the other hand, for the next four runs, the feed rate was constant at 1100 mm/min while the spindle speed varies between 1,000 rpm and 4,000 rpm. It should be noted after trimming, the quality of each sample was different due to the layer binding. Table 6 shows the range of R_a value when the spindle speed is increasing. In this section, at 1,000 rpm and 2,000 rpm spindle speed, 90° sample had the

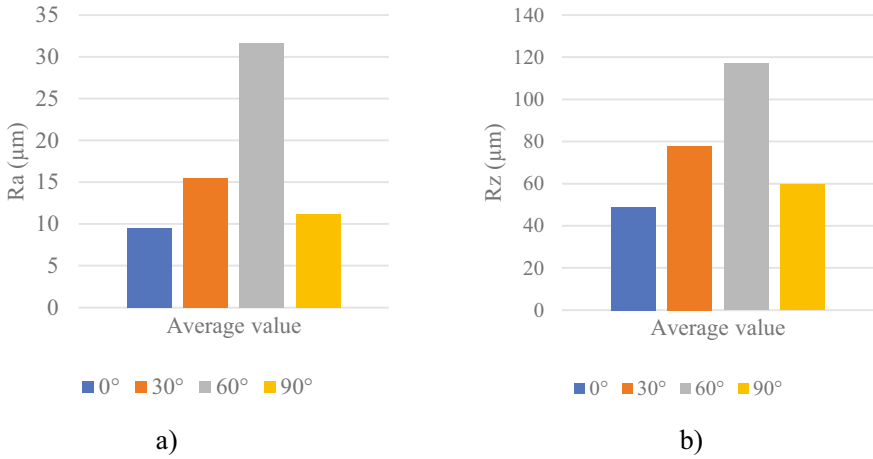


Fig. 5 a R_a values in different build orientations and **b** R_z values in different build orientations

Table 4 R_a value for different feed rates in machining

Parameter		Build (degree)	R_a (μm)					Average (μm)
Spindle speed (rpm)	Feed rate (mm/min)		1	2	3	4	5	
3,500	600	0	0.91	1.02	1.24	1.02	1.09	1.05
		30	1.4	2.14	1.59	1.01	1.05	1.43
		60	2.2	1.04	1.43	1.54	1.33	1.50
		90	1.29	1.53	1.05	1.18	0.82	1.17
	800	0	0.95	0.87	1.02	0.99	0.81	0.92
		30	0.85	1.034	0.9	0.83	1.5	1.02
		60	1.15	0.71	1.6	1.01	1.1	1.11
		90	0.76	0.92	0.88	0.99	1.3	0.97
	1,000	0	0.62	0.76	1.03	1.02	0.66	0.81
		30	1.5	0.92	0.83	0.77	0.8	0.96
		60	1.14	0.94	0.99	1.09	1.18	1.06
		90	1.01	1.04	0.68	1.07	0.7	0.90
	1,200	0	0.61	0.74	0.6	0.55	0.62	0.62
		30	0.59	0.62	1	0.73	0.7	0.72
		60	0.78	1.2	0.83	0.85	0.83	0.89
		90	0.82	0.67	0.68	0.6	0.75	0.70

worst surface quality due to the poor speed while the 0° had the lowest R_a and R_z among others with the value of 3.66 μm and 20.92 μm (see Fig. 8). However, at 3,000 rpm and 4,000 rpm the poorest surface quality was for 60° which were 1.83 μm and 1.32 μm, respectively. The surface quality was the smoothest at

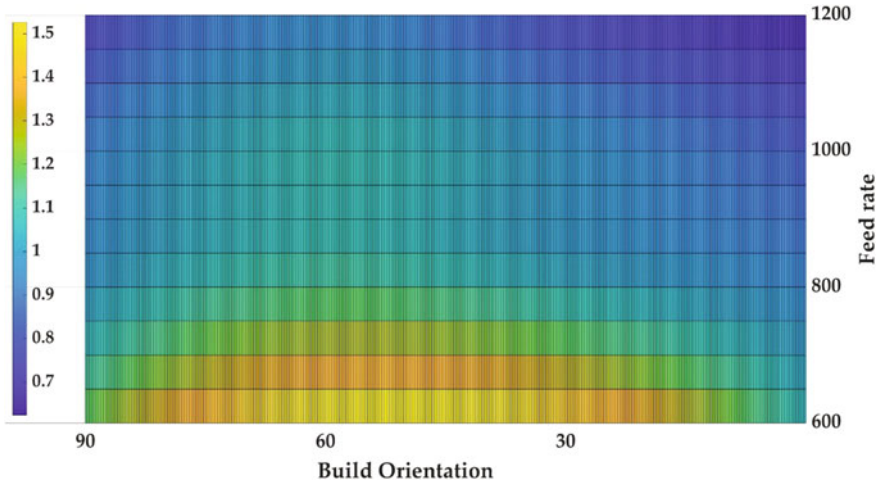


Fig. 6 2D graph of average R_a values for different feed rates

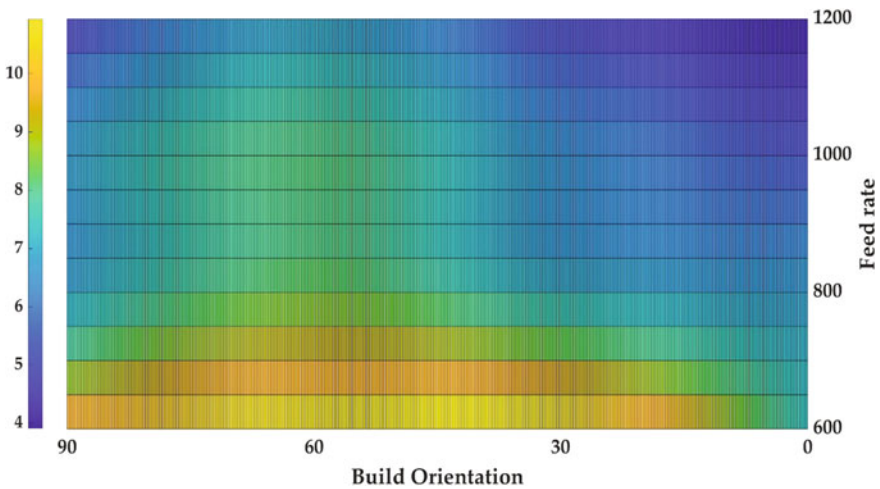


Fig. 7 2D graph of average R_z values for different feed rates

4,000 rpm but the problem was the process should be done twice due to the high-speed spindle to remove material completely from the surface. Table 7 and Fig. 9 show by increasing spindle speed the value of R_a and R_z decreases significantly. One of the issue during the trimming process was low feed rate and low spindle speed led to melting the sample. Further, finding optimum parameters in trimming process was vital to remove barriers and defects. It is noted that, a major improvement was observed for all samples step by step during the experiment.

Table 5 R_z value for different feed rates in machining

Parameter		Build (degree)	R_z (μm)					Average (μm)
Spindle speed (rpm)	Feed rate (mm/min)		1	2	3	4	5	
3,500	600	0	6.3	7.6	8.66	7.18	7.02	7.35
		30	9.29	14.7	11.8	8.7	8.66	10.63
		60	14	9.25	10.3	10.5	9.5	10.71
		90	11.5	12.02	9.5	8.6	7.2	9.76
	800	0	6.7	6.33	6.95	6.2	6.8	6.59
		30	6.8	6.77	7.4	6.95	6.85	6.95
		60	7	6.44	12	9.13	6.7	8.25
		90	6.38	6.45	6.3	6.5	7.55	6.63
	1,000	0	3.8	4.26	7.48	6.03	4.3	5.17
		30	11.3	6.8	4.24	4.59	5.3	6.44
		60	8.33	5.24	7.92	9.91	8.7	8.02
		90	8.3	8.24	5.56	6.87	3.88	6.57
	1,200	0	3.93	4.08	4.64	3.44	3.46	3.91
		30	3.46	3.86	7.6	4.32	4.38	4.72
		60	4.72	11.2	5.33	5.8	5.21	6.45
		90	4.2	4.3	4.35	4.1	4.3	4.25

Hence, a comparison between the optimum trimming process and FDM process was conducted percentage improvement. Based on data that were provided from roughness measurement, spindle speed 3,500 rpm with 1,200 mm/min feed rate showed the best surface quality. Moreover, the surface texture after trimming was also investigated to find out the effects.

Analysing surface integrity and surface roughness showed how trimming and machining can increase quality and achieve tight tolerances. As shown in Fig. 10, there is no evidence of stairstep defects and layer structure after trimming. The surface of all specimens was smooth without picks and valleys. The layer structure vanished completely and surface integrity was impressive. Therefore, trimming can be a potential post-processing technique to eliminate FDM process defects and achieve high accuracy as needed for product quality improvement.

Meanwhile, a comparison between 3D printed and trimmed samples was conducted to examine the average R_a and R_z value and their differences. The average value and the percentage of differences between printing and trimming are shown in Table 8. The percentage of differences between these processes are calculated as follow (See Eq. 1)

$$\text{Error}(\%) = \frac{\text{Printed value} - \text{Trimmed value}}{\text{Printed value}} * 100 \quad (1)$$

Table 6 R_a value for different spindle speed in machining

Parameter		Build (degree)	R_a (μm)					Average (μm)
Feed rate (mm/min)	Spindle Speed (rpm)		1	2	3	4	5	
1,100	1,000	0	3.57	3.89	3.31	3.8	3.76	3.66
		30	4.04	3.7	4.37	4.16	3.86	4.02
		60	3.93	3.6	4.2	4.33	4.4	4.09
		90	6.04	6.7	6.14	6.7	6.08	6.33
	2,000	0	3.11	3.51	3.7	3.22	3.05	3.31
		30	4.3	3.11	3.51	3.8	4	3.74
		60	3.5	4.5	3.8	3.4	3.6	3.76
		90	4.27	5.18	4.47	3.87	3.12	4.18
	3,000	0	1.18	0.91	0.88	1.03	0.99	0.99
		30	1.93	1.8	1.3	1.64	1.42	1.61
		60	2.05	1.42	2.9	1.6	1.22	1.83
		90	1.75	1.5	2.03	1.5	1.8	1.71
	4,000	0	0.59	0.62	1	0.73	0.7	0.72
		30	0.73	1.14	1.61	1.4	1.6	1.29
		60	1.2	0.9	1.2	1.5	1.8	1.32
		90	0.63	0.75	0.6	0.9	0.8	0.73

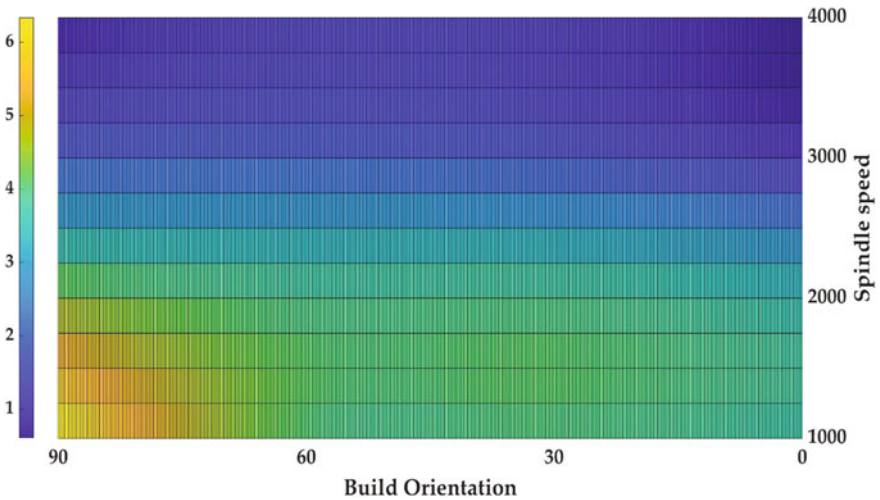


Fig. 8 2D graph of average R_a values for different spindle speed

Table 7 R_z value for different spindle speed in machining

Parameter		Build (degree)	R_z (μm)					Average (μm)
Feed rate (mm/min)	Spindle Speed (rpm)		1	2	3	4	5	
1,100	1,000	0	21.3	23	19.8	20.4	20.1	20.92
		30	25.1	19	24	22	20.6	22.14
		60	19.6	23	25.6	23.8	26	23.60
		90	29.3	29.8	32.1	30	29.5	30.14
	2,000	0	20.8	22.02	23.1	21.2	19	21.23
		30	22.1	23.2	21.3	25	26	23.52
		60	25.14	25.3	24.3	22.5	23.2	24.09
		90	27.3	28	26.2	24.1	22.2	25.56
	3,000	0	8.4	5.65	5.87	6.47	6.33	6.54
		30	11.2	9.84	8.25	8.95	6.83	9.01
		60	16.7	7.58	18.8	9.41	7.29	11.96
		90	14.23	8.62	15.4	10.1	7.33	11.13
	4,000	0	3.65	3.7	6	4.58	6.88	4.96
		30	4.11	7.68	11.9	9.25	10.6	8.71
		60	7.35	6.75	8.3	10.1	12.3	8.96
		90	4.22	7.28	5.66	4.12	5.75	5.41

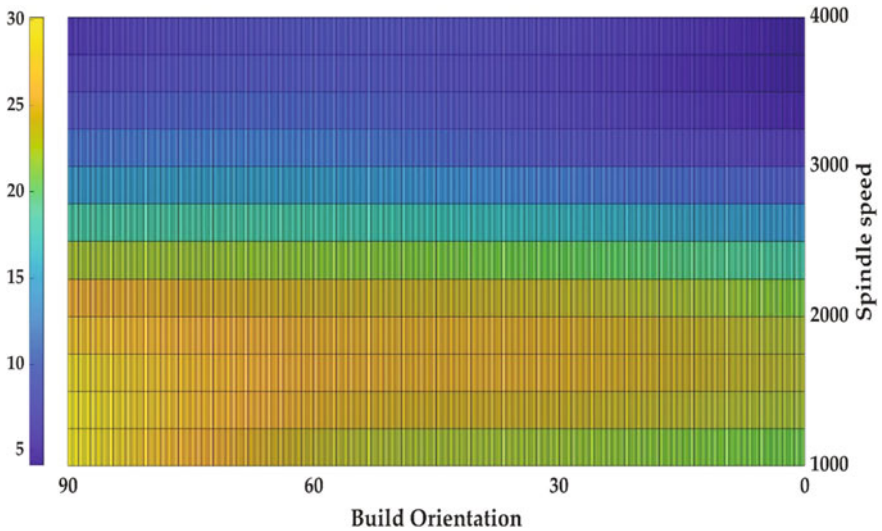


Fig. 9 2D graph of average R_z values for different spindle speed

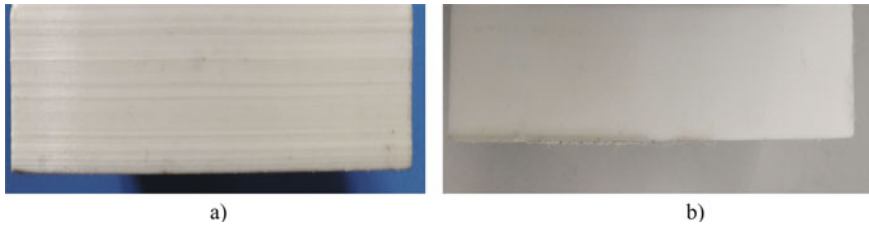


Fig. 10 Surface condition of sample **a** before trimming and **b** after trimming process

Table 8 Differences between printed and trimmed samples

Parameter	Build orientation (degree)	Print	Trimmed	Difference (%)
R _a (μm)	0	9.54	0.62	93.50
	30	15.45	0.72	95.33
	60	31.62	0.89	97.18
	90	11.16	0.7	93.72
R _z (μm)	0	48.88	3.91	92.00
	30	77.84	4.72	93.93
	60	117.1	6.45	94.49
	90	59.59	4.25	92.86

As shown in Table 8, a significant improvement is observed for all samples which are around 90%. It means the trimming process is highly effective to enhance products. On the other hand, the poorest surface was for 60° while the cutting process affected the surface quality dramatically. The largest difference between these samples is for 60° with 97.18%, selecting the proper range of variable and suitable cutting tool helps to increase mechanical properties and surface texture.

4 Conclusion

Extrusion and CNC trimming processes were investigated to determine their capabilities and features. Each process has specific requirements that need to be analysed separately to achieve better mechanical properties. In this study, the results showed how build orientation affected surface quality. It was found that horizontal and vertical printed products have better surface texture compared to perpendicular samples. Also, the effects of trimming process were examined as a post-processing technique to improve surface quality. Parameters like feed rate and spindle speed were studied to understand their influence on 3D printed PLA products. In printing process, 0° orientation sample had the best surface integrity compared to 30°, 60°, and 90°. In addition, the same result was conducted after trimming printed specimens. This means the 0° specimen had the best surface quality as well. Also, feed

rate with 1200 mm/min in this case and spindle speed with 3,500–4,000 rpm results showed the smoothest surface quality. Surface roughness was measured to analyse R_a and R_z parameters and examine the effects of trimming on parameters. A major improvement was observed for all samples. Besides, this technique is useful when it comes to a combination of machining and additive manufacturing which is known as Hybrid manufacturing (HM). Hence, these techniques are useful to improve the surface quality and removing defects in FDM process without wasting material. For further studies, changing printing parameters such as layer thickness or changing material are recommended.

References

1. Mwema FM, Akinlabi ET (2020) Basics of fused deposition modelling (FDM). In: Mwema FM, Akinlabi ET (eds) Fused deposition modeling: strategies for quality enhancement. Springer International Publishing, Cham, pp 1–15
2. Bikas H, Stavropoulos P, Chryssolouris G (2016) Additive manufacturing methods and modelling approaches: a critical review. *Int J Adv Manuf Technol* 83(1):389–405
3. Vyavahare S, Teraiya S, Panghal D, Kumar S (2020) Fused deposition modelling: a review. *Rapid Prototyping J* 26(1):176–201
4. Yap YL, Wang C, Sing SL, Dikshit V, Yeong WY, Wei J (2017) Material jetting additive manufacturing: an experimental study using designed metrological benchmarks. *Precision Eng* 50:275–285
5. Vock S, Klöden B, Kirchner A, Weißgärber T, Kieback B (2019) Powders for powder bed fusion: a review. *Progress Addit Manuf* 4(4):383–397
6. Gibson I, Rosen DW, Stucker B (2010) Sheet lamination processes. In: Gibson I, Rosen DW, Stucker B (eds) Additive manufacturing technologies: rapid prototyping to direct digital manufacturing. Springer US, Boston, MA, pp 223–252
7. Ziaee M, Crane NB (2019) Binder jetting: a review of process, materials, and methods. *Addit Manuf* 28:781–801
8. Dass A, Moridi A (2019) State of the art in directed energy deposition: from additive manufacturing to materials design. *Coatings* 9(7):418
9. Javaid M, Haleem A (2018) Additive manufacturing applications in medical cases: a literature based review. *Alexandria J Med* 54(4):411–422
10. Uriondo A, Esperon-Miguez M, Perinpanayagam S (2015) The present and future of additive manufacturing in the aerospace sector: a review of important aspects. *Proc Inst Mech Eng Part G J Aerosp Eng* 229(11):2132–2147
11. Ghaffar SH, Corker J, Fan MJAIC (2018) Additive manufacturing technology and its implementation in construction as an eco-innovative solution. 93:1–11
12. Steenhuis H-J, Pretorius L (2017) The additive manufacturing innovation: a range of implications. *J Manuf Technol Manag* 28(1):122–143
13. Gibson I, Rosen DW, Stucker B (2010) Development of additive manufacturing technology. In: Gibson I, Rosen DW, Stucker B (eds) Additive manufacturing technologies: rapid prototyping to direct digital manufacturing. Springer US, Boston, MA, pp 36–58
14. Olakanmi EO, Cochrane R, Dalgarno K (2015) A review on selective laser sintering/melting (SLS/SLM) of aluminium alloy powders: processing, microstructure, and properties. *Prog Mater Sci* 74:401–477
15. Calignano F et al (2017) Overview on additive manufacturing technologies. *Proc IEEE* 105 (4):593–612

16. Kumbhar NN, Mulay AV (2018) Post processing methods used to improve surface finish of products which are manufactured by additive manufacturing technologies: a review. *J Inst Eng (India): Series C* 99(4):481–487
17. Gebhardt A, Hötter JS (2016) 2—Characteristics of the additive manufacturing process. In: Gebhardt A, Hötter JS (eds) *Additive manufacturing*. Hanser, pp 21–91
18. Eyers DR, Potter AT (2017) Industrial additive manufacturing: a manufacturing systems perspective. *Comput Ind* 92:208–218
19. Osswald TA, Puentes J, Kattinger J (2018) Fused filament fabrication melting model. *Addit Manuf* 22:51–59
20. Zander NE (2019) Recycled polymer feedstocks for material extrusion additive manufacturing. In: *Polymer-based additive manufacturing: recent developments*. American Chemical Society, pp 37–51
21. Tlegenov Y, Hong GS, Lu WF (2018) Manufacturing, nozzle condition monitoring in 3D printing. *Robot Comput-Integr Manuf* 54:45–55
22. Wong KV, Hernandez A (2012) A review of additive manufacturing. *ISRN Mech Eng* 2012:208760
23. Taufik M, Jain PK (2013) Role of build orientation in layered manufacturing: a review. *Int J Manuf Technol Manage* 27(1–3):47–73
24. Salmi M, Ituarte IF, Chekurov S, Huutilainen E (2016) Effect of build orientation in 3D printing production for material extrusion, material jetting, binder jetting, sheet object lamination, vat photopolymerisation, and powder bed fusion. *Int J Collaborative Enterprise* 5(3–4):218–231
25. Pérez M, Medina-Sánchez G, García-Collado A, Gupta M, Carou D (2018) Surface quality enhancement of fused deposition modeling (FDM) printed samples based on the selection of critical printing parameters. *Materials (Basel, Switzerland)* 11(8):1382
26. Jaisingh Sheoran A, Kumar H (2020) Fused deposition modeling process parameters optimization and effect on mechanical properties and part quality: review and reflection on present research. *Mater Today: Proc* 21:1659–1672
27. Alsoufi MS, Elsayed AE (2017) How surface roughness performance of printed parts manufactured by desktop FDM 3D printer with PLA+ is influenced by measuring direction. *Am J Mech Eng* 5(5):211–222
28. Ariffin MM, Sukindar N, Baharudin BH, Jaafar C, Ismail M (2018) Slicer method comparison using open-source 3D printer. In: *IOP conference series: earth and environmental science*. IOP Publishing
29. Rodriguez Jose F, Thomas James P, Renaud John E (2000) Characterization of the mesostructure of fused-deposition acrylonitrile-butadiene-styrene materials. *Rapid Prototyping J* 6(3):175–186
30. Wickramasinghe S, Do T, Tran P (2020) FDM-based 3D printing of polymer and associated composite: a review on mechanical properties, defects and treatments. *Polymers* 12(7):1529
31. Alsoufi M, El-Sayed A (2017) Warping deformation of desktop 3D printed parts manufactured by open source fused deposition modeling (FDM) system. 17:7–16
32. Wulle F, Coupek D, Schäffner F, Verl A, Oberhofer F, Maier T (2017) Workpiece and machine design in additive manufacturing for multi-axis fused deposition modeling. *Procedia CIRP* 60:229–234
33. Lee W-C, Wei C-C, Chung S-C (2014) Development of a hybrid rapid prototyping system using low-cost fused deposition modeling and five-axis machining. *J Mater Process Technol* 214(11):2366–2374
34. Chohan JS, Singh R (2017) Pre and post processing techniques to improve surface characteristics of FDM parts: a state of art review and future applications. *Rapid Prototyping J* 23(3):495–513
35. Saloniitis K, D’Alvise L, Schoinochoritis B, Chantzis D (2016) Additive manufacturing and post-processing simulation: laser cladding followed by high speed machining. *Int J Adv Manuf Technol* 85(9–12):2401–2411

36. Adel M, Abdelaal O, Gad A, Nasr AB, Khalil A (2018) Polishing of fused deposition modeling products by hot air jet: evaluation of surface roughness. *J Mater Process Technol* 251:73–82
37. Kumar K, Ranjan C, Davim JP (2020) Non-conventional machining. In: Kumar K, Ranjan C, Davim JP (eds) *CNC programming for machining*. Springer International Publishing, Cham, pp 73–87
38. Boschetto A, Giordano V, Veniali F (2013) 3D roughness profile model in fused deposition modelling. *Rapid Prototyping J* 19(4):240–252
39. Hällgren S, Pejryd L, Ekengren J (2016) Additive manufacturing and high speed machining-cost comparison of short lead time manufacturing methods. *Procedia CIRP* 50:384–389
40. Taufik M, Jain PK (2016) CNC-assisted selective melting for improved surface finish of FDM parts. *Virtual Phys Prototyping* 11(4):319–341
41. Nsengimana J, Van der Walt J, Pei E, Miah M (2019) Effect of post-processing on the dimensional accuracy of small plastic additive manufactured parts. *Rapid Prototyping J* 25 (1):1–12
42. Abdul Shukor J, Said S, Harun R, Husin S, Kadir A (2016) Optimising of machining parameters of plastic material using Taguchi method. *Adv Mater Process Technol* 2(1):50–56
43. Pandey PM, Reddy NV, Dhande SG (2003) Improvement of surface finish by staircase machining in fused deposition modeling. *J Mater Process Technol* 132(1–3):323–331
44. Pang X, Zhuang X, Tang Z, Chen X. *Poly(lactic acid) (PLA): research, development and industrialization*. (1860–7314 (Electronic))
45. Alauddin M, Choudhury I, El Baradie M, Hashmi M (1995) *Plastics and their machining: a review*. *J Mater Process Technol* 54(1–4):40–46
46. Dhokia V, Kumar S, Vichare P, Newman S, Allen R (2008) Surface roughness prediction model for CNC machining of polypropylene. *Proc Instit Mech Eng Part B J Eng Manuf* 222 (2):137–157
47. Raju KVMK, Janardhana GR, Kumar PN, Rao VDP (2011) Optimization of cutting conditions for surface roughness in CNC end milling. *Int J Precis Eng Manuf* 12(3):383–391
48. Prakashvudhisarn C, Kunnappadeelert S, Yenradee P (2009) Optimal cutting condition determination for desired surface roughness in end milling. *Int J Adv Manuf Technol* 41(5–6):440
49. Lalegani Dezaki M, Mohd Ariffin MKA, Ismail MIS (2020) Effects of CNC machining on surface roughness in fused deposition modelling (FDM) products. *Materials* 13(11):2608
50. Pămărac R, Petrus R (2018) Study regarding the optimal milling parameters for finishing 3D printed parts from ABS and PLA materials. *ACTA Universitatis Cibiniensis* 70:66–72
51. Quinten M (2019) Capacitive and inductive surface metrology. In: Quinten M (ed) *A practical guide to surface metrology*. Springer International Publishing, Cham, pp 57–65
52. Brown CA (2002) A practical approach to understanding surface metrology and its applications, in atomic force microscopy/scanning tunneling microscopy 3. In: Cohen SH, Lightbody ML (eds) Springer US, Boston, MA, pp 1–10
53. Garlotta D (2001) Environment, a literature review of poly (lactic acid). *J Polym Environ* 9 (2):63–84
54. Sin LT, Rahmat AR, Rahman WAWA (2013) 5—Mechanical properties of poly(lactic Acid). In: Sin LT, Rahmat AR, Rahman WAWA (eds) *Poly(lactic acid)*. William Andrew Publishing, Oxford, pp 177–219
55. Bhushan B (2000) Surface roughness analysis and measurement techniques. In: *Modern tribology handbook*, vol 2. CRC press, pp 79–150
56. Taufik M, Jain PK (2016) A study of build edge profile for prediction of surface roughness in fused deposition modeling. *J Manuf Sci Eng* 138(6)
57. Reddy V, Flys O, Chaparala A, Berrimi CE, Amogh V, Rosen BG (2018) Study on surface texture of fused deposition modeling. *Procedia Manuf* 25:389–396

Sustainable Product Development by Fused Deposition Modelling Process



**R. Keshavamurthy, Vijay Tambrallimath, G. Ugrasen,
and D. P. Girish**

Abstract Sustainability in the field of manufacturing is the need of the hour. Global climate mitigations have affected the manufacturing industry on a larger scale. Increased resource utilization has led to depletion in the availability of raw material for the manufacturing process. The amount of impact in terms of deteriorating environment, economical imbalances, and inefficient manufacturing methods of complex geometries has led to the development of an advanced manufacturing process known as Additive Manufacturing (AM). This manufacturing process's scope and ability are vast and forward compared to conventional systems with respect to utilization of materials, build time, efficient supply chain, reduction in material usage, and freedom of forms. AM exhibits the sustainable approach in the manufacturing cycle and in reusing the materials through recycling and remanufacturing. This chapter discusses the sustainable approaches of the AM process leading towards green manufacturing. The study also indicates the feasibility of the process to play a significant role in sustainability and the recovery of a deteriorating environment.

R. Keshavamurthy (✉)

Mechanical Engineering, Dayananda Sagar College of Engineering, Bangalore 560078, India
e-mail: keshavamurthy.r@gmail.com

V. Tambrallimath

Automobile Engineering, Dayananda Sagar College of Engineering, Bangalore 560078, India
e-mail: vijay.tambrallimath@gmail.com

G. Ugrasen

Mechanical Engineering, BMS College of Engineering, Bangalore 560019, India
e-mail: ugrasen.g@gmail.com

D. P. Girish

Mechanical Engineering, Government Engineering College, Ramnagara 562159, India
e-mail: omganesha16@gmail.com

1 Introduction

Sustainability is a term that is being heard frequently in this period. Focus and necessity to have an insight on large consumption and wastage of products is of prime importance. United Nations has termed the statement of sustainability as “*Sustainable development is a development that meets the needs of the present without compromising the ability of future generations to meet their own need*” [1]. The impact of increased population and necessities for large consumption of materials has led to exponential raw materials consumption. The extinction of specific material from the earth is seen to be effective. The research states that raw materials extraction has seen an upscale from 20 to 70 billion tons from 1970 to 2010. As the increment in population and standard of living is reaching greater heights, the requirement for large consumption of products will be high. The economy of the country also plays an essential role in determining the consumption of raw material utilization [2].

However, a certain study conducted by the Commonwealth Scientific Industrial and Research Organization (CSIRO) indicates the shift from just production and consumption to various other forms. The global trends encompass developing goods with available resources and enhancing the quality and life span. Inclusive growth by protecting the natural habitats, more of societal connections in the virtual world, and increased cost of health care will utilize the resources more largely [3]. The scarcity of energy production is not alone the foremost concern; potential mineral scarcity is also a threat in the present scenario. Hence, recycling and remanufacturing will be the option for extracting the required materials from the disposed products.

The manufacturing process involves many procedures to be followed that could emit certain amounts of pollutants during the course and at the end of the product development. The variation in global scenario due to enhanced population, scarcely available resources, and impacts of climate change has led global organizations like UN to roll out Sustainable Development Goals which should be adhered in the process of manufacturing for the reduction in environmental footprints. The long-term goals aim to achieve the least dependence on natural resources and cause minimal or no damage to the ecology by reusing, recycling and remanufacturing [4]. The present conventional manufacturing system uses the concept of make-use-dispose by creating the demand by the consumers and focusing on large volume creations. Circular economy, a new trend in understanding the sustainable manufacturing approach, focuses more on generative and restorative models than the previous. This approach leads to the maintenance of value to the product throughout its lifecycle [5]. This strategy involves repairing, remanufacturing, and reusing the products by adding initial face value and maintaining the desired properties as initially developed.

The sustainable manufacturing process involves the process of Additive Manufacturing in its category [6]. Additive Manufacturing is an advanced manufacturing process of developing required parts by building one layer at a time.

In AM process, the part to be developed is initially developed in any CAD software and converted to .stl format and sent for printing in the machine by giving the specified layer thickness and orientation [7, 8]. The usage of materials in the process of additive manufacturing is optimal. In metal additive manufacturing, the raw material is saved unto 40% compared with the conventional manufacturing system. Also, 95–98% of the unused raw material is recycled and reused [9].

The remanufacturing ideology is basically producing the product back into utilization by following approved steps to provide the warranty for the product and maintain the required standard quality [10]. Figure 1 shows the general procedure followed in remanufacturing. When seen through the perspective of optimal energy and material utilization, remanufacturing is finer than recycling. Compared to the manufacturing of new products, the energy saved by remanufacturing is almost 90% [11]. The remanufacturing plays a vital role in extensively using the hidden values to develop a higher economic margin. Few countries have already exercised the importance of remanufacturing, which provides an added advantage in economic growth and opens job creation as it is labour intensive.

The remanufacturing process is considered an essential aspect of sustainable development in providing the circular economy's key aspect. The cyclic flow of material attains closed-loop, reduces energy usage, and nullifies the waste

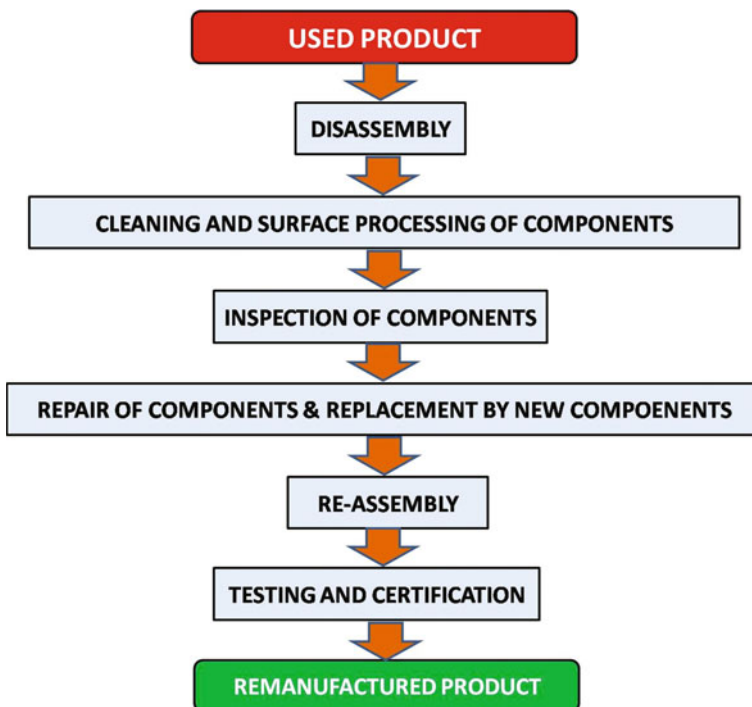


Fig. 1 Remanufacturing process

disposal [12]. The method is well suited for aerospace products, heavy-duty off road vehicles, various parts of the automobile, and numerous machinery technology products. In this chapter, a detailed description of polymer product development by Fused Deposition Modelling will be discussed. Sustainability aspects in the FDM process and environmental and economic impact will be put forth in the chapter.

The possibility of developing complex parts with the utilization of single machines and as a single job has made businesses adopt AM technology as an adoptable end-user manufacturing technique. The advancement in research and industrial acceptance of AM has led to its utilization from rapid prototyping to rapid tooling and direct manufacturing [13]. AM’s feasibility in creating complex geometries and enhanced design freedom and fewer parts and a wide range of materials is an added benefit. The advantages of utilizing AM in the process of whole life cycle of the developed product are shown in the Fig. 2.

In a broader sense, the manufacturing sector can be classified based on three basic attributes that make a process acceptable. The first attribute is advantages in complexity; this is the categorical implementation of complex parts and the feasibility of utilizing the method in numerous aspects. Customization is the second attribute that focuses on the simplicity of features and provides variability of each manufactured component with a quantifiable customized feature [14]. The third attribute refers to volume, wherein the parts produced could be in small or large volumes. The advancement in its growth and shift from just prototyping to tooling and manufacturing has led to advancement in AM technology to wider manufacturing sectors. Certain factors to be considered in choosing to manufacture are the cost, complexity of parts, utilization of various materials, time, energy usage, sustainability and so on. The parts developed by traditional manufacturing system enables the parts to have restricted complexity and customization options. The scope of customer preference is very minimal for variations in traditional manufacturing. AM has the scope of manufacturing complex parts with similar cost as of conventional system [15]. The method of conventional manufacturing is best suited for mass productions in relation to cost analysis; however, AM’s process is well

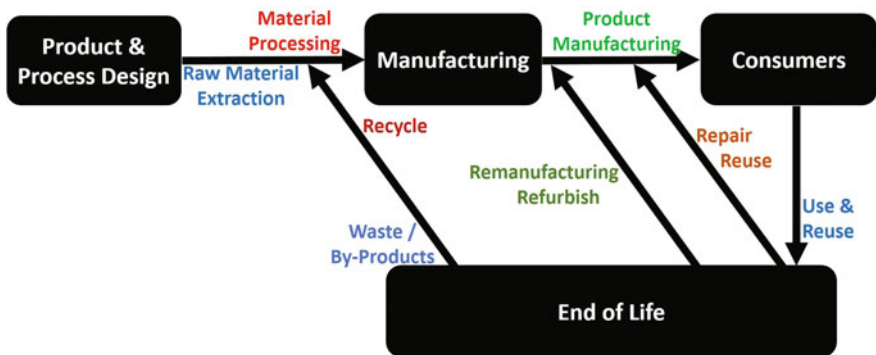


Fig. 2 Life product life cycles

suited for developing tools required for fabrication and fixtures that are used for conventional manufacturing system [16, 17]. Lean production parts can be manufactured with greater ease using the process of AM [18]. AM has simplified the supply chain and has efficiently used for producing single unit and low volume production in wide sectors. These sectors range from the highest implementer of metallic AM Aerospace products [19], to plastic FDM printed AM prosthetics [20], customized for the individual hearing aids [21], medical implants [22] and brace moulds, unique complex patterned art and fashion. AM machines offer production flexibility; the machines do not require expensive set-up arrangements, making the technology economical for smaller batch production [8].

In general, AM is categorized as a method of production with less waste generation compared to conventional subtractive manufacturing. The approach of AM is recognized as a sustainability friendly approach of manufacturing. Numerous studies have shown the AM method to improving the resources, beneficial in extending the product life, and structuring the value chains [23]. Hence, this technology of manufacturing can advance the sustainable society of the future [8]. In this chapter, a detailed discussion of sustainable approaches in development of parts through Fused Deposition Modelling (FDM) will be discussed. This manufacturing process involves extrusion of polymer materials through the nozzle in which it is melted and deposited on the build platform.

2 Materials and Methods Towards Sustainable Approach

The major role of environmental impact by using AM technology is related to materials usage [24, 25]. The materials used in AM technologies are similar to those used in conventional systems. Sustainable approaches and environmentally stable materials could be developed by optimization of process parameters. This will reduce waste materials and reduce energy consumption; however, there remain different optimized process parameters to be adopted for various designs [26].

Polymers, the most widely used materials that possess great challenge in recycling for numerous reasons. The primary difficulty in recycling this material is its diversity of mixtures, variety of reinforcements, availability in diversified colours, loss of original quality, and large energy requirement to carry this process [27]. However, there are numerous recycling methods are numerous ways to recycle and reuse polymeric materials by grinding and extrusion to use it as raw material. This method is also adopted in dire necessity of reduction in plastic consumption during manufacturing [28, 29]. Numerous researchers have shown a positive intent in the usage of recycled materials towards the development of local and domestic products [30].

Commercial filament usage is way costlier than the raw polymer that could be overcome by recycling the plastic to develop the filament. This reusing method to extract a new filament will reduce 90% energy consumption than the manufacturing of new filament. Many waste materials have been converted back to filament

successfully, such as polylactic acid (PLA), acrylonitrile butadiene styrene (ABS), polycarbonate (PC), polypropylene (PP), polystyrene (PS) and low-density polythene (LDPE). Matthew et al. [31], exhibited the use of recycled polymers in the development of 3D printed models while retaining the required mechanical properties. They recycled high strength and good heat resistant material polycarbonate (PC) to develop fused particle fabrication (FPF). ASTM standard tests were used to analyse the recycled polymers tensile and compression strengths and were compared with virgin filaments. The measure of tensile strength for recycled PC was 64.9 MPa and for commercially available desktop printed PC it was 62.2 MPa. Hence the potential for reusing and remanufacturing the components will not deter the values of mechanical properties by optimizing the process parameters.

Considering the largest manufacturing sector such as the automotive industry, has played a great role in using polymer parts. Numerous well known companies are working on utilizing recycled, remanufactured and biopolymer parts for their vehicles. Toyota a major automotive manufacturing company globally, has certain measures or challenges in its vision towards sustainability. One among them is the utilization of recycled parts. One of the first imitative in this direction is PLA plastic development in bio form [32]. This bio-based PLA plastic was widely used up to 80% in the SAI model's interiors released in 2013. This company has also been a major process developer in having precise measures in collection and recycling of numerous polymers parts especially bumpers [33]. Similarly, other automotive companies have been using the process of the rethe automotive sector and recycling in various parts made of polymers. Nissan, Ford, BMW and Volkswagen are some of the manufacturers that use either recycled plastic or bio plastic [34, 35]. Martin et al. [36] have discussed the issues of continual usage of polymer filament as raw material for developing models through FDM. To overcome the impact on environment due to unsustainable approach by using polymers has led to usage of remanufactured polymer filaments which would reduce the cost as well as contribute towards the circular economy. Most of the remanufactured polymers tend to be losing their properties due to chain scission or cross linking of molecular chains. However, polypropylene (PP) materials can withstand the multiple formalities of chemical reactions and showcase the original stability through thermal and mechanical properties. Hence, remanufacturing of filaments with PP as the base can be used to manufacture desired parts. The study focused on mechanical, thermal and tribological parameters. The filament was extruded iteratively for 15 long times and the value of these parameters remained unaltered. The variation of heat and stress during reusing has not very much impacted the samples' desired properties. Hence, PP can withstand the process-ability of extruding and FDM.

Van et al. [30] have proposed using biomaterials towards reaching the demands of sustainable and circular economy. However, the focus has also been given on the statement that all biomaterials are not biodegradable in nature. Most widely and commonly used biodegradable polymer is Polylactic acid (PLA) [37]. The other perspective of usage of this material in terms of toxicity emission should also be a point of concern [23]. Properties of PLA are in the upper hand compared to widely used ABS polymer for FDM applications, as ABS requires higher temperatures

during processing and generates the unpleasant odour. Lately, most commonly used biomaterials are biome 3D which has a base material as starch, nylon 11 developed by castor oil and amitel eco co-polyester developed by synthesis of rapeseed oil [30].

3 Sustainability Concerns of Additive Manufacturing and Future Trends

The need for a sustainable ecosystem in manufacturing has caused the development of research to develop a sustainable ecosystem in manufacturing, which has caused the development of research to develop sustainable and environmentally friendly goals. Brudtland commission have precisely quoted the definition of sustainability as “Sustainable development is the development that meets the needs of the present without compromising the ability of future generations to meet their own needs” [38]. In the development stage, development stage, the process of AM has various hindrances in terms of economic viability, environmental concerns, and societal impacts [39, 40]. Improvised research and development in reaching sustainable goals of AM are necessary to meet AM’s adaptation in present-day industries. As an emerging technology, AM still has high costs and there remain many technical problems that affect the productive system’s efficiency. As per Chen et al. [41], there is strong linkage between the conventional manufacturing systems, these kind of interlinks holds well for AM as well. The techniques of AM can be a legible contender for conventional manufacturing systems towards manufacture of medium to small scale parts. The cost involvement towards machines and materials is on a higher range in AM which would see a reduction with more usage of this technology at all manufacturing stages. However, the notion that the materials used in AM are greener than conventional materials does not hold good. The variation of energy consumption depends on various parameters [23].

Energy consumption is a prime concern in the manufacturing sector, numerous studies have suggested that, the shift of industries towards additive manufacturing will help in reduction of 5% energy consumption globally by the year 2025 [42]. AM’s certain acclaimed benefits are reduced waste generation compared to conventional systems, iterative methods to optimize the process parameters and product design. The freedom of design is wide in AM, enabling it to be optimized topographically and the process use resources more efficiently to develop desired components. Large manufacturing areas’ requirement will be reduced as the feasibility of the development of multi-material and complex geometries can be performed in a single machine.

Design for Manufacturing (DfM) has played a significant role in the emergence of new materials, paved the path for optimal design methods and enhanced the societal necessity for manufactured parts. However, the concept of DfM holds inefficient for AM technologies and hence has given rise to Design for Additive

Manufacturing (DfAM) that plays a larger role in encapsulating the needs of modern manufacturing system. The overall objectives of DfAM is categorically characterised into three sections. Initially, the process orients itself in providing the necessary techniques, tools and methodologies for numerous manufacturing hindrances. Secondly, it is used to clarify the effects of the design process on manufacturing and viceversa to analyse the performance of the process and its quality. Finally, to establish the relation between design process and manufacturing, also to characterize the impact of this process on designer, the practices and process followed [43]. In general, the purpose of DfAM is to support designers in developing desirable quality and cost-efficient parts to meet the desired functional needs by ensuring its development through AM. Fabrication of any form of geometry can be easily carried out using the process of FDM. There still remains certain geometrical constraints using the current FDM technologies which limits the size of part, usage and removal of support structures, development of thin sections, features related to geometry, build orientation and path planning [44]. Table 1 shows the constraints and possible solutions using DfAM for development of optimal products using FDM. The number of advantages of using AM's process is well defined in all aspects; however, the practicality of understanding its possibility to greater area is still not fully analysed. A comparative study in understanding the energy utilization for injection moulding and AM process is carried out [45]. The studies of general aspects in concluding with the remark that AM utilizes less energy than conventional system is not feasible and has to be dealt carefully with considering certain process aspects [23]. The availability of large scale materials in the form of filament

Table 1 DfAM strategies for FDM constraints

Constraint	Solution
Structural support for overhangs, difficulty in breaking, leads to distortion of surfaces	The overhangs to be maintained at length of 1.8 mm, gap in combines elements to be less than 0.4 mm to have higher dimensional accuracy [46]
Limitation in build size	Combination of fabricating process could be considered [47], development of smaller parts using FDM and assembling [48]
Difficulty in developing thin sections	Wall thickness of 1–1.5 mm to be used. Post processing strategies could be used for attaining final dimension [49]
Accuracy and resolution	Present accuracy is in the range of 0.1–0.3 mm. Geometrical features should not be placed too closely, not to develop tolerances and geometrical stability beyond system capabilities.
Build orientation	Fabricating the parts with minimal surface contact along support structures [50]. Orientation to be chosen that has minimal build layers [51]
Planning of internal and external path	The internal path with spiral and curved ways leads in reduction of anisotropic effects and enhances the mechanical properties [52]

for fused deposition modelling is still not to be seen in the market. Many new start-ups provide the new feasible filaments and some remanufactured filament that are not being readily accepted by all printing industries. The existing printing mechanism development of parts with remanufactured filament and obtaining a similar quality as originally manufactured products is difficult to match.

The complete retaining of the remanufactured plastic parts strength is difficult to be maintained for FDM parts. In one study conducted for remanufactured FDM though PLA it was observed that the mechanical properties of the samples deteriorate with every recycle like all common plastics [53]. The need for research studies in understanding the reasons for deterioration of remanufactured parts through FDM has to be explored along with providing better qualities of remanufactured parts [54]. In totality, FDM's process to meet the sustainable goals has to inculcate the design of parts that are durable, usage of recycled materials, analysis and selecting highly efficient manufacturing process, methods in reduction of toxic substances, and investigation of bonding between the user and product. Parts developed with these techniques have longer life and minimal environmental impacts.

4 Summary

The general perspective of manufacturing is conversion of raw materials into useful forms. The major concern of this process is the efficiency involved in the process of conversion to products with the impact on environment [55]. There is a strong interlink between manufacturing and environmental effects in both conventional and AM processes [41]. To realize the sustainable product development by fused deposition modelling, Issues related to development of environmental friendly raw materials, environmental impact are to be addressed.

The AM processes available in present scenarios are economically convenient and can meet the requirements of production for small and medium scales. The machine cost per part is a major component of total cost. The cost analysis of AM in present stage is on higher side due to its infancy stage, however, with prolonged usage and market capturing ability, the cost of these manufacturing units will drop down drastically. At later stages of manufacturing the cost involvement related to AM would find reduction due to greater embracement of this technology. The process of AM plays an important role in freedom of design and redesign. The utilization of AM in integrated assembly plays an important role in reducing fabrication time, minimal cost, and eliminating the flaws of assembly.

The analysis of product through life cycle plays a greater role in using AM technology as there is notable savings in goods produced. Savings are estimated at \$113 to 370 billion by 2025, with these arising from reductions in material inputs and handling, along with shorter supply chains [56]. In broader perspective advantages related to efficiency and improvements in process design are more profitable than the thought of tooling investment [57].

Over and above the increase in recycling capability of AM process, the materials used in this process are yet to reach the greener side as conventional manufacturing materials [58]. AM's full environmental performance must consider the energy demand from a system perspective and not just the process itself [59, 60]. The impact of AM process on the society is yet to be understood at a precise scale. The most detailed study concerning social issues focuses on work conditions and workers' health as social indicators [8].

The combination of ICT, widely available CAD software and 3D printers is changing consumption patterns. There is a shift seen with the advent of AM process from being a passive consumer to becoming the advent of AM process from being a passive consumer to becoming producers and consumers with the help of the global manufacturing community [41]. Certain group of producers and consumers are well aware of the shared maker facilities related to AM and its effects on the environment. However, large group of people are still unaware of this. Sustainability issues are not integrated into their practices [61, 62]. The utilization of DfAM methodologies has been incorporated to help designers appropriately decide the optimal strategies to meet the functional needs and been incorporated to help designers appropriately decide the optimal strategies to meet the functional needs and meet the properties of manufacturing using FDM.

References

1. Brundtland GH (1987) Report of the world commission on environment and development: our common future. United Nations
2. UNEP. Global material flows and resource productivity—summary for policymakers. The International Resource Panel, Paris
3. Hajkowicz S, Cook H, Littleboy A (2012) Our future world: global megatrends that will change the way we live. The 2012 revision. Commonwealth Scientific Industrial Research Organisation (CSIRO), Brisbane, Australia
4. United Nation. Sustainable development goals, 2015, consulted 01 Oct 2017. Available <http://www.un.org/sustainabledevelopment/sustainable-developmentgoals/>
5. Tolio T et al (2017) Design, management and control remanufacturing and remanufacturing systems. *Manuf Technol* 66(2):585–609
6. Keshavamurthy R, Tambrallimath V, Prabhakar K, Sekhar N (2018) Additive manufacturing processes and their applications for green technology. In: Paulo Davim J, Kumaran ST, Taw Jo Ko, Arvind Raj S, Uthayakumar M (eds) Handbook of research on green engineering techniques for modern manufacturing, Nov 2018. IGI Global, USA. <https://doi.org/10.4018/978-1-5225-5445-5>. 2019
7. ASTM F2792—10e1 (2010) Standard terminology for additive manufacturing technologies
8. Huang SH, Liu P, Mokasdar A, Hou L (2013) Additive manufacturing and its societal impact: a literature review. *Int J Adv Manuf Technol* 67(5–8):1191–1203
9. Petrovic V, Vicente Haro Gonzalez J, Jordá Ferrando O, Delgado Gordillo J, Ramón Blasco Puchades J, Portolés Griñan L (2011) Additive layered manufacturing: sectors of industrial application shown through case studies. *Int J Prod Res* 49:1061–1079
10. ERN (2015) Remanufacturing market study. <https://www.remanufacturing.eu/wp-content/uploads/2016/01/study.pdf>

11. Steinhilper R (1998) Remanufacturing: the ultimate form of recycling. Fraunhofer IRB Verlag, Stuttgart
12. Nasr N, Thurston M (2006) Remanufacturing: a key enabler to sustainable product systems. In: *Procedia of 13th CIRP international conference on life cycle engineering*, pp 15–18
13. Gausemeier J et al (2011) Thinking ahead the future of additive manufacturing—future applications
14. Da Silveira G, Borenstein D, Fogliatto FS (2001) Mass customization: literature review and research directions. *Int J Prod Econ* 72(1):1–13
15. Conner BP et al (2014) Making sense of 3-D printing: creating a map of additive manufacturing products and services. *Addit Manufact* 1:64–76
16. Upadhyay M, Sivarupan T, El Mansori M (2017) 3D printing for rapid sand casting—a review. *J Manuf Process* 29:211–220
17. Levy GN, Schindel R, Kruth J-P (2003) Rapid manufacturing and rapid tooling with layer manufacturing (LM) technologies, state of the art and future perspectives. *CIRP Ann Manuf Technol* 52(2):589–609
18. Gero J (1995) Recent advances in computational models of creative design. In: *Computing in civil and building engineering*, p 21. Balkema
19. Lyons B (2014) Additive manufacturing in aerospace: examples and research outlook. *The Bridge* 44(3)
20. Zuniga JM et al. (2017) The development of a low-cost three-dimensional printed shoulder, arm, and hand prostheses for children. *Prosthet Orthot Int* 41(2):205–209
21. Petrick IJ, Simpson TW (2013) 3D printing disrupts manufacturing: how economies of one create new rules of competition. *Res Technol Manag* 56(6):12–16
22. Ventola CL (2014) Medical applications for 3D printing: current and projected uses. *Pharm Ther* 39(10):704
23. Ford S, Despeisse M (2016) Additive manufacturing and sustainability: an exploratory study of the advantages and challenges. *J Clean Prod* 137:1573–1587
24. Cunico MWM, Kai DA, Cavalheiro PM, de Carvalho J (2019) Development and characterisation of 3D printing finishing process applying recycled plastic waste. *Virtual Phys Prototyping* 14(1):37–52
25. Fullenwider B, Kiani P, Schoenung JM, Ma K (2019) Two-stage ball milling of recycled machining chips to create an alternative feedstock powder for metal additive manufacturing. *Powder Technol* 342:562–571
26. Griffiths CA, Howarth J, De Almeida-Rowbotham G, Rees A, Kerton R (2016) A design of experiments approach for the optimisation of energy and waste during the production of parts manufactured by 3D printing. *J Clean Prod* 139:74–85
27. Exrecycling (2018) Plaståtervinning. Available <http://www.exrecycling.se/>
28. Van Den Bossche W, Peeters JR, Devoldere T, Duflou JR, Dewulf W (2014) Proof of concept of an elastomer based fastener enabling rapid disassembly. *Procedia CIRP* 15:234–238
29. Jiang J, Xu X, Stringer J (2019) Optimization of process planning for reducing material waste in extrusion based additive manufacturing. *Robot Comput Integr Manuf* 59:317–325
30. Van Wijk AJM, Van Wijk I (2015) 3D printing with biomaterials: towards a sustainable and circular economy. IOS Press, Incorporated
31. Reich MJ, Woern AL, Tanikella NG, Pearce JM (2019) Mechanical properties and applications of recycled polycarbonate particle material extrusion-based additive manufacturing. *Materials* 12:1642. <https://doi.org/10.3390/ma12101642>
32. Toyota Motor Corporation (2015) Respect for the planet—Toyota’s environmental initiatives. Toyota Environmental Affairs Division
33. Toyota Motor Corporation (2017) Vehicle recycling. Toyota Environmental Affairs Division
34. Ford Motor Company (2017) Sustainability report 2016/17, Ford Motor Company
35. Akampumuza O, Wambua PM, Ahmed A, Li W, Qin X-H (2017) Review of the applications of biocomposites in the automotive industry. *Polym Compos* 38(11):2553–2569

36. Spoerk Martin, Arbeiter Florian, Raguž Ivan, Holzer Clemens, Gonzalez-Gutierrez Joamin (2019) Mechanical recyclability of polypropylene composites produced by material extrusion-based additive manufacturing. *Polymers* 11:1318. <https://doi.org/10.3390/polym11081318>
37. Faludi J, Bayley C, Bhogal S, Iribarne M (2015) Comparing environmental impacts of additive manufacturing vs traditional machining via life-cycle assessment. *Rapid Prototyping J* 21(1):14–33
38. Brundtland G, Khalid M, Agnelli S, Al-Athel S, Chidzero B, Fadika L, Hauff V, Lang I, Shijun M, Morino de Botero M et al (1987) *Our common future* ('Brundtland Report'). Oxford University Press, New York, NJ, USA. ISBN 9780192820808
39. Kellens K, Yasa E, Dewulf W, Dufflou JR (2010) Environmental assessment of selective laser melting and selective laser sintering. *Methodology* 4:5
40. Lindemann C, Jahnke U, Moi M, Koch R (2012) Analyzing product lifecycle costs for a better understanding of cost drivers in additive manufacturing. *Int Solid Free Fabr Symp* 23:177–188
41. Chen D, Heyer S, Ibbotson S, Saloniis K, Steingrímsson JG, Thiede S (2015) Direct digital manufacturing: definition, evolution, and sustainability implications. *J Clean Prod* 107:615–625
42. Gebler M, Schoot Uiterkamp AJ, Visser C (2014) A global sustainability perspective on 3D printing technologies. *Energ Policy* 74:158–167
43. Thompson MK, Moroni G, Vaneker T et al (2016) Design for additive manufacturing: trends, opportunities, considerations, and constraints. *CIRP Ann Manuf Technol* 65:737–760
44. Levy GN, Schindel R, Kruth JP (2003) Rapid manufacturing and rapid tooling with layer manufacturing (LM) technologies, state of the art and future perspectives. *CIRP Ann Manuf Technol* 52:589–609
45. Baumers M, Tuck C, Bourell DL, Sreenivasen R, Hague R (2011) Sustainability of additive manufacturing: measuring the energy consumption of the laser sintering process. *J Eng Manufact* 225(12):2228–2239
46. Adam GAO, Zimmer D (2014) Design for additive manufacturing—element transitions and aggregated structures. *CIRP J Manuf Sci Technol* 7:20–28
47. Dimitrov D, Schreve K, Taylor A et al (2007) Rapid prototyping driven design and realisation of large components. *Rapid Prototyping J* 13(2):85–91
48. Medellin H, Lim T, Corney J et al (2007) Automatic subdivision and refinement of large components for rapid prototyping production. *J Comput Inf Sci Eng* 7:249–258
49. Fodran E, Koch M, Menon U (1996) Mechanical and dimensional characteristics of fused deposition modeling build styles. In: *Solid freeform fabrication symposium*, University of Texas, Austin, USA, pp 419–442
50. Allen S, Dutta D (1994) On the computation of part orientation using support structures in layered manufacturing. In: *Solid freeform fabrication symposium*, pp 259–269
51. Mohamed OA, Masood SH, Bhowmik JL (2016) Mathematical modeling and FDM process parameters optimization using response surface methodology based on Q-optimal design. *Appl Math Model* 40(23–24):10052–10073
52. Pei E, Campbell RI, de Beer D (2011) Entry-level RP machines: how well can they cope with geometric complexity? *Assembly Autom* 31:153–160
53. Cruz F, Lanza S, Boudaoud H, Hoppe S, Camargo M (2015) Polymer recycling and additive manufacturing in an open source context: optimization of processes and methods. In: *Annual international solid freeform fabrication symposium—an additive manufacturing conference*, Austin
54. Pakkanen J, Minetola P, Manfredi D, Iuliano L (2017) About the use of recycled or biodegradable filaments for sustainability of 3D printing. In: *4th International conference on sustainable design and manufacturing*, Bologna
55. Gutowski TG, Branham MS, Dahmus JB, Jones AJ, Thiriez A (2009) Thermodynamic analysis of resources used in manufacturing processes. *Environ Sci Technol* 43(5):1584–1590

56. Gebler M, Schoot Uiterkamp AJM, Visser C (2014) A global sustainability perspective on 3D printing technologies. *Energ Policy* 74(C):158–167
57. Atzeni E, Salmi A (2012) Economics of additive manufacturing for end-usable metal parts. *Int J Adv Manuf Technol* 62(9–12):1147–1155
58. Faludi J, Bayley C, Bhogal S, Iribarne M (2015) Comparing environmental impacts of additive manufacturing versus traditional machining via life-cycle assessment. *Rapid Prototyping J* 21(1):14–33
59. Hao L, Raymond D, Strano G, Dadbakhsh S (2010) Enhancing the sustainability of additive manufacturing. In: *Proceedings of the 5th international conference on responsive manufacturing e green manufacturing (ICRM 2010)*
60. Sreenivasan R, Goel A, Bourell DL (2010) Sustainability issues in laser-based additive manufacturing. *Phys Procedia* 5:81–90
61. Kohtala C (2015) Addressing sustainability in research on distributed production: an integrated literature review. *J Clean Prod* 106:654–668
62. Kohtala C, Hyysalo S (2015) Anticipated environmental sustainability of personal fabrication. *J Clean Prod* 99:333–344

Sustainability Analysis of Fused Deposition Modelling Process



Faladrum Sharma and U. S. Dixit

Abstract Fused deposition modelling (FDM) is a popular additive manufacturing technology. This chapter discusses FDM process from the perspective of sustainability. Sustainability is one of the main concerns in the present era of manufacturing. The assessment of sustainability is important for comparison of the productivity and efficiency of FDM with other manufacturing processes. All the three facets of sustainability, i.e., economic, environmental and societal need to be addressed. In this article, the cost-analysis of FDM is carried considering it to be the first pillar of sustainability-analysis. The necessary cost variables and their importance are discussed for developing the cost model. For environmental sustainability, an analytical approach for the estimation of energy consumption, highlighting various energy-consuming elements, is discussed. Initially, deterministic cost and energy consumption models are presented, which are later converted to fuzzy set based models for handling uncertainties. The main uncertain variables are considered as fuzzy and the output values are obtained by carrying out fuzzy arithmetic operations. The values obtained from the fuzzy set based models are in the form of triplets (low, most likely and high), from which linear triangular membership functions can be constructed. Amongst the three aspects, the societal aspect is the least explored by researchers. This article makes an attempt to study the impact of FDM based additive manufacturing processes on the society. The overall sustainability analysis of two parts, manufactured by FDM, is presented.

F. Sharma · U. S. Dixit (✉)

Department of Mechanical Engineering, Indian Institute of Technology Guwahati,
Guwahati, India

e-mail: uday@iitg.ac.in

F. Sharma

e-mail: fds80@iitg.ac.in

1 Introduction

Increased environmental considerations and market competitiveness have compelled the manufacturing industries to update their production systems and explore sustainable technologies. One such technology is additive manufacturing (AM). It refers to the practice of making a product layer by layer based on a digital model prepared by a computer-aided design (CAD) software. The layer by layer method of manufacturing was patented by George J. Peacock in 1902 for making laminated horseshoes [1]. At that time, computers were not available, but Peacock's method can be considered as an initiator to AM. AM emerged as a rapid prototyping (RP) technology in 1980s. The purpose was to build a prototype before final configuration for commercialization. RP technology has been referred by numerous names, e.g., layer-based manufacturing, freeform fabrication, automated fabrication, digital fabrication, rapid manufacturing, rapid tooling, rapid prototyping and 3D Printing. Amongst these, the most commonly used term is 3D Printing. Though there is still a dispute on the acceptance of a universal name, the recently adopted ASTM standards use the name '*Additive Manufacturing*' (ASTM 2012 Standard F2792) to refer to a process in which product is manufactured layer by layer directly from the CAD model. AM enables a computerized three-dimensional (3D) solid model to directly transform into a finished product without the aid of any tooling system unlike conventional manufacturing. This disruptive technology efficiently uses raw material and produces lesser waste as compared to conventional manufacturing [2, 3]. Some key considerations for a successful and viable AM are material development and characterisation, proper design methodology, modelling and process monitoring, and certification [4].

Different AM processes developed over the years can be classified into three categories—powder-based, liquid-based and solid-based [5]. The following subsections briefly discuss common AM processes with a special focus on their operating principles. Altogether, six different technologies, viz., stereolithography (SLA), laminated object manufacturing (LOM), selective laser sintering (SLS), fused deposition modelling (FDM), laser engineered net shaping (LENS) and 3D printing (3DP) are discussed. The latter part of the article focuses on FDM only; however, in order to make a suitable background for sustainability analysis, it is essential to have basic idea of other competitive processes.

1.1 Stereolithography

Stereolithography apparatus (SLA) or vat polymerization is the first patented and commercialized AM technology [6]. This technique relies on the use of liquid photopolymers and curable resins. The ultraviolet laser traces and forms a layer of the resin according to the CAD model. The layer is formed by the process of cross-linking of monomers involving complex kinetics and reaction mechanism.

After the layer is formed, the platform (substrate) is lowered as per the layer thickness set by the operator. A new layer of resin is coated by the blade in the previously formed solid layer. The tracing by the laser beam continues until the entire part is built. For parts having complicated features, support structures attach the part to the platform. After removal of the part from the platform, necessary post-processing operations comprising support removal and cleaning are performed. The high cost of the polymer resin, less variety of raw material and handling issues are the main limitations of SLA [7].

1.2 Laminated Object Manufacturing (LOM)

LOM is one of the earliest AM processes that is based on the continuous supply of raw material sheet from a feed roll. A heated roller is passed over the layer and activates the heat-sensitive adhesive present on the surface of the sheet. The sheets are glued together due to the application of heat and pressure. The high-intensity CO₂ laser performs the cutting operation. The parameters of the laser are set in such a way that the cutting depth is equal to the desired layer thickness. Once the layer is built, the built platform is lowered. The excess (waste) material is wound by a second roller to allow fresh material to come over the build platform. LOM is an encouraging AM technology for fabricating large-sized products that are not feasible for other AM [8].

1.3 Selective Laser Sintering (SLS)

SLS is a laser based powder bed fusion (PBF) technology where a CO₂ laser beam fuses polymeric powder in the required area of the build material. A roller helps in spreading the powder in the platform. Subsequently, the laser beam sinters the powder and forms a layer of particular thickness. The platform is then lowered by one-layer thickness with the help of a movable piston in the z direction. The roller is fed with powder by another movable piston to spread the new layer of powder above the previously built layer. The principle is almost similar for selective laser melting (SLM). However, in SLM, instead of polymeric powder metallic powder is used that is heated completely up to the melting temperature. Thus, a high intensity laser beam is required.

1.4 Fused Deposition Modelling (FDM)

Extrusion technology in the form of fused deposition modelling (FDM) was patented by S. Scott Crump of the US in 1992 [9]. A thermoplastic filament

material is fed from the spool to the nozzle. The filament gets heated to the temperature just above the melting point (1–2 °C higher than the melting point). The semi-liquid material is then extruded from the nozzle and bonds to the previously built layer. The layer thickness is mainly dependent on the material extrusion rate and speed of the head. The material is deposited in a layer-by-layer fashion in the platform until the entire part is built. Usually, the build platform moves in z direction, while the extrusion nozzle continues to move in x – y plane. For producing complicated geometries, FDM equipment with two nozzles, one for the part material and the other for support material, is used.

1.5 Laser Engineered Net Shaping (LENS)

This popular process comes under the category of direct energy deposition (DED). LENS is a relatively new process patented in the year 2000 [10]. It uses an extremely powerful source of either laser or electron beam that is focused on a particular area. The nozzle is mounted on a multi-axis (3–5) arm that can move in multiple directions. Instead of a powder bed, unlike in SLS process, the metallic powder is injected in the substrate by a powder nozzle. For creating a layer through melting and solidification, the substrate is moved underneath the laser beam. The entire process is carried out in an inert atmosphere. The uniqueness of this process lies in its ability to use multiple materials at the same time.

1.6 3D Printing (3DP)

This jet based technology was developed by Sachs et al. [11] of the United States. In this process, a roller spreads and levels the powder on the platform. A nozzle sprays the binder in the required cross-sectional area to bind the powder and form a layer. To avoid distortion, the powders are misted with water droplets. The process of fusion takes place by capillary action. After the layer is formed, the piston lowers down the platform as per the layer thickness and the roller spreads a new layer of powder. This process continues until the last layer of the part is generated. The final fabricated part is removed from the platform and is subjected to proper heat treatment to strengthen the bonding and remove the unbound powder.

Among all the aforementioned processes, FDM is the most popular and user-friendly AM process [12]. The market share of FDM is the highest in terms of the number of AM machinery sold [13], thanks to the economy of this extrusion-based technology [14]. The affordability and simplicity of FDM make it the most favorable process for the training and initial exposure in an educational institution or any organization. The commonly used raw materials for this process are acrylonitrile butadiene styrene (ABS) and poly lactic acid (PLA). These are available in the form of filament spool and fed to the heated nozzle for extrusion as

shown in Fig. 1. Although the raw materials are readily available in the market, there exist certain limitations. During the printing of a part, ABS emits toxic fumes that are hazardous for the user as well as the environment. Apart from this, there are some other issues specific to FDM. If a complex and a large-sized part is to be fabricated that involves continuous movement of the nozzle as well as continuous material extrusion, the machine may abruptly stop during the middle of the printing. Sometimes, the clogging of the nozzle also results in the failure of the part. Hence, frequent cleaning of the nozzle tip and timely maintenance of the machine is highly recommended. Another notable limitation of FDM like other AM processes is that it is not competitive enough for mass production. Legal issues on intellectual property (IP) protection are also a concern [15]. Certified objects like weapons and implants can be easily manufactured that might disobey IP and patent law.

It is evident that the implementation of FDM technology should be done judiciously to obtain the overall benefit of sustainability. This chapter discusses the sustainability of FDM addressing its economic, environmental and social impact. The issues of cost, energy consumption, and societal considerations of FDM in the presence of uncertainties are discussed.

The origin of sustainability can be traced back to the eighteenth century, where the focus was on environmental protection [17]. This perception has gained enormous attention due to increasing environmental concerns. Sustainable development, as reported by the Brundtland Commission in 1987, is “to meet the need of the present as well as safeguarding the need of future generation” [18]. Since then, several concepts were proposed over the years. The World Summit held in 2005 put forward a universally acceptable concept of sustainability as a combination of economic, environmental and societal aspects [19]. These are considered as three pillars of sustainability. In the context of AM, its birth and development took place by the drive of sustainability. The coaction of AM with sustainability can lead to a new dawn in the coming era of manufacturing. It is claimed that AM will be the most promising campaigner for sustainable development. For economic aspects of sustainability, the cost analysis is carried out in Sect. 2. For environmental

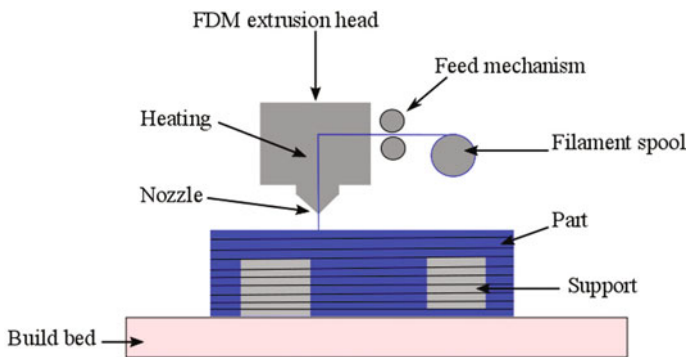


Fig. 1 A schematic of FDM [16] (Under a Creative Commons License, CC BY-NC-ND)

sustainability, an analytical approach of energy consumption highlighting various energy-consuming elements is discussed in Sect. 3. The third facet, i.e., the societal aspect and its importance, is emphasized in Sect. 4.

2 Cost Analysis in Presence of Uncertainty

Every organization aims to make profit from the products that it manufactures. To ensure profitability, it is necessary that an organization fix the price of the product by using a proper cost estimation approach. Apart from fixing the price of a product, cost estimation helps in identifying business potential, prepare production budgets, access the sustainability of the process and perform a break-even analysis. It guides the management in making important decisions and choosing better alternatives. To estimate the cost of a product, it is necessary to find the cost involved in various manufacturing operations. This section describes the procedure to estimate the cost of a part manufactured by FDM process. The list of some cost elements for an AM process is given in Table 1 [20].

The raw material for fabricating the part including the support structures is available in the form of filament plastic that is extruded through the nozzle. However, some FDM machines also employ different raw materials for the part and support structures. In such cases, two different nozzles are present. The operator is involved in operating the machine and inspecting during printing of the part. Although AM processes are claimed to be automatic, it is necessary to engage an operator during the process. After building the part, the operator removes the part from the build platform and performs necessary post processing operations like removal of the support structures and proper surface finishing of the part. A designer is involved in changing the format of CAD model and setting the necessary parameters. The orientation and position of the part are to be properly set for building the part properly. A slicing software is required to convert the digital CAD model to standard tessellation language (STL) format. STL is standard file format especially for AM. The designer sets the parameters such as layer thickness, extrusion velocity, printing velocity, bed temperature and orientation in the slicing software. Proper setting of the parameters is important for efficient printing and preventing any kind of failure. In some cases, operators are also trained to handle

Table 1 Cost elements of FDM

Cost element	Sub-elements
Material cost	Main product, support and post-processing costs
Operator cost	Machine set-up, operating and post-processing costs
Slicing cost	Software and designer costs
Overhead cost	Depreciation, annual maintenance, electricity, factory rent costs

Modified with permission from Sharma and Dixit [20], Copyright KSME and Springer (2019)

the slicing software. One of the most crucial steps in cost estimation of any AM process is to determine the build-time. This is the time period where the product is fabricated by the deposition of raw material in a layer-by-layer fashion.

2.1 Build Time Estimation in FDM

An early and accurate estimation of build time is a crucial task for proper cost estimation. The build time differs based on the operating principle of AM, type of machinery and geometrical parameters of the part. The build time, t_{build} of an AM process is given by [21, 22]:

$$t_{build} = t_{dep} + t_{idle}, \quad (1)$$

where t_{dep} is the deposition time where the molten material is extruded via the nozzle to generate the layers in the part and t_{idle} is the non-productive time during the printing process. The non-productive time or the idle time comprises the time involved in lowering down the build platform, repositioning the nozzle to start a new path or layer, delay and cooling. Proper setting of the parameters in the STL file is necessary for minimizing the build time and finally the overall cost of the part. An important parameter for minimizing the build time is to choose the proper orientation of the part. Choosing the proper orientation reduces the overall height of the part. This may increase the cross-sectional area of the layer but this also reduces the number of layers, thus reducing the time required for lowering the platform. It is evident from several research findings that minimizing the number of layers in a part reduces the build time. However, specific to some geometries and process parameters, the orientation having less number of layers took more time to build as compared to the orientation of the part having relatively more layers [23]. High printing speed and feed rate may increase the deposition rate of the material, but in such cases, the repositioning of the nozzle takes time due to the effect of acceleration and deceleration.

Specific to FDM, Thrimurthulu et al. [24] proposed a simple methodology to estimate the build time based on fundamental machine and geometrical parameters. However, their study ignored the non-productive time and the effect of orientation of the part in the printing process. Assuming continuous deposition of the molten material, the build time, t_{build} , is given by

$$t_{build} = \frac{V_p}{a_n v_e}, \quad (2)$$

where V_p is the volume of the part to be fabricated, a_n is the cross sectional area of the nozzle and v_e is the extrusion velocity of the filament. The build time obtained from this method will be different than the actual build time due to the non-productive time.

2.2 Cost Calculation

This section proposes the cost model considering the cost elements described in Table 1 and the cost incurred in different activities as mentioned earlier. Sharma and Dixit [20] proposed a cost model for selective laser sintering (SLS) AM process. The procedure can also be developed for other AM process if a build time estimation procedure is available. Algebraic summation of the cost elements provides the total cost, C_{FDM} of the part:

$$C_{FDM} = C_{material} + C_{operator} + C_{slicing} + C_{overhead}, \quad (3)$$

where $C_{material}$, $C_{operator}$, $C_{slicing}$, $C_{overhead}$ are the material, operator, slicing and overhead costs, respectively. Considering the material cost per unit mass and other time-dependent cost elements, the total cost, C_{FDM} is given by

$$C_{FDM} = (c_{material} \times m_r) + (c_{slicing} \times t_{design}) + \{(c_{operator} + c_{overhead}) \times t_{build}\} + (c_{operator} \times t_{pp}), \quad (4)$$

where $c_{material}$ is the material cost per kg, m_r is the mass of the plastic filament, t_{design} is the time required to set necessary parameters and transform the CAD model to proper STL format and t_{pp} is the time for performing finishing operations on the part. It should be noted that Eq. (4) is applicable only when a single quantity of the part is built in the machine bed. For building n quantities of the same part, the cost per part C_{FDM} is given by

$$C_{FDM} = (c_{material} \times m_r) + \left(c_{slicing} \times \frac{t_{design}}{n}\right) + \{(c_{operator} + c_{overhead}) \times t_{build}\} + (c_{operator} \times t_{pp}), \quad (5)$$

Slicing cost per hour $c_{slicing}$ in Eq. (3) is given by

$$c_{slicing} = \frac{\text{Annual slicing software cost}}{\text{annual operating hours}} + \frac{\text{monthly salary of the designer}}{\left(\begin{array}{l} \text{working days in a month} \\ \times \text{effective working hours in a day} \end{array}\right)}. \quad (6)$$

Operator cost per hour $c_{operator}$ is given by

$$c_{operator} = \frac{\text{monthly salary}}{\left(\begin{array}{l} \text{working days in a month} \\ \times \text{effective working hours in a day} \end{array}\right)}. \quad (7)$$

Overhead cost per hour $C_{overhead}$ is given by

$$C_{overhead} = \frac{1}{\text{annual operating hours}} \left(\frac{\text{machine cost} - \text{salvage value}}{\text{machine life}} + \text{annual maintenance cost} + \text{annual factory rent} + \text{annual electricity charge} \right) \tag{8}$$

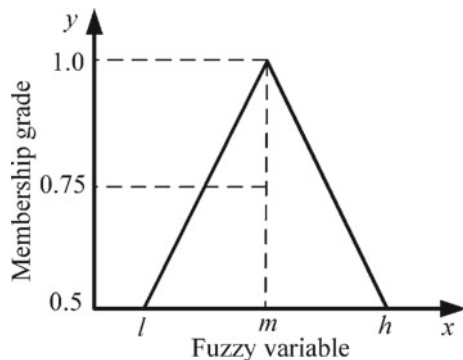
The procedure described in this section is illustrated through case studies in Sect. 5.

2.3 Incorporation of Uncertainty in Cost Estimation

The procedure described in Sect. 2.2 to estimate the cost is deterministic in nature. It gives only a single value of cost. However, in practice, most of the cost elements have an element of uncertainty. Hence, considering the uncertainty, the cost of the part is obtained in a particular range. One of the most common approaches to tackle uncertainty is by adopting a fuzzy set theory. It is a well-recognised soft computing based method that handles uncertainties and provides reasonable solution [25]. The concept of fuzzy set and fuzzy numbers is described in sequel.

A fuzzy variable is represented by a quantity whose value is imprecise instead of a single crisp value. In a fuzzy set based model, the uncertain as well as imprecise variables are considered as fuzzy. These uncertain variables are represented as various interval numbers. Each interval number is assigned a membership grade varying between 0 and 1. A common way to obtain membership functions is to obtain them from experts' opinion. Based on an expert's opinion, one can obtain the low (l), most likely (m) and high (h) estimates of a parameter. By this, a linear triangular membership function can be constructed where the low and high estimates are assigned a membership grade of 0.5 and the most likely estimate is assigned a membership grade of 1. The representation of a fuzzy number is shown in Fig. 2. It is clearly seen that corresponding to each membership grade, there is an interval in which the variable may lie.

Fig. 2 A triangular membership function



A fuzzy number A at a particular value of α -cut can be represented by

$$A_\alpha = [a_1^\alpha, a_2^\alpha], \quad (9)$$

where A_α is the interval for the membership grade α , a_1^α and a_2^α are the lower and upper limits of the interval, respectively. Arithmetic operations of two fuzzy numbers at a particular membership grade (α -cut) is carried out in the following manner:

$$\text{Summation: } (a_1^\alpha, a_2^\alpha) + (b_1^\alpha, b_2^\alpha) = (a_1^\alpha + b_1^\alpha, a_2^\alpha + b_2^\alpha), \quad (10)$$

$$\text{Subtraction: } (a_1^\alpha, a_2^\alpha) - (b_1^\alpha, b_2^\alpha) = (a_1^\alpha - b_2^\alpha, a_2^\alpha - b_1^\alpha), \quad (11)$$

$$\text{Multiplication: } (a_1^\alpha, a_2^\alpha) \times (b_1^\alpha, b_2^\alpha) = (a_1^\alpha \times b_1^\alpha, a_2^\alpha \times b_2^\alpha), \quad (12)$$

$$\text{Division: } (a_1^\alpha, a_2^\alpha) \div (b_1^\alpha, b_2^\alpha) = (a_1^\alpha/b_2^\alpha, a_2^\alpha/b_1^\alpha). \quad (13)$$

As the cost is always obtained as a positive real number, it is assumed that the arithmetic operations are carried out only for a set of positive real numbers. The addition and subtraction of two fuzzy numbers result in a linear triangular fuzzy number; this is not the case for multiplication and division. However, as an approximation, a nonlinear triangular fuzzy number can also be considered as a triangular fuzzy number. The procedure described in this section is illustrated with examples in Sect. 5.

3 Impact on Environment

The environmental impact of a manufacturing process is assessed on the basis of the consumption of natural resources and the energy consumed during the conversion of the raw material to the final commercialized part. Although AM is claimed to be sustainable and environmental friendly, it can have adverse environmental impact if not utilized judiciously. If the temperature of the machine chamber is not controlled properly during the manufacturing phase, the extra energy usage is unfavorable. Proper estimation of energy consumption and minimizing it is one of the main strategies for obtaining environmental benefits. This section describes a method to estimate the energy consumed to produce a part by a popular AM process, i.e., FDM. The energy consumption in FDM can be categorized in the following stages:

- Energy consumed during melting of filament
- Energy consumed during extrusion
- Energy consumed in heating the baseplate
- Energy consumed by the movable platform
- Miscellaneous energy consumption (standby, losses).

3.1 Energy Consumed During Melting of the Filament

The thermoplastic filament is extruded in the molten form through the nozzle of the machine. The molten extruded material is maintained at a temperature 1 °C above the melting point [7]. After extrusion, the material is fused with the previously formed layer. The total heat energy, Q_m required during melting of the filament is given by

$$Q_m = m_e c_{ps}(T_m - T_i) + m_e q_f + m_e c_{pm}(T_f - T_m), \quad (14)$$

where m_e is the mass of the extruded material, c_{ps} is the specific heat of solid polymer, T_m is the melting temperature of the material, T_i is the initial temperature, q_f is the heat of fusion, c_{pm} is the specific heat of melted polymer and T_f is the final temperature. The heat input is provided by the heater and its energy consumption $E_{melting}$ is given by

$$E_{melting} = \frac{Q_m}{\eta_r}, \quad (15)$$

where η_r is the efficiency of the heater.

3.2 Energy Consumed During Extrusion

At this stage, the molten thermoplastic material is pushed through the nozzle to the baseplate. The required force for extrusion should overcome the pressure drop across the extruder. The pressure drop is dependent on the viscosity of the molten material and geometry of the extruder and nozzle. The material behaviour of thermoplastic filament obeys shear thinning where the viscosity of the material decreases with an increase in the shear rate [26]. A power law is adopted to model the dependence of viscosity on shear rate [27]:

$$\eta = K \dot{\gamma}^{n-1}, \quad (16)$$

where η is the viscosity of the material, $\dot{\gamma}$ is the shear rate, K and n are the power law fit parameters. Also, the flow of the molten material in the extruder is non-isothermal. Hence, the dependence of viscosity on temperature should also be considered along with shear rate dependence [26, 27]:

$$\eta = H(T)\eta_{T_0}(\dot{\gamma}), \quad (17)$$

where $H(T)$ is the temperature-dependent term for viscosity. The term T_0 is the reference temperature at which the power fit parameters K and n are determined. The Arrhenius relation to model the temperature-dependent term is given by [27]

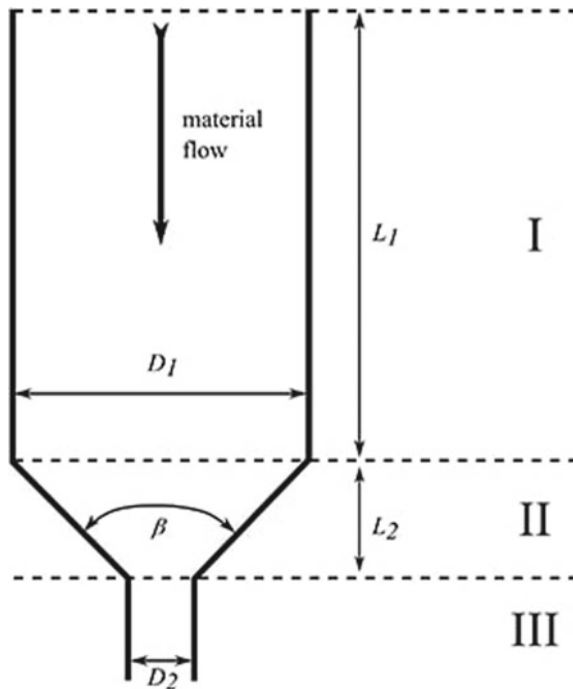
$$H(T) = \exp\left\{\alpha\left(\frac{1}{T} - \frac{1}{T_0}\right)\right\}, \quad (18)$$

where α is the activation energy and T is the temperature at the end of the extruder.

Applying Eqs. (17) and (18) to the momentum balance on the extruder, Bellini et al. [26] estimated the pressure drop in the extruder by dividing into three different zones as illustrated in Fig. 3. For simplicity, the model was developed considering several assumptions: (a) the melt, i.e. the molten material, is incompressible, (b) no-slip boundary condition is applicable at the wall of the extruder, and (c) the flow of the melt is uniform, steady and laminar.

The pressure drops are given by [26, 27]

Fig. 3 Different zones of the extruder. With permission from Turner et al. [27]. Copyright 2014, Emerald Publishing Company



$$\begin{aligned}
\Delta P_1 &= 2L_1 \left(\frac{v}{\phi} \right)^{1/m_f} \left\{ \frac{m_f + 3}{(D_1/2)^{m_f + 1}} \right\}^{1/m_f} \exp \left\{ \alpha \left(\frac{1}{T} - \frac{1}{T_0} \right) \right\}, \\
\Delta P_2 &= \left\{ \frac{2m_f}{3 \tan(\beta/2)} \right\} \left(\frac{1}{D_2^{3/m_f}} - \frac{1}{D_1^{3/m_f}} \right) \left\{ \left(\frac{D_1}{2} \right)^2 (m_f + 3) 2^{m_f + 3} \right\}^{1/m_f} \exp \left\{ \alpha \left(\frac{1}{T} - \frac{1}{T_0} \right) \right\}, \\
\Delta P_3 &= 2L_3 \left(\frac{v}{\phi} \right)^{1/m_f} \left\{ \frac{(m_f + 3)(D_1/2)^2}{(D_1/2)^{m_f + 1}} \right\}^{1/m_f} \exp \left\{ \alpha \left(\frac{1}{T} - \frac{1}{T_0} \right) \right\},
\end{aligned} \tag{19}$$

where ΔP_1 , ΔP_2 and ΔP_3 are the pressure drops in zone I, II and III, respectively, L_1 and L_3 —are the length of the liquefier corresponding to zone I and III, respectively, v is the velocity of the filament at the entry, β is the nozzle angle, ϕ and m_f are the power law fit parameters, and D_1 and D_2 are diameters of the filament and nozzle, respectively. The total pressure drop, ΔP is given by the algebraic summation of the pressure drops at all the three zones:

$$\Delta P = \Delta P_1 + \Delta P_2 + \Delta P_3. \tag{20}$$

The force F_e required to push the molten thermoplastic material through the liquefier is given by

$$F_e = \Delta P A_f, \tag{21}$$

where A_f is the cross sectional area of the filament. The energy required in extrusion $E_{extrusion}$ is given by

$$E_{extrusion} = F_e S, \tag{22}$$

where S is the distance travelled by the molten material in the liquefier. The distance travelled S is given by

$$S = v_e t_e, \tag{23}$$

where v_e is the extrusion velocity and t_e is the extrusion time. The extrusion time t_e is assumed to be equal to the printing time. The energy required in extrusion $E_{extrusion}$ is provided by the motor:

$$E_{extrusion} = \frac{E_e}{\eta_m}, \tag{24}$$

where η_m is the efficiency of the motor.

3.3 Energy Consumed in Heating the Baseplate

The extruded material is deposited in a baseplate that is heated by the resistive heater. The baseplate where the printing takes place is made of a thermosetting plastic. The heat input, Q_b to raise the temperature of the base plate during printing is given by

$$Q_b = m_b c_{pb} (T_f - T_i), \quad (25)$$

where m_b is the mass of the base plate, c_{pb} is specific heat of the baseplate, T_f is the final attainable temperature by the baseplate and T_i is the initial temperature of the baseplate. The heat input provided by the resistive heater and the energy consumption $E_{base\ plate}$ is given by

$$E_{base\ plate} = \frac{Q_b}{\eta_r}. \quad (26)$$

3.4 Energy Consumed by the Movable Platform

After a layer is formed, the baseplate moves in the downward direction according to the predetermined layer thickness. The base plate along with the platform moves and stops repeatedly according to the number of layers present in the part. Assuming that no energy is required in stopping, the mechanical energy of the movable platform, E_p is given by the summation of potential and total kinetic energies:

$$E_p = m_p g h + \frac{1}{2} m_p v_p^2 N_l, \quad (27)$$

where m_p is the mass of platform, g is the acceleration due to gravity, h is the total height travelled, v_p is the velocity of the platform and N_l is the number of layers present in the part. The energy required by the platform, $E_{platform}$ is provided by the motor:

$$E_{platform} = \frac{E_p}{\eta_m}, \quad (28)$$

where η_m is the efficiency of the motor.

3.5 *Miscellaneous Energy Consumptions*

Apart from the energy consumption sources mentioned in Sects. 3.1–3.4, energy is also consumed by the computer, workstation and some energy is also lost in the form of heat and machine error [28, 29]. The energy consumed by miscellaneous sources E_{misc} is approximated as 5% of the total energy consumed by all other sources, i.e.,

$$E_{misc} = 0.05(E_{melting} + E_{base-plate} + E_{platform} + E_{extrusion}). \quad (29)$$

The deterministic model described in this section can also be developed for uncertain conditions by considering the variables as fuzzy. This is illustrated through examples in Sect. 5.

4 **Social Issues**

Specific to additive manufacturing (AM), the societal aspect has received less attention as compared to environmental and economic aspects of sustainability [19, 30–33]. Some aspects of social sustainability of AM are discussed in Sects. 4.1–4.4:

4.1 *Employment and Working Conditions*

The implementation of AM technology can drastically change the workforce structure of an organization. Due to the automatic characteristics of AM, the workload associated with production and manufacture of goods is significantly reduced. Several changes are seen in the working parameters including working hours and conditions, intensity of labor and type of work. AM machinery needs less involvement of operators; thus, the same operator can be engaged in other activities as well. Owing to this, the need for human labor reduces, which in turn leads to loss of employment opportunities. Also, it requires comparatively less skill to operate as compared to CNC lathe or mill [34]. Hence, workers have to settle with the salary of low skilled jobs. The working environment of AM has relatively less detrimental health effect on workers as compared to conventional manufacturing (CM). Unlike CM, it does not generate waste chips, coolant spills and mist. Also, the risk of occurrence of injuries to the operators is relatively less. However, material handling in AM may cause certain health issues. Huang et al. [7] reported that the direct contact of AM based chemicals could cause skin allergies. They also emphasized that the biodegradability of these chemicals is poor and they remain in the environment for a considerable amount of time. The breakdown of these

long-chained molecules emits poisonous gases like carbon dioxide and carbon monoxide.

4.2 Health and Wellness

One of the major societal challenges is to provide efficient and quality health care. AM has proven to be helpful during medical emergencies. Its ability to produce customized products is the main motive for medical sector to procure AM [35]. Bio-medical products such as orthosis, artificial limbs, and implants can be effectively fabricated as per patients' requirements [7]. In the process of drug delivery, AM is capable of producing ready-to-use oral tablets in high quantity [36]. This technology also enables production of safety equipment such as helmet, protective garment as per the user's comfort and mass production of medical equipment for the prevention of various diseases and ailments. After the outbreak of Corona Virus disease (COVID-19) in December 2019, there was an urgent need of personal protective equipment (PPE) in the form of facemask and face shield, and testing kits [37, 38]. These were required in large volumes throughout the globe especially for the healthcare workers handling COVID-19 cases. During this urgent need, a fused deposition modelling based 3D printer was able to manufacture 112 ready-to-use face shields in 72 h [39].

4.3 Education and Training

The development of this technology has given rise to opportunities in the educational field as well. With these opportunities, the need for education, training, and accumulation of a new set of technical skills has also risen [40]. Students and trainees who understand how to use this technology can benefit from the same in numerous ways. This will provide trained individuals to test their creativity. Also, it will act as compensation for the problems caused due to the reduction in the demand for manual labor by creating new opportunities in the education and training department as well as giving rise to new self-employment opportunities. Creative designers who wish to work independently can also use this technology to manufacture their own products. In addition to the increase in creative opportunities and reduction in operational costs, the range of 3D printers in general is wide. Hence, low-cost 3D printers are available for hobbies, personal use or small businesses [32]. Owing to this, it is possible for countries employing this technology to operate independently for the production and distribution of goods and services instead of relying on imports and exports thereby promoting their economic and social well-being.

4.4 *Authorization and Legal Issues*

AM is instrumental in making the manufacturing process easier by reducing distance limitations and cutting unnecessary costs. However, the increasing popularity of AM has raised several issues on the interpretation of intellectual property rights (IPR) system [40]. IPR is a legal right that aims to protect the creations and inventions resulting from intellectual efforts in the field of technology, design, artistry and literary works. Some concerns of IPRs specific to AM comprise copyright, patent and trademark [41]. The digital feature of this technology permits everyone to re-design an existing model, produce the product and even sell the product along with its associated CAD model. The ability of a 3D scanner to scan innovative products such as implants and produce the model digitally also raises questions on patent infringement. Production of certain items such as guns and weapons that are illegal as per government directives can be easily created in the CAD format. The circulation of such files and their availability in the internet also pose threats to the defence of a country. Hence, some restrictions must be imposed on the legality of CAD files to avoid misuse of AM.

4.5 *A Quantitative Method for Evaluating the Penalty Due to Reduction in Employment*

AM is well suited for making parts having complex geometrical features. The parts that are difficult to manufacture by conventional manufacturing can be easily manufactured by 3D printing owing to the automatic characteristics. This may have an adverse impact on the labor in terms of employment. However, if the job of the labor is permanent and there is no policy of salary reduction, the organization has to pay full salary to the labor or the operator in spite of their reduced involvement in the production process. Government may also enforce the organization to pay some unemployment allowance to state exchequer as a part of corporate social responsibility (CSR).

The time taken to manufacture a complex part by 3D printing is less than that by conventional manufacturing. However, the salary payable to the labor will be same for both conventional and 3D printing although the latter involves less labor engagement. The amount payable to the manpower head can be referred as labor penalty cost. Let t_c be the time for conventional manufacturing and t_{3D} the time for 3D printing for a product. The labor penalty cost attributed to a product can be obtained as

$$\text{Labour penalty cost} = \left(\frac{t_c}{t_{3D}} - 1 \right) \times (\text{Labour cost}). \quad (30)$$

The organization can reduce the labor penalty cost by enhancing the production, provided there is sufficient market for the product. Define a ratio r as

$$r = \frac{\text{Demand potential}}{\text{Current annual production}}. \quad (31)$$

Incorporating r in Eq. (30), the modified labor penalty cost is obtained as

$$\text{Labour penalty cost} = \left(\frac{t_c}{t_{3D}r} - 1 \right) \times (\text{Labour cost}). \quad (32)$$

Maximizing the value of r , the labor penalty cost can be minimized. It is to be noted that in some cases, the penalty cost may be negative also, implying that AM is in fact going to provide more employment.

5 Case Studies

The deterministic models described in Sect. 2.2 and 3 are implemented for estimating the cost and energy consumption of two parts in FDM. Figure 4 shows two parts (Part 1 and Part 2) printed by FDM. The geometrical parts shown in Fig. 4 were printed in Riwell RL 200A, an FDM based desktop 3D printer [42]. The volume and height of Part 1 are 8266.06 mm^3 and 39 mm, respectively. Part 2 is relatively large, of volume $15,831.47 \text{ mm}^3$ and height 15 mm. The actual time to print those parts (54 min for Part 1 and 88 min for Part 2) will be used for estimating the overall cost and energy consumption of the parts. The raw material used was thermoplastic ABS filament of density 1.21 gm/cm^3 .

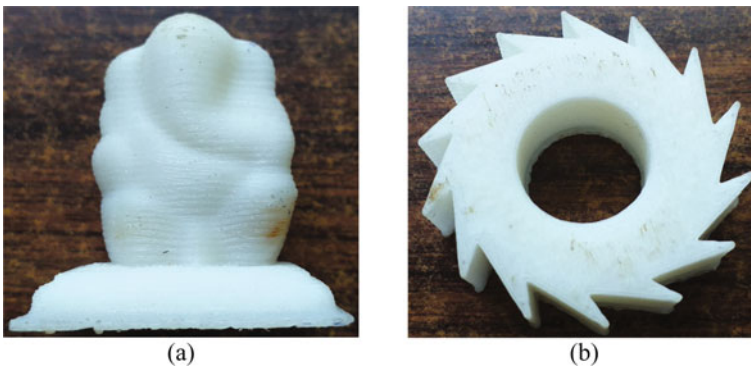


Fig. 4 Printed parts in FDM based 3D printer: **a** part 1, and **b** part 2

5.1 Cost Estimation

The details of the cost elements, viz., the material, operator, slicing and the overhead costs are shown in Table 2. The same cost elements were also considered for estimating the cost of another AM process, i.e., selective laser sintering (SLS) in Ref. [20].

The cost is estimated as per the procedure described in Sect. 2.2. Initially, the material cost is determined. In practice, some filament always gets wasted. Hence, an additional 20% is included with the volume of the part to consider the material loss. Then, the slicing, operator and overhead costs are determined as per Eqs. (6), (7) and (8), respectively. In Eq. (8), the dominating cost element is the machine cost. The useful life of the 3D printer is considered as 8 years and straight line depreciation is followed. In Eq. (4), t_{design} and t_{pp} are considered as 30 min each. Finally, the overall costs of Part 1 and Part 2 are obtained as \$3.16 and \$4.34, respectively.

Table 2 Details of cost elements considered in this study

Cost elements	Most likely value	Basis
Raw material cost per kg (\$)	16.44	Ref. [43]
<i>Operator cost</i>		
Monthly salary of an operator (\$)	205.48	Ref. [44]
Monthly working days	25	Typical industrial practice
Effective daily hours (hr)	7	Typical industrial practice
<i>Slicing cost</i>		
Slicing software fee (\$)	205.48	Ref. [45]
Annual operating hours (hr)	2100	Seven hours usage in 300 days
<i>Overhead cost</i>		
Machine cost (\$)	6849.32	Ref. [46]
Machine life (year)	8	Ref. [20]
Salvage value (\$)	684.93	10% of the cost of the machine
Annual maintenance cost (\$)	342.47	5% of the cost of the machine
Annual floor rent (\$)	394.52	Ref. [47], assuming 200 ft ² of floor space
Annual electricity charge (\$)	71.92	Electricity price of \$ 0.14 per kWhr and electricity consumption of 250 Whr
Annual operating hours (hr)	2100	Seven hours usage in 300 days
Indian currency (₹) is converted to US dollar (\$) [48]		

5.2 Application of Fuzzy Arithmetic in Cost Estimation

In Sect. 5.1, the cost is obtained as a single value. This section considers the uncertain cost related parameters as fuzzy variables. The fuzzy variables are represented in the form of low (l), most likely (m) and high (h) as described in Sect. 2.3. The list of fuzzy parameters considered is given in Table 3. The material cost per kg, monthly salary of the operator, slicing software cost, machine cost and the salvage values are considered to vary by 10%. However, for yearly maintenance cost of the 3D printer, the lower and higher estimates are considered to vary by 10% and 20%, respectively. Lastly, for annual floor rent and electricity charge, both the lower and higher estimates are considered by 5%. Applying suitable fuzzy arithmetic operations as per Eqs. (10)–(13), the estimates of cost are obtained as fuzzy numbers. The cost (in \$) for Part 1 is obtained as $l = 2.83$, $m = 3.16$ and $h = 3.51$, whereas for Part 2, it is obtained as $l = 3.95$, $m = 4.34$ and $h = 4.93$. The variation of cost of the parts with different membership grades is shown in Fig. 5.

5.3 Estimation of Energy Consumption

The energy consumption for the parts is estimated as per the procedure described in Sect. 3. The first step is to estimate the energy consumed during melting of the filament as per Eq. (14). The necessary parameters for estimating the energy in melting are listed in Table 4. An extra 20% is included in the mass of the extruded material to consider the material loss. The next step is to estimate the energy consumed during extrusion. It depends on several parameters including the geometry of the liquefier, pressure drop in the liquefier, cross sectional area of the filament, extrusion velocity and extrusion time. The parameters for estimating the extrusion energy are listed in Table 5. The next step comprises the estimation of energy consumption in heating the base plate. The resistive heater consumes energy for heating the base plate during the entire printing process. Lastly, the energy consumed by the movable platform in the vertical direction is estimated as per

Table 3 Fuzzy parameters considered in cost estimation

Cost elements	(l, m, h)
Material cost per kg (\$)	(14.79, 16.44, 18.08)
Monthly salary of an operator (\$)	(184.93, 205.48, 226.03)
Slicing software fee (\$)	(184.93, 205.48, 226.03)
Machine cost (\$)	(6164.38, 6849.32, 7534.25)
Salvage value (\$)	(616.44, 684.93, 753.42)
Yearly maintenance cost (\$)	(308.22, 342.47, 410.96)
Annual floor rent (\$)	(374.79, 394.52, 414.25)
Annual electricity charge (\$)	(68.32, 71.92, 75.51)

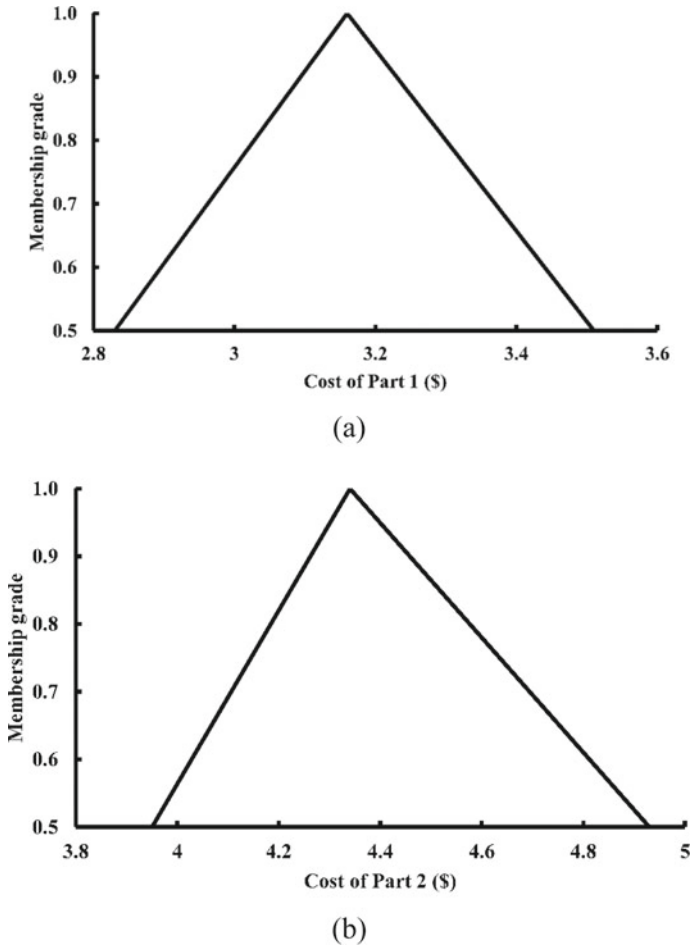


Fig. 5 Representation of cost as a fuzzy number for **a** part 1 and **b** part 2

Eq. (27). The movable platform lowers down vertically according to the layer thickness of the part. The total vertical distance travelled by the platform is equal to the height of the part.

The energy consumed by different sources for the parts is listed in Table 6. It is observed that the maximum energy is consumed during heating the base plate. The mass of the parts, printing time and the geometrical features give indication on the energy consumption.

Table 4 Parameters for estimating the energy consumed during melting of the filament and heating the base plate

Parameters	Most likely value	Basis
Specific heat of solid ABS, c_{ps} (kJ/kg °C)	1.92	Ref. [49]
Specific heat of melted ABS, c_{pm} (kJ/kg °C)	2.4	Ref. [49]
Melting temperature of ABS, T_m (°C)	230	Ref. [50]
Initial temperature, T_i (°C)	25	Room temperature
Heat of fusion of ABS, q_f (kJ/kg)	205	Ref. [51]
Final temperature, T_f (°C)	231	Refs. [7, 50]
Efficiency of the heater, η	0.9	Assuming 10% heat loss
Mass of the baseplate, m_b (gm)	500	Assumption
Specific heat of the base plate, c_{pb} (kJ/kg °C)	1.3	Ref. [52]
Initial temperature of the base plate, T_i (°C)	25	Room temperature
Final temperature of the base plate, T_f (°C)	110	Ref. [53]

Table 5 Parameters for estimating the energy consumed during extrusion of the molten filament and the movable platform

Parameters	Most likely value	Basis
Length of zone I (mm)	97.5	Ref. [26]
Length of zone II (mm)	37.5	Ref. [26]
Length of zone III (mm)	15	Ref. [26]
Velocity of the filament at the entry, v (mm/s)	3.1	Ref. [54]
Flow exponent, m_f	1.54	Ref. [54]
Fluidity, ϕ	1.19×10^{-3}	Ref. [54]
Diameter of zone I (mm)	1.75	Ref. [20]
Diameter of zone II (mm)	0.4	Ref. [20]
Nozzle angle, β (°)	120	Ref. [27]
Temperature at the end of the extruder, T (K)	540	Ref. [26]
Temperature, T_0 (K)	500	Ref. [55]
Energy of activation, α	19,800	Ref. [56]
Mass of the platform, m_p (kg)	5	Assumption
Velocity of the platform, v_p (mm/s)	40	Ref. [20]

5.4 Application of Fuzzy Arithmetic in Energy Consumption

Similar to Sect. 5.2, this section considers the uncertain energy related parameters as fuzzy. The fuzzy parameters are represented in the form of low (l), most likely (m) and high (h) as listed in Table 7. In the estimation of energy consumed during melting, the lower of the extra material consumed is assumed to vary by 5% whereas the upper limit by 20%. For estimating the pressure drop in the liquefier,

Table 6 Energy consumption by various sources for the parts

Energy consuming source	Most likely value	
	Part 1	Part 2
Energy consumed during melting of the filament (kJ)	8.01	15.35
Energy consumed in heating the baseplate (kJ)	61.39	61.39
Energy consumed during extrusion (kJ)	22.25	36.26
Energy consumed by the movable platform (J)	2.4	1.73
Miscellaneous energy consumption (kJ)	4.58	5.64
Total energy consumption (kJ)	96.24	118.65
Total energy consumption (Whr)	26.73	32.96
Total energy consumption per unit mass (kJ/kg)	8018.38	5161.57
Total energy consumption per unit build time (kJ/hr)	106.93	80.9

the lower and upper limit of the length of the liquefier is considered to vary by 10%. Assuming heat loss in different forms, the lower and upper limit of efficiency of the heater is considered as 80% and 95%, respectively. The total energy consumption (in kJ) of Part 1 is obtained as $l = 90.07$, $m = 96.24$ and $h = 123.30$, whereas for Part 2, it is obtained as $l = 110.42$, $m = 118.65$ and $h = 132.44$. The variation of energy consumption of Part 1 and Part 2 with different membership grades is shown in Fig. 6.

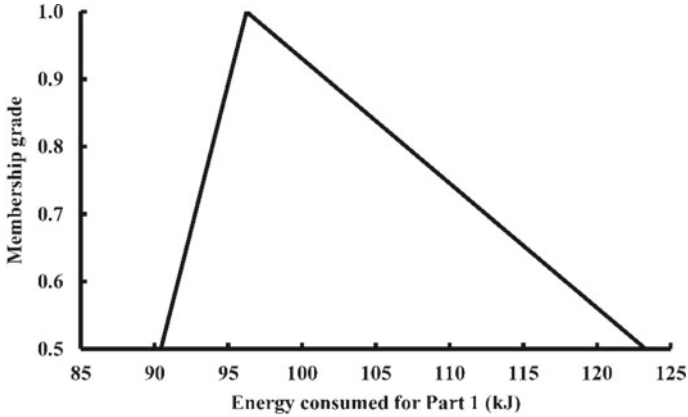
5.5 Overall Sustainability Analysis

It is considered that an industry works effectively for 300 days in a year and the 3D printer operates for 6 h a day, i.e., 1800 h is available in a year. Based on this assumption, the maximum quantities of Part 1 and Part 2 that can be manufactured in a year can be estimated. The printing times for Part 1 and Part 2 are 54 min and 88 min, respectively. Hence, a maximum of 2000 quantities of Part 1 and 1227 of Part 2 can be manufactured annually. Finally, the manufacturing cost on an annual basis can be estimated.

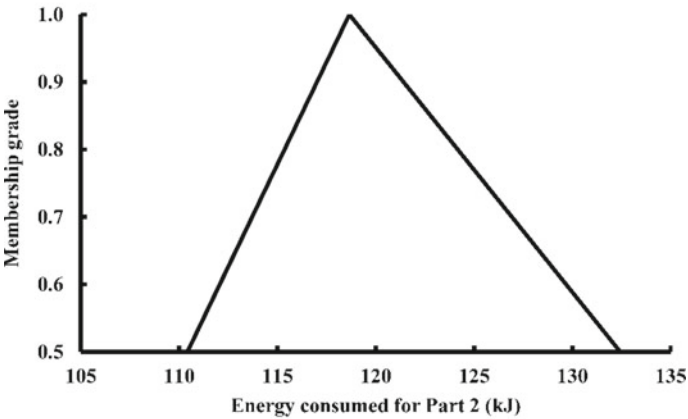
The energy consumption of the parts can be used to estimate the environmental cost and the amount of CO₂ emission. The environmental cost is estimated based on the values of energy consumption and electricity rate given in Tables 6 and 2,

Table 7 Fuzzy parameters considered in energy estimation

Parameters	(l, m, h)
Extra material consumed during extrusion (%)	(5, 20, 30)
Efficiency of the heater (%)	(80, 90, 95)
Total length of liquefier (mm)	(148.5, 150, 151.5)
Efficiency of the motor (%)	(70, 75, 80)



(a)



(b)

Fig. 6 Variation of energy consumption as a fuzzy number for **a** part 1 and **b** part 2

respectively. For simplicity, it is taken as cost of electricity. The amount of CO₂ emission (in kg) based on the energy input is given by [57]:

$$\text{Amount of } CO_2 \text{ emission} = \text{Energy input} \times \text{Emission factor}, \quad (33)$$

where the energy input is considered in terms of kWhr/year and emission factor is taken as 0.85. Table 8 shows the manufacturing cost, environment cost, energy usage and amount of CO₂ emission for Part 1 and Part 2.

The calculation of labor penalty cost for a product needs t_c , t_{3D} and r . Depending on these values, labor penalty cost can be positive or negative. As these parts have been chosen for the purpose of illustration and are not being produced in industry,

Table 8 Cost, energy usage and CO₂ emission of the parts on an annual basis

Parts	Annual production (quantities)	Manufacturing cost (\$)	Energy usage (kWhr/year)	Energy cost (\$)	CO ₂ emission (kg)
Part 1	2000	6320	53.47	7.48	45.45
Part 2	1227	5325.18	40.44	5.66	34.37

there is no information available regarding t_{3D} and r . With the availability of the values of t_{3D} and r , labor penalty cost can be easily estimated. Finally, the overall cost of a product can be computed as the sum of manufacturing, environmental cost and penalty cost. One can also add penalty due to CO₂ emission to environmental cost.

6 Conclusion

This chapter attempts to address the sustainability of a popular additive manufacturing process, i.e., fused deposition modelling (FDM). Different additive manufacturing processes are briefly described and the specialty of FDM is highlighted. Initially, in the context of economic sustainability, the cost model of FDM is proposed by considering several cost elements. This can also be generalized for other additive manufacturing process if the procedure for estimating the build time is provided. In context of environmental aspect, an energy consumption model is proposed where the role of several energy consuming elements is described. From the energy analysis of the parts, it is observed that the maximum energy is consumed in heating the base plate where the molten thermoplastic material is deposited to produce the part. To tackle uncertainty, the deterministic models of cost and energy consumption are upgraded to fuzzy set based models by considering uncertain or imprecise variables as fuzzy. The values obtained by the fuzzy set based models are in the form of interval as a function of membership grade and give an idea about the upper and lower bound of the estimates. Some aspects of social sustainability, viz., the impact of AM on workforce structure, benefits availed by the medical sector, opportunities for starting small-scale business and legal matters are described. The ease of manufacturing provided by this disruptive technology sometimes raises concern about intellectual property rights protection.

This article also illustrates a procedure to quantify the overall sustainability based on overall cost, CO₂ emission and the involvement of workforce in the production phase. The methodology is illustrated by manufacturing two parts in an FDM based 3D printer. The overall procedure presented in this work can be implemented in industrial scenario to compare with conventional manufacturing processes. This will help in assessing the sustainability of FDM and quantify its

competitiveness with other processes. Based on this, the management can take decision under which circumstances FDM or other additive manufacturing process is preferable to conventional manufacturing.

References

1. Yang L, Hsu K, Baughman B, Godfrey D, Medina F, Menon M, Wiener S (2017) Additive manufacturing of metals: the technology, materials, design and production. Springer, Cham
2. Kruth JP, Leu MC, Nakagawa T (1998) Progress in additive manufacturing and rapid prototyping. *CIRP Ann* 47(2):525–540
3. Levy GN, Schindel R, Kruth JP (2003) Rapid manufacturing and rapid tooling with layer manufacturing (LM) technologies, state of the art and future perspectives. *CIRP Ann Manuf Technol* 52(2):589–609
4. Dixit US, Hazarika M, Davim JP (2016) A brief history of mechanical engineering. Springer, Switzerland
5. Chua CK, Wong CH, Yeong WY (2017) Standards, quality control, and measurement sciences in 3D printing and additive manufacturing. Elsevier, Cambridge
6. Hull CW, UVP Inc (1986) Apparatus for production of three-dimensional objects by stereolithography. U.S. Patent 4,575,330
7. Huang SH, Liu P, Mokasdar A, Hou L (2013) Additive manufacturing and its societal impact: a literature review. *Int J Adv Manuf Technol* 67:1191–1203
8. Liu Q, Leu MC, Schmitt SM (2006) Rapid prototyping in dentistry: technology and application. *Int J Adv Manuf Technol* 29:317–335
9. Crump SS, Stratasys Inc (1992) Apparatus and method for creating three-dimensional objects. U.S. Patent 5,121,329
10. Jeantette FP, Keicher DM, Romero JA, Schanwald LP (2000) Method and system for producing complex-shape objects. U.S. Patent 6,046,426
11. Sachs E, Cima M, Williams P, Brancazio D, Cornie J (1992) Three dimensional printing: rapid tooling and prototypes directly from a CAD model. *J Eng Indus* 114(4):481–488
12. Masood SH (1996) Intelligent rapid prototyping with fused deposition modelling. *Rapid Prototyping J* 2(1):24–33
13. Kumar S, Czekanski A (2018) Roadmap to sustainable plastic additive manufacturing. *Mater Today Commun* 15:109–113
14. Vyavahare S, Teraiya S, Panghal D, Kumar S (2020) Fused deposition modelling: a review. *Rapid Prototyping J* 26(1):176–201
15. Kurfess T, Cass WJ (2014) Rethinking additive manufacturing and intellectual property protection. *Res Technol Manag* 57(5):35–42
16. Qattawi A, Alrawi B, Guzman A (2017) Experimental optimization of fused deposition modelling processing parameters: a design-for-manufacturing approach. *Procedia Manuf* 10:791–803
17. Michelsen G, Adomßent M, Martens P, von Hauff M (2016) Sustainable development—background and context. In: Heinrichs H, Martens P, Michelsen G, Wiek A (eds) *Sustainability science*. Springer, Dordrecht, pp 5–29
18. <https://sustainabledevelopment.un.org/content/documents/5987our-common-future.pdf>. Accessed 5 Aug 2020
19. Ma J, Harstvedt JD, Dunaway D, Bian L, Jaradat R (2018) An exploratory investigation of additively manufactured product life cycle sustainability assessment. *J Clean Prod* 192:55–70
20. Sharma F, Dixit US (2019) Fuzzy set based cost model of additive manufacturing with specific example of selective laser sintering. *J Mech Sci Technol* 33(9):4439–4449

21. Alexander P, Allen S, Dutta D (1998) Part orientation and build cost determination in layered manufacturing. *Comput Aided Des* 30(5):343–356
22. Zhu Z, Dhokia V, Newman ST (2016) A new algorithm for build time estimation for fused filament fabrication technologies. *Proc Inst Mech Eng [B]: J Eng Manuf* 230(12):2214–2228
23. Chacón JM, Caminero MA, García-Plaza E, Núñez PJ (2017) Additive manufacturing of PLA structures using fused deposition modelling: effect of process parameters on mechanical properties and their optimal selection. *Mater Des* 124:143–157
24. Thrimurthulu KPPM, Pandey PM, Reddy NV (2004) Optimum part deposition orientation in fused deposition modeling. *Int J Mach Tools Manuf* 44(6):585–594
25. Dixit PM, Dixit US (2008) Modeling of metal forming and machining processes: by finite element and soft computing methods. Springer, London
26. Bellini A, Guceri S, Bertoldi M (2004) Liquefier dynamics in fused deposition. *J Manuf Sci Eng* 126(2):237–246
27. Turner BN, Strong R, Gold SA (2014) A review of melt extrusion additive manufacturing processes: I. Process design and modeling. *Rapid Prototyping J* 20(3):192–204
28. Song R, Telenko C (2017) Material and energy loss due to human and machine error in commercial FDM printers. *J Clean Prod* 148:895–904
29. Yosofi M, Kerbrat O, Mognol P (2018) Energy and material flow modelling of additive manufacturing processes. *Virtual Phys Prototyping* 13(2):83–96
30. Ford S, Despeisse M (2016) Additive manufacturing and sustainability: an exploratory study of the advantages and challenges. *J Clean Prod* 137:1573–1587
31. Matos F, Godina R, Jacinto C, Carvalho H, Ribeiro I, Peças P (2019) Additive manufacturing: exploring the social changes and impacts. *Sustainability* 11(14):3757
32. Matos F, Jacinto C (2019) Additive manufacturing technology: mapping social impacts. *J Manuf Technol Manag* 30(1):70–97
33. Naghshineh B, Lourenço F, Godina R, Jacinto C, Carvalho H (2020) A social life cycle assessment framework for additive manufacturing products. *Appl Sci* 10(13):4459
34. Faludi J, Bayley C, Bhogal S, Iribarne M (2015) Comparing environmental impacts of additive manufacturing vs traditional machining via life-cycle assessment. *Rapid Prototyping J* 21(1):14–33
35. Niaki MK, Torabi SA, Nonino F (2019) Why manufacturers adopt additive manufacturing technologies: the role of sustainability. *J Clean Prod* 222:381–392
36. Shahrubudin N, Koshy P, Alipal J, Kadir MHA, Lee TC (2020) Challenges of 3D printing technology for manufacturing biomedical products: a case study of Malaysian manufacturing firms. *Heliyon* 6(4):03734
37. Ishack S, Lipner SR (2020) Applications of 3D printing technology to address COVID-19 related supply shortages. *Am J Med* 133(7):771–773
38. Novak JI, Loy J (2020) A quantitative analysis of 3D printed face shields and masks during COVID-19. *Emerald Open Res* 2:42
39. Armijo PR, Markin NW, Nguyen S, Ho DH, Horseman TS, Lisco SJ, Schiller AM (2020) 3D printing of face shields to meet the immediate need for PPE in an anesthesiology department during the COVID-19 pandemic. *Am J Infect Control*. <https://doi.org/10.1016/j.ajic.2020.07.037>
40. Hornick J, Roland D (2013) 3D printing and intellectual property: initial thoughts. *The Licensing J* 33(7):12
41. Ballardini RM (2019) Intellectual property rights and additive manufacturing. In: Pei E, Monzon M, Bernard A (eds) *Additive manufacturing—developments in training and education*. Springer, Cham, pp 85–97
42. <http://thepeco.in/show-product.php?id=2>. Accessed 13 March 2020
43. https://www.amazon.in/s?k=abs+filament+1.75mm+1kg&crd=1SCZW8MH9AY4&srefix=ABS+filament%2Caps%2C496&ref=nb_sb_ss_i_4_12. Accessed 15 Sept 2020
44. <https://www.indeed.co.in/salaries/machine-operator-Salaries>. Accessed 10 Sept 2020
45. <https://all3dp.com/1/best-3d-slicer-software-3d-printer/>. Accessed 17 Sept 2020

46. <http://www.myriwell.com/en/>. Accessed 11 Sept 2020
47. <https://www.99acres.com/rent-factory-land-in-india-ffid>. Accessed 10 Sept 2020
48. <https://www.xe.com/currencyconverter/convert/?Amount=1&From=USD&To=INR>. Accessed on September 17, 2020.
49. <https://dielectricmfg.com/knowledge-base/abs/>. Accessed 11 Sept 2020
50. <https://www.plastikcity.co.uk/useful-stuff/material-melt-mould-temperatures>. Accessed 11 Sept 2020
51. https://www.hanserpublications.com/SampleChapters/9781569903988_9781569903988_Polymer%20Processing_Oswald_Hernandez-Ortiz.pdf. Accessed 10 Sept 2020
52. <https://dielectricmfg.com/knowledge-base/glass-epoxy/>. Accessed 12 Sept 2020
53. Rahman H, John TD, Sivadasan M, Singh NK (2018) Investigation on the scale factor applicable to ABS based FDM additive manufacturing. *Mater Today: Proc* 5(1):1640–1648
54. Sukindar NA, Ariffin MKA, Baharudin BHT, Jaafar CAN, Ismail MIS (2016) Analyzing the effect of nozzle diameter in fused deposition modeling for extruding polylactic acid using open source 3D printing. *Jurnal Teknologi* 78(10):7–15
55. Qaiser AA, Qayyum A, Rafiq R (2009) Rheological properties of ABS at low shear rates: effects of phase heterogeneity. *Malays Polym J* 4(2):29–36
56. Bellini A (2002) Fused deposition of ceramics: a comprehensive experimental, analytical and computational study of material behavior, fabrication process and equipment design. Doctoral dissertation, Drexel University, United States
57. <https://greencleanguide.com/calculate-your-carbon-footprint/>. Accessed 13 Oct 2020

Fabrication of Composite Structures via 3D Printing



Madhukar Somireddy

Abstract 3D printing technologies are advanced manufacturing techniques, and fabricate three-dimensional parts additively meaning that material is deposited layer upon layer to get finished parts. The production process of the latest fabrication techniques is contrary to the traditional machining method, where the material is removed to get finished products. 3D printing process, also referred as additive manufacturing (AM), has revolutionized the way how materials and parts are designed and manufactured in many industries. Fabrication of composite structures using 3D printing techniques is an emerging field in recent years and is because of the benefits associated with the technologies. Furthermore, the usage of composite structures in many engineering applications has gone up due to their high structural efficiency. Therefore, the chapter is focused on different AM technologies and their fabrication process. Also, the fabrication of composite structures using material extrusion AM is presented in detail and further, challenges and future perspectives of the fabrication process are discussed.

1 Introduction

Fabrication of composite structures via additive manufacturing technologies is gaining popularity and is because of the benefits associated with the technologies [1, 2]. The composite structures are in more demand than ever before, especially in the aerospace and automotive industries, and is due to their high strength to weight ratio [3]. Furthermore, 3D printing is a very viable fabrication technology for the production of smart structures using responsive composite materials/smart materials [4–6]. Additive manufacturing, also commonly known as 3D printing, fabricates three-dimensional (3D) parts by material deposition layer upon layer. The AM process is contrary to conventional manufacturing methods, where the material is

M. Somireddy (✉)

Department of Mechanical Engineering, York University, 4700 Keele St,
M3J1P3 Toronto, Canada
e-mail: madhukar@yorku.ca

removed to get the final finished part. The primary benefit of 3D printing technology is more freedom in the design of structures besides many other benefits including ease of fabrication, minimal wastage of material, rapid production, and no extra tooling [7]. Moreover, the advanced fabrication technology enables the material design to tailor final properties of 3D printed parts, and also the fabrication of topologically optimized structure is made easier [8].

AM technologies can be further classified into different methods based on the printing technology used in 3D printers that comprise of type of heat source, material dispensing manner, printing axes and the material state. Different methods of AM technologies include material extrusion, powder bed fusion, binder jetting, material jetting, vat photopolymerization, directed energy deposition, and sheet lamination [7]. However, these latest manufacturing techniques fabricate parts in the same way. The AM technologies are materials specific meaning that different materials can not be processed using these technologies. For instance, vat photopolymerization or material jetting AM technology can only process photopolymers. Materials synthesis for the production of parts is mainly governed by the architecture of the 3D printer including the heat source, build chamber characteristics, materials deposition strategy, and the state of the material. Polymer-based composite materials can be synthesized for the production of composite structures via AM technologies [9–15].

In this chapter, we focused on additive manufacturing technologies and their fabrication process. Also, pros and cons of each of the technologies were discussed. Then, traditional manufacturing techniques for fabrication of composite structures were briefly presented and further, differences of the technologies were discussed. A special emphasis on material extrusion additive manufacturing and its different configurations for the production of composite structures were discussed in detail. Finally, applications of the AM technologies and their future perspectives were presented.

2 AM Technologies for Fabrication of Structures

This section focuses on different additive manufacturing technologies and the production process of these methods, materials, and their applications are discussed in detail.

2.1 Material Extrusion Additive Manufacturing

The material extrusion AM process is also referred as fused filament fabrication (FFF), fused deposition modeling (FDM) by Stratasys Ltd. In this process, polymeric filament material is fed using drive wheels and is melted in a liquefier, and the liquefied material is then extruded via nozzle. The extrudate from the nozzle is

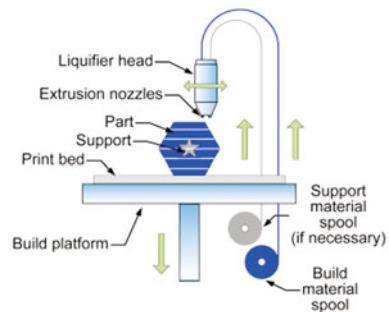
deposited on the machine build platform systematically layer upon layer, and subsequently the material undergoes solidification process and then diffuse with the previously deposited material. Machine configuration of desktop FFF 3D printers can be seen in Fig. 1 and most machines are generally equipped single nozzle to extrude the filament material and, an additional nozzle is used in some machines for extruding only support material.

The filament materials used in these 3D printers are can either be only polymer or polymer and other reinforcements in the form of short fibers and particulates. Commonly used materials in these 3D printers are polymeric materials that include ABS, PLA, PA, Nylon, PC, and high-grade polymers including PEEK, PVDF, PEI, and reinforcements material include metal particulates, carbon fiber, and glass fiber. Figure 2 provides a list of polymeric materials of different grades available for material extrusion AM technology.

2.2 Powder Bed Fusion Additive Manufacturing

In powder bed fusion AM technology, a thin layer of powder is spread on the build platform using a roller/blade, and then a laser beam is focused systematically in desired areas to fuse the powder particles together. Then, the build platform is lowered for a new layer of powder to spread on the previously deposited layer. This procedure is repeated until a 3D part is built. Commercial names of 3D printers based on this technology go with different names; selective laser sintering (SLS), selective laser melting (SLM), direct metal laser sintering (DMLS), electron beam melting (EBM). Although the printing process is the same in these technologies, the main difference between them lies in the heat source used for fusing the powder particles. For instance, SLS uses low laser power for sintering powder particles whereas DMLS and SLM use high laser power to melt powder particles, and EBM employs an electron beam to melt the powder and it operates in a vacuum environment. In general, these technologies are used to produce metal parts. Selective laser sintering technology is mainly employed for 3D printing of parts with polymers and polymer-based composite materials. However, the SLS technology can

Fig. 1 Material extrusion additive manufacturing process [16]



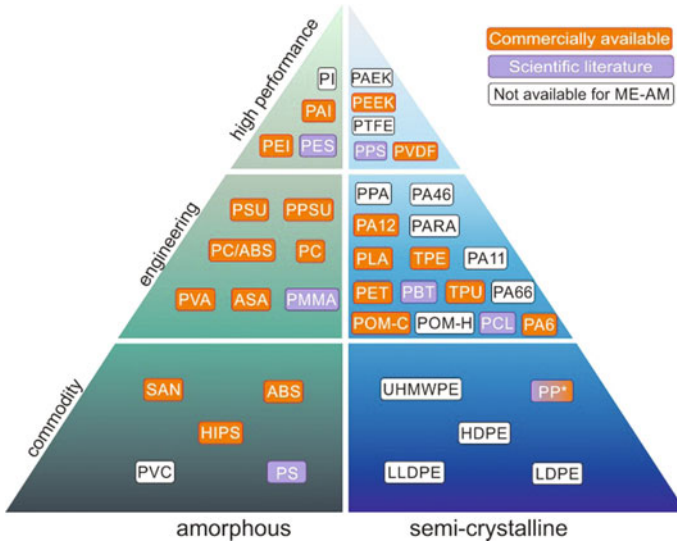


Fig. 2 Polymeric materials available for material extrusion additive manufacturing [17] (license CC BY 4.0)

also accommodate metal and ceramics powder particles coated with a polymeric material. The polymer phase on metal and ceramic powders is used only for sintering particles and consolidating 3D printed part. The schematic diagram of the SLS process can be seen in Fig. 3a.

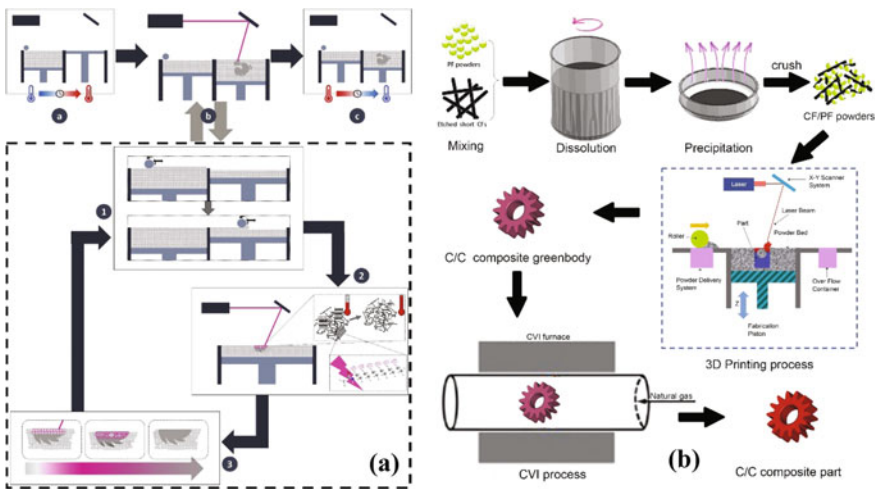


Fig. 3 Powder bed fusion additive manufacturing **a** fabrication procedure [18], **b** selective laser sintering with chemical vapor infiltration process [19]

A novel 3D printing procedure, SLS technology combining with chemical vapor infiltration thermal treatment process, is proposed for the fabrication of high-performance carbon/carbon (C/C) composite parts, and the fabrication procedure is shown in Fig. 3b. In this, the carbon fibers (CF) were treated by oxidation method to etch the surface of CFs, and then etched CFs were mixed with polymeric resin powders in acetone solution. After removing the acetone, the composite mixture (CF with polymer powders) were obtained by a mechanical crush. Then this mixture is used in the SLS printing process to make C/C composite green body, and then post-heat treatment is carried out to get the consolidated composite part. Materials commonly employed in SLS 3D printers are nylon-based materials PA-11 and PA-12, and TPU, PEEK, and HDPE also available for use. These polymers with additional discontinuous fiber reinforcements such as glass, carbon, and aluminum fillers are also used for better material properties in 3D printed parts [9]. A list of polymers available for SLS 3D printing is presented in Fig. 4.

2.3 Binder Jetting Additive Manufacturing

The binder jetting (BJ) process is formerly known as 3D printing (3DP). In the BJ process, a layer of powder material is deposited on the build platform using rollers

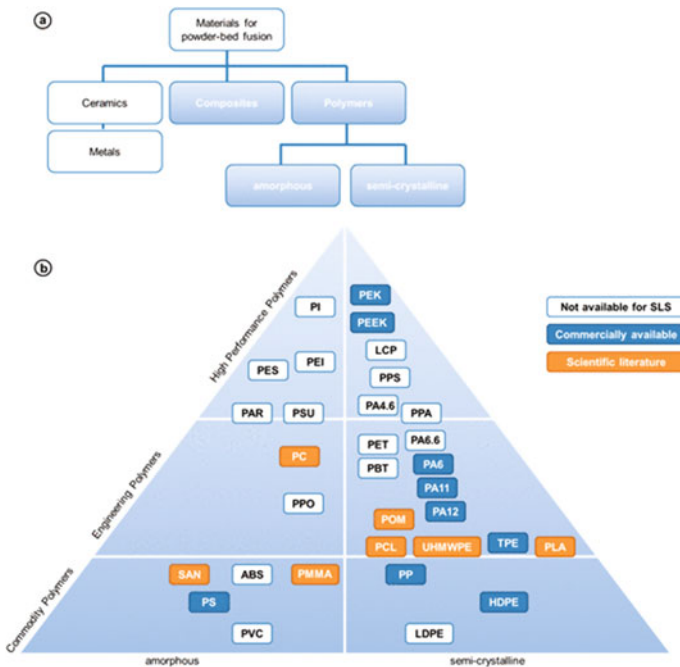


Fig. 4 Polymeric material available for selective laser sintering process [9] (license CC BY 4.0)

similar to that of the powder bed fusion process. Then, the liquid binder material is jetted from the print head in desired areas of the powder bed to bind powder particles together. Once the printing of a layer is done, then the build platform is lowered for another layer and then the same process is repeated until a complete part is built. The main difference between binder jetting and powder bed fusion processes is the binding method used to fuse the powder particles. A high power laser is used to melt the powder particles to form a part cross-section in powder bed fusion whereas the BJ uses liquid binder to fuse the powder particles together. Furthermore, only a portion of material is jetted through the print head in the BJ process, and the most of material is comprised in the powder bed.

The fabrication process of binder jetting AM is illustrated in Fig. 5. Once the printing process is completed, 3D printed part is then annealed to cure the binder and the resulting part is referred as a 'green part'. The green part is fragile and porous (50–60% density) and therefore, the part is not ready for functional use at this stage. The green parts need to undergo a critical post-processing procedure, called densification, to attain full density. Densification is a very crucial process for these 3D printed parts, and it is done in two ways (infiltration/sintering) to achieve the desired density and mechanical properties [20]. Densification using the infiltration method involves eliminating the residual porosity of 3D printed part by infiltrating low melting metal (e.g. bronze) and achieves a full density with negligible dimensional changes. The other prominent densification method is sintering, this increases the density of the green part by diffusion at high temperature. This method drastically changes the dimensions of the part by shrinkage ($\approx 20\text{--}35\%$) as no additional metal alloy is used to eliminate porosity in the part. However, the sintering results into a single alloy 3D printed part with a higher density ($\approx 98\%$), and the same is not possible with the infiltration method. Binder jetting 3D printing can process a broad range of materials including metals, ceramics, and composite materials. Materials available for the binder jetting technology can be seen in Fig. 6.

2.4 Material Jetting Additive Manufacturing

In material jetting technology, a resin material is jetted either a continuous or drop-on-demand approach onto the build platform using a print head. In this 3D printing method, all the part material is jetted from the print head, once material is dispensed, and then it is solidified using ultraviolet light. Unlike binder jetting, where only a binder material is jetted from the print head on powder bed to fuse powder particles. The material jetting printing process can be seen in Fig. 7. The material with low viscosity is used in this technology as the material must be deposited in drops and therefore, the number of materials used in this process are limited because of this limitation. Commonly used materials for this process are photopolymers with wax.

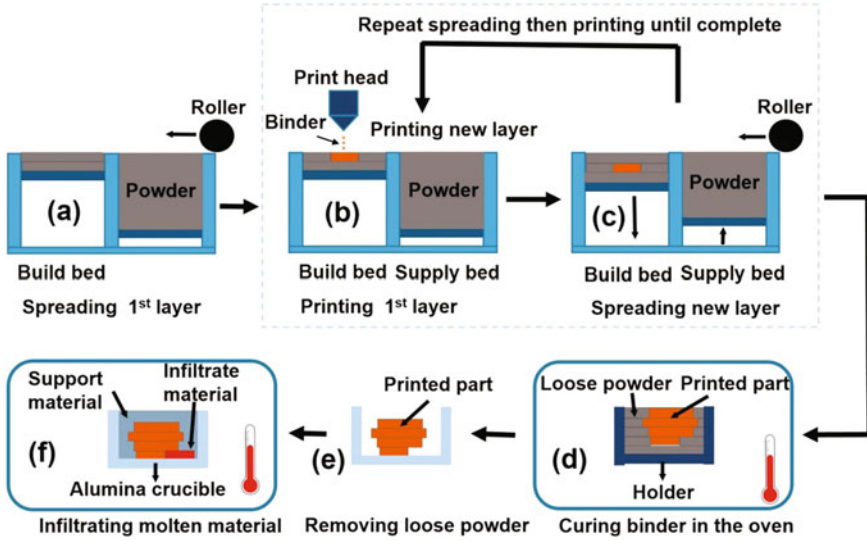


Fig. 5 Fabrication process of binder jetting additive manufacturing [21]

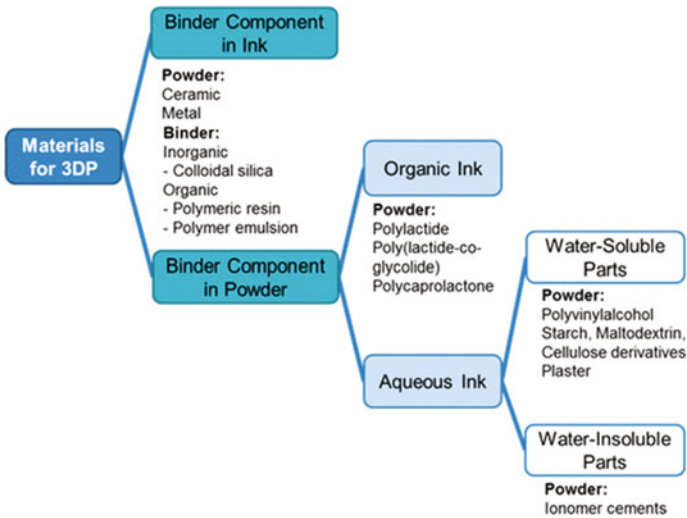
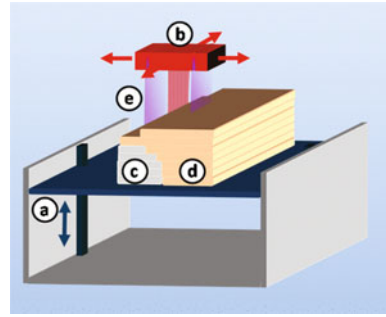


Fig. 6 Materials available for binder jetting process [9] (license CC BY 4.0)

Fig. 7 Material jetting additive manufacturing [9] (license CC BY 4.0)



2.5 Vat Photopolymerization Additive Manufacturing

In this 3D printing process, a vat of photopolymer resin is exposed to UV radiations to the selected area to solidify a layer of resin material. Once the top layer of resin in a vat undergoes the photopolymerization process to solidify and then, the platform is lowered, and again fresh liquid photopolymer resin is exposed to radiations to solidify. This process is repeated until the final 3D part is built. The schematic diagram of the printing process can be seen in Fig. 8. This printing process is also known as stereolithography (SLA) 3D printing process. Materials for this process are limited since the 3D printing process is based on photopolymerization. The photopolymer resin commonly used for 3D printing is a composite mixture of acrylates and epoxy.

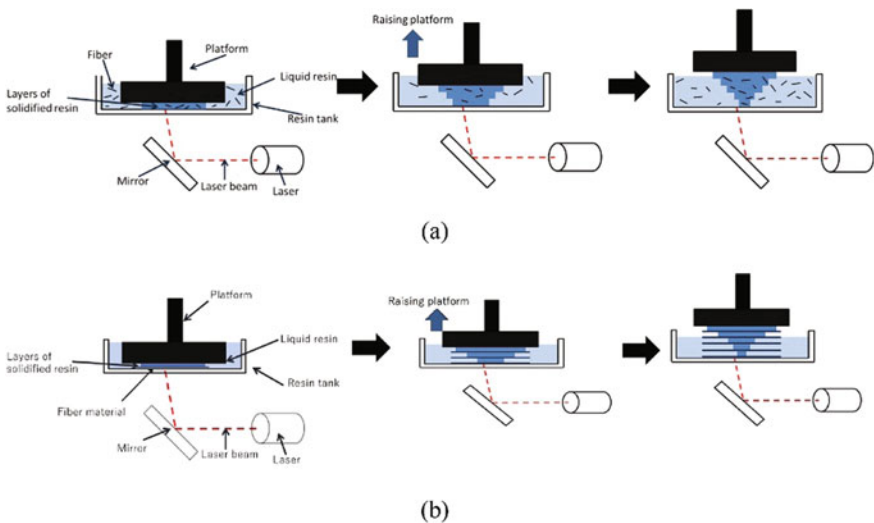


Fig. 8 Vat photopolymerization additive manufacturing **a** top-down short glass fiber process **b** top-down continuous glass fiber printing process [22]

2.6 Directed Energy Deposition Additive Manufacturing

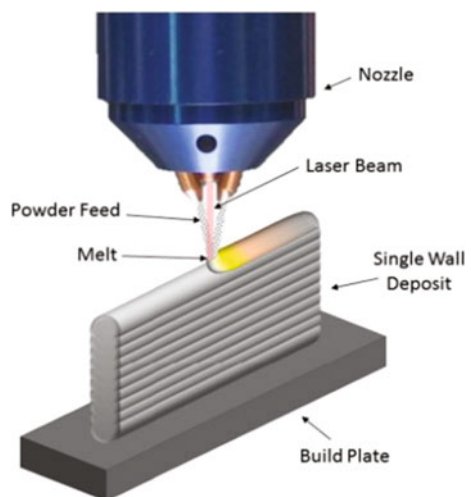
In directed energy deposition (DED) process, the parts are produced by liquefying material while depositing it. This 3D printing process is predominantly used for metals in the form of either powder or wire. However, the printing process can also accommodate other materials including ceramics, metal composites and polymers. In this technology, the energy is directed into a fine and focused region to melt the substrate, and simultaneously melting print material is deposited into the melt pool of the substrate. This process is contrary to the powder bed fusion techniques, where a pre-laid powder particles in a powder bed are melted to print a part. The working principle of the DED 3D printing method is shown in Fig. 9.

2.7 Sheet Lamination Additive Manufacturing

Sheet lamination AM process involves layer upon layer lamination of material sheets, and then a low power laser is employed to cut each sheet representing one cross-sectional layer of the CAD model of the part. The sheet lamination process also referred as laminated object manufacturing (LOM). The bonding between the layers is achieved using several methods; gluing or adhesive bonding, thermal bonding, and ultrasonic welding. The fabrication of LOM is shown in Fig. 10.

The above AM technologies are unique in filling different needs of industries, and each technology has pros and cons. A list of the advantages and disadvantages of each AM technique is presented in Table 1. Furthermore, a comparison of the AM technologies on six primary parameters related to cost and quality of 3D printed parts is provided in Table 2.

Fig. 9 Directed energy deposition additive manufacturing [23]



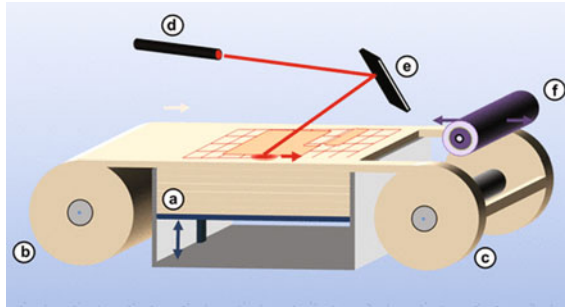


Fig. 10 Sheet lamination additive manufacturing process [9] (license CC BY 4.0)

Table 1 Advantages and disadvantages of AM technologies

AM process	Advantages	Disadvantages
Material extrusion	Large build volume, lower production cost, less expensive machine, affordable materials, multi-material printing	Poor surface, dimensional accuracy, inhomogeneity in material properties
Powder bed fusion (SLS)	Higher dimensional accuracy, homogeneity in material properties, as printed parts ready functional use	Small build volume, limited materials, expensive materials, expensive machine, production cost
Binder jetting	Can process wide range of materials, large build volume, no thermal residual stresses, cheaper production, faster production	Multi-steps i.e. extensive post processing, poor surface finish, very porous structure
Material jetting	Highly accurate parts, multi colours, no post processing required	Limited material, mechanical properties not suitable for functional use, limited build volume, slow production rate
Vat photopolymerization	Highly accurate parts, faster production rate, no post processing required	Limited materials, small build volume
Directed energy deposition	Useful for repairs, can process different materials, high deposition rate, uniform material properties	Thermal stress, slower production, poor surface finish, poor dimensional accuracy, internal cavities difficult to produce, limited materials
Sheet lamination	High quality parts, faster production, no residual stresses	Limited flexibility on part design, limited materials

Table 2 Comparison of AM technologies

AM process	Production rate	Investment cost	Part quality	Part design freedom	Material design freedom	Reinforcement type (fiber)
Material extrusion	***	**	**	*****	*****	Continuous/ discontinuous
Powder bed fusion	**	*****	****	*****	*****	Discontinuous
Binder jetting	***	***	***	***	***	Discontinuous
Material jetting	**	****	*****	*****	**	N/A
Vat photopolymerization	*****	***	*****	*****	**	N/A
Directed energy deposition	**	*****	**	***	***	Discontinuous
Sheet lamination	*****	**	***	**	***	Continuous

Note Parameters on scale 1–5 stars, more stars indicate higher value; N/A denotes not applicable

3 Conventional Manufacturing Techniques for Composite Structures

Traditionally composite structures are fabricated using different manufacturing methods [1, 24, 25]. Some of the prominent processes include hand lay-up, spray-layup, filament winding, vacuum bag, vacuum infusion, and resin transfer molding, pultrusion, compression, and injection molding.

Hand lay-up and spray lay-up: Hand lay-up and spray lay-up are open molding fabrication methods, where mold is open and exposed to the atmosphere to cure the resin. In the hand lay-up process, the resin is applied to laminae fabrics laid in the mold, as shown in Fig. 11a, and whereas spray lay-up process, a spray gun is employed to deposit the chopped fibers and resin to the mold as shown in Fig. 11b. These are manual fabrication methods and the quality of fabricated structures depends on the skill of the technician.

Filament winding: This fabrication method is commonly used to produce hollow composite structures. In this process, continuous fiber reinforcements pass through the hot resin bath and then, the resin-infused fibers are wrapped around the rotating mandrel, as shown in Fig. 11c. Although, the process produced quality composite parts but limited to symmetrical hollow shapes only.

Pultrusion fabrication: This method is employed for producing symmetrical hollow composite tubes/channels. In this process, the continuous fiber reinforcements are steered through a resin impregnation unit. Then, the impregnated continuous fibers are drawn through a forming die in which consolidates the part. The fabrication process can be seen in Fig. 11d.

Vacuum bag, vacuum infusion and resin transfer molding: The open molding methods produce composite structures with inferior quality and therefore, a closed molding procedure is developed. In vacuum processes, a vacuum bag is placed

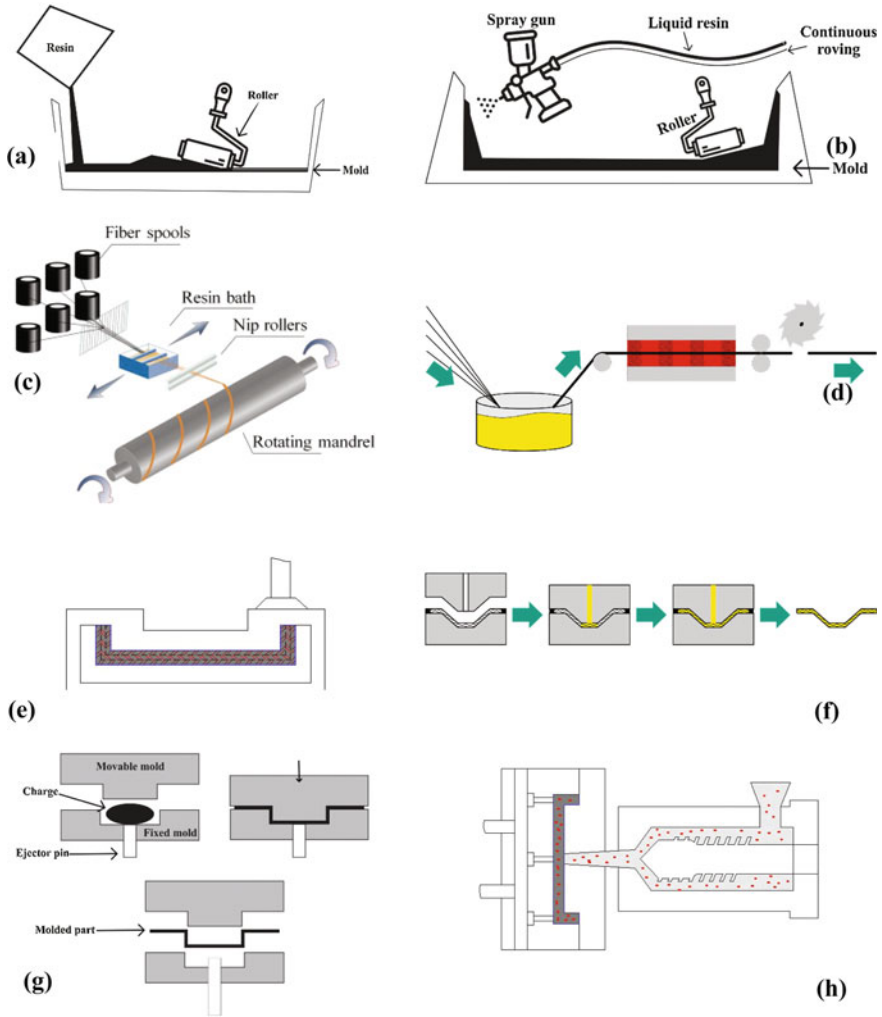


Fig. 11 Traditional fabrication techniques for composite structures [1, 24, 26] **a** hand lay-up, **b** spray lay-up, **c** filament winding, **d** pultrusion, **e** vacuum bag, **f** resin transfer molding, **g** compression molding, **h** injection molding

around the perimeter of the mold to remove entrapped air during the molding process, the manufacturing process can be seen in Fig. 11e. In the vacuum infusion process, a vacuum is applied before introducing the resin and this is in contrast with the vacuum bag method. In the resin transfer molding (RTM) technique, the resin is injected into a closed mold. The fabrication process of RTM is shown in Fig. 11f. *Compression and injection molding:* The injection and compression molding processes are used to produce the composite parts with the particulate or short fiber

reinforcements. In compression molding, the bulk composite mixture is placed in a fixed part of the mold, and the other movable part of the mold is compressed to take the material mold shape. On the other hand, the injection molding technique uses a high-pressure injection unit to inject the composite material into the mold, once the part is cured and the part is ejected from the mold.

Although the above traditional technologies produce quality composite parts but have a few major limitations. Firstly, most of these techniques require expensive tooling and machinery besides labor costs. Secondly, the fabrication procedure of these methods involves tedious manual work, and requires a skill set to produce high-quality parts and further, more time-consuming. Finally, less design freedom in part design and tailoring material properties. However, some of the above techniques produce highly dimensional accurate parts with very good surface quality. Figure 12 presents the material property of composite structures fabricated with different traditional technologies and AM technology. Furthermore, a comparison of these technologies on different parameters related to the cost and quality of 3D printed parts is provided in Table 3.

4 Material Extrusion AM for Fabrication of Composite Structures

Material extrusion AM is the most versatile advanced fabrication process among the AM technologies and is a very promising technique for the fabrication of composite structures. This AM technology can process different materials including polymers and composites, and recently the same technology is also employed to produce metal parts [28]. 3D printers based on this technology are the most commonly used for 3D printing of parts [29] and is because of several additional benefits associated with the technology over others. The additional benefits include large build volume,

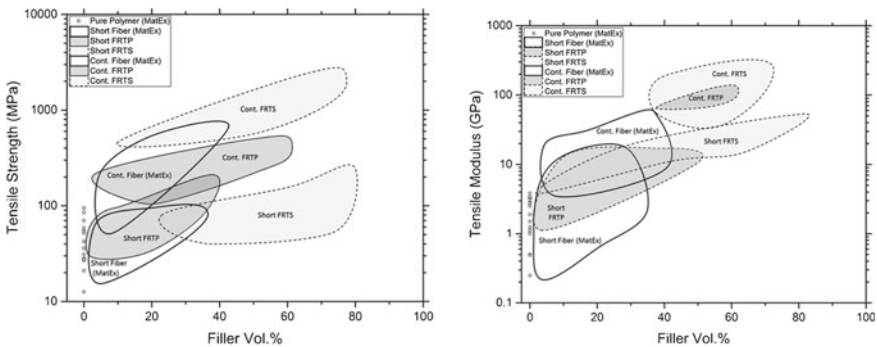


Fig. 12 Tensile properties versus filler volume ratio of parts fabricated via traditional and material extrusion (MatEx) AM technology [27]

Table 3 Comparison of traditional technologies for fabrication of composite structures

Process	Production rate	Investment cost	Surface quality	Part design freedom	Material design freedom	Reinforcement type (fiber)
Hand lay-up	**	**	**	**	**	Continuous
Spray lay-up	**	**	**	**	**	Discontinuous
Filament winding	***	*****	***	**	**	Continuous
Vacuum bag moulding	**	***	***	***	***	Continuous
Resin transfer moulding	**	***	***	***	***	Continuous
Pultrusion	*****	***	***	**	***	Continuous
Compression moulding	*****	*****	*****	*****	**	Discontinuous
Injection moulding	*****	*****	*****	*****	**	Discontinuous

Note Parameters on scale 1–5 stars, more stars indicate higher value

low production cost, low cost of 3D printers, multi-material printing, faster production, low material cost and accommodates different materials. Such advantages increased the demand for FFF technology in many engineering applications [25]. In general, the desktop 3D printers are equipped with a single nozzle as seen in Fig. 1. However, different configurations of 3D printers are available in the market. Therefore, this section emphasizes the details of the material extrusion method for the fabrication of composite structures.

The printing parameter governs the quality of 3D printed parts. Table 4 presents different printing parameters of the process and their definitions, and also approximate values of the parameters are given in the table. The final material properties of parts synthesized via 3D printing are influenced by mesostructure, which in-turn governed by printing parameters. The printing parameters namely layer thickness, raster angle/printing direction, and overlap between fibers, are the key parameters that influence the properties of 3D printed part [26, 30]. Fully dense parts can be produced using standard printing practice as shown in Fig. 13a; such printed parts resemble architecture of laminates [31]. Also, other parameters of printing process viz. shells and infill pattern and infill density can be seen in Fig. 13b.

Different configurations of 3D printers of this technology are shown in Fig. 14. The main difference between them lies in the material feeding system. Industrial 3D printers are equipped with two nozzles (Fig. 14a); one for extrusion of material for printing the part and the other nozzle for supporting material. Soluble materials are generally used for printing support structures, which are needed while 3D printing overhangs of the main part. Therefore, such materials are extruded from a different nozzle, and on the other hand, single nozzle 3D printers use the same printing

Table 4 Printing/process parameters of material extrusion additive manufacturing method

Printing parameter	Meaning	Values (approx. values)
Layer thickness, t	Thickness of material deposition	100–500 μm
Printing/raster direction θ°	Direction of extrudate deposition	$0^\circ, 15^\circ, 30^\circ, 45^\circ, 60^\circ, 90^\circ$
Infill pattern	Printing pattern which defines the internal architecture of part	Line, rectilinear, grid, triangle, cubic, concentric, honeycomb, gyroid
Infill density	Amount of material to deposit	10–100%
Print speed	Speed of nozzle movement	10–100 mm/s
Feed rate	Material flow rate from the nozzle, it is synchronized with print speed	5–20 mm^3/s
Overlap	Gap between adjacent extrudate	0–20%
Shell	Number of perimeters of the part	1–10

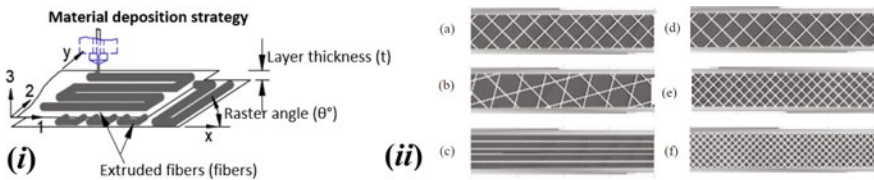


Fig. 13 Process parameters of material extrusion additive manufacturing, **i** material deposition strategy, **ii** different infill patterns with different infill densities [32] (CC BY 3.0)

material for support structures. Two different feed systems are available for feeding the continuous reinforcements as shown in Fig. 14c, d. It can be seen in Fig. 14c that the continuous fibers are feed through the nozzle, which is used for a polymer material, and this type of FFF printers commonly found in research laboratories. On the other hand, Fig. 14d employs a separate nozzle for continuous fiber reinforcements and such printers are industrial-grade 3D printers. The material feed system of the FFF 3D printer for the fabrication of large structures is entirely different from the other three configurations, and such printers employ a single screw extruder to extrude the pellets (Fig. 14b), and these systems also are known as big area additive manufacturing (BAAM) [33, 34]. The material used in BAAM 3D printers is in the form of pellets and short fiber reinforcements. The material deposition rate of BAAM is up to 50 kg/hr and the desktop printer’s feed rate is usually around 15–85 cm^3/hr [35]. Metal 3D printers based on this technology for industrial applications were developed by different companies; Markforged, DigitalAlloys, and Rapidia Inc. However, these metal 3D printers were limited with small build volume at this moment.

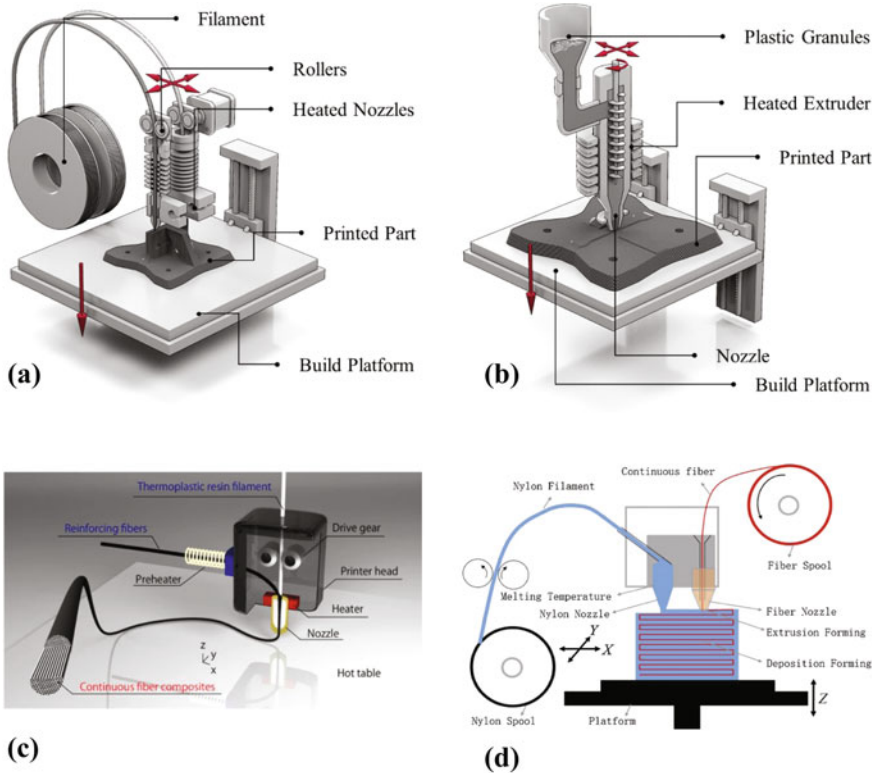


Fig. 14 Different configurations of 3D printers based on material extrusion additive manufacturing technology **a** material feed system with two nozzles, **b** single screw extruder [33], **c** feed system with a nozzle for continuous fibers [36] (CC BY 4.0), **d** system with two nozzles for continuous fiber composites [37]

Composite materials usage in 3D printing of engineering applications has risen in the recent decade [12] and this is because of advantages with these materials. Further, composite materials development for the fabrication of structures is an emerging research area of the AM field. Smart composite and sandwich structures for many engineering applications also can be produced via material extrusion AM technology, and the production of composite/sandwich structures with different microstructure configurations is possible to obtain desired mechanical properties [38, 39]. This means that the AM technology enables the design of materials, and tailoring of material properties in 3D printed composite structures. The microstructure of composites and orientation of fibers greatly influence the performance of the structures. Figure 15 illustrates different 3D printed preforms for composite structures and infill patterns for the core of sandwich structures.

The mechanical behavior of 3D printed structures is similar to that of the behavior of traditional composite laminates [40]. This is mainly because of the

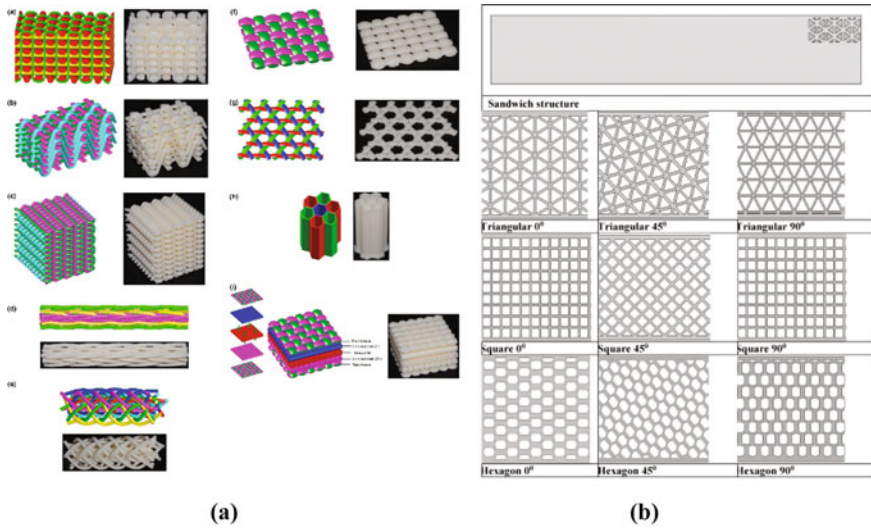


Fig. 15 Microstructures of 3D printed composite parts **a** different multi-directional preforms for composites [38] (CC BY-NC-ND 4.0), **b** different infill patterns for core of sandwich structure [39]

internal architecture of the printed parts and traditional laminates is similar. Therefore, structures fabricated with continuous fiber as discontinuous fibers can be treated with mechanics of laminates. Further, these mechanics of composites can be employed to characterize the mechanical behavior of 3D printed structures [31].

Although the material extrusion AM can able to make complex geometric composite structures, however, the quality of 3D printed structures is poor when compared to the quality of structures produced via traditional manufacturing processes. Dimensional accuracy and surface finish of 3D printed structure is very limited. Also, consistency in the quality of printed parts is another concern. Furthermore, anisotropy in the material properties of parts is one of the primary concerns with AM technologies in general. The quality of the 3D printed parts is governed by many factors including design features of parts, printing parameters, and materials used for synthesizing parts. However, recent advances in the field enhancing the final quality of 3D printed structure and very promising fabrication technology among AM technologies for producing composite structures of any size.

5 Applications of 3D Printing Technologies

3D printing technologies have been employed in many industries including mechanical, space, electronic, civil structures, health, medical, and fashion. Here we focus on applications of 3D printed composite structures. Initially, these fabrication

technologies were employed for making prototypes but are now used for producing functional parts of different engineering applications. In recent years with advances in technologies, complex and critical parts of space industries have been fabricated using metal 3D printers [41]. The technologies, especially material extrusion AM is leveraged to fabricate smart structures using responsive material [4], and material jetting is also used for fabrication of functional parts and printed circuit boards [9]. One of the established applications in the mechanical field is the production of machine tools e.g. jigs, fixtures, molds, and dies. Also, health and medical industries are using these technologies to fabricate patient-specific medical devices and parts. One of the growing applications of material extrusion AM is the fabrication of large molds and functional consolidated products [42]. Recently, a composite research group at UMaine 3D printed the entire boat ‘3Dirigo’ [43]. Fabrication of car bodies using the material extrusion AM was attempted by several researchers and industries [44, 45] however, fabrication of molds for boats and windmill was successful (Fig. 16).

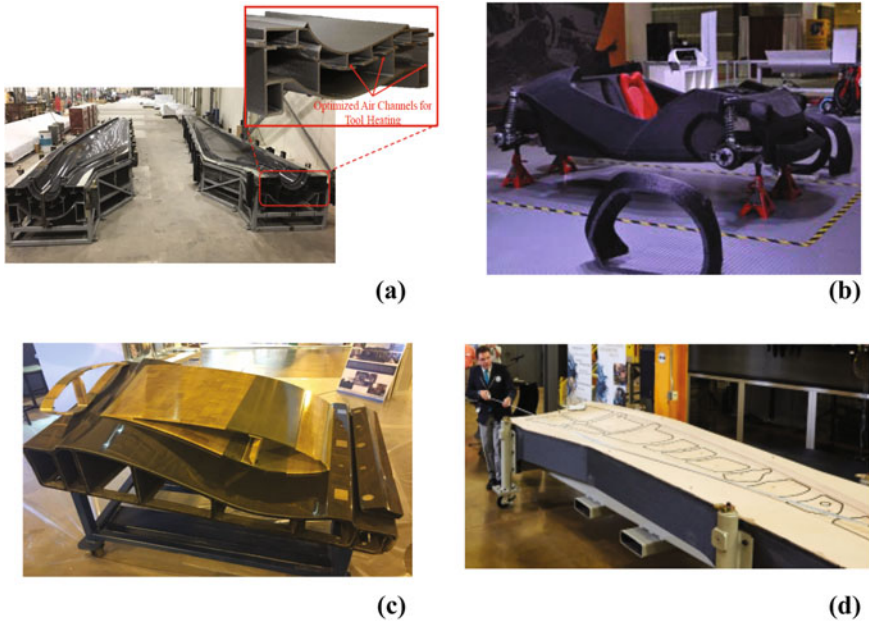


Fig. 16 Applications of 3D printed composite structures via material extrusion additive manufacturing **a** molds for windmill blades [44], **b** car body [45], **c** mold [46], **d** large trim tool for composites [44]

6 Conclusions and Future Perspectives

AM technologies are revolutionizing the way how the structures are designed and fabricated in many industries. These advanced technologies are unique in fulfilling the different needs of the industries. Although these techniques offer several benefits over conventional fabrication technologies but, as printed parts require additional post-processes to improve their quality for functional use. Also, the production rate of 3D printing is lower when compared to conventional methods. One of the concerns is limited build volume and therefore restricted to the production of small composite parts. However, material extrusion AM is a promising fabrication technique for the production of composite structures of any size, but several challenges remain unaddressed. A few primary concerns related to material, design, and process are mentioned below for further work in this field.

- *Anisotropic material properties:* Anisotropy in final material properties is observed and is one of the major concerns with 3D printed parts. This is caused by a change in microstructure, which is produced while deposition of material. A comprehensive understanding of process-structure-property relationship can provide predictable behavior of 3D printed parts.
- *Fabrication of large structures:* Although the BAAM produces large structures, but issues related to inter layer bonding and internal defects are major concerns with the technology. Further enhancement of the technology is required to produce high-quality large structures.
- *Quality of 3D printed parts:* Dimensional accuracy and surface quality of 3D printed parts are poor, especially with large parts. The quality of printed parts is mainly governed by process, materials, and design. Improvement in the areas including printing process, design for AM, and post-processing methods is required.
- *Composite materials:* Materials for fabrications are limited and moreover, certain materials are difficult to process because of material characteristics e.g. material with high shrinkage leading to poor dimensional accuracy and poor interlayer bonding. A wide variety of printable materials for different engineering applications need to be developed.
- *Computational models:* Computational tools are not yet available for simulation of the printing process and mechanical behavior of 3D printed parts for different loadings. Furthermore, tools for design for additive manufacturing are needed for effective design as well as production of reliable and durable composite structure parts.

References

1. Fleischer J, Teti R, Lanza G, Mativenga P, Möhring HC, Caggiano A (2018) Composite materials parts manufacturing. *CIRP Ann* 67(2):603–626
2. Parandoush P, Lin D (2017) A review on additive manufacturing of polymer-fiber composites. *Compos Struct* 182:36–53
3. Gay D (2014) Composite materials design and applications. CRC Press, Boca Raton
4. Shafraneck RT, Millik SC, Smith PT, Lee CU, Boydston AJ, Nelson A (2019) Stimuli-responsive materials in additive manufacturing. *Prog Polym Sci* 93:36–67
5. Kuang X, Roach DJ, Wu J, Hamel CM, Ding Z, Wang T, Dunn ML, Qi HJ (2019) Advances in 4D printing: materials and applications. *Adv Func Mater* 29(2):1805290
6. Rayate A, Jain PK (2018) A review on 4D printing material composites and their applications. *Mater Today: Proc* 5(9):20474–20484
7. Gibson I, Rosen DW, Stucker B (2015) Additive manufacturing technologies. Springer, New York
8. Li N, Link G, Wang T, Ramopoulos V, Neumaier D, Hofele J, Walter M, Jelonnek J (2020) Path-designed 3D printing for topological optimized continuous carbon fibre reinforced composite structures. *Compos B Eng* 182:107612
9. Ligon SC, Liska R, Stampfl J, Gurr M, Mülhaupt R (2017) Polymers for 3D printing and customized additive manufacturing. *Chem Rev* 117(15):10212–10290
10. Ngo TD, Kashani A, Imbalzano G, Nguyen KT, Hui D (2018) Additive manufacturing (3D printing): a review of materials, methods, applications and challenges. *Compos B Eng* 143:172–196
11. Schmid M, Amado A, Wegener K (2015) Polymer powders for selective laser sintering (SLS). In: *AIP Conf Proceedings* 1664(1):160009. AIP Publishing LLC
12. Valino AD, Dizon JR, Espera AH Jr, Chen Q, Messman J, Advincula RC (2019) Advances in 3D printing of thermoplastic polymer composites and nanocomposites. *Prog Polym Sci* 98:101162
13. Balla VK, Kate KH, Satyavolu J, Singh P, Tadimeti JG (2019) Additive manufacturing of natural fiber reinforced polymer composites: processing and prospects. *Compos B Eng* 174:106956
14. Kalsoom U, Nesterenko PN, Paull B (2016) Recent developments in 3D printable composite materials. *RSC advances* 6(65):60355–60371
15. Tan LJ, Zhu W, Zhou K (2020) Recent progress on polymer materials for additive manufacturing. *Adv Func Mater* 6:2003062
16. Ning F, Cong W, Qiu J, Wei J, Wang S (2015) Additive manufacturing of carbon fiber reinforced thermoplastic composites using fused deposition modeling. *Compos B Eng* 80:369–378
17. Spoerk M, Holzer C, Gonzalez-Gutierrez J (2020) Material extrusion-based additive manufacturing of polypropylene: a review on how to improve dimensional inaccuracy and warpage. *J Appl Polym Sci* 137(12):48545
18. Chatham CA, Long TE, Williams CB (2019) A review of the process physics and material screening methods for polymer powder bed fusion additive manufacturing. *Prog Polym Sci* 93:68–95
19. Yi X, Tan ZJ, Yu WJ, Li J, Li BJ, Huang BY, Liao J (2016) Three dimensional printing of carbon/carbon composites by selective laser sintering. *Carbon* 96:603–607
20. Mostafaei A, Elliott AM, Barnes JE, Li F, Tan W, Cramer CL, Nandwana P, Chmielus M (2020) Binder jet 3D printing—process parameters, materials, properties, and challenges. *Prog Mater Sci* 100707
21. Do T, Kwon P, Shin CS (2017) Process development toward full-density stainless steel parts with binder jetting printing. *Int J Mach Tools Manuf* 121:50–60
22. Sano Y, Matsuzaki R, Ueda M, Todoroki A, Hirano Y (2018) 3D printing of discontinuous and continuous fibre composites using stereolithography. *Addit Manuf* 24:521–527

23. Reichardt A, Dillon RP, Borgonia JP, Shapiro AA, McEnerney BW, Momose T, Hosemann P (2016) Development and characterization of Ti-6Al-4V to 304L stainless steel gradient components fabricated with laser deposition additive manufacturing. *Mater Des* 104:404–413
24. Rajak DK, Pagar DD, Kumar R, Pruncu CI (2019) Recent progress of reinforcement materials: a comprehensive overview of composite materials. *J Mater Res Technol* 8(6):6354–6374
25. Frketic J, Dickens T, Ramakrishnan S (2017) Automated manufacturing and processing of fiber-reinforced polymer (FRP) composites: an additive review of contemporary and modern techniques for advanced materials manufacturing. *Addit Manuf* 14:69–86
26. Somireddy M, Czepakanski A (2020) Anisotropic material behavior of 3D printed composite structures—material extrusion additive manufacturing. *Mater Des* 195:108953
27. Fallon JJ, McKnight SH, Bortner MJ (2019) Highly loaded fiber filled polymers for material extrusion: a review of current understanding. *Addit Manuf* 30:100810
28. Gibson MA, Mykulowycz NM, Shim J, Fontana R, Schmitt P, Roberts A, Ketkaew J, Shao L, Chen W, Bordeenithikasem P, Myerberg JS (2018) 3D printing metals like thermoplastics: fused filament fabrication of metallic glasses. *Mater Today* 21(7):697–702
29. The State of 3D Printing Report (2019). <https://www.sculpteo.com/en/ebooks/state-of-3d-printing-report-2019/>. Accessed 20 Nov 2020
30. Somireddy M, Singh CV, Czepakanski A (2020) Mechanical behaviour of 3D printed composite parts with short carbon fiber reinforcements. *Eng Fail Anal* 107:104232
31. Somireddy M, Singh CV, Czepakanski A (2019) Analysis of the material behavior of 3D printed laminates via FFF. *Exp Mech* 59(6):871–881
32. Rismalia M, Hidajat SC, Permiana IG, Hadisujoto B, Muslimin M, Triawan F (2019) Infill pattern and density effects on the tensile properties of 3D printed PLA material. *IOP Publishing J Phys Conf Ser* 1402(4):044041
33. van de Werken N, Tekinalp H, Khanbolouki P, Ozcan S, Williams A, Tehrani M (2020) Additively manufactured carbon fiber-reinforced composites: state of the art and perspective. *Addit Manuf* 31:100962
34. Sánchez DM, de la Mata M, Delgado FJ, Casal V, Molina SI (2020) Development of carbon fiber acrylonitrile styrene acrylate composite for large format additive manufacturing. *Mater Des* 191:108577
35. Kishore V, Ajinjeru C, Nycz A, Post B, Lindahl J, Kunc V, Duty C (2017) Infrared preheating to improve interlayer strength of big area additive manufacturing (BAAM) components. *Addit Manuf* 14:7–12
36. Matsuzaki R, Ueda M, Namiki M, Jeong TK, Asahara H, Horiguchi K, Nakamura T, Todoroki A, Hirano Y (2016) Three-dimensional printing of continuous-fiber composites by in-nozzle impregnation. *Sci Rep* 6:23058
37. Mei H, Ali Z, Yan Y, Ali I, Cheng L (2019) Influence of mixed isotropic fiber angles and hot press on the mechanical properties of 3D printed composites. *Addit Manuf* 27:150–158
38. Quan Z, Wu A, Keefe M, Qin X, Yu J, Suhr J, Byun JH, Kim BS, Chou TW (2015) Additive manufacturing of multi-directional preforms for composites: opportunities and challenges. *Mater Today* 18(9):503–512
39. Rajpal R, Lijesh KP, Gangadharan KV (2018) Parametric studies on bending stiffness and damping ratio of sandwich structures. *Addit Manuf* 22:583–591
40. Somireddy M, Czepakanski A, Singh CV (2018) Development of constitutive material model of 3D printed structure via FDM. *Mater Today Commun* 15:143–152. <https://doi.org/10.1016/j.mtcomm.2018.03.004>
41. DebRoy T, Wei HL, Zuback JS, Mukherjee T, Elmer JW, Milewski JO, Beese AM, Wilson-Heid AD, De A, Zhang W (2018) Additive manufacturing of metallic components—process, structure and properties. *Prog Mater Sci* 92:112–224
42. Post BK, Chesser PC, Lind RF, Roschli A, Love LJ, Gaul KT, Sallas M, Blue F, Wu S (2019) Using big area additive manufacturing to directly manufacture a boat hull mould. *Virtual Phys Prototyping* 14(2):123–129

43. UMaine News. Advanced structures & composites center, 3Dirigo: The world's largest 3D printed boat. <https://composites.umaine.edu/3dirigo-the-worlds-largest-3d-printed-boat/>. Accessed 10 Oct 2020
44. Kunc V, Hassen AA, Lindahl J, Kim S, Post B, Love L (2017) Large scale additively manufactured tooling for composites. In: Proceedings of 15th Japan international SAMPE symposium and exhibition
45. Love LJ (2015) Utility of big area additive manufacturing (BAAM) for the rapid manufacture of customized electric vehicles. Oak Ridge National Lab (ORNL), Oak Ridge, TN (United States). Manufacturing Demonstration Facility (MDF). <https://www.osti.gov/biblio/1209199>
46. Post BK, Richardson B, Lind R, Love LJ, Lloyd P, Kunc V, Rhyne BJ, Roschli A, Hannan J, Nolet S, Veloso K (2017) Big area additive manufacturing application in wind turbine molds. In: Solid freeform fabrication symposium

Use of FDM Technology in Healthcare Applications: Recent Advances



Irene Buj-Corral, Aitor Tejo-Otero, and Felip Fenollosa-Artés

Abstract Additive Manufacturing (AM) technologies, which were developed around 30 years ago, are still evolving. They are applied in different sectors such as aeronautics, automotive, health, etc. There are different AM technologies: binder jetting, direct energy deposition, material extrusion, material jetting, powder bed fusion, sheet lamination and vat photopolymerisation. Amongst all of them, material extrusion is the most common technique used nowadays, due to several reasons: manufacture of parts is easy and cost-effective, desktop 3D printers are affordable, and they allow the use of many different materials. Within this AM category, two main techniques can be highlighted: FFF (Fused Filament Fabrication), also known as FDM (Fused Deposition Modelling), and DIW (Direct Ink Writing). FFF is the most typical technology which can offer multimaterial 3D printed parts. In addition, it can be mixed with other AM technologies in order to build hybrid 3D printers. Main applications of the FFF technology in the medical sector, which are explained in detail in the present chapter, are the manufacture of training models and surgical planning prototypes, medical devices, surgical guides, bio-active scaffolds, and cell 3D-bioprinting, etc. During the global pandemic of COVID-19, the FDM technology allowed to print different devices such as face masks or artificial breathers, among others.

I. Buj-Corral (✉) · F. Fenollosa-Artés

Mechanical Engineering Department, School of Engineering of Barcelona (ETSEIB),
Universitat Politècnica de Catalunya (UPC), Av. Diagonal 647, 08028 Barcelona, Spain
e-mail: irene.buj@upc.edu

A. Tejo-Otero · F. Fenollosa-Artés
Centre CIM, Universitat Politècnica de Catalunya (CIM UPC),
Carrer de Llorens i Artigas, 12, 08028 Barcelona, Spain
e-mail: atejo@cimupc.org

F. Fenollosa-Artés
e-mail: ffenollosa@cimupc.org

1 Introduction

Additive Manufacturing (AM), also known as 3D printing, is defined as the process by which the materials are joined layer-upon-layer in order to manufacture different objects. AM has existed for more than 30 years, but its popularity has mainly grown during the last years. Most AM technologies are still under evolution. The ISO/ASTM 52900 Standard [1] classifies AM technologies into seven categories: binder jetting, direct energy deposition, material extrusion (which includes FFF-Fused Filament Fabrication), material jetting, powder bed fusion (which includes SLS-selective laser sintering), sheet lamination and vat photopolymerisation (which includes SLA-stereolithography).

Regarding the FFF technology, also known as Fused Deposition Modelling (FDM), it was patented in 1989 by Scott Crump, co-founder of Stratasys [2]. The patent did not expire until 2009. From that point on, it has grown steadily as an open source technology.

In the FFF process a continuous filament of a thermoplastic material is used, such as PLA (Polylactic Acid), ABS (Acrylonitrile Butadiene Styrene), PVA (Polyvinyl Alcohol), etc. The filament is melted thanks to a resistance, it is then extruded through a nozzle and subsequently deposited layer by layer [3]. Direct Ink Writing (DIW) is another technology within the material extrusion category. It is based on pushing a paste, for example made of ceramic, through a nozzle, and later depositing it in order to manufacture 3D printed samples [4]. This is the main technology used in bioprinting [5].

Most of the 3D printers that use FFF are easy-to-use and low-cost. They can be employed both at home and in the work environment. However, larger FFF printers are used in industry, which are also capable of meeting different user requirements, for example concerning the use of materials with different melting temperatures. As a result of this, AM technologies started to bloom up in different fields such as aeronautics, industry or health. The latter mentioned has undergone an important transformation, since it is currently used in different applications: surgical planning prototypes, surgical guides, scaffolds, medical devices, etc.

In this book chapter, different medical applications in which the FFF technology is used are introduced. But, prior to that, not only the technology evolution from monomaterial to multimaterial is explained, but also the relationship of FFF with other AM technologies.

2 Technology Evolution: From Monomaterial to Multimaterial

The FFF technology has undergone an important step forward with the development of the multimaterial 3D printers. The multimaterial concept is based on the mobilization of different printing heads, each one designed to provide a different

material, in order to manufacture a multimaterial prototype. Multimateriality can be achieved in two main ways, namely mosaic colour/material print or mixed colour/material print [6].

Regarding mosaic colour, i.e., non-mixed colours, multimateriality comprises two main different concepts, which are explored in Sect. 2.1:

- Exploration of the variants of the independent head concept.
- Exploration of the tool changer concept.

The idea of mixed colour material/print is explained in Sect. 2.2 and comprises two different concepts:

- Mix of colours based on sequential pass of filaments.
- Mix of colours based on mixture-based nozzle approach.

2.1 Mosaic Colour or Non-mixed Colours

2.1.1 Independent Head Concept

Some FFF machines use parallel extruders, in which two [7] or more nozzles [8] are placed in the same carriage. However, in this case the heads are constrained to describe parallel paths. The independent head concept goes a step beyond the IDEX (Independent Dual Extruder) concept, which is used, for example, in the Sigma[®] printer from BCN3D (Fig. 1). It has two independent heads that allow printing with two different materials, for example when the supports of a part are to be obtained in a hydrosoluble material or in order to print two parts at the same time. Both printing heads are mounted on the same bar (X axis) and can move together along the Y axis. The Z movement is provided by the printing bed in this case. The transition from one to two independent heads showed that it is possible to increase the number of heads to more than two. This path is explored in the present section. The arrangement of new independent heads is a way to increase the variety of materials integrated into a sample.

Despite the great mechanical complexity involved in the use of independent nozzle heads, each one with its own drives, the theoretical number of heads is not limited. This complexity is corroborated by the fact that commercial developments of this idea are scarce. Therefore, it is necessary to carry out an in-depth research on this concept, in order to build 3D printers with a higher number of independent heads [9].

Firstly, it is possible to add more independent heads in a bar, as can be seen in Fig. 2. In this way, it would be necessary to increase the length of the X axis as does the Sigmax[®] printer from BCN3D, which doubles this length with respect to the Sigma[®], and to ensure that the arrangement of more end sensors between the heads

Fig. 1 Schematic of the assignment of degrees of freedom to the BCN3D Sigma printer [9]

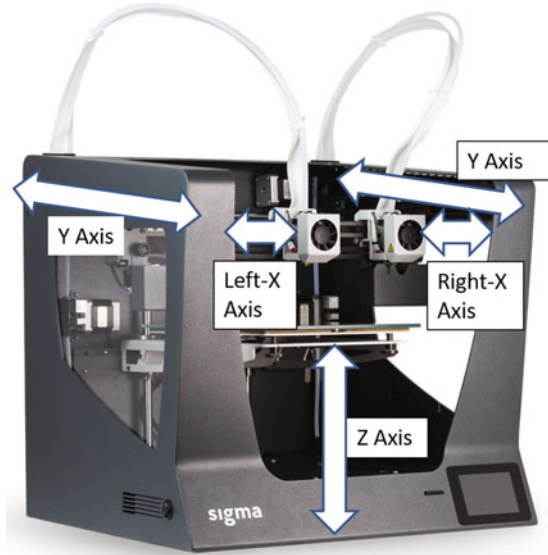


Fig. 2 Simulation of a BCN3D Sigmax printer with 4 heads in the X-axis movement guide [9]



(which are mobile elements) does not lead to a reduction in the precision of the process.

Secondly, another concept to be considered is to add another bar, in order to duplicate the number of independent heads. However, some precautions should be considered about the development of this concept. It will be necessary: (1) to duplicate the end system for the X axes, as there is now only one at the rear for the single X-axis; (2) to adjust the length of the Y guides, so as not to lose printing area with respect to the current solution of a single X-axis; (3) to redesign the machine so

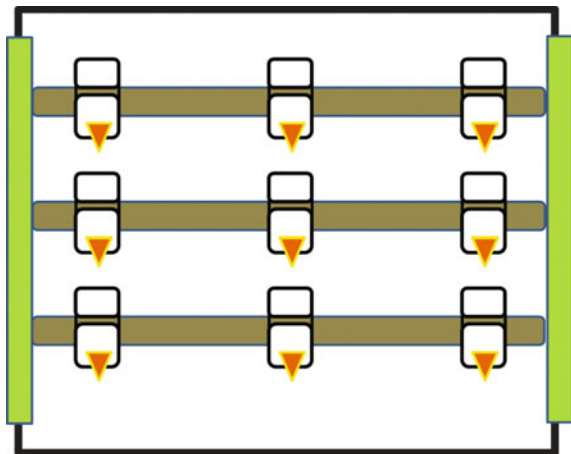
that it incorporates two new filament guidance and pushing systems, and to redesign the electronic and control (more motors to be managed, and adjustment of the software for the management of more than two heads); (4) to develop a new software to generate the g-codes, that takes advantage of the independence of the two bars in terms of *Y* movement, to make two heads work simultaneously, thus shortening the printing time.

Finally, the two ideas explained above lead to a concept of *n* bars and *m* heads per bar that would have ($n \times m$) independent heads (Fig. 3).

The scenario of having so many heads available opens the door to a wide range of possibilities, such as advancing in the 3D printing of surgical planning prototypes. Up to 9 printing heads are proposed in the following list, which could be integrated in a hypothetical 3D printer such as the one conceptualized in Fig. 3:

1. Rigid material colour A (modelling bones, organs ...).
2. Rigid material colour B (same as above).
3. Rigid material colour C (same as above).
4. Rigid translucent or transparent material, to show other structures.
5. Soft material to represent the tumour mass, with a level of hardness adjusted to facilitate the extraction test and, if necessary, with the maximum possible transparency.
6. Soft material (low hardness) colour D (blood vessels, organs).
7. Soft material (medium hardness) colour E (same as above).
8. Soft material (high hardness) colour F (same as above).
9. Soluble material to serve as a support in construction (PVA-polyvinyl alcohol).

Fig. 3 Schematic of a system with 9 independent heads (3 bars and 3 heads per bar) [9]

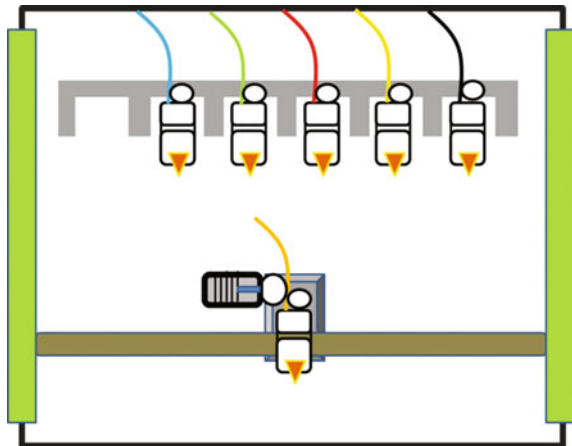


2.1.2 Tool Changer Concept

This new paradigm in 3D printing, with independent heads in which the concept of interchangeable tool during the work process is applied, takes into account the experience of numerical control (NC) machine-tools [10]. In a similar way to a revolver head for a NC machine, the main head of the printer would incorporate the motor for the extrusion of the filament. When a nozzle is placed in the working position, it will connect with the main motor. Figure 4 shows a diagram of this concept, based on the following points [9]:

- A stationary warehouse of nozzles, each one with its own filament already assembled. In the example, the traced positions are 6, but they could be more, if the head has enough work area to allow them to go to their fixed positions.
- Several nozzles that, in addition to the filament, will incorporate a part of its traction system. They will require the power to be supplied from the nozzle holder to be functional.
- Any system that allows the movement of the nozzle holder head, for example the XY system of the Sigma[®] 3D printer already shown.
- A nozzle holder head that includes a system for locking and unlocking the 3D printing nozzles. For example, it could use magnets or fast, precise and simple spring type clips.
- The extrusion motor should also be engraved with the thread-pulling means incorporated in the nozzles.
- An external complementary system to arrange the filament coils, probably in a lateral plane or in a plane over the printing one, to facilitate the unwinding operation. For incorporating heads having pastes instead of filament, it is

Fig. 4 Schematic of a system with nozzle changer [9]



necessary to use tubes fed by a fixed tank to the structure, in an analogous way to the use of a coil.

Some examples of tool changers are: (1) the beta 30 [11], and (2) the Mark2 [12], which is a magnetic tool changer.

2.2 *Mixed Colours or Single Head Multicolour Management*

This is a possible solution for the manufacture of complex 3D printed shapes in the event that the use of several extruders is to be avoided. There are two different approaches: (1) mix of colours based on the sequential passage of filaments; (2) mixture-based nozzle approach.

2.2.1 **Mix of Colours Based on the Sequential Passage of Filaments**

In this case, the nozzle can receive different filaments sequentially and, therefore, there is no direct mixing of filaments. Only different filaments pass, one after the other, through the same nozzle (Fig. 5), in contrast to the previous section, in which each nozzle was intended for a single type of filament.

This system is designed to vary the colour of the part in the same layer, without changing the extruder and without having to purge in the head to remove the transition material.

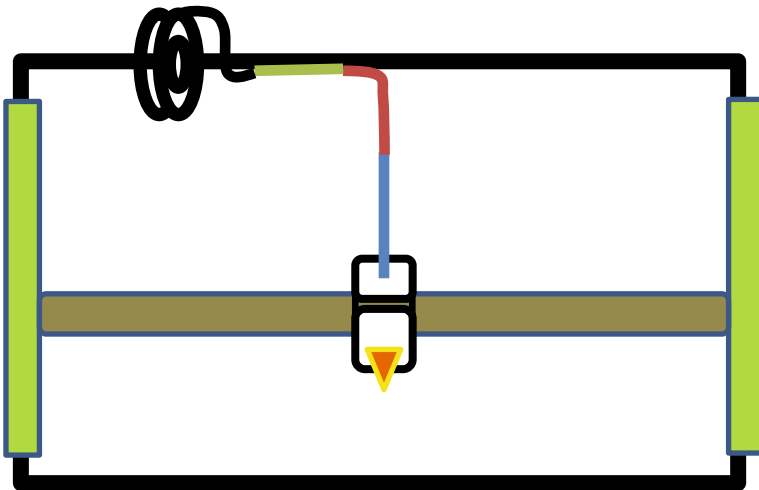


Fig. 5 Schematic of a system with a FFF approach based on the sequential passage of filaments

There are different 3D printers developed according to this concept, for instance: (1) the Mosaic Manufacturings® device [13] that composes a single filament from several ones, from the programming of a multicoloured figure; (2) the Prusa i3 MK3® [14] with the update of a multimaterial kit, in which different colours pass through a single head.

2.2.2 Mix of Colours Based on Mixture-Based Nozzle Approach

In this case, a premix of more than one filament is produced within the nozzle, and the colour and characteristics of the mix depend on the materials being mixed (Fig. 6). The main advantage of this approach is that the mixed materials have different properties than the original filaments. In terms of colour, combining 5 filaments (blue, magenta, yellow, white, black) will theoretically result in any hue. The same goes for other features such as elasticity, where different combinations of hard and soft materials can be obtained. The main disadvantage is that, inevitably, when looking for a specific mixture colour, a transition material is formed in the chamber of the nozzle, which needs to be purged. This purge means, in many cases, spending more material and time in the process. Thus, for example, if a barcode is to be printed in three dimensions, in the most unfavourable orientation it would be necessary to change many times from each layer of the filament white to black (unless software defines paths that complete the intervention of each colour per layer). Once a few millimetres of one colour have been completed, the other colour will be given way, but it should be done in a purge area so that the head is clean of

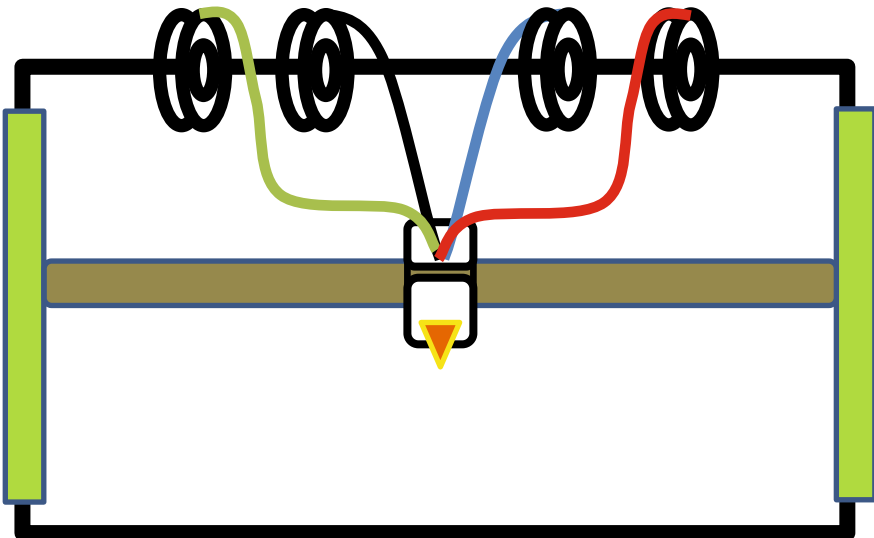


Fig. 6 Schematic of a system with FFF mixture-based nozzle approach

remnants of the previous colour. The solution to this problem is the same that is applied to the printers with independent heads to reactivate the extrusion when the head that was inactive has to be restarted: to extrude a few millimetres of wire forming a purge tower in a corner of the platform.

So far, different examples of 3D printers that use this concept can be listed: (1) E3D® supplies the Cyclops® head [15], in which two filaments converge in a single nozzle; (2) BotObjects [16] proposed a machine, the Prodesk3D, with a mixing chamber for five filaments (blue, magenta, yellow, white and black) to obtain the full range of colours. To these materials a sixth filament for soluble support was added, which was provided by a second extruder in the same head. Some authors have also studied this concept [9, 17, 18].

3 Relationship Between FFF and Other AM Technologies

In the present section, the relationship between FFF and other printing technologies, either or not within the extrusion group of technologies, is addressed.

As was mentioned in the introduction (Sect. 1), when mimicking tissues, it is usual to combine both the extrusion of filament with FFF and the extrusion of pastes with DIW. On this last case, the paste is extruded through a syringe and a nozzle, and then deposited layer by layer. It can be applied to different materials such as ceramics, food, drugs, etc. It can also be applied to silicones for medical applications [19]. Different systems are employed to push the paste, for example plungers, screws and pumps [20, 21].

On the other hand, in recent years some filaments used in FFF started combining plastics with powdered metals like copper [22], stainless steel [23] or titanium [24], among others, in order to improve their conductivity and/or mechanical strength. Other filaments have been filled with ceramics, wood, carbon fibre, etc. [22].

The FFF technology mainly allows printing commercial hard plastics and rubber-like materials (for example Polylactic Acid-PLA, Polystyrene-PS or Ninjaflex). For this reason, a different approach has been used to print soft materials such as silicones, gelatine and hydrogels, which allow mimicking the tactile sensation, mechanical properties and colour of the tissues in a more precise way [25]. It is a reverse process that consists of using FFF to manufacture moulds and then to fill them with the soft materials. For example, the liver was mimicked by casting silicones in PLA FFF printed moulds [26].

A similar reverse process called EMB3D (Embedded Three-Dimensional Printing) involves 3D printing of an ink, normally a silicone, using a capillary needle in a transparent and photocrosslinkable support medium. This new 3D printing technique is an avant-garde technology that was first mentioned in 2011 [27]. During this time, different supporting gels have been developed and studied such as carbopol [28], Pluronic® F-127 [29, 30] and gelatin [31, 32]. After printing, the part and the support medium are cured to obtain a solid part at a specific

temperature, depending on the materials used. Once the curing is finished, the printed object is peeled off along with the closed shell [33].

4 Training Models and Surgical Planning Prototypes

In the present section, the development of FFF training models and surgical planning prototypes is addressed.

Surgeons need to fulfil complex technical tasks during the operation: finding appropriate methods for removing the tumour, trying not to cause any haemorrhage, etc. Additionally, this needs to be done in a short period of time. Those are the reasons why using 3D printed surgical planning prototypes can be vital, since they can give an idea on how to deal with the procedure. These prototypes are 3D realistic models used by surgeons to improve their rehearsal experience, since they are able to visualize the affected organs and even to practice surgery before performing it.

In different research studies it has been demonstrated that doctors who had the opportunity to train with physical models showed better skills in comparison with those who did not have the same chance [34]. In this way, the surgery time is decreased and, hence, the risks are reduced.

In recent years, the surgical planning prototypes have been used in different procedures such as oncology, hepatectomy, cardiology, etc. The increase in their use is partly due to the development of the AM technologies [35, 36].

4.1 Oncology

Oncology is the specialization of medicine that studies the prevention, diagnosis and treatment of cancer. In this area of the medicine, it is important to have highly realistic 3D models that can differentiate the different anatomical structures (blood vessels, for example) and the tumours. Figure 7 shows an example of an FFF printed training model with the anatomical structures printed in white and the tumour in yellow.

Additionally, it is important to clarify that, currently, FFF printed prototypes cannot mimic the properties of the tissues. However, the tactile properties and feeling of the tissues are important for surgeons. Thus, ideally the materials should mimic the correspondent soft living tissue as closely as possible. Therefore, in order to fulfil the requirement, two different methods have been employed during the last years, as was explained in Sect. 3. On the one hand, DIW has been applied to print silicone, with properties similar to those of the corresponding tissues. On the other hand, the moulding technique has been used, usually with FFF printed moulds. After printing, the moulds are fixed together so that a material, either a silicone or a hydrogel, can be cast.

Fig. 7 Example of an FFF training model with the anatomical structures printed in white and the tumour in yellow



Tumours can be found in different soft living tissues such as lungs or liver. The latter organ mentioned may suffer from biliary tract rhabdomyosarcoma, which is a soft tissue malignant musculoskeletal tumour. As sometimes it is a difficult task to remove the tumour, a hepatectomy is then carried out, which is the surgical removal of part of the liver. It is interesting to mention that, if the hepatectomy is done to a child, its liver mass can regenerate until around 90%.

The hepatectomy is normally planned before the surgery because, by using DICOM (Digital Imaging and Communication On Medicine) images and 3D printed prototypes. Figure 8 shows a prototype which was manufactured using both Selective Laser Sintering (SLS) for the internal parts (tumour and blood vessels), and FFF, to print a mould in which transparent silicone was cast. [37]. Different

Fig. 8 Liver 3D printed prototype [9]



materials were tested and it was observed that 1wt% agarose was the most appropriate composition for mimicking the liver tissue.

4.2 Cardiology

Within the cardiology field, it is also possible to manufacture prototypes [38], although prospective studies are still required to demonstrate their clinical utility. For example, Fig. 9 shows two different prototypes: one printed with SLS and the other one with FFF. Regarding the FFF process, it was necessary to use support material (yellow colour), while for SLS it was not necessary. However, the FFF prototype is cheaper than the SLS one.

Although both prototypes are able to show anatomical structures of the heart such as the superior vena cava or the aorta, it would be necessary to use more nozzles to print other important areas in case of need, for example, the tumour.

4.3 Osteology

Osteology is the science that studies the human skeleton. The FFF prototypes cannot currently mimic the hard bone tissue. In addition, unlike silicones and hydrogels, they cannot be cast in moulds. That is why, in this field, phantoms are mainly used as anatomical models for education, for instance.

For manufacturing 3D models like the ones in Fig. 10, the oozing problem needs to be taken into consideration. Oozing happens when small parts of plastic are left behind in a printed model. This problem is solved with independent head systems,

Fig. 9 Heart 3D printed prototype: SLS (left), FFF (right) [9]

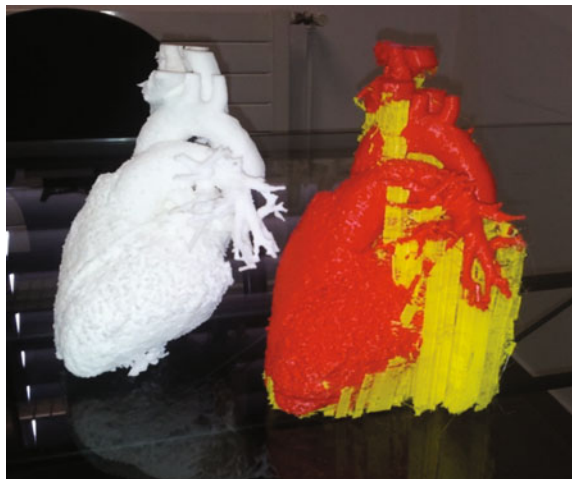




Fig. 10 Knee joint manufactured with two materials, with and without oozing effect: 3D printer with two non-independent extruders (left) 3D printer with independent double extruder–IDEX–(right) [9]

as one independent head is at rest during the work of the other head, as is the case with single-head multinozzle systems.

5 Surgical Guides

Surgical guides are the latest developed tools in order to get more safety and precision in complex surgery cases such as dental implants or in relation to cervical and lumbar diseases and tumours [39]. Rubio-Pérez et al. [40] manufactured surgical guides with the FFF technology, using PLA (Polylactic Acid). They verified

Fig. 11 Example of surgical guide used in dentistry



that the use of personalized patient models like surgical guides helps to manage the presence of sacral anomalies. Figure 11 shows an example of a surgical guide used in dentistry.

It is worth mentioning that, if these guides are only used for rehearsal experience, they do not need to meet any criteria. However, if they are used for interacting with patients (the materials and devices are in contact with the patients) during a surgery, it is necessary to use materials that follow the ISO 10993 [41] (a series of standards used to evaluate the biocompatibility for medical devices in order to manage the biological risks).

6 3D Bio-Printing

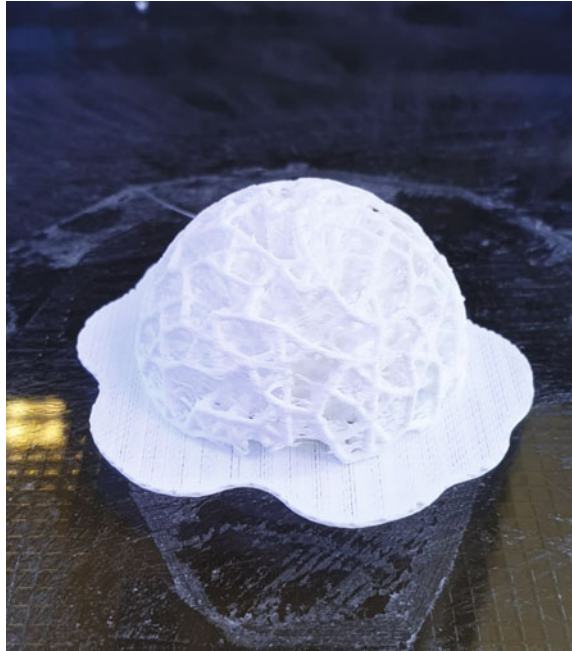
3D bio-printing consists of using different 3D printing techniques to manufacture biomedical parts that imitate the natural tissues. This is achieved by combining cells, growth factors and biomaterials. 3D bio-printing consists usually of three steps: pre-bioprinting, bioprinting and post-bioprinting. In pre-bioprinting, it is necessary to obtain a model of a tissue or organ. This can be done, for example, with computer tomography (CT) or magnetic resonance (MR). Then, in the bioprinting step the information of the geometry is transferred to a printer. Later, the cells are mixed with a liquid material that provides oxygen and other nutrients. The mixture, which is known as bioink, is placed in a cartridge and deposited. Then, the obtained pre-tissue is transferred to an incubator, where the pre-tissue is transformed into a tissue. Finally, the post-bioprinting stage allows to create a stable structure of the biomedical material, by means of both mechanical and chemical stimulations [42].

Among the main applications of 3D bio-printing, two can be highlighted: manufacture of bio-active scaffolds and cell 3D bio-printing [13].

As for the first application, 3D printed scaffolds have extensively been used in tissue engineering, drug delivery and cell viability tests [43]. Currently, some hard tissues such as bones can be printed [44]. However, it is difficult to print complicated shapes. For example, the trabecular structure of bones has been simulated in plastic material with the FFF technology [45]. Figure 12 shows a simulated PLA hip prosthesis with a trabecular porous structure for the external area that would favour its fixation by means of osseointegration. Required porosity and pore size values can be obtained from the appropriate selection of printing parameters. The manufacture of 3D printed parts made of ceramics is also blooming up since they can be used in different medical solutions. For example, Minguella-Canela et al. [46] manufactured porous bone spacers using hydroxyapatite (HA) with β -TCP (tricalcium phosphate) ceramics.

Cell 3D bio-printing allows mimicking native tissues. Cell-derived matrices (CDMs) are a new type of modifiable extracellular matrices for a variety of tissues [47]. Currently, it is possible to fabricate tissues and organs by depositing live cells with ink droplets, although they may lack some elements. For example, Jakab et al.

Fig. 12 FDM 3D printed hip prosthesis using PLA



[48] printed blood vessels and cardiac valves. In another example, Rabionet et al. [49] printed tubular parts for vascular tissue engineering. On the other hand, biocompatible and biodegradable materials can be used to reduce incompatibilities with the human body [50].

7 Medical Devices

Medical device is a term that includes both simple (tongue depressors and bedpans) and more developed (pacemakers) medical instruments. Some of these devices cannot be 3D printed, especially those that are very complex and need an in-depth research study. However, more simple medical devices such as stents are easier to be 3D printed. On the other hand, since medical devices are normally implanted in the human body, they have two main prerequisites: (1) the materials used must be biocompatible and non-toxic; and (2) the device must be sterilized.

Already in 1996, a patent presented the possibility to print different medical devices by means of solid free-form fabrication methods such as SLA, SLS, FDM, etc. Specifically, the patent claims the fabrication of matrices with interconnected porous structures for drug delivery [51]. An example of this was carried out by Holländer et al. [52], in which T-shaped prototypes of intrauterine system (IUS) that

contain drugs within the entire backbone of the medical device were printed by means of FFF. The material used was PCL (poly(ϵ -caprolactone)).

Other medical devices were manufactured using the material extrusion concept either by FDM or by DIW. For instance, wearable pulse oximeters have been printed in silicone [53]. Regarding the stents, two different examples can be highlighted: (1) a first step into the manufacturing of different tracheal stent prototypes (ABS, non-implantable silicone stent, acetic silicone mold) was carried out by Melgoza et al. [54], (2) Jia et al. [2, 55] manufactured self-expandable biodegradable vascular stents by FDM, using shape memory PLA, due to the high number of in-stent restenosis and stent thrombosis rate observed in stent implantation with balloon angioplasty.

8 FDM Against COVID-19

Very recently, the large 3D printing community has shown a great responsiveness to help in the fight against COVID-19 (Coronavirus Disease) through the printing of different devices such as face masks or door openers. These devices do not only reduce the likelihood of suffering COVID-19, but also open the possibility to future FDM 3D printed parts in order to deal with new problems, either medical or social.

For example, at CIM UPC, a door opener was 3D printed in order to avoid the use of the professional hands. It is commonly known that, in case of being infected by COVID-19, it can be easily spread into different surfaces like the door handle, which is touched at every moment when a door is opened. Additionally, the virus can live for a few days on surfaces [56]. That is why this FFF 3D printed part is a medical solution in the fight against the pandemic (Fig. 13).

Moreover, as mentioned above, a part of face shields can be easily 3D printed using FFF. Then, the front transparent plastic part is added, and a face shield is finished (Fig. 14). These devices are useful for preventing from the saliva drops of



Fig. 13 CIM UPC design of a door opener to fight the spread of Covid-19: 3D printed sample (left) and its use (right)



Fig. 14 Face shield 3D printed using FFF. The visor is 3D printed using PP (PolyPropylene) and the screen material is PVC (PolyVinyl Chloride), not 3D printed

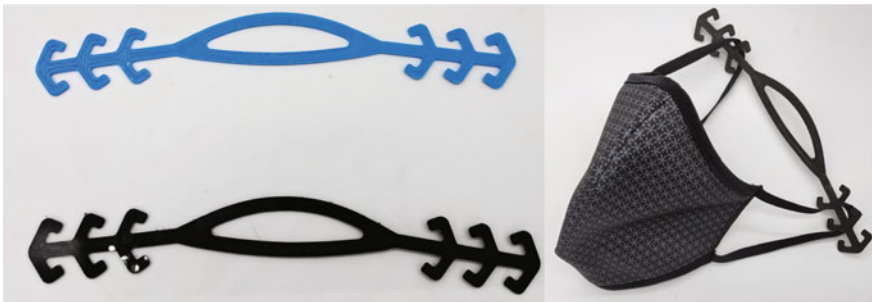


Fig. 15 3D printed ear guards using PLA by means of FFF

other people, because there is a slight chance of developing a disease if the virus drops get in touch with the eyes.

Another interesting object is the use of ear guards for the facemask, which had a high significance in the fight against COVID-19. Although this is a simple thing, it is ingenious, since its aim is to reduce the discomfort of the masks that are held behind the ears. Many face masks have a design problem because they are either too big or too small. The ear guard allows the elastic bands of each ear to join in a flat piece behind the neck, with serrations to regulate the tension (Fig. 15).

9 Conclusion

The present book chapter summarizes different applications of the FFF technology in the medical sector. First, a brief description of the evolution of the technology, from monomaterial to multimaterial, is presented. Then, the relationship between FFF and other printing technologies is addressed. Finally, different applications of FFF in the medical field are analysed, such as the manufacture of training models, surgical planning prototypes, medical devices, surgical guides, etc.

Main conclusions of the chapter are as follows:

- The FFF technology is currently moving towards multi-material printing, using two main concepts based on either the mosaic colour or the mixed colour concepts.
- FFF is widely used in medical applications, for instance the manufacture of training models and of surgical planning prototypes. In this case, it is recommended to combine FFF with other extrusion techniques such as DIW, in order to incorporate both rigid thermoplastic materials and softer materials like silicones in the same prototype. Reverse 3D printing processes, in which a mold obtained with the FFF technique is filled with a softer material have also been reported.
- Surgical guides, which help doctors to perform surgery, can be obtained in an easy and economical way with the FFF technique.
- 3D bio-printing has two main applications: manufacture of bio-active scaffolds and cell 3D-bioprinting. In both cases, an FFF printed structure can be used as a base for cell growth.
- Medical devices such as stents or wearable pulse oxymeters have been manufactured with success by means of the FFF technique.
- During the global pandemic of COVID-19, FFF has been proven to be a fast and effective technique to manufacture different devices such as door openers or face masks.

The FFF or FDM process is still under development and will most likely lead to new applications in the medical area in the years to come.

Funding The present chapter was co-financed by the European Union Regional Development Fund within the framework of the ERDF Operational Program of Catalonia 2014-2020, with a grant of 50% of total cost eligible, project BASE3D, grant number 001-P-001646.

References

1. ISO/ASTM (2015) International Standard ISO/ ASTM 52900 Additive manufacturing—general principles—Terminology. Int Organ Stand. <https://doi.org/10.1520/ISOASTM52900-15>
2. Scott Crump S, Minnetonka M (1989) Apparatus and method for creating three-dimensional objects, 15. US5121329A

3. Gibson I, Rosen DW, Stucker B (2010) Additive manufacturing technologies. Springer, US, Boston, MA
4. Buj-Corral I, Domínguez-Fernández A, Gómez-Gejo A (2020) Effect of printing parameters on dimensional error and surface roughness obtained in direct ink writing (DIW) processes. *Materials* 13:2157.1–2157.11
5. Guzzi EA, Bovone G, Tibbitt MW (2019) Universal nanocarrier ink platform for biomaterials additive manufacturing. *Small* 15(51):1905421
6. Boulaala M, Elmessaoudi D, Buj-Corral I et al (2020) Towards design of mechanical part and electronic control of multi-material/multicolor fused deposition modeling 3D printing. *Int J Adv Manuf Technol* 110:45–55
7. Keller P (2016) Designing a compact dual head for FLM 3D printing technology. *MM Sci J* 2016:1560–1564
8. Löffler R, Koch M (2019) Innovative extruder concept for fast and efficient additive manufacturing. In: IFAC-Papers OnLine, pp 242–247
9. Fenollosa-Artés F (2018) Contribució a l'estudi de la impressió 3D per a la fabricació de models per facilitar l'assaig d'operacions quirúrgiques de tumors—Contribution to the study of 3D printing for the manufacture of models to facilitate the testing of tumour surgery. PhD thesis, Universitat Politècnica de Catalunya (UPC)
10. Xu X (2009) Integrating advanced computer-aided design, manufacturing, and numerical control: Principles and implementations. Information Science Reference, Hershey, PA
11. E3D-online. ToolChanger: the update you've all been waiting for <https://e3d-online.com/blogs/news/toolchanger-the-update-youve-all-been-waiting-for>. Accessed 10 Oct 2020
12. Mark2. The smart way to multi-extrusion. <https://magnetic-tool-changer.com/>. Accessed 10 Oct 2020
13. Mosaic. Simple, multi-material 3D printing. <https://www.mosaicmfg.com/>. Accessed 10 Oct 2020
14. The original PRUSA I3 MK3S 3D printer. <https://www.prusa3d.com/original-prusa-i3-mk3/>. Accessed 10 Oct 2020
15. E3D. Cyclops+. <https://e3d-online.com/products/cyclops>. Accessed 10 Oct 2020
16. BotObject announces the world's first full-color 3D printer. <https://www.pcworld.com/article/2037094/botobjects-announces-the-world-s-first-full-color-3d-printer.html>. Accessed 10 Oct 2020
17. Pascale D, Simion I (2018) Multi-material 3D printer extruder concept. *J Ind Des Eng Graph* 13(1):25–28
18. Guan Y, Shen B, Zhang Y, Fu Z (2017) Design of color mixing 3D printing system based on LabVIEW. *J Comput* 28(6):277–287
19. Luis E, Pan HM, Sing SL et al (2020) 3D direct printing of silicone meniscus implant using a novel heat-cured extrusion-based printer. *Polymers* 12(5):1031
20. Pusch K, Hinton TJ, Feinberg AW (2018) Large volume syringe pump extruder for desktop 3D printers. *HardwareX* 3:49–61
21. Mesbahi JEL, Buj-Corral I, Mesbahi AEL (2020) Use of the QFD method to redesign a new extrusion system for a printing machine for ceramics. *Int J Adv Manuf Technol* 111(1–2):227–242
22. Liu Z, Lei Q, Xing S (2019) Mechanical characteristics of wood, ceramic, metal and carbon fiber-based PLA composites fabricated by FDM. *J Mater Res Technol* 8:3743–3753
23. Liu B, Wang Y, Lin Z, Zhang T (2020) Creating metal parts by fused deposition modeling and sintering. *Mater Lett* 263:127252
24. Lee J, Lee H, Cheon KH et al (2019) Fabrication of poly(lactic acid)/Ti composite scaffolds with enhanced mechanical properties and biocompatibility via fused filament fabrication (FFF)-based 3D printing. *Addit Manuf* 30:100883
25. Qiu K, Zhao Z, Haghshastiani G et al (2018) 3D printed organ models with physical properties of tissue and integrated sensors. *Adv Mater Technol* 3(3):1700235

26. Estermann SJ, Pahr DH, Reisinger A (2020) Quantifying tactile properties of liver tissue, silicone elastomers, and a 3D printed polymer for manufacturing realistic organ models. *J Mech Behav Biomed Mater* 104:103630
27. Wu W, Deconinck A, Lewis JA (2011) Omnidirectional printing of 3D microvascular networks. *Adv Mater* 23(24):H178–H183
28. Bhattacharjee T, Zehnder SM, Rowe KG et al (2015) Writing in the granular gel medium. *Sci Adv* 1(8):e1500655
29. Muth JT, Vogt DM, Truby RL et al (2014) Embedded 3D printing of strain sensors within highly stretchable elastomers. *Adv Mater* 26:6307–6312
30. Liu W, Heinrich MA, Zhou Y et al (2017) Extrusion bioprinting of shear-thinning gelatin methacryloyl bioinks. *Adv Healthc Mater* 6(12):1601451
31. Hinton TJ, Jallerat Q, Palchesko RN et al (2015) Three-dimensional printing of complex biological structures by freeform reversible embedding of suspended hydrogels. *Sci Adv* 1(9): e1500758
32. Hinton TJ, Hudson A, Pusch K et al (2016) 3D printing PDMS elastomer in a hydrophilic support bath via freeform reversible embedding. *ACS Biomater Sci Eng* 2:1781–1786
33. Zhao J, Hussain M, Wang M et al (2020) Embedded 3D printing of multi-internal surfaces of hydrogels. *Addit Manuf* 32:101097. <https://doi.org/10.1016/j.addma.2020>
34. Tejo-Otero A, Buj-Corral I, Fenollosa-Artés F (2020) 3D printing in medicine for preoperative surgical planning: a review. *Ann Biomed Eng* 48:536–555
35. Muguruza Blanco A, Krauel L, Fenollosa Artés F (2019) Development of a patients-specific 3D-printed preoperative planning and training tool, with functionalized internal surfaces, for complex oncologic cases. *Rapid Prototyping J* 25:363–377
36. Krauel L, Fenollosa F, Rianza L et al (2016) Use of 3D prototypes for complex surgical oncologic cases. *World J Surg* 40:889–894
37. Tejo-Otero A, Lustig-Gainza P, Fenollosa-Artés F et al (2020) 3D printed soft surgical planning prototype for a biliary tract rhabdomyosarcoma. *J Mech Behav Biomed Mater* 109:103844
38. Celi S, Gasparotti E, Capellini K et al (2020) 3D printing in modern cardiology. *Curr Pharm Des* 26:1
39. Wilcox B, Mobbs RJ, Wu A-M, Phan K (2017) Systematic review of 3D printing in spinal surgery: the current state of play. *J Spine Surg* 3:433–443
40. Rubio-Pérez I, Lantada AD (2020) Surgical planning of sacral nerve stimulation procedure in presence of sacral anomalies by using personalized polymeric prototypes obtained with additive manufacturing techniques. *Polymers* 12(3):581
41. Wallin RF, Upman PJ (1998) A practical guide to ISO 10993-3: carcinogenicity. *Medical Device and Diagnostic Industry*
42. Gu Q, Hao J, Lu YJ et al (2015) Three-dimensional bio-printing. *Sci China Life Sci* 58:411–419
43. Jakab K, Norotte C, Marga F et al (2010) Tissue engineering by self-assembly and bio-printing of living cells. *Biofabrication* 2(2):02201
44. Zhang L, Yang G, Johnson BN, Jia X (2019) Three-dimensional (3D) printed scaffold and material selection for bone repair. *Acta Biomater* 84:16–33
45. Buj-Corral I, Bagheri A, Petit-Rojo O (2018) 3D printing of porous scaffolds with controlled porosity and pore size values. *Materials* 11:1532
46. Minguela-Canela J, Calero JA, Korkusuz F et al (2020) Biological responses of ceramic bone spacers produced by green processing of additively manufactured thin meshes. *Materials* 13 (11):2497
47. Rubi-Sans G, Castaño O, Cano I et al (2020) Engineering cell-derived matrices: from 3D models to advanced personalized therapies. *Adv Funct Mater* 30(44):2000496
48. Jakab K, Norotte C, Damon B et al (2008) Tissue engineering by self-assembly of cells printed into topologically defined structures. *Tissue Eng—Part A* 14:413–421
49. Rabionet M, Guerra AJ, Puig T, Ciurana J (2018) 3D-printed tubular scaffolds for vascular tissue engineering. In: *Procedia CIRP*, vol 68, pp 352–357

50. Billiet T, Vandenhaute M, Schelfhout J et al (2012) A review of trends and limitations in hydrogel-rapid prototyping for tissue engineering. *Biomaterials* 33:6020–6041
51. Cima LG, Cima MJ (1996) Preparation of medical devices by solid free-form fabrication methods, 11. USOO5490962A
52. Holländer J, Genina N, Jukarainen H et al (2016) Three-dimensional printed PCL-based implantable prototypes of medical devices for controlled drug delivery. *J Pharm Sci* 105:2665–2676
53. Abdollahi S, Markvicka EJ, Majidi C, Feinberg AW (2020) 3D printing silicone elastomer for patient-specific wearable pulse oximeter. *Adv Healthc Mater* 9(15):1901735
54. Melgoza EL, Vallicrosa G, Serenó L et al (2014) Rapid tooling using 3D printing system for manufacturing of customized tracheal stent. *Rapid Prototyping J* 20:2–12
55. Jia H, Gu SY, Chang K (2018) 3D printed self-expandable vascular stents from biodegradable shape memory polymer. *Adv Polym Technol* 37:3222–3228
56. Van Doremalen N, Bushmaker T, Morris DH et al (2020) Aerosol and surface stability of SARS-CoV-2 as compared with SARS-CoV-1. *N Engl J Med* 382:1564–1567

Fused Filament Fabrication for External Medical Devices



C. P. Paul, K. Dileep, A. N. Jinoop, A. C. Paul, and K. S. Bindra

Abstract Fused Filament Fabrication (FFF) is the most commonly used additive manufacturing process primarily used to build polymer-based components. FFF finds wide applications in various fields, like—prototyping, tooling, automotive, medical, etc. Among them, the applications of FFF is expanding widely in medical sector mainly due to the customization freedom offered by the technology complying with the unique shape, size and clinical requirement as opposed to conventional manufacturing techniques. The development of orthoses and prostheses are the two major applications of FFF for external medical devices. Orthoses devices are used for either the correction or restoration of the functionality of organs, while prostheses are artificial devices/appliances used for replacement of natural body parts lost or damaged due to illness or injury. However, there are certain challenges associated with the development of accurate medical devices using FFF due to several process-induced limitations. This chapter briefly introduces the FFF process and subsequently focus on its various applications to develop external devices in the medical sector, like—orthosis and prosthesis. It also elucidates the development of bionic prosthesis. The various stages involved in the development of customized medical devices using FFF is discussed. The chapter

C. P. Paul (✉) · K. Dileep · A. N. Jinoop · K. S. Bindra

Laser Technology Division, Raja Ramanna Centre for Advanced Technology,
Indore 452013, Madhya Pradesh, India

e-mail: paulcp@rrcat.gov.in

K. Dileep

e-mail: mail.dileepkr@gmail.com

A. N. Jinoop

e-mail: anjinoop@gmail.com

K. S. Bindra

e-mail: bindra@rrcat.gov.in

C. P. Paul · K. Dileep · A. N. Jinoop · K. S. Bindra

Homi Bhabha National Institute, Anushaktinagar, Mumbai 400094, Maharashtra, India

A. C. Paul

Nitte Meenakshi Institute of Technology, Bengaluru 560064, Karnataka, India

e-mail: alinipaul@gmail.com

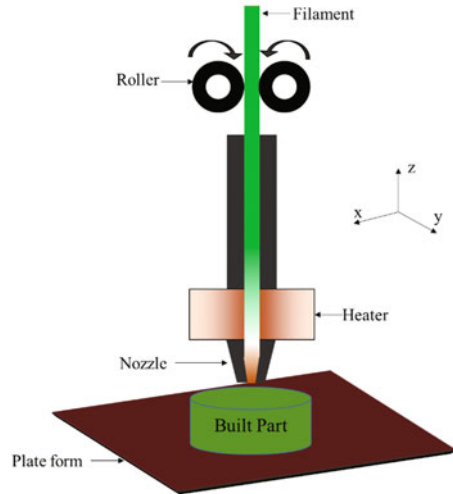
also addresses the various issues associated with the deployment of FFF to build medical devices. Case studies and recent advances associated with the development of customized orthosis and prosthesis are also included in the chapter. This chapter will serve as quick-start for novices to appreciate the innovations with FFF technology and as a compiled reference document for practising researchers.

1 Introduction

Additive Manufacturing (AM) techniques have evolved significantly in the last few decades and have changed the way designs are conceived. Thus, AM became “a game-changer technology” that can build complex geometry parts/components rapidly, with significant cost savings [1]. The ability to build intricate geometries directly from digital model data attracts the applications of AM in various sectors, like—medical, tooling, prototyping, aerospace and many other industries since its evolution in 1986 through stereolithography process. Among the various AM techniques, the most commonly used technique in industries and academia is Material Extrusion technique. Material extrusion is commonly known by the names Fused Filament Fabrication (FFF) and Fused Deposition Modelling (FDM™) [2]. FFF is extensively used mainly due to the availability of low-cost machines; expiration of patents; low maintenance and material cost; availability of open source systems and software; RepRap projects etc. FFF is commonly used for building polymer components. However, recent literature shows the fabrication of polymer composites and metallic components using FFF. Indirect techniques are generally used for building metallic components using FFF. It includes fabrication of green components (mix of polymer and metal) using FFF, which is followed by post-processing treatments, like—de-binding, infiltration and sintering to build dense metallic components.

Figure 1 presents the typical schematic of a FFF process. The system consists of a spool carrying feedstock material in the filament form, roller for pulling the filament from the spool, heater for bringing the material to a molten state, XY manipulation system for depositing material in a layer and Z direction manipulation system to deposit material in a layer by layer fashion. Similar to other AM processes, FFF starts with a 3-dimensional (3D) model data that can be a CAD model or output from reverse engineering or output from numerical analysis. The 3D model is converted to a machine-specific format for communication between the developed 3D model and FFF system. Some of the common machine-specific formats used for AM are STL, OBJ and Additive Manufacturing File (AMF). Among them, STL and OBJ are most commonly used in FFF systems commercially. Prior to conversion to machine-specific format, the model is sliced into several layers and the tool path is generated for each layer, which allows for material addition as per the model design. XYZ manipulation is generally achieved by one of the combinations of movement of the nozzle and build plate. The preferred choice is the nozzle movement in the XY plane and build plate in the z-direction or by moving the nozzle head in the XYZ direction with a fixed build plate.

Fig. 1 Typical schematic of FFF system



FFF is extensively used in various sectors, like—automotive, aerospace, tooling, education, medical, etc. Among them, the medical sector widely uses FFF techniques for developing the anatomical models for education/training, performing surgical rehearsal and medical diagnosis, developing implant for surgery, etc. Other applications of FFF in the medical sector are the fabrication of bone scaffold, hearing aids, dental braces, implants and artificial cosmetic organs, like—nose, ear, breast, hips etc. FFF is also employed in the development of drug delivery devices and surgical aids [3, 4].

The development of orthoses and prostheses (O&P) using FFF are emerging areas in the field of external medical devices. Orthoses are used for either the correction or restoration of the functionality of organs, while prostheses are artificial devices/appliances used for replacement of natural body parts lost or damaged due to illness or injury. This chapter is focussed on the manufacturing of externally used medical devices such as O&P. The various stages involved in the development of customized medical devices using FFF is discussed along with the various issues associated with the deployment of FFF to build medical devices. Case studies and recent advances associated with the development of customized orthosis and prosthesis using FFF are included.

2 Orthoses and Prostheses

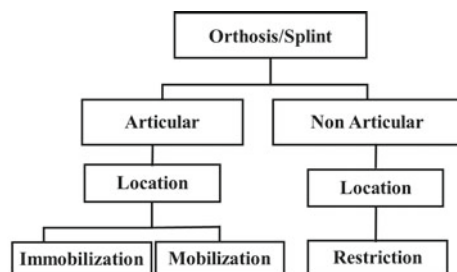
The word orthosis is a Greek word, which means ‘making straight’. Orthoses are used for aligning, supporting, immobilizing, or treating muscles, joints or skeletal parts. Orthoses include braces, splints, or other artificial assistive devices serving to support the limbs or spine or to prevent or to assist its relative movement.

According to ISO standards, an orthosis is an externally applied device used to modify structural and functional characteristics of the neuromuscular skeleton system. Orthoses devices assist patients to fulfil their biomechanical need during neuromuscular and musculoskeletal impairment that causes functional limitation and disability [5]. These devices increase the ability and boost the value of living. Each orthosis device is named according to the location of the injured body part. The most common orthoses used in orthopaedics are shown in Fig. 2. The ‘articular’ orthoses cross one or more body joints. Wrist immobilization orthosis, proximal interphalangeal (PIP) joint extension mobilization orthosis, and elbow flexion restriction orthosis are the most common examples of articular orthoses. ‘Non-Articular’ devices do not cross a joint and these devices are used to stabilize the applied body segment. The orthosis can also be classified based on the position of application [6]. Upper extremity orthosis is used in the upper body segment, like—shoulder–arm—elbow orthosis, wrist orthosis, hand orthosis, etc. Lower extremity orthosis is used in the lower body segment, like—foot orthosis, ankle–foot orthosis, hip–knee–ankle–foot orthosis, etc.

The word prosthesis is a Greek word, which means “addition, application or attachment”. Prostheses are artificial devices that replace missing or amputated body parts and can restore their functionality, which may be lost due to trauma, disease, or a congenital disorder (condition present at birth) or cosmetic appearance [7]. Prostheses can be divided based on the position of the body, like—upper limb (arm, wrist, finger etc.) and lower limb (leg, foot etc.). Based on the design consideration some prostheses can be categorised as exoskeletal and endoskeletal. An exoskeletal prosthesis gains its structural strength from the outer laminated shell through which the weight/force of the body transmit, while endoskeletal prostheses are the tubular central supporting structure, usually having modular or interchangeable connectors with other components such as knees and feet [8].

Bionic prostheses are replacement of a body part by an artificial device and are an area of building artificial systems similar to living systems. Bionic prostheses are functional prosthesis, capable of nearly duplicating natural limb functionality. The deployment of these devices improves mobility and improve the quality of living of a person suffering from an amputated limb. Some bionic prostheses are

Fig. 2 Orthosis classification in orthopaedics



myoelectric-controlled and use external electrical power without using the body/muscle power of the patient/user. These devices use electromyography (EMG) signals and controlled with microcontroller/computer. Figure 3 presents the general structure of myoelectric prostheses. Generally, EMG signals are collected from exoskeleton muscles using specific EMG sensors. Further, these signals are processed for controlling the prosthesis [9]. Myoelectric arm prostheses are the most widely used bionic prostheses. In arm prostheses, muscle tension signals from the residual limb of patient/user are sensed with sensors. These signals are myoelectrical impulses in microvolt order, which is amplified and sent to the control system of the device for controlling the motion [10]. The functional assistances of these prostheses system have a key influence on the rehabilitation as bionic/myoelectric prostheses offer customised design along with better comfort. In case of lower-limb amputees, these devices allow the user to climb stairs and move along the slopes and uneven ground, which significantly reduces their risk of falling as well as reducing stress on the rest of their body parts [11]. *Hero arm* is an example of the myoelectric brain-controlled prosthesis arm of ‘Open Bionics’—a UK based company developing low-cost bionic hands. They used AM to fabricate the prostheses arm that can perform difficult tasks, like—brushing hair/teeth, opening a lip balm or putting clothes on a hanger [12].

3 Need for FFF Built O&P Devices

Globally millions of people suffer from congenital limb disorder, whereas many people lost their limbs in accidents, military war or the amputation of a limb during the trauma of critical disease diagnosis like—foot ulcers in diabetes, cancer, etc. It is estimated that 0.5% of any population globally requires prostheses, orthoses, and rehabilitation treatment. According to a study carried out in United States,

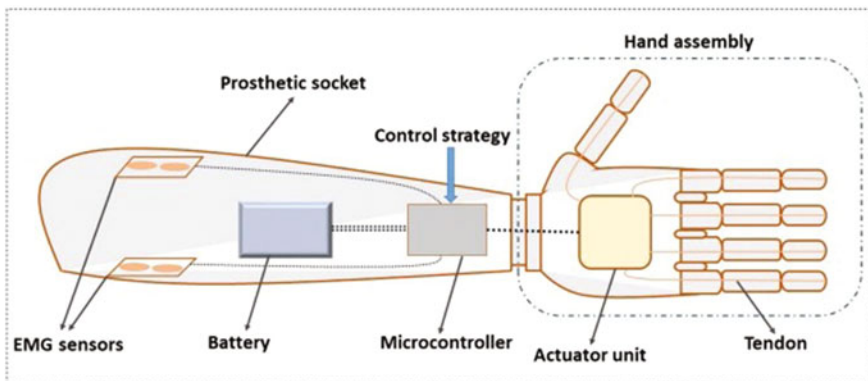


Fig. 3 Basic structure of a myoelectric prosthesis [13]

approximately 185,000 amputations occur each year and nearly 2 million people live with limb loss. It can be projected that this estimation can be doubled by the year 2050 [14]. Every year millions of people suffer from bone and muscle injury/fracture and various minor injury requires rehabilitation and restoring the functionality of affected organs. In 2013, Medicare-approved payment for nearly 2.4 million orthotic codes, 2.07 million prosthetic services, and 5.9 million pedorthic codes that accounted for more than \$734 million, \$664 million, and \$255 million, respectively [15]. These data indicate that the global demand for these sectors is very high and the industry is “a billion-dollar industry”.

One of the sectors that demand wide application of O&P is the orthopaedics field as it needs new ways to adapt orthoses to individuals for hand, leg, foot, ankle, shoulder, etc. In the case of fracture, rupture, or dislocation, the affected limb is immobilized with plaster in traditional methods. Pasting plaster generates discomfort to patients during daily work routine. Some patients suffer from odour generation, excessive itching and sweating, skin diseases, etc. due to the difficulty in maintaining proper hygiene.

Some traditional O&P devices are pre-fabricated and readily available. To fit in patient size, these devices are generally adjusted to meet the required fit. However, adjustment for fit is not possible in many cases and it leads to an increase in rehabilitation time and patient discomfort [16]. For example, in the case of limbs amputee, socket prosthetic is used to attach the amputated limb with prostheses. Traditionally, the fabrication of the socket involves several steps. Plaster casting of a socket is the common practice in prosthetics. In plaster casting, a negative cast is built using patient amputee organ (residue portion of leg/arm) and this negative pattern is used to cast a positive plaster pattern, which is further modified by Prosthetist. Subsequently, the prosthetic socket is made to fit on positive plaster cast [17]. During negative socket casting, if soft tissues (muscles) are pressed, it can generate the fitting error, which can lead to failure of prosthesis operation or discomfort during use. Also, traditional methods do not provide a cost-effective and rapid solution [18]. As the device design is artistic and created manually, a highly skilled workforce is required during manufacturing. Therefore, tailor-made accurate manufacturing techniques with the scientific approach are required in manufacturing O&P devices. Besides, O&P devices require tailor-made devices for each patient as the requirement changes with growing age, weight, size, functionality and updated rehabilitating necessity for each patient for his or her unique problem. These reasons engender requirements for every new change in patient's need. Further, lightweight O&P devices also helps to develop customised lattice designs helping with the designs having permeability for taking liquid medicine over the skin. Thus, it is necessary to deploy advanced manufacturing techniques like FFF for fabricating customized O&P devices [19].

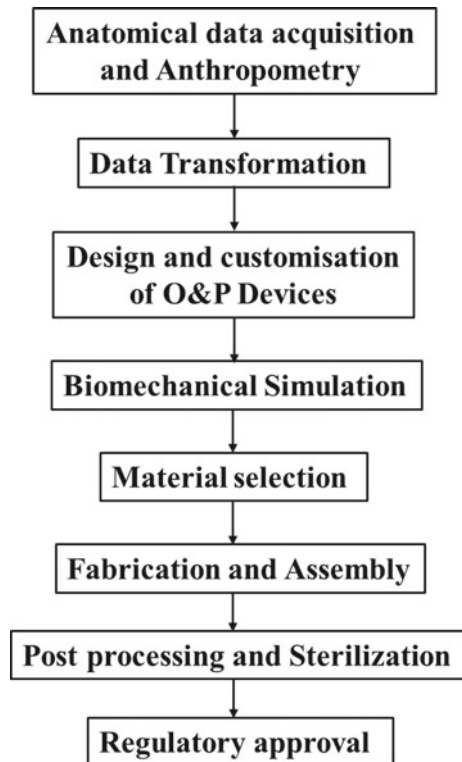
4 Stages in Manufacturing of O&P Devices

Medical applications require a combination of design and manufacturing tools to build customised medical O&P devices. The various steps involved in the development of O&P devices are shown in Fig. 4, which includes anatomical data acquisition and measurement, data transformation, design and customisation, biomechanical simulation, material selection, fabrication, post-processing, sterilization and regulatory approval. The different stages are explained in the following subsections.

4.1 Anatomical Data Acquisition and Measurement

The primary step in the manufacturing of O&P devices is the anatomical measurement of the affected area of the patient body. Standard anatomical measurements techniques utilise tools, like—measuring scale/tape, the goniometer is not sufficient to build all O&P devices as most of them require customization as per the

Fig. 4 Manufacturing steps for O&P devices



patient requirement. To achieve the above, advanced techniques, like—reverse engineering, 3D scanning and medical imaging technique (like—ultrasound, X-ray/MRI/PET scanning techniques) are used to develop a digital model of human anatomy [20].

3D scanning is the most commonly used technique for capturing external anatomy of an object in a non-contact manner. The technique collects data points (coordinate points) from the surface of scanned objects. These coordinates/data points are used to regenerate a digital model of the scanned object. These captured data points accurately describe the shape and size of a scan in terms of 3D digital model. This digital model can be utilised for different purposes, like—designing, modelling, analysis etc. The technique is fast, accurate and widely used in reverse engineering. The most widely used non-contact 3D scanning techniques are discussed below:

- (a) **Laser triangulation 3D scanning:** This method uses the principle of triangulation for measuring distance. It consists of a point or line beam of laser light and the laser source, object and detector form a triangle. The detector detects diffused reflections of laser beam impinging on a surface. This method capture data with high speed and accuracy and are suitable for capturing human anatomy.
 - (b) **Structured light 3D scanning:** Structured light 3D scanning works on trigonometric triangulation principle of distance measurement by projecting a pattern of light onto the object to scan. In this method, LCD projector or some other light source is set up along with two/more cameras/sensors at certain angles on either side. One or more cameras/sensors placed slightly offset from the projector, capture the shape of the pattern of light and calculate the distance of every point in its field of view. This data is used to create extremely precise digital models of the scanned object. The structured light used in the scanning process can be white or blue and the pattern of the light consists of a series of stripes and a matrix of dots or other shapes. Accuracy and quality depend on the colour of light used in projection, with blue light giving a better result.
 - (c) **Photogrammetry:** In photogrammetry methods, the object (for the 3D scan) is kept in a well-illuminated region. Several photographic images of the object are captured from various views with common reference points in each image. Photographic images are captured such that it includes all points of the object to be scanned. These captured images are processed using dedicated photogrammetry software to create a digital 3D model.
 - (d) **Laser pulse-based 3D scanning technology:** This type of scanner operates based on the time of flight of laser pulse. The time of flight of laser light is used to measure accurate co-ordinate position and generate 3D model data suitable for large object scan with a slower speed.
- For O&P devices manufacturing, laser triangulation and structured light 3D scanning are the most suitable and economic methods for capturing 3D geometry of the external body.

4.2 Data Transformation

The geometrical data collected from different scanning techniques are processed using dedicated software. The software are used to create a 3D model and convert the file formats to machine-specific formats, like—‘.STL’, ‘.OBJ’ or ‘.AMF’ etc. Generally, the software is used for rendering, cleaning, smoothing, editing and manipulating of generated 3D models. Materialise ‘Magics’, ‘Mimics suits with 3-matic’ and Geomagics of 3D-System are the most widely used commercial software for medical image data processing, and also for editing and repairing of ‘.stl’ file. Open/free-licence software like ‘Meshlab’, ‘Meshmixer’ (of Autodesk), ‘InVesalius’ are some alternative resource for editing, repairing, and file format conversion. After required modification, dimensional measurement is taken from the 3D model of the scanned human body part for creating the O&P device design as per the diagnosis requirements.

4.3 Design and Customization

To design a suitable O&P device, several factors should be considered including the diagnosis goal, biomechanical functionality, etc. In most common instances of a limb prosthesis, weight, muscle tonicity, skin conditions, residual limb stability and behaviour (i.e. activities and goal of a patient) of patients/users have an important role [16, 21]. Different rules and guidelines are used for different devices for a specific user. For instance, the foot care professional prescribes the custom foot orthosis design after finding the full clinical assessment, biomechanical examination, and gait analysis. Figure 5 presents the various steps involved in designing O&P devices.

In one of the published literature, Bahler presented the design principles and factors to be considered for lower limb orthotics. These rules are necessary during CAD modelling so that natural body axes and orthotic joint axes match as close as possible. A non-coinciding orthosis joint with natural joint creates shear stress that limits the natural motion. The report by Bahler also suggested various rule of thumb for heel, knee, hip and thigh related devices design [22].

Kinematics should be considered during the device design such that the effect of these devices on the other limb functionality should be minimal to achieve maximum comfort. Also, designing of O&P and bionic prosthesis devices is a multi-disciplinary problem. It requires the support of orthopaedician/orthopedist, CAD designer and material science expert along with specialists from electronics, signal processing, computational programming, etc. for designing bionic prostheses. Customisation of devices is based on measurements, diagnoses and service goals of a patient/user. In designing prosthesis devices of amputated limb socket, measurement with high accuracy is required as the part is critical since it directly comes in contact with residue limb. The socket shape and shell thickness is

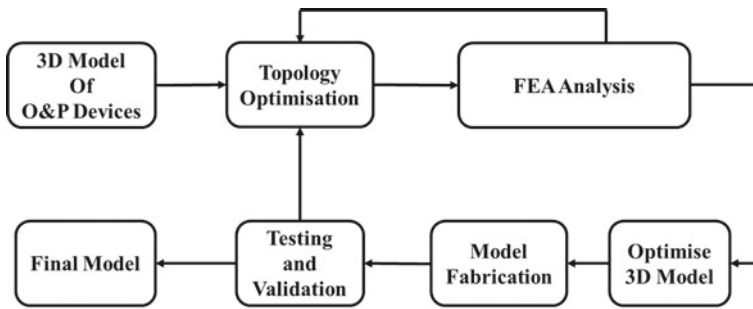


Fig. 5 Steps involved in designing O&P device

designed as per the input received from pressure analysis at different points and various proprietary software along with Socket Modelling Assistant (SMA) tools are deployed in complete design of the socket [23]. Various commercial CAD software like ‘Bioshape’, ‘Rodin4D NEO’, ‘PandoFit’, ‘Canfit’, ‘Cyborg Design Studio’, etc. are specially programmed for O&P devices modelling. These software packages provide specific tools like altering the volume scale parameters of positives and rapid device modelling. ‘Meshmixer’ along with ‘Tinkercad’ are widely used free software package for O&P device modelling. The design expert can edit positives (scanned external anatomy) and can generate 3D models of devices.

4.4 Biomechanical Simulation

Before production of devices it is important to simulate the device functionality and mechanical characteristics. CAE-CAD tools are generally used to simulate kinematics of devices. The biomechanical simulation will aid to select the suitable design and material. In order to perform effective reconstruction of muscles and bone model for biomechanical simulation, MRI and CT scan are used. Various Finite Element Analysis (FEA) software packages are implemented to simulate stress, deformation, wear of a prosthesis devices, etc. [24]. Non FEA/FEA based topology optimization software packages like ‘Magics’, ‘Netfabb’, ‘nTopology’, etc. help to enhance design aesthetics and reduce the weight of O&P device. Static and dynamic performances of O&P devices could be analysed and verified for different designs/materials to choose optimum design/materials. Otepergenov et al. performed FEA simulation for stress and deformation studies on three different device models of ankle foot orthosis. Based on the simulation results, decisions on altering the design and material of the device are taken before manufacturing. Nylon is used as the build material at high stress region, while PLA is used for other regions of the device [25]. Subsequently, in order to verify structural strength,

mechanical test can be executed, if necessary. These approaches help to reduce the time and material wastage and it will allow the fabrication of O&P devices with best comfort and faster rehabilitation.

4.5 *Material Selection*

Material selection is one of the important stages in the development of O&P devices. Static strength, hardness, fatigue strength, density, flexibility, compressibility, and resilience are the properties considered while selecting the material. It is also a function of the combination of physical and mechanical properties, which depends on the final objectives and application of O&P devices. A hard material can cause discomfort or be biomechanically injurious to users/patients. Traditionally, wood, leather, polymers, plaster, epoxy, steels and aluminum alloy are used for fabrication of O&P devices. However, low-density materials like—thermoplastics, polymer composites, and foams are now commonly used to manufacture O&P devices using FFF.

The most commonly used thermoplastic polymers for developing O&P devices are Acrylonitrile Butadiene styrene (ABS), Polylactic acid (PLA), polycarbonate (PC), Polyamide, Nylon etc. [26]. ABS is a polymer commonly used to produce prosthesis due to its toughness and strength. PLA is a biodegradable thermoplastic and is derived from natural resources like starch. PLA filament with antimicrobial copper/silver oxide nano-particle are also used in few studies for orthosis device making [27]. Carbon fibre composite filaments are a very good choice due to its high strength to weight ratio for orthosis devices, but clinical trials are necessary before the deployment as it should not seriously affect patients/users. In addition, it should be biocompatible in case of direct contact with human body. FFF can process multi-materials to develop devices with colour and texture similar to human skin for cosmetic appearance. Flexible thermoplastic elastomer or rubber like soft polymer is used at pressure points sections, wherever the devices interact with skin at high load. Soft rubber like thermoplastic elastomer made by combining plastic polymer with rubber polymers are also used in fabricating prosthetic sockets [28].

4.6 *Fabrication and Assembly*

The final design of O&P devices is converted to machine specific file format. Generally, machine build volume and building criterion decide the build orientation. Some of the building criteria that determine the build orientation are structural strength of builds, part quality, support structure, built time and build cost of part. After selecting the build-orientation, other data preparation steps, like—selection of support structures, process parameters, bed temperature etc. are carried

out as they critically influence the build quality. Figure 6 presents the typical image of an arm splint orthosis imported in CURA (a free software of Ultimaker) indicating the common process parameters and process conditions used in FFF, like—layer height, infill density, shell thickness, extruder and bed temperature, printing speed, etc.

The most common criterion for the selection of the build orientation and process parameters are provided below:

- (a) **Structural strength:** As FFF follows the layer-by-layer building, the components are generally anisotropic in nature i.e. the properties are direction dependent. Generally, the tensile strength of a component along the build direction (z-direction) is lower than the tensile strength of the component along other directions due to the layer wise stacking in FFF [29]. Fast cooling and low build chamber temperature causes improper adhesion between deposited layers, which causes lower tensile strength along the build direction. In some cases, low extruder temperature can also be a reason for weak bonding between layers. Shear strength parallel to build plane (i.e. x-y) is minimum for FFF built parts [30]. Thus, a fine tuned process parameter selection and build orientation selection is required to build O&P devices.
- (b) **Build quality:** Device quality comprises of various attributes, like—surface quality, dimensional accuracy and tolerances, smallest feature size, build distortion etc. There are several sources of errors associated with FFF process that deteriorate the build quality. It is possible to minimize them by systematic process parameter optimisation. Surface quality is a function of process parameters, build geometry and process conditions. Dimensional resolution and accuracy of features depend on the machine architecture, nozzle diameter, printing speed, material shrinkage and build orientation. Distortion or warping during the build depends on material shrinkage, bed temperature and chamber

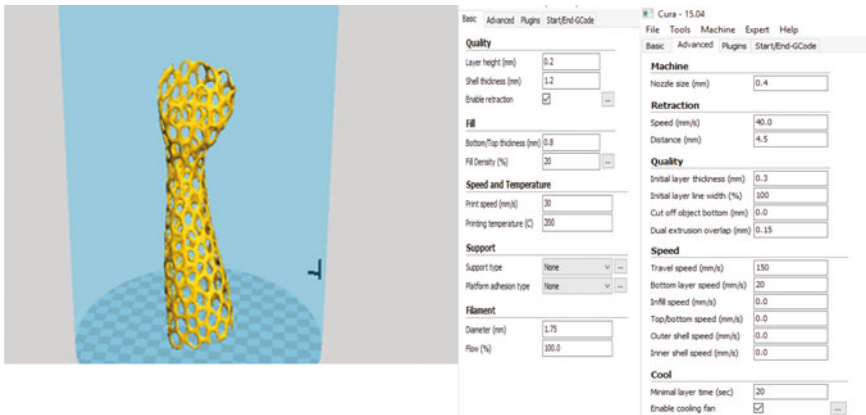


Fig. 6 Arm splint orthosis imported in CURA

temperature. For every new stock of material, calibration and optimisation is necessary to reduce the build error. Figure 7 shows the various possible sources of errors occurring in the O&P device built using FFF.

- (c) **Support structure:** Supports structures are necessary for building overhang sections of a part beyond a certain angle. Build preparation software and FFF machine software packages have several types of the inbuilt support library. Some of them provide control over the type of contact with part and density of supports. Treelike, linear and grid are the commonly used support types. Support structure volume depends on overhang support type, support density, and build orientation. Support structure volume affects the built time and directly affects the build cost. The selected build orientation should use only minimal supports and facilitate fabrication satisfactorily.
- (d) **Built time and cost:** Build time of O&P devices in FFF machine depends on the build and support volume i.e. the material utilised and FFF process parameters. Build time is directly related to build speed and build orientation. The typical cost of an O&P device depends on the total material volume used and the built time and thus, the optimized cost is a function of material and FFF machine utilization time. Maso et al. estimated total cost (C) of ankle-foot orthosis on three cost factors, (i) Cost associated equipment ownership/operation (E), (ii) Cost of material/filament used (M), (iii) Labour Cost (L) [19].

$$C = E + M + L \tag{1}$$

Thus, the process parameter and conditions should be selected in such a way that the optimal property/quality O&P devices are built as per the requirements. Generally, post-processing is required to achieve the final build quality requirements. In some cases, these devices are fabricated in parts due to either machine build volume limitations or requirement for multi-material devices, which attracts post-processing to assemble parts using suitable mechanical methods like fasteners, adhesives, cable, belt etc.

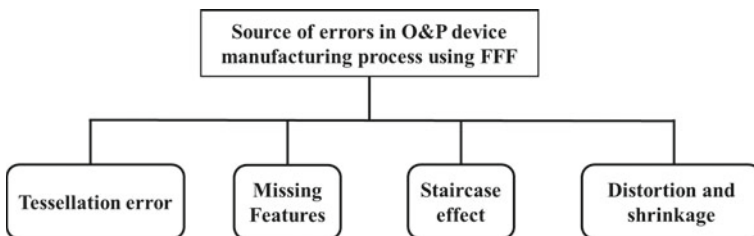


Fig. 7 Sources of errors in O&P device during FFF

4.7 *Post-processing and Sterilisation*

Post-processing is required for O&P devices built using FFF to make the device suitable for final deployment [31]. It involves removal of support structures; improving surface quality; enhancing aesthetic appearance; cleaning and sterilization. The most common post-processing techniques used to finish FFF produced parts are:

- (a) **Support structure removal:** As discussed earlier, the overhang portion of the parts requires a support structure. However, these structures should be removed before the final deployment. Supports used in FFF are of two types: soluble and insoluble. The most common soluble supports used in FFF are: Polyvinyl alcohol (PVA) used with PLA build material, High impact polystyrene (HIPS) used with ABS build material. PVA and HIPS are dissolved in water chemicals, like—D-limonene, respectively for support removal. Insoluble supports are generally built using a lower filling density as compared to build material to allow easy removal of the support. These supports are removed using mechanical force with the help of hand tools, like—X-acto knives, scrapper knives, and needle nose plier.
- (b) **Sanding and polishing:** Surface of FFF built devices are rough due to staircase effect and support contacts. Thus, surfaces should be smoothed using medium and fine-grit sandpaper. Wood and jewellery crafting tools (like Dremel tools) and polishing tools are commonly used to enhance the surface quality of builds.
- (c) **Acetone vapour smoothing:** Acetone smoothing is a popular technique for smoothing ABS. In this techniques, part/device is kept in an acetone vapour chamber, where acetone reacts with the outer layer of ABS and melt it. During this reaction, the surface roughness reduces and smooth and shiny surface is produced.
- (d) **Priming and painting:** Priming and painting help to enhance the aesthetic look as well as to protect the device from the environmental chemical effect and reduces the degradation of the material. Before priming and painting, smoothing of the surface is always recommended. It should be taken care that paint should have good adherence with device materials.
- (e) **Hydro dipping:** Hydrographic or hydro dipping is a relatively new technique for painting solids, which is applied to FFF built parts to make their appearance better. It provides the aesthetic and customised appearance to O&P devices.
- (f) **Joining and glueing:** Large size parts cannot be built with small volume FFF machines. Thus, 3D model of the device will be sectioned into several parts. These parts should be joined together so that the device can perform its intended function. This is generally carried out by using a good quality adhesive. The adhesive is selected by considering its compatibility with the part material. One of the examples is using acetone for joining ABS parts to obtain joints with very good strength.

- (g) **Cleaning and sterilization:** It is necessary before and during use regularly. Soap and water cleaning along with commonly used sterilization methods, like —exposure to hydrogen peroxide vapour, ultraviolet and gamma radiation, ethylene oxide etc. are used to sterilise the devices.

5 Standards and Regulatory Approval

There are various national and international guidelines for O&P device manufacturers. The World Health Organization has published new standards for Prosthetics and Orthotics in the year 2017. They published it in 2 parts (part 1 for standards and part 2 for implementation manual). It aims to ensure that prosthetic and orthotic services are people-centred and responsive to every individual's personal and environmental needs. There are 60 standards in the following four areas. (a) policy (b) products (c) personnel (d) provision [32]. *These standards include effective, efficient, high-quality service provision in a user-friendly, barrier-free safe clinical environment with health and safety regulations and training to personals* etc. The four areas are explained below:

- (a) **Policy:** This area shows the responsibility of member states to encourage the availability and use of O&P at an economical cost to users or the State. This section states that funding of O&P services should be considered when moving towards universal health coverage. Suitable financing should be provided to provide access to O&P specially through national health and/or social insurance.
- (b) **Products:** This area highlights that O&P products and working methods should be suitable for the situation in which the products are fabricated, fitted, used and funded. This segment suggests that O&P materials, components, tools etc. should be exempted from import taxes and customs for developing cheap and accessible products. It requests stakeholders to develop substitute and cheap products that are affordable, good quality and situation suitable.
- (c) **Personnel:** This area identifies the needs to be considered in planning, developing, and promoting professional recognition of the workforce. It describes the significance of training various types of O&P people to see national requirements and urges the announcement of State regulations to confirm that service users are safe from misconduct and poor-quality amenities. O&P clinicians should be accepted as autonomous health professionals with a different professional title, profile and job depiction. It states the significance of a multi-disciplinary team method in O&P, particularly for people with extreme or complex physical damages.
- (d) **Provision:** This area highlights the significance of people or user-centred O&P services. Users should be considered as equivalent participants of the treatment team and should be given the essential data to authorize them to make decisions regarding their care and final product selection. They must be consulted and

involved in policy development and planning, implementing, monitoring and evaluating services. The section keeps O&P services as an essential portion of health services, closely related to medical, surgical and rehabilitation services. It increases the significance of synchronization with other segments, like—labour, social welfare and education, for complete health and restoration outcomes.

ISO/TC 168 and related standards provide various rules including definition and nomenclature of O&P devices. ISO 10328:2016 includes structural testing of lower-limb prosthetics, prostheses requirements and their test methods [33]. Food and Drug Administration (FDA), USA have provisions for the approval of medical/clinical devices including O&P devices [34]. Biocompatibility of the material for making a device with various safety measures is required along with the clinical trial. Before the use of any O&P devices, patient/user should consult with trained and certified orthotist/prosthetist.

6 Challenges in FFF for Building External Medical Devices

Some of the major challenges associated with FFF of external medical devices are:

- (a) Although FFF is a promising method to build customised solutions for clinical aids, the parts have highly anisotropic structural property, which is difficult to predict and are highly dependent on the process parameters.
- (b) Limited accuracy and higher surface roughness limit the direct deployment of FFF built devices. Dimensional accuracy of FFF built parts are lower than conventionally machined components. Dimensional accuracy of FFF also depends on the machine architecture, hardware and shrinkage of the material. Generally, x-y resolution is limited by the stepper motor step angle and nozzle diameter, while z resolution is controlled by the layer height and lead screw movement. Higher surface roughness can be rectified by appropriate post-processing techniques.
- (c) The production speed of FFF is very slow as compared to injection moulding, CNC machining etc. Typically, it takes several hours to build a small part of 100 mm³, which includes time for data preparation also. The building time of an O&P device depends on the size, orientation and building parameters. Although large built time makes FFF unsuitable for very large-scale production, smaller lead-time as compared to injection moulding make it suitable for customised solutions.
- (d) Another challenge associated with FFF is material limitation. Presently, limited materials are available for medical aids. As biocompatibility is important, only specially designed and modified materials are suitable for O&P devices.

- (e) The higher cost of feedstock material (typically 3–4 times) as compared to commercially available polymers is another major challenge. Overall cost includes material, manpower, machine operation costs, that make it costlier. However, the technology is cost-effective for a customised solution as mould/die making for injection moulding for single part production is not justified.

7 Case Studies

7.1 Orthoses

7.1.1 Hybrid Model for the Customized Wrist Orthosis

Kim and Jeong used a hybrid manufacturing procedure that uses FFF and injection moulding technology to produce wrist orthosis that rectifies the difficulties of the plaster casts [35]. As compared to the wrist orthosis developed using FFF and 3D scanning, hybrid model considerably decreases the build time and cost. The major objective of using hybrid model is to separate the plastic cast into two parts: an inner structure and an outer cover. The inner structure is built using FFF that surrounds the skin, while the outer structure is attached to the inner structure for protecting the injured part from external forces. The outer cover is made in advance using injection moulding with three sizes as per the wrist sizes. The major steps involved in the hybrid process are as follows:

- The scanning of the fractured body part using photometric or laser 3D scanner.
- The obtained data from the scanning is processed using a surface modelling software for connecting surfaces, smoothing the surfaces, covering the holes etc.
- Subsequently, the surfaces are refined to the best possible way in a short span
- Outer cover is made by injection moulding using the patient wrist size
- Once the outer cover selection is completed, the 3D model of the outer cover is taken in a 3D modelling software to create the inner frame. The solid model of the inner frame is created using the skin geometry and 3D data of outer cover.
- After the design finalization of the inner cover, the 3D model of the inner cover is converted to STL file format and built using FFF.
- Post-processing is carried out by using support removal, polishing and painting.

It is confirmed from the test results that the new wrist orthosis has appropriate strength, good ventilation, and lightweight. The time cost for development is observed to be 1/3 of other methods. It is expected that the hybrid method can be an optimum solution for developing customized FFF built plastic orthosis for reduced manufacturing time and cost.

7.1.2 FFF Built Ankle-Foot Orthosis

FFF provides numerous benefits as compared to conventional manufacturing technologies, particularly when high-level customization is required. Maso and Casmo developed a procedure to develop a completely customized FFF built ankle-foot orthosis (AFO) for a 21-year-old woman with an injured ankle [19]. Figure 8a shows the pictorial view of the foot and its 3D model. AFO development started with geometric data acquisition from the patient's foot using photogrammetry. Subsequently, the acquired data is converted and imported to 3D modelling software. AFO model is developed parametrically around the foot mesh and optimized for resisting the predicted mechanical stresses using FEA. Lastly, the device is built using a FFF machine and tested on the patient. Figure 8b presents the photographic view of AFO developed using FFF. The geometrical correspondence between the AFO and the patient's foot is found to be excellent, which results in great comfort and improved medical functionality. The procedure has several advantages, like—versatility due to wide applicability, lower time and reduced costs. The use of FFF as a manufacturing technique allows the fabrication of extremely cheap devices without large investments.

7.2 *Prosthetics*

7.2.1 Prosthetic Hand for Children

This is a case study for kids suffering from unilateral congenital or traumatic limb reductions at the distal carpal or trans-metacarpal level or children with peromelic symbrachydactyly, or amniotic band syndrome resulting in complete loss of all digits. Kids suffering from congenital or traumatic hand reduction require unique prosthetics. Due to physical growth and psychosocial development, the required prosthetic size changes continuously. The conventional prosthetic is less suitable for kids due to weight and high cost. FFF fabricated rugged, lightweight, easily replaceable, the low-cost assistive hand is alternative to the conventional hand. Measurement of patient limbs is used for customised fabrication. A cyborg hand-design is shown in Fig. 9 is selected for prosthesis and fabricated using FFF [36]. During assembly, additional parts like elastic thread, nylon line, screw/bolts and Velcro are used. A custom orthoplast socket is bonded to the inside of the palm component of orthoses with hot glue. It gives better comfort along with efficient force transmission. It took 15–20 h to fabricate the hand prosthesis. Thus, FFF can produce low-cost lightweight, durable, and easily changeable prostheses device that can be customised for an individual child's growth and changing requirements [36]. The technology has an incredible ability to deliver effective customised solutions in hand prosthesis fabrication. The success of the above depends on the cooperative work of engineers, clinicians, patients/users and their families.

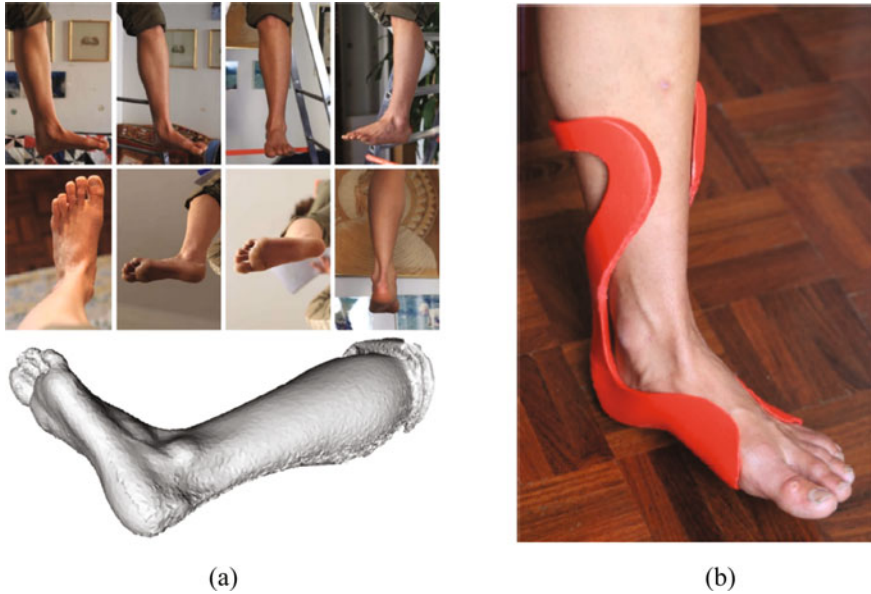


Fig. 8 Photographs of **a** actual foot and developed model, **b** developed AFO [19]

7.2.2 Prosthetic Glove for Hand Rehabilitation

Anirudh et al. developed a prosthetic glove (refer Fig. 10) for physiotherapy of patients [37]. Patients/users consider numerous factors, like—level of amputation, functionality, cosmetic appearance and cost of the device while choosing a prosthetic glove. The aim of this prosthesis glove is physiotherapy training of patients to perform regular exercises at home for curing the physical dysfunctions. This prosthetic prototype helps in rehabilitation to conduct the flexion and extension in fingers movement. Three kinds of designs; half ring, full ring and phalange design are commonly used in glove prosthesis. These designs are modelled and analysed using FEA software package for selecting the best one. Half ring based prosthetic glove is found to be most suitable for Arduino controlled motor. In this, the motion of the links and forces are transmitted through the threads of good tensile strength [37]. Prosthetic glove parts are fabricated on FFF machine using PLA material. The individual servo motor is provided for fingers and thumb movement.

8 Research Trends

Customisation in manufacturing of O&P devices in the last decade is significant. These devices are more comfortable, lightweight with improved functionality and have improved service period with better cosmetic appearance. The combination of



Fig. 9 Prosthetic hand for children [36]

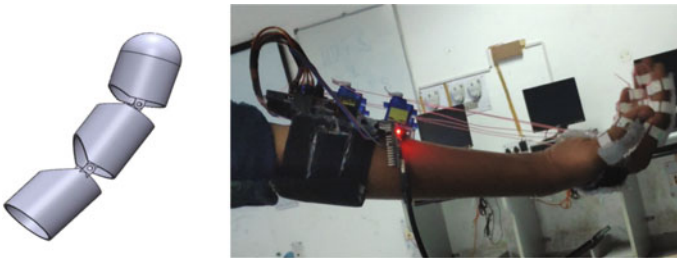


Fig. 10 Prosthetic glove for hand rehabilitation [37]

advanced manufacturing technologies such as FFF and data acquisition methods such as 3D scanning, medical imaging etc. are improving the way O&P devices are being built by improving the speed of fabrication along with a reduced cost. Advanced CAD-CAM and CAE tools aid to simulate the devices with aesthetic and customised designs in static and dynamic conditions [25]. Further, advanced gait dynamics studies are also utilised for improving the designs for providing better functionality and reducing rehabilitation period [38].

Cloud-based manufacturing is another approach in which the patient can consult with doctors and experts using web [15]. Anatomy of a patient can be captured at his/her living place using a hand scanner. Orthotist/prosthetist along with a designer

can model the required device on cloud-based platforms and manufacturing of the device can be done at AM hub near to patient or by the using AM system available with them. It reduces logistic costs, enhances the quality and improves the customisation. Research is underway to develop advanced materials with enhanced structural strength and low density (biocompatible carbon fibre/graphene composite polymers). The use of devices with shape memory actuators, embedded sensors with neuromuscular control along with advanced myoelectric bionic prosthesis technology are continuously evolving in the research field. In this section, some of the latest advancements in the field of O&P devices are discussed.

8.1 Orthosis Using Smart Memory Alloys and FFF

Toth et al. developed the prototype of a smart ‘powered’ orthosis for stroke patients with spastic hand paralysis by using AM technology [39]. The team used FFF fabricated parts along with nitinol shape memory alloy (SMA) for post-stroke patients suffered from spastic hand paralysis. Orthosis device is made of two parts; thermoplastic polyurethane (TPU) attached with SMA plate and a polyamide passive frame covering the finger parts and the forearm part (Fig. 11). The major advantage derived from this device is that the SMA part provides motion of orthosis without stepper motors/actuators and can be controlled by ‘Arduino’ based controller. These prototypes used on six patients showed significant recovery in functionality during rehabilitation [39]. The lightweight design of the smart orthosis is cost-effective and suitable for spastich and paralysis patient for home use.

8.2 Antibacterial Prostheses Using FFF

The use of antibacterial and antimicrobial polymer filaments is a promising solution to fabricate medical devices generally subjected to bacterial development, like—

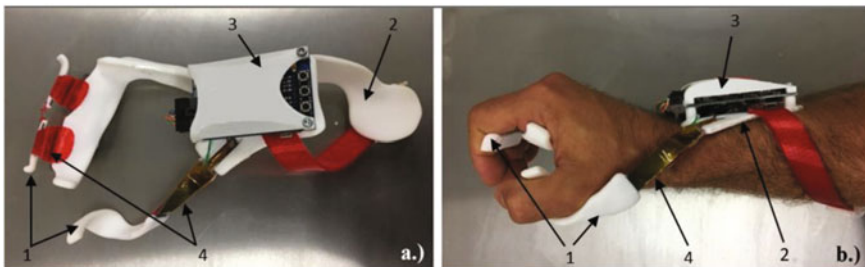


Fig. 11 SMA based orthosis **a** prototype, **b** application onto a volunteer’s hand. The various parts are: 1—Finger arts; 2—Forearm part; 3—control unit (3); 4—active SMA part [39]

O&P devices. Zuniga developed prosthesis device using antibacterial material (PLACTIVE™—PLA with antibacterial copper nanoparticles). Finger prostheses fabricated using FFF are tested on two adults suffering with left index finger amputations [27]. Box and Block test performance of the patient with prosthesis confirmed significant enhancement in the functionality. Patient satisfaction was assessed using the Quebec User Evaluation of Satisfaction with assistive technology (QUEST 2.0). Bacterial analysis of the prostheses was performed by two independent laboratories against *Staphylococcus aureus* and *Escherichia coli* (ISO 22196). The bacterial analysis revealed that PLACTIVE™ with 1% copper nanoparticles additives was found to be 99.99% effective against *Staphylococcus aureus* and *Escherichia coli*.

9 Conclusions

Orthoses and Prostheses (O&P) are external medical devices that are used for correction or restoration of the functionality of organs, and replacement of natural body parts lost or damaged due to illness or injury, respectively. Traditionally, O&P devices are handcrafted, where the quality is primarily dependent on the expertise of orthotist. One of the major limitations is the discomfort and pain suffered by the patient due to inefficient design and lack of precise fit. FFF is an advanced manufacturing platform that can potentially change the way the O&P devices are designed and manufactured. FFF along with the 3D scanning techniques aids to develop most suitable O&P devices for the patient. The various steps involved in the development of O&P devices using FFF are anatomical data acquisition and measurement, data transformation, design and customisation, biomechanical simulation, material selection, fabrication, post-processing, sterilization and regulatory approval. However, O&P devices built using FFF technique suffer from various issues such as anisotropy, dimensional inaccuracy, lower build rate, availability of limited materials, etc. Efforts are being made by the researchers to improve the process of building high-quality devices. Latest advancements indicate the deployment of shape memory alloy-based device and devices with antibacterial material. With further advancements in design tools and manufacturing capabilities, the wide adoption of FFF built O&P devices are possible.

Acknowledgements K. Dileep and A. N. Jinoop acknowledge the financial support of Raja Ramanna Centre for Advanced Technology (RRCAT), Department of Atomic Energy, Government of India and Homi Bhabha National Institute, Mumbai. A. C. Paul acknowledges the constant encouragement from Prof. Sudheer Reddy, Head and other faculty members of the Department of Mechanical Engineering, Nitte Meenakshi Institute of Technology, Bengaluru. The authors express their sincere gratitude to Mr. Debashis Das, Director RRCAT for his constant support and encouragement. Thanks are due to Mr. S. V. Nakhe, Director—Laser Group for constant encouragement in this evolving program at RRCAT. The authors are also thankful to our colleagues at Laser Additive Manufacturing Laboratory for their support.

References

1. Guo N, Leu MC (2013) Additive manufacturing: technology, applications and research needs. *Front Mech Eng* 8:215–243. <https://doi.org/10.1007/s11465-013-0248-8>
2. Vyavahare S, Teraiya S, Panghal D, Kumar S (2020) Fused deposition modelling: a review. *Rapid Prototyp J* 26:176–201
3. Tan DK, Maniruzzaman M, Nokhodchi A (2018) Advanced pharmaceutical applications of hot-melt extrusion coupled with fused deposition modelling (FDM) 3D printing for personalised drug delivery. *Pharmaceutics* 10:203. <https://doi.org/10.3390/pharmaceutics10040203>
4. Yoo TS, Morris J, Chen DT, Burgess J, Richardson AC (2001) Template guided intervention: interactive visualization and design for medical fused deposition models. *Interact Med Image Vis Anal* 18:45–48
5. Hsu JD, Michael J, Fisk J (2008) *AAOS Atlas of orthoses and assistive devices*, 4th edn. Elsevier Health Sciences, Pennsylvania
6. Belokar RM, Banga HK, Kumar R (2017) A novel approach for ankle foot orthosis developed by three dimensional technologies. In: *IOP conference series: materials science and engineering*. IOP Publishing, p 12030
7. Kotov A (1945) Osteoplastic re-amputation of thigh. *Br Med J* 1:179–180
8. McGimpsey G, Bradford TC (2008) *Limb prosthetics services and devices*
9. Nachtigall W, Wissler A (2014) *Bionics by Examples: 250 scenarios from classical to modern times*, 1st edn. Springer International Publishing, Switzerland
10. Clement RGE, Bugler KE, Oliver CW (2011) Bionic prosthetic hands: a review of present technology and future aspirations. *Surg* 9:336–340
11. Chelle P, Mathijssen G, Wang Q, Vanderborcht B, Lefeber D (2014) Advances in propulsive bionic feet and their actuation principles. *Adv Mech Eng* 6:984046
12. Hero Arm—an affordable, advanced and intuitive bionic arm. <https://openbionics.com/hero-arm/>. Accessed 4 Oct 2020
13. Prakash A, Sahi AK, Sharma N, Sharma S (2020) Force myography controlled multifunctional hand prosthesis for upper-limb amputees. *Biomed Signal Process Control* 62:102122. <https://doi.org/10.1016/j.bspc.2020.102122>
14. Kozak LJOM (1998) *Ambulatory and inpatient procedures in the United States, 1995*. United States Department of Health and Human Services, Maryland
15. Shih A, Park DW, Yang YY, Chisena R, Wu D (2017) Cloud-based design and additive manufacturing of custom orthoses. *Proc CIRP* 63:156–160. <https://doi.org/10.1016/j.procir.2017.03.355>
16. Chen RK, Jin Y, Wensman J, Shih A (2016) Additive manufacturing of custom orthoses and prostheses—a review. *Addit Manuf* 12:77–89. <https://doi.org/10.1016/j.addma.2016.04.002>
17. Ng P, Goh JCH (2002) Prosthetic sockets fabrication using rapid prototyping technology. *Rapid Prototyp J* 8:53–59. <https://doi.org/10.1108/13552540210413310>
18. Jin Y, Plott J, Chen R, Wensman J, Shih A (2015) Additive manufacturing of custom orthoses and prostheses—a review. *Proc CIRP* 36:199–204. <https://doi.org/10.1016/j.procir.2015.02.125>
19. Dal Maso A, Cosmi F (2019) 3D-printed ankle-foot orthosis: a design method. *Mater Today Proc* 12:252–261. <https://doi.org/10.1016/j.matpr.2019.03.122>
20. Comey J, Hieu LC, Zlatov N, Vander Sloten J, Bohez E, Khanh L, Binh PH, Oris P, Toshev Y (2005) Medical rapid prototyping applications and methods. *Assem Autom* 25:284–292
21. Supan TJ (2019) Principles of fabrication. In: Webster J, Douglas M (eds) *Atlas of orthoses and assistive devices*, 5th edn. Elsevier, Pennsylvania, pp 42–48
22. Bahler A (1982) Principles of design for lower-limb orthotics. *Orthot Prosthet* 36:33–39
23. Colombo G, Facoetti G, Gabbadini S, Rizzi C (2013) Socket modelling assistant for prosthesis design. *Int J Comput Aided Eng Technol* 8:216–241

24. Debta S, Kumar K (2018) Static structural analysis of a powered ankle foot prosthesis mechanism. *Mater Today Proc* 5:11616–11621
25. Otepbergenov T, Smagulov Z, Abilgazyev A (2020) Numerical and experimental analysis of the 3D printed multi-material ankle-foot orthosis numerical and experimental analysis of the 3D printed multi- material ankle-foot orthosis. *J Phys Conf Ser* 1510:012012. <https://doi.org/10.1088/1742-6596/1510/1/012012>
26. Barrios-Muriel J, Romero-Sánchez F, Alonso-Sánchez FJ, Rodríguez Salgado D (2020) Advances in orthotic and prosthetic manufacturing: a technology review. *Materials (Basel)* 13:295
27. Zuniga JM (2018) 3D printed antibacterial prostheses. *Appl Sci* 8:1–10. <https://doi.org/10.3390/app8091651>
28. Devine DM (2019) *Polymer-based additive manufacturing: biomedical applications*. Springer Nature, Switzerland
29. Rajpurohit SR, Dave HK (2018) Effect of process parameters on tensile strength of FDM printed PLA part. *Rapid Prototyp J* 24:1317–1324. <https://doi.org/10.1108/RPJ-06-2017-0134>
30. Samykano M, Selvamani SK, Kadirgama K, Ngui WK, Kanagaraj G, Sudhakar K (2019) Mechanical property of FDM printed ABS: influence of printing parameters. *Int J Adv Manuf Technol* 102:2779–2796. <https://doi.org/10.1007/s00170-019-03313-0>
31. Ahn S-H, Lee CS, Jeong W (2004) Development of translucent FDM parts by post-processing. *Rapid Prototyp J* 10:218–224. <https://doi.org/10.1108/13552540410551333>
32. World Health Organization (2017) *Standards for prosthetics and orthotics*
33. International Organization for Standardization (2016) *ISO 10328:2016(en) Prosthetics—structural testing of lower-limb prostheses—requirements and test methods*. Switzerland
34. Larsen J (2004) Orthotic treatment protocols for plagiocephaly. *J Prosthet Orthot* 16:31–34. <https://doi.org/10.1097/00008526-200410001-00010>
35. Kim H, Jeong S (2015) Case study: Hybrid model for the customized wrist orthosis using 3D printing. *J Mech Sci Technol* 29:5151–5156
36. Burn MB, Ta A, Gogola GR (2016) Three-dimensional printing of prosthetic hands for children. *J Hand Surg Am* 41:e103–e109. <https://doi.org/10.1016/j.jhsa.2016.02.008>
37. Sareen A, Singh A, Sinha A, Arya A, Arya A, Sapra G, Kumar R, Kumar P, Singh D (2020) Design and fabrication of prosthetic glove for hand rehabilitation. *Mater Today Proc* 28:1612–1615. <https://doi.org/10.1016/j.matpr.2020.04.849>
38. Rigney SM, Simmons A, Kark L (2016) A prosthesis-specific multi-link segment model of lower-limb amputee sprinting. *J Biomech* 49:3185–3193. <https://doi.org/10.1016/j.jbiomech.2016.07.039>
39. Toth L, Schiffer A, Nyitrai M, Pentek A, Maroti P (2020) Developing an anti-spastic orthosis for daily home-use of stroke patients using smart memory alloys and 3D printing technologies. *Mater Des* 195:109029. <https://doi.org/10.1016/j.matdes.2020.109029>

Potential Advanced Drug Delivery Systems Based on Hydrogels in 3D Printing Technology for Cancer Treatment



Agnieszka M. Jankowska , Magdalena B. Łabowska ,
Izabela Michalak , Patrycja Szymczyk-Ziółkowska ,
Julita Kulbacka , and Jerzy Detyna 

Abstract Cancer is a significant public health problem worldwide, therefore it is important to find appropriate treatment methods. In addition to surgical treatment, chemotherapy, and radiotherapy, drugs are increasingly employed. Drugs and their delivery systems have a significant role in the treatment of cancer, hydrogels find wide application there. Hydrogels may easily be modifiable by physicochemical reactions in order to obtain the desired functional properties and porous structure adapted to the appropriate application. Properties like solubility and degradation, make hydrogels suitable for use as drug in drug delivery systems (DDS). Properly selected methods of drug delivery minimize side effects and maximize drug efficacy. Three-dimensional (3D) printing may replace traditional fabrication tech-

A. M. Jankowska · M. B. Łabowska · J. Detyna (✉)

Department of Mechanics, Materials and Biomedical Engineering, Faculty of Mechanical Engineering, Wrocław University of Science and Technology, Smoluchowskiego 25, 50-372 Wrocław, Poland
e-mail: jerzy.detyna@pwr.edu.pl

A. M. Jankowska
e-mail: agnieszka.jankowska@pwr.edu.pl

M. B. Łabowska
e-mail: magdalena.labowska@pwr.edu.pl

I. Michalak
Department of Advanced Material Technologies, Faculty of Chemistry, Wrocław University of Science and Technology, Smoluchowskiego 25, 50-372 Wrocław, Poland
e-mail: izabela.michalak@pwr.edu.pl

P. Szymczyk-Ziółkowska
Faculty of Mechanical Engineering, Centre for Advanced Manufacturing Technologies, Wrocław University of Science and Technology, Łukasiewicza 5, 50-371 Wrocław, Poland
e-mail: patrycja.e.szymczyk@pwr.edu.pl

J. Kulbacka
Department of Molecular and Cellular Biology, Faculty of Pharmacy, Wrocław Medical University, Borowska 211A, 50-367 Wrocław, Poland
e-mail: julita.kulbacka@umed.wroc.pl

niques as it has an ability to fabricate complex shapes that can meet individual patient needs, improve compliance and availability, using a wide variety of materials. The new 3D printing inks based on alginate or methylcellulose are successfully used to produce high-quality 3D structures. This chapter describes the problem of cancerous diseases, as well as an overview of treatment methods, especially with a focus on hydrogel drug carriers. Several selected routes of administration of hydrogel carriers were presented. The chapter also contains information on the materials used to create the drug carrier, especially in additive technologies.

1 Introduction

Polymeric hydrogels are three-dimensionally cross-linked networks made up of hydrophilic macromolecules, which are able to retain large amounts of an aqueous solution. The liquid absorption capacity of these viscoelastic materials depends on the number of hydrophilic groups in the polymer chains, such as amino, carboxyl, and hydroxyl groups. Thus, the liquid content of hydrogels can vary between 10% to thousands times of their dry weight [1–4]. Polymeric materials intended for hydrogel production can be obtained from natural (e.g. alginate, collagen, chitosan, fibrin, hyaluronic acid) and synthetic sources (e.g. poly(acrylamide), poly(ethylene glycol) diacrylate, poly(vinyl alcohol)) or as a combination of both. The process of hydrogel production can be accomplished by chemical, physical, or radiation cross-linking methods, but also grafting polymerization [4–6]. Obtained hydrogels can be easily modified by physio-chemical reactions to achieve porous structure (i.e., macroporous, microporous, nanoporous) and desired mechanical properties customized for the relevant applications. However, the strength capabilities of hydrogels are limited due to their typically soft nature. They are usually described as a highly flexible, but low strength material [4, 7]. Hydrogels allow the controlled and targeted release of drugs (the hydrogel is formed after the injection and holds the drug for a longer period) in response to various triggers and therefore become attractive for targeted drug therapy [8].

Cancer is a major health problem worldwide and more than half of all cases and deaths are caused by potentially preventable risk factors (such as smoking, unhealthy diet, high alcohol consumption, lack of physical activity and excess weight). The most commonly diagnosed cancers were dominated by lung, breast, colorectal, prostate, skin cancer (non-melanoma), stomach [9]. The most common causes of cancer death are cancers of lung, colorectal, stomach, liver, and breast [10]. Cancer might be treated in three stages: primary treatment [11], adjuvant treatment [12] and palliative treatment [13]. The first two should cause complete removal of the cancer cells and reduce the chance of cancer recurrence. Palliative treatment, often used simultaneously with primary and adjuvant treatment, may help relieve side effects of treatment and cancer symptoms and relieve pain. Cancer treatment methods are surgery [14], chemotherapy [12], radiation therapy [15], bone marrow transplant [16], immunotherapy [17], hormone therapy [18], targeted

drug therapy [19], cryoablation [20], radiofrequency ablation [21], nanotechnology [22]. Broader application of existing cancer treatment methods and clinical trials would undoubtedly accelerate progress in the struggle against cancer [23]. Most of the chemotherapeutic agents applied in the cancer treatment are cytotoxic and lead to numerous side effects (e.g. nausea, hair loss, bone marrow suppression and loss of appetite) [24, 25]. Majority of drugs spread rapidly after implementation, causing drug levels to increase and decrease rapidly, while targeted drug delivery maximizes the effectiveness of the drug, releasing it slowly based on its physiological condition. The targeted drug delivery to a specific location minimizes side effects and maximizes drug efficacy, while hydrogels fulfill such requirements, therefore they are used in such systems [26].

Unique biological properties such as biocompatibility, biodegradability, bio-functionality make hydrogels widely applicable in the biomedical field. Hydrogels exhibit the ability to mimic the nature of most soft tissues. Their structure enables easy transport of oxygen, nutrients and metabolic products. Thus, they are an attractive material used in tissue engineering to create a synthetic extracellular matrix (ECM) that can be applied for cell cultures [27, 28]. The soft nature of the hydrogel and its lack of toxicity make it suitable for contact with sensitive tissues and organs, such as wounds, organs, eyeballs. Therefore they are used for production, inter alia, wound dressings that are capable of absorbing huge amounts of exudate from the wound. Moreover, due to their form, they are able to relieve pain, especially during their removal and even accelerate the process of healing [29, 30]. Transparency, flexibility, high hydration and permeability make hydrogels ideal materials for contact lenses [31]. All of the above-mentioned applications can also be combined with active substances to create drug delivery systems [3, 32, 33]. The design of solubility and degradation of hydrogels by hydrolytic, enzymatic or environmental factors such as temperature, pH, electric field, makes drug carriers suitable for use in the majority of drug administration. Drug delivery systems can therefore be applied for instance by transdermal, ocular, oral cavity, gastrointestinal tract, vaginal route and rectal routes; whereas drugs employed in them may be successfully manufactured by three-dimensional printing technology [6, 34, 35].

Additive manufacturing technologies (AM), commonly known as 3D printing, have gained wide interest as they offer significant benefits in the medical sector by enabling the personalization of products [36]. The manufacturing capabilities of these methods allow for production of three-dimensional porous structures (scaffolds), that promote faster tissue regeneration, performing a support function until complete recovery. Degrading polymeric scaffolds provide mechanical support pending the replacement of new tissue [37, 38]. Technological advances can lead to the design and manufacture of 3D formulations with specific architecture and dosages, enabling targeted drug delivery [39]. This technology allows releasing the drug in a regulated manner by controlling the geometry of the structure [40]. An additional advantage of these methods is the possibility of simultaneous use of several biomaterials in one process, as well as shortening the production time by appropriate selection of spatial structure [41]. The 3D-printed structures with incorporated drugs can also be used after surgical resection for local treatment of

different types of cancers (prostate, colon, uterus and breast cancer in women diagnosed at an early regional stage) and for palliative treatment (alleviating treatment side effects and improving the quality of life of patients suffering from late-stage cancer) [42]. Despite surgical resection, the tumour leaves undetected microscopic cancer cells that can lead to cancer recurrence. The use of such 3D structures in that case allows for local treatment to eliminate the surgically unrecovered cells [40]. Inks used for 3D printing have to be suitable for a range of key requirements for processing with 3D printing machines. Printability should be determined by rheological properties, ink consistency measurements and sample dimensions and predicted mechanical properties [43].

The present chapter provides information about cancer morbidity in recent years, possible reasons of patient's disease, as well as an overview of current treatment methods. One of them is the application of 3D printing technology with biomaterials such as hydrogels in order to propose advanced drug delivery systems for cancer treatment. A special attention was paid to hydrogels—the most commonly used materials for the production of drug carriers for cancer therapy. These materials are easily processed on bioplotters and enable the production of personalized medications by selecting the appropriate dose adjusted to the patient's needs.

2 Selected Cancers and Treatment Methods

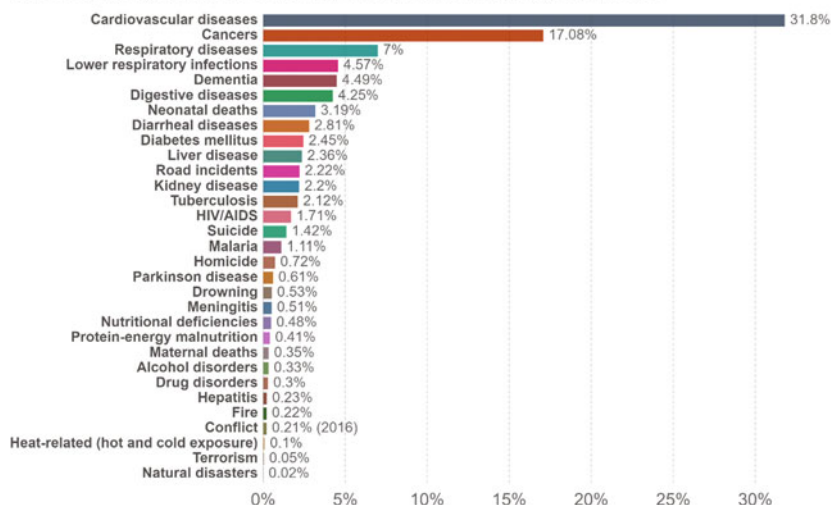
Cancers are malignant neoplasms (carcinoma and sarcoma) that are caused by abnormal and uncontrolled cell division and invade and destroy the surrounding tissue [44]. Cancer is considered not as a disease-focused solely on the basic population of cancer cells, but rather as a condition characterized by a fundamental imbalance in the entire cellular environment [45]. Every second person in their life develops some form of cancer. There are more than 200 different types of cancer, and each is diagnosed and treated in a specific way. The symptoms and signs of cancer depend on the specific type and severity of the disease. Symptoms that may indicate cancer that is not very specific include pain, fatigue, weight loss, unusual bleeding, fever, change in bowel or bladder function, skin lesions, persistent coughing, hoarseness, or voice change [46].

2.1 *Cancer in Statistics*

Every sixth death worldwide is caused by cancer, making it the second leading reason of death (Fig. 1), right after death in case of cardiovascular diseases. It is estimated that 9.6 million people died from various forms of cancer in 2018 [47]. This section presents cancer statistics worldwide. There is a large variation between different geographical areas due to varying exposure to risk factors, the screening

Share of deaths by cause, World, 2017

Data refers to the specific cause of death, which is distinguished from risk factors for death, such as air pollution, diet and other lifestyle factors. This is shown by cause of death as the percentage of total deaths.



Source: IHME, Global Burden of Disease

CC BY

Fig. 1 Causes of death worldwide [49]

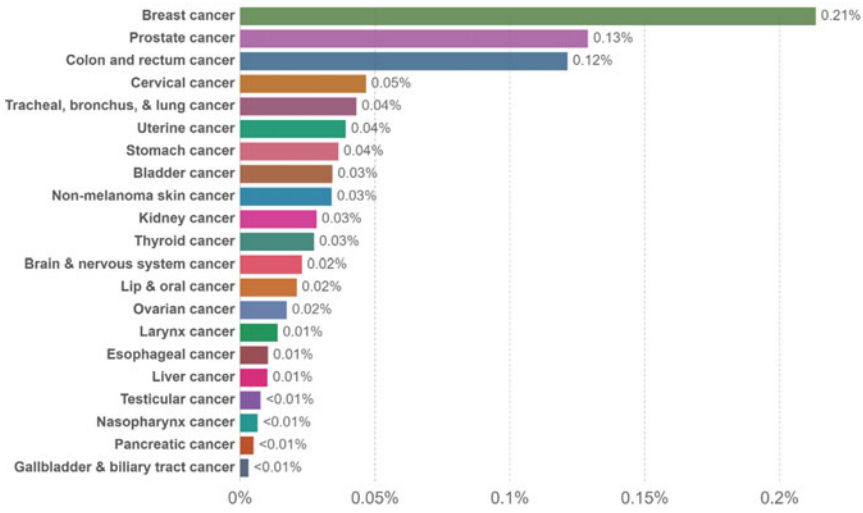
application as well as access to appropriate treatment services (a large part of the differences can be attributed to socioeconomic status) [48].

Breast cancer is the most commonly diagnosed cancer and the main cause of death from cancer (among women), followed by colorectal, cervical and lung cancer (in terms of incidence) and vice versa (in terms of mortality). However, it varies significantly by country or region and depends on the degree of economic development and related social and lifestyle factors [48]. The share of population with cancer is shown in Fig. 2.

The total number of deaths from cancer, by its type, in 2017 is shown in Fig. 3. Total number of deaths is decreasing, both among men and women for all major racial and ethnic groups. Rates have decreased for males and females for lung, colorectal, breast and prostate cancer. In addition, mortality rates increased for liver cancer, pancreatic and brain cancer in men and liver and uterine cancer in women. Overall incidence rates of lung and colorectal cancer have decreased in men but have stabilized in women, while rates have increased for liver, myeloma, melanoma, oral cavity and thyroid cancer in both men and women, and pancreatic cancer in men. Survival rate increased significantly overall and for both early and late-stage diseases, and survival differs statistically significantly by race/ethnicity and state [50].

It is widely acknowledged that many cancers may be explained by a two-stage process, initiation by one or a series of mutations and blood diseases. Replication of the mistake may proceed at different rates in a variety of tissues [51]. Mutations are

Share of population with cancer, World, 2017



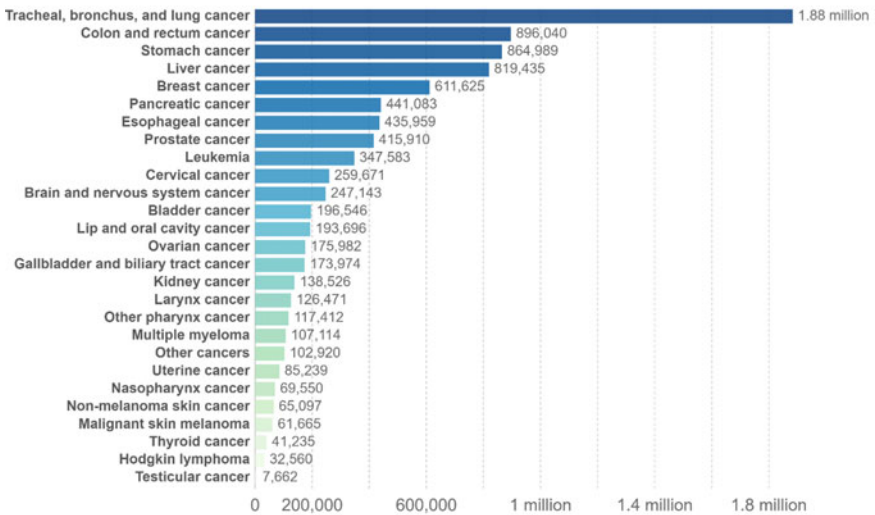
Source: IHME, Global Burden of Disease
 Note: To allow comparisons between countries and over time this metric is age-standardized.
 OurWorldInData.org/cancer • CC BY

Fig. 2 The population contribution with cancer [49]

Cancer deaths by type, World, 2017



Total annual number of deaths from cancers across all ages and both sexes, broken down by cancer type.



Source: IHME, Global Burden of Disease (GBD) CC BY

Fig. 3 Total number of deaths from cancer by its type in 2017 worldwide [49]

the result of the interaction between genetic factors and external agents: physical carcinogens (e.g. ultraviolet and ionizing radiation), chemical carcinogens (e.g. asbestos, components of tobacco smoke, aflatoxin, and heavy metals such as arsenic) and biological carcinogens (e.g. infections from certain viruses, bacteria, or parasites) [52]. However, most cancers are caused by many overlapping factors, so the combined effect of individual factors can be more than 100% [53]. Smoking is the biggest risk factor for lung cancer, the trend for lung cancer follows the trend for smoking with a delay of about 20 years [54]. Lung cancer mortality trends are due to the trend in smoking as the percentage of smokers decreases, and lung cancer mortality rates also fall [55]. Mortality from lung cancer peaked in many countries in the 20th century (the United States in the 1980s, Spain in the 1990s). In 2017, about 7 million people worldwide died prematurely from smoking [56].

2.2 *Cancer Types*

Types of cancer are usually called for organs or tissues in which the cancer is formed (e.g. lung cancer from lung cells and brain cancer from brain cells) and their distribution in the worldwide population was shown in the previous subsection (Fig. 2). Cancer can also be classified by the type of cell that originates from it. This division allows to differentiate such types of cancers as carcinoma, sarcoma, leukemia, lymphoma, multiple myeloma, melanoma, brain and spinal cord tumors and other rare types of cancers. The following subsections describe cancer types distinguished by cell type [57].

2.2.1 **Carcinoma**

The most common type of cancer is carcinoma. It is formed from epithelial cells, the cells that cover the internal and external surface of the body. Carcinoma types can be divided into: adenocarcinoma, basal cell carcinoma, spiny cell carcinoma and transitional cell carcinoma. Adenocarcinoma occurs in epithelial cells that produce fluids or mucus (most cancers of the breast, colon and prostate are adenocarcinomas) [58]. Basal cell carcinoma occurs in the lower or basal layer of the epidermis, which is the outer skin layer [59]. Squamous cell carcinoma is formed in squamous cells, which are located just below the outer surface of the skin and in many organs (such as stomach, lungs, intestines, kidneys and bladder) [60]. Transitional cell carcinoma is formed in the transitional epithelium (urothelium), which is located e.g. in the linings of the bladder, ureters and kidney parts (renal pelvis) [61].

2.2.2 Sarcoma

Sarcomas represent a heterogeneous group of mesenchymal cancers. They can be divided into two categories: soft tissue sarcoma and primary bone sarcoma. Sarcoma forms in bone and soft tissues of the body (muscles, tendons, ligaments, fat, blood vessels, lymph vessels, nerves and tissue around the joints) [62]. The most common types of soft tissue sarcoma are leiomyosarcoma, Kaposi sarcoma, synovial sarcoma, angiosarcoma, malignant fibrous histiocytoma, liposarcoma, dermatofibrosarcoma protuberans, rhabdomyosarcoma and primary alveolar soft-part sarcoma [63]. Primary bone sarcomas include osteosarcoma, Ewing sarcoma, giant cell tumor, and chondrosarcoma [64].

2.2.3 Leukemia

Leukemia is a tumor occurring in hematopoietic bone marrow tissue. During leukemia, no solid tumor is formed and instead, large numbers of abnormal white blood cells (leukemia cells and blast leukemia) accumulate in the blood and bone marrow, displacing normal blood cells [65]. Low levels of normal blood cells do not allow the organism to oxygenate the tissues, control the bleeding or struggle with infections. There are four common types of leukemia, which are grouped according to how quickly the disease deteriorates (acute or chronic) and according to the origin of the blood cells (lymphoblastic or myeloid) [66, 67]. Leukemia has an uncommon etiology and is phenotypically and genetically heterogeneous. The potential etiological factor is the interaction between genetic factors and environmental factors. Leukemia is the most common cancer in children, accounting for one third of all childhood cancers [68].

2.2.4 Lymphoma

Lymphoma is a cancer that begins in lymphocytes (T or B lymphocytes), which are components of the immune system. In lymphoma abnormal lymphocytes build up in lymph nodes and vessels as well as in other organs [69]. There are two main types of lymphoma: Hodgkin lymphoma and Non-Hodgkin lymphoma. Hodgkin lymphoma is characterized by abnormal lymphocytes—Reed-Sternberg cells (formed from B lymphocytes). Non-Hodgkin's lymphoma is a large group of cancers that start in lymphocytes. Cancers can have different rates of growth from either B or T lymphocytes [70, 71].

2.2.5 Multiple Myeloma

Multiple myeloma—a bone marrow neoplasia is a haematological condition characterised by the abnormal proliferation of clonal, terminally differentiated B

lymphocytes in the bone marrow [72]. The etiology of the disease remains unknown, the genetic impact is mainly suspected and may also be a consequence of environmental factors (such as exposure to toxic chemicals, exposure to pesticides, ionizing radiation (e.g. survivors of the Chernobyl disaster or the Nagasaki atomic bomb). Multiple myeloma is the one of the most common hematological malignancy in the World, and this disease remains incurable (an incidence of 6/100,000/yr in Europe). Multiple myeloma is also called plasma cell myeloma and Kahler disease [73].

2.2.6 Melanoma

Melanoma is developed as a result of a number of abnormalities in the genetic pathways within the melanocyte [74]. This promotes cell proliferation and block apoptosis responsive to DNA damage and stimulate the growth of blood vessels, avoiding immune response, tumor invasion and metastasis. Most melanomas appear on the skin, but melanomas can also form in other pigmented tissues, such as the eye [75].

2.2.7 Brain and Spinal Cord Tumors

The most common cytogenetic changes in primary brain tumors are losses of chromosomes and the presence of double minute chromosomes. The identification of specific cytogenetic abnormalities in human brain tumors has created a framework for the identification of genes that may inhibit tumor development, and their loss or inactivation causes tumor development [76]. Most malignant gliomas contain gains of chromosome 7 and losses of chromosome 10; losses of chromosome 22, 9p, and the sex chromosomes occur in subgroups of cases. Brain tumors can be benign or malignant. Spinal cord tumors are relatively rare. The most common spinal cord tumors are: astrocytomas, ependymomas, and hemangioblastomas [77].

2.2.8 Other Types of Tumors

In addition to the above mentioned, other cancers such as germ cell tumor, neuroendocrine tumor or carcinoid tumor may also occur. Germ cell tumors are a type of tumor that starts in the cells that produce sperm or ovum [78]. Neuroendocrine tumors are formed from cells that release hormones into the blood in response to a signal from the nervous system (they produce larger amounts of hormones than normal) [79]. Carcinoid tumor is a type of neuroendocrine tumor. This is a slow-growing tumor that usually occurs in the digestive system (they secrete substances such as serotonin or prostaglandins). These tumors can occur almost anywhere in the body and can be either benign or malignant [80, 81].

2.3 Cancer Treatment Methods

Cancer treatment methods are an intensively developed field of medicine. Among the most popular methods of cancer treatment can be distinguished surgery (one or more), radiotherapy and systemic therapy [82]. In the early stages of the disease, patients are usually treated only surgically, in other cases a combination of treatments is necessary. In metastatic diseases, systemic therapy is the main method of treatment (easier access to the disseminated sites of cancer). Systemic therapies include hormone therapy, targeted therapy, immunotherapy and chemotherapy [83]. The treatment of metastatic diseases is mainly palliative in nature, except for germ cell tumors [83]. Despite great improvements in oncology and surgical skills, the overall cancer survival rate has been improved only slightly over the last few decades [84]. With targeted treatment, we can adjust the diagnosis and management of the disease at the cellular level. This approach creates new opportunities in oncology because in the past cancer detection and treatment have included non-specific contrast agents and systemic chemotherapeutics that damage healthy tissue [82].

2.3.1 Surgery

Surgery is a major intervention and provides an opportunity to cure patients with cancer. By completely removing the tumor, surgeons have a radical impact on the course of the patient's cancer [82]. On the other hand, the period of perioperative occurs, marked by an increased risk of accelerated disease development and new metastatic foci. Factors in the perioperative period (such as anesthesia, transfusion, hypothermia and postoperative complications) are also important as likely harmful agents contributing to early relapse [85]. Appropriate visualization of the tumor remains a limitation often preventing complete removal of the tumor tissue. The usage of white light by surgeons mainly limits the differentiation between healthy tissue and the tumor and may lead to leaving the tumor cells at the border of resection. Fluorescence-guided imaging and intraoperative guidance can improve surgical field navigation to completely remove the tumor and avoid critical structures [82].

2.3.2 Chemotherapy

Chemotherapy is a common method of treating various types of cancer which was inspired by the usage of a DNA alkylating agent called nitrogen mustard as an idea to use toxic drugs to treat cancer during World War II. More than four hundred chemotherapeutic drugs have been discovered and manufactured since then to treat different types of cancers [86]. Chemotherapy drugs work by interfering with the cell cycle. Cancer cells differ from normal cells in their ability to grow and survive, they become insensitive to growth inhibitory signals and avoid cell death.

Chemotherapy drugs cause cell death: by apoptosis, by direct interference with DNA, or by targeting key proteins required for cell division. Chemotherapy drugs are classified by their action in the cell cycle or by their biochemical properties. The ability to cause a higher percentage of killing cells in cancer cells, as opposed to normal cells, allows the therapeutic use of chemotherapeutics. Unfortunately, they can also be harmful to normally divide cells (such as bone marrow and mucous membranes). Understanding cancer biology, pharmacology and resistance patterns will enable more effective treatment of chemotherapy. In the future it is likely that chemotherapy will be used in combination with biological agents for most types of cancer and will be less toxic and more targeted [83].

2.3.3 Radiation Therapy

Radiation therapy (external beam radiotherapy and internal radioisotope therapy) is widely used in the clinical treatment of cancer. Radiotherapy leads to serious damage to normal tissues surrounding cancer, by requiring high doses of ionizing radiation, due to the low absorption of radiation by the cancer. The development of nanotechnology has enabled the use of nanomedicine strategies to increase tumor response to radiation, these nanomedicines can act as a radio-sensitizer that deposits radiation energy within cancer and increases the effectiveness of treatment [87]. External beam radiotherapy is widely used to treat local solid tumors (breast, colorectal, esophageal, head and neck, lungs, prostate and brain tumors), internal radioisotope therapy is used to treat local tumors as well as metastatic tumors spread throughout the body [84].

2.3.4 Another Therapies

In addition to surgery, chemotherapy and radiotherapy, other methods and combinations of different types of therapy are used to cure cancer. The therapeutic potential of cancer chemotherapy is unsatisfactory due to inaccurate drug delivery, multi-drug resistance and heterogeneity of cancer. Currently there is a tendency to combine chemotherapy with nanotechnology, which can lead to a significant increase in therapeutic efficacy with few side effects for normal tissues [87]. A bone marrow transplantation is an effective method of treating several of the increasingly common hematological malignancies [88]. Anticancer immunotherapy is a validated and extremely important approach in the treatment of cancer patients. Scientific and clinical research aims to develop both endogenous and synthetic approaches to immunotherapy, basic understanding and clinical progress [89]. Immunotherapy is a powerful clinical strategy in the treatment of cancer. A key challenge in the treatment of cancer is the controlled modulation of the immune system, because drugs for these diseases have severe negative effects. Advanced biomaterials and drug delivery systems, including hydrogels, can effectively use immunotherapy while reducing toxic side effects of the treatment [90].

3 Drug Delivery Systems

Hydrogels have become very popular in the biomedical sector, especially in manufacturing of the Drug Delivery Systems. Compared to regular drug formulations, hydrogel-based drug carriers should deliver the Active Pharmaceutical Ingredient (API) (e.g. protein peptides, high molecular weight drugs) to its destination and release it in a controlled manner at an effective rate. Three-dimensional structure of hydrogels and their ability to water retention enable to keep the active substance inside the carrier and its gradual and sustained distribution [33, 34]. DDS overcomes the major drawbacks of conventional drug administration, such as a frequent application or high doses in order to increase efficacy. As a result, the use of DDSs can eliminate side-effects, increase efficacy and not cause toxicity, as traditional medicines do [26]. The combination of benefits of constant and extended drug release with the achievable structure of hydrogels allow the placement of any size of substance from small molecules as non-steroidal anti-inflammatory drugs to large peptides and proteins [91]. On the other hand, the low tensile strength of the hydrogels or too large pore size may result in premature release of part of the active substance contained in the carrier, before reaching its destination. To avoid these situations, a chemical modification of the hydrogels can be undertaken, for example by controlling hydrogel cross-linking density or by using hydrogels capable of degrading after an external signal is received (temperature change, pH or electrical signal) [34, 35].

The basic phenomenon during the incorporation of the active substance and its release from the hydrogel carrier is diffusion. This results from the high permeability of hydrogels, their hydrophilic nature and their ability to degrade. Encapsulated molecules can be released from the carrier by cleavage of polymer chains via hydrolytic or enzymatic degradation or stimulation by external factors. The API release rate is influenced by parameters such as the type of polymer used for the hydrogel carrier, its cross-linking density and degradation rate, but also the molecular size of the drug [92, 93]. Hydrogel DDS can be manufactured in several ways and this depends on the specific utilization of the product (form of administration).

The potency of hydrogel carriers in the medical sector is used extensively in cardiology, immunology, oncology, wound healing but also pain management [26]. Based on the hydrophilic nature of the hydrogel functional groups, DDSs are suitable to deliver drugs characterized by their hydrophilic nature. Unfortunately, most drugs effective in disease therapy, especially anti-cancer agents, do not show such features and are poorly soluble in an aqueous medium. This problem is overcome through hydrogel modifications, in order to effectively integrate the active substance into the carrier [35, 94].

3.1 *Stimuli-Responsive Hydrogels*

Hydrogel materials exhibit a tendency to swell in water presence and shrink in its absence. Among hydrogel materials, there are also those that can change the swelling degree under the influence of other external factors. These materials are known as “smart” hydrogels and are sensitive to stimuli such as temperature, light, electrical signal or pH change [92]. There are also hydrogels that are sensitive to factors such as ultrasound, pressure, magnetic field and also responsive to glucose [95, 96]. This creates many opportunities in drug delivery. The release of a therapeutic agent may be induced by changes in the environment. For example, it is possible to release the drug gradually, in a controlled manner or at a specific location, with a change of one of the above listed parameters [2, 32, 92].

Materials sensitive to pH changes are very useful in carriers administered orally, due to pH fluctuations at each stage of the digestive system, but also they are used for drug delivery in cancer treatment, where pH of the diseased tissues is more acidic than normal tissue. These materials can be used to deliver insulin or to create kits for blood glucose detection. The most commonly used polymer for this purpose is alginate [1, 26]. Among the materials responding to temperature, we can distinguish those that form gel after lowering the temperature, as well as those that undergo reverse thermogelation, i.e. they gel after raising the temperature. The example of first group includes gelatin, a natural polymer. The second group uses synthetic polymers such as poly(ethylene oxide)-poly(propylene oxide)-poly(ethylene oxide) (PEO-PPO-PEO) and poly(N-isopropylacrylamide) (PNIPAm). These materials may also be used in cancer therapy, where temperature of the affected area is slightly higher than the standard body temperature (e.g. breast cancer) [26]. Polymeric hydrogels sensitive to electric-stimuli usually consist of polyelectrolytes, reacting to the influence of an electric field by shrinking and swelling under the influence of an anode and cathode [3]. In Table 1 hydrogel materials are gathered, which have the ability to change under the influence of external factors with an example of the use of API in DDS.

3.2 *Route of Administration*

There are many ways to deliver the drug to the human body. The route of drug administration determines the bioavailability, i.e. the specific time after which the product will start to release and the length of its pharmacological effect, but also the manner of activity (locally or generally systemic). The systemic absorption of drugs can include the intestinal route of administration (release of the substance takes place at the desired section of the digestive system) and the parenteral route (subcutaneous injection, bypassing the digestive system). The pulmonary and nasal routes are another examples of the administration of a systemic drug but are less commonly used [99]. Hydrogel carriers have a universal purpose, as they can be

Table 1 The use of hydrogels sensitive to external stimuli in different drug delivery systems

Stimulus	Polymeric material	Active pharmaceutical ingredient (API)	References
Electric-field-sensitive	Poly(methacrylic acid) (PMA), hydrolysed polyacrylamide, sodium acrylic acid acrylamide, poly (2-acryl-amido-2-methylpropanesulfonicacid-co-n-butylmethacrylate)	Pilocarpine and raffinose, edrophonium chloride, hydrocortisone	[95, 97]
pH-sensitive	Alginate poly(methacrylic-g-ethylene glycol) (p(MMA-g-EG)), hydroxyl-propyl methylcellulose (HPMC), covalently cross-linked chitosan-poly (ethylene glycol) (PEG), guar gum cross-linked with glutaraldehyde	Insulin protein peptides, high molecular weight drugs	[3, 97, 98]
Thermo-sensitive	Layer of chitosan pluronic on poly(lactide-co-glycolide) (PLGA) microparticles, gelatine, poly(ethylene oxide)-poly(propylene oxide)-poly (ethylene oxide) (PEO-PPO-PEO), poly(N-isopropylacrylamide) (PNIPAm)	Indomethacin, doxorubicin	[26, 97]

easily formed into various shapes reaching every size, but through physicochemical modification, it is also possible to achieve arbitrary structure (i.e. required pore size or their absence) [26].

3.2.1 Ocular

The first soft contact lenses, formed from poly-hydroxyethyl methacrylate (pHEMA) hydrogels, appeared in the 1960s and became the first media for ophthalmic delivery of the drug. One of the methods of lens production containing API was soaking the lens in a solution with a drug. In this way, the active agent was absorbed by the lenses. However, they were not sufficient due to the small amount of the drug capacity and the high release rate. They lose most of the API contained in it usually in one day [31, 100]. A combination of pHEMA with 4-vinylpyridine (VP), which is a hydrophobic monomer, was used to reduce diffusion of the active substance. The second method was to combine pHEMA with an ionic monomer such as N-(3-aminopropyl)methacrylamide (APMA). This allowed to increase the drug capacity and to extend the lens's activity, providing sustained release of active substances [31]. An improved pHEMA lens with a polymer-drug encapsulated film can release API for up to 4 weeks [101]. Generally, the drug administered through the cornea is less biologically available in the posterior ocular tissues, such as the choroid and retina. Therefore, therapies for intraocular cancers such as uveal melanoma and retinoblastoma (Rb) require a completely different approach and a lot of research [102]. Hydrogels based on APMA are currently used together with anticancer drugs [103].

3.2.2 Oral

One of the most widespread routes of drug administration is the oral route. This is caused by the simplicity of intake pharmaceuticals, a significant amount of available medicines, high patient compliance, large surface area for systemic absorption, cost-effectiveness and ease of production. It is generally a safe method, due to the slowness of active substances absorption, but unfortunately, it also has certain disadvantages. Pharmaceuticals administered orally are generally characterized by poor bioavailability of the drug, low solubility and reduced permeability across intestinal biological membranes [6, 104, 105]. Hydrogel DDSs were designed to overcome the disadvantages of conventional oral medicines by increasing effectiveness and bioavailability, as well as enabling sustained and controllable delivery of the API [97]. However, factors such as microbial colonization and enzymes, autonomic and hormonal activity, but also pH in different parts of the digestive tract can influence the drug's behaviour in the gastrointestinal tract. This fact should be taken into account during designing the DDS [105, 106]. Depending on the location where the absorption process should take place, different materials are used. Some medicines disintegrate immediately after being inserted inside the mouth

(fast-dissolving tablets with dissolution time up to 60 s), but there are also those, which have to deliver API into the gastrointestinal tract or the colon [98]. The oral DDS also includes long-term gastric retention mechanisms for prolonged release of drugs in the stomach (with time-release of 6–12 h). The maintenance of this carrier in the stomach can be achieved by the utilization of mucoadhesive polymers or floating drug release systems, as well as by changing the drug particle density. They are used, for example, to deliver antibiotics, antacids [98, 106]. The administration of selected APIs to the small intestine is associated with their instability at earlier stages of the digestive system and the difficulty of their absorption [98]. Smart hydrogels can protect encapsulated molecules from shear stresses caused by flowing gastric juices and low pH. Examples of materials used for hydrogel drug carriers are alginate, hydroxypropyl methylcellulose (HPMC), covalently cross-linked chitosan-poly (ethylene glycol) (PEG), guar gum cross-linked with glutaraldehyde [91, 98, 106].

3.2.3 Vaginal and Rectal

Another way of transmucosal administration of the drug is vaginal and rectal routes. The dense network of blood vessels and permeability to a wide range of compounds make the vaginal administration of medicine suitable not only for the local administration of medicines but also for systemic. The unquestionable advantage of using this route is the length of time the drug is held in the vagina. This allows a sustained and prolonged release of API, which minimizes the frequency of its dosing. This pathway guarantees a quick absorption of drug and an almost immediate effect. In addition, the gastrointestinal tract is bypassed, therefore the interaction of several drugs in the stomach, degradation by enzymes and gastric acid is avoided [107, 108]. Zaman et al. [97] mentioned the anti-cancer drug bleomycin contained in the flat disk of hydroxypropyl cellulose, which releases the active substance almost around 24 h.

3.2.4 Transdermal

One of the alternatives to oral administration and hypodermic injection is transdermal drug delivery. The large skin surface area provides many possibilities to place the transdermal drug carrier and pharmacokinetic profiles of controlled release of drug minimize the risk of overdosing and thus, toxic side effects. Moreover, this is a painless, non-invasive way of drug delivery and most crucially eliminates the first-pass effect of the liver [109–111]. These systems include adhesive patches, which release the API in a controlled manner to the systemic circulation, but also local use as active wound dressings. The hydrogel ability to retain large amounts of liquid is a useful feature in wound healing applications, where the hydrogel used as a dressing absorbs excess exudate. In addition, they may contain substances that affect the healing process [97, 109]. The second method of drug administration by

the skin are patches for systemic treatment applied onto intact and healthy skin. It can increase the effectiveness of the drug and its bioavailability [97]. Understanding the diffusion of drugs through the stratum corneum, deeper epidermis and dermis is the first step in the proper design of this carrier. Due to the skin barrier, transdermal DDSs can derive mainly small lipophilic drugs. The size of the patch determines the amount of active substance contained in it, therefore API molecules should be potent enough to be delivered in a limited amount. On the market there are available drug carriers such as estradiol, testosterone, fentanyl and lidocaine, as well as a combination of several drugs for contraception in a single patch [109, 112]. Currently, transdermal DDSs containing anti-cancer agents are a promising treatment for skin cancer (i.e. melanoma). Vishnubhaktula et al. [113] indicated that there is ongoing research on targeted administration of paclitaxel to eliminate cancer cells. The authors also described the permanent retention of 5-fluorouracil, incorporated in polyethylene glycol, polycaprolactone and poly-L-lactic acid copolymers hydrogel, which significantly inhibited melanoma growth in *in vitro* and *in vivo* tests.

3.2.5 Brain Treatment

The blood-brain barrier is difficult to cross, only about 2% of the synthesized medical therapeutics are able to overcome this barrier. Zaman et al. [97] reported that one such system is the hydrogel microsphere of PLGA with camptothecin content. The experiment was conducted on rats with malignant gliomas. Their survival period increased after the administration of the drug. Israr et al. [114] described the use of photopolymerizable PEG-DMA-based hydrogel in the form of micelles filled with Temozolomide for glioblastoma (GBM) treatment. The author also mentioned an example of glioma treatment, where a combination of hydrogel and paclitaxel (PTX) nanoparticles was used. Another example was described by Basso et al. [94] about the application of hydrogel nanoparticles to GBM treatment. Nanogels, as they can also be identified by this term, exhibit features of both hydrogels and nanoparticles, thus they are perfect for the use in intravenous or intratumoral injection. In contrast, macroscopic hydrogels are recommended for the use for *in situ* drug delivery, after surgical resection. Most of the medications administered have increased the survival of GBM patients. In addition to using hydrogels as DDS, their injection directly into the stroke cavity can provide mechanical properties similar to those of the brain and serve as a local storage of a therapeutic agent [115, 116]. Hydrogels are also used as mimicking structures in 3D *in vitro* tumor microenvironment models to improve research related to tumor cell biology, cellular proliferation, migration, motility and angiogenesis behavior [117].

4 Hydrogel-Based Inks for 3D Printing in Cancer Treatments

3D printing technology is based on layer-by-layer manufacturing based on prepared 3D CAD models, thus enabling the creation of complex 3D geometries [40, 118] and formulation of customized drugs with a release profile designed for a specific patient and condition to be treated [119]. One of the representatives of layered methods, which is widely used in medical applications, is bioprinting technology, a developed branch of 3D printing in which living cells, extracellular matrix (ECM) components, biomaterials and biochemical agents are printed on a suitable substrate. This technology is applied in biochemical surface modelling, wound healing, three-dimensional tissue design, regenerative medicine, disease modelling and pharmaceutical research [120] and has significant potential for application in cancer research [118]. Previously used 2D models are not sufficient and until the 3D cancer models mimic the complexity of their structure and facilitate the assessment of physiologically significant cell–cell and cell–matrix interactions. Such cancer microenvironmental models provide a platform for a deeper understanding of cancer pathology, cancer drug delivery screening and cancer treatment development [121]. 3D printed structures are widely utilized in various fields, including drug delivery, tissue engineering, in vitro drug screening and tissue or cancer models. Cross-linked 3D hydrogel structures are developed to increase drug loading or to sustain drug release [122]. The evolving 3D printing technology allows for the improvement of some disadvantages such as high costs and speed, and this technology is becoming more widely used. Modern 3D printing based drug delivery systems can launch a new era of treatment of various diseases [123].

4.1 *Materials and Forms of Applications in Cancer Treatment*

4.1.1 **Materials**

Materials for 3D printing as inks differ due to the potential application of the printed structure. Bioglass is used to kill cancer cell remains as well as to repair bone defects. Fibers and hollow microspheres were developed for the treatment of skin tumors/bodies and wound healing. However, these materials are not suitable for use as soft tissue fillers (e.g. graphene oxide may be toxic) [124]. Alginate, due to its biocompatibility and gelation with cations (such as Ca^{2+} or Mn^{2+}), is widely used in soft tissue engineering and fat tissue regeneration. Due to its low stiffness and poor cell adhesion, it is often used with additives [30]. Nanohydrogels have potential applications in cancer therapy as a drug delivery system because they are characterized by low toxicity, impressive biodegradation, acute double reactivity, adequate drug loading capacity and high containment efficiency [26]. Injected chitosan

Table 2 Examples of materials for 3D printing used in cancer treatment

Material with drug	Application	Function	References
Hyaluronic acid (HA)-based hydrogel, doxorubicin, paclitaxel, cisplatin	Drug delivery systems	Active targeting of malignant tumors, improved antitumor activity and reduction of systemic side effects	[126]
Methacrylated HA with di(ethylene glycol) diacrylate, doxorubicin	Drug delivery systems	Penetration of nanogels in tumor cell lines that over-express CD44 receptors	[127]
HA-doxorubicin	Drug delivery systems	Excellent cytotoxic activity against tumor cell lines that overexpress CD44 receptor and a high affinity targeting to the lymph nodes for the treatment of local and metastatic tumors	[128]
PLGA-polyethylene glycol-poly (lactide-co-glycolide) (PCL), paclitaxel	Drug delivery systems; tissue engineering	Long drug release time, suppression of the remnant microscopic tumor, inhibition of the tumor recurrence	[40]
Alginate-polydopamine (Alg-PDA)	Tissue engineering	Great flexibility and similar modulus with normal breast tissues, facilitating the adhesion and proliferation of normal breast epithelial cells, photoacoustic imaging ability in vivo	[123]

hydrogel with graphene nanoparticles can be used in controlled drug administration (e.g. methotrexate) as a potential breast cancer therapy system [125]. Examples of materials for 3D printing used in cancer treatment are shown in Table 2.

4.1.2 Forms of Applications

3D printing systems provide flexibility in the selection of supporting materials and drugs, a wide range of concentrations of drugs contained in them, continuous dosing of material containing the drug and even distribution of the drug [40]. Three-dimensional printing technology may be successfully implemented in the development of personalized dosage forms, due to its high precision and accuracy [129]. Structures manufactured with the assistance of 3D printing can be in various forms, these can include printlets (printed tablets), 3D scaffolds and surface coatings (e.g. implants coatings). Hydrogel systems available for the drug delivery include bulk hydrogels, porous or fibrous scaffolds, hydrogel microspheres, hydrogel sandwich systems, microwells and 3D bioprinted constructs [130].

4.2 3D Printed Structures as In Vitro Cancer Models

Cancer models are widely used in research contributing to the expansion of basic knowledge of cancer biology (gene expression, protein expression and protein gradient profiles, morphology, vitality, proliferation, migration, organization and signalling also response to drugs) [131]. Significant differences between 2D and 3D models of cancers can be observed. 2D cell cultures offer hypothetical results on cancer pathogenesis, but they lack cell-cell and cell-matrix interactions [132]. On the other hand, 3D models have achieved a more accurate representation of tumor tissues in terms of cancer microenvironment and biological behavior, which allows for more accurate analysis and application of such structures to study the anticancer effect of particular drugs [120]. The implementation of 3D printing and 3D bioprinting is excellent for producing 3D cancer models [36]. Bioprinting is used to produce complex vascularized tissue structures (e.g. for organ printing and for research on a potentially anti-cancer drug) using various materials, including hydrogels. 3D bioprints are used to produce complex vascularized tissue structures (e.g. for organ printing and for research on a potentially anti-cancer drug) [133]. Bioprinted hydrogels are also commonly used for microflow devices or more complex lab-on-a-chip (LOC) [130].

5 Future Outlook and Concluding Remarks

Advanced hydrogel-based drug delivery systems manufactured with additive manufacturing methods can be successfully applied in cancer treatment. Their hydrophilic nature makes it possible to include certain drugs directly or after physicochemical modification. Hydrogel degradation enables the controlled release of drugs, which is an excellent alternative to conventional methods of administration. The control of the release of the active substance eliminates the need for frequent dosing, which reduces the accumulation of the drug in the body as well as overdosing. Furthermore, versatility of the hydrogel DDSs allows them to be used in most application routes.

It would be valuable to consider the use of 3D printing in personalized medicine, for example, to print custom made drugs for patient (including cancer drugs), in regenerative and tissue medicine (filling in cavities after cancer resection), in targeted drug therapy using nanotechnology (precise tumor treatment) or in wound healing. In addition, it should be noticed that 3D printed hydrogel structures are used in the research on the manufacturing and introducing to treatment of potentially anticancer drugs, this technology allows to produce porous, multi-material structures both in single batches and on an industrial scale. The main obstacle to the introduction of universal access to 3D printed treatment is the insufficient development of technology and materials applied for 3D printing, as well as the relatively high cost of technology.

Funding The research is a part of the Statutory Subsidy No. 8201003902 at the Department of Mechanics, Materials and Biomedical Engineering (K58), Faculty of Mechanical Engineering, Wrocław University of Science and Technology, Smoluchowskiego 25, 50372 Wrocław, Poland. This work was also supported by the National Centre for Research and Development in Poland (Grant No. LIDER/23/0098/L-9/17/NCBR/2018).

References

1. Pal K, Banthia AK, Majumdar DK (2009) Polymeric hydrogels: characterization and biomedical applications. *Des Monomers Polym* 12(3):197–220
2. Laftah WA, Hashim S, Ibrahim AN (2011) Polymer hydrogels: a review. *Polym Plast Technol Eng* 50(14):1475–1486
3. Bahram M, Mohseni N, Moghtader M (2016) An introduction to hydrogels and some recent applications. In: Majeed SB (ed) *Emerging concepts in analysis and applications of hydrogels*. InTech, UK, pp 9–38
4. Lim KS, Martens P, Poole-Warren L (2018) Biosynthetic hydrogels for cell encapsulation. In: Li J, Osada Y, Cooper-White J (eds) *Functional hydrogels as biomaterials*. Springer, Berlin, Heidelberg, pp 1–29
5. Chirani N, Yahia L, Gritsch L, Motta FL, Chirani S, Fare S (2015) History and applications of hydrogels. *J Biomed Sci* 4(2):1–23
6. Bharskar GR (2020) A review on hydrogel. *World J Pharm Pharm Sci* 9(7):1288–1298
7. Okay O (2009) General properties of hydrogels. In: Gerlach G, Arndt KF (eds) *Hydrogel sensors and actuators*. Springer, Berlin, Heidelberg, pp 1–14
8. Senapati S, Mahanta AK, Kumar S, Maiti P (2018) Controlled drug delivery vehicles for cancer treatment and their performance. *Signal Transduct Targ Ther* 3(7):1–19
9. Feng R-M, Zong Y-N, Cao S-M, Xu R-H (2019) Current cancer situation in China: good or bad news from the 2018 Global Cancer Statistics? *Cancer Commun* 39(1):22
10. Mattiuzzi C, Lippi G (2020) Cancer statistics: a comparison between World Health Organization (WHO) and Global Burden of Disease (GBD). *Eur J Pub Health* 30(5):1026–1027
11. Tewari KS, Burger RA, Enserro D et al (2019) Final overall survival of a randomized trial of bevacizumab for primary treatment of ovarian cancer. *J Clin Oncol* 37(26):2317–2328
12. Masuda N, Lee S-J, Ohtani S et al (2017) Adjuvant capecitabine for breast cancer after preoperative chemotherapy. *New Engl J Med* 376(22):2147–2159
13. Palma DA, Olson R, Harrow S et al (2019) Stereotactic ablative radiotherapy versus standard of care palliative treatment in patients with oligometastatic cancers (SABR-COMET): a randomised, phase 2, open-label trial. *Lancet* 393(10185):2051–2058
14. Harlan LC, Clegg LX, Trimble EL (2003) Trends in surgery and chemotherapy for women diagnosed with ovarian cancer in the United States. *J Clin Oncol* 21(18):3488–3494
15. Shipley WU, Seiferheld W, Lukka HR et al (2017) Radiation with or without antiandrogen therapy in recurrent prostate cancer. *New Engl J Med* 376(5):417–428
16. Lee SJ, Logan B, Westervelt P et al (2016) Comparison of patient-reported outcomes in 5-year survivors who received bone marrow vs peripheral blood unrelated donor transplantation long-term follow-up of a randomized clinical trial. *JAMA Oncol* 2(12):1583–1589
17. Pinter M, Jain RK (2017) Targeting the renin-angiotensin system to improve cancer treatment: implications for immunotherapy. *Sci Transl Med* 9(410):eaan5616
18. James ND, de Bono JS, Spears MR et al (2017) Abiraterone for prostate cancer not previously treated with hormone therapy. *New Engl J Med* 377(4):338–351
19. Liang C, Xu L, Song G, Liu Z (2016) Emerging nanomedicine approaches fighting tumor metastasis: animal models, metastasis-targeted drug delivery, phototherapy, and immunotherapy. *Chem Soc Rev* 45(22):6250–6269

20. McArthur HL, Diab A, Page DB et al (2016) A pilot study of preoperative single-dose ipilimumab and/or cryoablation in women with early-stage breast cancer with comprehensive immune profiling. *Clin Cancer Res* 22(23):5729–5737
21. Rajyaguru DJ, Borgert AJ, Smith AL, Thomes RM, Conway PD, Halfdanarson TR, Truty MJ, Kurup AN, Go RS (2018) Radiofrequency ablation versus stereotactic body radiotherapy for localized hepatocellular carcinoma in nonsurgically managed patients: analysis of the national cancer database. *J Clin Oncol* 36(6):600–608
22. Tran P, Lee SE, Kim DH, Pyo YC, Park JS (2020) Recent advances of nanotechnology for the delivery of anticancer drugs for breast cancer treatment. *J Pharm Investig* 50(3):261–270
23. Siegel RL, Miller KD, Jemal A (2019) Cancer statistics, 2019. *CA Cancer J Clin* 69(1):7–34
24. Oun R, Moussa YE, Wheate NJ (2018) The side effects of platinum-based chemotherapy drugs: a review for chemists. *Dalton Trans* 47(19):6645–6653
25. Yang C, Lee A, Gao S, Liu S, Hedrick JL, Yang YY (2019) Hydrogels with prolonged release of therapeutic antibody: block junction chemistry modification of ‘ABA’ copolymers provides superior anticancer efficacy. *J Controll Release* 293:193–200
26. Li J, Mooney DJ (2016) Designing hydrogels for controlled drug delivery. *Nat Rev Mater* 1(12):16071
27. Geckil H, Xu F, Zhang X, Moon S, Demirci U (2010) Engineering hydrogels as extracellular matrix mimics. *Nanomedicine* 5(3):469–484
28. Jabbari E, Leijten J, Xu Q, Khademhosseini A (2016) The matrix reloaded: the evolution of regenerative hydrogels. *Mater Today* 19(4):190–196
29. Francesko A, Petkova P, Tzanov T (2018) Hydrogel dressings for advanced wound management. *Curr Med Chem* 25(41):5782–5797
30. Łabowska M, Michalak I, Detyna J (2019) Methods of extraction, physicochemical properties of alginates and their applications in biomedical field—a review. *Open Chem* 17(1):738–762
31. Hu X, Hao L, Wang H, Yang X, Zhang G, Wang G, Zhang X (2011) Hydrogel contact lens for extended delivery of ophthalmic drugs. *Polym Biomater Tissue Eng Appl* 2011(814163)
32. Sosnik A, Seremeta K (2017) Polymeric hydrogels as technology platform for drug delivery applications. *Gels* 3(3):25
33. Aswathy SH, Narendrakumar U, Manjubala I (2020) Commercial hydrogels for biomedical applications. *Heliyon* 6(4):e03719
34. Hoare TR, Kohane DS (2008) Hydrogels in drug delivery: progress and challenges. *Polymer* 49(8):1993–2007
35. Narayanaswamy R, Torchilin VP (2019) Hydrogels and their applications in targeted drug delivery. *Molecules* 24(3):603
36. Trenfield SJ, Awad A, Madla CM, Hatton GB, Firth J, Goyanes A, Gaisford S, Basit AW (2019) Shaping the future: recent advances of 3D printing in drug delivery and healthcare. *Expert Opin Drug Deliv* 16(10):1081–1094
37. Hamid ZA, Blencowe A, Palmer J, Abberton KM, Morrison WA, Penington AJ, Qiao GG, Stevens G (2011) Hydrogel scaffolds: advanced materials for soft tissue re-growth. *IFMBE Proc* 831–835
38. Jeong KH, Park D, Lee YC (2017) Polymer-based hydrogel scaffolds for skin tissue engineering applications: a mini-review. *J Polym Res* 24(7). <https://doi.org/10.1007/s10965-017-1278-4>
39. Kotta S, Nair A, Alsabeelah N (2018) 3D printing technology in drug delivery: recent progress and application. *Curr Pharm Des* 24(42):5039–5048
40. Yi HG, Choi YJ, Kang KS, Hong JM, Pati RG, Park MN, Shim IK, Lee CM, Kim SC, Cho DW (2016) A 3D-printed local drug delivery patch for pancreatic cancer growth suppression. *J Controll Release* 238:231–241
41. Szymczyk-Ziółkowska P, Łabowska MB, Detyna J, Michalak I, Gruber P (2020) A review of fabrication polymer scaffolds for biomedical applications using additive manufacturing techniques. *Biocybern Biomed Eng* 40(2):624–638

42. Li Y-C, Zhang YS, Akpek A, Shin SR, Khademhosseini A (2016) 4D bioprinting: the next-generation technology for biofabrication enabled by stimuli-responsive materials. *Biofabrication* 9(1):012001
43. Ouyang L, Yao R, Zhao Y, Sun W (2016) Effect of bioink properties on printability and cell viability for 3D bioplotting of embryonic stem cells. *Biofabrication* 8(3):035020. <https://doi.org/10.1088/1758-5090/8/3/035020>
44. Martin E (2015) Concise medical dictionary. *Concise Med Dict.* <https://doi.org/10.1093/acref/9780199687817.001.0001>
45. Nurmik M, Ullmann P, Rodriguez F, Haan S, Letellier E (2020) In search of definitions: cancer-associated fibroblasts and their markers. *Int J Cancer* 146(4):895–905
46. Koo MM, Swann R, McPhail S, Abel GA, Elliss-Brookes L, Rubin GP, Lyratzopoulos G (2020) Presenting symptoms of cancer and stage at diagnosis: evidence from a cross-sectional, population-based study. *Lancet Oncology* 21(1):73–79
47. Cai Z, Liu Q (2019) Understanding the global cancer statistics 2018: implications for cancer control. *Sci China Life Sci* 1–4
48. Bray F, Ferlay J, Soerjomataram I, Siegel RL, Torre LA, Jemal A (2018) Global cancer statistics 2018: GLOBOCAN estimates of incidence and mortality worldwide for 36 cancers in 185 countries. *CA Cancer J Clin* 68(6):394–424
49. Roser M, Ritchie H (2015) Cancer. In: *Our world data.* <https://ourworldindata.org/cancer>. Accessed 01.11.2020
50. Jemal A, Ward E, Thun MJ (2007) Recent trends in breast cancer incidence rates by age and tumor characteristics among U.S. women. *Breast Cancer Res* 9(3):R28
51. Ashford NA, Bauman P, Brown HS, Clapp RW, Finkel AM, Gee D, Hattis DB, Martuzzi M, Sasco AJ, Sass JB (2015) Cancer risk: role of environment. *Science* 347(6223):727
52. Rojas K, Stuckey A (2016) Breast cancer epidemiology and risk factors. *Clin Obstet Gynecol* 59(4):651–672
53. Song M, Giovannucci EL (2015) Cancer risk: many factors contribute. *Science* 347(6223):728–729 (New York, NY)
54. Siegel RL, Jacobs EJ, Newton CC, Feskanich D, Freedman ND, Prentice RL, Jemal A (2015) Deaths due to cigarette smoking for 12 smoking-related cancers in the United States. *JAMA Intern Med* 175(9):1574–1576
55. Lortet-Tieulent J, Sauer AG, Siegel RL, Miller KD, Islami F, Fedewa SA, Jacobs EJ, Jemal A (2016) State-level cancer mortality attributable to cigarette smoking in the United States. *JAMA Intern Med* 176(12):1792–1798
56. Stanaway JD, Afshin A, Gakidou E et al (2018) Global, regional, and national comparative risk assessment of 84 behavioural, environmental and occupational, and metabolic risks or clusters of risks for 195 countries and territories, 1990–2017: a systematic analysis for the Global Burden of Disease Study 2017. *Lancet* 392(10159):1923–1994
57. Mimeault M, Batra SK (2006) Concise review: recent advances on the significance of stem cells in tissue regeneration and cancer therapies. *Stem Cells* 24(11):2319–2345
58. Haggitt RC (1994) Barrett's esophagus, dysplasia, and adenocarcinoma. *Hum Pathol* 25(10):982–993
59. Rubin AI, Chen EH, Ratner D (2005) Basal-Cell Carcinoma. *New Engl J Med* 353(21):2262–2269
60. Alam M, Ratner D (2001) Cutaneous squamous-cell carcinoma. *New Engl J Med* 344(13):975–983
61. Vlahou A, Schellhammer PF, Mendrinos S, Patel K, Kondylis FI, Gong L, Nasim S, Wright GL (2001) Development of a novel proteomic approach for the detection of transitional cell carcinoma of the bladder in urine. *Am J Pathol* 158(4):1491–1502
62. Skubitz KM, D'Adamo DR (2007) Sarcoma. *Mayo Clin Proc* 82(11):1409–1432
63. Grünewald TGP, Cidre-Aranaz F, Surdez D, Tomazou EM, De Álava E, Kovar H, Sorensen PH, Delattre O, Dirksen U (2018) Ewing sarcoma. *Nat Rev Dis Prim* 4(1):5
64. Cesarman E, Damania B, Krown SE, Martin J, Bower M, Whitby D (2019) Kaposi sarcoma. *Nat Rev Dis Prim* 5(1):9

65. Ferrando AA, López-Otín C (2017) Clonal evolution in leukemia. *Nat Med* 23(10):1135–1145
66. Lowenberg B, Downing JR, Burnett A (1999) Acute myeloid leukemia. *New Engl J Med* 341(14):1051–1062
67. Hernández A, Menéndez P (2016) Linking pesticide exposure with pediatric leukemia: potential underlying mechanisms. *Int J Mol Sci* 17(4):461
68. Iacobucci I, Mullighan CG (2017) Genetic basis of acute lymphoblastic leukemia. *J Clin Oncol* 35(9):975–983
69. Rueffer U, Josting A, Franklin J, May M, Sieber M, Breuer K, Engert A, Diehl V (2001) Non-Hodgkin's lymphoma after primary Hodgkin's disease in the German Hodgkin's Lymphoma study group: incidence, treatment, and prognosis. *J Clin Oncol* 19(7):2026–2032
70. Armitage JO, Gascoyne RD, Lunning MA, Cavalli F (2017) Non-Hodgkin lymphoma. *Lancet* 390(10091):298–310
71. Cortelazzo S, Ferreri A, Hoelzer D, Ponzoni M (2017) Lymphoblastic lymphoma. *Critic Rev Oncol/Hematol* 113:304–317
72. Kyle RA (1975) Multiple myeloma. Review of 869 cases. *Mayo Clin Proc* 50(1):29–40
73. Diaz-delCastillo M, Chantry AD, Lawson MA, Heegaard A-M (2020) Multiple myeloma—a painful disease of the bone marrow. *Semin Cell Dev Biol*. <https://doi.org/10.1016/j.semcdb.2020.10.006>
74. Thompson JF, Scolyer RA, Kefford RF (2005) Cutaneous melanoma. *Lancet* 365(9460):687–701
75. Miller AJ, Mihm MC Jr (2006) Melanoma. *New Engl J Med* 355(1):51–65
76. Bigner SH, Mark J, Bigner DD (1990) Cytogenetics of human brain tumors. *Cancer Genet Cytogenet* 47(2):141–154
77. Balériaux DLF (1999) Spinal cord tumors. *Eur Radiol* 9(7):1252–1258
78. Lobo J, Gillis AJM, Jerónimo C, Henrique R, Looijenga LHJ (2019) Human germ cell tumors are developmental cancers: impact of epigenetics on pathobiology and clinic. *Int J Mol Sci* 20(2):258
79. Oronsky B, Ma PC, Morgensztern D, Carter CA (2017) Nothing but NET: a review of neuroendocrine tumors and carcinomas. *Neoplasia* 19(12):991–1002
80. Kulke MH, Mayer RJ (1999) Carcinoid tumors. *New Engl J Med* 340(11):858–868
81. Papaxoinis G, Lamarca A, Quinn AM, Mansoor W, Nonaka D (2018) Clinical and pathologic characteristics of pulmonary carcinoid tumors in central and peripheral locations. *Endocr Pathol* 29(3):259–268
82. Tringale KR, Pang J, Nguyen QT (2018) Image-guided surgery in cancer: a strategy to reduce incidence of positive surgical margins. *Wiley Interdiscip Rev Syst Biol Med* 10(3): e1412
83. Dickens E, Ahmed S (2018) Principles of cancer treatment by chemotherapy. *Surgery* 36(3):134–138
84. Song G, Cheng L, Chao Y, Yang K, Liu Z (2017) Emerging nanotechnology and advanced materials for cancer radiation therapy. *Adv Mater* 29(32):1700996
85. Tohme S, Simmons RL, Tsung A (2017) Surgery for cancer: a trigger for metastases. *Cancer Res* 77(7):1548–1552
86. Qin SY, Cheng YJ, Lei Q, Zhang AQ, Zhang XZ (2018) Combinational strategy for high-performance cancer chemotherapy. *Biomaterials* 171:178–197
87. Zhao CY, Cheng R, Yang Z, Tian ZM (2018) Nanotechnology for cancer therapy based on chemotherapy. *Molecules* 23(4):826
88. Douglas CM, Jethwa AR, Hasan W, Liu A, Gilbert R, Goldstein D, De Almedia J, Lipton J, Irish JC (2020) Long-term survival of head and neck squamous cell carcinoma after bone marrow transplant. *Head Neck* 42(11):3389–3395
89. Hegde PS, Chen DS (2020) Top 10 challenges in cancer immunotherapy. *Immunity* 52(1):17–35
90. Riley RS, June CH, Langer R, Mitchell MJ (2019) Delivery technologies for cancer immunotherapy. *Nat Rev Drug Discov* 18(3):175–196

91. Amin S, Rajabnezhad S, Kohli K (2009) Hydrogels as potential drug delivery systems. *Sci Res Essay* 3(11):1175–1183
92. Lin C-C, Metters AT (2006) Hydrogels in controlled release formulations: Network design and mathematical modeling. *Adv Drug Deliv Rev* 58(12–13):1379–1408
93. Satish C, Satish K, Shivakumar H (2006) Hydrogels as controlled drug delivery systems: synthesis, crosslinking, water and drug transport mechanism. *Indian J Pharm Sci* 68(2):133–140
94. Basso J, Miranda A, Nunes S, Cova T, Sousa J, Vitorino C, Pais A (2018) Hydrogel-based drug delivery nanosystems for the treatment of brain tumors. *Gels* 4(3):62
95. Kashyap N, Kumar N, Kumar MNVR (2005) Hydrogels for pharmaceutical and biomedical applications. *Critic Rev Ther Drug Carr Syst* 22(2):107–149
96. Podstawczyk D, Nizioł M, Szymczyk P, Wiśniewski P, Guiseppi-Elie A (2020) 3D printed stimuli-responsive magnetic nanoparticle embedded alginate-methylcellulose hydrogel actuators. *Addit Manuf* 34:101275
97. Zaman M, Siddique W, Waheed S, Sarfraz RM, Mahmood A, Qureshi J, Iqbal J, Chughtai FRS, Rahman MSU, Khalid U (2015) Hydrogels, their application and polymers used for hydrogels: a review. *Int J Biol Pharm Allied Sci* 4(12):6581–6603
98. Gupta H, Bhandari D, Sharma A (2009) Recent trends in oral drug delivery: a review. *Recent Pat Drug Deliv Formul* 3(2):162–173
99. Ruiz ME, Scioli Montoto S (2018) Routes of drug administration. In: Talevi A, Quiroga PAM (eds) *ADME process in pharmaceutical science*. Springer International Publishing, Cham, pp 97–133
100. Kompella UB, Kadam RS, Lee VHL (2010) Recent advances in ophthalmic drug delivery. *Ther Deliv* 1(3):435–456
101. Edelhauer HF, Rowe-Rendleman CL, Robinson MR et al (2010) Ophthalmic drug delivery systems for the treatment of retinal diseases: Basic research to clinical applications. *Investig Ophthalmol Vis Sci* 51(11):5403–5420
102. Weng Y, Liu J, Jin S, Guo W, Liang X, Hu Z (2017) Nanotechnology-based strategies for treatment of ocular disease. *Acta Pharm Sinica B* 7(3):281–291
103. Kurniawansyah IS, Sriwidodo S, Ravi SMK (2018) Drug delivery system by hydrogel soft contact lens materials: a review. *J Pharm Sci Res* 10(2):254–256
104. Magalhães J, Vieira A, Santos S, Pinheiro M, Reis S (2017) Oral administration of nanoparticles-based TB drugs. In: Grumezescu AM (ed) *Multifunctional systems for combined delivery biosensing diagnostics*. Elsevier, Netherlands, pp 307–326
105. Viswanathan P, Muralidaran Y, Ragavan G (2017) Challenges in oral drug delivery: a nano-based strategy to overcome. In: Andronescu E, Grumezescu AM (eds) *Nanostructures oral medicine*. Elsevier Inc., pp 173–201
106. Indurkha A, Patel M, Sharma P, Abed SN, Shnoudeh A, Maheshwari R, Deb PK, Tekade RK (2018) Influence of drug properties and routes of drug administration on the design of controlled release system. In: Tekade RK (ed) *Dosage form design considerations*, vol. I. Elsevier, pp 179–223
107. Vermani K, Garg S (2000) The scope and potential of vaginal drug delivery. *Pharm Sci Technol Today* 3(10):359–364
108. Krishna SV, Ashok V, Chatterjee A (2012) A review on vaginal drug delivery systems. *Int J Biol Pharm Allied Sci* 1(2):152–167
109. Prausnitz MR, Langer R (2008) Transdermal drug delivery. *Nat Biotechnol* 26(11):1261–1268
110. Tanwar H, Sachdeva R (2016) Transdermal drug delivery system: a review. *Int J Pharm Sci Res* 7(6):2274–2290
111. Alkilani AZ, McCrudden MTC, Donnelly RF (2015) Transdermal drug delivery: innovative pharmaceutical developments based on disruption of the barrier properties of the stratum corneum. *Pharmaceutics* 7(4):438–470
112. Rastogi V, Yadav P (2012) Transdermal drug delivery system: an overview. *Asian J Pharm* 6(3):161–170

113. Vishnubhaktula S, Elupula R, Durán-Lara EF (2017) Recent advances in hydrogel-based drug delivery for melanoma cancer therapy: a mini review. *J Drug Deliv* 2017(ID 7275985):1–9
114. Ahmed I, Elsharif M, Omar A et al (2020) Usage of hydrogels for brain imaging and diagnostics. *Glob J Eng Sci* 4(3):1–7
115. Danhier F (2016) Local delivery of nanomedicines-loaded hydrogel for the treatment of glioblastoma. 8th International Conference and Exhibition on Pharmaceuticals & Novel Drug Delivery System
116. Nih LR, Carmichael ST, Segura T (2016) Hydrogels for brain repair after stroke: an emerging treatment option. *Curr Opin Biotechnol* 40:155–163
117. Bastiancica C, Danhier P, Préata V, Danhier F (2016) Anticancer drug-loaded hydrogels as drug delivery systems for the local treatment of glioblastoma. *J Controll Release* 243:29–42
118. Draganescu D, Lupuliasa D, Dragomiroiu GTAB, Rosca AC, Hincu L, Cioaca D (2019) 3D printing pharmaceutical formulation of drugs in personalized therapy. *Farmacia* 67(1):1–9
119. Stewart S, Domínguez-Robles J, McIlorum V, Mancuso E, Lamprou D, Donnelly R, Larrañeta E (2020) Development of a biodegradable subcutaneous implant for prolonged drug delivery using 3D printing. *Pharmaceutics* 12(2):105
120. Knowlton S, Onal S, Yu CH, Zhao JJ, Tasoglu S (2015) Bioprinting for cancer research. *Trends Biotechnol* 33(9):504–513
121. Zhang YS, Duchamp M, Oklu R, Ellisen LW, Langer R, Khademhosseini A (2016) Bioprinting the cancer microenvironment. *ACS Biomater Sci Eng* 2(10):1710–1721
122. Haleem A, Javaid M, Vaishya R (2020) 3D printing applications for the treatment of cancer. *Clin Epidemiol Glob Health* 8(4):1072–1076
123. Wei X, Liu C, Wang Z, Luo Y (2020) 3D printed core-shell hydrogel fiber scaffolds with NIR-triggered drug release for localized therapy of breast cancer. *Int J Pharm* 580:119219
124. Luo Y, Wei X, Wan Y, Lin X, Wang Z, Huang P (2019) 3D printing of hydrogel scaffolds for future application in photothermal therapy of breast cancer and tissue repair. *Acta Biomater* 92:37–47
125. Saeednia L, Yao L, Cluff K, Asmatulu R (2019) Sustained releasing of methotrexate from injectable and thermosensitive chitosan-carbon nanotube hybrid hydrogels effectively controls tumor cell growth. *ACS Omega* 4(2):4040–4048
126. Trombino S, Servidio C, Curcio F, Cassano R (2019) Strategies for hyaluronic acid-based hydrogel design in drug delivery. *Pharmaceutics* 11(8):407
127. Yang C, Wang X, Yao X, Zhang Y, Wu W, Jiang X (2015) Hyaluronic acid nanogels with enzyme-sensitive cross-linking group for drug delivery. *J Controll Release* 205:206–217
128. Jhan HJ, Liu JJ, Chen YC, Liu DZ, Sheu MT, Ho HO (2015) Novel injectable thermosensitive hydrogels for delivering hyaluronic acid-doxorubicin nanocomplexes to locally treat tumors. *Nanomedicine* 10(8):1263–1274
129. Shi K, Aviles-Espinosa R, Rendon-Morales E, Woodbine L, Maniruzzaman M, Nokhodchi A (2020) Novel 3D printed device with integrated macroscale magnetic field triggerable anti-cancer drug delivery system. *Coll Surf B Biointerfaces* 192:111068
130. Liaw C-Y, Ji S, Guvendiren M (2018) Engineering 3D hydrogels for personalized *in vitro* human tissue models. *Adv Healthc Mater* 7(4):1701165
131. Swaminathan S, Hamid Q, Sun W, Clyne AM (2019) Bioprinting of 3D breast epithelial spheroids for human cancer models. *Biofabrication* 11(2):025003
132. Wang Y, Mirza S, Wu S, Zeng J, Shi W, Band H, Band V, Duan B (2018) 3D hydrogel breast cancer models for studying the effects of hypoxia on epithelial to mesenchymal transition. *Oncotarget* 9(63):32191–32203
133. Szekalska M, Puciłowska A, Szymańska E, Ciosek P, Winnicka K (2016) Alginate: current use and future perspectives in pharmaceutical and biomedical applications. *Int J Polym Sci* 1–17. <https://doi.org/10.1155/2016/7697031>

3D Printed Personalized Orthotic Inserts Using Photogrammetry and FDM Technology



T. Ravi, Rajesh Ranganathan, S. P. Ramesh,
and Devendra Singh Dandotiya

Abstract Orthotic shoe inserts are the most prominent fixtures used in shoes/sneakers of the sportspersons to accurate biomechanical foot issues. One size fits all doesn't work in these cases, as foot shape, curvature, and arch height from person to person differs. As of now, personalized inserts are very expensive due to the conventional manufacturing approach. With improved manufacturing technology, additive manufacturing the future is looking bright and promising. Manufacturing of inserts requires the need for soft or flexible material, which can be exploited conveniently using fused deposit modelling (FDM) technology. In this chapter, inserts have been modeled using unique android phone cameras and free computer software's based on photogrammetry technology, which has the capability to converts a series of 2D images into 3D models with STL file format. Then, the scanned model is smoothed in Mesh mixer software. Subsequently, upon making the changes in the model, the final product is printed and tested for its appropriateness for use. While the product developed is a low cost due to the simple, yet customized manufacturing method, the comfort delivered by the inserts are highly satisfactory.

T. Ravi (✉) · R. Ranganathan
Department of Mechanical Engineering, Coimbatore Institute of Technology,
Coimbatore 641014, Tamil Nadu, India
e-mail: travi.cit@gmail.com

R. Ranganathan
e-mail: drrijeshranganathan@gmail.com

S. P. Ramesh · D. S. Dandotiya
Department of Mechanical Engineering, Presidency University, Bangalore 560064,
Karnataka, India
e-mail: rameshspr@gmail.com

D. S. Dandotiya
e-mail: devendradandotiya@presidencyuniversity.in

1 Introduction

Orthotic Inserts are the biomechanical devices that are embedded into shoes to help feet or “foot curve” to ingest stun and torment bringing about an agreeable way other than remedying inborn anomalies of foot and giving appropriate distribution of pressure while walking. The inserts are helpful devices to lessen the complications because of deformities caused by different human foot profiles.

Prefabricated orthotic inserts are available off shelves and less expensive, as they are manufactured in large quantities, However one size fits all doesn’t work in these cases, as foot shape, curvature, and arch height vary from person to person [1]. Major challenge is the absence of proper basis for combined technologies with the AM process and the necessity to come with a prosthetic or orthotic product design that can satisfy the functional and comfort needs. Conventional approach to manufacture orthotic insoles/inserts call for creating the mould as per the specifications of one’s foot based on the medial longitudinal arch as shown in Fig. 1. The outcome appeared in Fig. 1 were taken using emed pressure distribution platform and clearly shows that there is a no contact of zone at the arch. This work fundamentally proposed to improve arch support utilizing the recent technological advancements. One being, FDM technology that allows the manufacturer to print the personalized

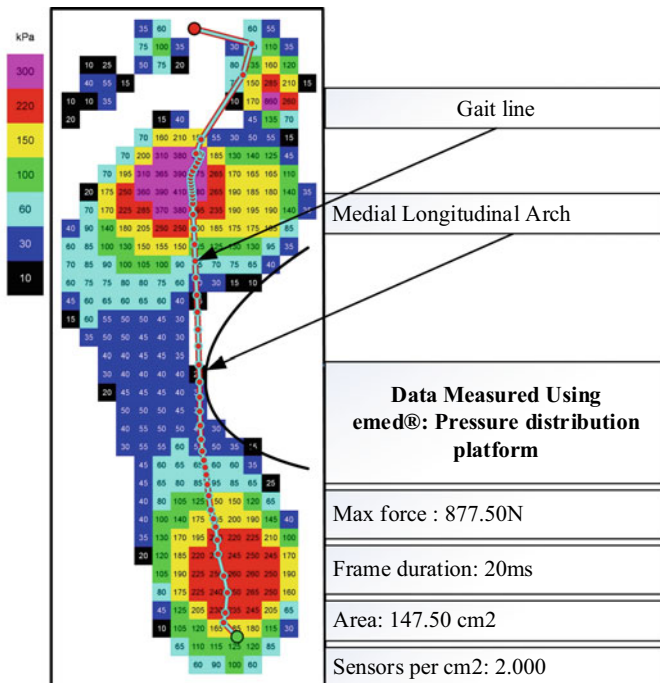


Fig. 1 Human foot medial longitudinal arch using emed

models based on the 3D geometry obtained from photogrammetry technology with the help of multiple series of 2D images.

Number of investigations have been carried out in assessing the outcomes of customized insoles on reduction of plantar pressure and their quantifiable approximations [2]. There is an exponential surge in research work carried in field of fused deposition modeling applied to manufacturing totally functional parts straightaway from a 3D CAD model. The classical fabrication method for producing the prosthetics or orthotic devices involves wastage of material, time, and labor demanding. Due to the exponential evolution of RPT, a drastic transformation in manufacturing of fully functional orthotic devices is witnessed in the recent periods [3]. FDM technique, due to its multifaceted style of adoption to varieties materials, lead to greater acceptability. Application of ADM in biomedical engineering to produce customized complex parts, insoles and orthoprosthesis, has attracted many.

FDM technique finds wide application in the manufacturing of spinal braces [4] and exoskeleton parts [5]. Also, due to its application in the medical and dental industry signifies it being the biggest serving industries in the domain [6]. FDM offers greater flexibility in producing personalized orthotic device. The orthotic inserts and prosthetic devices are highly customizable [7], and is used for appropriate fit for the devices to intricate geometrical features, with a greater accuracy. Adding to these, devices are fabricated economically with better lead-time, and product quality [8].

1.1 Subtractive Manufacturing Versus Additive Manufacturing

Competition in manufacturing field, cost saving and complex product design has led to the need of new technologies to improve design processes. Traditional machining is based on the theme regulated material removal called as subtractive manufacturing as shown in Fig. 2a. Some applications in technologically advancing world, where traditional method of machining become impractical and uneconomical, time consuming and takes too much effort. Additive Manufacturing (AM) is the nontraditional method of manufacturing. Manufacturing is classified as shown in Fig. 3. Additive manufacturing process under Rapid prototyping, is the exact reverse process in which materials are manipulated so that they are successfully combined to form the desired product as shown in Fig. 2b. The awareness of AM has triggered progress in conventional manufacturing methods. In short time, the product can be built with better accuracy and required strength. However, for specific applications, metals, machining will continue to be a major manufacturing process [9].

“Rapid Prototyping” can automatically construct physical models with the aid of Computer-Aided Design data. Fast computing has brought a revolution in the RP manufacturing. More intricate control systems, and better-quality materials,

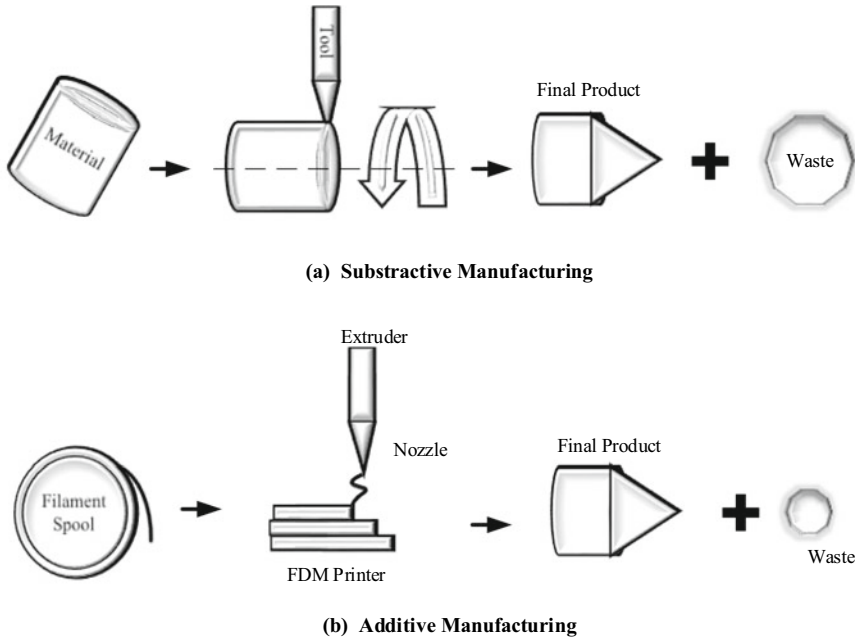


Fig. 2 Subtractive manufacturing versus additive manufacturing

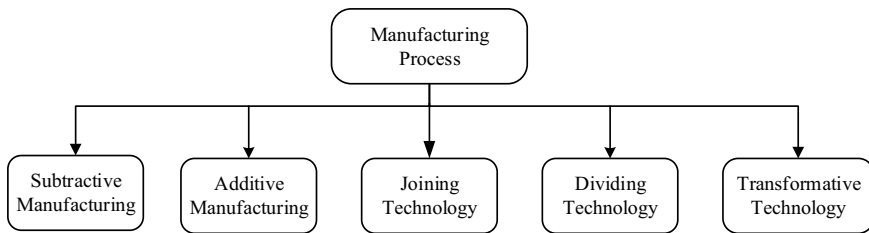


Fig. 3 Classification of manufacturing processes

enhanced RP manufacturing affectedly reduced build time, increased the speed and accuracy of machining. Development of RP has encouraged development in classical subtractive methods [10]. RP will not make conventional machining outdated, but rather accompaniment it. A usual extension of RP is rapid manufacturing of products from the CAD data prepared. RP will improve the lead time of prototyping, will never totally supplant other assembling procedures, particularly in enormous creation runs where large scale manufacturing is more practical. For short creation runs and prototyping, notwithstanding, RM is a lot less expensive, as it doesn't need tooling. Because of nature of manufacturing, it does not require any special/expensive tooling. This is one of the biggest contribution of additive manufacturing.

1.2 Trends in Additive Manufacturing

AM was initially demonstrated in the late 80s, leading to a published article titled Three-Dimensional Data Display by Automatic Preparation of a Three-Dimensional Model [10]. Development of AM occurred in 1987 by Chuck Hull with STL (courtesy: 3D Systems), a procedure which sets layers of ultraviolet (UV) light-sensitive liquid polymer utilizing a laser. It can effectively fabricate complex and personalized models with limited skill employed, shorter conveyance time, and shorter product life cycles. However, AM will never totally supplant other assembling strategies, particularly in productions runs where large scale manufacturing is more affordable [11]. As of now only polymer/plastic materials have been in use as raw materials in AM. However, metals are also used in manufacturing small components through the use of metal powder metallurgy. But there is still a long way to go to achieve full success in manufacturing of real life size and high strength components.

2 FDM Technology

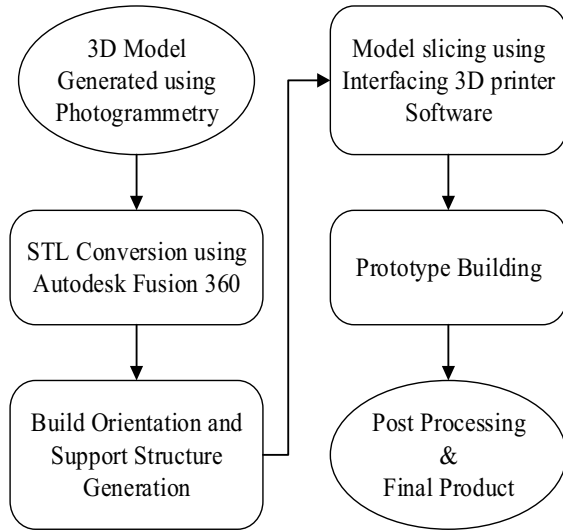
FDM can be suitably employed to build a part or geometry of complex surfaces or volumes by layering material on the build plate in a consecutive manner. The procedure utilizes a nozzle to extrude the warmed ABS fibers in semi-fluid state and permitted to store on the build plate (X-Y plane) in an organized manner with indistinguishable cuts and permits to set at compartment temperature. The quality or cost of the fabricated part absolutely rely upon the boundary conditions employed during the process.

Here, the AM machine employed is FDM uPrint SE wherein the boundary conditions stay fixed according to the vendor defaults. The fundamental determinations of the FDM uPrint SE are, manufacture volume of $8 \times 6 \times 6$ in., the layer thickness of 1.24 mm, ABS P430 fiber with a thickness of 1.78 mm and Catalyst Ex being the interfacing programming software for this technology [12]. FDM fabrication process is shown in Fig. 4.

2.1 Limitations of FDM Technology in 3D Printing

Like every technology, FDM has also has its share of limitation in terms of materials used, applications etc. These limitations will have an impact while printing an object. Despite advances, FDM can bring exceptional results to the industry due to its vast advantages. There are limitations that make additive manufacturing technologies [13] not extensively applied in many areas. Limitations are due to the AM processes itself, which can be improved, as well as to auxiliary

Fig. 4 FDM Uprint SE build process



processes (previous manipulations of material, post-processing, quality control etc.,) that in many cases condition their viability. These limitations are undoubtedly are challenges for research, technological development and innovation. Few of major challenges that 3D printing facing are;

1. Technologies in development
2. Availability and cost of the raw material
3. Initial investment
4. Size of the pieces
5. Non-profitable mass production
6. Finishes and precision of the final product
7. Obtaining digital files
8. Wrapping.

With technological advances, FDM will never be the same and challenges would be resolved. Recent advances in availability of raw materials used for 3D printing are being revived. One of the advantages of FDM include; fast alteration of the filling of the 3D printed models. Which means, it is easy to print a prototype for checking modification and concluding. With less internal filling, or hollow core, we can save on the material cost. Additionally, FDM materials can be of high strength, it is of low cost and waterproof, it can utilize ABS material for its impact resistance and toughness, and different material shades are accessible. 3D printing is upsetting the manufacturing industries in days to come. It makes fabricating more nearby consequently creating more employment/entrepreneur opportunities.

2.2 *Quality Issues*

The limitations of FDM has an impact while printing an object. FDM technology adopts printing of required product, layer by layer of molten filament material. Adhesion and fusion properties between adjacent layers are very critical for quality printed parts. Additionally, the extrusion conditions of the filament material during the printing process affect the accuracy, quality and performance characteristics of the printed product. The surface roughness of the FDM products is one of the major drawbacks of the quality of this process [14]. This will result in higher surface roughness. High levels of roughness ranges hinder the application of the FDM manufactured products in certain fields such as dentistry, biomedical and sensing Components (with high roughness) would be dangerous to use as prosthesis or dental implants due to their reactive property with body fluids. This would cause early implant failure. Sometimes, improper extrusion (over- or under-extrusion) can cause lack of enough adhesion between the adjacent layers of the filament material that promotes high roughness and other structural defects such as porosity and cracks [15].

2.3 *FDM Process Parameters*

FDM technique depends not only on machine but also on material parameters. Machine parameters are essential parameters that the 3D printer client will indicate on the slicing programming during G-code file generation [16]. Other machine parameters include, printing rapidity, raster angle, melt flow rate, air gap, thickness of layer, infill density, build path and temperature [11]. Thermal and mechanical properties of properties influence both the extrusion and performance of the printed product.

3 *Methodology*

This segment is focused on the precise strategy to accomplish the motivation behind the study. Firstly, it begins getting CAD information from the foot geometry and study with respect to the 3D reconstruction utilizing photogrammetry software's and designing using conventional modelling/sculpting software's. Next, the STL format created from CAD programs empowers FDM interfacing software (CatalystEx) to read it.

3.1 Photogrammetry Technology

Additive manufacturing (AM) technology is the most accepted techniques among rapid prototyping. When integrated with the abilities of drone-mapping and photogrammetry software, it speeds up the procedure of creating 3D models of objects and reconstructing them at any measure. Using AM technology, an object can be replicated as it is, through post processing of subject model formed by a smart phone camera and printing out of the fully rectified file using 3D printer.

An approach for personalized orthotic inserts development is driven by employing the photogrammetry and a FDM built 3D Printer is made in this chapter. Here FDM ABS material is only used to making model. The photogrammetry technology and 3D printer is utilized to lessen the expenses and built-up time in comparison with the conventional style of orthotic manufacturing. The schematic outline of methodology is summed up in Fig. 5.

3.2 Technique for 3D Reconstruction of Orthotic Inserts

This effort includes progressive steps which are fundamental for creation of specially crafted insert intended to improve the helpless stride capacities (gait) and stance of individuals (posture). As a beginning, so as to acquire 3D model of the subject foot, a series of photographs need to be taken utilizing an android smart phone which works with the three photogrammetric softwares. In photogrammetry technology, the nature of photographs conveyed by the camera shoulders a crucial job hence so as to fulfill this, a 48MP smart phone camera has been used to choose the colossal factor for the best photogrammetry result.

The camera is utilized to take photographs from all sides of the subject’s lower leg and foot framing 360° round the direction. The photos were taken using auto mode at 10° and 30° shooting edge with 20° augmentations, achieving 50 pictures

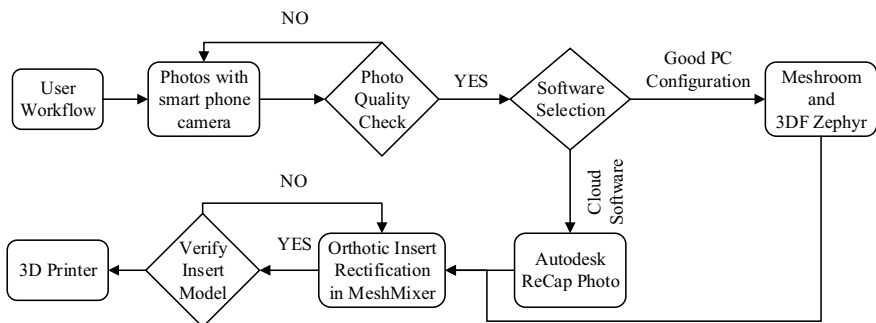


Fig. 5 User systematic workflow for personalized 3D printed orthotic inserts

from all sides of the foot with each individual camera. The technique used for taking the picture is given in Fig. 6. Taking or using less number of pictures would result in low quality model building leading erroneous result. At the same of time quality of picture/images must be good to ensure basic result.

In the wake of taking the photographs, the photographs will be set up in the photogrammetry PC programs. The products used in this chapter are Autodesk Recap Photo 2020, which are cloud based and does not require high end systems. To make it further simple, this light software can be used on a smart phone. Meshroom and 3DF Zephyr listed in Table 1, need to be installed and used on a system. Among these the initial two are Autodesk products and the latter is made by 3DFLOW. These programs are good for making a 3D model from series of photographs with least number of pictures that are required for preparing is 20 numbers. Another software, Autodesk Meshmixer is also employed in this project for editing purposes.

On a basic level, the proposed approach for picture based 3D virtual remaking of a foot could be figured as to cover the accompanying advances as shown in Fig. 7.

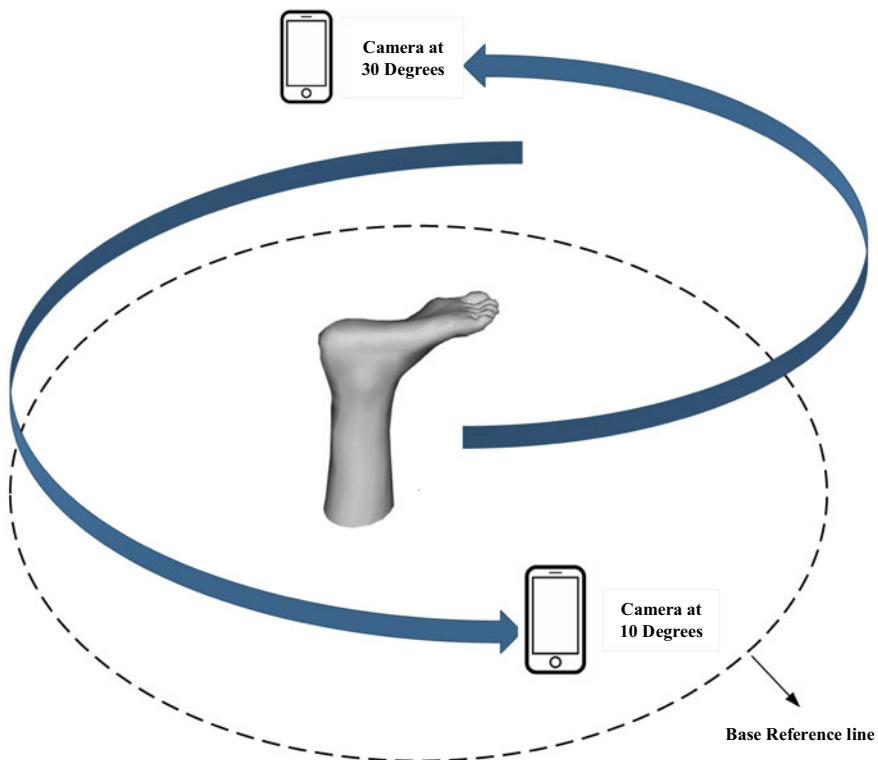


Fig. 6 Procedure utilized for taking series of foot images around the leg

Table 1 Software products used in the chapter

S. No.	Product name	License type	Purpose
1.	Autodesk Recap Photo 2020	Educational	3D reconstruction (photogrammetry)
2.	Autodesk Meshroom	Free	
3.	3DF Zephyr	Free trial	
4.	Autodesk Meshmixer	Free	Editing/refinement

**Fig. 7** Proposed approach for image based 3D virtual reconstruction

The photographs were handled utilizing three photogrammetric software as listed in Table 1. Among the three software's, Autodesk ReCap photo 2020 was found to be giving a superior photogrammetric results and furthermore it is preparing the series of uploaded photos on their cloud servers so, one need not to stress over the PC graphics configuration because, the last render is very intensive and requires NVIDIA CUDA graphic cards. Autodesk Recap photo took a time span around an hour to generate 3D model based on the uploaded series of images. The model comprised by the software could incorporate a few imperfections started from lighting conditions in which photographs of the lower leg and foot were taken as shown in Fig. 7. It is important to play out a cleaning activity to dispose imperfections. The same could be accomplished by utilizing different open-source programs as per the user's wish. In this examination, Autodesk Recap editing tool and Meshmixer software's were used.

The altered lower leg and foot underside is as yet an unpleasant surface. The perfection activity was carried out to improve the surface quality and this progression was likewise executed by using Meshmixer. The surface external to foot bottom and the internal surface of the planned insert ought to have a similar topology to support a decent fit and to fulfill the subject explicitness. So as to acquire a similar topology of foot for inserts design, Autodesk ReCap open-source program was utilized. The yield of this progression is as yet a surface in stereolithography (STL) format and must be changed to a CAD format so as to perform required modeling operations as shown in Fig. 8.

Outside of the insert, which has a similar topography with the foot surface, was later changed over to a water tight model using a regular modeling software. Later,

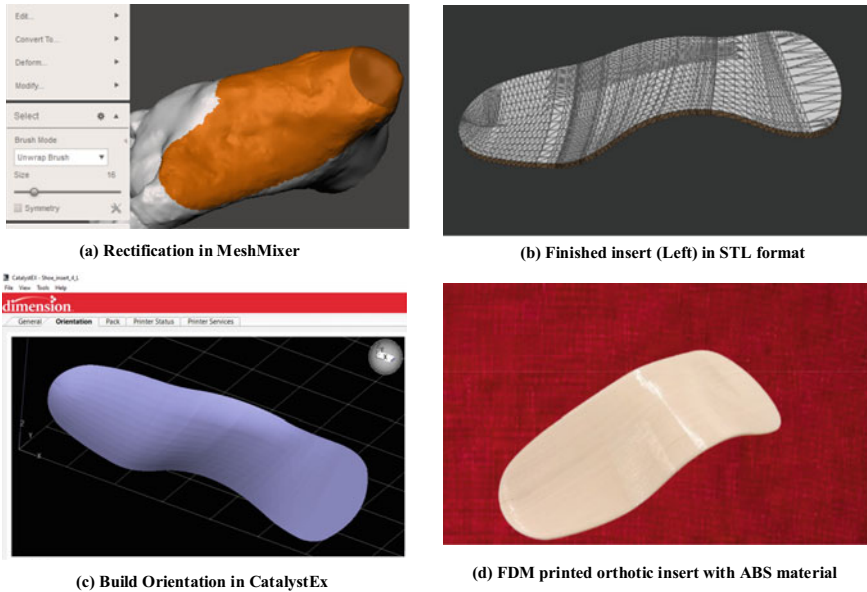


Fig. 8 Rectification of the photogrammetric model and final 3D print

making the suitable corrections, the model was found to be a fit to be printed by a 3D printer. Prior to the final print, build path analysis is suggested for the particular 3D printer for additional material sparing and cost.

4 Results and Discussions

Conventionally, one can acquire the foot geometry by the process of molding, which is laborious and time consuming. Latest advancements in scanning technologies, uncovered another method of generating 3D meshed models with exact shape, size and texture using photogrammetry technology. Generated 3D meshed models could be imported to various open source and educational licensed software's and can be utilized to get explicit calculations for various purposes. Hence, labor, fabrication time and costs that are identified with process of molding or 3D Scanners are perceptibly decreased by using photogrammetry technology. Different 3D scanning software products and gadgets are available in the market for 3D reconstruction. However, these software's are significantly expensive and require skilled persons.

The investigation demonstrated the possibility for utilization of photogrammetry software's and additive manufacturing technology (FDM) for design and development of personalized orthotic insert. The product was successfully built as per the functional prerequisites such as ensuring complete contact, less labor intensive, low

cost and effectively producible. Also, the delivered insert has indicated a decent match with the foot surface of the subject. As the transformation of foot underside to insole surface is the basis for comfort in stance (posture) and stride (gait), a suitable match is a significant outcome for the research.

5 Conclusion

The techniques portrayed in the chapter can be opted for researches wherein 3D scanning or image acquisition of 3D object is an agenda. After 3D printing the orthotics to coordinate explicit subjects and their findings, one could direct an investigation to assess and look at the mechanical properties of a 3D printed orthotic versus that of an orthotic created utilizing a traditional strategy so as to get a reliable and custom fit products. Also, for future examination bearings, inserts could be made by means of various materials. Flexible 3D printable materials and the comfort levels could be contrasted and can be sorted out for the materials which offer improved support for subjects. Various CAE products can be adopted to explore the strength and surface properties of insoles during loading conditions arising from the static and dynamic conditions.

References

1. Webster Joseph MD (2018) Atlas of orthoses and assistive devices. *Phys Med Rehabil*
2. Ganesan S, Ranganathan R (2018) Design and development of customised split insole using additive manufacturing technique. *Int J Rapid Manuf* 7(4):295. <https://doi.org/10.1504/ijrapidm.2018.095783>
3. Tofail SAM, Koumoulos EP, Bandyopadhyay A, Bose S, O'Donoghue L, Charitidis C (2018) Additive manufacturing: scientific and technological challenges, market uptake and opportunities. *Mater Today* 21(1):22–37. <https://doi.org/10.1016/j.mattod.2017.07.001>
4. Ravi T, Ranganathan R, Arumugam S (2020) A conceptual method for developing a Torso Assisted Orthopedic Support Brace (TAOSB) device for people with spinal deformities. *IOP Conf Ser Mater Sci Eng* 788(1). <https://doi.org/10.1088/1757-899x/788/1/012025>
5. Redaelli DF, Storm FA, Biffi E, Reni G, Colombo G (2020) A virtual design process to produce scoliosis braces by additive manufacturing. In: *Design Tools and Methods in Industrial Engineering*, pp 860–870
6. Douglas C, Vito G, Robert R, Sheku K, Xue-Cheng L (2010) Additive fabrication of custom pedorthoses for clubfoot correction. *Rapid Prototyp J*. 16(3):189–193. <https://doi.org/10.1108/13552541011034852>
7. Zuniga J et al (2015) Cyborg beast: a low-cost 3d-printed prosthetic hand for children with upper-limb differences. *BMC Res Notes* 8:10. <https://doi.org/10.1186/s13104-015-0971-9>
8. de Carvalho Filho IFP, Medola FO, Sandnes, FE, Paschoarelli, LC (2020) “Manufacturing technology in rehabilitation practice: implications for its implementation in assistive technology production. In: *Advances in additive manufacturing, modeling systems and 3d prototyping*, pp 328–336
9. Sharma KR, Anand D (2019) Additive and subtractive manufacturing. *Addit Subtractive Manuf* 2(2):174–177. <https://doi.org/10.1515/9783110549775>

10. Mahindru DV, Mahendru P, Mahindru V, Mahendru P (2013) Review of rapid prototyping-technology for the future. *Glob J Comput Sci Technol Graph Vis* 13(4):27–38. ISSN:0975-4172
11. Chua CK, Leong KF, Lim CS (1998) Rapid prototyping principles and applications in manufacturing
12. Ravi T, Ranganathan R (2020) Topology and build path optimization for reducing cost in FDM uPrint SE, pp 189–198. https://doi.org/10.1007/978-981-32-9433-2_16
13. Fernandez-Vicente M, Cayada M, Conejero A (2015) Identifying limitations for design for manufacturing with desktop FFF 3D printers. *Int J Rapid Manuf* 5(1):116–128. <https://doi.org/10.1504/IJRAPIDM.2015.073551>
14. Hsin-Chieh W, Toly CT-C (2018) Quality control issues in 3D-printing manufacturing: a review. *Rapid Prototyp J* 24(3):607–614. <https://doi.org/10.1108/RPJ-02-2017-0031>
15. Gordeevm EG, Galushko AS, Ananikov VP (2018) Improvement of quality of 3D printed objects by elimination of microscopic structural defects in fused deposition modeling. *PLoS One* 13(6):e0198370. Available: <https://doi.org/10.1371/journal.pone.0198370>
16. Popescu D, Zapciu A, Amza C, Baciu F, Marinescu R (2018) FDM process parameters influence over the mechanical properties of polymer specimens: a review. *Polym Test* 69:157–166. <https://doi.org/10.1016/j.polymertesting.2018.05.020>

Manufacturing of Watertight Housing for Electronic Equipment by Fused Deposition Modeling



Pablo E. Romero, Antonio Agulló, and Esther Molero

Abstract In the present work, the influence of different printing parameters (number of perimeters, flow, extrusion temperature, layer height and printing speed) on the watertightness of 3D printed parts has been studied. The vessels have been printed on polyethylene terephthalate glycol (PETG) by fused filament deposition modeling (FDM). A total of 27 prismatic vessels have been manufactured, following a fractioned experimental design. By means of a simple test, the quantity of water that has leaked from each vessel after seven hours has been measured. After analyzing the results obtained, using Taguchi method and analysis of variance (ANOVA), it can be stated that the number of perimeters and the flow are the most influential parameters in the watertightness of the vessels. One of the vessels tested had zero leakage. With the printing parameters of this vessel, an housing has been printed for an ARDUINO board. The watertightness of the housing has been tested by immersion at a depth of 1 m for 30 min, according to the UNE-EN 60529:2018 standard. Although it did not pass the test, the quantity of water that entered the casing was less than 0.5 g.

1 Introduction

Additive manufacturing (AM) technologies were initially developed with the intention of manufacturing prototype products or components that would later be mass produced by other manufacturing processes [1]. After this initial stage, AM is now perceived as a way to manufacture fully functional end products [2].

P. E. Romero (✉) · A. Agulló · E. Molero
Department of Mechanical Engineering, Campus of Rabanales,
Leonardo Da Vinci Building, 14014 Cordoba, Spain
e-mail: p62rocap@uco.es

A. Agulló
e-mail: p22agraua@uco.es

E. Molero
e-mail: z72moreo@uco.es

Although there are different AM technologies, the most extended at present is fused deposition modeling (FDM) [3]. This is due to several reasons [4]: the cost of the equipment is low; the portfolio of filaments available in the market is broad; the learning curve is short; the information available in the network is abundant; there are many spare parts for the 3d printers at affordable prices.

To perform certain functions, parts manufactured by FDM must meet different properties: resistance to mechanical loads, ultraviolet (UV) radiation resistance, resistance to chemical solvents, watertightness, among others. The mechanical characteristics of parts printed using FDM have been widely studied in the literature [5]. UV radiation resistance is achieved by using the appropriate filaments, such as polyethylene terephthalate glycol (PETG) [4]. The resistance to certain chemical products has been studied by some authors, interested in the use of 3D printing tools in chemical processes [6].

Al-Hasni and Santori [7] have carried out watertightness tests on printed parts by FDM, using air equipment that allows them to carry out both pressure and vacuum tests. Test pieces were printed and tested in both polylactic acid (PLA) and acrylonitrile butadiene styrene (ABS) and the influence of the layer height and extrusion flow on the tightness was studied. The authors concluded that, due to the manufacturing process, parts printed using the FDM technique have pores through which air enters or exits under pressure. To improve the sealing results, they propose the use of epoxy resin infusion to fill the voids.

Gordeev et al. [6] have analyzed the possibilities of 3D printed recipients using FDM in an organic chemistry laboratory. The authors printed diverse elements (Erlenmeyer flask, round-bottom flask, funnel, test tubes, and beaker) using different filaments (PETG, PLA, ABS, polypropylene -PP-). The test results showed that the permeability depended on the geometry of the vessel, the wall thickness and the material used for printing. The authors attribute the lack of watertightness to the layered structure and propose subjecting the printed vessels to thermal post-treatment (fritting) to eliminate leaks.

On the other hand, Shaghghi and Mayer [8] have manufactured an FDM housing for the electronic equipment used in the automation of an irrigation system. The authors subjected the housing to a series of showers from different angles for 15 min (according to the UNE-EN 60529:2018 standard [9]). The results of the tests were positive, so they replaced a standard housing with IP65 protection with a customized housing printed in 3D. The material used to manufacture the enclosure was PETG, due to its resistance to environmental elements [4].

In the present work, the influence of five parameters (number of perimeters, flow, extrusion temperature, layer height and printing speed) on the degree of tightness achieved in prismatic vessels printed on PETG by means of FDM is evaluated. For this purpose, a fractioned design of experiments (DOE) has been drawn up, consisting of a total of 27 tests. An equal amount of water has been deposited in each vessel, and the amount that each vessel has lost after a period equal to seven hours has been measured. The information obtained in this initial test has been used to print an enclosure for an ARDUINO electronic board. The filament chosen has been PETG because the housing is going to be used outdoors.

2 Materials and Method

The methodology followed in this work is shown in Fig. 1. First, the vessel was modeled in three dimensions with the help of SolidWorks software. Secondly, the input variables to the problem were selected and the design of experiments was elaborated. Thirdly, the G-code files needed to print the part were generated. Then, the vessels were printed using a fused filament deposition modeling (FDM) 3D printer. Fifthly, the watertightness tests were carried out; from the results obtained, using the Taguchi and ANOVA method, the influence of the different printing parameters on this watertightness was analyzed. Finally, a housing for electronic equipment was designed, printed, and evaluated.

2.1 3D Modeling of the Vessel

The model of the vessels was made using the SolidWorks parametric software (release 2018) (Fig. 2). The inner dimensions of each vessel were $25 \times 25 \times 50 \text{ mm}^3$. Once the digital model of the vessel was created, it was exported as STL (stereolithography).

2.2 Design of Experiment

The printing variables studied in this work are number of perimeters, flow, extrusion temperature, layer height and printing speed. For each of these variables, three

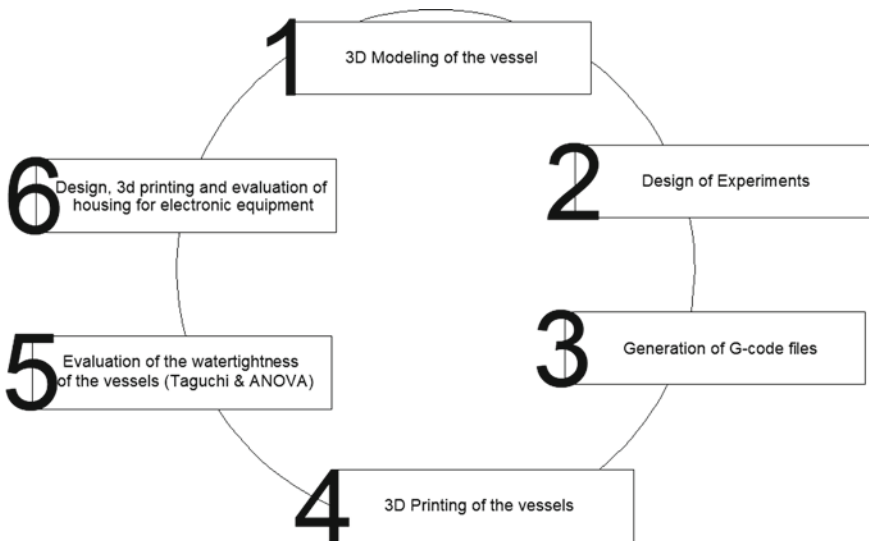
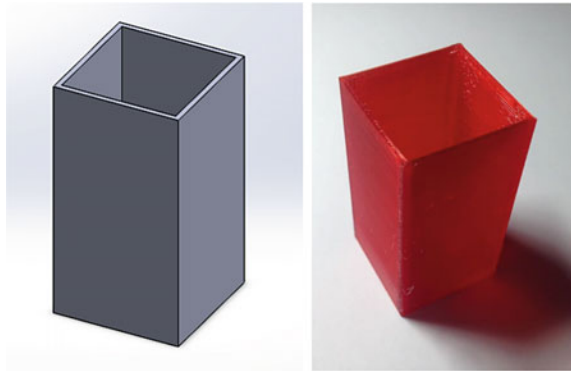


Fig. 1 Diagram showing the methodology followed in this work

Fig. 2 Vessel used in waterproofing tests: design made in SolidWorks (release 2018) (left); actual picture of the vessel (right)



levels were established (Table 1). From these levels, a design of L27 experiments was elaborated (Table 2).

2.3 Generation of G-Code Files

The CURA software (release 4.3.0) was used to generate the G-code files corresponding to the 27 vessels. The STL file created in the first step was imported from CURA. For each vessel, the corresponding printing parameters were defined in each case, using the information indicated in Table 2.

2.4 3D Printing of the Vessels

The vessels were printed on a common FDM printer (Creality Ender 3). The 3D printer has a heated bed measuring $220 \times 220 \text{ mm}^2$ and is equipped with an extruder. The filament used to print the vessels was PETG, supplied by FormFutura. This filament was chosen for its excellent properties (it is waterproof, corrosion and impact resistant). Using the printer's clock timer, the time needed to Print each vessel was measured.

Table 1 Levels of the design of experiment (DOE)

Print parameters	Unit	Level 1	Level 2	Level 3
Perimeters	Number	2	3	4
Flow	%	100	105	110
Extrusion temperature	°C	215	225	235
Layer height	mm	0.16	0.20	0.24
Print speed	mm/s	50	70	90

Table 2 Design of experiments

Test	Perimeters (#)	Flow (%)	Extrusion temperature (°C)	Layer height (mm)	Print speed (mm/s)
1	2	100	215	0.16	50
2	2	100	215	0.16	70
3	2	100	215	0.16	90
4	2	105	225	0.20	50
5	2	105	225	0.20	70
6	2	105	225	0.20	90
7	2	110	235	0.24	50
8	2	110	235	0.24	70
9	2	110	235	0.24	90
10	3	100	225	0.24	50
11	3	100	225	0.24	70
12	3	100	225	0.24	90
13	3	105	235	0.16	50
14	3	105	235	0.16	70
15	3	105	235	0.16	90
16	3	110	215	0.20	50
17	3	110	215	0.20	70
18	3	110	215	0.20	90
19	4	100	235	0.20	50
20	4	100	235	0.20	70
21	4	100	235	0.20	90
22	4	105	215	0.24	50
23	4	105	215	0.24	70
24	4	105	215	0.24	90
25	4	110	225	0.16	50
26	4	110	225	0.16	70
27	4	110	225	0.16	90

2.5 Evaluation of the Watertightness of the Vessels

To measure the watertightness of each vessel, a digital scale, a plate and a sheet of absorbent paper were used (Fig. 3): first, the plate was located on the scale; on the plate, the sheet of paper was placed and the scale was tared; then, the vessel was situated on the paper and 30 ml of water were deposited by means of a syringe; after 7 h, the vessel was removed; the value marked on the digital scale was taken (this value is equal to the mass of water lost by the vessel).



Fig. 3 Tightness test: the digital scale with the absorbent paper sheet is set to zero, the vessel is filled with 30 ml of water and the stopwatch is activated (left); after 7 h, the weight of the amount of water that has leaked and been absorbed by the paper is determined (right)

2.6 Design, 3D Printing and Evaluation of Housing for Electronic Equipment

The goal of this work is to manufacture a waterproof housing for an Arduino Uno board by means of FDM 3D printing. To do this, the measurements of the electronic board were taken, using a caliper. From the measurements taken ($75 \times 55 \times 15 \text{ mm}^3$), a housing prototype was drawn in SolidWorks. As shown in Fig. 4, the proposed design consisted of two parts (a male and a female), each with four lugs. In these lugs are provided through holes that serve to accommodate four M4 \times 25 mm screws. The closure is achieved by means of the tightening provided by these screws and the corresponding nuts (Fig. 5, left). To guarantee the watertightness of the joint, a slot has been provided in one of the parts to house a rubber seal. The rubber seal was also printed using thermoplastic elastomer (TPE) filament.

Once printed, the casing was subjected to a test in accordance with the UNE-EN 60529:2018 standard [9]. To do this, it was immersed in water for 30 min at a depth of one meter (Fig. 5, right). A total of three tests were carried out. To measure the amount of water that entered the enclosure, a system similar to that explained for the vessels was used: (i) a sheet of absorbent paper was taken and weighed on the scale; (ii) the sheet of paper was then placed inside the casing; (iii) the casing was closed and the four screws were placed; (iv) the casing was placed into the water, one meter deep, with a weight on top to prevent it from floating; (v) after 30 min, the casing was dried well on the outside and opened carefully; (vi) the paper was removed and weighed on the digital scale.

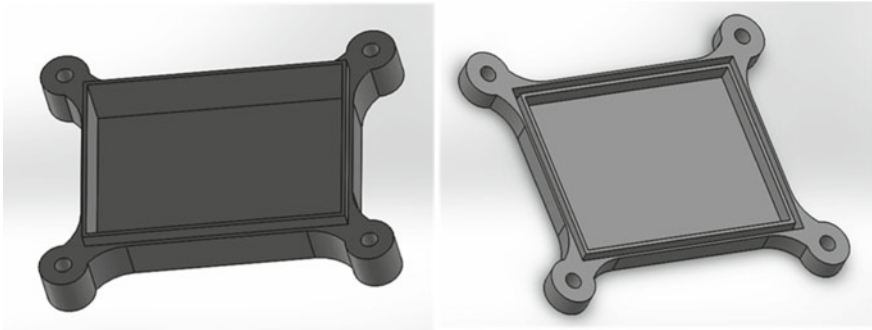


Fig. 4 Design of the Arduino electronic board housing: inferior case (left); superior case (right)

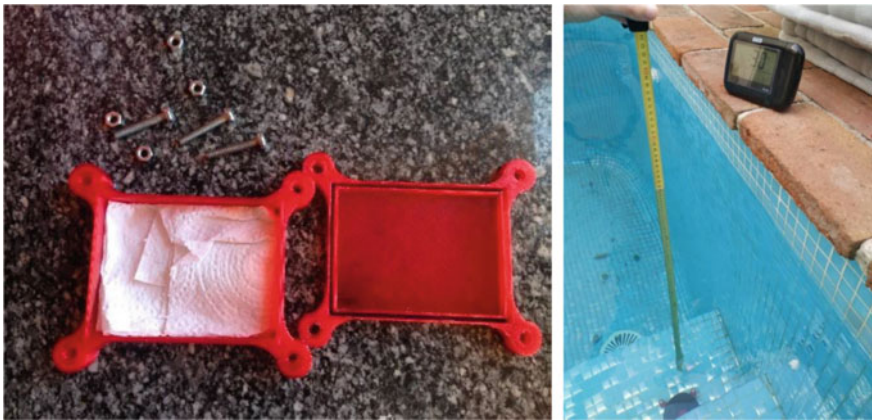


Fig. 5 Housing watertightness test: housing before immersion (left); immersion at 1 m depth for 30 min (right)

3 Results

3.1 Watertightness Tests on Vessels

Table 3 summarizes shows the results obtained in the tests. In the first column, the printing time of each vessel is indicated. The second column shows the length of filament used during the printing of each vessel. The third column present the amount of water, in grams, that each vessel has lost after 7 h.

Figure 6 shows the relationship between the time spent printing each vessel and the different printing parameters studied. This graph has been generated from the data in Tables 2 and 3, using the Taguchi method. On the other hand, Table 4 presents the results of an ANOVA analysis. In this case, the results coincide with what is expected: the vessels with the highest number of perimeters, with the lowest

Table 3 Design of experiments (DOE)

Test	Printing time (min)	Filament used (mm)	Leaked water (g)
1	62	1.98	6.60
2	60	1.98	23.05
3	60	1.98	23.22
4	50	2.07	12.41
5	49	2.07	20.02
6	48	2.07	6.60
7	42	2.19	14.90
8	41	2.19	6.59
9	41	2.19	11.57
10	61	3.10	14.69
11	50	3.10	18.06
12	50	3.10	16.73
13	91	3.26	11.54
14	73	3.26	9.74
15	73	3.26	10.4
16	73	3.43	14.07
17	60	3.43	4.12
18	59	3.43	16.73
19	87	4.09	15.39
20	66	4.09	12.23
21	57	4.09	9.08
22	75	4.30	8.16
23	57	4.30	6.14
24	49	4.30	13.35
25	110	4.51	0.00
26	83	4.51	4.46
27	72	4.51	5.97

layer height and with the lowest printing speed are those that take the longest time to print. There are combinations that allow printing times of less than 50 min, while others exceed 100 min (Table 3 and Fig. 7).

Figure 8 shows the relationship between the quantity of water leaked from each vessel and the different printing parameters studied. As in the previous case, the results obtained using the Taguchi method have been contrasted using an ANOVA (Table 5). As can be seen, the parameters that have a higher contribution and a lower p-value are the number of perimeters and the flow. The vessels that have been printed with a higher number of perimeters have low average leaks. Similarly, vessels printed with a high flow value have low average losses. To achieve maximum tightness, it is necessary to print the vessels with 4 perimeters and a flow equal to 110% (Fig. 9).

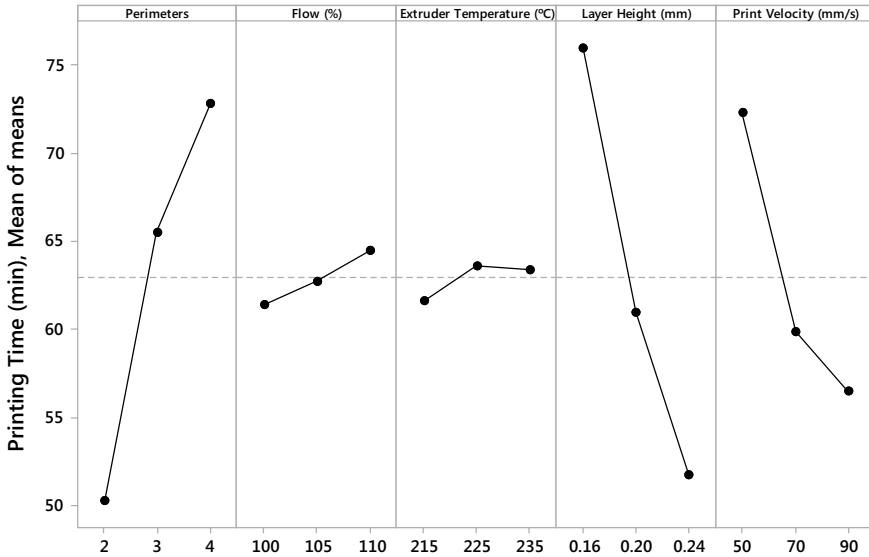


Fig. 6 Results obtained via Taguchi method for printing time of the vessels

Table 4 Results obtained via ANOVA for printing time of the vessels

Parameters	Contribution (%)	p-value
Perimeters	33.30	0.00
Flow (%)	0.61	0.64
Extruder temperature (°C)	0.30	0.80
Layer height (mm)	37.60	0.00
Print velocity (mm/s)	17.39	0.00
Error	10.80	*

Figure 10 shows simultaneously the printing time needed to produce each vessel, as well as the water losses for each one during the tests. As you can see, there are combinations of printing parameters that require high printing times, but that allow to reach a total watertightness. If the printing time is a priority factor, and the watertightness condition can be relaxed, certain interesting combinations can be found in the graph, which allow to reduce the printing times between 45% and 63%.

3.2 Watertightness Tests in Housing for Electronic Equipment

The combination of parameters that obtained the best results in the watertightness tests performed on the specimens was (Fig. 10): number of perimeters equal to 4,

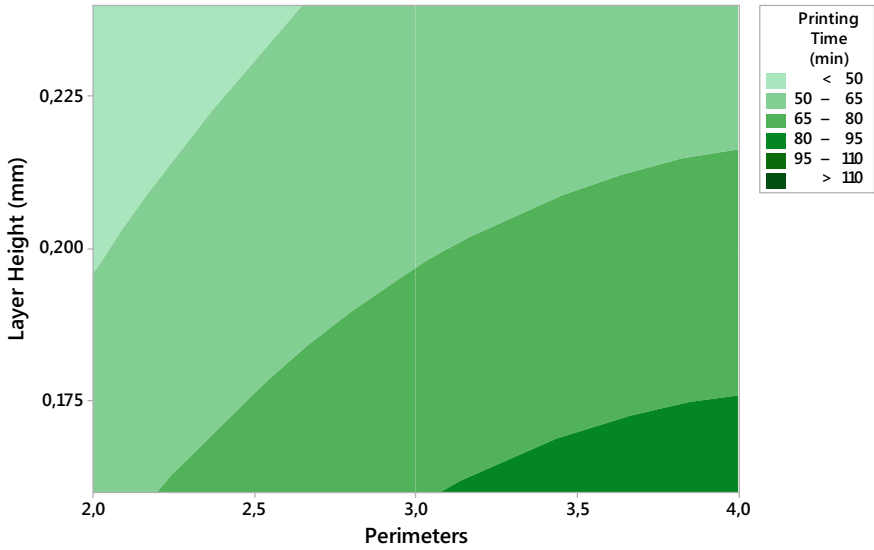


Fig. 7 Vessels printing time of the vessels as a function of the number of programmed perimeters and layer height

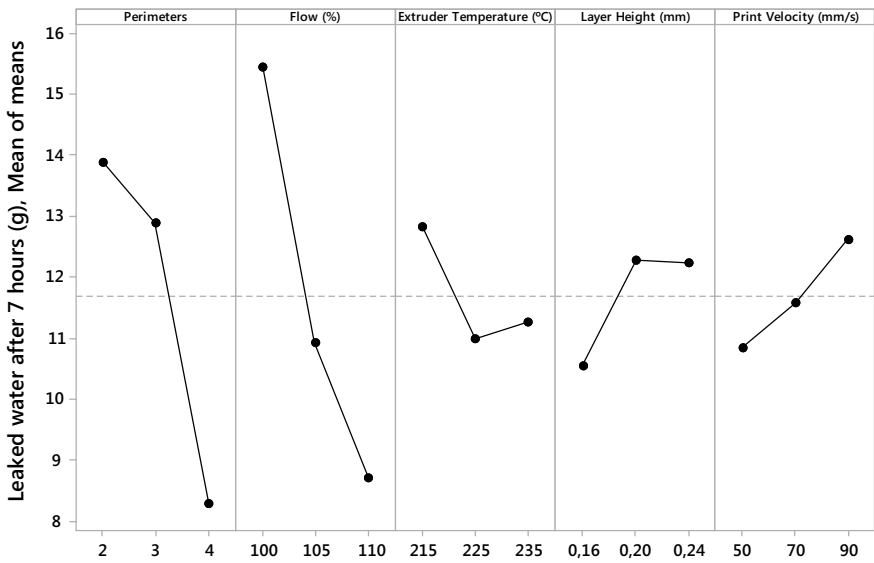


Fig. 8 Results obtained via Taguchi method for leaked water from vessels after 7 h

Table 5 Results obtained via ANOVA for leaked water from vessels after 7 h

Parameters	Contribution (%)	p-value
Perimeters	18.16	0.09
Flow (%)	24.19	0.04
Extruder temperature (°C)	2.00	0.73
Layer height (mm)	2.01	0.73
Print velocity (mm/s)	1.61	0.78
Error	52.01	*

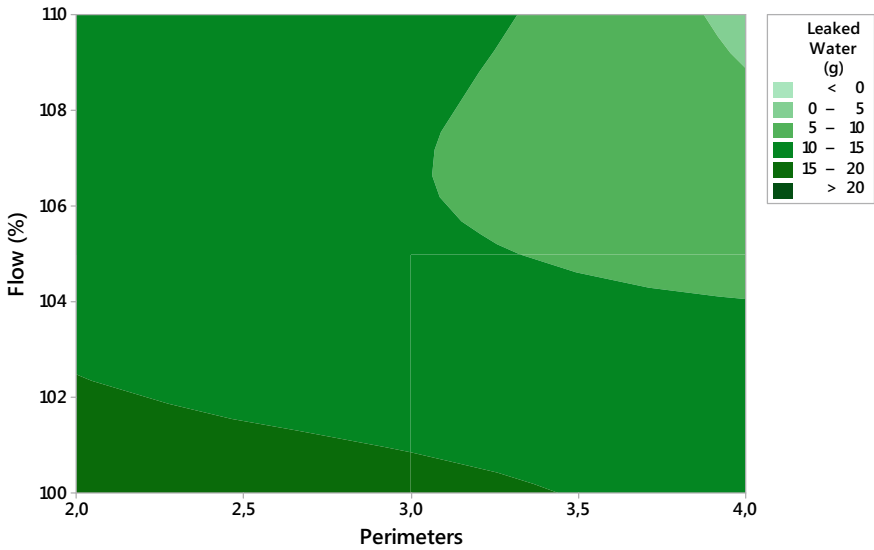


Fig. 9 Leaked water from the vessels as a function of the number of programmed perimeters and flow

flow equal to 110%, extrusion temperature equal to 225 °C, layer height equal to 0.16 mm and printing speed equal to 50 mm/s. Using these printing parameters, a housing was fabricated for an Arduino Uno board. The housing is formed by two pieces that fit into each other (Fig. 5, left). To ensure the closure of both parts, a gasket made using TPE filament was printed.

The watertightness tests were carried out according to the UNE-EN 60529:2018 standard [9]. A total of three dives were carried out. The results obtained, as well as the arithmetic mean of them, are shown in Table 6. As can be seen in this table, the average amount of water entering the housing is less than 0.5 g half a gram.

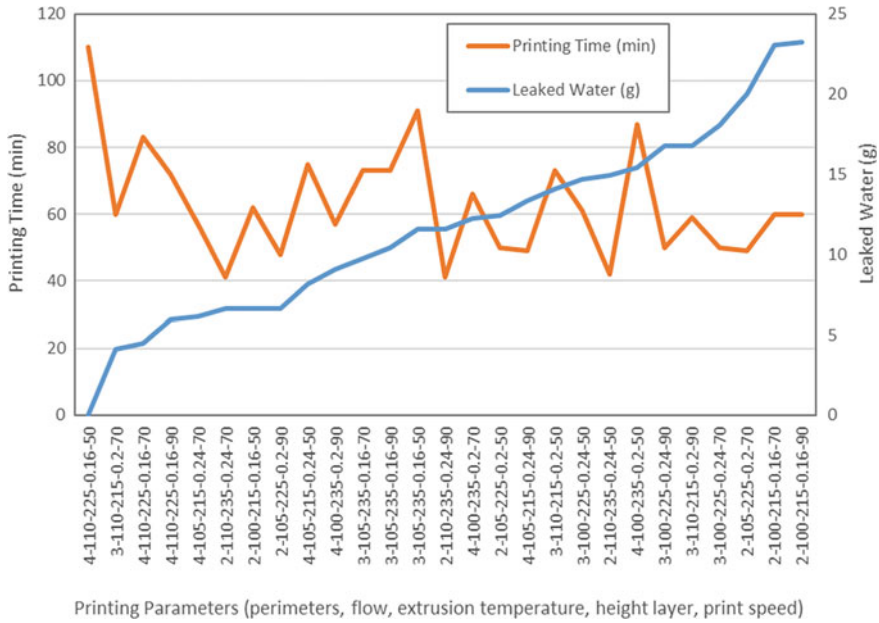


Fig. 10 Printing time and leaked water from the vessels as a function of the printing parameters used

4 Discussion

In the present work, the relationship between different printing parameters in FDM (perimeters, flow, extrusion temperature, layer height and printing speed) and the watertightness of 3D printed parts has been analyzed. For this purpose, a fractioned DOE has been elaborated (Table 2), and a total of 27 prismatic vessels have been printed (Fig. 2). The same volume of water has been deposited in each vessel, and the mass that each one has lost after 7 h has been measured (Fig. 3). From the results obtained, which have been analyzed by Taguchi and ANOVA, it can be stated that the most influential parameters in the watertightness of the printed vessels are the number of perimeters and flow (Fig. 8): a higher number of perimeters and a higher flow value are associated with higher watertightness (Fig. 9). On the other hand, it has been proven experimentally that a higher number of perimeters means a longer printing time (Figs. 6 and 7).

One of the printed vessels has been completely sealed (Fig. 10). This vessel was printed with the following printing parameters: number of perimeters equal to 4, flow equal to 110%, extrusion temperature equal to 225 °C, layer height equal to 0.16 mm and printing speed equal to 50 mm/s. The time needed to print this specimen was 110 min and 4.51 m of filament were needed to complete its manufacture (Table 3). Setting the printing parameters previously mentioned, a housing

Table 6 Results of the tests carried out on the housing according to the UNE-EN 60529:2018

Test	Water entering the housing
1	0.56
2	0.35
3	0.41
Mean	0.44

was fabricated for an ARDUINO electronic board (Fig. 5, left). This housing was subjected to an immersion test at a depth of one meter for 30 min, as required by the UNE-EN 60529:2018 standard [9] (Fig. 5, right). The test was performed three times, and the average quantity of water that penetrated the housing was less than 0.5 g (Table 6).

The results of the present work are consistent with those obtained by other authors of the literature. Al-Hasni and Santori [7] printed six test pieces by means of FDM, with different values of layer height and flow, and carried out watertightness tests with pressurized air. After analyzing the results, they concluded that the extrusion flow is an influential parameter in the tightness, while the layer height is not. The number of perimeters is a variable that these authors did not study.

The housing fabricated in this work does not completely pass the immersion test. The authors believe that water entered the enclosure due to a poor design of the socket between the upper and lower housing. In any case, this result is like that obtained by Champion et al. [10], who tried to manufacture a housing to house electronic equipment in an underwater robot. The degree of protection required in that case was IP68 (resistance to prolonged immersion), according to the UNE-EN 60529:2018 standard [9]. The authors used both PLA and ABS and tested different designs of the enclosure. However, they were not able to reach the initially set goal.

In any case, even if the housing fabricated in the present work does not reach the IP68 protection degree, the requirements for the IP65 degree (completely sealed against dust and protects the equipment against water jets) are exceeded. This result is similar to that obtained by Shaghaghi and Mayer [8], who produced an enclosure using FDM for electronic equipment used in the automation of an irrigation system. They subjected the housing to 15 min showers from different angles, as required by the UNE-EN 60529:2018 standard [9], with satisfactory results. In this way, the printed housing replaced a conventional generic housing with an IP65 degree of protection. In this work, the printing parameters used during the printing of the enclosure were not detailed.

Gordeev et al. [6] stated in their paper that ABS, PLA and PP are more watertight than PETG. Furthermore, they indicate that to guarantee the watertightness of a piece printed in FDM, the piece must be subjected to thermal post-treatment (fritting) in order to reduce the porosity of the printed material. For the same reason, Al-Hasni and Santori [7] also recommend the use of a chemical post-treatment (resin infusion) to guarantee the watertightness of parts printed using FMD. The authors of the present work want to emphasize that one of the printed vessels has passed a simple watertightness test without the need to use any type of post-treatment, simply with an adequate selection of the printing parameters.

5 Conclusion


In the present work, the relationship between several printing parameters and the watertightness of pieces printed on PETG via FDM has been studied experimentally. For this purpose, 27 vessels have been fabricated following a fractioned DOE. Each printed vessel has been subjected to a watertightness test during seven hours. The results obtained have been statistically analyzed, using the Taguchi and ANOVA methods. In this way, it has been demonstrated that the most influential parameters in the watertightness of the vessels are the number of perimeters and the flow. One of the test pieces has managed to pass the watertightness tests, without the need to apply any type of thermal or chemical post-treatment. Using the printing parameters corresponding to the aforementioned vessel, an housing has been printed for an ARDUINO electronic board. This housing has been subjected to an immersion test according to UNE-EN 60529:2018, corresponding to an IP67 degree of protection. Although the housing has not passed the demanding test, it has come close: due to deficiencies in the design of the joint between the two parts of the housing, a small amount of water (less than 0.5 g) has entered the enclosure. In future work, an attempt will be made to improve the design of this joint and to achieve resistance to prolonged immersion (IP68).

References

1. Gibson I, Rosen DW, Stucker B (2014) Additive manufacturing technologies: 3D printing, rapid prototyping, and direct digital manufacturing. Springer, New York
2. Dawoud M, Taha I, Ebeid SJ (2016) Mechanical behaviour of ABS: an experimental study using FDM and injection moulding techniques. *J Manuf Process* 21:39–45
3. Ngo TD, Kashani A, Imbalzano G, Nguyen KTQ, Hui D (2018) Additive manufacturing (3D printing): a review of materials, methods, applications, and challenges. *Compos Part B Eng* 143:172–196
4. Barrios JM, Romero PE (2019) Improvement of surface roughness and hydrophobicity in PETG parts manufactured via fused deposition modeling (FDM): an application in 3D printed self-cleaning parts. *Materials* 12(15):1–15
5. Chacón JM, Caminero MA, García-Plaza E, Núñez PJ (2017) Additive manufacturing of PLA structures using fused deposition modelling: effect of process parameters on mechanical properties and their optimal selection. *Mater Des* 124:143–157
6. Gordeev EG, Degtyareva ES, Ananikov VP (2016) Analysis of 3D printing possibilities for the development of practical applications in synthetic organic chemistry. *Rus Chem Bull* 65 (6):1637–1643
7. Al-Hasni S, Santori G (2019) 3D printing of vacuum and pressure tight polymer vessels for thermally driven chillers and heat pumps. *Vacuum* 171:109017
8. Shaghghi N, Mayer J (2019) A sustainable 3D-printed casing for hydro-system automation sensing units. In: IEEE global humanitarian technology conference. Seattle
9. UNE-EN 60529:2018 degrees of protection provided by enclosures (IP Code)
10. Champion BT, Jamshidi M, Joordens MA (2016) 3D printed underwater housing. In: Proceedings of the biannual world automation congress, Rio Grande

4D Printing by Fused Deposition Modeling (FDM)



Mohammad Aberoumand, Davood Rahmatabadi,
Ahmad Aminzadeh, and Mahmoud Moradi 

Abstract 4D printing is a pioneer field to produce functional smart devices. The combination of 3D printing and smart material is called as 4D printing. The extra dimension refers to time in order to shape transformation of the printed part during time. FDM is a universal process to 3D printing of thermoplastic polymers. Therefore, for successful and typical 4D printing a deep understanding of every aspect of shape memory polymers especially thermoplastic polymers is necessary. So, in this chapter, shape memory polymers, printing preparation such as filament production and FDM printing parameters, finally applications, previous finding and functional printed parts by FDM have been studied detailed.

1 Introduction

Additive manufacturing (AM) or 3D printing is a type of manufacturing of solid part by layer-by-layer material deposition from a computer-aided design (CAD) model that have been sliced to number of layers in respect of its accuracy,

M. Aberoumand · D. Rahmatabadi
School of Mechanical Engineering, University of Tehran, Tehran, Iran
e-mail: m.aberoumand@ut.ac.ir

D. Rahmatabadi
e-mail: d.rahmatabadi@ut.ac.ir

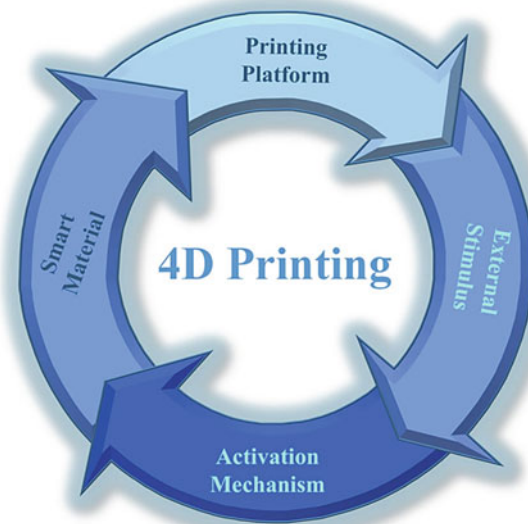
A. Aminzadeh
Department of Mathematics, Computer Science and Engineering,
Université du Québec à Rimouski, Rimouski, Québec, Canada
e-mail: ahmad.aminzadeh@uqar.ca

M. Moradi (✉)
School of Mechanical, Aerospace and Automotive Engineering, Faculty of Engineering,
Environment and Computing, Coventry University, Gulson Road, Coventry CV1 2JH, UK
e-mail: moradi@malayeru.ac.ir; moradi.malayeru@gmail.com

Department of Mechanical Engineering, Faculty of Engineering, Malayer University,
Malayer, Iran

surface roughness and resolution. A vast of AM processes have been developed for any type of materials such as metals, polymers, ceramics and their composites. Main 3D printing uses was for comprehensive prototyping at first but nowadays, researches and industries tried to use it as final part for aerospace, automotive, electronics and specially for customized uses for health care and biomedical applications such as stents, scaffolds, artificial tissues and etc. [9, 14, 18, 23]. Among of various techniques for printing polymers, fused deposition modeling (FDM) or fused filament fabrication (FFF) is most popular 3D printing technique in comparison with Polyjet and other liquid-AM techniques because of its low cost and easiness to use and maintenance so that even home version is available in market. In the FDM technique, a thermoplastic material filament is fed into a machine via a pinch roller mechanism then is melted in a heated liquefier and the solid portion of the filament acting as a piston to push the melt through a print nozzle [9, 18, 23, 28, 36]. Shape memory effect (SME) of some materials can be described as the ability of recover a deformation via some stimulus at a certain pre-defined condition and the common stimuluses are temperature, electricity, magnetic field, moisture, UV or light and etc. Among all the shape memory materials, SMPs and SMPCs are most popular due to light weight, higher deformation, higher tendency for strain recovery, lower and programing temperature, easier process ability, variety of materials, biocompatibility and biodegradability [10, 19, 20]. 4D printing is combination of 3D printing and SME that one more dimension is related to the time that is provided by dynamic shape changing of 3D printed part. In fact, 4D printed part can alter the shape, property, or functionality of a 3D printed structure as a function of time. 4D printing has benefits of 3D printing and beside that it has shape the ability to self-assembly, self-adaptation, actuating

Fig. 1 Four necessary conditions for 4D printing [27]



and sensing [14, 18, 20, 21]. As shown in Fig. 1, at least for successful 4D printing, we must have four condition that are best known for us. These are 3D printing facility, external stimulus, smart material and activation mechanism or programing.

2 Shape Memory Polymers

SMPs are a type of smart materials that exhibit SME. SMPs always can remind the original shape which has been created by initial forming process such as molding, extrusion, curing mold for thermosets. 3D printing process are composed by above-mentioned initial forming process like extrusion in FDM. In fact, shape memory polymers can fix deformation in a proper special thermomechanical condition that is named as temporary shape and can recover its initial before deformation shape in a special condition by an appropriate stimulus that is named as permanent shape. This behavior is an intrinsic property of this type of materials that is not covered to us and it has its special mechanisms that will discussed in next section [19]. It can be noted that all semi crystalline polymers exhibit SME but majority of then cannot exhibit strong SME and most of them need to be modified. The more common SMP type is thermal responsive one that temperature acts as trigger. Programing of temperature responsive SMPs consists of main four step as Fig. 2. The first step is rising of temperature above T_{trans} make a deformation in material. In second step, the sample must be cooled under the T_{trans} while the load is remained to fix the deformation then the load can be eliminated after quenching for the third step. In the final step, the temperature will be raised above T_{trans} and the permanent shape is recovered. There are some parameters for quantification of fixing and recovery ability of the smart material that are named as shape fixing ratio (Rf) and shape recovery ratio (Rr), respectively. Based on data in Fig. 2:

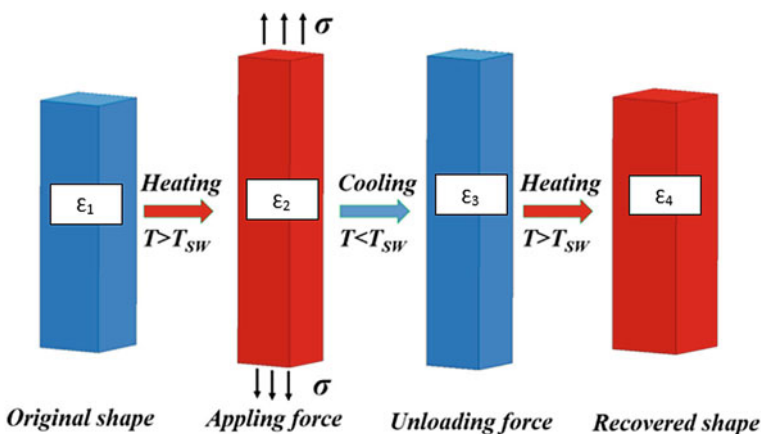


Fig. 2 The shape memory polymer programing [32]

$$\%Rf = \frac{\epsilon_3 - \epsilon_1}{\epsilon_2 - \epsilon_1} * 100 \tag{1}$$

$$\%Rr = \frac{\epsilon_4 - \epsilon_3}{\epsilon_1 - \epsilon_3} * 100 \tag{2}$$

Figure 3 shows the relation between temperature-strain and stress during programming of a SMP. Shape recovery ratio never get 100% and always there is unrecoverable hysteresis due to molecular architecture on smart polymer that discussed in the next section. In fact, in shape memory effect, an elastic force is saved to the material ad under proper stimulation, the saved elastic force releases and make recovery of deformation. The unrecoverable strain is related to the ability of molecular architecture to behave to the deformation as elastic with lowest relaxation tendency. However, whatever the tendency of relaxation of a polymer increase, the recovery ratio will decrease [25].

2.1 Mechanisms

SMPSs consist of two main part, a part which is responsible for storing elastic energy without relaxation and keeps the permanent shape of the sample and the second one is responsible for keeps the stored energy and releases it with switching

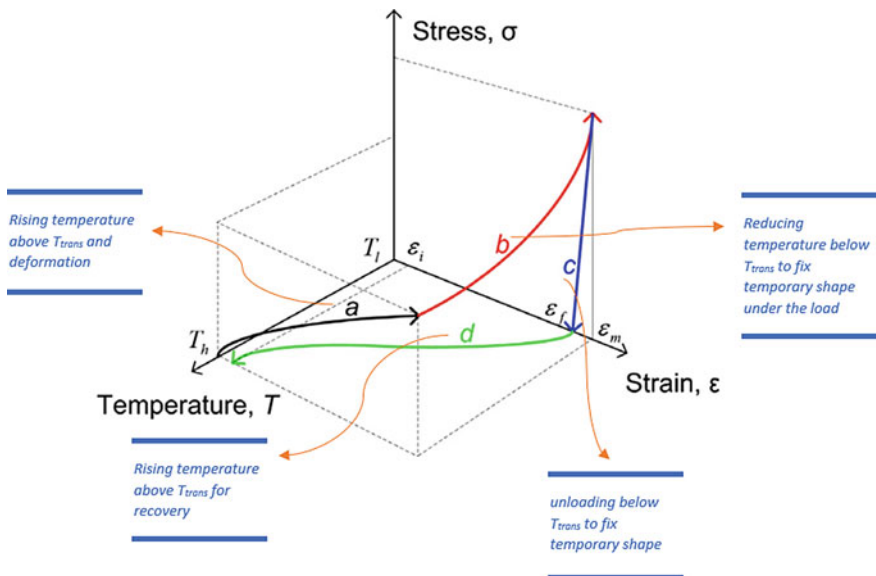


Fig. 3 Temperature-strain-stress relation in SMP programming cycle [15]

in concerning temperature change. This switching phase are the energy barriers. For storing the elastic deformation without significant relaxation, the polymer chains must be connected to each other. The connections are called as net points. A switching phase must exist to not let the elastic strain has been recovered before the switching phase has been removed. The net points or permanent network is called as hard segments because are responsible for retaining the permanent shape and does not change at the transition temperature and the switching phase is called as soft segment. This was the general concept of SMPs that can be seen in Fig. 4. As noted, good SME needs proper connection between chains to store the elastic deformation with a slight relaxation. It can be obtained by crosslinking which are two type of crosslinking. The first is chemical or covalent crosslinking that made by direct covalent bond between chains and the another is physical crosslinking that provide by crystallization and connects the tie molecules between crystalline. In fact, the “physical” refers to connection between chains without any chemical bonding that can be in the form of phase segregation in block copolymers or vast physical entanglement in high molecular weight polymers and any similar physical phenomenon. All the common net point formation phenomenon is shown in Fig. 4. With subdividing the crosslinking mechanisms into chemical and physical types, SMPs can be subdivided into thermoset and thermoplastic SMPs [11, 15].

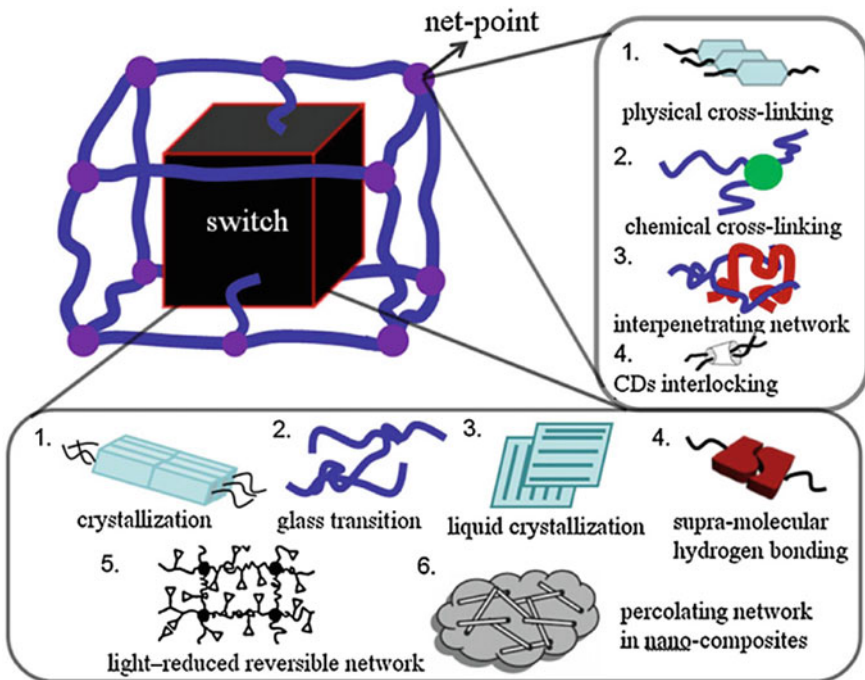


Fig. 4 Overall architecture of shape memory polymer mechanism

The switching phase, the most common transitions in polymers are glass transition temperature (T_g) and crystalline melting temperature (T_m). glass transition temperature is related to amorphous an irregular part of a polymer that below this temperature micro Brownian motions for altering the conformation of the chains will be restricted and polymer is in “glassy” state. Above the glass transition temperature, the elastic modulus of a polymer drops by three order of magnitude of ten and microscopic motions can happen. Melting transition temperature is related to the melting of ordered crystalline domains that depends on intermolecular forces, crystalline thickness and etc. [26]. So, with above-mentioned interpretations, all SMPs are classified in four categories as physically cross-linked thermoplastics with $T_{trans} = T_g$; physically cross-linked thermoplastics with $T_{trans} = T_m$; chemically cross-linked amorphous polymers with $T_{trans} = T_g$; chemically cross-linked semi-crystalline polymer networks with $T_{trans} = T_m$ [15]. Figure 5 shows the microscopic model of SMPs mechanisms in different categories. The poly lactic acid (PLA) and thermoplastic polyurethane base SMPs (SMPUs) are the most familiar thermoplastic SMPs with physical crosslinking method. On the other hand, styrene based and epoxy SMPs are the most familiar thermoset SMPs with chemical crosslinking method.

It must be noted that chemical cross-linked SMPs exhibits less creep, thus the irreversible deformation during shape recovery is less. The SMPs with glass transition temperature switching temperature exhibits lower recovery rate because of broader temperature range for glass transition in comparison with melting transition temperature, even the modulus of elasticity in rubbery state is higher than molten state and has more resistance for recovery. But the slower recovery rate of glass transition temperature based SMPs has its benefits in biomedical device field that for avoiding insertion-induced tissue damage and self-assembly applications [15]. It seems that both of shape recovery ratio and shape fixing ratio can be improved when the degree of crystallinity increases because it can cause more elastic strain storing with heavy fixing function.

2.2 Reversible SMPs (Two-Way SME)

SMPs programing that discussed in the previous section needs to repeat the deformation for every cycle that is not practical in actuation applications such as hot programming that can be eliminates by cold programing. Thus, a new title was created under reversible SMPs or two-way SME that SMP can change its shape in two specific shape under and above transition temperature and by once deformation for the first programing, then can change its shape between two specific shape under the trigger, as reversible or two-way shape memory effect (TSME). Another common SMPs that needs re-deformation for programing new cycle are called as one-way shape memory effect (OSME). Figure 6 shows a comprehensive schematic of differences between two-way and one-way SME [10, 31].

Fig. 5 Different molecular mechanisms of thermally-induced shape memory effect **a** block copolymer with transition of melting of crystalline (T_m of soft segment), **b** cross-linked polymer with transition of melting crystalline (T_m of soft segment), and **c** an amorphous polymer network with transition of glassy state to rubbery state (T_g) [1]

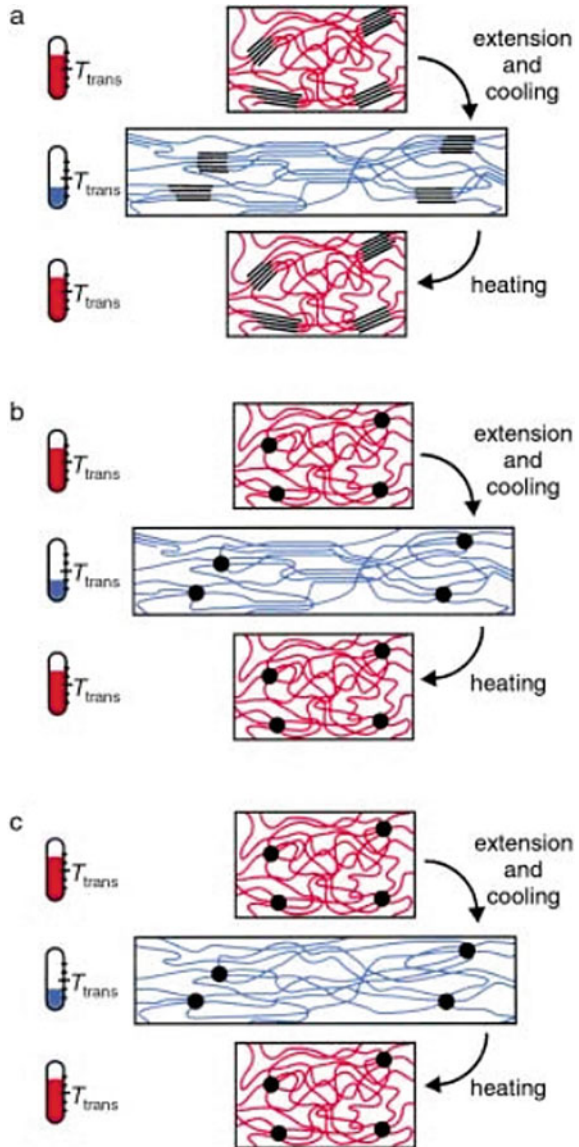


Figure 7 shows a comprehensive schematic of constant pressure type TSME programming procedure and the differences with one-way SME. There are some parameters for characterization the TSMEs. Because of the development of reversible SMPs for actuation applications, a quantitative parameter, as actuation magnitude, $R_{act} (\sigma)$ for any applied stress can be defined as the ratio of length difference between two specific shape over initial length of sample as below [24]:

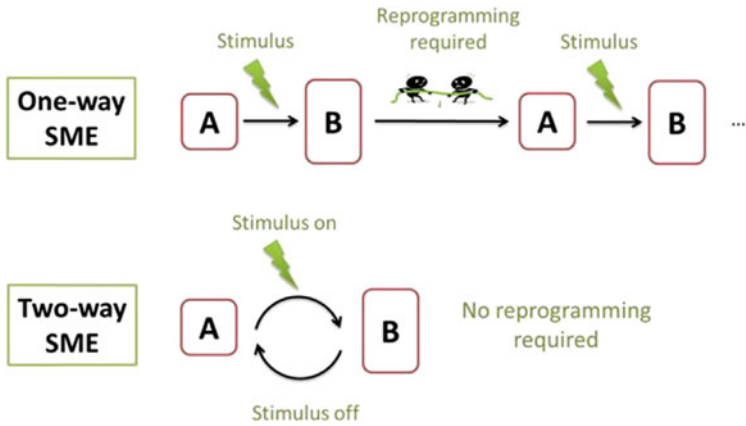


Fig. 6 Schematic definition of one-way and two-way SME [10, 14]

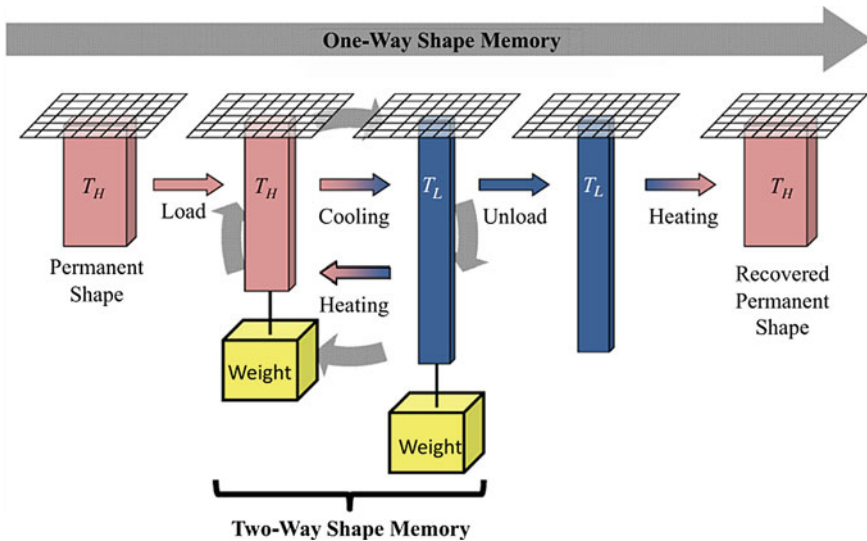


Fig. 7 Constant pressure type reversible (two-way) shape memory effects and its difference with one-way shape memory effect [29]

$$Ract(\sigma) = \frac{Llow(\sigma) - Lhigh(\sigma)}{L0} * 100 \tag{3}$$

And the recovery ratio can be calculated as the ratio of length difference between two special shape after cooling (beginning of cycle) over length difference between two special shape warming up cooling (end of cycle) below [24]:

$$Rr = \frac{L_{low} - L_{high}("final")}{L_{low} - L_{high}("initial")} * 100 \tag{4}$$

The second strategy to obtain reversible SMP is called as SMP laminate [7]. This strategy is based on thermal stress mismatch in thickness of a polymer ribbon that consists of two different layers [31]. In this strategy are included, two layers that one of them is OSMP like polyurethane-based SMP and the second one is an elastomer. The SMP layer should be stretched above T_{trans} and quenched before the sticking of elastomer as second layer, and in this situation, the SMP just need to warming up to recover its original shape. Then the programed SMP layer is stucked to the elastomer layer. When the laminate sample is warmed up, the SMP layer want to recover and the elastomer layer restrict the complete recovery and an elastic energy is stored in elastomer layer. Then with cooling down the sample, the elastic energy that was stored in elastomer, released and make reprogram in SMP layer automatically. It must be noted that, the modulus of elasticity of elastomer drops above T_{trans} can deform easily by large strain and below the T_{trans} the elastomer modulus of elasticity increased while the SMP module is still small and elastomer layer can recover almost its elastic strain and reprogram the SMP layer. As it can be seen, the strategy is based on each layer is under stress in a specific temperature while another layer is almost in stress free condition. There is a hysteresis unrecoverable strain in the first programming cycle because the force recovery that was stored in the SMP layer cannot overcome quietly the elastomer and there is a remained unrecovered strain in SMP. But form cycle two, the two shape in low temperature and high temperature can be in fixed shape with specific strain hysteresis from primary shape in the first cycle due to self-adaptation [7, 37]. Figure 8 shows a reversible smart polymer laminate in the first and second cycle. The programming procedure is like the other TSMEs and just is by warming up and cooling down the sample.

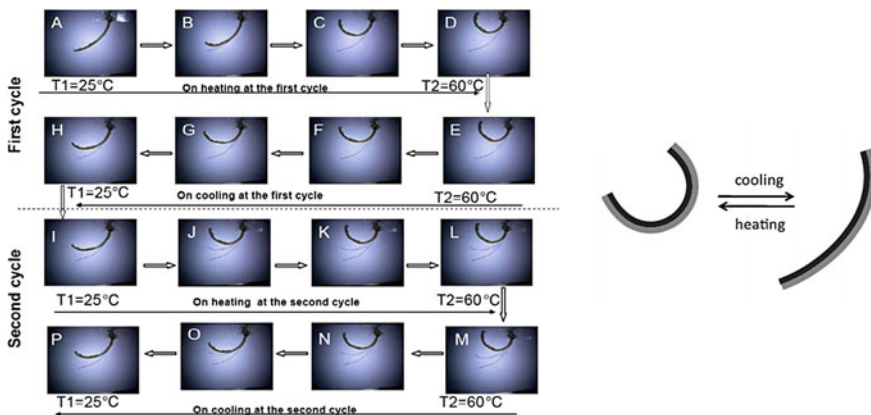


Fig. 8 a First and second cycle programming of reversible laminate SMP [7] b reversible laminate SMP behavior (black layer is pre-stretched SMP and gray layer is elastomer) [37]

2.3 Triple and Multi SME

One of the advancing researches in SMP belong to multi SMPs that started with a report of triple SME. The ordinary SMMs that is discussed previously, all have dual SME is defined as one permanent shape with one temporary shape in each programming cycle. In multiple SME, more than one temporary shape in a cycle in special distinct value of stimulus are seen. In fact, the multiple SME is the ability of a smart material that can memorize more than two distinct shape [6, 10]. Figure 9 shows the triple shape memory effect.

The programming of dual-SMMs consists of one step deformation of sample above T_{trans} and quenching then shape recovery by warming the sample up again, but, the deformation in triple SMPs programming consist of two steps, first deformation in specific highest temperature and another deformation in the middle temperature and then quenching below the middle temperature. Recovery process consists of two steps too. The first recovery step is warming sample up to middle temperature to gain the deformed shape at middle temperature and in another step, the temperature is raised above the highest temperature to obtain permanent shape [37]. Similar to dual-SMPs and reversible SME, triple and multiple SMPs need to quantitative parameters to be characterized. So, according to Fig. 10, Shape fixing ratio and shape recovery ratio must be calculated for each temporary shape.

There are two main strategies to design a triple and multiple shape memory polymer. If we have two or more transition phases with distinct temperatures, so we could deform the sample in each transition temperature as two or more switch phase and the triple or multiple shape memory effect can be obtained. So, the first strategy

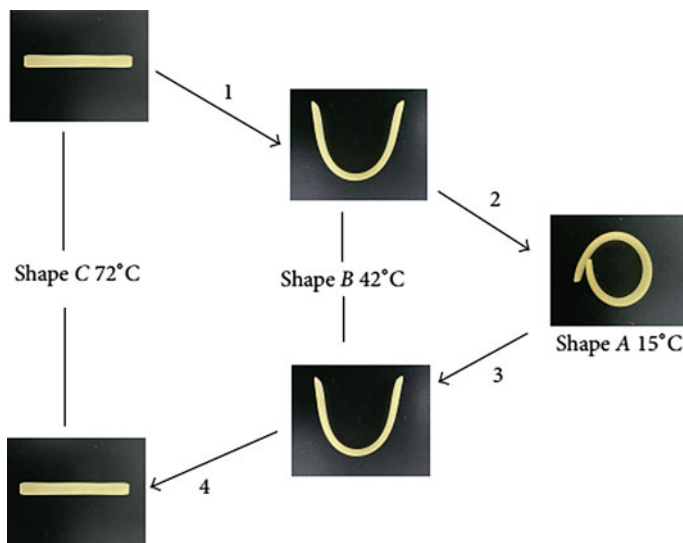


Fig. 9 Triple shape memory effect of an epoxy resin composite bilayers [16]

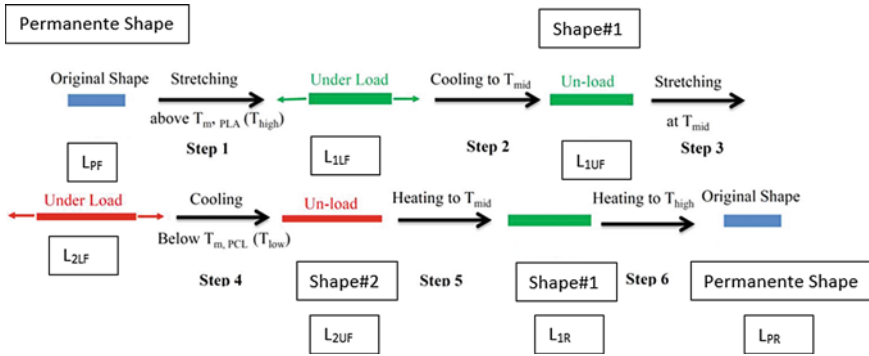


Fig. 10 Triple shape memory effect detailed programming procedure [13]

is two or more distinct transition. The second one is a broad transition temperature e.g. broad glass transition temperature (T_g) or broad crystalline melting transition temperature (T_m) [14]. There are several common ways to obtain distinct transitions for multi shape memory effect that one of them in copolymerization that each monomer has its transition temperature and it is better the transition temperatures is far from one another. Another way to obtain distinct transition temperature is blending of two immiscible polymer that have two far transitions and net point must exist too [14] can be obtained by blending of two miscible polymers with so far transition temperature. Another way is broad melting temperature by crystallization in various size and melting temperature [14]. Gradient copolymerization is another way to obtain broad glass transition temperature with two type of monomer that has a faraway glass transition temperature.

2.4 Stimulation

In the SMPs switch phase types, the major type is related to thermal transition nature that is the main trigger for switching is temperature but there are some stimulation methods that have different transition nature. In the general subdividing of stimulation methods, there is two thermal and athermal stimulation types. The thermal transition stimulation methods depend on the Joule heating but athermal stimulation may have chemical nature or etc. [15].

2.4.1 Thermal Stimulation

The thermal stimulation methods are subdividing to direct and indirect thermal stimulation. The direct thermal stimulation can be obtained by increasing surrounding temperature directly with a hot medium like warm water or hot gas and

etc. the indirect thermal stimulation is obtained by generating heat within the material via some physical phenomenon like electrical resistivity, alternative magnetic field, similar phenomenon. As most common stimulation methods, we can refer to electrical-induced SMP, magnetic-induced SMP, water and solution-induced SMP and photothermal-induced SMP as thermal indirectly stimulation. The majority of indirect thermal stimulation are related to raising the temperature by filler via external trigger like absorbing infrared light by carbon black to warm up for photothermal stimulation case. For transmitting generated the heat by the functional fillers, the design the microstructure of the composite should be in a way that a cluster of fillers are formed. A special concept is existed for solvent and moisture-induce SME that is related to drop the transition temperature to the ambient temperature for occurring the transition without any warming up but still it has a thermal nature. Also, some solvents can destroy the crystals for transition occurrence. For example, carbon base fillers and metallic powders can provide Joule heating by electrical resistivity and cause temperature rising. Therefore, the uses of SMP composites have been noticed. It must be noted that, using of functional fillers not only can provide us some indirect thermal stimulation or even athermal stimulation, but also can improve the mechanical and thermal properties of the SMP that was an issue for polymeric materials. Also, SMP composites can provide us multi functionality behavior devices that have been made of and can be use as strain sensor because the electrical resistivity of an electrically conductive sample can be altered by strain.

2.4.2 Athermal Stimulation

Photochemical-induced SMPs have photoactive groups that can make crosslinks when light of a special wavenumber light is applied. In fact, the crosslinks that are made during specific light emission can fix temporary shape and recovery can be occur when the wavenumber alters to a value that photochemical crosslinks are eliminated. In fact, photo-induced crosslinks act as the soft segment for switching. PH sensitive groups, such as amino, carboxyl and sulfonic are introduced into polymers to obtain pH-induced SMPs. PH-sensitive switching occurs via hydrogen bond interactions of pH sensitive groups in polymer. globule-to-coil transition can be done in response to changing in PH on solution in some cases and the sample turns to coil in lower PH due to excess H⁺ due to repulsion and on the other hands the chain can turn to globule due to attraction [6, 22]. Some advanced another chemical phenomenon are existed for athermal stimulation that is not in the scope of this chapter.

3 4D Printing by FDM

Main applications of SMPs and SMPCs was as sensor, mechanical actuator and multifunctional devices with self-adaptation, self-morphing, self-folding, self-bending, self-deployment and precisely shape controlling ability for mechatronic (soft robotics), personalized biomedical devices and drug delivery, smart textiles, electronics, aerospace, packing, micro and nano-electromechanics (MEMS) and automotive. Some exciting functionality can be given by SMPs structure such as self-folding boxes, interlocking components and active origamis and hinges. All above-mentioned applications are belonged to 4D printing too. Using 4D printing become important for SMP fabrication in the case of personalized, non-mass production, complex shapes and need to fabricate multi-material product [10, 18–21, 25, 34].

3.1 Challenges of 4D Printing by FDM

The researches on 4D printing by FDM was lower than other AM processes due to limited thermoplastic SMPs in order type of stimuluses and printability. It seems to be a good attempt to do more researches on extrusion base AM of thermoplastic SMPs due to greater mechanical behavior and durability than thermosets and cheapness of FDM process and materials. Some researches done for SMP filament preparation and printing conditions by discussing effective parameters in filament and part fabrication steps. Effective filament fabrication parameters consist of screw rotation speed (RPM), extruding temperature and winding speed. Mentioned parameters effect on the filament quality, density and diameter and filament quality influence on the printed part quality directly. Three common defects can be seen in filaments that are voids, coarseness and partial melted pellets. Voids cause by evaporation of trapped moisture and some voltaic component and can be eliminated by de-humidity of the pellets; screw rotation increase and extrusion temperature decrease. Partial melted pellets defect cause discontinuity in filament can be eliminated by screw rotation decrease and extrusion temperature increase. Coarseness of the filament surface cause by internal deformation of trapped air into the polymer filament in high temperature and can cause density reduction. So, the right choosing of extrusion parameters is necessary to obtain proper filament [18, 22]. Printing parameters and conditions can influence on the shape accuracy and shape memory behavior of the part. A specific pre-strain is created during material extrusion of nozzle and cause more shrinkage tendency of SMPs that exposed to high temperature for long time. Shrinkage tendency of SMPs must be controlled for accuracy and the only way is cooling that must be more for 4D printing by more air circulation that examined in previous researches. Reheating of each layer caused by depositing of new molten layer on the previous layer and contact of the hot nozzle. Lower printing speed causes more printing time and duration of the time that each

layer is exposed to high temperature, on the other hands, higher printing speed causes deposition of next layer sooner and suppress the cooling of each layer. So, it seems to be an optimum value of printing speed for best dimensional accuracy and lower shrinkage of printed SMP that is in near to the middle of standard range of speed. Part density can be altered by printing temperature and printing speed. Trapped air between layers can be reduce by better deposition of each layer. Greater temperature causes lower viscosity and better deposition. Lower printing speed also causes lower viscosity and better deposition too [34]. Some of SMPs with glass transition temperature between 30 and 70 °C have own extrusion issues in printing procedure such as buckling below the roller because the roller temperature is above glass transition temperature to eliminate filament buckling during printing, the roller cooling, higher distance between roller and hot end, lower printing temperature can be effective due to lower thermal conduction [18, 34]. Printing parameters can be effective in SME like shape recovery rate. The lower air trapped between the layers causes more thermal conductivity and higher recovery rate. Higher printing temperature causes lower viscosity to better layer deposition with an optimum layer thickness causes minimum trapped air between layers and provide greater recovery rate [30]. Also printing parameters can affect on the physical properties of SMPC with functional filler. Higher trapped air also can affect on the electrical conductivity of the printed conductive sample with electrical stimulation. Lower electrical conductivity provides more Joule heat to active the transition due to higher electrical current that pass the sample. So, optimum layer thickness with higher printing temperature can be provide lower electrical conductivity and greater shape recovery rate of 4D printed SMPC sample [18].

4 Application

In this section, first, researches are presented in summary form in Table 1 and then, based on different applications, they are examined and discussed in more detail.

4.1 Self-folding

A novel approach to obtain self-folding behavior without any deformation after fabrication was achieved by the role of FDM process parameters manipulation. During the extrusion process, aligned chains stretch along the extrusion direction by compression behind them. As the compression be higher and temperature be lower, chain slippage is limited, and pre-strain is increased. This pre-strain recovery can cause macroscopic shrinkage. As it can be concluded, by extrusion of the filament on a platform, a significant pre-strain can be preserved and the tendency of SMPs for pre-strain is higher than conventional polymers for 3D printing. As you know hot proگرامing of SMPs, the temporary shape stabilize step consists of warming up

Table 1 Organized chart of 4D printing by FDM pervious studies

No	Findings, printed parts and applications	Materials	Extra note	References
1	Obtain complex 3D structure, reversible self-folding flower, helical structure with different degree of spiral, corrugated structure by bidirectional folding, adaptable lattice metamaterial with switchable bandgap frequency	Polylactic acid (PLA)/ paper composite $T_g = 65\text{ }^\circ\text{C}$	Programing is during the FDM process by controlling printing parameters	[21, 35]
2	Self-conforming subtracts, self-tightening surgical sutures, self-conforming splint and self-coiling/ deploying stent	Polyurethane-based SMP filament $T_g = 60\text{ }^\circ\text{C}$	Programing is during the FDM process by controlling printing parameters	[2, 25]
3	Personalized and adoptable elbow protector, smart Kungfu panda and Terracotta warrior dull, recoverable “Bird’s Nest” stadium	UV cross-linkable linear PLA/PCL copolyesters $T_g = 60\text{ }^\circ\text{C}$	UV assisted FDM is adopted for crosslinking and making thermoset SMP	[8]
4	Variable stiffness hyper-redundant robotic arm	ABS for ball and socket SMP for the middle active part $T_g = 45\text{ }^\circ\text{C}$	–	[20, 33]
5	Dimensional increase of structure by self-bending feature (1D → 2D, 2D → 3D)/2D circle to cone and 2D square to doubly-curved shell/ 1D beam to curved beam	Polyurethane-based SMP filament $T_g = 60\text{ }^\circ\text{C}$	Programing is during the FDM process by controlling printing parameters	[12]
6	Filament production feasibility and effect of printing parameters on quality/4D printing feasibility by FDM and effect of printing parameters on shape memory behavior and electrical properties of electrical-induced SMP	SMP pellets (MM35200/ MWCNT) composite Recovery voltage = 30 V	–	[18]

(continued)

Table 1 (continued)

No	Findings, printed parts and applications	Materials	Extra note	References
7	Functionally graded sample for local actuation and multi-shape memory by different percent of plasticizing	PLA/PEG blend in three different PEG percentage of 0, 10 and 30%	–	[27]
8	Triple shape memory effect from a dual-shape memory polymer using FDM Self-assembly stent, mechanical gripper for treating strike and smart stemple	Polyurethane-based SMP filament $T_g = 55\text{ }^\circ\text{C}$	Triple shape memory effect was obtained by combination of hot programming during FDM and cold programing after that	[3]
9	Self-outer lock circular braided tube textile	PLA and silicone elastomer matrix $T_g = 63\text{ }^\circ\text{C}$	–	[36]
10	PH-responsive smart polymer for flow regulating valve and microporous catalyst substrate for reducing of 4-nitrophenol	Poly(2-vinylpyridine) (P2VP) + 12% wt ABS and other additives for crosslinking and quaternization $T_g = 120\text{ }^\circ\text{C}$	The sample was cured and quaternized after printing for crosslinking and be PH-response SMP respectively	[22]
11	4D printing feasibility and effect of FDM printing process on printed part quality such as part density, dimensional accuracy, tensile strength and surface roughness Smart flower and soft mechanical gripper have been printed	DiAPLEX MM-4520 pellets from SMP Technologies, Inc. (a family of TPU)	–	[34]
12	Reversible energy absorbing meta-sandwich via multi-material 4D printing	Polyurethane-based SMP filament $T_g = 60\text{ }^\circ\text{C}$ /FlexPro elastomer	–	[4]
13	4D printing of olefin ionomer feasibility and effect of 3d printing process and printing parameters on shape memory behavior Smart spiral spring	Zink-neutralized poly (ethylene-co-methacrylic acid) Melting transition is about 40–100 °C But $T_{\text{trans}} = 70\text{ }^\circ\text{C}$	Potential for multi-shape memory effect	

the sample and making a specific strain then finally cooling down the sample and unloading. By a simple comparison of printing process of a SMP and hot programming, it can be concluded that FDM process is very similar to hot programming. Higher temperature and slower printing speed, provide lower pre-strain due to more chain mobility and lower pressure behind the extruded raster. Much exposure to the higher temperature may provide a part of recovery energy besides the probability of relaxation and finally can decrease the pre-strain value. So, the pre-strain can release by heating the printed part. The left side of Fig. 11 shows a printed mono-layer raster leaf vessel-like geometry on a paper platform to make a flower-like PLA/paper composite and then printed part was heated up to release the pre-strain. The shape turns to a positive bend via stress mismatch between PLA printed pre-strained and paper and finally cooled down. Then the paper can be torn off and a 3D complex shape obtained. In fact, this designed 4D printed part exhibit a reversible behavior. Then by warming up again, the shape turns to flat by thermal expansion coefficient difference between PLA and paper which the thermal expansion coefficient of PLA is greater than those of paper. This is achievement to lightweight 3D reversible structure.

4.2 Functionally Graded 4D Printing

In another research series, self-folding and self-coiling ability was achieved by programming during printing. The above-mentioned pre-strain during FDM process is different along the specimen printed thickness. The cooling rate of the bottom layer is lower due to printing new layers on top of them, thus they are in higher temperature for longer time and this fact cause decrease in pre-strain value. The cooling rate of top layer is highest because no layer is deposited on the top of it. However, the pre-strain is variable through the thickness. The pre-strain is higher

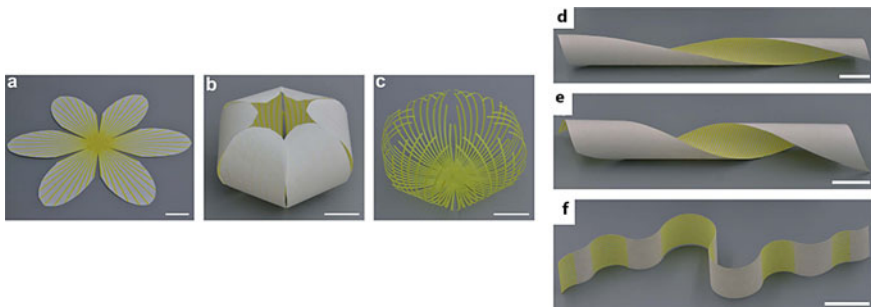


Fig. 11 **a** The two-dimensional initial shape of the 3D-printed composite sheet. **b** The final flower-like three-dimensional shape achieved by a process of heating and cooling. **c** A complex structure fabricated by tearing off the paper from the flower-like 3D structure. **d, e** Helical structures with different degrees of spiral. **f** Corrugated structures by bidirectional folding [35]

than on the top. This type of 4D printing type named as functionally graded 4D printing. As mentioned, the SMPs are programmed during FDM process and the pre-strain can be released by warming up the specimen above the transition temperature. In this special case, the stress mismatch causes the positive bend of the sample in along each raster. Figure 12 shows the self-bending feature of 4D printed part by FDM and the effect of printing speed and printing temperature on self-folding ability.

A different FG 4D printing have been adopted by different transition temperature in a specific direction of printed part by adding different amount of plasticizer for each section. With this FG adopted method, localized actuation and localized recovery can be achieved. By adopting mentioned method, it can be possible that the printed part be programmed in multi-SME manner to obtain multi shape memory effect via different transition temperature in each different location. In this method the specimen consists of three distinct part that was printed by three amount of plasticizer which are 0, 10 and 30%. Higher amount of plasticizer provides more chain movement and reduce spatial obstacle and can reduce glass transition temperature significantly [5, 27]. The main SMP material is PLA and polyethylene glycol were used as plasticizer.

4.3 *UV-Assisted FDM*

A novel 4D printing have been done to produce thermoset specimen by FDM. In this process crosslinking is done via UV during printing each layer. The crosslinking is occurred by embedding double bond in linear co-polyester that. The photo-crosslinking can be initiated by the irradiation of UV activation of photo-initiator. So, there is functional coupling agent in the linear copolyester with double bond that can be broken to make a chemical crosslinking by photo-initiator via UV radiation to make a network. The hard PLA phases is hard segment and PCL phases with strong low melting crystals is as soft segment and switching phase. The printing proper printing speed must be chosen considering PLA to PCL ratio. Because of the significant difference between printing temperature and crystallinity temperature of PCL, lower printing speed needed in higher PCL conte of Layer by layer photo-crosslinking can cause network formation between layers and more crosslinking efficiency because of crosslinking each thin layer separately. This is a feasible way to produce thermoset SMP with FDM. Two type of elbow protector for biomedical application have been designed and printed by this way.

4.4 *Self-deployable*

Tensegrity structures can be used in communication application such as antenna, solar array or other deployable structures. This deployment feature can reduce the

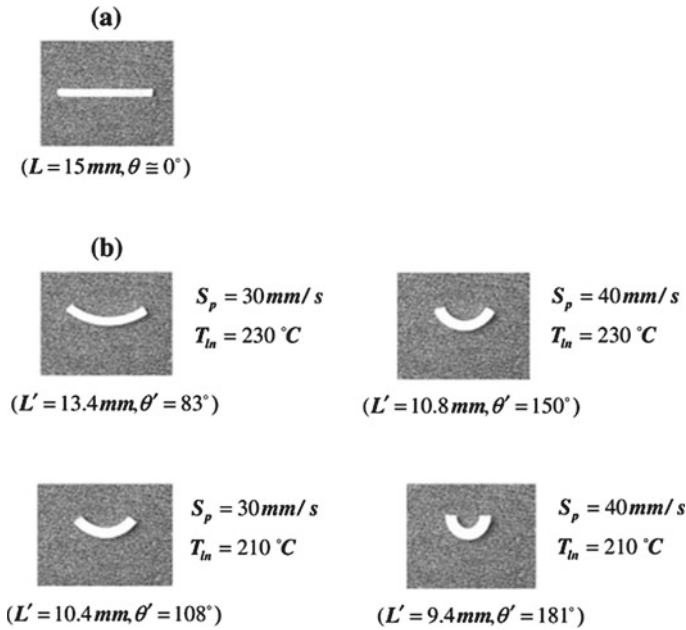


Fig. 12 Functionally graded assisted by 4D printing: **a** straight beam printed with different printing speed and temperature, **b** curved configuration of the printed beam after heating-cooling process [2]

risk of failure and less joining. The reliability and precision of deployment is an important thing in microgravity condition such as fixity, repeatability and reversibility. Another challenge is 4D printing feasibility in microgravity. The larger antennas will be folded in Vega launcher and deploy in space. So, self-deployment and printing in microgravity causes reduction of the failure probability, ease of transporting and lower dependence on earth therefore cheaper space missions can be obtained [20]. Figure 13 shows a deployable tensegrity structure with self-deployment feature.

4.5 Textile Applications

For textile applications, circular braided tube in single SMP material and silicone elastomer matrix multi-material form has been produced. The schematic of braided tube and thermal properties of PLA SMP that was printed by FDM is shown in Fig. 14. The influence of braiding angle, tube wall thickness and shape recovery temperature on shape memory behavior have been investigated. Inter or outer lock perform is the main application in textile smart parts. Three braiding angles as 20°, 30° and 40° with three wall thickness as two, three and five layers have been

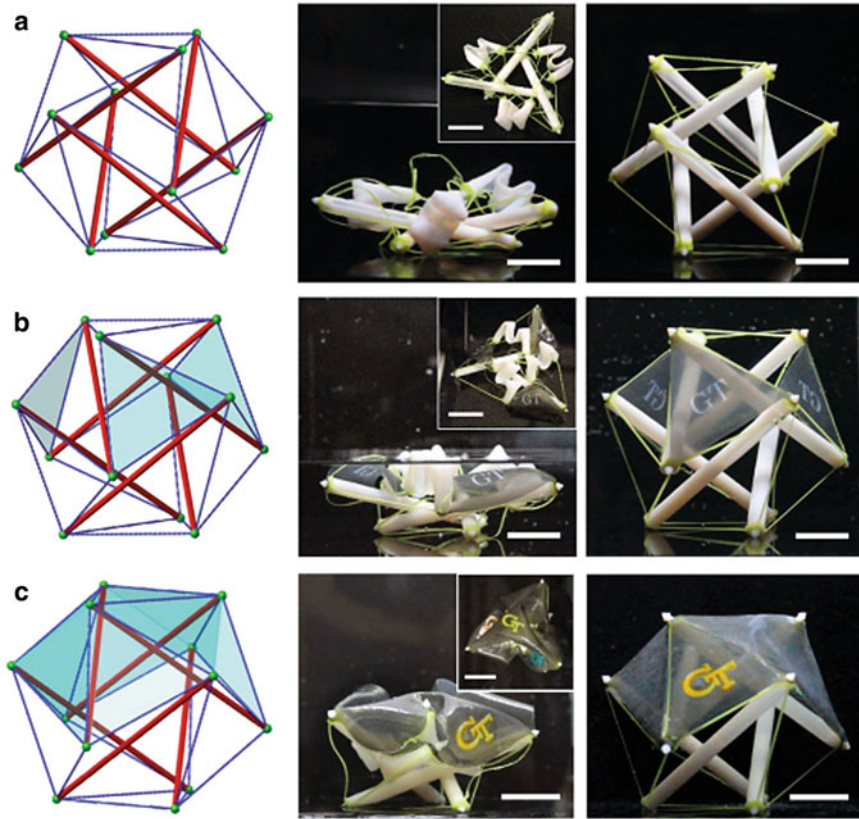


Fig. 13 Deployment of 6-strut spherical tensegrity. **a** Deployment of a spherical tensegrity using the partial folding strategy to improve reliability of deployment. **b** Positioning of three discrete pieces of surfaces into space. **c** Deployment of a continuous surface supported by the active tensegrity to form a tent [17]

checked. Deformation temperature was 90 °C and three recovery temperature as 70, 80 and 90 °C was chosen. A silicone elastomer matrix has been added to the printed braided tube in order to increase recovery ratio and recovery force. The recovery ratio is greater in higher braiding angle due to higher circumferential reinforcement. As the wall thickness increase the recovery ratio decreases due to lower thermal conductivity in thicker wall case. Higher recovery temperature provides higher recovery rate. The recovery force was increased in silicone elastomer matrix case and the recovery ratio was reaches to 100% but recovery rate was decreased because of lower thermal conductivity of silicone.

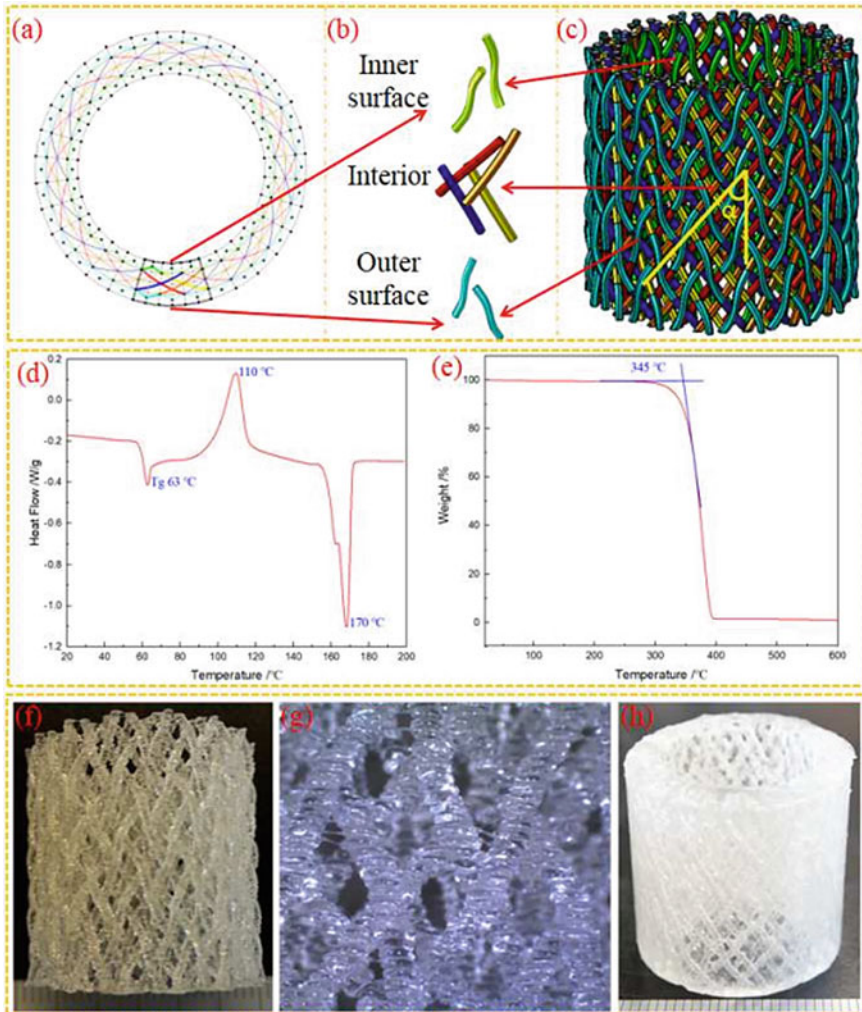


Fig. 14 Details of 3D circular braided tube model **a** yarn contour projection, **b** unit cell model, **c** tube geometrical model, **d** DSC curve and **e** TGA curve of SMP PLA filaments for 4D printing, **f** 4D printed circular braided tube preform, **g** enlarged optical image of preform surface and **h** 4D printed circular braided tube preform/silicone elastomer matrix composite [36]

4.6 Energy Absorber

4D printed sample can be in application of energy absorbing and recover to the original shape after energy absorption to re-use. A tunable meta-sandwich for reversible energy absorption is printed in the shape of Fig. 15 with dual extrusion FDM by four material types: polyurethane-based SMP, Flex pro elastomer filament,

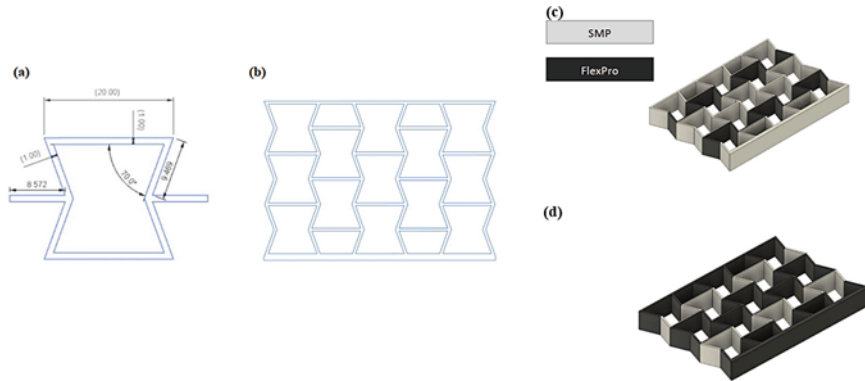


Fig. 15 **a** Unit cell of auxetic geometry, **b** lattice schematic. Dual-material auxetics: **c** SMP-elastomer (FlexPro) composed of pattern orientation SMP followed by FlexPro, **d** elastomer (FlexPro)-SMP composed of FlexPro followed by SMP [4]

SMP/Flex pro elastomer multi-material and Flex pro/SMP elastomer multi-material. Using 3D printing and specially FDM cheap method is a favorable way to fabricate such this sophisticated multi-material structure. Energy can be absorbed by elastic and plastic deformation, mechanical instability and structural collapse. The SMP is elasto-plastic and Flex pro is elastomer. So, the absorbed energy and caused deformation in elasto-plastic material is irreversible and only SMP can be recovered to its original shape under heating. The combination of elastomer and SMP can exhibit good recovery force, lower deformation and beside good energy absorption. Under deformation, a non-linear stiffness behavior such as softening and then hardening can be seen as a result of snap-through buckling for softening and densification and contact between beam-like members for hardening. The Flex pro/SMP sample that majority of sample is Flex pro exhibit best absorbed energy because of lower hysteresis deformation due to elastomer besides significant yielded force due to elasto-plastic SMP [4]. Figure 16 shows energy absorption and recovery process of The Flex pro/SMP sample.

5 Future Outlook

All above-mentioned process parameters show that 3D printing of shape memory polymers is sensitive to the processing conditions and parameters and the need of further study on the processing parameters of thermoplastic SMPs is needed to characterize the shape memory behavior of FDM printed parts. The hot programming of SMP during FDM process can be an advantage of 4D printed parts by FDM to exhibit spontaneous self-folding behavior to obtain 3D complex smart devices. 4D printing can uses for self-assembly in-body biomedical devices and self-adaptable devices specially for biomedical applications. Self-deployable smart structure can

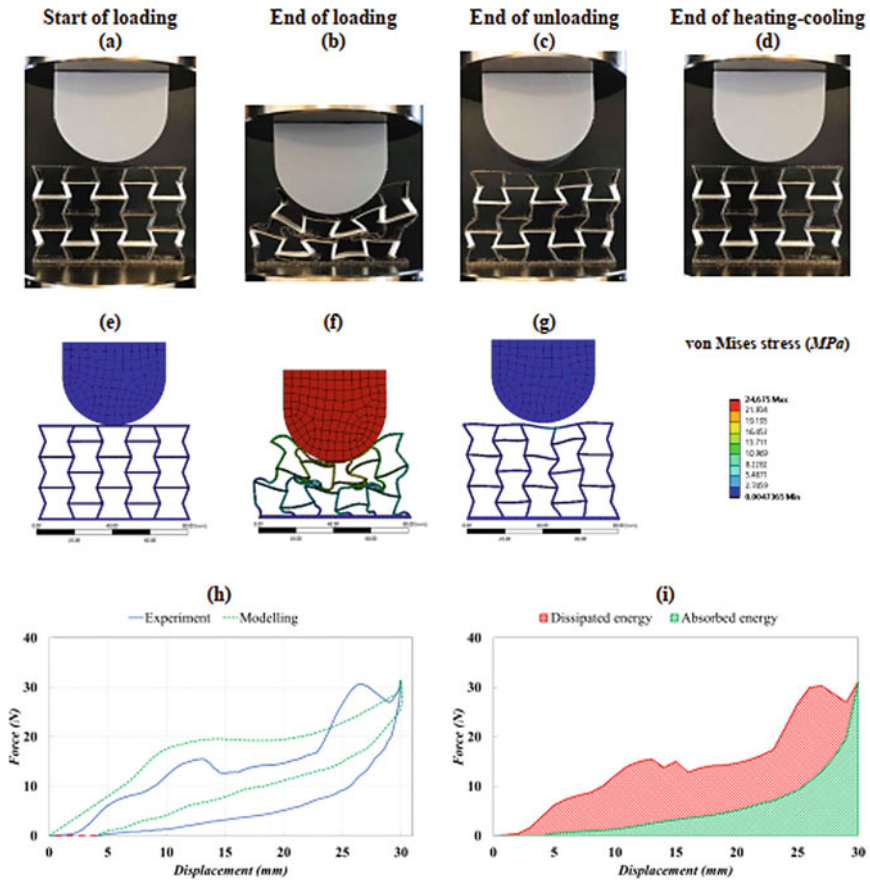


Fig. 16 Elastomer(FlexPro)-SMP sample of meta-sandwich structure: **a–g** experimental and computational configuration, **h** force and displacement for loading-unloading and thermal shape recovery, **i** dissipated and absorbed energy [4]

reduce the cost of transportation and failure and has a potential application in aerospace applications. 4D printing can provide freedom in design of robotic actuators and has a potential application in soft robotics too. The 4D printing also can provide us the freedom of designing multi-material design of a smart device to multi-activation and sophisticated meta-materials. The 4D printed composites can be used as sensor by monitoring physical properties changing during shape changing and reuse for further cycles.

6 Conclusion

4D printing is the combination of additive manufacturing (AM) and smart materials with an extra dimension of time that provides us a dynamic complex geometry. 4D printing is a pioneer field that has a potential application in biomedical, smart textiles, electronics, aerospace, packing, micro and nano-electromechanics (MEMS) and automotive by self-adaptation, self-morphing, self-folding, self-bending, self-deployment behavior and also can be used as mechanical actuator and sensors. Shape memory polymer is a type of smart material that can memorize a permanent shape and can recover its original shape after any deformation by means of temperature, electricity, magnetic field, moisture, light, PH and etc. fused deposition modeling (FDM) is an extrusion-based AM for polymers that is cheap and pervasive. We can just print thermoplastic materials in form of filament by FDM that is melted by a liquefier and deposits by extrusion through the nozzle. The majority of SMPs are thermosets and 4D printing of thermoplastics is sophisticated and rare but advantages of FDM encourage the researcher to work on it. For the successful 4D printing we need to know all aspects of SMPs first, such as SME mechanisms, the stimulus, shape memory polymer composites, reversible (two-way) SMPs and multi-shape memory polymers. We must use all above-mentioned aspects of SMPs considering what is desired of final smart printed part.

References

1. Atzrodt J, Derau V, Kerr W, Reid M (2017) Applications of hydrogen isotopes in the life sciences. *Angew Chemie Int Ed* 1–26. [https://doi.org/10.1002/\(ISSN\)1521-3773](https://doi.org/10.1002/(ISSN)1521-3773)
2. Bodaghi M, Damanpack AR, Liao WH (2017) Adaptive metamaterials by functionally graded 4D printing. *Mater Des* 135:26–36. <https://doi.org/10.1016/j.matdes.2017.08.069>
3. Bodaghi M, Damanpack AR, Liao WH (2018) Triple shape memory polymers by 4D printing. *Smart Mater Struct* 27:065010. <https://doi.org/10.1088/1361-665X/aabc2a>
4. Bodaghi M, Serjoui A, Zolfagharian A, Fotouhi M, Rahman H, Durand D (2020) Reversible energy absorbing meta-sandwiches by FDM 4D printing. *Int J Mech Sci* 173:105451. <https://doi.org/10.1016/j.ijmecsci.2020.105451>
5. Cai S, Sun YC, Ren J, Naguib HE (2017) Toward the low actuation temperature of flexible shape memory polymer composites with room temperature deformability via induced plasticizing effect. *J Mater Chem B* 5:8845–8853. <https://doi.org/10.1039/c7tb02068f>
6. Chen HM, Wang L, Zhou SB (2018) Recent progress in shape memory polymers for biomedical applications. *Chinese J Polym Sci* 36:905–917 (English ed)
7. Chen S, Hu J, Zhuo H, Zhu Y (2008) Two-way shape memory effect in polymer laminates. *Mater Lett* 62:4088–4090. <https://doi.org/10.1016/j.matlet.2008.05.073>
8. Cheng CY, Xie H, Xu ZY, Li L, Jiang MN, Tang L, Yang KK, Wang YZ (2020) 4D printing of shape memory aliphatic copolyester via UV-assisted FDM strategy for medical protective devices. *Chem Eng J* 396:125242. <https://doi.org/10.1016/j.cej.2020.125242>
9. Gebhardt A (2011) Understanding additive manufacturing. Carl Hanser Verlag GmbH & Co, KG
10. Hager MD, Bode S, Weber C, Schubert US (2015) Shape memory polymers: past, present and future developments. *Prog Polym Sci* 49–50:3–33

11. Hu J, Zhang C, Ji F, Li X, Han J, Wu Y (2016) Revealing the morphological architecture of a shape memory polyurethane by simulation. *Sci Rep* 6:1–9. <https://doi.org/10.1038/srep29180>
12. Jiyong H, Yinda Z, Hele Z, Yuanyuan G, Xudong Y (2017) Mixed effect of main electrospinning parameters on the β -phase crystallinity of electrospun PVDF nanofibers. *Smart Mater Struct* 26:085019. <https://doi.org/10.1088/1361-665x/aa7245>
13. Khademeh Molavi F, Ghasemi I, Messori M, Esfandeh M (2017) Nanocomposites based on poly(L-lactide)/poly(ϵ -caprolactone) blends with triple-shape memory behavior: effect of the incorporation of graphene nanoplatelets (GNPs). *Compos Sci Technol* 151:219–227. <https://doi.org/10.1016/j.compscitech.2017.08.021>
14. Lee J, Kim HC, Choi JW, Lee IH (2017) A review on 3D printed smart devices for 4D printing. *Int J Precis Eng Manuf-Green Technol* 4:373–383
15. Leng J, Lan X, Liu Y, Du S (2011) Shape-memory polymers and their composites: stimulus methods and applications. *Prog Mater Sci* 56:1077–1135
16. Li X, Zhu Y, Dong Y, Liu M, Ni Q, Fu Y (2015) Epoxy resin composite bilayers with triple-shape memory effect. Hindawi Limited
17. Liu K, Wu J, Paulino GH, Qi HJ (2017) Programmable deployment of tensegrity structures by stimulus-responsive polymers. *Sci Rep* 7:1–8. <https://doi.org/10.1038/s41598-017-03412-6>
18. Ly ST, Kim JY (2017) 4D printing—fused deposition modeling printing with thermal-responsive shape memory polymers. *Int J Precis Eng Manuf-Green Technol* 4:267–272. <https://doi.org/10.1007/s40684-017-0032-z>
19. Meng H, Li G (2013) A review of stimuli-responsive shape memory polymer composites. *Polymer (Guildf)* 54:2199–2221
20. Mitchell A, Lafont U, Holyńska M, Semprimoschnig C (2018) Additive manufacturing—a review of 4D printing and future applications. *Addit Manuf* 24:606–626
21. Momeni F, Mehdi Hassani.N MS, Liu X, Ni J (2017) A review of 4D printing. *Mater Des* 122:42–79. <https://doi.org/10.1016/j.matdes.2017.02.068>
22. Nadgorny M, Xiao Z, Chen C, Connal LA (2016) Three-dimensional printing of pH-responsive and functional polymers on an affordable desktop printer. *ACS Appl Mater Interfaces* 8:28946–28954. <https://doi.org/10.1021/acsami.6b07388>
23. Ngo TD, Kashani A, Imbalzano G, Nguyen KTQ, Hui D (2018) Additive manufacturing (3D printing): a review of materials, methods, applications and challenges. *Compos Part B Eng* 143:172–196
24. Pandini S, Baldi F, Paderni K, Messori M, Toselli M, Pilati F, Gianoncelli A, Brisotto M, Bontempi E, Riccò T (2013) One-way and two-way shape memory behaviour of semi-crystalline networks based on sol-gel cross-linked poly(ϵ -caprolactone). *Polymer (Guildf)* 54:4253–4265. <https://doi.org/10.1016/j.polymer.2013.06.016>
25. Rayate A, Jain PK (2018) A review on 4D printing material composites and their applications. In: *Materials today: proceedings*. Elsevier, Netherlands, pp 20474–20484
26. Sperling LH (2005) *Introduction to physical polymer science: fourth edition*. Wiley, New Jersey
27. Sun YC, Wan Y, Nam R, Chu M, Naguib HE (2019) 4D-printed hybrids with localized shape memory behaviour: implementation in a functionally graded structure. *Sci Rep* 9:1–13. <https://doi.org/10.1038/s41598-019-55298-1>
28. Turner BN, Strong R, Gold SA (2014) A review of melt extrusion additive manufacturing processes: I. Process design and modeling. *Rapid Prototyp J* 20:192–204
29. Westbrook KK, Mather PT, Parakh V, Dunn ML, Ge Q, Lee BM, Qi HJ (2011) Two-way reversible shape memory effects in a free-standing polymer composite. *Smart Mater Struct* 20:065010. <https://doi.org/10.1088/0964-1726/20/6/065010>
30. Wu W, Ye W, Wu Z, Geng P, Wang Y, Zhao J (2017) Influence of layer thickness, raster angle, deformation temperature and recovery temperature on the shape-memory effect of 3D-printed polylactic acid samples. *Materials (Basel)* 10:970. <https://doi.org/10.3390/ma10080970>

31. Wu X, Huang W, Zhao Y, Ding Z, Tang C, Zhang J (2013) Mechanisms of the shape memory effect in polymeric materials. *Polymers (Basel)* 5:1169–1202. <https://doi.org/10.3390/polym5041169>
32. Xin X, Liu L, Liu Y, Leng J (2019) Mechanical models, structures, and applications of shape-memory polymers and their composites. *Acta Mech Solida Sin* 32:535–565
33. Yang Y, Chen Y, Li Y, Zhiqiang Chen M (2016) 3D printing of variable stiffness hyper-redundant robotic arm. In: *Proceedings—IEEE international conference on robotics and automation*. institute of electrical and electronics engineers Inc., pp 3871–3877
34. Yang Y, Chen Y, Wei Y, Li Y (2016) 3D printing of shape memory polymer for functional part fabrication. *Int J Adv Manuf Technol* 84:2079–2095. <https://doi.org/10.1007/s00170-015-7843-2>
35. Zhang Q, Zhang K, Hu G (2016) Smart three-dimensional lightweight structure triggered from a thin composite sheet via 3D printing technique. *Sci Rep* 6:1–8. <https://doi.org/10.1038/srep22431>
36. Zhang W, Zhang F, Lan X, Leng J, Wu AS, Bryson TM, Cotton C, Gu B, Sun B, Chou TW (2018) Shape memory behavior and recovery force of 4D printed textile functional composites. *Compos Sci Technol* 160:224–230. <https://doi.org/10.1016/j.compscitech.2018.03.037>
37. Zhao Q, Qi HJ, Xie T (2015) Recent progress in shape memory polymer: new behavior, enabling materials, and mechanistic understanding. *Prog Polym Sci* 49–50:79–120

Computational Models: 3D Printing, Materials and Structures



Ashish R. Prajapati, Shilpesh R. Rajpurohit,
and Madhukar Somireddy

Abstract A comprehensive understanding of the 3D printing method—microstructure—material properties relationship of 3D printed parts is currently limited. In fused filament fabrication (fused deposition modeling/FDM) 3D printing technology, parts are fabricated by deposition of material layer upon layer. The printing process has a vital influence on the final quality of printed parts. Also, processing parameters control the microstructure of 3D printed components and thus, the parameters in-turn affect the component's material properties. Experimental evaluation of this relationship is challenging, and an alternative solution is computational modeling. The computational models based on multi-physics provide deeper insights into the relationship of process-structure-property of printed parts. This chapter explores different computational models available for modeling the FDM process, computational material models for 3D printed parts and models for characterizing part's material behavior.

1 Introduction

Fused Filament Fabrications (FFF), commonly known as Fused Deposition Modeling (FDM) by Stratasys, is a 3D printing process, which fabricates parts additively. This production process is opposing to traditional machining, where the raw material is cut to get finished parts. The FFF/FDM process is also referred to as material extrusion additive manufacturing (AM) by the community. The FDM process is a versatile advanced fabrication technology among other AM technologies. FDM is commonly used to produce parts with polymeric materials, but the technology can accommodate different materials, including composites, metals,

A. R. Prajapati · S. R. Rajpurohit
Department of Mechanical Engineering, S V National Institute of Technology,
Surat 395007, India

M. Somireddy (✉)
Department of Mechanical Engineering, York University, Toronto, ON M3J 1P3, Canada
e-mail: madhukar@yorku.ca

and ceramics. Furthermore, 3D printers based on this technology are affordable and can fabricate large structures, unlike other AM technologies, which have a limitation on build volume. Such additional benefits with technology increased its demand in many engineering applications. Although the FDM is the most widely used 3D printing technology, but the deeper understanding of the process and its impact on the material properties of final manufactured parts is currently limited. Such challenges can be explored using computational models.

Experimental investigation of parts synthesized via FDM revealed that the printing process has a major effect on the final quality of parts [1]. Mainly, the processing parameters such as extrusion temperature, speed of printing, melt flow rate, and chamber temperature govern the quality extrudates. Furthermore, the bonding strength between the adjacent extrudates also influences the mechanical strength of printed parts [2]. Moreover, the dynamics of melt flow and material deposition play an important role in bond formation [3]. Recently, computational models [4–6] have been in use to understand the printing process and its effect on the material properties of printed components.

The properties of 3D printed specimens are ruled by the microstructure, which in turn is governed by different types of printing process parameters such as layer height, angle of raster, printing direction, print orientation, overlap, infill pattern, and infill density [7–10]. Experimental works [11–13] revealed that the final material properties of 3D printed components are anisotropic, and the reason for that is due to variation in the microstructure due to change in printing parameters while building parts. Computational materials and analytical models [14–17] are available for estimation of material properties and further, these models enable modifying the material characteristics of final 3D printed parts. The results of mechanical testing revealed that the mechanical behavior of 3D printed components is comparable to that of laminates behavior and such printed structures can be handled as composite laminate structures [18]. Therefore, laminate mechanic can be used to depict the mechanical properties of 3D printed structures.

In this chapter, we initially explored different computational models available for modeling of the fused deposition process. Then, analytical and computational models for material modeling were presented for the 3D printed structures. Finally, material models were discussed to depict the mechanical behavior of FDM made parts.

2 Modeling of Material Extrusion Process

Currently, understanding of the process science of FDM process modeling is limited. The models that define the melt dynamics, extrusion technique and bonding between successive material layers are crucial for the development of advanced approaches for different 3D printers. Further, understanding the relationship between processing parameters and mechanical properties of printed parts is crucial in enabling the effective design of parts for manufacturing. Also, the relationship is

critical in producing reliable parts for industrial use and in facilitating more intelligent/smart materials. Key elements of the FDM process include the pinch rolled feed mechanism, liquefier dynamics, extrudate (road or bead) spreading, bonding between extrudates, and temperature of the chamber, substrate, and extrudates. This section analyzes the present state of the art in modeling each of these characteristics of FDM process.

The material extrusion process involves the extrusion of polymeric material through a nozzle and the melt flow, usually at higher rates of shear, and followed by quick cooling. This extrusion process significantly influences the geometry, porosity, and mechanical properties of final components. To understand the influence of the material extrusion process, it requires multi-scale multi-physics models that can include flow behaviour of polymer melt, heat transfer, viscoelastic effect, solidification, and crystallization [4]. The material flow deposition of the printing process can be seen in Fig. 1. The extrusion process can be described by governing equations; conservation of mass, conservation of momentum, and the heat equation, and modeling of the process using these governing equations was discussed in [19–21].

Computational models are available for analysis of liquefier dynamics of the modeling [22–24], and investigation of melt deposition and solidification [25]. The aforementioned computational models also provide insights on the effect of inlet velocity, nozzle diameter, and nozzle angle on the melt flow behaviour of fused deposition modeling. Furthermore, computational fluid dynamics models of the material flow and extrusion process helped to understand the influence of velocity ratio, feed rate, the gap between extruder and substrate on the extrudate, and its shape [26]. Numerical models [27] were also employed to investigate the effect of

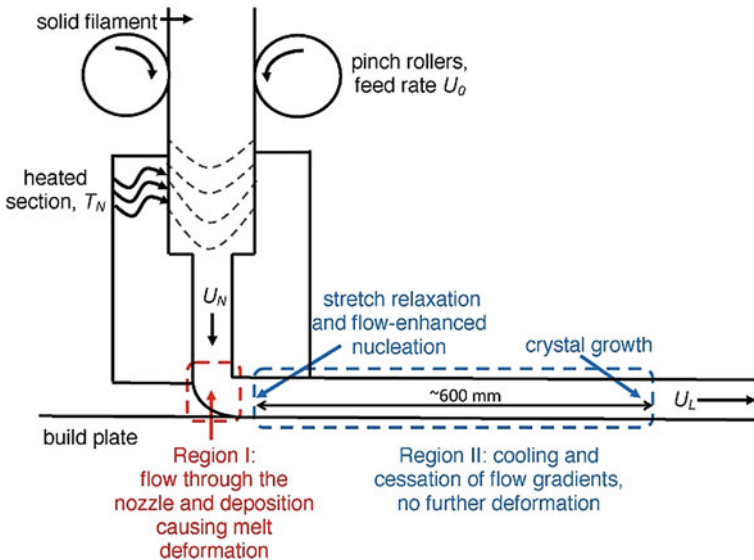


Fig. 1 Material extrusion process of fused deposition modeling [21]

printing speed and layer height on the shape of extrudate. Also, the influence of nozzle speed and nozzle temperature on material deposition was investigated using numerical models [28]. Computational modeling of material deposition also revealed that the deposition rate is greatly influenced by the heat transfer rate [29].

3 Modeling of Bond Formation

The bonding strength between the layers and adjacent extrudates (roads) governs the final strength of 3D printed structures. The bonding strength is ruled by printing process parameters and characteristics of the materials used in printing. In this section, we will see computational models used for simulation for bond formation.

Heat transfer and polymer sintering models were employed to investigate the evolution of neck growth during the formation of the bond [3]. Figure 2 illustrates the bond formation between the adjacent roads, and Fig. 3 shows the same for layers of printed parts. A similar study based on polymer sintering models was also investigated by [5]. The polymer sinter model was used to assess the influence of processing conditions viz. extrusion temperature and the dimensions of the filaments extruded from the nozzle. Extrusion temperature has an important influence on the neck growth between the extrudates and in-turn on the strength of bonding [1].

Thermomechanical simulations revealed that different tool-path patterns cause distortion in the part geometry [30, 31]. The computational model for this is based on three-dimensional transient heat conduction with heat generation due to phase change. A diffusion-controlled healing model was employed to predict the bonding strength between the layers [2]. It revealed that the Z-axis (or inter-layer) strength of 3D printed component depends on printer settings and material properties. In addition, one-dimensional transient thermal analysis of the temperature-dependent diffusion model of the interface between layers was used to predict bond strength.

Thermo-mechanical models [32, 33] were also considered to examine the effects of processing conditions viz. nozzle temperature, speed of the printing, layer height and thermal gradient of synthesized. Thermal analysis was performed to forecast the profile of temperature distribution of a model with similar dimensions of the

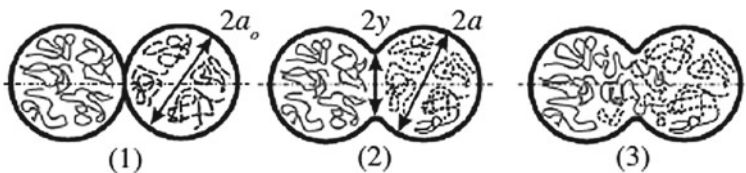
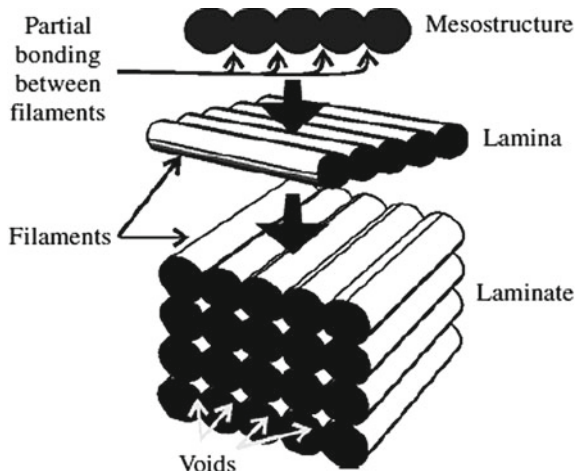


Fig. 2 Bond formation between adjacent extrudates [3] (1) surface contacting, (2) neck growth, (3) diffusion at interface

Fig. 3 Different levels (microstructure to structural level) of 3D printed parts via FDM [3]



part. Also, for the input of analysis, these profiles of temperature distribution were used for thermal stress. Later, it concluded that the developed model could forecast the effective diffusion time with fewer errors than the existing theoretical and numerical models. The numerical model also revealed that low values of temperature, speed of printing, and layer height were helpful for reducing the distortion and residual thermal stresses.

4 Material Modeling of 3D Printed Parts

Anisotropy in the characteristics of 3D printed parts is one of the main concerns for operative design and analysis, as final properties are differing from the properties of the material used for FDM process. This change in the characteristics is primarily because of variation in the mesostructure/microstructure that is built while depositing the material layer upon layer. Material properties are critical for the effective design of structures and consequently, the final properties need to be projected to produce reliable and durable components. The material behavior of 3D printed parts was found to be similar to that of laminate's behavior [13, 15, 34], and the layers of the specimens can be treated as an orthotropic material. The orthotropic material constitutes nine independent elastic moduli viz. E_1, E_2, E_3 (Young's modulus), G_{12}, G_{13}, G_{23} (shear modulus) and $\nu_{12}, \nu_{23}, \nu_{13}$ (Poisson's ratio). Experimental evaluation of nine elastic moduli is challenging and further, it is time consuming and tedious. An alternative to experimental work is analytical methods and computational methods. Constitutive relation of orthotropic material is given as

$$\left\{ \begin{matrix} \sigma_{11} \\ \sigma_{22} \\ \sigma_{33} \\ \tau_{12} \\ \tau_{13} \\ \tau_{23} \end{matrix} \right\} = \begin{bmatrix} C_{11} & C_{12} & C_{13} & 0 & 0 & 0 \\ C_{12} & C_{22} & C_{23} & 0 & 0 & 0 \\ C_{13} & C_{23} & C_{33} & 0 & 0 & 0 \\ 0 & 0 & 0 & C_{44} & 0 & 0 \\ 0 & 0 & 0 & 0 & C_{55} & 0 \\ 0 & 0 & 0 & 0 & 0 & C_{66} \end{bmatrix} \left\{ \begin{matrix} \varepsilon_{11} \\ \varepsilon_{22} \\ \varepsilon_{33} \\ \gamma_{12} \\ \gamma_{13} \\ \gamma_{23} \end{matrix} \right\}, \text{ simply } \{\sigma\} = [C]\{\varepsilon\} \tag{1}$$

$$\{\varepsilon\} = [S]\{\sigma\} \tag{2}$$

Here, compliance matrix is represented by S and different matrix coefficients are:

$$\begin{aligned} S_{11} &= \frac{1}{E_1}, S_{12} = -\frac{\nu_{12}}{E_2}, S_{13} = -\frac{\nu_{13}}{E_1}, S_{22} = \frac{1}{E_2}, S_{23} = -\frac{\nu_{23}}{E_2}, S_{33} = \frac{1}{E_3}, S_{44} \\ &= \frac{1}{G_{12}}, S_{55} = \frac{1}{G_{13}}, S_{66} = \frac{1}{G_{23}} \end{aligned} \tag{3}$$

The components C_{ij} of the C matrix have been found by inverting the compliance matrix. The elastic modulus in the above equation needs to be determined to consider material behavior while designing parts. In this section, we will see different analytical and computational models used in the modeling of FDM made components to estimate the material characteristics.

Rule of mixture: The rule of mixture is the popular and simplest method; this technique is based on the different material mechanics for estimating the overall properties of the composite parts. [15, 35] Mathematical formulation for calculating the overall elastic moduli of 3D printed parts is given below.

$$\bar{E}_1 = (1 - \rho_1)E \tag{4}$$

$$\bar{E}_2 = \bar{E}_3 = \left(1 - \rho_1^{1/2}\right)E \tag{5}$$

$$\bar{G}_{12} = \bar{G}_{13} = G \frac{(1 - \rho_1)(1 - \rho_1^{1/2})}{(1 - \rho_1) + (1 - \rho_1^{1/2})} \tag{6}$$

$$\bar{G}_{23} = \left(1 - \rho_1^{1/2}\right)G \tag{7}$$

$$\bar{\nu}_{12} = \bar{\nu}_{13} = (1 - \rho_1)\nu \tag{8}$$

$$\bar{v}_{13} = (1 - \rho_1^{1/2})v \tag{9}$$

$$\bar{v}_{21} = \bar{v}_{31} = \bar{v}_{32} = (1 - \rho_1^{1/2})v \tag{10}$$

where, the void density is ρ_1 on first plane in Fig. 4, and E , G and ν are the isotropic properties of the material, which are the elastic properties of the material used for 3D printing. The void density on a plane can be estimated from analysis of the microscopic image of 3D printed part. However, this method can not consider the influence of shape of voids on the properties.

Closed-form orthotropic constitutive model: In this analytical model [37], elastic modulus for a material can be estimated using the following equations. This method accounts for the influence of the void’s shape on final material properties. Figure 5 illustrates the unit cell of a 3D printed part with different void shapes.

$$E_{xx} = (1 - f)E \tag{11}$$

$$\nu_{xy} = \nu \tag{12}$$

$$\nu_{xz} = \nu \tag{13}$$

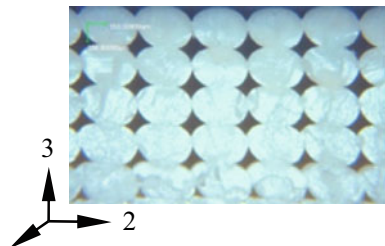
$$\frac{E_{yy}}{E} = \frac{(c - 1)(3c^2 - 1)}{(c - 1)(3c^2 - 1) - f(3c^3 - 3c^2 + c - 3)} \tag{14}$$

$$E_{zz} = E_{yy} \tag{15}$$

$$\nu_{yz} = \frac{\nu(-3c^3 + 3c^2 + c - 1) - f(3c^3 - 3c^2 + c + 1)}{f(3c^3 - 3c^2 + c - 3) - 3c^3 + 3c^2 + c - 1} \tag{16}$$

$$\frac{G_{yz}}{G} = \frac{(c + 1)(1 - 3c^2)}{(c + 1)(1 - 3c^2) + f(\kappa + 1)} \tag{17}$$

Fig. 4 Cross section of 3D printed part [36] (license CC BY 4.0)



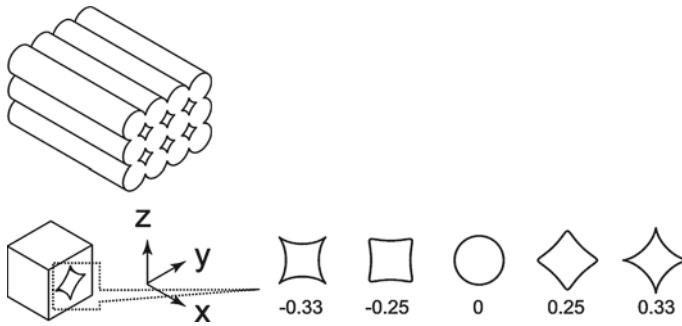


Fig. 5 Unit cell of square array mesostructure [37]

$$\frac{G_{xy}}{G} = \frac{1 - 3c^2}{2f - 3c^2 + 1} \tag{18}$$

$$G_{xz} = G_{xy} \tag{19}$$

Here, mesostructure’s porosity is represented by $f \in [0, 1]$, κ and G are Kolosov constant and shear modulus of the material respectively used for 3D printing. For an isotropic material, the relationship between G , E and ν is written as $G = \frac{E}{2(1+\nu)}$ and $\kappa = \frac{3-\nu}{1+\nu}$. Due to the symmetry of the shape of void, E_{yy} is equivalent to E_{zz} in the closed-form model, and also this model predicts that G_{xy} is equivalent to G_{xz} .

Computational models: In computational methods, the microstructure of FDM made components is used in the FE simulation, and also the material’s properties of the microstructure are considered in the material modeling. The homogenization technique [17, 38, 39] is used for computational material modeling, in this method the unit cell is considered as a homogeneous orthotropic material macroscopically. The fields of the unit cell viz. $\bar{\sigma}_{ij}$ (average stress) and $\bar{\epsilon}_{ij}$ (average strains) are computed by averaging of the all local stresses σ_{ij} and strains ϵ_{ij} over the V_{RVE} (volume of RVE) correspondingly. The average stress and strains are written as

$$\bar{\sigma}_{ij} = \frac{1}{V_{RVE}} \int_V \sigma_{ij}(x_1, x_2, x_3) dV \tag{20}$$

$$\bar{\epsilon}_{ij} = \frac{1}{V_{RVE}} \int_V \epsilon_{ij}(x_1, x_2, x_3) dV \tag{21}$$

The elastic constitutive relation for a RVE is given as

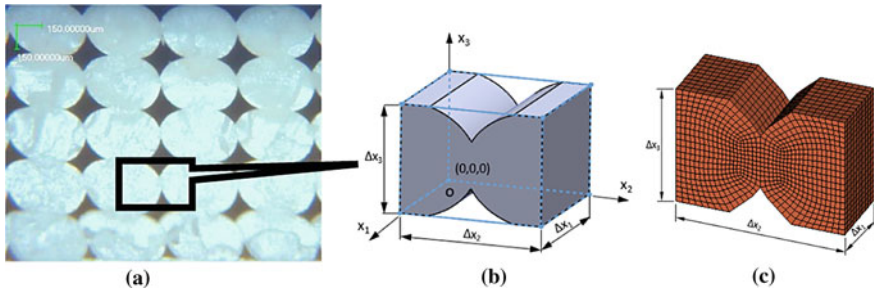


Fig. 6 Microstructure of 3D printed parts [16] **a** unit cell/RVE **b** finite element model

$$\{\bar{\sigma}\} = [C]\{\bar{\epsilon}\} \tag{22}$$

Here, orthotropic material’s constitutive matrix is represented by $[C]$ which is equivalent to $[S]^{-1}$. Then, the strain energy of homogenized RVE can be written as

$$U^* = \frac{1}{2} \{\bar{\epsilon}\}^T [C] \{\bar{\epsilon}\} V_{RVE} \tag{23}$$

The elements which are unknown in the design matrix are obtained with the help of various load conditions. For the deformation model, strain energy (U^*) is calculated using FE simulations and then different values of the stiffness are calculated. Unit cell/RVE plays an important role in determining the properties of FDM made components. Unit cell/RVE is a repetitive architecture of the microstructure of 3D printed parts and it is considered in the homogenization. The RVE is mainly comprised of the material of extrudates and voids between the extrudates, and also their geometry is considered in finite element modeling of RVE. The shape of RVE may vary based on the printing parameters (*e.g.* layer thickness, the orientation of extrudates) used for printing a part. Researchers [16, 17] considered RVE from a single layer of printed parts, refer to Figs. 6 and 7 and on the other hand, RVE is taken from two layers of printed parts [35, 40, 41]. However, these studies treated the RVE as orthotropic material in homogenization.

5 Modeling of Mechanical Behavior of 3D Printed Structures

The material behaviour of FDM made components is similar to the laminate parts [13]. This behaviour is primarily because of the alignment of extrudates (bead or roads) and the deposition of layers while 3D printing. This indicates that the extrudates in a particular printed layer act as a single laminate with several layers acting like a laminated composite part with different orientations of the extrusion.

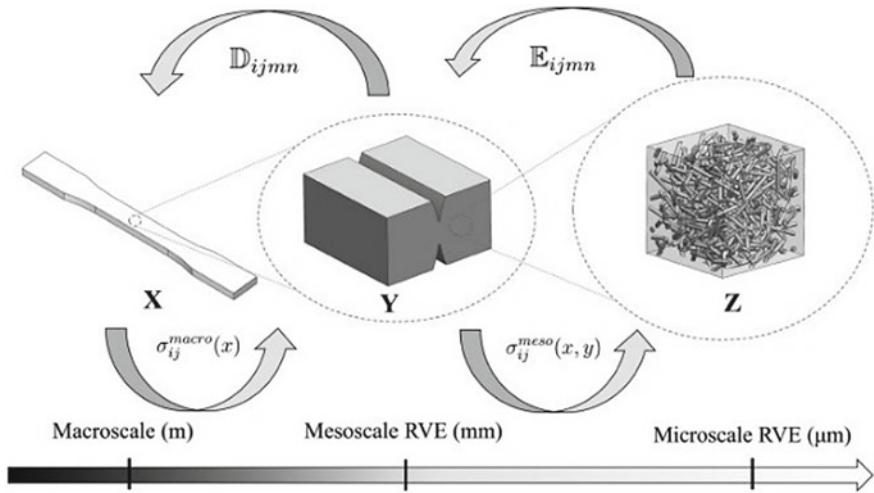


Fig. 7 Three-scale homogenization for 3D printed composite parts [17]

The different layers of the final FDM made part acts like orthogonal anisotropic material and therefore, these can be characterized as a unidirectional fiber reinforced layer. The material behavior of FDM made components can be considered with the help of laminate dynamics and CLT (classical laminate theory) methods. Therefore, CLT helps to characterize the behavior of FDM components that are exposed to various loads during stress analysis. Thus, final FDM made components can be viewed as laminated composite structures that characterize its mechanical behavior.

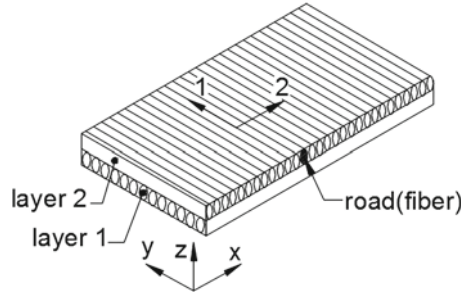
Thin layers of FDM made structures can be characterized with plane stress constitutive relation. Then, for a plane stress case, the constitutive relation of orthotropic materials (Eq. 1) reduces to

$$\begin{Bmatrix} \sigma_{11} \\ \sigma_{22} \\ \tau_{12} \end{Bmatrix} = \begin{bmatrix} Q_{11} & Q_{12} & 0 \\ Q_{12} & Q_{22} & 0 \\ 0 & 0 & Q_{66} \end{bmatrix} \begin{Bmatrix} \varepsilon_{11} \\ \varepsilon_{22} \\ \gamma_{12} \end{Bmatrix} \tag{24}$$

where Q_{ij} components of a constitutive matrix (\mathbf{Q}) of a lamina. The laminate coordinate system is referred to with x , y , and z , and the local coordinate system is denoted with 1, 2, and 3, as illustrated in Fig. 8.

Classical laminate theory: Figure 8 shows a 3D printed plate with two-layers, with the fibers (extrudates) oriented in layers 1 and 2 at 0° and 90° , respectively

Fig. 8 Plate made with FDM in different raster orientation



The displacement field for a lamina from CLT are given as

$$u(x, y, z) = u_0(x, y) + z\phi_x(x, y) \tag{25a}$$

$$v(x, y, z) = v_0(x, y) + z\phi_y(x, y) \tag{25b}$$

$$w(x, y, z) = w_0(x, y) \tag{25c}$$

For a thin layer the rotation terms in Eq. 25 converted into $\phi_x = -\frac{\partial w_0}{\partial x}$, $\phi_y = -\frac{\partial w_0}{\partial y}$, based on the Kirchhoff–Love hypothesis. The strains of the laminate are written as

$$\begin{Bmatrix} \varepsilon_{xx} \\ \varepsilon_{yy} \\ \gamma_{xy} \end{Bmatrix} = \begin{Bmatrix} \varepsilon_{xx}^0 \\ \varepsilon_{yy}^0 \\ \gamma_{xy}^0 \end{Bmatrix} + z \begin{Bmatrix} k_{xx} \\ k_{yy} \\ k_{xy} \end{Bmatrix}, \quad \text{or } \{\varepsilon\} = \{\varepsilon^0\} + z\{k\} \tag{26}$$

where ε_{xx}^0 and ε_{yy}^0 are strains at mid-plane; γ_{xy}^0 is the shear strain; z is the distance from the mid-plane; k_{xx} and k_{yy} are curvatures of bending and k_{xy} is curvature of twisting. The constitutive relation is depicted as:

$$\begin{Bmatrix} \sigma_{xx} \\ \sigma_{yy} \\ \tau_{xy} \end{Bmatrix} = \begin{bmatrix} \bar{Q}_{11} & \bar{Q}_{12} & 0 \\ \bar{Q}_{12} & \bar{Q}_{22} & 0 \\ 0 & 0 & \bar{Q}_{66} \end{bmatrix} \begin{Bmatrix} \varepsilon_{xx} \\ \varepsilon_{yy} \\ \gamma_{xy} \end{Bmatrix}, \quad \text{or } \{\sigma\} = [\bar{Q}]\{\varepsilon\} \tag{27}$$

where \bar{Q}_{ij} are constants of transformed material and the elements of \bar{Q}_{ij} are given as

$$[\bar{Q}] = [T]^{-1}[Q][T]^{-T} \tag{28}$$

Here, $[T]$ is a transformation matrix.

$$[T] = \begin{bmatrix} c^2 & s^2 & 2cs \\ s^2 & c^2 & -2sc \\ -cs & cs & c^2 - s^2 \end{bmatrix} \tag{29}$$

Here, c is $\cos \theta$, s is $\sin \theta$, and θ is the fiber orientation in an counter clockwise direction. The resultant force and moment are defined as

$$\begin{Bmatrix} N_{xx} \\ N_{yy} \\ N_{xy} \end{Bmatrix} = \int_{-h/2}^{h/2} \begin{Bmatrix} \sigma_{xx} \\ \sigma_{yy} \\ \tau_{xy} \end{Bmatrix} dz = \sum_{k=1}^n \int_{h_k}^{h_{k+1}} \begin{Bmatrix} \sigma_{xx} \\ \sigma_{yy} \\ \tau_{xy} \end{Bmatrix}_k dz, \quad \{N\} = \sum_{k=1}^n \int_{h_k}^{h_{k+1}} \{\sigma\} dz \quad (30)$$

$$\begin{Bmatrix} M_{xx} \\ M_{yy} \\ M_{xy} \end{Bmatrix} = \int_{-h/2}^{h/2} \begin{Bmatrix} \sigma_{xx} \\ \sigma_{yy} \\ \tau_{xy} \end{Bmatrix} z dz = \sum_{k=1}^n \int_{h_k}^{h_{k+1}} \begin{Bmatrix} \sigma_{xx} \\ \sigma_{yy} \\ \tau_{xy} \end{Bmatrix}_k z dz, \quad \{M\} = \sum_{k=1}^n \int_{h_k}^{h_{k+1}} \{\sigma\} z dz \quad (31)$$

Using Eqs. 26 and 27, Eqs. 30 and 31 become

$$\{N\} = \sum_{k=1}^n [\bar{Q}] \left[\int_{h_k}^{h_{k+1}} \{\varepsilon^0\} dz + \int_{h_k}^{h_{k+1}} \{k\} z dz \right] = [A] \{\varepsilon^0\} + [B] \{k\} \quad (32)$$

$$\{M\} = \sum_{k=1}^n [\bar{Q}] \left[\int_{h_k}^{h_{k+1}} \{\varepsilon^0\} z dz + \int_{h_k}^{h_{k+1}} \{k\} z^2 dz \right] = [B] \{\varepsilon^0\} + [D] \{k\} \quad (33)$$

Here, N_{xx} and N_{yy} signify the normal forces per unit width; N_{xy} represents the shear force; M_{xx} and M_{yy} represent the bending moments in the y - z and x - z planes, respectively; M_{xy} denotes the twisting moment. $[A]$, $[B]$, and $[D]$ are the stretch stiffness matrix, bond stiffness matrix, and flexural rigidity stiffness matrix, respectively.

$$[A] = \sum_{k=1}^N [\bar{Q}] \int_{h_k}^{h_{k+1}} dz, \quad [B] = \sum_{k=1}^N [\bar{Q}] \int_{h_k}^{h_{k+1}} z dz, \quad [D] = \sum_{k=1}^N [\bar{Q}] \int_{h_k}^{h_{k+1}} z^2 dz \quad (34)$$

The elongation and curvature can be obtained from Eqs. 32 and 33, once the values of normal force and moment are provided. The symmetric laminate structure have the same lamina material properties and fiber orientation evenly distributed above and below the median plane of the laminate. The above mechanics of laminates are useful in characterizing the mechanical behavior of FDM made components under different loadings.

6 Conclusions

Computation models of the extrusion process provided the significance of the different processing parameters on the quality of FDM made structures. The models based on fluid dynamics considered the influence of material flow behavior and the

extrusion process. Polymer sintering models and heat transfer models were employed to investigate the formation of the bonding between the layers, and these models revealed the effects of the temperature of extrusion and chamber environment on the evolution of neck growth. Computational homogenization models were used for material modeling of 3D printed parts, and the final properties of parts were estimated by considering the underlying microstructure of the parts. Finally, the 3D printed parts were treated as laminate structures and the mechanics of laminates were employed to investigate the mechanical behavior of 3D printed parts. In summary, the above computational models provided more insights on the process-structure-property relationship of 3D printed parts, and further, the models were useful to further enhance the quality of parts.

References

1. Sun Q, Rizvi GM, Bellehumeur CT, Gu P (2008) Effect of processing conditions on the bonding quality of FDM polymer filaments. *Rapid Prototyp J* 14(2):72–80
2. Coogan TJ, Kazmer DO (2017) Bond and part strength in fused deposition modeling. *Rapid Prototyp J* 23(2):414–422
3. Bellehumeur C, Li L, Sun Q, Gu P (2004) Modeling of bond formation between polymer filaments in the fused deposition modeling process. *J Manuf Process* 6(2):170–178
4. Das A, McIlroy C, Bortner MJ (2020) Advances in modeling transport phenomena in material–extrusion additive manufacturing: coupling momentum, heat, and mass transfer. *Progress Addit Manuf*. <https://doi.org/10.1007/s40964-020-00137-3>
5. Gurrala PK, Regalla SP (2014) Part strength evolution with bonding between filaments in fused deposition modelling: this paper studies how coalescence of filaments contributes to the strength of final FDM part. *Virtual Phys Prototyp* 9(3):141–149
6. Coogan TJ, Kazmer DO (2017) Healing simulation for bond strength prediction of FDM. *Rapid Prototyp J* 23(3):551–561
7. Tymrak BM, Kreiger M, Pearce JM (2014) Mechanical properties of components fabricated with open-source 3-D printers under realistic environmental conditions. *Mater Des* 58:242–246
8. Huang B, Singamneni S (2015) Raster angle mechanics in fused deposition modelling. *J Compos Mater* 49(3):363–383
9. Cantrell JT, Rohde S, Damiani D, Gurnani R, DiSandro L, Anton J, Young A, Jerez A, Steinbach D, Kroese C, Ifju PG (2017) Experimental characterization of the mechanical properties of 3D-printed ABS and polycarbonate parts. *Rapid Prototyp J* 23(4):811–824
10. Somireddy M, Czekanski A (2020) Anisotropic material behavior of 3D printed composite structures–material extrusion additive manufacturing. *Mater Des* 195:108953
11. Rajpurohit SR, Dave HK (2019) Analysis of tensile strength of a fused filament fabricated PLA part using an open-source 3D printer. *Int J Adv Manuf Technol* 101(5–8):1525–1536
12. Rezaayat H, Zhou W, Siriruk A, Penumadu D, Babu SS (2015) Structure–mechanical property relationship in fused deposition modelling. *Mater Sci Technol* 31(8):895–903
13. Somireddy M, Singh CV, Czekanski A (2019) Analysis of the material behavior of 3D printed laminates via FFF. *Exp Mech* 59(6):871–881
14. Ning F, Cong W, Hu Y, Wang H (2017) Additive manufacturing of carbon fiber-reinforced plastic composites using fused deposition modeling: effects of process parameters on tensile properties. *J Compos Mater* 51(4):451–462

15. Li L, Sun Q, Bellehumeur C, Gu P (2002) Composite modeling and analysis for fabrication of FDM prototypes with locally controlled properties. *J Manuf Process* 4(2):129–141
16. Somireddy M, Czekanski A, Singh CV (2018) Development of constitutive material model of 3D printed structure via FDM. *Mater Today Commun* 15:143–152
17. Nasirov A, Gupta A, Hasanov S, Fidan I (2020) Three-scale asymptotic homogenization of short fiber reinforced additively manufactured polymer composites. *Compos B Eng* 202:108269
18. Somireddy M, Singh CV, Czekanski A (2020) Mechanical behaviour of 3D printed composite parts with short carbon fiber reinforcements. *Eng Fail Anal* 107:104232
19. Turner BN, Strong R, Gold SA (2014) A review of melt extrusion additive manufacturing processes: I. Process design and modeling. *Rapid Prototyp J* 20(3):192–204
20. Turner BN, Gold SA (2015) A review of melt extrusion additive manufacturing processes: II. Materials, dimensional accuracy, and surface roughness. *Rapid Prototyp J* 21(3):250–261
21. McLroy C, Graham RS (2018) Modelling flow-enhanced crystallisation during fused filament fabrication of semi-crystalline polymer melts. *Addit Manuf* 24:323–340
22. Bellini A, Güçeri S, Bertoldi M (2004) Liquefier dynamics in fused deposition. *J Manuf Sci Eng Trans ASME* 126:237–246
23. Ramanath HS, Chua CK, Leong KF, Shah KD (2008) Melt flow behaviour of poly- ϵ -caprolactone in fused deposition modelling. *J Mater Sci-Mater Med* 19(7):2541–2550
24. Serdeczny MP, Comminal R, Mollah MT, Pedersen DB, Spangenberg J (2020) Numerical modeling of the polymer flow through the hot-end in filament-based material extrusion additive manufacturing. *Addit Manuf* 36:101454
25. Xia H, Lu J, Dabiri S, Tryggvason G (2018) Fully resolved numerical simulations of fused deposition modeling. Part I: fluid flow. *Rapid Prototyp J* 24(2):463–476
26. Comminal R, Serdeczny MP, Pedersen DB, Spangenberg J (2019) Motion planning and numerical simulation of material deposition at corners in extrusion additive manufacturing. *Addit Manuf* 29:100753
27. Serdeczny MP, Comminal R, Pedersen DB, Spangenberg J (2018) Experimental validation of a numerical model for the strand shape in material extrusion additive manufacturing. *Addit Manuf* 24:145–153
28. Xia H, Lu J, Tryggvason G (2018) Fully resolved numerical simulations of fused deposition modeling. Part II—solidification, residual stresses and modeling of the nozzle. *Rapid Prototyp J* 24(6):973–987
29. Phan DD, Swain ZR, Mackay ME (2018) Rheological and heat transfer effects in fused filament fabrication. *J Rheol* 62(5):1097–1107
30. Zhang Y, Chou YK (2006) Three-dimensional finite element analysis simulations of the fused deposition modelling process. *Proc Inst Mech Eng B J Eng Manuf* 220(10):1663–1671
31. Zhang Y, Chou K (2008) A parametric study of part distortions in fused deposition modelling using three-dimensional finite element analysis. *Proc Inst Mech Eng B J Eng Manuf* 222(8):959–968
32. Zhou Y, Nyberg T, Xiong G, Liu D (2016) Temperature analysis in the fused deposition modeling process. In: 2016 3rd international conference on information science and control engineering (ICISCE) IEEE, pp 678–682
33. Zhou X, Hsieh SJ, Sun Y (2017) Experimental and numerical investigation of the thermal behaviour of polylactic acid during the fused deposition process. *Virtual Phys Prototyp* 12(3):221–233
34. Parandoush P, Lin D (2017) A review on additive manufacturing of polymer-fiber composites. *Compos Struct* 182:36–53
35. Rodríguez JF, Thomas JP, Renaud JE (2003) Mechanical behavior of acrylonitrile butadiene styrene fused deposition materials modeling. *Rapid Prototyp J* 9(4):219–230
36. Somireddy M, Czekanski A (2017) Mechanical characterization of additively manufactured parts by FE modeling of mesostructure. *J Manuf Mater Process* 1(2):18
37. Chen R, Kaplan AF, Senesky DG (2020) Closed-form orthotropic constitutive model for aligned square array mesostructure. *Addit Manuf* 36:101463

38. Yuan Z, Fish J (2008) Toward realization of computational homogenization in practice. *Int J Numer Meth Eng* 73(3):361–380
39. Xia Z, Zhang Y, Ellyin F (2003) A unified periodical boundary conditions for representative volume elements of composites and applications. *Int J Solids Struct* 40(8):1907–1921
40. Anoop MS, Senthil P (2019) Homogenisation of elastic properties in FDM components using microscale RVE numerical analysis. *J Braz Soc Mech Sci Eng* 41(12):540
41. Calneryte D, Barauskas R, Milasiene D, Maskeliunas R, Neciunas A, Ostreika A, Patasius M, Krisciunas A (2018) Multi-scale finite element modeling of 3D printed structures subjected to mechanical loads. *Rapid Prototyp J* 24(1):177–187

Multi-Objective Optimization for FDM Process Parameters with Evolutionary Algorithms



Nita Yodo and Arup Dey

Abstract Fused deposition modeling (FDM) based three-dimensional (3D) printing process has become a popular and economical alternative to produce complex 3D structures without the necessity of expensive tooling. There are a set of process parameters involved in the FDM process that should be appropriately set to ensure the desired 3D part properties are achieved. The relationships between these process parameters are often complicated, conflicting, and interdependent. The selection of optimum process parameters combination is essential. Many approaches can be taken to optimize FDM process parameters. Although experimental methods are exhaustive, they are often expensive and time-consuming. Alternatively, numerical methods have gained a lot of traction in the application of optimizing FDM process parameters. This chapter will introduce multi-objective optimization and review the state-of-the-art optimization methods based on evolutionary algorithms that can be employed in optimizing FDM process parameters. Multi-objective optimization involves optimizing more than one objective function simultaneously and often results in many optimal solutions known as Pareto-optimal solutions. This Pareto-optimal set of solutions can help decision-makers make a robust optimal selection for FDM process parameters.

1 Introduction

Fused deposition modeling (FDM) or three-dimensional (3D) printing process is a rapidly growing additive manufacturing and rapid prototyping technology. The FDM process is a part of the additive manufacturing process based on material extrusion, initially known for making custom and complex 3D prototypes.

N. Yodo (✉) · A. Dey

Industrial and Manufacturing Engineering Department, North Dakota State University, 1410
14th Ave N, Fargo, ND 58102, USA
e-mail: nita.yodo@ndsu.edu

A. Dey

e-mail: arup.dey@ndsu.edu

The FDM process has slowly made its way to produce functional parts in recent years. The FDM process can be summarized as a continuous melted-filament (typically thermoplastic-based materials) deposited as lines and layer-by-layer to form predefined shapes. Thus, the FDM process is also known as the 3D printing process, filament-based process, fused-filament fabrication, or sometimes, freeform filament fabrication. The FDM process is popular among researchers, practitioners, and the general public because it can create complex 3D geometrical shapes without any expensive tooling or require additional assembly processes [1, 2]. Although the FDM process overcomes design complexity restriction, some challenges need to be addressed for the FDM process from being fully industrialized.

The FDM process begins with creating a 3D model in computer-aided design (CAD) software. Nowadays, 3D object scanners can also be used to convert any object to a 3D model. Prior to the printing (or deposition) process, a software that can digitally slice the CAD model into digital layers is required. The output of this process is a file format also known as the stereolithography (STL) file. The STL file is further inputted to the FDM process equipment or 3D printers. The 3D printer is set up with various printing parameters such as print speed, infill density, infill patterns, or melting temperature. The 3D printer then builds the model by depositing the melted thermoplastics materials layer-by-layer onto a printing platform, a build table, or the last printed layer. After completing a layer, the build table typically moves downward in the Z-direction to maintain a constant distance between the printing surface and the extrusion nozzle. Post-processing associated with the 3D printing process, such as removing support structures, polishing, cleaning, or painting, may be required depending on the use of the printed parts.

The FDM process or additive manufacturing, in general, offers various opportunities for advancing global manufacturing and innovation. The 3D printing process benefits vary from design freeform, customizable, no complex tooling required, and many more. However, many large companies and industries are still struggling to adopt the FDM process into their product development and manufacturing processes. FDM processes are often employed only up to the proof-of-concept or then product development stage, and then conventional manufacturing processes will take over the mass production.

The FDM process still has many challenges that need to be resolved before it can compete with traditional manufacturing processes, such as injection molding [3]. Some of the obstacles are equipment cost, limited accommodation for large part dimensions, manufacturing cost for self-replicated parts, lack of repeatability, and longer production timelines. Although many 3D printers for personal use are affordable, this is not applicable for large manufacturers such as automobile and aerospace industries. FDM process requires a dedicated place and may not always possible to be consolidated with conventional production processes or assembly lines. Thus, the more massive the dimension of a printed structure, the larger the required space is to set up the FDM equipment. This further translates to substantially higher equipment costs, investment costs, as well as manufacturing costs.

Although the FDM process may have an advantage in producing customize and complex structures, for self-replicated parts, the FDM process is behind the

injection molding process in terms of manufacturing costs, production repeatability, and production timelines. In addition, the FDM process often does not offer high build-to-build accuracy. This is because there are many sources of uncertainty (inherent or not) present in the overall FDM process [4]. The printed parts' quality depends on preprocessing activities, such as CAD and STL file conversion, multiple process parameter settings, and post-processing activities. Although the preprocessing and post-processing actions may affect the printed parts' quality, the input process parameters selection is known to significantly impact the printed part performance.

Much research efforts had been attempted to understand the relationship of FDM process parameters with the part properties. However, it was found that many trade-offs and sacrifices have to be made depending on the overall objective of the final printed parts. If a printed piece is required to have high mechanical properties such as impressive compression strength, good stability, and sturdiness, more materials should be used to build the printed part. This will eventually add to additional build time and higher manufacturing and material costs. Although process parameters can be adjusted to reduce build time, such as increasing the printing speed, this will further result in other problems such as weak adhesion between layers. Thus, to find a balance between conflicting process parameters, the FDM process parameters need to be optimized.

Multi-objective optimization is a part of the decision-making and optimization disciplines that simultaneously optimize more than one objective function [5, 6]. Multi-objective optimization has been applied in many fields of engineering, logistics/transportation, designs, and other applied science, where an optimal decision is a concern in the presence of multiple conflicting objectives. The FDM application can benefit from multi-objective optimization as well. The multi-objective optimization approach can be applied to obtain an optimal combination of process parameters to ensure desired part properties are being fulfilled.

Before dipping further into multi-objective optimization approaches in FDM application, this book chapter will initially discuss commonly known FDM process parameters in Sect. 2 and their influence on the 3D printed parts in Sect. 3. Section 4 introduces multi-objective optimization, evolutionary algorithms, related search algorithm, as well as hybrid algorithms. Section 5 will highlight some potential future work in the FDM field as concluding remarks of this chapter.

2 FDM Process Parameters

Process parameters are defined as variables related to the FDM process, which impact the production process and the produced parts. Like many other manufacturing processes, the FDM process has multiple process parameters that can be controlled or adjusted. To improve printed part properties such as surface quality, dimensional accuracy, thermal properties, and mechanical properties, selecting a proper combination of process parameters is necessary [7–9].

Additionally, process parameters also significantly impact the production time, energy consumption, waste of materials (in the form of support material), in addition to the properties of printed parts. Manufacturers, researchers, and practitioners should know adequate knowledge about the FDM process parameters and their appropriate settings level and combination to produce high-quality parts within a reasonable time. Extensive experiments and research efforts had been carried out to understand the influence of different process parameters on various part properties. Several commonly known process parameters are described in the following subsections.

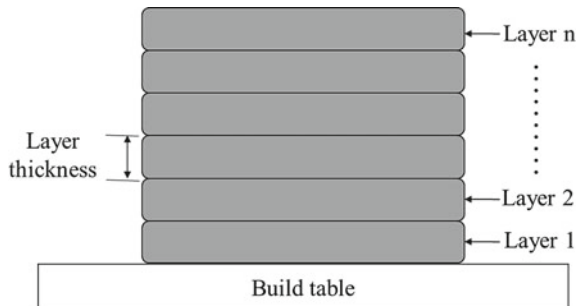
2.1 Layer Thickness

In the FDM process, a filament layer is deposited one at a time or layer-by-layer until a product is completed according to the input design. The height of the deposited layers is known as layer thickness, as shown in Fig. 1. Generally, the range of layer thickness is between 0.1 and 0.4 mm. However, the thickness may vary based on nozzle diameter and FDM machines. For an extrusion nozzle, the maximum layer thickness can be the same as the nozzle diameter. Layer thickness impacts visual appearance, surface quality, dimensional accuracy, and printing (build or production) time. Nowadays, adaptive slicing techniques are applied to convert a design to different layer thickness to improve the surface quality and reduce production time. The small value of layer thickness or the thinner the layer thickness is preferable to improve surface finishing for a part surface with a slight slope and printed on the XY -plane of a build table.

2.2 Build Orientation

Build orientation is the way to position a part on a build table with respect to the X , Y , and Z -axes. In most of the FDM equipment or 3D printers, the vertical axis

Fig. 1 Layer thickness and number of layers



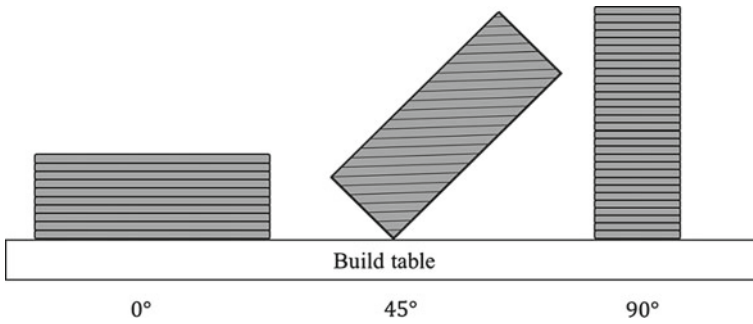


Fig. 2 Build orientation in 0° , 45° , and 90° angles

represents Z-axis. The amount of support material required to print a part depends on the build orientation settings. Selecting appropriate build orientation can reduce the waste of filament used as support materials. Build orientation is measured based on the angle of a printed part with respect to XY -plane. Build orientation can take any value between 0° and 90° . Some example of various build orientations are shown in Fig. 2. Also, build orientation may determine if support materials are required or not. As portrays in Fig. 2, printing parts with 0° and 90° build orientations may not require additional support materials. In contrast, printing parts on a 45° build orientation most likely may need some support materials.

2.3 Extrusion Temperature

According to the predefined designs and other printing instructions set from an FDM machine, the semi-molten filament is deposited through a nozzle on the build table. The temperature at which the filament is heated for deposition is called the extrusion temperature. The setting of extrusion temperature is often selected based on filament materials. Also, the extrusion temperature varies with different filament manufacturers' recommendations. A list of common filament materials and the typical extrusion temperatures are given in Table 1. Note that the list in Table 1 is not exhaustive. There are other composites or bio-based filaments in the market (e.g., wood composite PLA), and their extrusion temperature may vary from the materials listed in Table 1.

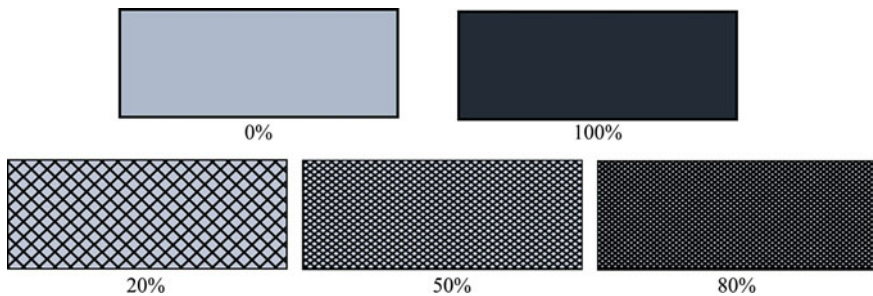
2.4 Infill Density

Infill density in the FDM process refers to the amount of support materials used inside the printed structure. Unlike traditional manufacturing processes such as injection molding, the inner support structure of FDM printed parts is not always

Table 1 Extrusion temperature for different filament materials

Filament materials	Extrusion temperature*, Celcius (°C)
Polylactic acid (PLA)	190–240
Acrylonitrile butadiene styrene (ABS)	230–270
Polycarbonates (PCs)	260–310
Polyether ether ketone (PEEK)	360–410
Polyetherimide (PEI)	350–390
Nylon	230–260

* It is always advised to follow the recommendation from the filament manufacturers

**Fig. 3** Different levels of infill density with a diamond infill pattern

necessary to be completely solid. Instead, the infill density can be adjusted between 0 and 100%. Infill density of 0 and 100% represent a hollow print (no infill) and a solid print inner structure, respectively [10]. Different levels of infill density with a diamond infill pattern are shown in Fig. 3.

A higher infill density makes a more solid print, which means that more materials are used inside the printed parts. This also translates to more material consumption, longer printing time required, and more weight on the final printed pieces. At the same time, a higher infill density offers more stability and durability. Infill density has a significant impact on different parts properties such as compressive strength. If the printed structure is not a concern, choosing lower infill density can reduce the final weight of the printed part, as well as the production time and filament consumption during the printing process. Therefore, it is essential to consider all factors before deciding on the best infill density. Lower infill density (10–15%) is preferable for the non-functional parts such as small prototypes because the visual appearance is a more vital factor than the structure.

2.5 Infill Pattern

Infill or the material inside the printed parts comes in various shapes, sizes, and patterns. The geometric design of the infill is called the infill pattern. When infill

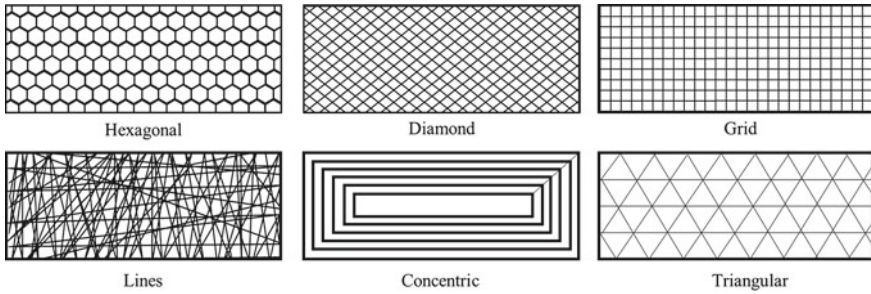


Fig. 4 Different infill patterns

density between 0 and 100% may exclude the infill pattern because the printed part is entirely a hollow or a solid piece, different infill patterns can take many forms in FDM printed parts. Commonly used infill patterns are hexagonal (also known as honey or honeycomb), diamond (or rectilinear), grid (or linear), concentric, and random lines. Note that the terms used for describing different infill patterns may vary with the FDM equipment or 3D printers utilized.

Similar to infill density, infill patterns may affect the printed part properties, especially when structure and mechanical properties are concerned and not the aesthetics. Each infill pattern has its advantages and disadvantages. Infill patterns, such as hexagonal, diamond, and linear, as shown in Fig. 4, offers a nice balance between structural properties and material usage.

2.6 Number of Shells

The outer layer of a printed piece is known as the shell. The minimum number of shells is one (01) layer. In many practical cases, a 3D printed part is produced with more than one shell to ensure more stability and sturdiness. The same concept with the infill pattern and infill density, the number of shells also impacts the printed parts' property. Although increasing the number of shells offers a better structural property, it also increases the printing costs due to more material consumption and longer printing time. The number of shells may also affect the aesthetics properties of the printed parts in addition to the structural properties. If post-processing is required, where the printed part's outer layer will be refined or polished to obtain a smoother surface, it is common to increase the shells' number to produce a thicker wall.

2.7 Raster Width

In 3D printing, the tool path width is known as the raster width. A layer of a printed piece consists of several deposited rasters (or also known as beads), and one pass of

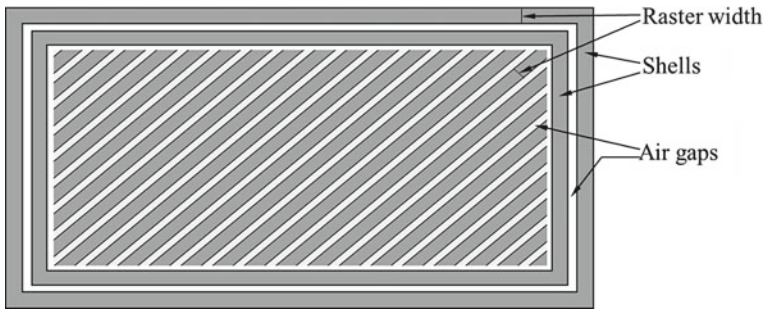


Fig. 5 Shells (outer layers), air gaps, and raster width in a printed part

the nozzle generates one raster. The width of the deposition path is known as raster width. Usually, the raster width depends on the nozzle diameter, and the size of the raster width is slightly larger than the nozzle (or tip) diameter. Thus, the raster width has an impact on the printed layer thickness. In addition, different part properties and build time may also depend on the raster width. The representation of the raster width for an FDM printed part is given in Fig. 5. The deposited raster angle with respect to the XY -plane or the build table is known as the raster angle.

2.8 Air Gap

The gap between two adjacent rasters is known as the air gap or the raster air gap. The air gap in the FDM process can be either negative, positive, or no air gap. A negative air gap means two adjacent rasters are overlapped together. A positive air gap indicates that two adjacent rasters are deposited but not overlapped, maintaining a distance between the deposited rasters. When two adjacent rasters touched each other, and no overlapping occurs, there is no air gap. In most cases, the air gap impacts the printed parts' shells more than the infills because generally, the infills are not set to be solid (100% infill density). The air gap is demonstrated in Fig. 5.

2.9 Print Speed

Printing speed is the speed at which the nozzle (or extruder motors) moves in the XY -plane during the filament deposition process. There are times during the printing; the nozzle also moves to take a position without depositing any filament. This speed is known as travel speed. Print speed and travel speed affects the overall printing time. They can be adjusted to reduce production time. However, improper adjustment of the print speed may significantly affect the quality of the printed parts.

The print speed that is too slow may cause printing deformation or failure in printing. Too slow of a print speed cause the nozzle to sit in the deposited filament for an unnecessary elongated time and may cause the nozzle to adhere to the deposited filament. The print speed that is too fast may cause the extruder to overheat, and weak layer adhesion on the printed part due to insufficient colling time between the deposited layers.

The print speed optimization is necessary to balance printing time without sacrificing too much on the quality of the printed parts. In some higher specification 3D printers, the print speed can be adjusted based on the printing stage. As an example, the outer walls and the infills can be printed with different print speeds. Typically, in practice, the print speed for the exterior walls is slightly decreased to improve the surface quality.

3 Process Parameters Influence on 3D Printed Parts

The FDM process or additive manufacturing, in general, offer numerous advantages—some of the benefits of the FDM process includes assembly cost reduction for complex-shapes parts production, improvement in prototyping abilities, highly skilled operators are not necessarily required to set up and operate a 3D printer, and other benefits in different aspects. Despite the advantages, the adoption of additive manufacturing processes is limited, and to this date, less than 1% of total worldwide manufacturing revenues come from additive manufacturing processes [11]. Inconsistent printed part properties, lack of accuracy from build-to-build parts, as well as insufficient replicability are significant causes behind the limited applications of the FDM process.

Selecting optimum process parameters are known to improve part properties such as surface finishing, dimensional accuracy, tensile strength, flexural strength, compressive strength, or build time. However, there are no exact rules on selecting optimal process parameters in the FDM process due to many conflicting process parameters. Several well-known correlations of process parameters with 3D printed part properties and build time are discussed in this section. The correlations discussed in this section are a summary of different researches findings. Depending on the design of the printed parts and the FDM equipment utilized, the process parameters influence on 3D printed parts discussed in this chapter may slightly vary. More information on the FDM process parameters influence the 3D printed objects can be found from these publications [7–9, 12–14].

3.1 Dimensional Accuracy

Dimensional accuracy is a vital property for replicable parts. It is a measure of how well a 3D printed part matches the size and the specification of the original design.

In addition to replicability, dimensional accuracy can be critical in printing large assemblies. In 3D printing application, a printed piece is often observed to have a higher dimensional accuracy when printed with low layer thickness and low extrusion temperature settings [15–17]. For FDM build parts, dimensional accuracy is comparatively better at the top surface (XY -plane) than at the side surfaces (XZ -plane or YZ -plane). Dimensional accuracy is observed to reduce when printing parts at high temperatures due to the fluidity of deposited rasters.

Dimensional accuracy also depends on shape complexity, size, and the requirement of support materials. Unlike most manufacturing processes, a smaller object (not microscale) can be printed with higher dimensional accuracy than a more massive object with the FDM process. This is because a more sizeable piece may have more room for printing errors. For the same process parameters settings, dimensional accuracy is typically higher for flat surface prints than curvy surface prints [18]. However, a large flat surface may be more prone to sagging, wrapping, or shrinking and require a support structure to hold up these kinds of structures. Although support materials can improve dimensional accuracy, it is traded-off with post-processing to remove the support structures. If not removed carefully, the support structure may affect the final dimensional accuracy of the printed parts.

3.2 Surface Topology

Surface topology is often associated with the aesthetics quality of printed parts. One of the measures of surface topology in the FDM application is the surface roughness. Although surface roughness is mainly considered aesthetics quality, it may also impact other mechanical properties such as crack initiation, wear resistance, and sealing. Due to the inherent FDM process, where a part is built layer-by-layer, 3D printed parts are considered to have a rough surface finish [19].

Similar to dimensional accuracy, lower layer thickness and low extrusion temperature settings are preferable for obtaining a smoother surface or lower surface roughness [20, 21]. Surface quality is often higher at low print speed as well. The staircase effect is a common phenomenon in 3D printed curvy surfaces, and it is infrequently observed for horizontal nor vertical printed surfaces. The staircase effect is more evident for inclined surfaces that are printed on the XY -plane of an FDM machine. The staircase effect can be minimized by choosing a lower layer thickness setting.

3.3 Mechanical Properties

One of the most common 3D printed part properties studied is the mechanical properties. Mechanical properties measure a physical property of the 3D printed part upon the application of forces. Some of the most common mechanical

properties studied are the modulus of plasticity, elasticity, tensile strength, elongation, compression strength, stiffness, and fatigue limit, and many others. Surface roughness can also be considered as one of the mechanical properties. Several published articles detail the mechanical properties of the 3D printed parts [9, 12, 14, 22]. The mechanical properties related to strength typically require more materials. This can be achieved by setting for a higher infill density and choosing a more solid infill pattern. On the other hand, this setting may reduce the elasticity, flexibility, plasticity, or elongation of the 3D printed objects.

FDM build parts are anisotropic [23], which means the tensile strength depends on the direction of the applied load. The tensile strength of the printed parts is typically observed to be higher when the direction of the applied load is parallel to the direction of the filament beads [12, 13]. Therefore, it is recommended to print a part by keeping the tensile load direction parallel to the *XY*-plane. Besides, the low layer thickness setting is often recommended for obtaining good tensile properties [24]. At higher extrusion temperature settings, the tensile properties are also found to be higher due to stronger bonding among the printed layers [24, 25]. A higher percentage of infill density [25, 26], higher print speed [24], and more number of shells [27] are also preferable to achieve good tensile properties.

Process parameters also have a significant impact on many other parts properties such as compressive strength [4], flexural strength [28], impact strength [28], modulus of elasticity [29], lattice structure [30], many others. Due to the limitation of space, other mechanical properties are not going to be detailed further. Interested readers are encouraged to refer to the provided references.

3.4 Build Time

Although build time does not directly impact the printed part properties, it is considered essential to measure the FDM process replicability properties. The shorter the build time means more parts can be printed in a given amount of time. The preferred FDM process parameter settings to reduce build time is the combination of low infill density, high layer thickness, and one shell [4, 31]. The build orientation is also an essential parameter to be considered to minimize the overall build time. Selecting a build orientation for which minimum support materials are required can reduce build time and material consumptions [32]. Another recommendation to shorten the build time is by choosing higher printing speed settings.

3.5 Optimal Process Parameters

For printing a part with the desired part properties, when multiple process parameters are involved, determining the right combination of process parameters is more crucial than selecting an optimum level of a single process parameter. This

approach is also valid for achieving the desired levels of multiple part properties. Therefore, choosing a combination of process parameters that is optimal for one part property may not be enough to fulfill all specific application requirements.

Due to inherent uncertainties exists in the FDM process, it is not always possible to directly select the levels of process parameters to obtain optimum part properties. The association and the combination of multiple process parameters on printed part properties are not always transparent and not easily comprehensible. For every two variables considered, the relationship may be linear or non-linear, positive or negative, or no relationship at all. Various relationships between one process parameters (x -axis) and one part property (y -axis) are shown in Fig. 6. Note that one process parameter does not only affect one part property. It can affect multiple part property as well.

In addition, there are also relationships that exist between multiple process parameters and one part property, or vice versa between one parameter and multiple part properties. When three variables are considered, the relationship can be portrayed in a 3D chart. Considering multiple process parameters and multiple part properties together results in endless combinations, and it is an inherently complex problem to solve. It can be expected that numerous conflicting process parameters and part properties are present in those infinite combinations of multiple process parameters and multiple part properties.

An experimental verification can be approached to understand how one or multiple process parameters influence the change in properties of the printed parts. However, most experimental approach is often labor-intensive, time-consuming,

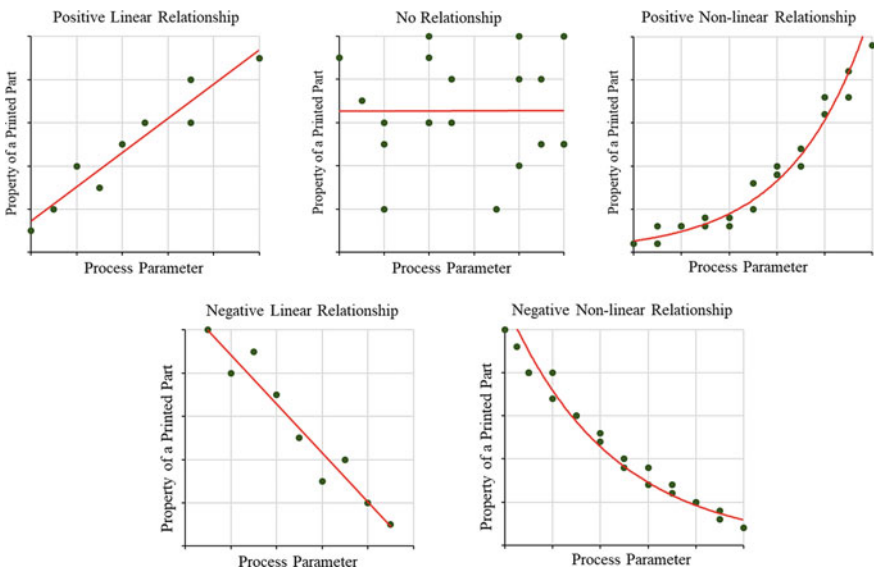


Fig. 6 Various relationships that may exhibit between one process parameter and one printed part property

and expensive. Many physical test samples need to be printed with multiple process parameter settings, and combinations of multiple process parameters can be endless. Various destructive testings are often required to obtain mechanical properties. The test samples used in destructive testing cannot be further reused for other testings. In addition, each testing may require different test samples with different dimensions and shapes according to the suggested test standards. Thus, the experimental approach is not always favorable when a lot of sample data is involved. Experimental methods are preferable for collecting initial sample data or conducting small-scale verification.

When a lot of sample data is involved, the numerical methods approach is more desirable in terms of time, cost, and resources required. Data analysis and optimization are two numerical methods that are widely used to obtain the answer to which combination of process parameters is optimal to ensure the desired part properties are achieved. When there are more than two objective functions or contradictory objective functions that are necessary to be optimized at once, multi-objective optimization can be employed. Assorted multi-objective optimization methods that had been applied to the FDM application will be summarized in the following section.

4 Multi-Objective Optimization for FDM Processes

This section will highlight the big picture of multi-objective optimization and review some commonly applied optimization methods based on evolutionary algorithms that can also be employed in optimizing FDM process parameters. The summary of multi-objective optimization for two conflicting objective functions is shown in Fig. 7. The problem definition begins from considering two conflicting objective functions, Objective 1 and Objective 2. The actual relationship between the objectives is called the Pareto-optimal front, which can be estimated with mathematical functions or an experimental approach by collecting sample data. If an evolutionary algorithm is employed, the optimization process begins by generating a set of feasible initial solutions [5, 6]. Sometimes search algorithms are also used to discover the Pareto-optimal front effectively.

The resulting solutions from multi-objective optimization are often called non-dominated solutions, meaning that there is no existence of a single solution that can, at the same time, optimize two conflicting objectives [5, 6]. As seen from Fig. 7, it can be interpreted as Solution A is not a better solution than Solution B or C. Similarly, Solution B cannot be considered as a better solution than Solution C, and vice versa. The set of non-dominated solutions that lies on the Pareto-optimal front line is also known as Pareto-optimal solutions. Since all the solution sets of Pareto-optimal are deemed equally optimal, an additional decision-making process is often carried out to decide one exact solution to be implemented in practice.

Different optimization techniques had been proposed to maximize or minimize one or more desired outputs. However, most optimization approaches attempted

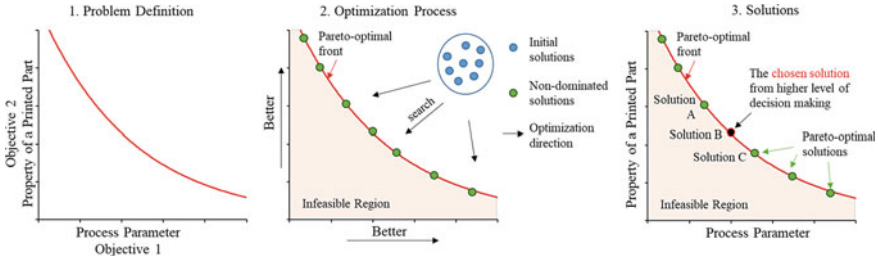


Fig. 7 Multiple-objective optimization overview

only for one single objective. Although if there is more than one objective function considered, these objective functions are optimized one at a time but not simultaneously [22]. Obtaining solutions for a multiple-objective optimization problem is inherently more complicated than a single-objective optimization problem. This section will introduce some evolutionary algorithms, heuristic search algorithms, and hybrid methods that had been employed to optimize multiple FDM process parameters.

4.1 Evolutionary Algorithms

Various evolutionary algorithms had been approached to optimize multiple FDM process parameters or multiple-objective optimization problems in general. The evolutionary algorithm is associated with a population-based metaheuristic optimization algorithm. Initially, a population is generated and goes through multiple genetic operators (crossover, mutation, or reproduction) to find the fittest individual based on a predetermined fitness function. The optimality (or quality) of the solution is evaluated through the fitness function. One or more than one individual in the population is the potential solution to the multiple-objective optimization problem. There are many forms of evolutionary algorithms. Some of the popular ones are summarized as follows.

Genetic Algorithm (GA). GA is one of the most popular evolutionary algorithms to this date. The basic flowchart of GA is portrayed in Fig. 8. GA approaches the optimization and search problem with biologically inspired operators. Mutation and crossover are the two most well-known operators, which are often known as GA operators. The five most common steps considered in GA are the initial population, fitness function, selection, crossover, and mutation. In the initial population generation, an individual in GA is presented as a set of parameters (or variables) known as a gene. Typically, the gene takes a binary value of 0 and 1. Genes are joined together into an exact number of strings called chromosomes (individual, solution). Depending on the application, the software employed, or how the problem is being set up, the flowchart of GA varies from case to case.

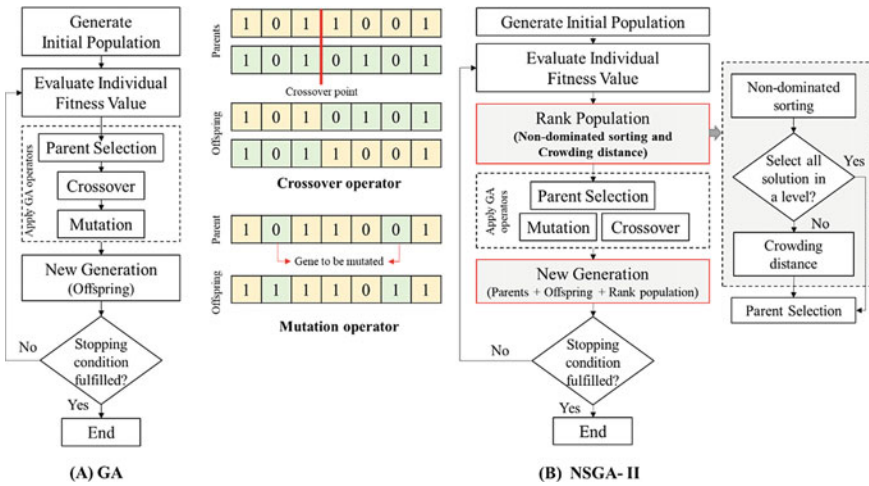


Fig. 8 Flowchart of GA and NSGA-II

GA has been applied to optimize multiple process parameters in the FDM applications for one or more than one printed part properties. Peng et al. [33] studied four controllable parameters (line width, extrusion velocity, filling velocity, and layer thickness) on three output responses (dimensional accuracy, warp deformation, and build time). They optimized the four controllable parameters to minimize the second-order response surface method. Their results showed that with the optimized process parameter, the dimensional error decreased by almost 20%, warp deformation decreased by around 3%, however the build time increases by 5%. It is showed that there is a trade-off between dimensional accuracy and warp deformation with the build time. This work was employed as a comparison by Rao and Rai [34]. Nguyen et al. [35] used GA in single and multiple-objective optimization. They chose to analyze the influence of layer height, infill percentage, print temperature, and print speed on the final product weight, total printing time, and tensile strength. Instead of one best combination, their solutions resulted in 17 Pareto solutions of process parameters combinations within a certain predefined range.

Non-Dominated Sorting Genetic Algorithm (NSGA-II). NSGA-II is currently one of the most favorable algorithms for the multi-objective optimization problem. It leverages GA capability to search for optimal solutions. Similar to GA, NSGA-II also begins by generating a set of the initial solution. The difference between NSGA-II and GA is selecting the parents, as highlighted in Fig. 8B. NSGA-II employed non-dominated sorting and crowding distance to choose the parent population [6].

NSGA-II is the most widely used multiple-objective optimization in FDM applications. Asadollahi-Yazdi et al. [1] employed NSGA-II to study layer thickness and part orientation with the relations to production time and material mass

used in the FDM process. In their problem formulation, they used surface roughness and tensile strength as a constraint for ensuring product quality. Their solution sets contain 18 Pareto-optimal combinations among the two controllable parameters. By utilizing NSGA-II, Gurralla, and Regalla [36] optimized infill density and print directions in both horizontal and vertical directions to achieve higher tensile strength and minimize volumetric shrinkage. Their optimization results obtained 100 combinations of non-dominated solutions. To ensure the Pareto-optimal solutions are valid, a validation experiment was carried out for three combinations and concluded that the results obtained from NSGA-II are accurate.

Surface roughness and build time are the two most conflicting part properties. The study of the FDM process parameters that affect surface roughness and build time had been carried out by Pandey et al. [37] by optimizing the CAD model axis and angle of rotations. They presented 40 sets of Pareto-optimal solutions for this problem formulations. Padhye and Deb [38] attempt similar research with different process parameters to optimize build orientation in *x*-direction and *y*-direction. Nguyen et al. [35] also employed NSGA-II in their study of optimizing four controllable parameters, as shown in Table 2.

Table 2 FDM process parameters optimization on multiple printed part properties case studies with evolutionary algorithms

References	Optimization Method	FDM Process Parameters	Printed Part Properties
Asadollahi-Yazdi et al. [1]	NSGA-II	Layer thickness Part orientation (in <i>x</i> , <i>y</i> , and <i>z</i> directions)	Production time Material mass
Rayegani and Onwubolu [2]	DE	Part orientation Raster angle Raster width Air gap	Tensile strength
Peng et al. [33] Rao and Rai [34]	GA	Line width compensation Extrusion velocity Filling velocity Layer thickness	Dimensional error Wrap deformation Build time
Nguyen et al. [35]	GA	Layer height Infill percentage Printing temperature Printing speed	Weight Printing time Tensile strength
Gurralla and Regalla [36]	NSGA-II	Model interior (infill density) Horizontal Direction Vertical Direction	Tensile strength Volumetric shrinkage
Pandey et al. [37]	NSGA-II	CAD model axis Angle of rotation	Surface roughness Build time

(continued)

Table 2 (continued)

References	Optimization Method	FDM Process Parameters	Printed Part Properties
Padhye and Deb [38]	NSGA-II	Build orientation (in x and y direction)	Surface roughness Build time
Panda et al. [39]	DE GP	Layer thickness Raster angle Raster width Air gap	Tensile strength
Vijayaraghavan et al. [40]	Multi-gene genetic programming (Im-MGGP)	Layer thickness Build orientation Raster angle Raster width Air gap	Wear strength

Note This table is not exhaustive

Genetic Programming (GP). GP is similar to GA. It applies the same evolutionary approach from the initial population generation, evaluating fitness function, genetic operations (crossover and mutation) until the stopping conditions are met. The main difference between the two is in the representation of the solution. GA represents a solution in a fixed string of numbers. The output of the GP is another set of computer functions. GP is represented by a tree-like structure with a mathematical function in every tree node and operand (or input parameters) in the terminal nodes. The functions can be any of the arithmetic functions (+, −, ×, ÷), non-linear functions (for example, the trigonometric functions of sine, cosine, and tangent), or Boolean operators (and, or, not) [39]. The simple representation of GP and the GP with mutation and crossover operators are shown in Fig. 9.

Panda et al. [39] employed GP to maximize tensile strength by optimizing four controllable parameters: layer thickness, raster angle and width, and air gap. As a continuous effort of this work, the multi-gene genetic programming (Im-MGGP) was used to study wear strength by optimizing the previous four controllable parameters with the addition of build orientation as the fifth parameter [40]. The proposed Im-MGGP approach is a GP-variant where, during the evolutionary phase, the model is combined with other sets of threes. From these two examples, the GP had been only applied for one objective function. There is room for future research direction to apply GP to maximize or minimize two or more part properties in the FDM process.

Differential Evolution (DE). DE is another evolutionary algorithm that presents variables with real numbers. The main idea behind DE is that the difference between two vectors yields a difference factor used as a scaling factor to transverse the search space. DE begins with generating a population of initial solution as vectors. Further, the initial solutions are improved by applying genetic operators such as crossover, mutation, and reproduction of a new generation [39]. This process is repeated continuously until the stopping criteria are fulfilled.

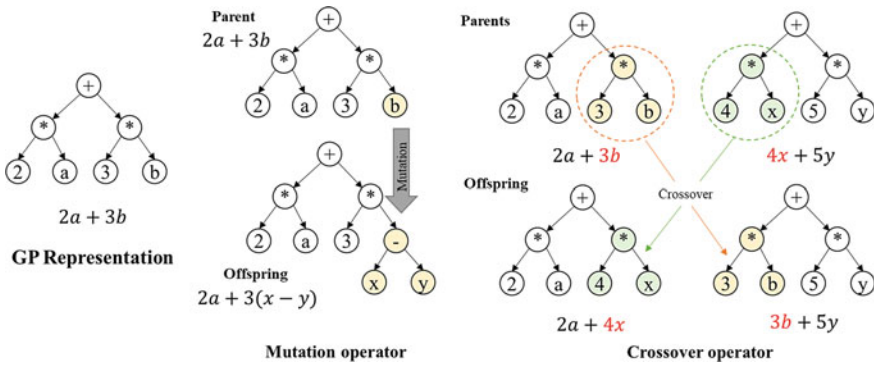


Fig. 9 General Representation of GP with mutation and crossover operators

Similar to GP, DE is only observed to be applied to one part properties. Rayegani and Onwubolu [2] used DE to maximize tensile strength by optimizing part orientation, raster angle, and air gap. Panda et al. [39] employed GP for similar purposes but with one different process parameter. Instead of part orientation, they were considering layer thickness in their study. In the future, DE can also be employed to study two or more part properties with multiple controllable process parameters.

In addition to GA, NSGA-II, GP, and DE, there are other evolutionary algorithms, such as evolutionary strategy and evolutionary programming. Depending on the size of the problem or on how the algorithms and the multiple-objective functions are being set up, some algorithms may work better than the others in some cases. Each of the evolutionary algorithms has its advantages. Similarly, when employing an evolutionary algorithm to investigate the effect or relationship of multiple process parameter combinations in the FDM process, no one algorithm is more superior to the other in all cases. However, NSGA-II seems to be more a more popular algorithm employed in this field. Table 2 lists some publications that employed an evolutionary algorithm to optimize multiple FDM process parameters and printed part properties.

4.2 Biologically-Inspired Optimization

Although there is no evolution involved, biologically-inspired algorithms are also related to the evolutionary algorithm to a certain extent because they are also inspired by natural phenomena. Some examples of biologically-inspired (or bio-inspired) optimization are ant colony optimization, particle swarm optimization, bee algorithm, cuckoo search, and many other algorithms. The two most common optimization algorithms employed in optimizing FDM process parameters that had been published are the particle swarm optimization and bacterial foraging optimization.

Particle Swarm Optimization (PSO). PSO belongs to the metaheuristic algorithm group. PSO solves a problem with the initial population solution represent as particles. These particles change position in a large search space corresponding to simple rules. The state of each particle is its velocity and position, and the movement is regulated by the particle's own best-known position and the best-known position of the entire swarm. PSO is an iterative method where each particle is expected to swarm to the best solutions. PSO is an excellent candidate to be employed in multiple objective-optimization problems, where the initial population of potential solutions should find the Pareto-optimal front. One of the drawbacks of PSO is that global convergence or the optimal solution cannot always be guaranteed [23].

Given multiple sets of process parameters, PSO had been utilized to optimize for single or multiple part properties. For single part property optimization, Panda et al. [39] employed PSO to maximize tensile strength by optimizing four FDM parameters (layer thickness, raster angle, raster width, and air gap). Saad et al. [41] studied the impact of four process parameters and their influence on surface roughness with PSO.

In the study of multiple-part properties, the authors had previously employed PSO to evaluate two conflicting part properties (compressive strength and build time) by optimizing four process parameters (layer thickness, build orientation, infill density, and extrusion temperature) [4]. Padhye and Deb [38] employed PSO for a bi-objective minimization problem to minimize surface roughness and build time by optimizing the build orientation in x - and y -direction only. Raju et al. [42] applied PSO in their multi-objective optimization study on the effect of four FDM parameters (layer thickness, support material, part orientation, and infill density) on four printed part characteristics (surface roughness, flexural modulus, hardness, and tensile strength). Li et al. [43] also employed PSO to optimize the build orientation in XY -plane and z -direction and studied the influence of build orientations on the support area and surface roughness of the printed parts, as well as, build time of the process.

There are also some variants of PSO that had been proposed, such as quantum-behaved particle swarm optimization (QPSO), that had been proposed to overcome the optimality issue. Sood et al. [23] proposed QPSO to maximize compressive strength by optimizing five process parameters (layer thickness, build orientation, air gap, raster angle, and raster width). The difference between the PSO and QPSO is the state of the particles is presented by wave function in QPSO instead of velocity and position in PSO [23].

Bacterial Foraging Optimization (BFO). BFO also belongs to swarm algorithms similar to PSO. It is motivated by the actions found in the *E. coli* bacteria that always strive to look for high levels of nutrients. The swarm of bacteria seeks to maximize its energy based on the foraging process and avoiding noxious substance [44]. The BFO algorithm begins with randomly distributed bacteria in a nutrient search space. Bacteria that contact a noxious substance or located in the low-nutrient area will eventually disperse. On the other hand, bacteria found in the high-nutrient area can attract other bacteria by generating chemical substances [44]. This is also how the bacteria move to the higher-nutrient location in the search space.

Raju et al. [42] applied BFO, in addition to PSO discussed previously, to analyze the effect of four FDM parameters (layer thickness, support material, part orientation, and infill density) on four printed part characteristics (surface roughness, flexural modulus, hardness, and tensile strength). Panda et al. [44] also employed BFO to optimize three responses in terms of the mechanical properties (tensile, flexural, and impact strength) of the printed parts by optimizing five FDM parameters (layer thickness, build orientation, raster angle, raster width, and air gap). Their results mentioned that the air gap is not applicable for impact strength.

Table 3 lists some publications that employed either PSO or BFO and their variants to optimize multiple FDM process parameters and printed part properties. PSO and BFO seem to be the two most popular algorithms in the FDM application. Thus, only these two algorithms are detailed in this book chapter. This does not mean that other algorithms cannot be applied to optimize FDM process parameters. One potential future research is to access the feasibility of other biologically-inspired algorithms to be employed in the FDM application.

Table 3 FDM process parameters optimization on multiple printed part properties case studies with search and hybrid algorithms

References	Optimization Method	FDM Process Parameters	Printed Part Properties
Dey et al. [4]	PSO	Layer thickness Build orientation Infill density Extrusion temperature	Compressive strength Build time
Sood et al. [23]	QPSO	Layer thickness Build orientation Raster angle Raster width Air gap	Compressive strength
Panda et al. [39]	PSO	Layer thickness Raster angle Raster width Air gap	Tensile strength
Padhye and Deb [38]	PSO	Build orientation (in x and y direction)	Surface roughness Build time
Saad et al. [41]	PSO	Layer height Print speed Print temperature Outer shell speed	Surface roughness
Raju et al. [42]	PSO, BFO, Hybrid PSO-BFO	Layer thickness Support material Build orientation Infill Pattern/Density	Surface roughness Flexural modulus Hardness Tensile strength
Li et al. [43]	PSO	Build orientation (in XY -plane and z -direction)	Support area Build time Surface roughness

(continued)

Table 3 (continued)

References	Optimization Method	FDM Process Parameters	Printed Part Properties
Panda et al. [44]	BFO	Layer thickness Build orientation Raster angle Raster width Air gap	Tensile strength Flexural strength Impact strength
Deswal et a. [45]	Hybrid-GA	Layer thickness Build orientation Infill density Number of contours	Dimensional accuracy (% variation in length, width, and thickness)

Note This table is not exhaustive

4.3 Hybrid Algorithms

Hybrid algorithms are developed by combining specific characteristics or desired features from two or more stand-alone algorithms to obtain better results than any of the stand-alone algorithms. Evolutionary algorithms or biologically-inspired optimization algorithms can also be fused with other algorithms. Hybrid algorithms, such as the hybrid between PSO and FBO (PSO-FBO) proposed by Raju et al. [42], can also be employed to find an optimal combination of FDM process parameters. Their results showed that the hybrid PSO-BFO algorithm achieved the highest overall responses improvement of more than 7%. In contrast, the stand-alone algorithm of PSO and BFO achieve lower overall responses improvement of around 4 and 2% only. Deswal, Narang, and Chhabra employed hybrid statistical tools based on GA for enhancing dimensional accuracy in the FDM 3D printing process. Their proposed approach is based on a hybrid between response surface methodology and GA and a hybrid between an artificial neural network and GA [45].

There are still many combinations between multiple part parameters and properties that have not been explored. Apart from the three types of algorithms discussed in this section (evolutionary algorithms, biologically-inspired optimization, and hybrid algorithms), advanced statistical methods and machine learning approaches can be employed to optimize conflicting FDM process parameters.

5 Potential Future Research Direction and Conclusions

As concluding remarks for this book chapter, this section will highlight a general potential future research direction for additive manufacturing and more focused research directions for continuously improving the FDM process parameter or FDM process in general.

5.1 *Potential Future Research Directions*

This book chapter only addressed a small portion of the potential improvement in the FDM process in terms of optimizing the controllable FDM processes parameters to ensure the desired part properties are achieved. In addition to optimizing FDM process parameters, there are many other potential future research directions to mature the additive manufacturing technology. Below are the three research areas that the authors are most interested in contributing to.

Design for Additive Manufacturing (DfAM). The scope of DfAM is related to the design for manufacturability exclusively for additive manufacturing processes. The goal of DfAM is minimizing time and cost while maximizing quality and profitability under the constraints of other design and manufacturing requirements [46]. Unlike the optimization of the process parameter, as discussed in this chapter, the optimization scope in DfAM is broader and involves commercializing additive manufacturing processes. In the macroscale, DfAM includes macro scale topology optimization, multi-color/multi-material design and assembly processes, mass production cost optimization, and custom-fit for customized mass products [46, 47]. In the microscale, DfAM includes lattice structure, metallurgy/material composition, or textures and properties on material-level (i.e., thermal, biodegradability, porosity, conductivity, etc.) [46, 48]. In addition to the macroscale and microscale subject area, the future research direction in DfAM is extensive. References [3, 49, 50] highlight some of the challenges and potential research directions.

Machine learning and deep learning. Machine learning and deep learning falls under the umbrella of artificial intelligence. Currently, machine learning has been implemented towards the near real-time condition monitoring or fault diagnostic [51] and prediction of the printed part properties such as mechanical properties [52], geometric accuracy [53], or surface roughness [54]. The opportunity of data analytics advances in machine learning, and deep learning is endless in the additive manufacturing application. It can be leveraged to material data harvesting to find new filament material properties. With the image processing capability, machine learning can be utilized to determine an optimal freeform and complicated geometry optimization, as well as ensuring manufacturability.

Uncertainty quantification. Although controllable FDM process parameters can be optimized, uncontrollable process parameters also impact the properties of the FDM build parts. Uncontrollable process parameters are associated with uncertainties. There are many uncertainties involves in each step of additive manufacturing processes. Moreover, the uncertainties aggregate at each processing stage from the generation of CAD and STL files up to the final printed parts. Before the uncertainties in the FDM process can be minimized, one has to be able to quantify how much uncertainties there are in the process [55]. This research direction is the personal interest of the authors in the near future to develop a framework for quantifying uncertainty in the FDM process.

5.2 Conclusions

The FDM process still has many rooms for technology improvements to be able to compete with conventional manufacturing processes in terms of cost and fabrication time. To improved the desired printed part quality, the FDM process parameters can be optimized. This chapter introduces multi-objective optimization disciplines that can be applied to optimize multiple FDM process parameters simultaneously. Any of evolutionary algorithms, biologically-inspired optimization algorithms, and hybrid algorithms can be employed. Each algorithm has its advantages. The algorithm's superiority can be influenced by aspects such as the application, the scope, the problem formulation, how the algorithm is being set up, or the simulation environment. Experimental verification can be conducted to verify the optimization results. Based on the published literature presented, NSGA-II and PSO are two of the most popular algorithms employed to this date. There are still many combinations of the FDM process parameter and printed part qualities that need to be analyzed further. Similarly, many other multi-objective optimization approaches have not been explored in optimizing FDM process parameters. Although this book chapter focuses on multiple-objective optimization, other approaches such as the advances in DfAM and machine learning can also be leveraged to improve the FDM process for it to be fully industrialized.

References

1. Asadollahi-Yazdi E, Gardan J, Lafon P (2018) Toward integrated design of additive manufacturing through a process development model and multi-objective optimization. *Int J Adv Manuf Technol* 96(9–12):4145–4164
2. Rayegani F, Onwubolu GC (2014) Fused deposition modelling (FDM) process parameter prediction and optimization using group method for data handling (GMDH) and differential evolution (DE). *Int J Adv Manuf Technol* 73(1–4):509–519
3. Stansbury JW, Idacavage MJ (2016) 3D printing with polymers: challenges among expanding options and opportunities. *Dent Mater* 32(1):54–64
4. Dey A, Hoffman D, Yodo N (2019) Optimizing multiple process parameters in fused deposition modeling with particle swarm optimization. *Int J Interact Des Manuf (IJIDeM)*, 1–13
5. Mao-Guo G, Li-Cheng J, Dong-Dong Y, Wen-Ping M (2009) Evolutionary multi-objective optimization algorithms
6. Deb K (2001) *Multi-objective optimization using evolutionary algorithms*, vol 16. Wiley, New Jersey
7. Dey A, Yodo N (2019) A systematic survey of FDM process parameter optimization and their influence on part characteristics. *J Manuf Mater Process* 3(3):64
8. Mohamed OA, Masood SH, Bhowmik JL (2015) Optimization of fused deposition modeling process parameters: a review of current research and future prospects. *Adv Manuf* 3(1):42–53
9. Popescu D, Zapciu A, Amza C, Baci F, Marinescu R (2018) FDM process parameters influence over the mechanical properties of polymer specimens: a review. *Polym Testing* 69:157–166

10. Chai X, Chai H, Wang X, Yang J, Li J, Zhao Y, Cai W, Tao T, Xiang X (2017) Fused deposition modeling (FDM) 3D printed tablets for intragastric floating delivery of domperidone. *Sci Rep* 7(1):1–9
11. Sargent JF, Schwartz RX (2019) 3D Printing: overview, impacts, and the federal role. Congressional Research Service. <https://fas.org/sgp/crs/misc/R45852.pdf>
12. Chacón J, Caminero M, García-Plaza E, Núñez P (2017) Additive manufacturing of PLA structures using fused deposition modelling: effect of process parameters on mechanical properties and their optimal selection. *Mater Des* 124:143–157
13. Vosynek P, Navrat T, Krejbychova A, Palousek D (2018) Influence of process parameters of printing on mechanical properties of plastic parts produced by FDM 3D printing technology. In: MATEC web of conferences. EDP Sciences, p 02014
14. Mazzanti V, Malagutti L, Mollica F (2019) FDM 3D printing of polymers containing natural fillers: a review of their mechanical properties. *Polymers* 11(7):1094
15. Mohamed OA, Masood SH, Bhowmik JL (2016) Optimization of fused deposition modeling process parameters for dimensional accuracy using I-optimality criterion. *Measurement* 81:174–196
16. Qattawi A, Alrawi B, Guzman A (2017) Experimental optimization of fused deposition modelling processing parameters: a design-for-manufacturing approach. *Procedia Manuf* 10:791–803
17. Beniak J, Krizan P, Šooš L, Matuš M (2019) Research on shape and dimensional accuracy of FDM produced parts. In: IOP conference series: materials science and engineering, vol 1. IOP Publishing, p 012030
18. Garg A, Bhattacharya A, Batish A (2016) On surface finish and dimensional accuracy of FDM parts after cold vapor treatment. *Mater Manuf Processes* 31(4):522–529
19. Li Y, Linke BS, Voet H, Falk B, Schmitt R, Lam M (2017) Cost, sustainability and surface roughness quality—a comprehensive analysis of products made with personal 3D printers. *CIRP J Manuf Sci Technol* 16:1–11
20. Pérez M, Medina-Sánchez G, García-Collado A, Gupta M, Carou D (2018) Surface quality enhancement of fused deposition modeling (FDM) printed samples based on the selection of critical printing parameters. *Materials* 11(8):1382
21. Valerga A, Batista M, Salguero J, Girof F (2018) Influence of PLA filament conditions on characteristics of FDM parts. *Materials* 11(8):1322
22. Sheoran AJ, Kumar H (2020) Fused deposition modeling process parameters optimization and effect on mechanical properties and part quality: review and reflection on present research. *Mater Today Proc* 21:1659–1672
23. Sood AK, Ohdar RK, Mahapatra SS (2012) Experimental investigation and empirical modelling of FDM process for compressive strength improvement. *J Adv Res* 3(1):81–90
24. Deng X, Zeng Z, Peng B, Yan S, Ke W (2018) Mechanical properties optimization of poly-ether-ether-ketone via fused deposition modeling. *Materials* 11(2):216
25. Rinanto A, Nugroho A, Prasetyo H, Pujiyanto E (2018) Simultaneous optimization of tensile strength, energy consumption and processing time on FDM process using Taguchi and PCR-TOPSIS. In: 2018 4th international conference on science and technology (ICST). IEEE, pp 1–5
26. Aw Y, Yeoh C, Idris M, Teh P, Hamzah K, Sazali S (2018) Effect of printing parameters on tensile, dynamic mechanical, and thermoelectric properties of FDM 3D printed CABS/ZnO composites. *Materials* 11(4):466
27. Crococo D, De Agostinis M, Olmi G (2013) Experimental characterization and analytical modelling of the mechanical behaviour of fused deposition processed parts made of ABS-M30. *Comput Mater Sci* 79:506–518
28. Fatimatuzahraa A, Farahaina B, Yusoff W (2011) The effect of employing different raster orientations on the mechanical properties and microstructure of fused deposition modeling parts. In: 2011 IEEE symposium on business, engineering and industrial applications (ISBEIA). IEEE, pp 22–27

29. Letcher T, Rankouhi B, Javadpour S (2015) Experimental study of mechanical properties of additively manufactured ABS plastic as a function of layer parameters. In: Proceedings of the ASME 2015 international mechanical engineering congress and exposition IMECE
30. Dong G, Wijaya G, Tang Y, Zhao YF (2018) Optimizing process parameters of fused deposition modeling by Taguchi method for the fabrication of lattice structures. *Addit Manuf* 19:62–72
31. Nancharaiha T (2011) Optimization of process parameters in FDM process using design of experiments. *Int J Emerg Technol* 2(1):100–102
32. Nidagundi VB, Keshavamurthy R, Prakash C (2015) Studies on parametric optimization for fused deposition modelling process. *Mater Today Proc* 2(4–5):1691–1699
33. Peng A, Xiao X, Yue R (2014) Process parameter optimization for fused deposition modeling using response surface methodology combined with fuzzy inference system. *Int J Adv Manuf Technol* 73(1–4):87–100
34. Rao RV, Rai DP (2016) Optimization of fused deposition modeling process using teaching-learning-based optimization algorithm. *Int J Eng Sci Technol* 19(1):587–603
35. Nguyen V, Huynh T, Nguyen T, Tran T (2020) Single and multi-objective optimization of processing parameters for fused deposition modeling in 3D printing technology. *Int J Automot Mech Eng* 17(1):7542–7551
36. Gurralla PK, Regalla SP (2014) Multi-objective optimisation of strength and volumetric shrinkage of FDM parts: a multi-objective optimization scheme is used to optimize the strength and volumetric shrinkage of FDM parts considering different process parameters. *Virtual Phys Prototyp* 9(2):127–138
37. Pandey PM, Thirumurthulu K, Reddy NV (2004) Optimal part deposition orientation in FDM by using a multicriteria genetic algorithm. *Int J Prod Res* 42(19):4069–4089
38. Padhye N, Deb K (2009) Multi-objective optimisation and multi-criteria decision making for FDM using evolutionary approaches. In: Multi-objective evolutionary optimisation for product design and manufacturing
39. Panda BN, Bahubalendruni MR, Biswal BB (2014) Comparative evaluation of optimization algorithms at training of genetic programming for tensile strength prediction of FDM processed part. *Procedia Mater Sci* 5:2250–2257
40. Vijayaraghavan V, Garg A, Lam JSL, Panda B, Mahapatra SS (2015) Process characterisation of 3D-printed FDM components using improved evolutionary computational approach. *Int J Adv Manuf Technol* 78(5–8):781–793
41. Saad MS, Nor AM, Baharudin ME, Zakaria MZ, Aiman A (2019) Optimization of surface roughness in FDM 3D printer using response surface methodology, particle swarm optimization, and symbiotic organism search algorithms. *Int J Adv Manuf Technol* 105(12):5121–5137
42. Raju M, Gupta MK, Bhanot N, Sharma VS (2019) A hybrid PSO–BFO evolutionary algorithm for optimization of fused deposition modelling process parameters. *J Intell Manuf* 30(7):2743–2758
43. Li A, Zhang Z, Wang D, Yang J (2010) Optimization method to fabrication orientation of parts in fused deposition modeling rapid prototyping. In: 2010 international conference on mechanic automation and control engineering. IEEE, pp 416–419
44. Panda SK, Padhee S, Anoop Kumar S, Mahapatra SS (2009) Optimization of fused deposition modelling (FDM) process parameters using bacterial foraging technique. *Intell Inf Manage* 1(02):89
45. Deswal S, Narang R, Chhabra D (2019) Modeling and parametric optimization of FDM 3D printing process using hybrid techniques for enhancing dimensional preciseness. *Int J Interact Des Manuf (IJIDeM)* 13(3):1197–1214
46. Thompson MK, Moroni G, Vaneker T, Fadel G, Campbell RI, Gibson I, Bernard A, Schulz J, Graf P, Ahuja B (2016) Design for additive manufacturing: trends, opportunities, considerations, and constraints. *CIRP Ann* 65(2):737–760
47. Plocher J, Panesar A (2019) Review on design and structural optimisation in additive manufacturing: towards next-generation lightweight structures. *Mater Des* 183:108164

48. Chu C, Graf G, Rosen DW (2008) Design for additive manufacturing of cellular structures. *Comput Aided Des Appl* 5(5):686–696
49. Doubrovski Z, Verlinden JC, Geraedts JM (2011) Optimal design for additive manufacturing: opportunities and challenges. In: *International design engineering technical conferences and computers and information in engineering conference*, pp 635–646
50. Salem H, Abouchadi H, El Bikri K (2020) Design for additive manufacturing. *J Theor Appl Inf Technol* 98(19)
51. Wu H, Yu Z, Wang Y (2017) Real-time FDM machine condition monitoring and diagnosis based on acoustic emission and hidden semi-Markov model. *Int J Adv Manuf Technol* 90(5–8):2027–2036
52. Panda BN, Bahubalendruni MR, Biswal BB (2015) A general regression neural network approach for the evaluation of compressive strength of FDM prototypes. *Neural Comput Appl* 26(5):1129–1136
53. Khanzadeh M, Rao P, Jafari-Marandi R, Smith BK, Tschopp MA, Bian L (2018) Quantifying geometric accuracy with unsupervised machine learning: using self-organizing map on fused filament fabrication additive manufacturing parts. *J Manuf Sci Eng* 140(3)
54. Vahabli E, Rahmati S (2016) Application of an RBF neural network for FDM parts' surface roughness prediction for enhancing surface quality. *Int J Precis Eng Manuf* 17(12):1589–1603
55. Nath P, Hu Z, Mahadevan S (2018) Modeling and uncertainty quantification of material properties in additive manufacturing. In: *2018 AIAA non-deterministic approaches conference*, p 0923

Application of Machine Learning in Fused Deposition Modeling: A Review



A. Eqbal, S. Akhter, Md. A. Eqbal, and A. K. Sood

Abstract Fused deposition modeling (FDM) is a paradigm of additive manufacturing (AM) which uses joining of materials in a layer by layer based methodology to fabricate a component. FDM can build complicated part geometries and intricacies in least time when compared to traditional manufacturing methods. It doesn't require any fixed process plan, special tooling and involve very little human intervention. FDM parts offer superb heat and chemical resisting behavior and shows excellent strength-to-weight ratios. Despite of all these advantages, FDM parts are facing inconsistency in part properties, reliability and accuracy. To meet the consistent quality standard and process reliability real time monitoring of FDM process is requisite. Research trend shows that machine learning (ML) aided models are proficient computational technology which enable AM processes to achieve the high quality standard, product consistency and optimized process response. In this direction, integration of machine learning (ML) and FDM process is relatively less explored. Though the researches are limited in number, a review based study on the application of ML in FDM process is lacking which can help the researchers to decide their areas of research. Authors got motivated to bridge this gap by presenting a state of art showing the applicability of ML methods in FDM process. FDM areas where ML can be applied or least explored are also discussed.

A. Eqbal (✉)

Department of Mechanical Engineering, Jamia Millia Islamia, New Delhi 110025, India

e-mail: azhr_eqbl06@yahoo.co.in

S. Akhter

Centre for Management Studies, Jamia Millia Islamia, New Delhi 110025, India

e-mail: sakhter1@jmi.ac.in

Md. A. Eqbal

Cambridge Institute of Technology, Ranchi 835103, Jharkhand, India

e-mail: eqbal.asif@yahoo.com

A. K. Sood

Department of Manufacturing Engineering, National Institute of Foundry and Forge Technology, Hatia, Ranchi 834003, Jharkhand, India

e-mail: anoopkumarsood@gmail.com

1 Introduction

Fused deposition modeling (FDM) is an additive process which fabricates the part by joining of extruded material from a nozzle in a layer based strategy [1, 2]. FDM process relied on the same building principle which drives all the other AM processes. The process chain in FDM process is depicted in Fig. 1. Here, a computerized model of the required product is first constructed using any of modeling software and then it is transformed to machine acceptable STL (stereolithography) file. The model is then sliced into number of 2-dimensional (2D) cross sections and these 2D data are transmitted to AM machine [3]. Similar to all AM machine, FDM process has its own pre-processing software where the suitable process parameters are defined. Depending on the complexity and sectional thickness of the part, location and volume of support structure is also decided. The part is then fabricated in form of fine layers which are joined subsequently [2]. Sometimes, to support the overhung structures, support structure is deposited in between the layers too. A simplified diagram of the FDM machine is depicted in Fig. 2. Materials are drawn from spool and guided into liquefier where it is heated by surrounding heater coil. Melted materials are then extruded by nozzle and are deposited over the platform by two working rollers: support material and part material depositing roller. For better understanding on FDM process working and build mechanism author's previous work can be referred [2].

Engineering grade plastics like ABS (acrylonitrile butadiene styrene), Polycarbonate (PC), PC-ABS and PC-ISO are widely used for part fabrication. However, with the advancement in technology and progress in material science new materials like metals and ceramic slurry also find their application in FDM but with limitation in size of nozzle diameter [4]. Important areas of application include tooling industries, mold and die sectors, automobiles, implant models in medical and casting industries. However, industrial applications of FDM demand closer dimensional tolerance, smooth surface finish and enough mechanical strength and FDM technologies are unable to meet the consistency in part properties, process

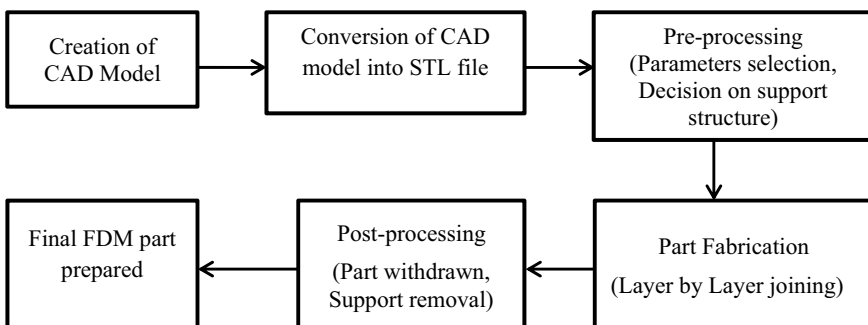


Fig. 1 Process chain for part fabrication in FDM

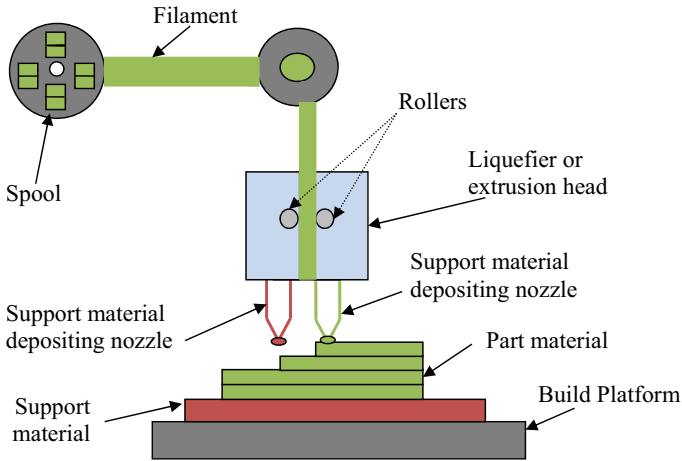


Fig. 2 A Simple diagram of FDM machine

reliability and part accuracy because they primarily dependent on building conditions such as layer thickness, build orientation and printing speed. Proper selection of these parameters with the varying process requirement is a big challenge. To minimize the variation in part quality and process reliability, basic understanding of the FDM process is pre-requisite.

Every step in the process chain of FDM process must be precisely monitored which can be either achieved by 3D simulations of FDM process to meticulously optimize the FDM process or doing number of experimental trials for inspection and monitoring of the process [5]. Doing number of experimental trials is an expensive and time consuming and conducting number of FDM process simulations requires an effective method which uses multiple data like images, signals and thermal histories for analyzing the process. Earlier methods using empirical techniques and analytical tools don't meet the requirements and hence advanced computational techniques are required to perform the precise analysis. Methods based on artificial analysis can meet the requirements. In this direction, research trend shows that machine learning (ML) is very much capable of doing the job. However, research trend also presents that use of ML method in FDM is relatively less explored. A state of art is thus required which can aid the research community to identify the areas in FDM where ML can be applied. Review study will also help in identification of other possible FDM areas where ML can be applied but not investigated by the researchers.

2 Machine Learning and Their Models

Machine learning is a technique of artificial intelligence (AI) where initial training of the machine is done by human and thereafter, machines will automatically learn from their past experience. The human interface is very less which is only used for initially training of machine. Learning of the machine from its past experience provide fast, accurate and an effective ways to study and analyze the data [6]. Machine learning models requires large number of data to train them but the process can be begin with moderate dataset and doesn't have to wait for large dataset. This section of the paper will present in brief the basic of ML and their related models. Figure 3 presents that ML can be categorized into: (1) Supervised learning (2) Unsupervised learning and (3) Reinforcement learning [7]. Though there is one more ML algorithm known as semi-supervised algorithm (combination of supervised and unsupervised algorithm) but that is relatively less used [8]. Further, categorization of supervised and unsupervised learning is shown in Fig. 3. Brief description related to learning algorithms are discussed as under.

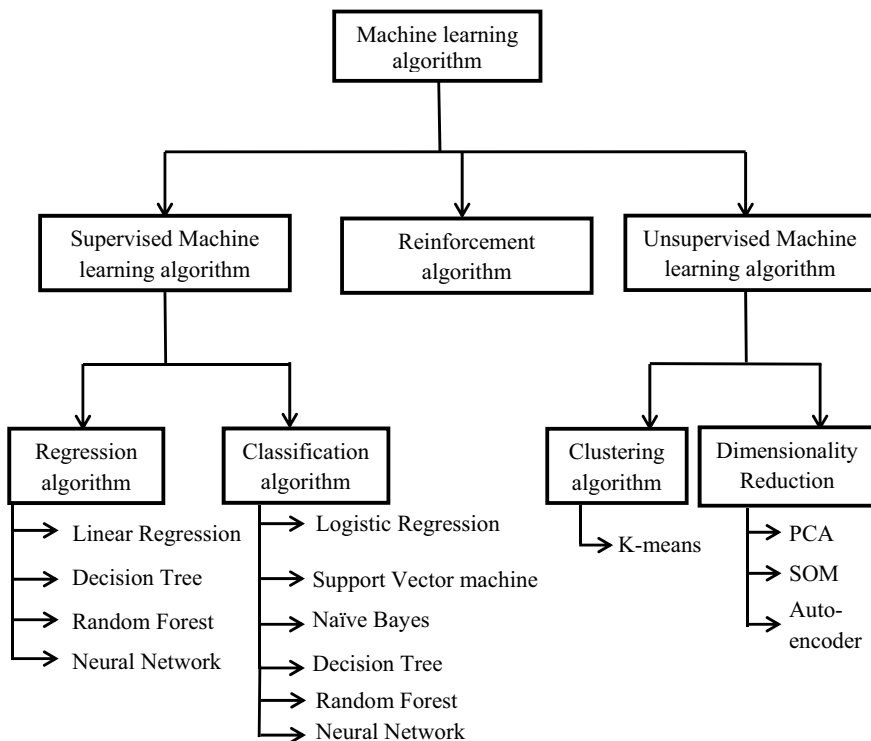


Fig. 3 Machine learning and models

2.1 Supervised Algorithm

In the supervised algorithm, set of classified training data or labeled data (input and output) are available, based on which a model is prepared. New data set are input into the model to predict the response. It can be classified into regression model and classification model [7, 8]. List of ML algorithms [9, 10] that worked on the supervised algorithms are given in Fig. 3. A best example can of supervised learning model is the exit poll used before the final result of any election where feedback from different people are regarded as training dataset and based on which result can be predicted.

2.2 Unsupervised Algorithm

In the unsupervised algorithm, no pre-knowledge is available and unclassified or unlabeled data are used. Based on the physical behaviour of the dataset they are grouped. Initially the output is unknown. This learning algorithm will learn from itself and determines the output. It is not essential that they will predict the right output but dataset or unlabeled data are explored to suggest output [8]. It can be further classified into clustering and dimensionality reduction. Some of the important algorithms categorized under unsupervised learning are logistic learning, support vector machine, k- means clustering, decision tree, random forest model and principal component analysis (PCA) [11, 12]. The details about the various learning algorithms under supervised and unsupervised algorithm are described elsewhere in literature [13, 14]. Most machine falls under unsupervised learning.

2.3 Reinforcement Learning

Reinforcement algorithm is based on reward and penalty. It produces an action by interacting with the environment and discover some reward (+) and penalty (-) with the change in environment. Based on the learning it proposed a policy which is used next time to perform the learning [10]. This learning algorithm is widely used in policy making in sports and gaming.

Literature manifest that these intelligent learning algorithms are very effective in observing and monitoring of FDM process but they find limited application in FDM process. A knowledge based review study is thus proposed which will aware the researchers about the possible application of ML models in FDM process. The study will also present the possible areas in FDM where ML is less explored or have not been investigated but can be suitably applied. Research papers relating the ML in FDM are collected from Scopus, Publons and Google scholar using ML in FDM or fused deposition modeling in machine learning as the search keywords.

The survey showed that ML in FDM process is relatively less explored and thus limited researchers are available showing the application of ML in FDM process.

3 Machine Learning in FDM Process

This study attempted to present an insight on the latest applications of ML in the AM. For better understanding of readers this section shows the applicability of ML in FDM process in categories.

3.1 Surface Roughness Prediction

Surface roughness of the parts fabricated by FDM process was predicted by three different ML models namely J48 (C4.5), random forest, and random tree [15]. Five different process parameters each at three levels are used for fabricating twenty seven FDM models using a fractionated orthogonal design. Average roughnesses of the fabricated parts were measured using profilometer. Measured dataset are divided and used for training and validation of the model and performance of the models were compared. Various performance indicators were used to compare the models and it was experienced that random tree provide the better result. It was experienced that random tree provide highest accuracy and area under ROC (receiver operating characteristic). Moreover it was also witnessed that random tree appears to be the fastest algorithm among the three investigated algorithms. Different ML based predictive models were used by Wu et al. [16] for demonstrating a data fusion method for estimation of surface texture in FDM processes. Real data were generated by multiple sensors (thermocouples, accelerometers and IR non-contact sensors) were used as input to the models. Integration of the data is done by means of a feature-level data fusion method for improvement in the prediction performance. Performance of the predictive model was evaluated. It was experienced using experimental result that different models trained using ML algorithms can accurately envisage the roughness of FDM parts. ML models provide comparable performance in terms of error %. It was suggested that increase in training data will improve the accuracy of the predictive models. They recommended that the same approach can be used by other AM process like powder bed fusion and direct energy deposition for prediction of surface roughness. Considering the surface integrity as one of the vital requirement in FDM parts, data-driven roughness prediction model was proposed in extrusion-based AM by Li et al. [17]. PLA (Poly lactic acid) samples were fabricated using commercial FDM machine. Temperature and vibration data were collected using multiple sensors. Average surface roughnesses of the samples were taken using a profilometer. To validation the predictive model eighty one experiments were conducted varying three factors at three levels. Monitoring data (104 features) were extracted and collected during each test. For

improving the computational efficacy and to avoid the overfitting, features based on their importance were selected using RF algorithm. Based on redundancy 40 out of 104 features were chosen for model training. Root mean-square-error (RMSE) and relative error (RE) were used as criterion to measure the performance of the predictive models. Criterion based ranking of the model were done as: ridge regression (RR), support vector regression (SVR), Classification and regression trees (CART), random forest (RF), Random vector functional link (RVFL) and AdaBoost. It was observed that ensemble learning algorithm i.e. RF and Adaboost outperforms the individual algorithm.

Surface roughness prediction of FDM parts was done by Molero et al. [18] employed 10 data mining algorithms. Experimental data were generated using 27 horizontally and 27 vertically fabricated specimens at various parameters and they were used for the training of the model. Among all, best cross-validation results were presented by models based on multilayer perceptron and logistic trees model. J48 algorithm (as decision trees) does not illustrate optimal results but determines the parameters influencing on the surface roughness. It was experienced that for XY specimens, roughness taken perpendicular to the extruded path depends only on the flow whereas in parallel to the extruded track it is affected by flow and some other parameters. For XZ specimen, roughness parallel to the extruded path depends only on the print speed and roughness measured perpendicular to the extrusion depends on the layer height and the extrusion temperature. Most reliable set up showed roughness of 0.46, 1.18, 0.45 and 11.54 μm in parallel to XY, perpendicular to XY, parallel to XZ and perpendicular to XZ. Prediction of printed qualities of FDM parts was done using data mining (DM) techniques via the machine vision method [19] employed. ANN was used to determine [20] the connection between five FDM parameters with surface roughness of the ABS part. Vahabli and Rahmati [21] showed an ANN model based to estimate the roughness in FDM parts with four medical case studies. Table 1 presents some important studies relating ML and surface roughness prediction in FDM parts.

Table 1 Some prominent studies relating ML and surface roughness prediction in FDM

Investigation with reference no.	ML Tools used	Conclusion
Prediction of surface roughness of the FDM printed parts [15]	J48 (C4.5), random forest and random tree	Random tree provides the highest accuracy and appears to be the fastest algorithm
Data-driven roughness prediction model was proposed in extrusion-based AM [17]	Ridge regression (RR), support vector regression (SVR), Classification and regression trees (CART), random forest (RF), Random vector functional link (RVFL) and AdaBoost	It was observed RF and Adaboost outperform the other algorithms
Data mining methods were used for roughness prediction of FDM parts [18]	J48 algorithm, multilayer perceptron and logistic trees	Best results were presented by models based on multilayer perceptron and logistic trees

3.2 *Quality Monitoring System*

Deep convolutional neural networks (DCNN) was used by Banadaki et al. [22] to propose an automated quality monitoring system for FDM process, sterelithography and selective laser sintering processes. Defects related images (surface, internal and arising due to layer wise deposition) are used for training of the CNN model. Performance of detection and classification of failure in AM process at different extrusion speeds and temperatures was studied using online testing of the model. Real time analysis of CNN model showed an accuracy of 94% and specificity of 96%. *F*-score, sensitivity and precision measures were above 75% for classifying the quality of the printing process. They recommended that predictive quality monitoring model will help as a basis for other AM machines. They also suggested that automated inspection of AM quality can improve the speed, material waste, reliability and productivity. System monitored by sensors was also developed by Rao et al. [23] demonstrated that Bayesian Dirichlet mixture model and evidence theory can detect the failure in FDM process with an accuracy of 85%.

An online monitoring and diagnostic system for FDM was proposed by Nam et al. [24]. PLA filament was used as the working material for part fabrication and data collection was done using sensors. Accelerometers, AE sensor connected to pre-amplifier and K-type thermocouples were used. An IR camera was also used in anterior of the FDM to regulate heating of the nozzle head and the printed layers. Experiments were performed under even levelling (better dimensional accuracy) and uneven levelling (deviation, warpage and bad adhesion) of bed and data collections from sensors are categorized in terms healthy and faulty states. Data were used to obtain the RMS values which are used to construct two models using SVM algorithm. 60 RMS values were used for building model to detect uneven levelling of FDM bed and 60 RMS values for showing the second levelled model and the diagnosis accuracies were compared. Training, Testing and validation of support vector model was done and comparison of result showed that non-linear SVM-based model using acceleration signals was more accurate in diagnosing the FDM process. Yoon et al. [25] used AE signals and piezoelectric strain sensors for fault detection and quality control of the FDM. Collected signals were processed to determine the running state of the belt. Rao et al. [26] also collected signals from online sensors for detecting the FDM process drifts.

Zhang [27] proposed a FDM printer optimization based on vibration test. They build the FDM based vibration test system. Application theory and experiments were combined for studying the vibration features of FDM printer jet. A fault diagnosis of FDM process based on semi-Markov model and ensemble empirical mode decomposition was also proposed by Zhang [28]. Bonding mechanism of printed fused filament was combined to investigate the fault progression process of defects. Analysis of belt's stress was done to produce a stress model of timing belt. Kantaros et al. [29] suggested the utilization of an optical sensor with a small fibre Bragg grating for learning the T.E (thermal expansion) coefficient for fault monitoring of printing apparatus.

Liao et al. [30] stated that when there is fault as motor damage, belt slip and printing fault during operation signals of different nature will be generated by FDM process in comparison to normal operation is performed. Method based on vibrational signal acquisition is used and reductions in dimensions are performed using principal component analysis technique. Features extracted using reduced dimensions are then evaluated against normal operation status using correlation coefficient technique, correlation ratio method and gram matrix method. If the degree of correlation is on higher side then the operation is normal else printer has fault and doesn't perform normal and warning is indicated. It was further added that development in intelligent theory will play a crucial role in indication of FDM printer failure. Identification of collection of characteristic signals from printer helps in early fault warning detection. Features are compared with normal running printer status to determine the fault running of printer [31, 32].

Fault diagnosis method based intelligent learning of sensor signal in FDM 3D printer was also proposed [30]. A fault signature database was prepared by labeling the known fault features. Continuous additions of known feature sets to database establish the base of intelligent learning and fault diagnosis. When it was observed that there is large deviation in the feature set from normal working condition the machine performed fault diagnosis and feature signals are substituted into different fault criterion of the system. The coherence of high degree showed that printer has a known fault whereas correlation of lower degree represents new type of fault and machine warning level was reduced. The sample data are then stored in the system leading to expansion of fault database showing the intelligent learning for fault diagnosis of machine. Sharing of fault databases feature set of independent device can be expanded. They added that a factory can have number of printers to perform printing and fault warning system can collect large dataset per day.

AE sensor-based monitoring of FDM was suggested by Wu et al. [33]. Use of AE hits showed ominously reduction in the volume of data to be processed. It was observed that SVM based on one feature is effective for machine state classification. It was recommended that more features will increase detection sensitivity. It was also proposed that reduced signals proposed by PCA technique provide better efficiency of the classification process [34]. In another study, signal produced by vibration of the extruder is collected for diagnosis of fault [35]. Collected AE signal contains the information of state of the machine. Time and frequency features were extracted to form hybrid feature space system which helps in avoiding the loss of the information. Linear discriminant analysis method (LDA) was used as a dimensional reduction technique for hybrid feature space system. Clustering is used as an unsupervised learning algorithm for identification of reduced hybrid features. Condition of extruder in the FDM is then recognized and categorized for diagnosis of fault. Density based clustering was experienced as an effective method for classification. Comparative studies with classification methods showed that the suggested method is a consistent, reliable and effective method for real time monitoring of the FDM machine particularly for the extruder. They recommended that addition of more AE sensors will improve the efficiency of the system and can be suggested as future work.

Jin et al. [36] employed computer vision and deep learning method for real-time monitoring of FDM printers. In the training phase, training of CNN model is done by ResNet 50 and actual images are fed to the model and printing condition is obtained. 70% of collected images were used for training and 30% are used for validation or testing. Detection of over extrusion will inevitably execute modifying commands to alter the printing parameters via a controlling graphical user interface (GUI). Feedback detection was embedded into the system and new input images settings are iterated till a better image is achieved. ML model is trained and transferred into the monitoring and refining system. Image acquisition rate is selected for balance of testing accuracy and the operational efficiency of the system. Printing condition was adjusted till 5 better quality results are received in continuation. A quick response is added to detect quality of print and variation will be adjusted to enhance performance before printing. 98% accuracy was achieved in predicting the part quality of FDM process. Table 2 presents some important studies relating ML and quality monitoring system.

Table 2 Some prominent studies relating ML and quality monitoring system

Investigation with reference no.	ML Tools used	Conclusion
Automated quality monitoring system for FDM, sterelithography and selective laser sintering processes [22]	CNN and DCNN	Predictive quality monitoring model serves as a basis for other AM machines. They can also improve the speed, material waste, reliability and productivity
Development of an online monitoring and diagnosis system for FDM [24]	Support Vector machine (SVM)	Non-linear SVM-based model using acceleration signals was more accurate in diagnosing the FDM process
Vibrational signal acquisition method is used and reductions in dimensions are performed [30]	Principal component analysis	Identification of characteristic signals from FDM machine helps in early fault warning detection
Use of AE sensor as a fault detection method for FDM [35]	Linear discriminant analysis	Density based clustering was experienced as an effective method for classification. It was recommended that more AE sensors will improve the efficiency of the system
A real-time monitoring and autonomous correction system for FDM printer [36]	Computer vision and deep learning method, CNN, ResNet 50	98% accuracy was achieved in predicting the part quality of FDM process

3.3 *Mechanical Properties*

Tensile test was performed at room temperature by Barrionuevo et al. [37] to discover the vital printing parameters for improving the mechanical properties of PLA based wooden composite filament in FDM process. The experiments were conducted in accordance with L27 orthogonal array using each parameter at three different levels. Experimentation was followed by ANFIS (Fuzzy inference system) ML optimization algorithm to explore the maximum yield strength. 21 trials were used for training of the model and testing and validation was performed using remaining of 6 dataset. Analysis revealed that yield strength of wooden composite relied on orientation of fibers during the test. Greater resistance was experienced that when raster angle was aligned in the direction of the load. They recommended that, 100% fill density, higher layer thickness and raster angle in the direction of load provided the highest yield strength. Printing speed was found to be insignificant for FDM of wood composite filaments.

Long short-term memory (LSTM) model and in-process sensing data were used for tensile strength prediction in FDM process [38]. Layer wise building data was collected using an IR sensor and a thermocouple was used to measure the temperature outside the chamber and compute its effect on the part property. These recorded data serves as input to the LSTM cells linked to printing layers. Data from each LSTM cell are then allied with the working parameters and material property to estimate the tensile strength of FDM parts. 144 testing specimens were under mechanically tested on an Instron 4411 machine following the ASTM D638-14. Metrics were used to evaluate the performance of strength prediction using LSTM model, RF model and support vector regression model. It was observed that in-process sensing significantly improve the prediction tensile strength in FDM where, predicted RMSE is reduced by 44% and increases the variation predictability by 22.6% as shown by R^2 . Comparative study showed LSTM model outperformed the other two models.

Pazhamannil et al. [39] used an artificial neural network (ANN) for prediction of tensile strength of PLA models fabricated using FDM. Experimentations were done in accordance with Taguchi L9 orthogonal array. Test specimens were fabricated as per the ASTM D638-14 and by input of G-code to fabricate the samples. Effective parameters influencing tensile strength were determined by ANOVA. Experimentally investigated dataset is used for training the ANN for predicting the tensile strength at varying process parameters. Correlation coefficient of 99.9% was obtained from regression plots drawn using ANN. Tensile strength predicted using ANN was validated using confirmation experiments performed at confidence interval of 95% and the result was found to be in reasonable agreement. It was observed that an inverse relation appears between layer thickness and tensile strength and influence of Infill speed on tensile strength is not significant. They recommended the use of lower layer thickness and high nozzle temperature for high tensile strength. A review study showing the effect of parameters on mechanical properties and part quality was shown by Sheoran et al. [40]. In addition to

traditional optimization technique they also showed the importance of modern ML based technique including ANN and fuzzy logic. It was observed that ML based design techniques has limited application in improvement in quality of FDM part. They recommended that there is a need to develop more ML based studied on FDM process. Table 3 demonstrated prominent studies relating ML and mechanical properties of FDM process.

3.4 Geometric Deviations

Sandhu et al. [41] employed ML based methods to examine the influence of processing parameters on the shrinkage of PLA parts printed by FDM process. 20 FDM samples were fabricated and examined for their dimensional accuracies. Analysis of result showed that part build orientation angle significantly affects the angular shrinkage of the resulted parts. Scanning electron micrographs also validated the effect of the input process parameters on the printed specimens. Performance of four ML models: decision tree, random forest, linear model and artificial neural network (ANN) were used for their prediction and investigation. 70% data are used for training and testing of models and validation of the models are done by 30% data. Different metrics were used for all the tested. Based on the observed result, neural network model perform the best with minimum error of 0.111628. Ji [42] recommended the FEM simulation and optimization of FDM process and suggested an accuracy prediction for FDM products based on wavelet NN. Geometric accuracy of FDM parts was tested using self-organizing map (SOM) [43]. Scanned data obtained by laser scanner is compared to the original

Table 3 Studies relating ML and mechanical properties of FDM process

Investigation with reference no.	ML Tools used	Conclusion
To discover the vital printing parameters for improving the mechanical properties of PLA based wooden composite filament in FDM [37]	ANFIS (Fuzzy inference system)	It was recommended that 100% fill density, higher layer thickness and raster angle in the direction of load provided the highest yield strength
Tensile strength prediction in FDM technology [38]	LSTM model, RF model and Support vector regression)	Comparative study showed that LSTM model outperformed the other two models
Prediction of tensile strength of PLA models fabricated using FDM [39]	Artificial neural network (ANN)	It was recommended that the use of lower layer thickness and high nozzle temperature for high tensile strength
A review study showing the effect of parameters on mechanical properties and part quality of FDM parts [40]	ANN and Fuzzy logic method	It was observed that ML based design techniques has limited application in improvement in quality of FDM parts

design data and the subsequent change is used to describe the dimensional deviations of the fabricated part. Clustering of point cloud data are done using direction and magnitude of geometric deviations using SOM and this method was evaluated against the experimental data measured from scanning of parts. It was experienced that clustering using SOM can differentiate between parts made with different processing state and can recognize the magnitude and direction of geometric deviation. They described that their method was not only suitable for recognizing the effect of processing conditions on geometric accuracy but also on explicit types of deviations. They said that a small portion of the surface area can be scanned and used for analysis can significantly increase the scan and processing speed. The authors recommended that SOM based clustering approach can be extended to predict the geometric accuracy of other AM process.

3.5 *Mixed Studies*

A deep neural network model (DNN) was proposed to calculate the connection between paths in a FDM process [44]. Process parameters such as filament extrusion speed, print speed, line distance and layer height were varied and four hundred experiments were conducted to obtain the status between line connections. Majority of the data obtained from the experimentation were used for the training of DNN model and remaining data is used for performance evaluation of the model. Connection status were classified into five classes where 0 represents large air gap (space between printed lines) and class 4 shows large spaces between lines allowing material overflow between the printed lines. Based on the analyzed result it was established that DNN model shows 83% accuracy in predicting the connection status between printed lines. It was further recommended that trained DNN model can predict the best combinations of parameters which results in better path connections. Garg and Tai [45] used genetic programming and least squares method based neural network (NN) algorithm for predicting the wear strength of aerospace part produced by FDM. For every fabricated part building material and their final structure are known in advance. Varied parameters used for part fabrication were layer thickness, part orientation, raster angle, raster width and air gap. Corresponding values of these parameters are fed as input to the genetic programming and NN algorithm. Observation showed that prediction of wear strength using the combined approach is better when compared to prediction made by any single machine learning algorithm. Dimensional accuracy in FDM was predicted and compared using six machine learning techniques by Tootooni et al. [46]. Based on the achieved results and their comparison with regard to the dimensional variation the sparse representation approach appears to be technique in terms of classification performance.

Nagar et al. [47] demonstrated a technical report presenting the use of digital twin technique in FDM through a case study. Modeling of FDM process can be done by using various working parameters from multiple sensors used as input to

the digital twin. They also proposed that use of cyber physical system and big data on FDM will enable new start-ups to enrich productivity in manufacturing industries using data generated through their system. RF based machine learning approach was used by Yi et al. [48] for energy simulation of the FDM process. The research was conducted in three phases where a part was first printed using FDM machine with power analyzer attached to capture the power data. In the 2nd phase power data in form of G-code is used for training and testing of the model using five models based on RF algorithm Python is use for training of the models. Lastly, trained RF simulator was used for the simulation of the energy consumption in FDM. Evaluation of the training process was done using different indicators: mean square error (MSE), mean absolute error (MAE) and R-squared value (R^2). Comparison of RF models showed that extreme gradient boosting model (XGB) provide the best performance in training and the light gradient boosting machine (LGB) model exhibit the best prediction accuracy.

Multi-nozzle extrusion based AM system was proposed by Chen et al. [49] for fabricating a sandwich structure with soft and hard material. A DA controller was used to control the air pressure of different injected flow speed. Python was used to process the G-code data sent to the multi-nozzle pneumatic extrusion AM system. A tiny nozzle was used for extruding out the liquid material and cured by a UV source. Better printing performance was experienced and print width is very finer (observed under microscope) when tested with materials with different viscosity. Gardner et al. [50] demonstrated a framework as an end-to-end tool for integrating ML into fused filament fabrication (FFF). Optimum parameter selection at each location is specified by the tool considering all important factors. Usefulness of tool was showed by correcting common visual flaws in parts made by FFF technology. To generate training data neural network relying on image recognition classified the local flaws in parts. For prediction of flaws in newly fabricated parts depending on location, geometry and parameters, a gradient boosting classifier was proposed. It was observed that optimum parameters determination was selected by tool based on discussed factors. It was finally experienced that quality of printed parts showed enhanced quality.

A new method was proposed, tested and validated to fabricate thin shell parts using no support in FDM process [51]. By fabrication and characterizing multiple parts they observed that NN-based recompensed path determination method upgraded the correctness and time delay error for multi-manipulator setup and enable the fabrication of thin shell accurate parts. It was recommended that reduction in build time and less use of support material was possible in the extrusion-based AM while building the thin shell parts. A knowledge based-ANN method was proposed to reduce the number of tests to train and validate ANNs for describing a FDM system [52]. The method was used for prediction of control factors of FDM. The results established the advantage of their method over traditional full-connected ANNs for the similar performance and equal number of training samples. Table 4 displays some important studies relating ML and mixed studies in FDM process.

Table 4 Some prominent studies relating ML and mixed studies in FDM process

Investigation with reference no.	ML Tools used	Conclusion
To calculate the connection between paths in a FDM process Geometric accuracy of FDM parts was tested [44]	Deep neural network model (DNN)	It was recommended that trained DNN model can predict the best combinations of parameters which results in better path connections
Prediction of the wear strength of aerospace part produced by FDM [45]	Genetic programming and least squares method based neural network	Prediction of wear strength using the combined approach is better when compared to prediction made by any single ML algorithm
Energy simulation of the FDM process [48]	Gradient boosting regressor (GBR), Light gradient boosting machine (LGB), Bagging regressor (BGG), RF regressor (RFR) and Extreme gradient boosting model (XGB)	Comparison of RF models showed that XGB model provide the best performance in training and the LGB model exhibit the best prediction accuracy
A framework as an end-to-end tool for integrating ML into fused filament fabrication [50]	Neural Network	Quality of printed parts showed enhanced quality

4 Discussions and Future Scope

Fused deposition modeling also known as fused filament fabrication (FFF) is a known AM technique capable of fabricating complex products with reduced cycle time. It doesn't require any specific tooling and definite process plan. The process also allows minimized human intervention. It is widely used in different engineering and medical applications. Instead of widespread application of FDM products, FDM process lack in providing consistency in part properties, process reliability and part accuracy. Advancement in computing technology enable the use of machine learning techniques to satisfy the FDM reliability and part accuracy but a review study showing the importance of ML in FDM process is still not established. To bridge this gap, authors tried to present an insight of ML in FDM process. The state of art presented the applicability of ML in different areas of FDM process. Based on the presented review Fig. 4 shows the important areas in FDM areas where ML has been successfully applied. Based on review carried out and pi-chart as presented in Fig. 4, it can be concluded that maximum application of ML is in quality monitoring system of FDM process. The review study accounts for around 40% of researches related to quality monitoring system in FDM process.

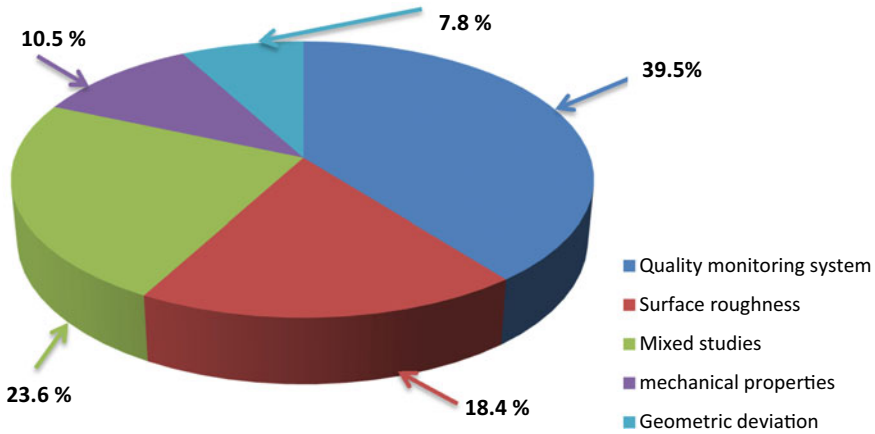


Fig. 4 ML applications in FDM areas

Next to quality monitoring system, ML is effectively applied in other miscellaneous areas (energy simulations, FEM simulation and use of support less extrusion AM system) of FDM followed by surface roughness prediction of FDM parts. It can also be witnessed from pie-chart that minimum studies are related with application of ML in geometric deviations or dimensional accuracy of FDM parts. Based on the literature survey as presented above prominent studies showing the application of ML in FDM process are shown in Tables 1, 2, 3, 4.

Applications of ML techniques in improving the dimensional accuracy of FDM parts is least reported. In addition use of ML in FDM simulation, support less extrusion AM system, tool for integrating ML into fused filament process, multi-nozzle extrusion system and wear prediction is also less explored. These areas are thus best choice for future investigations. Research gaps can also be identified by papers relating the use of ML in roughness prediction, tensile strength prediction and others to increase the applicability of ML in FDM process. It was also realized that limited number of ML techniques are used in FDM process and thus use of other popular ML techniques specially belonging to supervised algorithms can be integrated into the researches and comparative studies can be done. The comparative study can also help in determining the best suitable learning techniques for FDM process. ML is a subset of artificial algorithm (AI) and other AI techniques like use of IoT (internet of things), cloud computing and big data analysis is suggested for future direction.

References

1. Eqbal A, Eqbal MI, Sood AK (2019) An investigation on the feasibility of fused deposition modelling process in EDM electrode manufacturing. *CIRP J Manufact Sci Technol* 26:10–25
2. Eqbal A, Eqbal MI, Sood AK (2019) PCA-based desirability method for dimensional improvement of part extruded by fused deposition modelling technology. *Progress Addit Manuf* 4:269–280
3. Eqbal A, Eqbal MI, Sood AK, Pranav R (2018) A review and reflection on part quality improvement of fused deposition modeled parts. In: *IOP Conference Series Mater Science and engineering*, vol 455, pp 1–9
4. Giberti H, Strano M, Annoni M (2016) An innovative machine for fused deposition modeling of metals and advanced ceramics. Paper presented at 4th international conference on nano and materials science, MATEC web of conferences, 43, New York, USA, 7–9 January 2016
5. Razvi SS, Feng S, Narayanan A, Lee YT, Witherell P (2019) A review of machine learning applications in additive manufacturing. Paper presented at international design engineering technical conferences and computers and information in engineering conference, Anaheim, CA, USA, 18–21 August 2019
6. Omar S, Ngadi MA, Jebur HH, Benqdara H (2013) Machine learning techniques for anomaly detection: an overview. *Int J Comput Appl* 79(2):33–41
7. Simon A, Selvam V, Babu R, Deo MS (2016) An overview of machine learning and its applications. *Int J Electr Sci Eng* 1:22–24
8. Meng L, McWilliams B, Jarosinski W, Park H, Jung Y, Lee J, Zhang J (2020) Machine learning in additive manufacturing: a review. *J Miner Metals Mater Soc* 72(9):2363–2377
9. Reddy YCAP, Pulabaigari V, Reddy BE (2018) Semi-supervised learning: a brief review. *Int J Eng Technol* 7:81–85
10. Gosavi A (2009) Reinforcement learning: a tutorial survey and recent advances. *INFORMS J Comput* 21(2):178–192
11. Nguyen L, Buhl J, Bambach M (2020) Continuous eulerian tool path strategies for wire-arc additive manufacturing of rib-web structures with machine-learning-based adaptive void filling. *Addit Manuf* 35:1–17
12. Chen Z (2020) Understanding of the modelling method in additive manufacturing. In: *IOP conference series: materials science and engineering*, vol 711, pp 1–6
13. Korneev S, Wang Z, Thiagarajan V, Nelaturi S (2020) Fabricated shape estimation for additive manufacturing processes with uncertainty. *Comput Aided Des* 127:1–13
14. Di Angelo L, Di Stefano P (2011) A Neural Network-based build time estimator for layer manufactured objects. *Int Jo Adv Manuf Technol* 57(1–4):215–224
15. Barrios JM, Romero PE (2019) Decision tree methods for predicting surface roughness in fused deposition modeling parts. *Materials* 12(16):1–10
16. Dazhong W, Wei Y, Terpenney J (2018) Surface roughness prediction in additive manufacturing using machine learning, manufacturing equipment and systems. Paper presented at ASME 13th international manufacturing science and engineering conference, 3, MSEC, US, 18–22 June 2018
17. Lia Z, Zhanga Z, Shia J, Wu D (2019) Prediction of surface roughness in extrusion-based additive manufacturing with machine learning. *Robot Comput Integr Manuf* 57:488–495
18. Molero E, Fernández JJ, Rodríguez-Alabanda O, Guerrero-Vaca G, Romero PE (2020) Use of data mining techniques for the prediction of surface roughness of printed parts in polylactic acid (PLA) by fused deposition modeling (FDM): a practical application in frame glasses manufacturing. *Polymers* 12:840–856
19. Sohnius F, Schlegel P, Ellerich M, Schmitt RH (2019) Data-driven prediction of surface quality in fused deposition modeling using machine learning. In: *Wulfsberg J, Hintze W, Behrens B (eds) Production at the leading edge of technology*, Hamburg 2019. Springer, Germany, p 473

20. Mahapatra SS, Sood AK (2012) Bayesian regularization-based Levenberg-Marquardt neural model combined with BFOA for improving surface finish of FDM processed part. *Int J Adv Manuf Technol* 60:1223–1235
21. Vahabli E, Rahmati S (2017) Improvement of FDM parts surface quality using optimized neural networks-medical case studies. *Rapid Prototyp J* 23:825–842
22. Banadaki Y, Razaviarab N, Fekrmandi H, Sharifi S (2020) Toward enabling a reliable quality monitoring system for additive manufacturing process using deep convolutional neural networks. *Computer Vision And Pattern Recognition*, pp 1–8. [arXiv:2003.08749](https://arxiv.org/abs/2003.08749)
23. Rao PK, Liu JP, Roberson D, Kong ZJ, Williams C (2015) Online real-time quality monitoring in additive manufacturing processes using heterogeneous sensors. *J Manuf Sci Eng* 137(6):061007
24. Nam J, Jo N, Kim JS, Lee SW (2020) Development of a health monitoring and diagnosis framework for fused deposition modeling process based of a machine learning algorithm. *Proc Inst Eng B J Eng Manuf* 234(1–2):324–332
25. Yoon J, He D, Van Hecke B (2014) A PHM approach to additive manufacturing equipment health monitoring, fault diagnosis, and quality control. Presented at the annual conference of the prognostics and health management society, Fort Worth, TX, 2014
26. Rao PK, Liu JP, Roberson D, Kong Z, Williams C (2015) Sensor-based online process fault detection in additive manufacturing. Presented at Internal manufacturing science and engineering conference, Charlotte, North Carolina, USA, June 8–12, 2015
27. Zhang XY (2016) Research on 3D printing optimized technology based on vibration test system. M.A Thesis, Harbin Institute of Technology, Harbin, 2016
28. Zhang H (2017) Study on fault diagnosis of FDM 3D printing process based on HSMM and EEMD. M.A Thesis, Zhejiang University, Zhejiang 2017
29. Kantaros A, Karalekas D (2013) Fibre Bragg grating based investigation of residual strains in ABS parts fabricated by fused deposition modelling. *Mater Des* 50:44–50
30. Liao J, Shen Z, Xiong G, Liu C, Luo C, Lu J (2019) Preliminary study on fault diagnosis and intelligent learning of fused deposition modelling (FDM) 3D printer. In: Presented at 14th IEEE conference on industrial electronics and applications, pp 2098–2102
31. Xiong G, Wang FH, Nyberg TR et al (2018) Free mind to products: towards social manufacturing and services. *IEEE/CAAA J Automatica Sinica* 5(1):47–57
32. Lei Y, Jia F, Lin J, Xing S, Ding SX (2016) An intelligent fault diagnosis method using unsupervised feature learning towards mechanical big data. *IEEE Trans Ind Electron* 63(5):3137–3147
33. Wu H, Wang Y, Yu Z (2016) In situ monitoring of FDM machine condition via acoustic emission. *Int J Manuf Technol* 84(5–8):1483–1495
34. Wu H, Yu Z, Wang Y (2017) Real-time FDM machine condition monitoring and diagnosis based on acoustic emission and hidden semi-Markov model. *Int J Manuf Technol* 90(5–8):2027–2036
35. Liu J, Hu Y, Wu B, Wang Y (2018) An improved fault diagnosis approach for FDM process with acoustic emission. *J Manuf Process* 35:570–579
36. Jin Z, Zhang Z, Gu GX (2019) Autonomous in-situ correction of fused deposition modeling printers using computer vision and deep learning. *Manuf Lett* 22:11–15
37. Barrionuevo GO, Ramos-Grez JA (2020) Machine learning for optimizing technological properties of wood composite filament-timberfill fabricated by fused deposition modeling. In: Presented at 1st international conference, ICAT, Quito, Ecuador, 3–5 December 2020, pp 119–132
38. Zhang J, Wang P, Gao RX (2019) Deep learning-based tensile strength prediction in fused deposition modeling. *Comput Ind* 107:11–21
39. Pazhamannil RV, Govindan P, Sooraj P (2020) Prediction of the tensile strength of polylactic acid fused deposition modeling models using artificial neural network technique. *Mater Today Proc.* <https://doi.org/10.1016/j.matpr.2020.01.199>

40. Sheoran AJ, Kumar H (2019) Fused deposition modeling process parameters optimization and effect on mechanical properties and part quality: review and reflection on present research. *Mater Today Proc.* <https://doi.org/10.1016/j.matpr.2019.11.296>
41. Sandhu K, Singh S, Prakash C (2019) Analysis of angular shrinkage of fused filament fabricated poly-lactic-acid prints and its relationship with other process parameters. In: IOP conference series: materials science and engineering, vol 561, no 1–12, pp 012058
42. Ji LB (2011) Research on the finite element simulation and process optimization in fused deposition modelling. M.A Thesis, Nanchang University, Nanchang 2011
43. Khanzadeh M, Rao P, Jafari-Marandia R (2017) Quantifying geometric accuracy with unsupervised machine learning: using self-organizing map on fused filament fabrication additive manufacturing parts. *J Manuf Sci Eng* 140(3):1–12, 031011
44. Jiang J, Yu C, Xu X, Ma Y, Liu J (2020) Achieving better connections between deposited lines in additive manufacturing via machine learning. *Math Biosci Eng* 17(4):3382–3394
45. Garg A, Tai K (2014) An ensemble approach of machine learning in evaluation of mechanical property of the rapid prototyping fabricated prototype. *Appl Mech Mater* 575:493–496
46. Tootooni MS, Dsouza A, Donovan R, Rao P (2017) Classifying the dimensional variation in additive manufactured parts from laser-scanned three-dimensional point cloud data. *J Manuf Sci Eng* 139(9):091005
47. Nagar SV, Chandrashekar AC, Suvarna M (2020) Optimized additive manufacturing technology using digital twins and cyber physical systems. In: Auer M, Ram BK (eds) *Cyber-physical systems and digital twins. REV2019. Lecture Notes in Networks and Systems*, vol 80. Springer, Cham pp 65–73
48. Yi L, Glaßner C, Krenkel N, Aurich JC (2019) Energy simulation of the fused deposition modeling process using machine learning approach. *Procedia CIRP* 86:216–221
49. Chen KW, Tsai MJ, Lee HS (2020) Multi-nozzle pneumatic extrusion-based additive manufacturing system for printing sensing pads. *Inventions* 5(3):29–34
50. Gardner JM, Hunt KA, Ebel AB, Rose ES, Zylich SC, Jensen BD, Wise KE, Siochi EJ, Sauti G (2019) Machines as craftsmen: localized parameter setting optimization for fused filament fabrication 3D printing. *Adv Mater Technol* 1–10:1800653
51. Bhatt PM, Malhan RK, Rajendran P, Gupta SK (2019) Building free-form thin shell parts using supportless extrusion-based additive manufacturing. *Addit Manuf.* <https://doi.org/10.1016/j.addma.2019.101003>
52. Nagarajan HPN, Mokhtarian H, Jafarian H, Dimassi S, Bakrani-Balani S, Hamed A, Coatanea E, Wang GG, Haapala KR (2019) Knowledge-based design of artificial neural network topology for additive manufacturing process modeling: a new approach and case study for fused deposition modeling. *J Mech Des* 141(1–12):021705

Tool-Path Optimization in Material Extrusion Additive Manufacturing



Neri Volpato  and Tiago Rodrigues Weller

Abstract Manufacturing time is an important topic in Material Extrusion Additive Manufacturing (MEAM) mainly because of the thin filament deposited and the need to interrupt deposition during head repositioning (or jump). Depending on the part/build geometry, there might be a large number of jumps during deposition. Tool-path optimization can be applied to choose the best deposition sequence, but the amount of data can be quite large in such a problem. In this work, a framework for tool-path airtime optimization has been presented where the main idea is to reduce the problem size. The new methods to decompose the problem allow reducing its computational complexity, speeding up its solution, and then, larger instances of the problem can be solved. The CPU time savings when applying the framework proposal combining two basic heuristics, the Nearest Insertion, and 2-OPT, were remarkable. Additionally, the proposal is generic and suitable for different operational research methods.

1 Introduction

The ISO/ASTM standard separated the Additive Manufacturing (AM) according to the material addition principle into seven categories, among them is that based on material extrusion [1]. In general, the technologies in this group use a nozzle to extrude and deposit a filament of material in each layer of the part (Fig. 1). The Fused Deposition Modeling (FDM), developed by Stratasys Ltd, was the first material extrusion AM technology available on the market, and sometimes it is taken as a synonym of this principle. In the maker space, it is also common to refer

N. Volpato (✉) · T. R. Weller

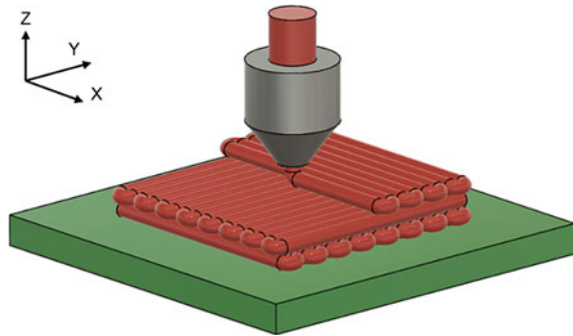
Federal University of Technology—Paraná (UTFPR), Additive Manufacturing and Tooling Group (NUFER), R. Deputado Heitor Alencar Furtado, 5000, Curitiba, PR CEP 81280-340, Brazil

e-mail: nvolpato@utfpr.edu.br

T. R. Weller

e-mail: weller@utfpr.edu.br

Fig. 1 Schematic representation of MEAM



to this technology as the Fused Filament Fabrication or Filament Freeform Fabrication (FFF), mainly when a filament spool feedstock is used. It is also possible to find reference to this principle as Direct Wright Ink or Robot Casting, mainly when dealing with the extrusion of ceramic or other biomaterials. In this chapter, a more generic term, which encompasses all possible materials and application of this category of process, is preferred, therefore Material Extrusion Additive Manufacturing (MEAM) is used.

Manufacturing time is a particular issue in MEAM mainly because the extrusion head produces a thin filament of material that needs to fill the entire areas of each layer. Additionally, the extrusion needs to be interrupted to allow head repositioning (or jump) to continue filling in another region [2, 3]. The layer filling is not continuous, and depending on the part/build geometry, there might be a large number of jumps during deposition. Due to these aspects, the process can be considered very slow when compared to other methods [4–6], and, therefore, time-saving can be considered an important issue in such AM technologies.

In this work, we discuss an approach to deal with the tool-path optimization problem, aiming to minimize the route length of head repositioning by choosing a good sequence of entities to be filled. Although the same approach, with few adaptations, can be used with other AM categories, this chapter is focused in MEAM, considering its peculiarities.

2 Particularities of the Path Planning for MEAM

The path planning is the step responsible to create the trajectory that the nozzle needs to follow to deposit the material. It is performed after the slicing step, which generates a stack of layers containing the closed polygons indicating where material should be added. The tool-path is required to deposit not only the part material but also for the support structures when needed. The support structures can be built using the same part material (same nozzle) or by a different one (with a specific nozzle). In the following sections, the entities (data) generated by the path planning to be processed during optimization are presented in detail.

2.1 Contour and Continuous Raster Segments

A contour (C) is obtained from offsetting a closed polygon to compensate for the filament width (Fig. 2a). As a closed polygon limits the area to be filled with material, a C will be also a closed polyline. A valid C is then a set (or list) of connected contour points (C-points), where the start and endpoints are the ‘same’. The AM process planning software determines the number and position of the C-points, which are affected by the part geometry and the accuracy of the 3D mesh. When depositing a C, any C-point of the list can be used as the entry/exit point. When setting the process parameters, it is possible to choose depositing multiple Cs, which creates a shell or part skin (Fig. 2b).

In general, a layer is composed of at least one C and its respective internal filling. The internal filling can be done with many strategies, such as raster filling (also referred to as rectilinear), honeycomb, line, grid, triangular, wiggle, concentric, Hilbert Curve, Octagram Spiral, etc. Many of these strategies have in common the fact that they are formed by an open polyline (an open path), usually due to a zigzag approach to cover the whole area to be filled. This means that the filling tool-path contains at least one continuous segment or section with a distinct start and end-points. This entity is referred to here as a Continuous Raster Segment (CRS) (Fig. 2c). For simplicity’s sake, the raster filling strategy, which is very popular, is used in this work to represent the internal filling. However, the open path effect is the same for other similar strategies. When a C is derived from a non-convex polygon (C2 in Fig. 2) or when there is one or more internal Cs in the layer (C1 and C3 in Fig. 2), a single CRS is not enough to fill in the entire area [4]. This is illustrated in Fig. 2c, where C1 and C2 require two and three CRSs to be filled, respectively.

The CRSs are symmetrical, which means that both directions of deposition between the two points are considered valid. The part geometry and the process parameters (for instance: raster angle, airgap, nozzle diameter, and filament width)

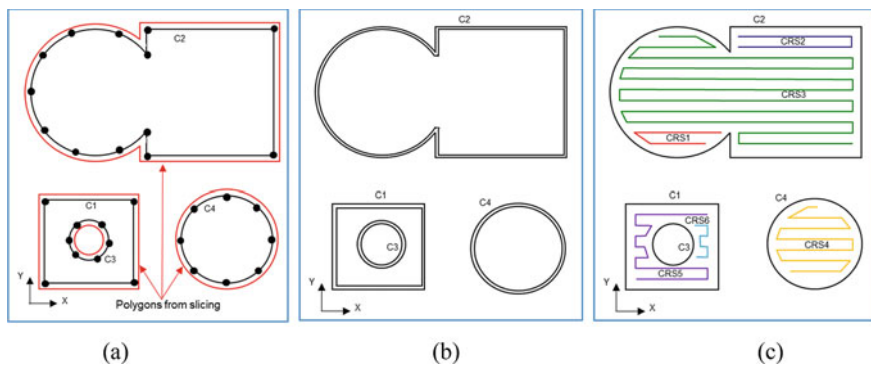


Fig. 2 Schematic of a layer containing Cs (a), shell with 2 Cs (b) and CRSs (c) in the MEAM

define the number and shape of the CRSs. Some optimization techniques may also be applied during filling calculation, and some works related to that can be found elsewhere [3, 7, 8].

If support structures are required to build a part, the AM process planning software might create Cs and CRSs that vary according to the shape of the used structures. These entities need to be considered in the analysis and are treated similarly to the Cs and CRSs from the part.

2.2 Head Repositioning or Idle Movements

It is common to have many Cs and CRSs in a layer (part or support structure), therefore the number of jumps of the extrusion nozzle to start a new deposition can be quite large. These jumps are called here head repositioning, also known as idle movements, meaning a non-productive airtime. They are drawn as dashed lines in Fig. 3 and are performed by the machine with rapid movements without material deposition. The jumps are also required when the extrusion head departs from the start (or cleaning) point, and when it needs to move to the next layer (or to the cleaning point), at the end of a layer. Even though the speed of the head repositioning is higher than that of the material deposition, time spent on idle movements can be considerable [9–11]. The total route length of head repositioning is affected by the part geometry (the number of Cs and CRSs) and size, the process parameters (the internal filling strategy), the need or not of support structures, and by the number of layers required to manufacture the part.

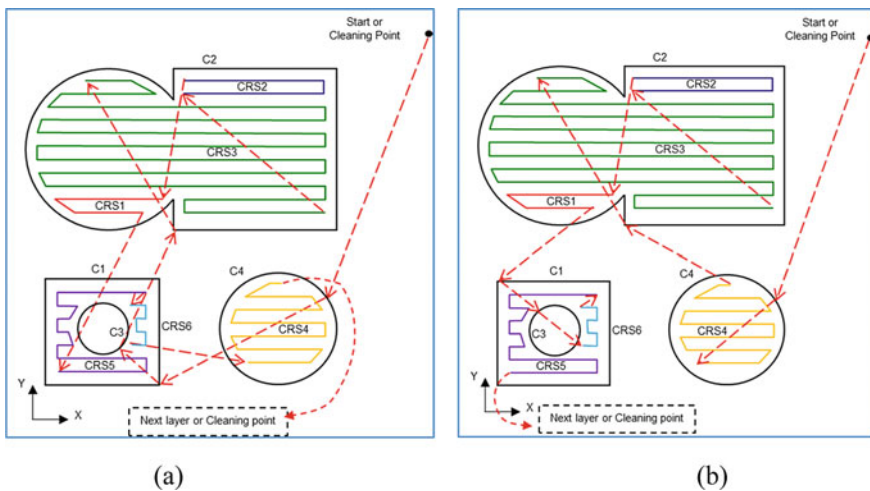


Fig. 3 Schematic of a tool-path showing the sequential (a) and intercalated (b) deposition sequence

Some commercial machines, such as the one from Stratasys Ltd, have a tip cleaning cycle, which is executed at the beginning of the process and at a predefined number of layers. This cleaning is used to avoid any burned material (which remained attaching to the tip) ending up deposited in the part, which would affect the quality of the printing. This cycle is done by moving the head to a point, where a cleaning brush is installed, extruding a small amount of material, and then passing the tip through the brush.

The cheaper desktop printers do not use this cycle, prioritizing time and material consumption. The inclusion of such a cycle will increase the number of idle movements and the length of head reposition route, and as consequence, the build time.

2.3 Part Deposition Sequence (Sequential and Intercalated)

Another important option in the path planning is the deposition sequence adopted to build the part, which can follow a sequential or an intercalated approach (Fig. 3). In the sequential approach, first, all Cs in a layer are deposited and, only after that, the fillings of the internal areas are executed. Figure 3a shows the possible sequential deposition: C4, C1, C3, C2, CRS3, CRS2, CRS1, CRS5, CRS6, and CRS4. The sequential deposition is usually the default option in the process planning software.

In the intercalated sequence, right after a particular external C is deposited, its respective CRS(s) can already be done. Figure 3b shows one possible intercalated sequence: C4, CRS4, C2, CRS3, CRS2, CRS1, C1, C3, CRS6, and CRS5. As can be seen, if there is any internal C inside an external one, it must be deposited before the respective CRSs, which is the case of C3 in Fig. 3b.

The deposition sequence directly affects the idle movements because, once an isolated region (Cs and respective CRSs) has been visited in the intercalated option, the extrusion head does not need to return to it anymore (see, for instance, C4 in Fig. 3b). On the other hand, in the sequential deposition, this region will be visited twice, first to deposit the Cs and later on to deposit the CRSs (compare with the same C4 in Fig. 3a).

3 Problem Definition

In this section, the precedence constraints related to the process and the similarities and dissimilarities with the classic optimization problems are discussed.

3.1 Precedence Constraints

The sequence of events when printing a part can vary a little between the first and the remaining layers, according to the user's choice. For instance, it is possible to use a skirt, a brim, and a base to accommodate the part in the platform, and all these entities are deposited first. After that, in each layer, it starts with the extrusion head leaving the home position, or any start point (last point of the previous entity), and moving fast to the first entity to be deposited. If support structures are required, their respective C and/or CRS are usually deposited before the part material. If no support structures are required, the first entity will be a part C. Once the first part C is deposited, it goes either to the next C or the respective CRSs (according to the deposition sequence), and this is done up to the last CRS. The extrusion head then moves up (or the platform moves down) by a layer thickness and jumps to the first C of the next layer (belonging to the support or the part), and so on, repeating the process. If a cleaning cycle is to be used, after a certain number of layers, before moving to the next layer, the extrusion head goes to a cleaning point. After depositing all layers, it returns to the home position.

This sequence defines some precedence constraints in this technology. The first one, and quite straightforward, is that the layer sequence can not be overlooked. Another precedence is that a C (or Cs) of a specific area must be deposited before its respective CRSs, and this is true either for the sequential or the intercalated deposition sequence and also for the support structures. The deposition sequence also sets a precedence constraint in a layer because it defines if all Cs must be deposited before the CRSs or if the CRSs can be deposited intercalated with the Cs. This is a hierarchy feature in the problem, which must be addressed. The connection between layers is done by going straightway to the first C of the next layer or, if a cleaning cycle is used, by passing through the cleaning point before. This is a user decision and also depends on the machine used.

3.2 Relevant Data and Data Size

The data to be considered in the analysis are the set of layers, the Cs and CRSs of each layer (part and support structure, if any), start point (home), cleaning point, if any, and the head repositioning (jumps). The lengths of each Cs and CRSs are not considered in the optimization problem, because only the non-productive displacements (idle movements) are analyzed. As mentioned before, all C-points must be considered as candidates to be used as the start point to deposit the respective C. For the CRSs, only the start and the endpoints need to be analyzed, all the intermediate points can be ignored. Also as mentioned above, both senses of a CRS, from the start to the endpoint and backward, need to be considered.

For simplicity, the head repositioning connecting any two points are assumed as straight lines (shown as dashed lines in Fig. 3), so the Euclidean distance is computed between these two points.

This optimization can be considered as a combinatorial non-polynomial hard (NP-hard) problem due to the large number of points forming the tool-path, that can easily reach more than 200 points. Then it makes it difficult to be solved optimally in an acceptable computing time [12, 13].

3.3 Similarities and Dissimilarities with the Classic Optimization Problems

The sequencing optimization described in this work has been compared to the classic optimization problems, especially the Travelling Salesman Problem (TSP) and the Chinese Postman Problem (CPP), and more specifically to some of their corresponding variants, such as the Generalized Traveling Salesman Problem (GTSP) and the Rural Postman Problem (RPP) [11, 14, 15].

In the classic TSP, the aim is to find the shortest possible route to visit a list of cities exactly once, having the distances between each pair of cities, and returning to the origin city. Because of that and, as it returns to the start point, the final route is called a Hamiltonian cycle. If the cities can be grouped in clusters, the problem can be thought of as the GTSP, where, one point from each cluster is required to create the main route [11]. In the GTSP, the salesman has to find a minimum length tour that includes exactly one of n cities of each m disjoint districts (clusters). In this case, finding an adequate route inside the clusters can be seen as another TSP. In this direction, if the ordering of places (points) within each cluster and the ordering of clusters have to be optimized simultaneously, this is considered another variant of the TSP called the Clustered Traveling Salesman Problem (CTSP) [16].

In the classic CPP, it is relevant to visit the edges connecting the points, therefore it is required to find a minimum weight tour such that each edge is visited at least once, then returning to the original city. When the postman does not need to travel all the edges of the graph but only some of them, identified as the required ones, it becomes a special instance of the CPP, known as the Rural Postman Problem. This was the option to model the path optimization problem by Iori and Novellani [15].

Once the precedence constraints mentioned above are respected, the connections (edges) between Cs and between CRSs are not relevant, i.e., what really matters is the point (or vertex) to start a deposition. There is nothing along the edges (reposition path) that need to be considered and there are not any predefined or preferential edge to be followed. Therefore, the tool-path optimization seems closer to the TSP than to the CPP. During the material deposition, the extrusion nozzle must move exactly once to all Cs and CRSs, and the displacement between two points has the same cost, regardless of the motion direction, which is a characteristic of

symmetrical TSP [9, 17]. The head repositioning is considered symmetric then, which means that both senses are considered valid and the direction of movement is not a constraint.

However, the Hamiltonian cycle would imply into find a route leaving the start point, going through all layers, and returning to the start point. Due to the amount of data, this is not practical to be solved. Nevertheless, because of the layers' precedence, each layer can be analyzed individually, and the problem can be seen as the Open Traveling Salesman Problem (OTSP). In such a variant, the solution is not concerned whether the salesman returns to the start point, i.e., the traveling costs between the last customer and the start point is not considered. In our problem, after finishing a layer, the extrusion head does not need to return to the starting point, and it does not matter the position of the last point to be deposited because it will be considered the start point of the next layer. Another fact is that the Cs and CRSs can be seen as clusters (of C-points and CRS-points) and the problem can be treated as a special case of GTSP. It is worth to point out that the clusters and the sequence of C-points within these are pre-defined by the process planning software. More details about this are presented in the next section.

A relevant difference concerning the TSP is how the CRSs are treated. When the extrusion head "visits" one point (start of a CRS), it does not depart from that point, as observed in traditional TSP, because the start and endpoints of a CRS are not coincident.

Regardless of the approach, to realistically characterize a MEAM process, the optimization method must consider Cs and CRSs, must consider the process restrictions, and has to be able to deal with a large number of points (many layers and many Cs and CRSs per layer). Based on this, the objective of this optimization is to minimize the head repositioning route length required to visit once each C, choosing just one of its C-points, and then each CRS, choosing one of the two CRS-points. This must be done in each layer and for the whole part. A proposal to deal with this problem in such a way is presented below.

3.4 Problem Variation According to the Layers

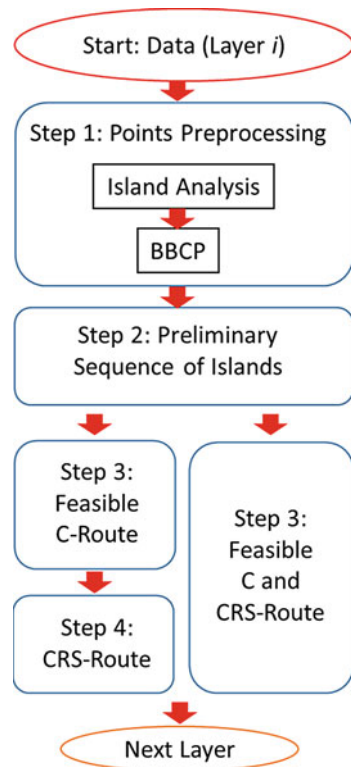
According to the layer being processed, the problem should be solved by having a different procedure because of the process requirements. There is a slight variation between the first, the intermediate, and the last (or cleaning) layer. For the first and all the intermediate layers, the initial route starts from a fixed point (home position or the last CRS-point of the previous layer) and the endpoint is free (not fixed). So, the problem can be seen as an OTSP with a fixed start point. However, for the last and any cleaning layer, the route starts from a fixed point (last CRS-point of the previous layer) but must finish at the home or cleaning point, respectively. In this case, the problem can be seen as an OTSP with fixed start and endpoints.

4 A Proposed Framework to Deal with the Problem

Bearing in mind that the problem data can be quite large, it is natural to look for alternatives to make it smaller. In this section we present an optimization framework, which breaks the problem into four steps (Fig. 4), making it easier to solve and allowing the use of many heuristics [14]. The first step is a preprocessing one, which aims to simplify the problem by taking advantage of momentarily reducing the data size using a sort of judgmental data sampling. This term was used here making an analogy to a similar procedure used in statistics [18]. In the second step, a preliminary sequence of C is generated based on the data sampling of step 1. Then, in step 3, a feasible C-route is created using all the original data, but applying a local search. If the sequential deposition is used, step 4 is responsible to create a CRS-route. Otherwise (intercalated sequence), the CRSs are included in the analysis in step 3, therefore, step 4 is not required.

The steps in Fig. 4 can also be applied to identify a good repositioning route to deposit support structures (Cs and/or CRSs). Once this route is ready, the process of creating the repositioning route for the part can start.

Fig. 4 Main steps of the optimization framework



4.1 Points Preprocessing (Step 1)

In this step, the problem data are decomposed and simplified aiming to reduce the number of points to be considered. Based on the researchers' knowledge and judgment, some criteria are defined, in a kind of judgmental sampling, to extract important information of the data that will reduce the amount of computing later on. By doing this, good solutions (non-optimal) can be obtained in a reasonable computing time. This is a generic step because it can be applied regardless of the heuristics used to solve Steps 2, 3, and 4.

4.1.1 Islands Analysis

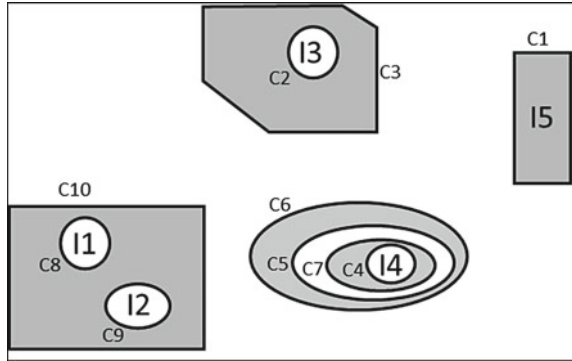
The data to be analyzed can be clustered in regions where material must be deposited. In this work, we named these clusters as 'islands', which are defined as regions in a layer where the extrusion head must jump to, in order to deposit material. An island is then a set of Cs (it may also contain CRSs), which encompasses this region. The number of elements in each set will vary according to the geometry of the region. Strictly speaking, the island concept proposed here may not represent an actual island definition, because an isolated region can originate many 'islands'. This is clarified in the next paragraph.

As an external C (C-points oriented counter-clockwise) always defines the limits where material should be deposited, it would be the first choice to generate an island. However, an external C might be inside other external and internal Cs. Then, a better way to identify an island is first to find its inner C, which can be either an external or an internal C, and then identify all Cs outside this inner one. The inner C is considered as the island generator and is used to represent the set of island-data. Figure 5 schematically shows an example of a layer containing five islands, originated by different situations. Island 5 (I5) is the simplest case because it is formed by the external C1 (I5{C1}). Island 3 (I3) is generated by the internal C2 and is a set of two Cs (I3{C2,C3}). If an external C has multiples internal Cs (not inside each other), each of them will generate islands, which is the case of I1{C8,C10} and I2{C9,C10}. The fact that C10 belongs to two different islands is not an issue in this proposal. If an external C has multiple levels of internal and external Cs, just the inner one will generate an island. This is the case of I4, which is a set of four Cs (I4{C4,C5,C6,C7}).

If a shell (many Cs) is selected, the extra Cs will be also included in the island set and will follow the analysis as any other normal C.

Once the islands are identified, it is possible to take advantage of the fact that the head repositioning must cross all the outside Cs of an island to reach the inner one. In other words, just the inner Cs could be enough to represent the optimization problem. Following this idea, in Fig. 5, there are ten (10) Cs in the layer, but only five (5), which are C1, C2, C4, C8, and C9, are relevant points where the extrusion must jump to. In this way, the problem size is reduced and, as it can be inferred, the

Fig. 5 Example of islands formation



efficiency of this proposal increases as the number of islands formed by a large number of Cs (such as I4 in the example) increases. Later on, in step 3, all Cs of each island will be inserted between the linear path that connects two islands, causing a minimum route deviation.

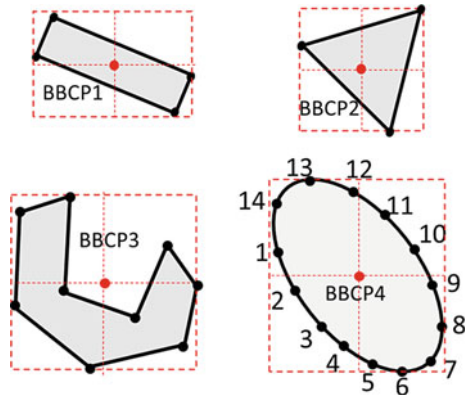
When the intercalated deposition sequence is considered, the island will include the respective CRSs belonging to it. In this way, each island will have a set of Cs and CRSs grouped in a cluster.

All Cs and CRSs within a specific island can be identified and mapped by applying the point in polygon test [19, 20], searching for the inner C and all Cs members of the set. Other important information in the set is the Cs' sorting, indicating the sequence from the inner to the outer one. This can be organized by the quick sort method [21], which compares the maximum X (or Y) coordinates of the C-points of each C in the set. In the example of Fig. 5, after been sorted, I4 will be represented as I4{C4,C7,C5,C6}. How this information can be useful is presented in step 3.

4.1.2 Pruning the Island Points

The problem data can be further reduced by choosing one point to represent the inner C in each island. A simple suggestion is to choose its Bounding Box Center Point (BBCP), as shown in some examples presented in Fig. 6. As a result, all C-points are transformed into just 1 (one) point. In other words, all clusters are transformed in singletons, therefore the problem coincides with the TSP [16]. Other options to represent the inner C have been explored by Weller et al. [14], but not proving to be more efficient than the BBCP. In the example of Fig. 5, only the five (5) BBCPs shown in Fig. 7 will be considered in the second step of the proposed framework. As can be seen, this data pruning is more efficient when the inner C has a large number of C-points. For instance, see BBCP4 in Fig. 6, where 14 points were reduced to 1.

Fig. 6 Examples of calculated Bounding Box Center Points (BBCP)



4.2 Preliminary Sequence of Islands (Step 2)

Even with the problem reduction, if all layers are considered together in the analysis this is still a quite hard problem to solve due to the large number of layers. As mentioned before, an alternative is to consider each layer individually as an open route, and then connecting it to the next layer, and so on. The issue related to different types of layers, pointed out in Sect. 3.4, must be considered at this point. In this case, for each type of layer, the problem can be treated as an OTSP with a fixed start point and either free or fixed endpoint. The home position will be included in the problem only at the last layer as the final destination of the extrusion head or in each cleaning layer.

As the number of points per layer became quite low at this stage, many heuristics can be applied to find a good preliminary sequence of island. The solution found in this step is crucial for the final result because once defined, the sequence of islands will be kept constant. It is worth emphasizing that this sequence obtained is not a

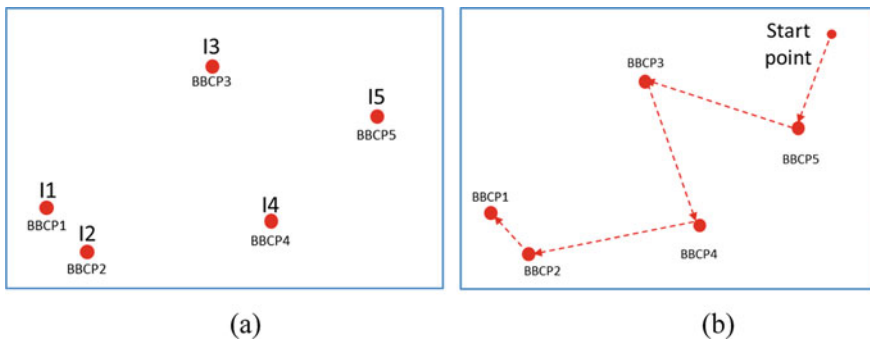


Fig. 7 BBCP of the islands from Fig. 5 (a) and a possible sequence of islands for the first layer (b)

real route, as the extrusion head does not need to go to the BBCP coordinates of each island. Figure 7b shows a possible open sequence of islands for the first layer based on Fig. 5. A feasible C-route must yet to be created in the next step, but this can be done by taking advantage of this sequence of islands.

4.3 Feasible Contour Route (Step 3)

In this step, a feasible C-route is generated based on the preliminary sequence of island generated in step 2. To achieve that, all Cs that were previously removed are brought back to the analysis. The procedure to achieve that can be quite simple because it needs to perform a local search. First, it needs to replace the BBCP for a C-point of the respective inner C and then, include the rest of the Cs of the specific island in the route. Many options can be used to do that, but one low-cost suggestion is to consider three consecutive points of the preliminary sequence of islands at a time. A preliminary route is then created between points one and three, and the cost to include the inner C of the second point (island) is calculated for all its C-points. The lowest cost route corresponds to the C-point to be included in the route. If the island has more than one C, each of them should be included in finding its best point, i.e., the one that will disturb less the route to reach the inner C. At the end of each iteration (island insertion), the analysis moves forward by one island in the sequence and the second island is inserted. This procedure goes on until all islands are included in the route. Any other local search procedure can be used.

Figure 8 schematically shows some of the steps to create a feasible C-route based on the sequence of islands obtained from Fig. 5 and applying the procedure suggested above. It starts by taking the first three consecutive points, i.e., the starting point, BBCP5 and BBCP3 in Fig. 8a, and creating an initial local route between the first and the last point (i.e., the starting point and BBCP3). A local search procedure is then used to include C1 (I5) in this initial local route, which, in this example, was P4(C1) (Fig. 8b). A new local route between P4(C1) and BBCP4 (I4) is established to include C2(I3). To include C3(I3), two options need to be analyzed, when entering the island or when leaving it (Fig. 8c). In the example, P4 (C3) was chosen. For the next island, a local route between P4(C3) and BBCP2(I2) is used to insert C4(I4) as shown in Fig. 8d. And the procedure goes on. If the start point is inside a C, which will be the case of any intermediate layer, then the C insertion will only be considered when leaving the first island.

If the intercalated deposition sequence is used, in each iteration, once the C-point of the inner C is included, the other Cs of the island are included when entering the island. After that, all the CRSs can be included choosing the lowest cost route leaving the island. In this case, step 4 of the framework is not required. The last CRS-point will become the initial point of the next layer and the process is repeated.

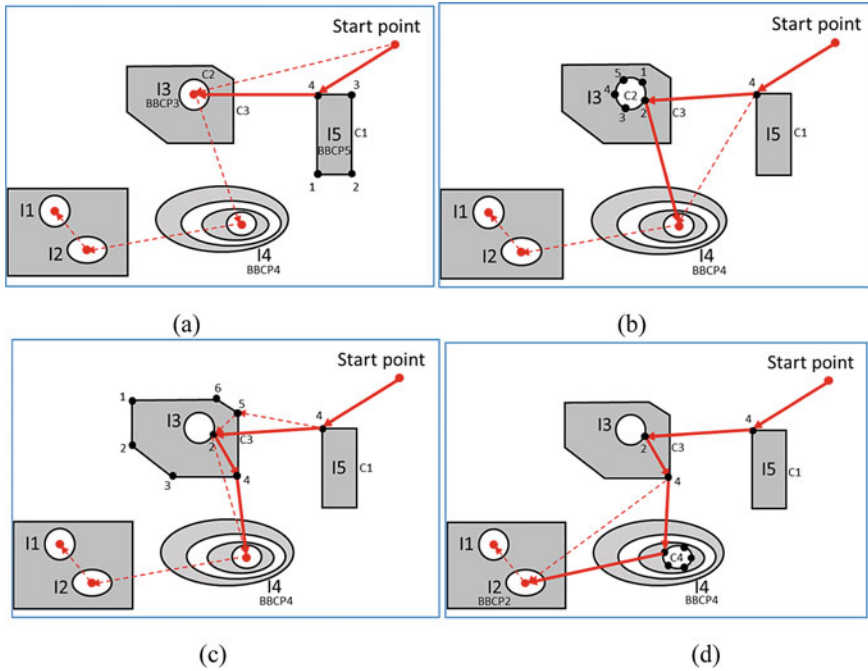


Fig. 8 Procedure to insert the set of Cs to obtain a feasible C-route based on the preliminary sequence of islands. Insert: C1(I5) (a), C2(I3) (b), C3(I3) (c) and C4(I4) (d)

4.4 Continuous Raster Segments Route (Step 4)

If the sequential deposition is chosen, this step 4 is required to create a separated CRS-route. The process will start from the last point of the C-route in each layer. Similar to step 3, many options can be applied here if the sequence of islands (step 2) is considered a good option. Again, a local search procedure can be easily done by following the sequence of island backward to include all CRSs of each island similarly, as suggested in step 3. As each CRS has a pair of points and the entry and exit points are not coincident, both options need to be checked for the lowest cost. If preferred, other heuristics can be used to find a better CRS-route at a relatively low cost, because of the reduced number of points involved, when compared to the C-points.

The last CRS-point to be visited becomes the starting point for the next layer. From this point, the iteration can start repeating step 1, and so on.

5 The Optimization Framework with the Nearest Insertion and 2-OPT Heuristics

The toolpath optimization using the combination of two basic heuristics, the Nearest Insertion (NI) and 2-OPT, in an algorithm called NI2OPT was implemented in the past [2]. The NI heuristic is based on the insertion of a point into an initial linear route which will cause less disturbance to this initial route [17]. It was considered a good option for this open route problem because the initial route can be set pointing to a desired location. This brought some advantages to the analysis because the initial route can easily direct the extrusion head to the home or the cleaning point [2]. In the same work, a Nearest Neighbour Procedure, also known as Greedy heuristic, was used to compare results. The Greedy heuristic creates a route by including the next point as being the closest point to the last stop [17]. Even though it may not yield good results for many cases, it was chosen to compare the methods due to its low computing cost. Only the sequential deposition was implemented in that work [2].

The same NI and 2-OPT heuristics were combined to implement the proposed framework described above, in an algorithm called NI2OPT-F. Without describing the detail of the implementation, which can be found in a recent work [22], it is interesting to point out the time saving achieved with the new implementation. The same 8 (eight) 3D parts chosen in [2] were used to compare the time performance of the methods. These parts represent different deposition path configurations (contours and islands), such as single contours, single contours with holes, multiple contours, multiple contours spread diversely. The parts were sliced with 1000 layers (layer thickness of 0.1 mm) and only one contour was used (no shell). Table 1 presents some information about the parts including the number of Cs, CRSs, and islands considering the 1000 layers processed. To help the analysis, the parts were sorted according to the number of Cs per layer. All details about process parameters can be found in [22].

The CPU time was computed by running the same part 100 times and calculating the average. This assessment was done in a personal computer with Intel 5, 7th generation, processor and 4 Gb memory, running on Windows®10 operating system.

Table 2 presents the results for the CPU time to run with the Greedy, the previous method (NI2OPT) and the new one (NI2OPT-F), and respective time savings.

As can be seen, the time saving achieved by the NI2OPT-F over the previous method is remarkable, yielding similar final routes [22]. The options to reduce the problem size were effective. As expected, the CPU time-saving increases as the number of Cs and C-points increases, and also as the number of islands increases. The reasons for this were discussed in detail in Sect. 4. Unsurprisingly, it is quicker to run the Greedy than the NI2OPT-F method, but the latter can still solve large cases with a better route in a reasonable time (a few seconds). It is expected that, if the proposed framework is implemented with better heuristics, the repositioning distance results will be more expressive [22].

Table 1 Data information of the parts considering 1000 layers

Part	Total number of Cs	Total number of C-points	Total number of CRS-points	Total number of Island
1	6000	333,000	14,000	4000
2	6000	300,000	13,000	4000
3	6000	348,000	15,000	4000
4	9000	450,000	20,000	7000
5	13,000	725,000	15,000	7000
6	14,000	480,000	28,000	8000
7	22,000	792,000	44,000	13,000
8	25,000	772,000	53,000	17,000

Table 2 CPU time for each optimization method (no cleaning)

Part	Greedy	NI2OPT	NI2OPT-F	Time-saving over NI2OPT (%)
	CPU time (s)	CPU time (s)	CPU time (s)	
1	0.21	2.08	1.14	45.2
2	0.18	1.64	0.97	40.9
3	0.21	1.90	1.34	29.5
4	0.37	6.22	2.44	60.8
5	0.83	42.31	5.24	87.6
6	0.55	22.33	4.08	81.8
7	1.48	124.18	10.95	91.2
8	1.47	170.99	14.56	91.5

6 Conclusions

This work presented a framework for tool-path airtime (non-productive time) optimization in material extrusion AM processes. The main idea is to reduce the problem size based on simplifications originated from its observation and understanding. The computational complexity of the optimization problem was reduced by introducing innovative and novel methods to decompose it. This allows to solve larger instances of the problem. The CPU time savings when applying the framework proposal combining two basic heuristics, the Nearest Insertion and 2-OPT, were extraordinary. Additionally, the proposal is generic and suitable for different operational research methods. These are some of the main strengths of the framework.

Due to the simplifications adopted in step 1 and the fixed sequence of islands generated in step 2, the framework does not allow the optimal solution to be obtained. Although good solutions have been found, the impact of these options has yet to be analyzed, comparing it to the optimal solution.

Finally, the importance of having a good and fast tool-path optimization method is paramount in large cases (a large amount of data). The data size might increase due to many aspects, such as intricate part geometry, the number of parts to be produced (production), the number of pieces packed in the same building, and with the process parameters refinement, for instance, the number of layers used. In these cases, even a small reduction in the idle movements can yield a significant time and money-saving.




References

1. 52900:2015 A (2015) Standard terminology for additive manufacturing—general principles—terminology. ASTM Int i:1–9
2. Volpato N, Galvão LC, Nunes LF, Souza RI, Oguido K (2019) Combining heuristics for tool-path optimisation in material extrusion additive manufacturing. *J Oper Res Soc* 0:1–11. <https://doi.org/10.1080/01605682.2019.1590135>
3. Jin Y, He Y, Fu G, Zhang A, Du J (2017) A non-retraction path planning approach for extrusion-based additive manufacturing. *Robot Comput Integr Manuf* 48:132–144. <https://doi.org/10.1016/j.rcim.2017.03.008>
4. Gibson I, Rosen D, Stucker B (2015) Additive manufacturing technologies—3D printing, rapid prototyping, and direct digital manufacturing, 2nd edn. Springer, New York
5. Agarwala MK, Jamalabad VR, Langrana NA, Safari A, Whalen PJ, Danforth SC (1996) Structural quality of parts processed by fused deposition. *Rapid Prototyp J* 2:4–19. <https://doi.org/10.1108/13552549610732034>
6. Han W, Jafari MA, Seyed K (2003) Process speeding up via deposition planning in fused deposition-based layered manufacturing processes. *Rapid Prototyp J* 9:212–218. <https://doi.org/10.1108/13552540310489596>
7. Jin Y, He Y, Fu JZ, Gan WF, Lin ZW (2014) Optimization of tool-path generation for material extrusion-based additive manufacturing technology. *Addit Manuf* 1:32–47. <https://doi.org/10.1016/j.addma.2014.08.004>
8. Zhang Y, Gupta RK, Bernard A (2016) Two-dimensional placement optimization for multi-parts production in additive manufacturing. *Robot Comput Integr Manuf* 38:102–117. <https://doi.org/10.1016/j.rcim.2015.11.003>
9. Wah PK, Murty KG, Joneja A, Chiu LC (2002) Tool path optimization in layered manufacturing. *IIE Trans (Institute Ind Eng)* 34:335–347. <https://doi.org/10.1080/07408170208928874>
10. Weidong Y (2009) Optimal path planning in rapid prototyping based on genetic algorithm. In: 2009 Chinese control and decision conference (CCDC 2009). Institute of Electrical and Electronics Engineers (IEEE), Guilin, pp 5068–5072
11. Castelino K, D'Souza R, Wright PK (2003) Toolpath optimization for minimizing airtime during machining. *J Manuf Syst* 22:173–180. [https://doi.org/10.1016/S0278-6125\(03\)90018-5](https://doi.org/10.1016/S0278-6125(03)90018-5)
12. Woeginger GJ (2003) Exact algorithms for NP-hard problems: a survey. In: Jünger M, Reinelt G, Rinaldi G (eds) *Combinatorial optimization—Eureka, You Shrink!*. Springer, Berlin, Heidelberg, pp 185–207
13. Khan WA, Hayhurst DR, Cannings C (1999) Determination of optimal path under approach and exit constraints. *Eur J Oper Res* 117:310–325. [https://doi.org/10.1016/S0377-2217\(98\)00263-X](https://doi.org/10.1016/S0377-2217(98)00263-X)
14. Weller TR, Weller DR, de Rodrigues LC, Volpato N (2021) A framework for tool-path airtime optimization in material extrusion additive manufacturing. *Robot Comput Integr Manuf* 67:101999. <https://doi.org/10.1016/j.rcim.2020.101999>

15. Iori M, Novellani S (2020) Optimizing the nozzle path in the 3D printing process. *Lect Notes Mech Eng* 912–924. https://doi.org/10.1007/978-3-030-31154-4_78
16. Laporte G, Palekar U (2002) Some applications of the clustered travelling salesman problem. *J Oper Res Soc* 53:972–976. <https://doi.org/10.1057/palgrave.jors.2601420>
17. Bodin LD, Golden BL, Assad AA, Ball MO (1983) Routing and scheduling of vehicles and crews: the state of the art. *Comput Oper Res* 10:63–211. [https://doi.org/10.1016/0305-0548\(83\)90030-8](https://doi.org/10.1016/0305-0548(83)90030-8)
18. Sego LH, Shulman SA, Anderson KK, Wilson JE, Pulsipher BA, Sieber WK (2010) acceptance sampling using judgmental and randomly selected. Oak Ridge, TN, USA
19. Schneider PJ, Eberly DH (2003) Geometric tools for computer graphics. Morgan Kaufmann Publishers, San Francisco, USA
20. Shimrat M (1962) Algorithm 112: position of point relative to polygon. *Commun ACM* 5:434. <https://doi.org/10.1145/368637.368653>
21. Cormen TH, Leiserson CE, Rivest RL, Clifford S (2009) Introduction to algorithms, 3rd edn. MIT Press, Massachusetts, USA
22. Volpato N, Wolter, FN, Minetto, R, da Silva, RD, Weller TR, Rodrigues LC Improving a tool-path optimization method in additive manufacturing by applying an optimization framework. *J Oper Res Soc.* (in preparation)

Metaheuristic Approaches for Modeling and Optimization of FDM Process



Ahmad Aminzadeh , Mohammad Aberoumand,
Davood Rahmatabadi , and Mahmoud Moradi 

Abstract According to the fact that the FDM process has several input parameters that should be optimized toward a zero-defect manufacturing production. In this chapter, at first statistical analysis and mathematical methods used in the design of the experiment and optimizing printing parameters, which are used in FDM printing parameters are defined, and then they are reviewed, discussed and categorized. In this regard, the application of different methods such as statistical modelling, design of experiments (DOEs), Artificial Neural Networks (ANN), Genetic Algorithms (GA), and Hybrid approaches are discussed. In the next section, using the results of researches in this field, they are reviewed on a case-by-case basis and the optimal printing parameters with different conditions, materials and goals are introduced in FDM 3D printing.

A. Aminzadeh

Department of Mathematics, Computer Science and Engineering,
Université du Québec à Rimouski, Rimouski, Québec, Canada
e-mail: ahmad.aminzadeh@uqar.ca

M. Aberoumand · D. Rahmatabadi
School of Mechanical Engineering, University of Tehran, Tehran, Iran
e-mail: m.aberoumand@ut.ac.ir

D. Rahmatabadi
e-mail: d.rahmatabadi@ut.ac.ir

M. Moradi (✉)
School of Mechanical, Aerospace and Automotive Engineering, Faculty of Engineering,
Environment and Computing, Coventry University, Gulson Road, Coventry CV1 2JH, UK
e-mail: moradi@malayeru.ac.ir; moradi.malayeru@gmail.com

Department of Mechanical Engineering, Faculty of Engineering, Malayer University,
Malayer, Iran

1 Introduction

The fused deposition modeling (FDM) technique has been hailed as the widely used method of additive manufacturing (AM) processes in recent years. In this inexpensive and available process, the thermoplastic filament is used as the raw material. By melting filament and extrusion into the heated nozzle, the material and the final design are printed layer by layer on a flat plate. FDM has initially been used as a method for rapid prototyping and mold making, but in recent years due to the use of advanced high-strength filament such as fiber and Nano-particles reinforcement filament and strengthening mechanical properties with various methods, it is considered as a manufacturing method in different industries. One of the main issues for the entry of different techniques into various industries is reducing cost, used materials, and the quality of produced samples. In FDM models, despite the cheapness and availability of equipment, the variety of raw materials, there are also some challenges such as mechanical properties, dimensional accuracy, and manufacturing speed. The main challenge concerning mechanical properties, unsuitable surface roughness, and low dimensional accuracy is a lack of proper bonding between fibers and layers, the presence of cavities, stair-stepping, and voids.

All the mentioned issues and even the printing speed can be achieved significantly by adequately adjusting the printing parameters. In FDM parts, despite the simplicity of working with them, have a lot of complexity to achieve the desired properties, and the most important is the effect of many printing parameters on these goals. Generally, all of the printing parameters are classified into three main categories: extruder geometry, processing, and structural parameters. The most important printing parameters that have been researched and studied by many researchers are diameter and width nozzle, raster and angle, gap, orientation, printing and retraction speed, infill density, pattern, nozzle and bed temperature, thickness layer, and overlapping. For most routine materials such as PLA, ABS, PEEK, PC and etc. the relationship between printing parameters and desired outputs such as strength, toughness, and surface roughness is mostly determined. However, because of the large number of printing parameters, their interaction, and the various goals, they sometimes are set against each other and complicate the setting of the printing parameters. From the industrial perspective, the primary goals are to achieve mechanical properties and higher dimensional accuracy, reducing time and cost. For example, with increasing infill density, dimensional accuracy and mechanical properties increase, but on the other hand, it increases the cost and speed of production, or as the layer thickness increases, the mechanical properties decrease but the stair stepping (surface roughness) increase and the costs decrease with increasing production speed. There are various solutions to this problem. To this end, using modeling and multi-objective optimization methods to predict the behavior of the material and offer a collection of optimal printing parameters can be a good option. Recently, these methods have been used to achieve the range of each printing parameter, especially for new filament materials (raw material for FDM), using less testing and save time and money. Nowadays, many mathematical and

statistical models have been proposed in this field, and the use of these tools has led to the faster growth of the 3D printing process. In FDM printer, due to the wide range of materials used, the utilizing design of experimental methods is essential because the new materials used in this method are expanding day by day and one of the ways to achieve mechanical and multifunctional properties is to use composite filaments reinforced with different metals, ceramics and carbon-based fibers and nanoparticles. In this chapter, the most widely used mathematical and statistical methods are introduced and then previous researches are reviewed aiming to introduce optimum printing parameters in different condition.

2 Design of Experiment (DOE)

The term of the design of experiments (DOE) is associated with the arrange an efficient amount and combination of experiments that required to achieve an optimum solution. Design of experiment is an analysis tool and systematic methodology that permits researchers to determine how inputs affect outputs as well as data collection to well understand a process's nature and condition. According to the fact that in the industrial applications experiment is an extraordinary costly and also time-consuming process. To this end, it is necessary arrangement, analyzing and cause-and-effect relationship to evaluate the elements that control the importance of a factor or collection of factors and manage the number of experiments and select the sufficient one. Therefore, performing practical tests that provide the most information with affordable and economic efficiency is the primary goal of every industry, company, engineer, and academic institution. As a result, as an essential requirement for a method in which the most information about the process can be obtained in the least cost and time, logical conclusions can be presented, and documentary evidence about the process can be obtained. In this regard, DOEs offer is a brilliant solution as a branch of applied statistics and a series of organized experiment investigation by full factorial, all possible mixtures, or fractional factorial, only a portion of the possible mixtures. The effects of systematic changes by considering the input variable on objectives parameters are then estimated. From the practical perspective, the right and thriving application of statistical test design is vital to achieving efficiency, decreasing unpredictability, decreasing delays in designing and developing a product's quality, and thus improving client service. Experimental design methods have three main applications: comparison, screening, and modeling of significant process parameters.

2.1 Response Surface Methodology (RSM)

Due to the nature of the manufacturing operation, there are several complicated parameters with a diverse level so that in order to enhance the production quality, it

is mandatory to apply DOE systematic strategy. Usually, manufacturing companies also work on processes or products where not satisfy by any principles or scientific theory that are straight applicable. From a practical perspective, the optimization tasks are divided into five main section, Randomization, Replication, Blocking, Orthogonality, Factorial experimentation [1]. Typically, in addition to recognizing the parameters that affect the response, there are other goals that we need to model the process to meet. For example, in all additive manufacturing processes, the printing parameters and their interaction in the production of the part are considered in order to reach the remarkable output, including strength, surface roughness. In this respect, there is usually an elaborate association between the printing terms and conditions as well as the desired output characterization. Thus, the most appropriate technique is applied design of experiment techniques to simulate, formulate, and modeling the process then be easily predicted using the model to achieve specific properties such as strength and stiffness. In modeling the process, these goals include; maximize or minimize the response surface and optimize multiple goals. In the optimization, the engineering departments look for efficient variables, which are the aim of the optimum points for each objective function. In statistics science, Response surface methodology (RSM) is a gathering of mathematical techniques for invention optimization between several explanatory variables [2]. Response surface methodology is usually applied together with a factorial design to reduce the cost of experimentation [3–7]. This method has a long history and nowadays has numerous applications in the field of industrial and manufacturing; it is specifically used in combination with finite element models. [8, 9]. In general, In the case of manufacturing and modeling uncertainty, RSM is found to be a good solution. Response surface methods usually include the following stages:

- Experiments need to change the setting to the range of the functioning circumstances where the outcome is optimum.
- In the optimum zone, the experiment needs to fit a more elaborate model between the response and the parameters.
- Some responses may have to be optimized simultaneously.

This method is able to estimate the curvature of the design space. Regarding the approximation of the true input-output function, the following polynomial models were used:

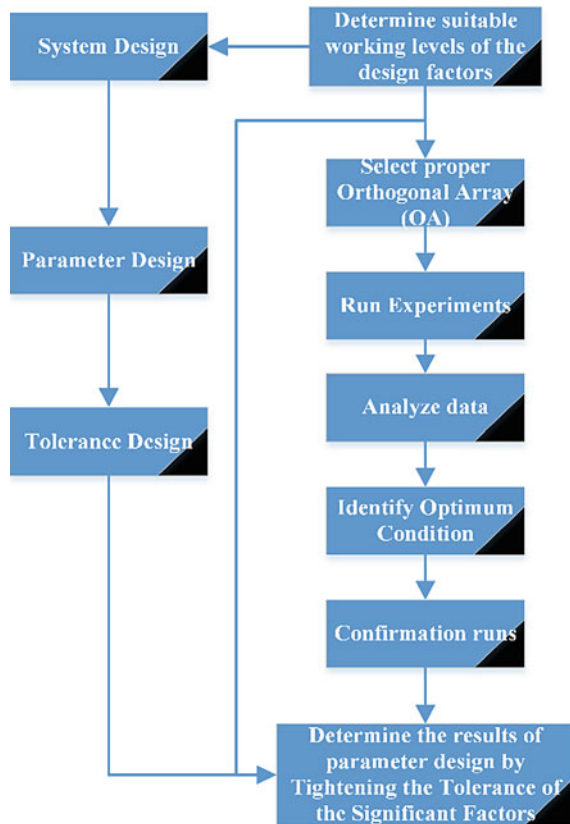
$$\eta = b_0 + \sum_{i=1}^k b_j X_j + \sum_{j=1}^k \sum_{i=1}^k b_{ij} X_i X_j \quad (1)$$

where b_0 , b_j , and b_{ij} are the regression constants with $i, j = 1, 2, \dots, k$ and X_i are the k input variables.

2.2 Taguchi Robust Design

Taguchi method focuses on manufacture economical, efficient, and remarkable production by decreasing the deviation in a process over the rational and powerful design of experiments and simultaneously reduce development interval. Generally, once the middle number of variables (3–50) are considered, this method will design based on the best output so that minimum interactions between input and output parameters are set [10]. In this arrangement, the independent distribution and level among factors are controlled by the elements matrix. To this end, in order to discover the ideal factors, the signal-to-noise ratio (S/N) of each process parameter in each level must be assessed for all outputs function. Then, the optimal level has the highest S/N value indicates. The standards ratio is demonstrated to define the problem criteria is maximization (Eq. (2), SNL) or (minimization (Eq. (3), SNS) objective. Where stands n and Y_i is the number of repeat observations and the response value, respectively. For instant, an orthogonal array with L18 (36) tests means it is necessary to do eighteen experiments, which are six factors with three

Fig. 1 Taguchi design procedure



levels (36). However, Taguchi's robust method will be suggested for an efficient number of experiments (18 runs). Figure 1 illustrates the procedure of the Taguchi design.

$$SN_L = -10 \log \left[\frac{1}{n} \sum_{i=1}^n \frac{1}{y_i^2} \right] \quad (2)$$

$$SN_S = -10 \log \left[\frac{1}{n} \sum_{i=1}^n y_i^2 \right] \quad (3)$$

3 Industrial Artificial Intelligence

In the modern world, human life deal with several new expressions like Blockchain, cyber manufacturing, Internet of things (IoT), Artificial Intelligence (AI), and Industry 4.0 that is gradually used. In this regard, big data in manufacturers is becoming a vital point for improving manufacturing competitiveness and make a new strategy for product lifecycle management. Actually, this revolution is having an enormous influence on today's existing production systems and the economy. Among them, combine Artificial Intelligence (AI), and industry 4.0 is an intellectual science to enables human to discover numerous brilliant methods to model our reasoning and sensing manufacturing process. Actually, the AI method is divided into two major sections, symbolic learning and machine learning. The first method, symbolic learning, is the pioneer of smart systems that based on symbolic computer science assumption. On the other hand, deep learning as a pinnacle of AI method that works with complex data and a wide verity of input factors. Form the deep learning point of view, the most powerful strategy in order to design the parameter distribution is Convolution Neural Network (CNN) [11], Recurrent Neural Networks (RNN) [12], Long Short-Term Memory (LSTM) [13], and Reinforcement Learning [14]. In the scope of manufacturing, several options are available based on the priority of production, limitation, and customer service. Generally, industrial AI is logical self-control to support engineers to systematically improve and deploy AI algorithms with repeating and then success. For such unique manufacturing works, AI is the core-driving engine of 5C- architecture (Connection, Conversion, Cyber, Cognition, and Configure) and is fully utilized through implementation and adaptation of Industrial AI [15]. Currently, among the artificial intelligence (AI) methods, the most significant well-known algorithms in manufacturing science are fuzzy logic systems [16], artificial neural networks [17], particle swarm optimization [18], genetic algorithm [19], colony optimization [20], simulated annealing [21], and evolutionary computing [22].

Regarding the combination of 3D printing and AI, it is still developing and getting more important every day that is increased the performance of a 3D printer by facilitating automated production and reducing the risk of error. Our research is

revealed how these two can come together in order to reach an adequate level of precision in the additive manufacturing process. In addition, trial and error approaches are not a fast enough solution or sustainable since AM contains several and elaborate input parameters to be controlled and monitored during the process. In that case, to enhance print efficiency and economic savings by using generative design and testing in the pre-fabrication stage, machine learning is currently being used to solve this problem. By doing so, this reconstruction is based on the training gained from previous results that have effectively integrated additive manufacturing and AI. For instance, automation of the 3D printing workflow, broaden the range of compatible materials, optimizing the 3D printing process, improving efficiency in the prototype phase, real-time monitoring, damage and defect detection, and production maintenance, especially in the aerospace sector. It is strongly believed that this study will work as a roadmap and guideline for researchers and industries towards the real-world implementation of Industrial AI. In the following paragraph, the significant strategies for machine learning will be discussed.

3.1 Artificial Neural Network (ANN)

Artificial Neural Networks (ANNs) as a core part of AI, are built like the animal brains that computing systems with neuron nodes interconnected like a web could transfer a signal to other neurons are called edges [23]. An ANN is formed based on two main parts, processing elements (PE) or neurons connection and a weight value, which establish the neural network construction and are arranged layer by layer. Naturally, neurons are gathered into layers, and this benefit can be estimated altogether, thereby acquisition massive information and improve the processing speed. There are several layers, the input layer and the output layer, in a complex network that transmit the signals in a diverse orientation; these layers could be hidden layers. Distillation layer or hidden layers are the significant features/patterns from the input layer, removing the dismissed information and forwards those features to the next layer for improving the decision. Figure 2 displays biological and artificial neurons and also a noticeable similarity between the two types of neurons. Moreover, backpropagation, backward propagation of error, as a brilliant strategy to achieve more accurate output, is applied in some complex processes like laser material processing and smart manufacturing system. To put in other words, the data are connected from the output units to the input units to modify the weight of its associates between the units. In the concept of smart manufacturing, there are diverse classifications such as multi-scale dynamic modelling, strong cybersecurity, intelligent automation, and simulation, as well as networked sensors in which AI plays a vital role as a powerful simultaneous solution. Obviously, big data processing capabilities, which are collected by industrial connectivity devices and services, and advanced robotics, is a core of this mechanism. To more specific, numerous applications of ANNs can be brief into pattern recognition, modeling, real-time monitoring, and prediction.

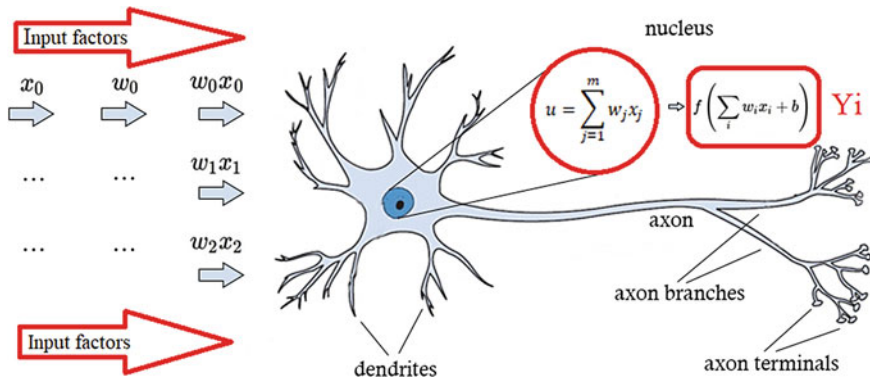


Fig. 2 Principle of a neuron calculation

According to Fig. 2, the main mechanisms of the neural network are neurons, connections, and the learning algorithm, where a neuron (j) is the elementary processing unit of a NN. All neurons in the network take several inputs (xi) and make an output (yi). It worth mentioning that outputs could be either input to additional neurons or output to the outside of NNs. Any association between two neurons(kj) has a weight (wkj) or weighting factor, which is absolutely essential in the computing process and solution time. From a mathematical perspective, the value of a single neuron could be calculated based on formulas from the following equations [24].

$$u = \sum_{j=1}^m w_j x_j \tag{4}$$

$$V = u + b \tag{5}$$

$$y = \varphi(v) \tag{6}$$

The term of x is a neuron with m inputs and one output y(x), and \$w_j\$ are weighted defining as for each input, which is weighted, and \$\varphi\$ is an activation function to define the non-linearity of the neural network.

3.2 Genetic Algorithm (GA)

Genetic algorithms (GAs) as an eventual method in the mathematical optimization or programming was suggested by Holland [24] as a concept of appropriate genetic processes that proved reasonably fast and robust in finding reasonable solutions and optimization technique. This method successfully has been used to a wide variety of real-world complications of significant elaborate. Nowadays, GA has been

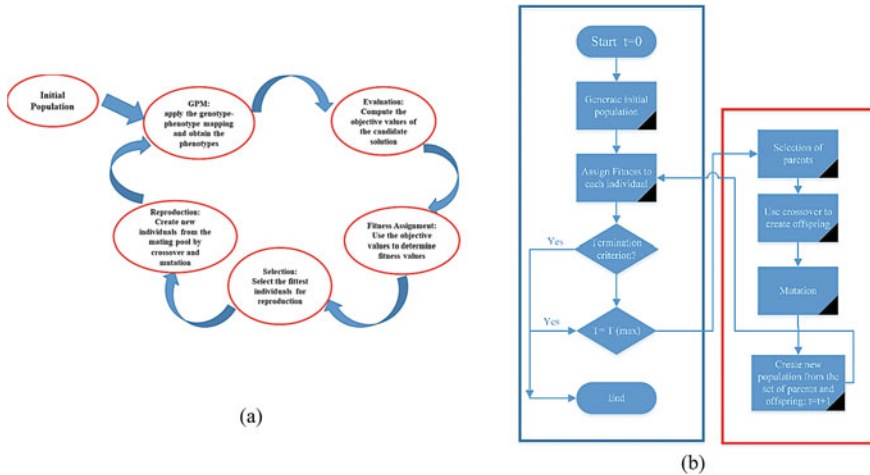


Fig. 3 The systematic procedure of (a) basic cycle of EAs and (b) Genetic algorithm [25]

developed as one of the main fast-growing areas of big data collection and informatics fields, especially in the manufacturing process. The basic construction of the eventual method is illustrated in Fig. 3. Generally, there are two main steps to deal with in eventual methods. Firstly, generate the initial population of individuals randomly. Second, repeat the following procedure:

- Evaluation of the fitness
- Selection of the fittest parents
- Breed new individuals
- Substitute with new individuals once.

As a significant advantage of GA, it could be applied in order to find the optimum condition for complex problems which is possessed ‘bad’ characteristics by manipulating a population and training the good enough response and performs their search for better output. By discovering all areas of the solution, space, and manipulating favorable zones, GAs is solved linear and non-linear problems [29].

3.3 Hybrid Methods

Nowadays, computer science engineering offers a new concept of optimization as a hybrid method, which is able to mix different methods from different categories to solve a complex problem in engineering and business plans. These methods could be suggested for the optimization of other process parameters and precise prediction and also outcomes for any industrial and academic applications. Figure 4, shows one of the excellent mixtures of hybrid optimization. In the following paragraph, the most significant sectors in manufacturing technology will be discussed.

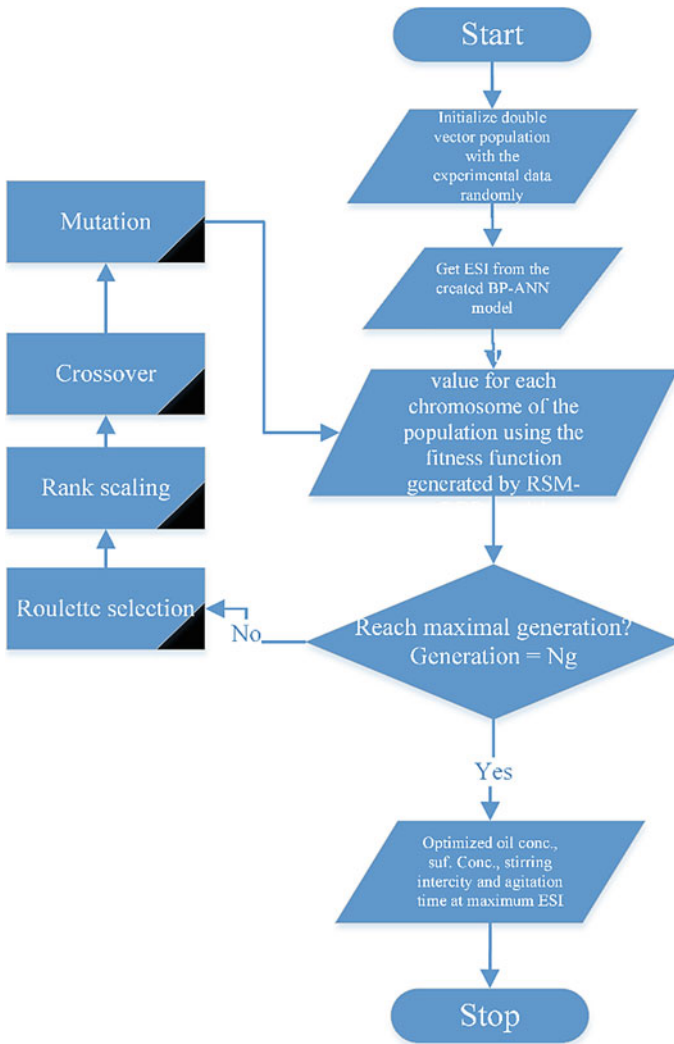


Fig. 4 Hybrid algorithm genetic configuration; (ANN-GA [GA], BP-ANN and [RSM-BBD])

3.3.1 GA-RSM

Based on the literature, one of the successful combinations between a statistical and Evolutionary method is GA-RSM. There are five steps in order to generate a GA-RSM model [26]:

1. Selection of random population.
2. Definition of the range of process parameters.

3. Using the RSM equation to create the Fitness function for GA.
4. Using a mutation to create a new population.
5. Finally, getting the optimum process parameters in the acceptable range of fitness function and the chromosomes.

3.3.2 GA-ANN

As mentioned before, based on Darwinian fight law for survival and natural biological evolution, one of the novel biological inspired intelligence techniques is proposed as Genetic algorithm (GA). This novel method is strongly recommended by scholars for solving the complex process parameters. In contrast, designing and train set in the Artificial Neural Network (ANN) is as another inspiring biological system is problematic and complicated. To this end, recently, some researchers proposed a novel approach to the combination of these methods as well know universal function approximates (GA-NNA) (Fig. 5). The main benefit of this configuration is a resolved network developed with the most acceptable weights would be able to yield the output with predicted accuracy comparable [26–28].

3.3.3 GA-ANFIS

Adaptive Neuro-Fuzzy Inference System (ANFIS) is a novel solution for the “black box” issue in Artificial Neural Networks (ANNs); also, it could be affected in a broader range of real-world applications. This brilliant idea is a mixture of artificial intelligence (AI) and the fuzzy system, which has the benefits of both

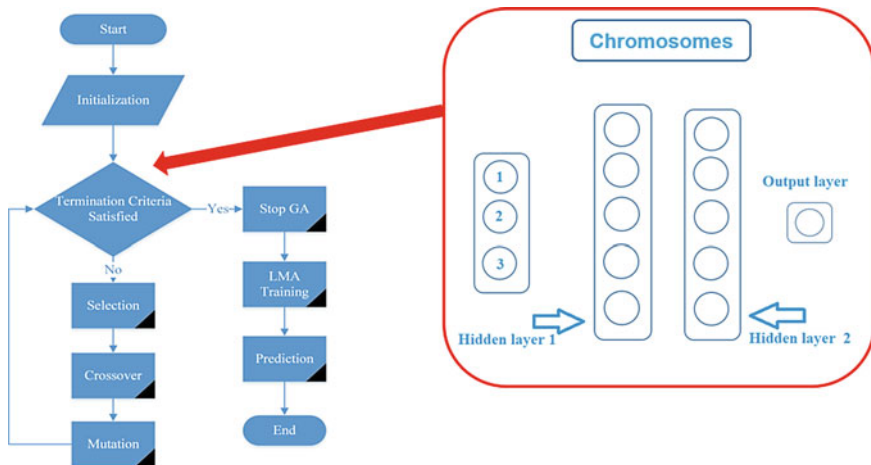


Fig. 5 Artificial neural network and genetic algorithm hybrid technique [28]

simultaneously. Generally, ANFIS network builds on five main phases, involving input fuzzification, applying the fuzzy methodology, application system, data gathering, and defuzzification [29]. In that case, an association between inputs and response are generated by the fuzzy part. On the other hand, the neural network training algorithms will create a relationship between parameters. Again, GA-ANFIS is also a hybrid method for statistical modelling where ANFIS carries out the task of data training, followed by its Genetic Algorithm [26]. In fact, the nominal rate of the error verifies the accurate training model performance.

4 FDM Challenges

In the FDM process for the production of the final part, there are usually several fundamental challenges, which can be summarized as anisotropy, low mechanical properties, surface roughness and manufacturing time. Each of these challenges is strongly influenced by the printing parameters, and with the right choice, the desired properties can be considered. Therefore, in most of the work done, the goal is to improve one or more of these challenges while adjusting the print parameters. As long as the effect of printing parameters on these challenges is the same and improves all of them in a specific direction or the goal is to consider only one of them, the task is simple and according to knowing the effect of printing parameters on the target, they can be selected and adjusted. For example, by reducing the layer thickness, better mechanical properties are obtained for the final parts of all filament polymers in FDM, and as long as the goal is only mechanical properties, as mentioned, the task is simple. But when consumables, geometric complexity, surface roughness are also added to our goals, the choice of this one parameter becomes more complicated because as the layer thickness decreases, the consumables and manufacturing time increase sharply. However, in the FDM process, the number of printing parameters is large, and most of them also affect the printing challenges. Therefore, the selection of printing parameters by considering the interaction between them and considering all the objectives requires optimal selection, and this is necessary for most materials, especially new materials are used in FDM. In Table 1, some of these researches are categorized according to the studied parameters, materials, design of experiment and optimization methods, and final objectives. In the following, in order to study more accurately and in more detail, we will review the effect of print parameters on each of the printing challenges and describe them on a case-by-case basis.

4.1 *Surface Roughness*

Khan and Mishra studied the role of printing parameters and post-processing on the surface roughness of parts produced by FDM, comprehensively and experimentally

Table 1 Summary of printing parameters and influence on the mechanical characterization

Material	First author	Inputs	Levels	Outputs	Optimization method	Reference
ABS	Wankhede	Layer thickness (mm) Infill density (%) Support style	0.254, 0.3302 High, low Smart, Sparse	Build time Surface roughness	Taguchi	[30]
ABS	Khan	Raster width (mm) Air gap (mm) Raster angle (°) Surface	0.3556, 0.5306, 0.7306 0, 0.05, 0.1 0, 45, 90 Flat, Curved, Inclined	Surface roughness	Taguchi	[31]
ABS	Dev	Orientation (°) Layer thickness (mm) Infill density (%)	0, 45, 90 0.2, 0.3, 0.4 20, 50, 80	Compressive strength Consumables	NSGA-II	[32]
ABS	Srinivasan	Layer thickness (mm) Infill density (%) Infill pattern	0.1, 0.15, 0.2 60, 70, 80 Cubic, Triangular, Grid	Tensile strength	CCD-RSM	[33]
ABS	Al-Ghamdi	Layer thickness (mm) Printing speed (mm/min) Infill density (%)	0.2, 0.5, 0.8 20, 50, 80 20, 60, 100	Build time Consumables Absorb energy	CCD-RSM	[34]
PC/ABS	Mohamed	Layer thickness (mm) Raster angle (°) Air gap (mm) Orientation (°) Number of contours Raster width (mm)	0.1270, 0.1778, 0.240, 0.3302 0, 15, 30, 45, 60, 90 0, 0.1, 0.2, 0.3, 0.4, 0.5 0, 30, 45, 60, 75, 90 1, 3, 5, 7, 8, 10 0.4572, 0.4814, 0.5056, 0.5298, 0.5540, 0.5782	Dynamic flexural strength Build time Consumables	Q-optimal-RSM	[35]
PC/ABS	Mohamed	Layer thickness (mm) Raster angle (°) Air gap (mm) Orientation (°)	0.1270, 0.1778, 0.240, 0.3302 0, 15, 30, 45, 60, 90 0, 0.1, 0.2, 0.3, 0.4, 0.5 0, 30, 45, 60, 75, 90	Toughness Storage modulus Loss modulus	FFD	[36]

(continued)

Table 1 (continued)

Material	First author	Inputs	Levels	Outputs	Optimization method	Reference
PLA	Sandeep	Number of contours Raster width (mm) Nozzle temperature (°C) Infill density (%) Printing speed (mm/s)	1, 3, 5, 7, 8, 10 0.4572, 0.4814, 0.5056, 0.5298, 0.5540, 0.5782 190, 200, 210 20, 60, 100 50, 100, 150	Tensile strength	GA-RSM GA-ANN GA-ANFIS	[26]
ABS	Samykano	Layer thickness (mm) Raster angle (°) Infill density (%)	0.35, 0.4, 0.5 45, 55, 65 40, 60, 80	Tensile strength Yield strength Elongation Toughness	RSM	[37]
ABS	Chin Ang	Air gap (mm) Raster width (mm) Orientation (°)	0, 1.27 0.305, 0.98 0, 90	Yield strength Compressive strength Porosity	RSM	[38]
ABS	Rayegani	Orientation (°) Air gap (mm) Raster angle (°) Raster width (mm)	0, 90 -0.0025, 0.5588 0, 45 0.2034, 0.5588	Tensile strength	GMDH	[39]
ABS	Sood	Layer thickness (mm) Orientation (°) Air gap (mm) Raster angle (°) Raster width (mm)	0.1270, 0.1780, 0.2540 0, 15, 30 0, 0.0040, 0.0080 0, 30, 60 0.4064, 0.4564, 0.5064	Tensile strength Impact strength Flexural strength	CCD-RSM	[40]
ABS/Cu	Nabipour	Nozzle temperature (°C) Raster angle (°) Nozzle diameter (mm) Layer thickness (mm)	230, 240, 250 +45/-45, 0/90, 30/60 0.5, 1, 1.5 0.1, 0.2, 0.3	Build time Tensile strength Density	Taguchi	[41]

(continued)

Table 1 (continued)

Material	First author	Inputs	Levels	Outputs	Optimization method	Reference
PLA	Moradi	Nozzle temperature (°C) Infill density (%) Layer thickness (mm)	190, 200, 210, 220, 230 10, 20, 30, 40, 50 0.1, 0.15, 0.2, 0.25, 0.3	Tensile strength Density Build time Elongation	RSM-CCD	[42]
PLA	Yang	Nozzle temperature (°C) Printing speed (mm/s) Nozzle diameter (mm) Layer thickness (mm)	200, 215, 230 20, 30, 40 0.2, 0.4, 0.6 0.1, 0.2, 0.3	Build Time Tensile strength Surface roughness	CCD-RSM	[43]
Bronze PLA	Moradi	Nozzle temperature (°C) Infill density (%) Layer thickness (mm)	190, 205, 220, 235, 250 15, 25, 35, 45, 55 0.15, 0.25, 0.35, 0.45, 0.55	Tensile strength Density Build time Elongation Fracture mechanism	CCD-RSM	[44]
PETC ABS PETC/ABS	Yadav	Nozzle temperature (°C) Layer thickness (mm)	210–240 0.05–0.14	Tensile strength	ANFIS	[45]
PEEK	El Magri	Nozzle temperature (°C) Printing speed (mm/s)	380, 390, 400, 410, 420 20, 30, 40	Tensile strength Elongation	RSM	[46]
Nylon	Kamoona	Air gap (mm) Raster angle (°) Orientation (°)	0, 0.1, 0.2 0, 30, 60 0, 45, 90	Flexural strength	RSM-FCCD	[47]
Nylon	Ramesh	Printing speed (mm/s) Infill density (%) Layer thickness (mm)	60, 65, 70 50, 75, 100 0.1, 0.2, 0.3	Tensile strength Flexural strength Impact strain Hardness	Taguchi	[48]

[31]. They used Taguchi and face-centered central composite design (FCCD) for design of experiment and relation between inputs and outputs, respectively [31]. Also, the printed specimens were manufactured via three different flat, curved and inclined geometry for both printing and post processing parameters. In this regard, air gap (0, 0.05 and 0.1 mm) raster angle (0, 45 and 90) and raster width (0.3556, 0.5306 and 0.7306 mm) as printing parameters. The smoothing involved spraying ABS solvent vapor (acetone) and the selected parameters were temperature (50, 60 and 70), time (10, 20 and 30 s) and cycle (one, two and three) [31]. The results show that all of the variable parameters for three surfaces were different. The optimum raster angle, raster width and air gap for curved surface were predicted in 37, 0.5102 mm and 0.02 mm, respectively [31]. These parameters for flat surface were calculated 10, 0.2832 mm and 0.05 mm and for inclined surface were predicted 8, 0.6213 mm and 0.02 mm, respectively. Also, as expected, the minimum and maximum amount of surface roughness in optimal conditions were calculated for flat and inclined surfaces, respectively [31]. The results are classified in Table 2.

Wankhede et al. studied the influence of three factors of infill density, layer thickness, and support style on the surface roughness and build time of ABS FDM samples. The ANOVA analysis showed that layer thickness has a leading role in build time (84.62%) and surface roughness (94.19%), respectively, but the support style has almost no effect on the outputs [30]. In summary, the main results are shown in Table 3.

4.2 Mechanical Properties

Deshwal and et al. comprehensively used three hybrid algorithms (GA-ANFIS, GA-ANN and GA-RSM) to find the optimum printing factors with the aim of

Table 2 Summary effect of printing and post processing factors on the surface roughness [31]

Surface	Optimized printing parameters			Optimized post processing			Surface roughness (µm)
	Raster angle (°)	Raster width (mm)	Air gap (mm)	Temperature (°)	Time (s)	Cycle no. (Magnitude)	
Flat	10	0.2832	0.05	63	15	2	0.526
Inclined	8	0.6213	0.02	46	15	1	1.824
Curved	37	0.5102	0.02	53	18	1	0.74

Table 3 Contribution of printing parameters on the surface roughness and build time [30]

Output	Contribution of printing parameters (%)		
	Layer thickness	Infill density	Support style
Surface roughness (µm)	94.19	0.60	3.02
Build time (s)	84.62	6.29	0.70

Table 4 Evaluation of accuracy of different hybrid method on the predicted tensile strength [26]

S. No	Optimization tools/method	Optimized printing parameters			Predicted UTS (MPa)	Experimental UTS (MPa)	Accuracy (%)
		Infill density (%)	Speed (mm/s)	Temperature (°C)			
1	Testing	100	100	210	–	45.27	–
2	GA-RSM	99.998	121.0404	209.656	45.66	45.34	99.30
3	GA-ANN	100	124.778	210	47.0724	47.0212	99.89
4	GA-ANFIS	100	116.322	203.585	46.4088	46.2012	99.55

increasing tensile strength for PLA parts. They also used CCD RSM, to combine parameters (temperature, infill density and printing speed) and modeling. The results of their work are summarized in Table 4 [26].

Recently, the influence of three factors, such as layer thickness, infill density and infill pattern for ABS samples was investigated using the statistical method of CCD of RSM, which showed that increasing the infill density and decreasing the layer thickness increases the strength, respectively. Also, the highest strength was obtained for triangular, cubic, and grid patterns, respectively [33]. Dev and Sirvasta investigated the influence of three printing parameters like infill pattern, layer thickness, and built orientation in three levels for ABS filament by FDM. They used Taguchi for design of experiment and empirical modeling and then the obtained model was optimized by NSGA method [32]. Finally, the authors suggest that to achieve higher mechanical properties while saving material, use 80% density, minimum layer thickness and medium to maximum construction angle.

4.3 Build Time and Volume of Material

Typically, the effect of layer thickness (four levels, 0.1270–0.3302 mm), raster angle (six levels, 0–90), build orientation (six levels, 0–90), raster width (six levels, 0.4572–0.5782 mm), number of contours (six levels, 1–10), and (air gap six levels, 0–0.5 mm) on the dynamic properties, build time and used materials experimentally and statistically with Q-optimal RSM. In that case, all parts were printed with PC/ABS filament. They used the perturbation diagram to find the effect of the parameters considered at the design points on the output to define the influence of each factor separately. The results showed a strong influence of layer thickness on fabrication time and air gap on material volume, and the gradual and continuous increase effect the number of contours of the outer layers on both output parameters. Also, were used cube diagram shows the role of interaction between three main parameters on the outputs. In short, it proved that as layer thickness increases: the flexural modulus at first decreases and then increases, build time severely decreased, and the volume of material slightly decreases. As the air gap increases,

Table 5 Investigations focused on the influence of various printing factors on the flexural strength, build time and volume of uses materials [35]

Output	Optimized printing parameters						Predicted	Experimental	Error (%)
	Layer thickness (mm)	Air gap (mm)	Raster angle	Raster width	Build orientation	Number of contours (no.)			
Build time	0.254	0.499	2.66×10^{-5}	0.484	3.39×10^{-5}	7	6.014	6	-0.233
Volume of material							1.595	1.621	1.604
Flexural modulus							640.768	639.301	-0.229

the flexural modulus decreases, the volume of material and build time severely decreases. By increasing the number of contours, the flexural modulus severely increases, build time increases and the volume of material slightly increased. For this reason, they used multi-objective optimization to achieve the most optimal factors and reported them: layer thickness 0.254 mm, raster angle 2.66×10^{-5} , build orientation 3.39×10^{-5} , raster width 0.484 mm, 0.4572–0.5782 mm, number of contours 7, and 0.499 mm air gap mm [35]. The results are summarized in Table 5.

5 Conclusion

In the FDM process for the production of the final part, there are usually several basic challenges, such as mechanical properties, surface roughness, the volume of used material and manufacturing time. Each of these challenges is strongly influenced by the printing parameters, and the interaction between these parameters complicates the selection and manipulation of parameters. Using outdated methods such as right and wrong also requires a lot of time and materials due to a large number of parameters. To this end, the use of optimization methods to consider the challenges of printing to set them, more importantly, the use of parts produced by FDM in different industries is necessary. In this chapter, first, the DOE, Taguchi, AI methods and its work process were introduced and then the researches in this field were categorized. In short, the influence of all printing parameters on the properties of the final parts is undeniable, and by fine-tuning the parameters, the desired properties can be approached, which requires the use of appropriate modeling and optimization methods.

References

1. Telford JK (2007) A brief introduction to design of experiments. Johns Hopkins APL Tech Dig (Applied Phys Lab 27:224–232
2. Moradi M, Abdollahi H (2018) Statistical modelling and optimization of the laser percussion microdrilling of thin sheet stainless steel. *Lasers Eng* 40:375–393
3. Aminzadeh A, Parvizi A, Moradi M (2020) Multi-objective topology optimization of deep drawing dissimilar tailor laser welded blanks; experimental and finite element investigation. *Opt Laser Technol* 125. <https://doi.org/10.1016/j.optlastec.2019.106029>
4. Moradi M, KaramiMoghadam M (2019) High power diode laser surface hardening of AISI 4130; statistical modelling and optimization. *Opt Laser Technol* 111:554–570. <https://doi.org/10.1016/j.optlastec.2018.10.043>
5. Moradi M, Salimi N, Ghoreishi M et al (2014) Parameter dependencies in laser hybrid arc welding by design of experiments and by a mass balance. *J Laser Appl* 26:022004. <https://doi.org/10.2351/1.4866675>

6. Moradi M, Arabi H, Shamsborhan M (2020) Multi-objective optimization of high power diode laser surface hardening process of AISI 410 by means of RSM and desirability approach. *Optik (Stuttg)* 202:163619. <https://doi.org/10.1016/j.ijleo.2019.163619>
7. Moskowitz HR, Maier A (2007) Response Surface Methodology and Consumer-Driven Product Optimization. In: *Accelerating New Food Product Design and Development*. pp 297–349
8. Mäkelä M (2017) Experimental design and response surface methodology in energy applications: A tutorial review. *Energy Convers Manag* 151:630–640
9. Mago J, Kumar R, Agrawal R, et al (2020) Modeling of Linear Shrinkage in PLA Parts Fabricated by 3D Printing Using TOPSIS Method. In: *Advances in Additive Manufacturing and Joining*. Springer, pp 267–276
10. Sheesley JH, Taguchi G, Elsayed E, Hsiang T (1990) Quality Engineering in Production Systems. *Technometrics* 32:457. <https://doi.org/10.2307/1270138>
11. Huang W, Qiao Y, Tang X (2014) Robust scene text detection with convolution neural network induced MSER trees. In: *Lecture Notes in Computer Science (including subseries Lecture Notes in Artificial Intelligence and Lecture Notes in Bioinformatics)*, pp 497–511
12. Graves A, Fernández S, Schmidhuber J (2007) Multi-dimensional recurrent neural networks. In: *International conference on artificial neural networks*, pp 549–558
13. Graves A (2012) Long short-term memory. In: *Supervised sequence labelling with recurrent neural networks*. Springer, pp 37–45
14. Jaśkowski W, Lykkebø OR, Toklu NE, et al (2018) Reinforcement Learning to Run... Fast. In: *The NIPS'17 Competition: Building Intelligent Systems*. Springer, pp 155–16
15. Lee J, Singh J, Azamfar M (2019) Industrial Artificial Intelligence. *J Intell Maint Syst*, 1–10
16. Kacprzyk J, Pedrycz W (2015) Springer handbook of computational intelligence. Springer
17. Gupta N, Khosravy M, Patel N, et al (2020) Evolutionary Artificial Neural Networks: Comparative Study on State-of-the-Art Optimizers. In: *Frontier Applications of Nature Inspired Computation*. Springer, pp 302–318
18. Khosravy M, Gupta N, Patel N, et al (2020) Particle swarm optimization of morphological filters for electrocardiogram baseline drift estimation. In: *Applied nature-inspired computing: algorithms and case studies*. Springer, pp 1–21
19. Katoch S, Chauhan SS, Kumar V (2020) A review on genetic algorithm: past, present, and future. *Multimed Tools Appl* 1–36
20. Price A, Joyce T, Herrmann JM (2020) 3 Ant colony optimization and reinforcement learning. *Comput Intell Theor Adv Adv Appl* 3:45
21. Suman B, Kumar P (2006) A survey of simulated annealing as a tool for single and multiobjective optimization. *J Oper Res Soc* 57:1143–1160
22. Hogarty DT, Su JC, Phan K et al (2020) Artificial Intelligence in Dermatology—Where We Are and the Way to the Future: A Review. *Am J Clin Dermatol* 21:41–47
23. Konar A (1999) *Artificial Intelligence and Soft Computing: Behavioural and Cognitive Modeling of the Human Brain*. CRC press
24. Goldberg DE, Holland JH (1988) Genetic Algorithms and Machine Learning. *Mach Learn* 3:95–99
25. Gregor M, Krajčovič M, Hnát J, Hančinsky V (2015) Genetic algorithms in the design and planning of production system. In: *Annals of DAAAM and Proceedings of the International DAAAM Symposium*. DAAAM International Vienna, pp 494–500
26. Deshwal S, Kumar A, Chhabra D (2020) Exercising hybrid statistical tools GA-RSM, GA-ANN and GA-ANFIS to optimize FDM process parameters for tensile strength improvement. *CIRP J Manuf Sci Technol*. <https://doi.org/10.1016/j.cirpj.2020.05.009>
27. Kumar V, Chhabra D, Shukla P (2017) Xylanase production from *Thermomyces lanuginosus* VAPS-24 using low cost agro-industrial residues via hybrid optimization tools and its potential use for saccharification. *Bioresour Technol* 243:1009–1019. <https://doi.org/10.1016/j.biortech.2017.07.094>
28. El-Dahshan E, Radi A, El-Bakry MY (2008) Artificial neural network and genetic algorithm hybrid technique for nucleon-nucleon collisions. *Int J Mod Phys C* 19:1787–1795. <https://doi.org/10.1142/S0129183108013382>

29. Termeh SVR, Khosravi K, Sartaj M et al (2019) Optimization of an adaptive neuro-fuzzy inference system for groundwater potential mapping. *Hydrogeol J* 27:2511–2534. <https://doi.org/10.1007/s10040-019-02017-9>
30. Wankhede V, Jagetiya D, Joshi A, Chaudhari R (2019) Materials Today: Proceedings Experimental investigation of FDM process parameters using Taguchi analysis. *Mater Today Proc* 27:2117–2120. <https://doi.org/10.1016/j.matpr.2019.09.078>
31. Khan MS, Mishra SB (2020) Minimizing surface roughness of ABS-FDM build parts: An experimental approach. *Mater Today Proc* 26:1557–1566. <https://doi.org/10.1016/j.matpr.2020.02.320>
32. Dev S, Srivastava R (2020) Experimental investigation and optimization of FDM process parameters for material and mechanical strength. *Mater Today Proc* 26:1995–1999. <https://doi.org/10.1016/j.matpr.2020.02.435>
33. Srinivasan R, Pridhar T, Ramprasath LS, et al (2020) Prediction of tensile strength in FDM printed ABS parts using response surface methodology (RSM). In: *Materials Today: Proceedings*. Elsevier Ltd, pp 1827–1832
34. Al-Ghamdi KA (2019) Sustainable FDM additive manufacturing of ABS components with emphasis on energy minimized and time efficient lightweight construction. *Int J Light Mater Manuf* 2:338–345. <https://doi.org/10.1016/j.ijlmm.2019.05.004>
35. Mohamed OA, Masood SH, Bhowmik JL (2016) Mathematical modeling and FDM process parameters optimization using response surface methodology based on Q-optimal design. *Appl Math Model* 40:10052–10073. <https://doi.org/10.1016/j.apm.2016.06.055>
36. Mohamed OA, Masood SH, Bhowmik JL et al (2016) Effect of Process Parameters on Dynamic Mechanical Performance of FDM PC/ABS Printed Parts Through Design of Experiment. *J Mater Eng Perform* 25:2922–2935. <https://doi.org/10.1007/s11665-016-2157-6>
37. Samykan M, Kanagaraj G, Selvamani SK et al (2019) Mechanical property of FDM printed ABS: influence of printing parameters. *Int J Adv Manuf Technol* 102:2779–2796. <https://doi.org/10.1007/s00170-019-03313-0>
38. Ang KC, Leong KF, Chua CK, Chandrasekaran M (2006) Investigation of the mechanical properties and porosity relationships in fused deposition modelling-fabricated porous structures. *Rapid Prototyp J* 12:100–105. <https://doi.org/10.1108/13552540610652447>
39. Rayegani F, Onwubolu GC (2014) Fused deposition modelling (fdm) process parameter prediction and optimization using group method for data handling (gmdh) and differential evolution (de). *Int J Adv Manuf Technol* 73:509–519. <https://doi.org/10.1007/s00170-014-5835-2>
40. Sood AK, Ohdar RK, Mahapatra SS (2010) Parametric appraisal of mechanical property of fused deposition modelling processed parts. *Mater Des* 31:287–295. <https://doi.org/10.1016/j.matdes.2009.06.016>
41. Nabipour M, Akhoundi B (2020) An experimental study of FDM parameters effects on tensile strength, density, and production time of ABS/Cu composites. *J Elastomers Plast* 009524432091683. <https://doi.org/10.1177/0095244320916838>
42. Moradi M, Meiabadi S, Kaplan A (2019) 3D printed parts with Honeycomb internal pattern by fused deposition modelling: experimental characterization and production optimization. *Met Mater Int* 25:1312–1325. <https://doi.org/10.1007/s12540-019-00272-9>
43. Yang L, Li S, Li Y et al (2019) Experimental investigations for optimizing the extrusion parameters on FDM PLA printed parts. *J Mater Eng Perform* 28:169–182. <https://doi.org/10.1007/s11665-018-3784-x>
44. Moradi M, Karami Moghadam M, Shamsborhan M et al (2020) The synergic effects of FDM 3D printing parameters on mechanical behaviors of bronze poly lactic acid composites. *J Compos Sci* 4:17. <https://doi.org/10.3390/jcs4010017>
45. Yadav D, Chhabra D, Gupta RK, et al (2020) Modeling and analysis of significant process parameters of FDM 3D printer using ANFIS. In: *Materials Today: Proceedings*. Elsevier Ltd, pp 1592–1604

46. El Magri A, El Mabrouk K, Vaudreuil S et al (2020) Optimization of printing parameters for improvement of mechanical and thermal performances of 3D printed poly(ether ether ketone) parts. *J Appl Polym Sci* 137:1–14. <https://doi.org/10.1002/app.49087>
47. Kamoona SN, Masood SH, Mohamed OA (2018) Experimental investigation on flexural properties of FDM processed Nylon 12 parts using RSM. In: *IOP Conference Series: Materials Science and Engineering*
48. Ramesh M, Panneerselvam K (2020) Mechanical investigation and optimization of parameter selection for Nylon material processed by FDM. *Mater Today Proc.* <https://doi.org/10.1016/j.matpr.2020.02.697>

Layout Optimization for FDM Process by Multi-objective Optimization Using RSM and GRA



Sandeep Rathee and Manu Srivastava

Abstract This chapter presents an overview of various aspects for quantitatively optimizing the fused deposition modelling (FDM) layout process. After initial introductory sections, a case study for utilizing hybrid optimization strategy by combining response surface methodology (RSM) with grey relational analysis (GRA) for optimizing multiple responses to achieve improved cost effectiveness for FDM process is presented. Spatial orientation (SO), air gap (AG), raster angle (RA) and contour width (CW) are taken as process variables. Also, build time (BT), model material volume (MV) and support material volume (SV) are considered as response in present work. Thirty experiments were performed for acrylo butadiene styrene (ABS) P400 on FDM machine for conical-shaped constructive solid geometry (CSG) primitives. Aim of the current case study is establishing a scientific reference for optimizing BT, MV and SV. Process parameter values of 0.654 mm CW, 0.0254 mm AG, 0° RA and 30° SO correspond to optimal process parameters.

1 Introduction

Additive manufacturing (AM) has established itself as a widely accepted technology to reduce processing time and facilitate fast product creation for further commercialization. In AM, any conceived part with manufacturing functionality is created directly from 3D digital data. This technology was initially utilized only for prototyping applications but has today extended itself to full-fledged tooling and manufacturing [1, 2]. Rapid prototyping (RP) was the original term used for AM processes and this term is still applied in many cases. However, the term RP is not

S. Rathee

Department of Mechanical Engineering, Amity University Madhya Pradesh, Gwalior, India
e-mail: rathee8@gmail.com

M. Srivastava (✉)

Department of Mechanical Engineering, Indian Institute of Information Technology,
Design and Manufacturing, Jabalpur, India
e-mail: manu@iiitdmj.ac.in

apt for these processes since it does not include the additive and layered nature of AM techniques. According to ASTM guidelines: AM is defined as a technique of producing objects by adding material in a layered fashion contrary to the conventional approach based upon material subtraction as per ASTM F42 standard. It is worth mentioning here that ASTM committee consensus advocated use of term AM. In general, AM processes require only detailed dimensions, materials and machine working details for part fabrication.

However, it needs to be kept into consideration that AM processes have not yet being fully explored owing to several challenges. Many aspects like quality, communication interface, material compatibility, mechanical properties, production speeds, design aspects, etc. need attention before AM can emerge as a full-fledged manufacturing option.

The present chapter is based upon a case study for quantitative layout optimization of FDM process that falls under the genre of extrusion-based processes. Details of extrusion-based processes are presented in the subsequent section.

2 Extrusion Based AM Processes

Extrusion based AM processes fundamentally utilize a basic principle of forcing semi-molten material with pressure from a nozzle at either continuous (fixed layer thickness) or variable rates (variable layer thickness) for obtaining layers which further consolidate/bond to make complete artefact after its solidification. The process can have two fundamental control mechanisms to enable layer formation. Temperature or chemical changes are the two basic control mechanism for enabling creation of layers. Temperature-based systems involve liquification of molten material in a reservoir for enabling its flow through nozzle and bonding with substrate. Chemical based systems involve chemical change driven solidification of layers by curing/residual solvents/reaction with air/drying. Extrusion based processes have manifold applications.

FDM has established itself as the most prominent extrusion-based process. Owing to the simplicity of principle, FDM process is a precursor technology for many rep rap techniques as well as commercial fused filament fabrication (FFF) techniques.

3 Fused Deposition Modelling (FDM)

S. Scott Crump in 1980s initially proposed FDM process which was subsequently made commercial by Stratasys. FDM as an AM technique has established strengths which includes features like robustness, ease of operation, part intricacy, etc. It does not require any tooling and human interference involved is also minimal. FDM can be utilized to fabricate models, prototypes as well as end parts. Its working involves

uncoiling of plastic filament from its spool which then goes into an extrusion nozzle. Choosing the nozzle and filament is specific need dependent. Heating element of the nozzle causes melting of the material. Machine bed moves in horizontal and vertical direction with the aid of an automated computational mechanism which in turn is directly under control of CAM software package. Layers are formed by extrusion of model materials directly either on substrate or upon the previously deposited layer. FDM offers a variety of choices ranging from legacy modelers to modern day machines. FDM prototypes/products may possess many applications like concept models, biomedical parts and so on [4–8].

Acrylonitrile butadiene styrene (ABS) plastic is a predominantly used FDM model material. In FDM, the basic concept of diffusion welding is utilized which is not continuous owing to which material is not uniformly distributed. This reduces part strength and additionally amounts to anisotropic FDM parts.

Figure 1 presents a FDM schematic. FDM process is based on the following working steps: First, three-dimensional CAD model is exported into FDM Insight™ in .stl format. This is followed by generating the process plan to control machine. The heating element brings the incoming ABS filament to a semi-molten form and subsequently it is forced out from a nozzle for deposition upon previous layer/substrate. The process is repeated until final part is obtained. Since the material is extruded in partially-molten state, fusion of newer material into previous layers takes place. Movement of head around x–y plane is followed by corresponding material deposition as per part geometry. After this, platform is lowered to enable deposition of new layer. The process is continued up to complete part fabrication as per CAD data.

Stratasys' FDM process gained huge popularity owing to their simple operation and robustness. However, there are a few challenges which include limited build speeds, accuracy and density. Also, fine layer thickness can only be achieved using extremely high-end expensive machines. Sharp corners and interiors are very difficult to obtain owing to round nozzle shape. FDM parts have high anisotropy also which may or may not be desirable based upon specific applications.

FDM process parameters are classified in four main classes which include operational, machine dependent, material dependent and geometry dependent. Each of them is in turn affected by many process parameters. A schematic relationship between these is presented in Fig. 2.

In present work, we have used four FDM parameters which include: width of contours, air gap, raster angle, spatial orientation as introduced below:

- Contour Width (A): As per Insight corollary, this is defined as “Contour width is the material bead width used for contours. Smaller values of contour width will build a part with a better surface finish. Larger values will require less time and material” [4].
- Air gap (B): As per Insight corollary, this is defined as “Air Gap sets the distance between the part and the supports when creating containment supports. Large values might position the support curve too far from the part to give

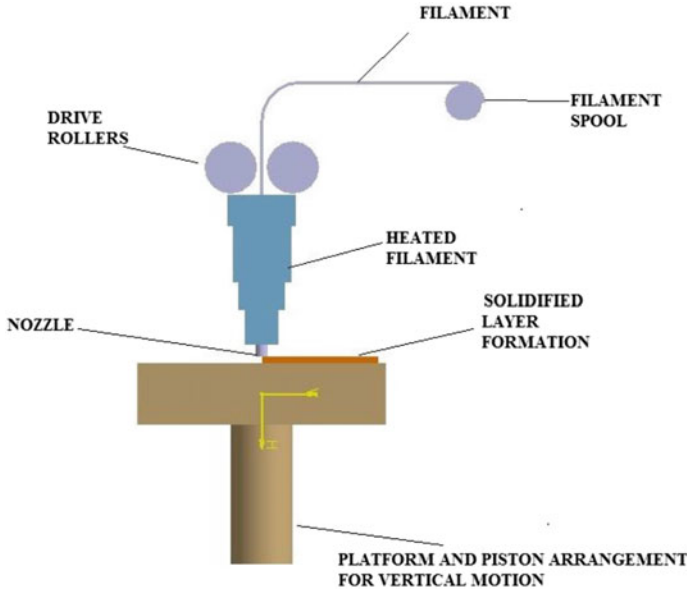


Fig. 1 FDM schematic [4]

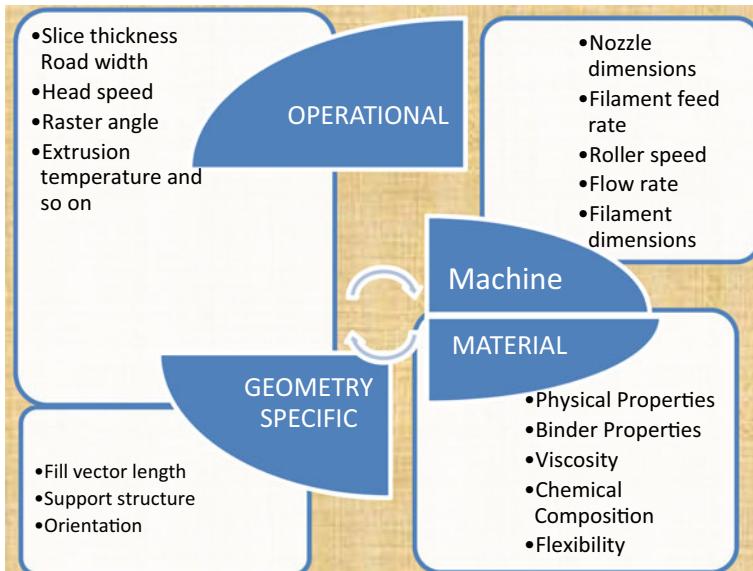


Fig. 2 FDM process parameters

support, while values that are too small might embed the support curves in the part” [4].

- Raster angle (C): As per Insight corollary, this is defined as “This angle is for rasters on the bottom part of layer. The angle is measured from the X axis of the current layer” [4].
- Orientation (D): As per Insight corollary, this is defined as “Part build orientation or orientation refers to the inclination of part in a build platform with respect to X, Y and Z axis where X and Y-axis are considered parallel to build platform and Z-axis is along the direction of part build” [4].

Remaining FDM parameters were kept constant (default values) during entire experimentation and modelling.

One can have two aspects for optimizing any given layout. One of these is quantitative and is based upon increasing volume of production and reducing cost. Another is qualitative measure and finds basis in quality enhancement of parts fabricated. A fine balance needs to be undertaken in both these aspects. In our study, we have mainly focused upon optimizing the quantitative aspects of FDM layout which mainly involves performance measures like BT, MV, SV and hence the overall production cost. These responses are briefly introduced as below:

Build Time (BT)

BT can be defined as the time spent on an AM machine in absence of bottle-necks. It should be clear that BT is not the same as process time or speed despite these two being direct indicators of each other. The same can be verified from Fig. 3 which clearly shows BT as a subset of process time.

A very important consideration is that superior parts might be desirable even at considerably high BT requirement. Lower BT should thus not be always preferable even when it means lower production cost in terms of money and time. Judicial weightage of BT against other design targets is thus mandatory before any final decision.

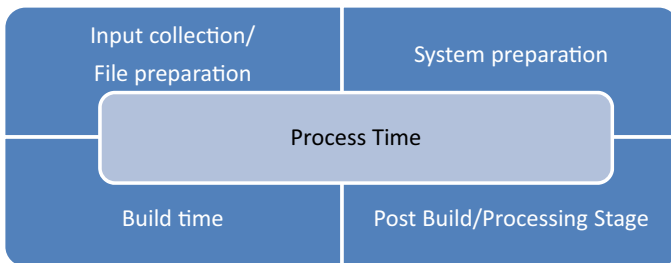


Fig. 3 FDM process time [1, 4]

Model Material Volume (MV)

As per Insight corollary, this is defined as “model material volume is the amount of raw material used for making component”. Most AM modelers including FDM utilize expensive MVs and its optimal utilization if of critical importance. Also, MVs requirement is different for every application. For example, porous scaffolds need minimal MV but service model parts need more of it, concept models might need lesser MV but structural parts require fully dense parts and so on.

Support Material (SM)

As per Insight corollary, this is defined as “support material volume is the amount of material used as support for making a component”. Significant savings are obtained by selecting optimal SM volume.

FDM Maxum powered by Insight software was utilized for experimentation and modelling in the present case study as shown as Fig. 4 (a) and (b) respectively.

In any FDM process, process performance is optimized based upon choice of correct parameters. In the current case study, selection of process parameters is based upon trial runs and previous experience [4–13]. Traditional methods including RSM and Taguchi methods give best performance when optimization of single response is desired but these are not preferred when multiple responses need to be simultaneously optimized. Techniques like grey relational analysis, fuzzy logic, etc. are frequently used for optimizing multi-response cases in addition to newer strategies including ant colony optimization, swarm optimization and so on [14–18]. A hybrid optimization strategy is used in the current case study where experimental design task is performed via RSM and GRA is used for simultaneous optimization of multiple responses. Both these techniques have been introduced in following section.

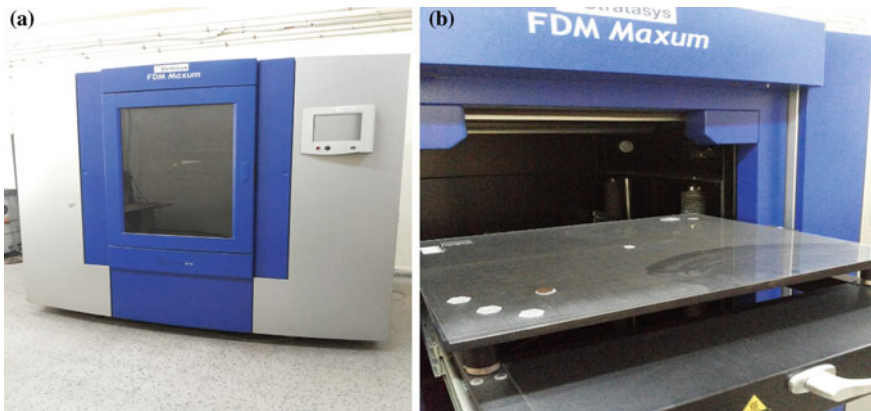


Fig. 4 a FDM maxum modeler, b built chamber of FDM maxum

4 Methodology

4.1 RSM Based Experimentation

Design Expert software is utilized to design experimental runs in this case study and the chosen design is CCD with three responses and four parameters having 30 total experimental runs.

Experiments were then conducted to establish effect of process parameters (CW, SO, RA and AG) on responses (BT, MV, SV) of conical ABS primitive for FDM process. The orientation of conical part about x-axis is kept in a manner to minimize z-height. This choice is because a part oriented in such a fashion results in least BT requirement. Dimensions of STL for cone shaped part are: X = 20, Y = 20, Z = 69.999 (all dimensions are in millimeters). Levels of input parameters for experimentation are presented in Table 1. 3D part drawing obtained from Solidworks software is saved in .stl format which was subsequently given as input to Insight of FDM maxum modeller. Results of experiments have been tabulated in Table 2.

4.2 Multi Response Optimization Using GRA

This case study involves studying the impact of varying process variables (CW, RA, SO, AG) on responses (BT, MV, SV). In all these responses, all the data sequences have lower-the-better nature. During normalizing experimental results for performance characteristics to arrive upon normalized values (NV), we normalize original experimental sequences in range of 0–1 owing to variation in units for measuring each. This step preprocesses data and is known as grey relational generating. Table 3 presents result of normalization as well as deviation sequence (DS) for each response. Further, grey relational coefficient (GRC) corresponding to response for every experimental run is evaluated for obtaining grey relational grade (GRG). This GRG is an overall indicator for least value of each response. The experiment which generates maximum value of GRG is then chosen (13th experiment in present case). It is thus observed that using GRA approach, a multi-response problem is converted into single equivalent objective function optimization case. Higher GRG implies the proximity of optimal combination of factors.

Table 1 Input variables with levels

S. No.	Parameters	Level 1	Level 2	Level 3
1	CW (A)	0.429 mm	0.5415 mm	0.654 mm
2	SO (D)	0°	15°	30°
3	RA (C)	0°	15°	30°
4	AG (B)	-0.0254 mm	0 mm	0.0254 mm

Table 2 Response table

Std	Run order	A	B	C	D	BT	MV	SV
		mm	mm	Deg	Deg	Hours	cm ³	cm ³
18	1	0.654	0	15	15	1.15	7.668	1.616
20	2	0.5415	0.0254	15	15	1.133	7.253	1.616
7	3	0.429	0.0254	30	0	1.283	7.256	1.632
10	4	0.654	-0.0254	0	30	1.133	8.121	1.593
29	5	0.5415	0	15	15	1.167	7.664	1.619
16	6	0.654	0.0254	30	30	1.267	7.279	1.621
3	7	0.429	0.0254	0	0	1.1	7.241	1.608
15	8	0.429	0.0254	30	30	1.283	7.255	1.617
8	9	0.654	0.0254	30	0	1.267	7.282	1.631
23	10	0.5415	0	15	0	1.167	7.663	1.616
6	11	0.654	-0.0254	30	0	1.317	8.144	1.629
11	12	0.429	0.0254	0	30	1.1	7.241	1.604
12	13	0.654	0.0254	0	30	1.083	7.264	1.591
1	14	0.429	-0.0254	0	0	1.15	8.149	1.59
22	15	0.5415	0	30	15	1.3	7.682	1.629
9	16	0.429	-0.0254	0	30	1.15	8.149	1.588
19	17	0.5415	-0.0254	15	15	1.183	8.139	1.621
21	18	0.5415	0	0	15	1.1	7.666	1.599
13	19	0.429	-0.0254	30	30	1.35	8.172	1.631
2	20	0.654	-0.0254	0	0	1.133	8.121	1.609
26	21	0.5415	0	15	15	1.167	7.664	1.621
30	22	0.5415	0	15	15	1.167	7.664	1.621
24	23	0.5415	0	15	30	1.167	7.666	1.619
14	24	0.654	-0.0254	30	30	1.317	8.141	1.619
28	25	0.5415	0	15	15	1.167	7.664	1.621
5	26	0.429	-0.0254	30	0	1.35	8.171	1.619
25	27	0.5415	0	15	15	1.167	7.664	1.621
17	28	0.429	0	15	15	1.167	7.666	1.621
4	29	0.654	0.0254	0	0	1.083	7.266	1.609
27	30	0.5415	0	15	15	1.167	7.664	1.621

5 Results and Discussion

Response values of experiments are tabulated in Table 2. RSM is utilized for checking sufficiency of models at 95 percent confidence interval. Calculation of normalized values (NV) is undertaken and deviation sequences (DS) are correspondingly estimated for every experiment on the basis of GRA principle. This is

followed by calculation of grey relational coefficient (GRC) for every response at each experimental run. Grey relational grade (GRG) is then found out. GRG ranks each run for prediction of optimal process parameters to achieve multi-objective optimization. A compilation of these results is presented as Table 3.

Table 3 Normalized values, deviation sequence, grey relation coefficient of BT, MV and SV. Calculation of GRG and rank for multi response optimization

Run order	NV			DS			GRC			GRG	Rank
	BT	MV	SV	BT	MV	SV	BT	MV	SV		
1	0.749	0.541	0.364	0.251	0.459	0.636	0.666	0.522	0.440	0.542	14
2	0.813	0.987	0.364	0.187	0.013	0.636	0.728	0.975	0.440	0.714	5
3	0.251	0.984	0.000	0.749	0.016	1.000	0.400	0.969	0.333	0.567	12
4	0.813	0.055	0.886	0.187	0.945	0.114	0.728	0.346	0.815	0.629	9
5	0.685	0.546	0.295	0.315	0.454	0.705	0.614	0.524	0.415	0.518	17
6	0.311	0.959	0.250	0.689	0.041	0.750	0.420	0.925	0.400	0.582	11
7	0.936	1.000	0.545	0.064	0.000	0.455	0.887	1.000	0.524	0.804	4
8	0.251	0.985	0.341	0.749	0.015	0.659	0.400	0.971	0.431	0.601	10
9	0.311	0.956	0.023	0.689	0.044	0.977	0.420	0.919	0.338	0.559	13
10	0.685	0.547	0.364	0.315	0.453	0.636	0.614	0.525	0.440	0.526	16
11	0.124	0.030	0.068	0.876	0.970	0.932	0.363	0.340	0.349	0.351	29
12	0.936	1.000	0.636	0.064	0.000	0.364	0.887	1.000	0.579	0.822	2
13	1.000	0.975	0.932	0.000	0.025	0.068	1.000	0.953	0.880	0.944	1
14	0.749	0.025	0.955	0.251	0.975	0.045	0.666	0.339	0.917	0.640	8
15	0.187	0.526	0.068	0.813	0.474	0.932	0.381	0.514	0.349	0.415	26
16	0.749	0.025	1.000	0.251	0.975	0.000	0.666	0.339	1.000	0.668	7
17	0.625	0.035	0.250	0.375	0.965	0.750	0.572	0.341	0.400	0.438	25
18	0.936	0.544	0.750	0.064	0.456	0.250	0.887	0.523	0.667	0.692	6
19	0.000	0.000	0.023	1.000	1.000	0.977	0.333	0.333	0.338	0.335	30
20	0.813	0.055	0.523	0.187	0.945	0.477	0.728	0.346	0.512	0.528	15
21	0.685	0.546	0.250	0.315	0.454	0.750	0.614	0.524	0.400	0.513	22
22	0.685	0.546	0.250	0.315	0.454	0.750	0.614	0.524	0.400	0.513	21
23	0.685	0.544	0.295	0.315	0.456	0.705	0.614	0.523	0.415	0.517	18
24	0.124	0.033	0.295	0.876	0.967	0.705	0.363	0.341	0.415	0.373	27
25	0.685	0.546	0.250	0.315	0.454	0.750	0.614	0.524	0.400	0.513	20
26	0.000	0.001	0.295	1.000	0.999	0.705	0.333	0.334	0.415	0.361	28
27	0.685	0.546	0.250	0.315	0.454	0.750	0.614	0.524	0.400	0.513	19
28	0.685	0.544	0.250	0.315	0.456	0.750	0.614	0.523	0.400	0.512	24
29	1.000	0.973	0.523	0.000	0.027	0.477	1.000	0.949	0.512	0.820	3
30	0.685	0.546	0.250	0.315	0.454	0.750	0.614	0.524	0.400	0.513	23

6 Conclusions

After a preliminary introductory section where AM processes are briefly outlined in addition to extrusion based and specially FDM process, a case study for quantitative optimization is provided in this chapter to provide the readers an in-depth process understanding.

A decision on process parameters and their levels followed by a seasoned choice of responses for quantitative layout optimization for FDM process, RSM and GRA are utilized for optimizing the process parameters that significantly affect process cost (BT, MV and SV). Multi objective optimization of responses via hybrid route is then attempted. Hybrid RSM-GRA approach yields the following optimal combination of parameters: 0.654 mm CW, 0.0254 mm AG, 0° RA and 30° SO. Optimal values of responses BT, MV and SV at this combination were 1.083 h, 7.264 cm³ and 1.59 cm³ respectively. These results if properly used can facilitate AM practitioners (research, academics and industry) as an effective guideline for quantitative layout optimization for FDM process.

References

1. Srivastava M, Rathee S, Maheshwari S, Kundra TK (2019) Additive manufacturing: fundamentals and advancements. CRC Press, Boca Raton, Florida
2. Rathee S, Srivastava M, Maheshwari S, Kundra TK, Siddiquee AN (2018) Friction based additive manufacturing technologies: principles for building in solid state, benefits, limitations and applications. CRC Press, Boca Raton, Florida
3. Tolio T, Ceglarek D, ElMaraghy HA, Fischer A, Hu SJ, Laperrière L, Newman ST, Váncza J (2010) SPECIES—CO-evolution of products, processes and production systems. *CIRP Ann* 59(2):672–693
4. Srivastava M (2015) Some studies on layout of generative manufacturing processes for functional components. Delhi University, India
5. Srivastava M, Maheshwari S, Kundra TK, Rathee S (2016) An integrated rsm-ga based approach for multi response optimization of FDM process parameters for pyramidal ABS primitives. *J Manuf Sci Prod*. <https://doi.org/10.1515/jmsp-2016-0012>
6. Srivastava M, Maheshwari S, Kundra TK, Rathee S, Yashaswi R, Sharma SK (2016) Virtual design, modelling and analysis of functionally graded materials by fused deposition modeling. *Mater Today Proc* 3(10):3660–3665
7. Srivastava M, Maheshwari S, Kundra TK, Rathee S, Yashaswi R (2016) Experimental investigation of process parameters for build time estimation in FDM process using RSM technique. In: Mandal DK, Syan CS (eds) *CAD/CAM, robotics and factories of the future*. Springer, India, pp 229–241
8. Srivastava M, Maheshwari S, Kundra TK, Yashaswi R, Rathee S (2016) Integration of fuzzy logic with response surface methodology for predicting the effect of process parameters on build time and model material volume in FDM process. In: Mandal DK, Syan CS (eds) *CAD/CAM, robotics and factories of the future*. Springer, India, pp 195–206
9. Srivastava M, Maheshwari S, Kundra TK, Rathee S (2017) Estimation of the effect of process parameters on build time and model material volume for FDM process optimization by response surface methodology and grey relational analysis. In: Wimpenny DI, Pandey PM,

- Kumar LJ (eds) *Advances in 3D printing and additive manufacturing technologies*. Springer Singapore, Singapore, pp 29–38
10. Srivastava M, Maheshwari S, Kundra TK, Rathee S (2017) Multi-response optimization of fused deposition modelling process parameters of ABS using response surface methodology (RSM)-based desirability analysis. *Mater Today Proc* 4(2):1972–1977
 11. Srivastava M, Rathee S (2018) Optimisation of FDM process parameters by Taguchi method for imparting customised properties to components. *Virtual Phys Prototyping* 13(3):203–210
 12. Srivastava M, Rathee S, Maheshwari S, Kundra TK (2018) Multi-objective optimisation of fused deposition modelling process parameters using RSM and fuzzy logic for build time and support material. *Int J Rapid Manuf* 7(1):25–42
 13. Srivastava M, Rathee S, Maheshwari S, Kundra TK (2019) Estimating percentage contribution of process parameters towards build time of FDM process for components displaying spatial symmetry: a case study. *Int J Mater Prod Technol* 58(2–3):201–224
 14. Lin C, Lin J, Ko T (2002) Optimisation of the EDM process based on the orthogonal array with fuzzy logic and grey relational analysis method. *Int J Adv Manuf Technol* 19(4):271–277
 15. Suresh Kumar B, Baskar N (2013) Integration of fuzzy logic with response surface methodology for thrust force and surface roughness modeling of drilling on titanium alloy. *Int J Adv Manuf Technol* 65:1501–1514
 16. Tarng YS, Yang WH, Juang SC (2000) The use of fuzzy logic in the Taguchi method for the optimization of the submerged arc welding. *Int J Adv Manuf Technol* 16:688–694
 17. StatEase (2014) *Design Expert*, Ed, F.I.T. package
 18. Bharti PS (2012) Optimization of process parameters of electric discharge machining based on neural networks and Taguchi's method. Guru Gobind Singh Indraprastha University, New Delhi